AN INTEGRATED FIELD, GEOCHEMICAL AND U-Pb GEOCHRONOLOGICAL STUDY OF THE SOUTHWEST HERMITAGE FLEXURE (NEWFOUNDLAND APPALACHIANS, CANADA) AND THE SIERRA DE GUADARRAMA (IBERIAN MASSIF, CENTRAL SPAIN): A CONTRIBUTION TO THE UNDERSTANDING OF THE GEOLOGICAL EVOLUTION OF CIRCUM-ATLANTIC PERI-GONDWANA

PABLO VALVERDE-VAQUERO

AN INTEGRATED FIELD, GEOCHEMICAL AND U-Pb GEOCHRONOLOGICAL STUDY OF THE SOUTHWEST HERMITAGE FLEXURE (NEWFOUNDLAND APPALACHIANS, CANADA) AND THE SIERRA DE GUADARRAMA (IBERIAN MASSIF, CENTRAL SPAIN): A CONTRIBUTION TO THE UNDERSTANDING OF THE GEOLOGICAL EVOLUTION OF CIRCUM-ATLANTIC PERI-GONDWANA

VOLUME I: Text

By:

© PABLO VALVERDE-VAQUERO; Lic.; M.Sc.

A thesis submitted to the School of Graduate Studies
in partial fulfilment of the requirements for the degree
of Doctor of Philosophy

Department of Earth Sciences
Memorial University of Newfoundland

September 1997

St. John's Newfoundland

ABSTRACT:

An integrated field and analytical study of three areas in Newfoundland and Spain was carried out to investigate the extent of the linkage between the geological evolution of the Peri-Gondwanan margin of the Iapetus Ocean, recorded in the southwest Hermitage Flexure of the Newfoundland Appalachians, and that of the Sierra de Guadarrama in the Central Iberian Zone of the Iberian Massif (European Variscan Belt). This study, while resolving the timing and character of the respective Appalachian and Variscan overprints, highlights the major importance of the Early Ordovician (ca. 480-470 Ma) magmatic events.

The Cinq-Cerf gneiss is part of the westernmost extent of the Late Precambrian basement block of the Hermitage Flexure. New data from the Cinq-Cerf gneiss demonstrates that this is a composite unit formed by highly strained metasedimentary rocks and 675+12/-11 Ma granitic orthogneiss, locally intruded by weakly defomed 584+7/-6 Ma Hbl-bearing granodiorite and a transitional/volcanic arc tholeiitic 557+14/-5 Ma metagabbro. Although variably deformed during the intrusion of the synkinematic 431.5±1 Ma Western Head granite and the subquent, 420 Ma, greenschist facies overprint, this set of rocks preserve evidence of pre-Silurian deformation. This is consistent with a basement-cover relationship between the Cinq-Cerf-gneiss and the nearby low-grade 583-570 Ma volcanosedimentary rocks. The 675 Ma intrusive event provides a strong link with the Avalon Zone further demonstrating that Avalonian rocks (*s.s.*) were involved in the Early Paleozoic evolution of the eastern margin of the Iapetus Ocean.

Further west the gneissic rocks of the Port-aux-Basques complex, generally adscribed to the Gander Zone, separate the Avalonian basement of the Hermitage Flexure from the

suture with the peri-Laurentian margin. New data shows that the oldest set of intrusives, the Margaree orthogneiss, represent a 20 km long, 474-465 Ma mafic-felsic igneous complex overprinted by Silurian (417-410 Ma) upper amphibolite facies metamorphism and deformation. The geochemical signatures of the Margaree orthogneiss suggest that it formed in a transitional arc/back arc setting at the time of the major Late Arenig-Llanvirn back-arc rifting event in the peri-Gondwanan margin of the Northern Appalachians.

In the Iberian Massif, the orthogneisses of the Sierra de Guadarrama form the southern portion of an enigmatic belt of pre-Variscan augen-gneisses that extends 600 km along the northern Central Iberian Zone (CIZ). Dating across the Berzosa-Riaza shear zone (BRSZ) demonstrates the presence of 468 Ma granites in the shear zone, 480±2 Ma volcanism in the low-medium grade hangingwall and coeval 488-477 Ma granitic batholiths in the high grade footwall. The 480 volcanism brackets the Sardic deformation in the CIZ between the Mid-Late Arenig. The BRSZ has an oblique extensional movement coincident with peak metamorphism (337-327 Ma), which developed during the Variscan D2 deformation (330-321 Ma), resulting in decompression and late-D2 growht of low P / high T assemblages (322 Ma) in the infrastructure. The shallow intrusion of the post-tectonic La Cabrera granite, dated at 292±2 Ma, seals the BRSZ and marks the end of the Variscan deformation. This new data demonstrates, for the first time, that the Early-Mid Carboniferous syn-collisional extension in the CIZ was coeval with extension along the entire hinterland of the Variscan belt.

These Ordovician orthogneisses of the Sierra de Guadarrama are interpreted as relicts of a short-lived magmatic arc coeval with the subduction-related break-up of Avalonia from Gondwana. This new data illustrates the striking parallelism between the Early Paleozoic events in the Peri-Gondwanan side of the Northern Appalachians and the southern portion of the European Variscan belt.

ACKNOWLEDGMENTS:

My deepest gratitude to the people of Canada who funded this project through the NSERC operating grant of Dr. Dunning and a Memorial University Graduate Scholarship. On a more personal level, I have to praise my thesis supervisor Prof. Greg Dunning and my co-supervisors Prof. Aphrodite Indares and Sean O'Brien (Newfoundland Department of Mines and Energy), for their continuous encouragement and guidance during all stages of this project, and their fanatic obsession with field relationships!! Also, I have to thank Dr. Peter Cawood for his guidance in the early stages of this project.

Laboratory training by Prof. Dunning, Jim Connelly and, especially, Kathy Manser was crucial to my mastering of the U-Pb geochronological technique. Kathy and Rod Churchill also shared the boredom and noise of the crushing room with me. Thanks to Pat Horan for keeping an eye on the mass-spectrometer and always being there to answer my questions. Pam King, Mike Turbett, Lakmali Hewa and Maggy Piranhan helped immensely with XRF, ICP-MS analyses and microprobe EDS determinations. Lloyd and Rick from the rock shop always had my thin sections ready on time. Pat Browne, Gerry Ford, Gerry Starkes, Maureen Moore, and Teresa Lannon helped me with all the university bureaucratic red tape.

It was, thanks to Cees van Staal (GSC, Ottawa), that I had the chance of having the true Canadian field experience with helicopter, tent, black-flies, wet boots and memorable open-water boat rides. He introduced me to the geology of the Port-aux-Basques area and was of great assistance and guidance during fieldwork in the Margaree orthogneiss. Shoufa Lin, Lindsay Hall and Dave Scholfield are thanked for field and general discussions on Port-aux-Basques geology. Discussions on the geology of the Cinq-Cerf gneiss and its surroundings with Brian O'Brien (Newfoundland Dept. of Mines and Energy) and Benoit

Dubé (GSC) were of great assistance. The boatmanship of Clyde Billard of Grand Bruit was greatly appreciated while navigating around Three Islands and Cinq-Cerf Bay.

Cecilio Quesada (Spanish Geological Survey, ITGE), Felix Bellido (ITGE), Enrique Martinez (Univ. Oviedo) and Florentino Diaz (Univ. de Oviedo) provided a crucial two-week field trip around the Ossa-Morena Zone, the Sierra de Guadarrama and NW Spain in 1993, during which the Sierra de Guadarrama was selected as a field area. Cecilio Quesada and Roberto Rodriguez (ITGE) were instrumental in organizing the close collaboration with the mapping crew of INYPSA, which partially covered field expenses in Spain. Pedro Pablo Hernaiz (INYPSA) and Javier Escuder (Univ. Complutense, Madrid) are thanked for interesting field discussion, free exchange of ideas and general friendship. Antonio Azor (Univ. de Granada) provided a copy of his unpublished "tesina de licenciatura". Luis Gonzalez (Univ. de Granada) photocopied and sent me a large amount of Spanish bibliography (I owe you one, Luis!). Also, thanks to the people of Montejo de la Sierra who enriched my field seasons with their animated character (specially to the patrons of "Meson el Hayedo" who provided occasional free-drinks!!) and to my sister Ana for allowing her car to be remorselessly abused during two full field-seasons

Thanks to Dave Corrigan and John Ketchum who were "assaulted" for geological advise and bibliography during the writing stages of this thesis. Special thanks to Ingo, Joy, Sandy, Steve, Arden, Jeroen, Jason, Adam and again to Dave for their friendship and companionship, and to my office-mate and fellow "lab rat" Richard Cox for making life easier with his corrosive sense of humour, friendship and fly-tying tips!!. .

Finally I would like to dedicate this work to my family and my girlfriend Pilar, who have endured with me the long separations, for their love and unconditional support.

TABLE OF CONTENTS

VOLUME I: Text

CHAPTER II

CHAPTER IV

CHAPTER VI

CHAPTER VII

APPENDIX

LIST OF TABLES

Volume I: Text

APPENDIX

Volume II: Tables, Maps and Figures

LIST OF MAPS

Volume II: Table, Maps and Figures

CHAPTER III.- THE CINQ-CERF GNEISS (SW Hermitage Flexure): The make up of a polyciclic Avalonian gneissic complex.

LIST OF FIGURES:

Volume I: Text

APPENDIX

Volume II: Tables, Maps and Figures

CHAPTER I: INTRODUCTION.

CHAPTER II: THE NEWFOUNDLAND APPALACHIANS.

CHAPTER III.- THE CINQ-CERF GNEISS (SW Hermitage Flexure)

LIST OF ABBREVIATIONS:

Symbols for rock-forming minerals (after Bucher and Frey, 1994)

Am	amphibole	Crd	cordierite	Qtz	quartz
An	anorthite	Ep	epidote	Sill	sillimanite
And	andalusite	Grt	garnet	St	staurolite
Bt	biotite	Kfs	K-feldspar	Ttn	titanite
Cam	clinoamphibole	Ky	kyanite	Tur	tourmaline
Chl	chlorite	Mnz	monazite	Zrn	zircon
Cld	chloritoid	Opx	orthopyroxene		
Cpx	clinopyroxene	Pl	plagioclase		

Other abbreviations (The rest of abbreviations are specified in the text):

cm	centimetre	Ls	stretching lineation
C°	degrees Celsius	m	meter
D	episode of deformation	mm	millimeter
		N	north
E	east	P	pressure
F	fold, episode of folding	ppm	parts per million
		S	south
HP	high pressure	T	temperature
HT	high temperature	W	west
Kb	kilobar	Ø	diameter
km	kilometer	≈	approximately
Lmin	mineral lineation	%	weight / modal percentage
LP	low pressure		

CHAPTER I

INTRODUCTION TO A STUDY OF THE PRECAMBRIAN AND PALEOZOIC GEOLOGICAL EVOLUTION OF PERIGONDWANA IN THE NEWFOUNDLAND APPALACHIANS AND THE IBERIAN MASSIF.

This thesis was originally conceived to assess the extent of the similarities between the Precambrian and Paleozoic geological evolution of the peri-Gondwanan elements of the Newfoundland Appalachians (e.g. O'Brien et al., 1996) and the Iberian Massif (Fig.1.1A) and, in doing so, to attempt to find the pre-Cadomian/Avalonian basement in both areas. Reported Late Precambrian events from the Iberian Massif and the Avalon Zone of the Newfoundland Appalachians suggested a similar Late Precambrian geological evolution (Fig.1.1B; Iberian Massif: Quesada, 1990a; Quesada, 1990b; Avalon Zone: O'Brien et al., 1983; O'Brien et al., 1990; O'Brien et al., 1996). This Precambrian evolution was connected with the development of the Pan-African orogens around the margins of Gondwana (Strachan and Taylor, 1990; Rogers, 1996). Two main areas, both with reported vestiges of Cadomian/Avalonian events, were selected for this study (Fig.1.1). The one in the Newfoundland Appalachians is in the western Hermitage Flexure (Williams et al., 1970; Brown, 1975; Dunning and O'Brien, 1989; O'Brien et al., 1991; O'Brien et al., 1993), which contains some of the most outboard relicts of Avalonian rocks of the Appalachian-Caledonian orogen (Fig.1.1). In the Iberian Massif, the medium- and high-grade rocks of the eastern Sierra de Guadarrama (Fig.1.1; Fernández Casals, 1979; Macaya et al., 1991;Vialette et al., 1986; Vialette et al., 1987; Wildberg et al., 1989; Azor et al.,

1992), in the Central Iberian Zone (Lotze, 1945; Julivert et al., 1972; Quesada, 1991) were selected for study. Additionally, the study involved the unraveling of the intensity and the character of the Appalachian and Variscan overprints in these different areas and offered an opportunity to further understand these Paleozoic events, responsible for the reamalgamation of the Late Precambrian peri-Gondwanan relicts of the North Atlantic.

This study also provides a series of different strategies to constrain absolute timing of deformation in medium- and high-grade terranes. These strategies are based on the combination of detailed classic field and petrographic work with high-precision U-Pb geochronology, which allows the integration of precise U-Pb protolith and metamorphic ages with clear field and petrographic relationships. Metamorphic conditions were assessed using stable mineral assemblages. It should be noted that the emphasis was placed more on assessing the conditions during deformation rather than having a precise estimation of the PT conditions. Additionally, whole rock major- and trace-element geochemistry of a selected number of samples was determined to maximize the information obtained from the protolith ages from the field areas in the Newfoundland Appalachians.

This thesis has three main parts. The first part deals with the areas in the southwest Newfoundland Appalachians (Chapters III and IV), and includes a general introduction to the geology of the Newfoundland Appalachians (Chapter II). The second part covers the Sierra de Guadarrama in the Central Iberian Zone (Chapter VI); an introduction to the geology of the Iberian Massif is also provided (Chapter V). The third and final part focuses on the significance of the contributions of the data from southwest Newfoundland and Central Spain to the understanding of the evolution of the Paleozoic circum-North Atlantic orogens (Chapter VII).

The following introductory sections provide justification for the field area selection, as well as a general geologic overview of the Paleozoic circum-North Atlantic orogens. Also, to clarify further discussions, a series of paleogeographic concepts are defined, followed by a synopsis of the evolution of the peri-Gondwanan circum-North Atlantic terranes, and an assessment of the possible connections between the Newfoundland Appalachians and the Iberian Massif.

1.1.- PURPOSE AND SCOPE.-

The rationale behind selecting gneissic complexes for this study is that these are in most cases blocks of lower or middle crust with a complex and in places prolonged tectonothermal evolution, constituting potential relicts of pre-orogenic crystalline basement in any orogenic belt. By unraveling the timing and character of the different deformational, metamorphic and intrusive events, it could be possible not only to assess the contemporaneity of the tectonic processes that operated at different crustal levels within the same segment of the orogen or along different parts of the orogen but to reconstruct part of its pre-orogenic evolution. It is this pre-orogenic evolution which forms the basis of this comparative study of the extent of the peri-Gondwanan linkage between gneissic complexes in the hinterland of the Newfoundland Appalachians and Iberian Massif.

Basement in the peri-Gondwanan margin of the Newfoundland Appalachians and most of the Iberian Massif is formed by Late Precambrian rocks deformed during the Avalonian/Cadomian orogeny and variably reworked during the subsequent Paleozoic orogenies (Fig.1.1). Archean-Proterozoic granulites outcrop offshore the Iberian Massif in the Cantabrian sea (northwest Spain; Guerrot et al., 1989) and 2.1 Ga gneisses are known from the Cadomian block in the Armorican Massif (Clavez and Vidal, 1978). Such pre-

Cadomian /Avalonian crystalline basement, although suspected, has yet to be identified in both the peri-Gondawanan margin of the Newfoundland Appalachians and the Iberian Massif. The gneissic complexes selected for this study offered the highest chance of finding such relicts, so a great deal of effort was put into searching for the oldest members of these complexes.

In the Newfoundland Appalachians, there is no evidence of gneissic basement to Late Precambrian volcanosedimentary sequences of the peri-Gondwanan Avalon Zone nor gneissic country rock to its Late Precambrian plutons, except for a small area of low P / high T metasedimentary rocks in the island of Miquelon (France) (Dunning et al., 1995). However, further west, gneissic rocks are described as the oldest members of a Late Precambrian Avalonian basement (Dunning and O'Brien, 1989) within the Hermitage Flexure (Fig.1.1). Of these gneissic rocks, the best candidate to host pre-Avalonian rocks was the Cinq-Cerf gneiss (Chapter III). This gneissic complex is in contact with a low-grade Late Precambrian volcanosedimentary sequence and its contact reportedly stitched by 570 Ma granite (Dunning and O'Brien, 1989; B.H. O'Brien et al., 1991; B.H. O'Brien et al., 1993). Separating the Cinq-Cerf gneiss from the suture with the Laurentian margin, there is a 100 Km wide belt of amphibolite to upper amphibolite facies rocks, metamorphosed during the Silurian Salinic orogeny (Dunning et al., 1990), with pre-Silurian intrusive rocks and local evidence for pre-477 Ma tectonic imbrication (Tucker et al, 1994). To investigate the evolution of this western extent of the peri-Gondwanan margin of the southwestern Newfoundland Appalachians a gneissic package with lithological resemblance to the Cinq-Cerf gneiss, the Margaree orthogneiss (Chapter IV) was selected for study. The combined new data from these two field areas is expected to further the understanding of the tectonothermal record of the marginal edge of Late Precambrian northwest Gondwana (Fig.1.1A) and its Paleozoic evolution.

In the Iberian Massif, Late Precambrian rocks and evidence for Late Precambrian events is widespread (Quesada, 1991). Cadomian gneissic rocks are known to outcrop as fault bounded blocks within a large megashear zone in the Ossa-Morena Zone (Fig.1.1; Badajoz-Cordoba shear zone; Schäfer, 1990), where Cadomian tectonothermal events are well documented (e.g. Quesada, 1991; Ochsner, 1993), and in the metamorphic complexes of the Central Iberian Zone (Lancelot et al., 1985; Wildberg et al., 1989). Stratigraphic and faunal evidence (chapter V) indicates that the Central Iberian (CIZ), West Asturian-Leonese (WALZ) and the Cantabrian Zones (CZ; Fig.1.1) formed a single Paleozoic Iberian terrane against which other elements like the Ossa-Morena (OMZ), the South Portuguese (SPZ) and Galicia-Trás-os-Montes (GTMZ) zones were accreted during the Late Paleozoic. Variscan deformation was transferred from the CIZ towards the more external WALZ and CZ. Work in the CIZ had a two fold objective, to resolve the timing of the pre-Variscan events while searching for relicts of a pre-Cadomian basement and to unravel the timing and character of the Variscan overprint.

The Sierra de Guadarrama in the CIZ was selected for this study (Fig.1.1) because it is the largest single massif of pre-Variscan orthogneisses in the Iberian Massif and it is part of an enigmatic 600 Km long belt of orthogneisses which extends from the Sierra de Guadarrama in central Spain to the NW coast of Spain (e.g., Azor et al., 1992). These orthogneisses are below an Ordovician unconformity (Sardic unconformity; Díez Balda et al., 1990). This Ordovician unconformitiy is characteristic of the CIZ. In the CIZ, there is also local evidence for a well-defined Late Precambrian Cadomian unconformity, which is also common to the WALZ and the CZ. The age of these orthogneisses in the Sierra de Guadarrama has remained controversial due to a limited and unreliable age data set (Early Ordovician, Rb-Sr; Vialette et al., 1986, 1987; vs. Precambrian-Cambrian, U-Pb; Wildberg et al., 1989). Zircon analyses with large degrees of Proterozoic-Archean

inheritance indicate the presence of 2.0 Ga crustal sources (Wildberg et al., 1989) and the potential for the presence of a pre-Cadomian basement (Quesada, 1992). Additionally the Sierra de Guadarrama contains a poorly dated (Wildberg et al., 1989) relict Barrovian metamorphic sequence, partially overprinted by a Variscan low P / high T metamorphic event, and Late Variscan post-collisional plutons (Bellido et al., 1981). Therefore, it provides the ideal area for a detailed combined investigation of the pre-Variscan and Variscan evolution of the CIZ.

Late Cretaceous paleogeographic reconstruction of the North Atlantic shows that the Avalon Zone of the Newfoundland Appalachians was facing the Iberian Massif prior to the opening of the North Atlantic ocean (Fig.1.1), indicating that Iberia collided against Avalonia during the Variscan orogeny. It is possible that exotic Appalachian elements were amalgamated to the Iberian Massif as a result of the Variscan collision. This thesis, however, attempts to explore if there was a common Precambrian-Early Paleozoic connection prior to the separation of Avalonia from Gondwana (see section 1.3).

1.2.-ANATOMY OF THE CIRCUM-NORTH ATLANTIC PALEOZOIC OROGENS.-

The Paleozoic geology of the circum-Atlantic realm is characterized by the presence of two Paleozoic orogenic belts, the Caledonian-Appalachian belt and the Variscan belt. These belts are separate and well defined to the north, but merge towards the south, as a result of the final amalgamation of Pangea (Fig.1.1 and 1.2). The following is a brief description of the most fundamental features of these belts, to familiarize the Appalachian reader with the Variscan and Iberian geology and vice versa.

1.2.1.- The Appalachian-Caledonian belt.-

The Appalachian-Caledonian belt (Fig.1.2) is a linear orogenic system that extends from southern Alabama (USA) through the eastern seaboard of the USA and Atlantic Canada to Newfoundland, Ireland, the U.K., Norway and eastern Greenland. This belt records the amalgamation of different elements to Laurentia (i.e. North American craton) as a result of Paleozoic development and closure of a proto-Atlantic ocean (Wilson, 1966), the Iapetus ocean (Harland and Gayer, 1972). Initiation of the Iapetus ocean is marked by Late Precambrian rifting in the Laurentian margin (e.g., Williams, 1979) and in the opposing margin in the Scandinavian Caledonides (e.g., Andréasson, 1994). The situation is however more complicated in the British Caledonides and the Northern Appalachians since the presently opposing margin, Avalon Zone (e.g., Williams, 1979; Nance and Thompson, 1996) was undergoing arc magmatism and deformation at that time (Avalonian-Cadomian events; e.g., O'Brien et al., 1996; D'Lemos et al.(eds.), 1990; Strachan and Taylor (eds.), 1990). During most of the Cambrian there was a pause in tectonic activity on all sides of the Iapetus Ocean and major paleontological differences were established between all margins of the Iapetus (Cocks and Fortey, 1982; Fortey and Cocks, 1986; Cocks and Fortey, 1990; Neuman and Harper, 1992; Williams S.H. et al., 1995; Landing, 1996). In the Ordovician tectonic activity was renewed. The Northern and Southern Appalachians record Ordovician accretion of volcanic arc elements to the Laurentian margin, known as the Taconic orogeny (Williams, 1979; Williams and Hatcher, 1983); the Grampian orogeny is the equivalent event in the British Caledonides (Rast and Crimes, 1969; Rast et al., 1988). Early-Mid Ordovician compressional events also took place in the opposing side, the Finnmarkian orogeny in the Scandinavian Caledonides (Sturt, 1978; Dallmeyer, 1988; Andréasson, 1994) and the Penobscottian orogeny in the Northern Appalachians (Neuman, 1967; Neumann and Max, 1989; Colman-Sadd et al., 1992a; Van Staal and de Roo, 1995;

Van Staal et al., 1996a). During the Late Ordovician-Silurian the final closure of the Iapetus involved a continent-continent collision which is responsible for the Salinic - late Caledonian - Scandian orogenies (Dunning et al., 1990; Barnes et al., 1989; Gee, 1975; Robinson et al., 1988). The collision in the Norwegian Caledonides was between Baltica and Laurentia whereas in the British Caledonides and the Northern Appalachians it was between Laurentia and Avalonia (a peri-Gondwanan terrane; Fig.1.1). This collision is apparently slightly diachronous in the New England Appalachians (USA) (Devonian Acadian orogeny, Dewey, 1969; Robinson et al., 1988; Eusden and Lyons, 1993) . However new precise geochronology from Maine (Stewart et al., 1995; Osberg et al., 1995) and Massachusetts (Hepburn et al., 1995) points to a Silurian peak of orogeny in parts of New England. The Southern Appalachians also record a Taconic event which is followed by a continent-continent collision between Laurentia and Gondwana (i.e. African craton) during the Carboniferous-Early Permian (Alleghenian orogeny; Bailey, 1935; Williams and Hatcher, 1983).

All the geological elements of the Northern Appalachians are best exposed in the island of Newfoundland (Canada). This island is located in the center of the orogenic belt and offers the most complete cross-section of the orogen, except for the Meguma Zone (Fig.1.2). The zones and subzones of the Newfoundland Appalachians can be traced along the Northern Appalachians and the British Caledonides (Dewey, 1969; Williams, 1978 a,b; Colman-Sadd et al., 1992b; Winchester and van Staal, 1995; van Staal et al., 1996a). For this reason tectonic models for both the Northern Appalachians and the British Caledonides have relied not only on the local geology but also on the constraints provided by the rocks exposed in the Newfoundland Appalachians (Wilson, 1966; Williams, 1978b; Williams and Hatcher, 1983; Colman-Sadd et al., 1992b; Williams, S.H. et al., 1995).

1.2.2.- The European Variscan belt (Fig.1.3 and 1.4).-

The Variscan Belt extends from Morroco to the Carpathian Mountains. Compared to the Appalachians, the European Variscides (Fig.1.3) are not a continuous belt but a series of massifs separated by Mesozoic-Cenozoic basins and areas with alpine deformation, containing a variably reworked Variscan basement (Betics, Pyrenees, Alps, Carpathians). The Iberian Massif is the largest of the Variscan blocks unreworked by the alpine orogeny. It is only in this part of the Variscan Belt that there is continuous outcrop showing the two-sided structural vergence of the belt (Parga Pondal et al., 1983; Dallmeyer and Martínez-García (eds.), 1990; Matte, 1995)

The Variscan belt is characterized by thrust nappe tectonics with opposite vergence towards opposite forelands, suggesting a continent-continent collision (Fig.1.4). Compared to the Appalachians the presence of oceanic sutures is quite conspicuous. True ophiolitic sequences are scarce, although mafic-ultramafic complexes throughout the belt have been interpreted as ophiolitic remanants (Ziegler, 1986; Matte, 1986; Pin, 1990; Menot and Paquette, 1993). These mafic/ultramafic complexes are commonly polydeformed and metamorphosed and they tend to occupy an axial position in the chain (Matte, 1986). The few reliable and precise ophiolite ages indicate two periods of ophiolite generation, Early-Mid Ordovician and Late Silurian-Early Devonian (Fig.1.4; Menot et al., 1988; Pin and Carme, 1987; Pin, 1990; Oliver, et al., 1993; Dunning, unpublished). Although the geochemistry of most of these ophiolites is indicative of a back-arc setting, they are generally interpreted as ocean floor spreading associated with continental rifting (Pin, 1990). Classic volcanic arc sequences are also absent of most places in the chain (Matte, 1995).

The opposite structural vergence and the metamorphic grade in the northern part of the belt has lead to the classic subdivision (Fig.1.4; Kosmatt, 1927; Franke, 1989) into: Rheno-Hercynian Zone (northern foreland); Saxo-Thuringian Zone (axial zone) and Moldanubian Zone (axial zone + southern margin). This classic subdivision is however difficult to follow in Central and Southern Europe, eventhough in the case of the Iberian Massif the two opposite forelands are particularly well developed (Lotze, 1945; Julivert et al., 1972; Matte, 1986). The Rheno-Hercynian Zone (RHZ) is correlated with the Ardennes Massif in Belgium and France and southern England; these areas, like parts of the RHZ, have recorded Caledonian deformation and have faunas with Mid Paleozoic Baltic affinities (Soper, 1988; Franke, 1989; Paris and Robardet, 1990). The Saxo-Thuringian and Moldanubian zones, the Central Massif, the Armorican Massif, the Iberian Massif, Sardinia and the Paleozoic of the Alps had paleontological similarities with those of Gondwana (Fig.1.4.; Paris and Robardet, 1990; Robardet et al., 1990; Young, 1990).

Cambrian-Early Ordovician faunal similarities along the belt progressively disappear during the Mid Ordovician - Silurian to be regained in the Late Devonian-Early Carboniferous (Paris and Robardet, 1990). Mid Paleozoic paleontological, sedimentological and paleomagnetic data suggest the presence of an ocean (Rheic ocean; Paris and Robardet, 1990), separating a northern domain (Rhenohercynian Zone) from a southern domain (Saxothuringian and Moldanubian zones and equivalents in southern Europe; Fig.1.4). The rocks of these two domains were amalgamated as a result of the Variscan orogeny.

Timing of Variscan orogenesis is classically defined as Late Devonian-Late Carboniferous (360-290 Ma; Stille, 1924). However, some authors (e.g., Perez Estaun et al., 1991) also consider Variscan the Late Silurian-Mid Devonian (≈420 Ma-380 Ma) deformation and metamorphism associated with the so called, Ligerian or Eo-Hercynian

event (e.g., Lefort, 1989). Throughout the chain there is evidence of earlier pre-Variscan events, including Late Precambrian Cadomian tectonothermal events (Fig.1.3; Strachan and Taylor (eds.), 1990; D'Lemos et al.(eds.), 1990) as well as Late Cambrian-Early Ordovician tectonothermal events of obscure significance (Ziegler, 1986; Matte, 1986; Gebauer, 1993).

1.3.- CONCEPTUAL FRAMEWORK FOR PRECAMBRIAN & PALEOZOIC NORTH ATLANTIC PALEOGEOGRAPHIC RECONSTRUCTIONS.-

The following is a definition of the paleogeographic terms that will be used in this thesis. The purpose of this description is to clarify further discussions and avoid confusion regarding the use of this terminology.

Gondwana (Fig.1.5): This term is used to define the supercontinent resultant of plate amalgamation during the Pan-African orogenic events (800-500 Ma; Rogers, 1995). These events lead to the formation of Late Neoproterozoic interior and exterior orogenic belts in Gondwana (Murphy and Nance, 1991). The core of this continent is formed by South America, Africa, Madagascar, India and Australia (du Toit, 1937; Scotese and McKerrow, 1990). Paleontological and paleomagnetic data indicate that during the Late Precambrian and Early Paleozoic, Gondwana was bordered by the peri-Gondwanan elements of the Appalachian-Caledonides (Hutchinson, 1962; Cocks and Fortey, 1982; Cocks and Fortey, 1990; Scotese and McKerrow, 1990; Williams S.H. et al., 1995), South and Central Europe (Southern Variscides; Robardet et al., 1990; Paris and Robardet, 1990; Young, 1990) as well as the Cimmerian terranes of the Middle East and Southeast Asia (Scotese and McKerrow, 1990).

Peri-Gondwana (Fig.1.1): This refers to the Late Precambrian-Early Ordovician Gondwanan margin of the Iapetus Ocean (Exploits subzone, Gander Zone, Avalon Zone and equivalents in the Newfoundland Appalachians). Peri-Gondwana also includes all Precambrian and Early Paleozoic elements with Gondwanan affinities in the Variscan Belt, since they are not proven to have been permanently attached to the African craton (Paris and Robardet, 1990).

Avalonian - Monian- Cadomian belts (Fig.1.1B): These are 680-540 Ma orogenic belts on the periphery of Gondwana (see general references in Strachan and Taylor (eds.), 1990; D'Lemos et al. (eds.), 1990). The Avalonian belt refers to the Late Precambrian - Cambrian rocks of the Avalon Zone (s.s; O'Brien et al., 1996) and their correlatives in the Northern Appalachians (Rast and Skehan, 1988) and British Isles (Tucker and Pharaoh, 1991; Strachan et al., 1996). The Monian Belt covers the Precambrian rocks of NW Wales and SE Ireland (Gibbons, 1990; Gibbons and Horák, 1990; Winchester et al., 1990). The Cadomian belt includes the Late Precambrian - Cambrian rocks of the northern Armorican Massif (D'Lemos et al.(eds.), 1990), the Iberian Massif (Ossa-Morena and Central Iberian Zones; Quesada, 1990), the Bohemian Massif (Chaloupsky, 1990) and the Eastern Alps (Frisch and Nebauer, 1989). The Avalonian / Cadomian events consist of a 680-620 Ma tectonothermal event (active margin ?) followed by 620-570 Ma development of an Andean-type arc with associated calc-alkaline magmatism and deformation (Cadomian I / Avalonian events) and 560-540 Ma crustal anatexis, calc-alkaline magmatism, H-P metamorphism and deformation (Cadomian II / Monian events). During the Cambrian, tectonic activity ceased in most of the belt (Quesada, 1990; Went and Andrews, 1990; Landing, 1995). However, Cambrian events in the Armorican Massif (magmatism; Brown et al., 1990) and the Ossa-Morena Zone of the Iberian Massif (Low P / high T metamorphism, deformation and magmatism; Ochsner, 1993) have been also ascribed to

the Cadomian cycle. Contemporaneity and similarity of events in these belts has lead to group them into an Avalonian superterrane (Rast and Skehan, 1988), although a direct connection between the Avalonian and Cadomian belts has yet to be demonstrated (Gibbons and Hórak, 1990). The basement of the Cadomian belt is formed by 2.7 Ga to 1.8 Ga gneisses (Clavez and Vidal, 1978; Guerrot et al., 1989; Wendt et al., 1993). Basement for the Avalonian belt is unknown.

Avalonia (Fig.1.5): The concept of Avalonia is based on a terrane with Late Precambrian peri-Gondwanan affinities (i.e. with Avalonian events) accreted to Laurentia during the final closure of the Iapetus ocean (Williams, 1979). According to Scotese and McKerrow (1990), Avalonia extends to the Ardennes (Belgium and France), England, SE Ireland, the Avalon Zone and the peri-Gondwanan margin of the Iapetus of the northern Appalachians (Fig.1.2. and 1.3). These areas are characterized by a Late Precambrian Avalonian basement, Cambrian to Early Ordovician cold water faunas with Gondwanan affinities and Baltic and Laurentian faunas during the Mid-Late Ordovician and Silurian (Cocks and Fortey, 1982; Cocks and Fortey, 1990; Williams S.H., et al., 1995). Paleomagnetic data indicates an Early-Mid Paleozoic movement of Avalonia towards warmer latitudes (Scotese and McKerrow, 1990; Torsvik et al., 1996)

Laurentia (Fig.1.1): This is North American craton formed by an Archean and Proterzoic basement, with distinctive Grenvillian (≈1000 Ma) events, against which different terranes were accreted during the development of the Appalachian-Caledonian belt (Williams, 1978). As a result of the opening of the Iapetus Ocean, Laurentia developed endemic faunas (Cocks and Fortey, 1982; Nowlan and Neuman, 1991 and ref, within; Williams et al., 1995). The warm water character of these faunas is consistent with a Late Precambrian-Paleozoic paleomagnetic position near the equator (Scotese and McKerrow, 1990; Torsvik et al., 1996)

Peri-Laurentia (Fig.1.1): This refers to the Laurentian Margin of the Iapetus Ocean (Humber Zone, Notre Dame subzone and equivalents; Fig.1.2).

Baltica (Fig.1.1): Late Precambrian to Mid Paleozoic continent rifted away from Laurentia during the opening of the Iapetus Ocean. This continent is bounded to the west by the Iapetus suture (Scandinavian Caledonides), to the SE by the Tornquist line (roughly the suture of the Tornquist sea; Cocks and Fortey, 1982) and to the East by the Urals (Devono-Carboniferous suture; Matte, 1995). According to Cocks and Fortey (1990), Baltica has its own distinctive Ordovician faunas. Paleomagnetic data (Torsvik et al., 1996), also, suggest a Late Precambrian to Ordovician paleogeographic position distinct from those of Gondwana, Laurentia and Avalonia.

Northern Variscides (Fig.1.3 and 1.4): This is used in the sense of Paris and Robardet (1990) and includes the Rheno-Hercynian Zone, the Ardennes, Brabant Massif, Cornwall and southern Ireland. The term refers to the areas of the Variscan Belt with Avalonian-Baltic faunal characteristics (Cocks and Fortey, 1990; Paris and Robardet, 1990) in the Mid to Late Paleozoic time.

Southern Variscides (Fig. 1.3 and 1.4): This is also used in the sense of Paris and Robardet (1990). It includes the Iberian Massif (with the possible exception of the South Portuguese Zone), the Armorican Massif, the Massif Central, Sardinia, Corsica, Vosges, Black Forest, external Alps, Saxothuringian and Moldanubian Zones. These areas are characterized by close faunal similarities with Morrocan Gondwanan faunas during the Early Paleozoic, indicating proximity with Gondwana. Middle-Late Paleozoic faunas from the Central Iberian Zone to the Bohemian Massif, however, have a distinct character. Asghill diamictites suggest a Mid Paleozoic lower latitude (Brenchley et al., 1991). Paleomagnetic data seem to support a lower latitude position, close to Gondwana, during

the Late Precambrian and Middle Paleozoic (Scotese and McKerrow, 1990). During the Devonian the Southern Variscides moved to higher paleomagnetic latitudes and warmer paleobiogeographic conditions (McKerrow and Scotese eds., 1990).

1.3.1.- Late Precambrian and Paleozoic Paleogeographic evolution of the circum-North Atlantic Gondwanan terranes (Fig.1.6).-

Gondwana is generally viewed as a supercontinent amalgamated during the Pan-African orogeny (800-550 Ma). This continent was assembled with pieces from the dismembered Rodinia (a single supercontinent formed as a result of the Grenvillian orogeny (≈1000 Ma); e.g., Hoffman, 1991). Most Late Proterozoic paleogeographic reconstructions show a collage of three major plates: Laurentia, Baltica and Gondwana (e.g., Torsvik et al., 1996). Laurentia and Baltica were rifted from each other as a result of the opening of the Iapetus Ocean (circa 650-580 Ma). During the same time an active margin was developed on the margin of Gondawana (680-540 Ma), the Avalonian-Cadomian Belt. This belt is a unique feature of Gondwana.

This plate configuration resulted in important faunal differences between these three major continents at the onset of the Cambrian. Landing (1996) points out that faunal differences between Avalonia (Fig.1.5) and Morrocan and Armorican faunas are significant enough to suggests that Avalonia was already detached from Gondwana. However, both paleontological and paleomagnetic data suggest that the peri-Gondwanan elements of the Appalachians and the southern Variscides were at similar latitudes and relatively close to Gondwana (McKerrow and Scotese eds., 1990; Cocks, 1993; Torsvik et al, 1996).

During the Early Paleozoic (Tremadoc, Arenig) faunal differences between peri-Laurentia and peri-Gondwana peaked, reflecting the widening of the Iapetus Ocean (Cocks and Fortey, 1982; Williams, S.H. et al., 1995). This coincides with island arc development

on both sides (Notre Dame and Exploits subzones of the Newfoundland Appalachians) and with Arenig ophiolite obduction and volcanic arc (Exploits Subzone)-passive margin (Gander Zone) collision in the Gondwanan margin of Iapetus (Penobscottian event; Colman-Sadd et al., 1992a; van Staal, 1996 and ref. within). The Mid Ordovician Taconic orogeny in the Laurentian side of Iapetus also represents a passive margin-volcanic arc collision (Williams, 1979; Williams ed., 1995). Contemporaneous events also took place in the Baltic side of Iapetus (Finnmarkian, high P events and ophiolite generation; e.g., Andréasson, 1994; Dunning and Pedersen, 1997). The Avalon Zone (s.s.) and similar correlatives in the British Isles (Midlands block; Tucker and Pharaoh, 1991) seem to have escaped these Early Ordovician events. However, the Southern Variscides registered granitic plutonism, ophiolite generation, high P metamorphism, calc-alkaline magmatism (Pin, 1990; Gebauer, 1990, 1993) and almost coeval alkaline magmatism within an apparent extensional setting (e.g., Ziegler, 1986; Ochsner, 1993). Therefore, the Early Ordovician seems to coincide with subduction along all margins of the Iapetus Ocean and with a period of major plate reorganization.

During the Mid and Late Ordovician, faunal differences between all sides of the Iapetus Ocean diminished as a result of ocean closure (McKerrow and Scotese eds., 1990; Williams S.H. et al., 1995). However, faunal differences between the Northern and Southern Variscides became apparent, indicating the presence of a faunal barrier (Rheic Ocean; Paris and Robardet, 1990). It is in this period that Avalonia and the northern Variscides migrated towards warmer latitutes (McKerrow and Scotese eds., 1990; Williams, S.H. et al., 1995) whereas the Southern Variscides remained at lower latitutes (Ashgill diamictites).

In the Silurian the Iapetus Ocean closed and a major continent-continent collision took place (Scandian, Late Caledonian and Salinic orogenies; Dunning et al., 1990 and ref.

within). As result of the collision between Laurentia, Baltica and Avalonia the Old Red Sandstone continent was formed (McKerrow and Scotese eds., 1990). The Northern Variscides show a continent-ocean trend which indicates they represent the external areas of such a continent (Paris and Robardet, 1990). Contemporaneously, (Silurian-Early Devonian) an event involving high P / high T metamorphism (subduction), ophiolite generation and obduction, deformation and plutonism took place in the Southern Variscides. This event is known in the Armorican Massif as the Ligerian event (e.g., Lefort, 1989) and in the Iberian Massif is considered as Eo-Variscan (Arenas et al., 1986; Santos Zalduegui et al., 1996). Silurian-Early Devonian faunal difference between the Northern and Southern Variscides disappear in the Mid Devonian (Givetian) suggesting the closure of the Rheic Ocean (Paris and Robardet, 1990). Variscan (s.s.) deformation, metamorphism and plutonism took place during the Late Devonian until the Permo-Carboniferous (Stille, 1924). The Variscan and Alleghenian orogenies resulted in the final amalgamation of Pangea (Rast, 1988).

CHAPTER II

THE NEWFOUNDLAND APPALACHIANS:

This thesis was partially conceived as a comparative study of the geological evolution of the peri-Gondwanan elements of the Newfoundland Appalachians and the Iberian Massif. Therefore, some of the readers might not be familiar with the most current understanding of the geology of the Newfoundland Appalachians. It is to those readers that the first introductory section is directed. The classic zonal divisions and subdivisions of the Newfoundland Appalachians have been grouped in two subsections, according to their linkage to the peri-Laurentian or the peri-Gondwanan margin of the Iapetus ocean. This concept of peri-Laurentian versus peri-Gondwanan margin is also used as a reference in the description of the main geological elements of the Southern Newfoundland Appalachians (Hermitage Flexure). This description is aimed at all readers, since it serves to place within a regional geological framework the elements of the Avalonian basement block of the Hermitage Flexure studied in chapter III (Cinq-Cerf gneiss), as well as the rationale behind their potential western extent into the Port-aux-Basque complex (Margaree orthogneiss, Chapter IV).

2.1.- LITHOTECTONIC ZONES OF THE NEWFOUNDLAND APPALACHIANS: GENERAL OVERVIEW.

The geology of the Newfoundland Appalachians can be viewed in terms of accretion of terranes with peri-Laurentian and peri-Gondwanan affinities to Laurentia, the North American craton (Williams, 1979; Cawood et al., 1988; Williams, 1995a,j). The pre-Silurian rocks allow the division of the belt into four classic lithotectonic zones, Humber, Dunnage, Gander and Avalon (Fig.2.1; Williams, 1979). Seismic reflection (Keen et al., 1986) indicates the presence of three crustal blocks: Grenville, Central and Avalon lower crustal blocks. The Grenville lower crustal block, which is expressed at the surface by the Humber Zone, extends from the North American craton under part of the Dunnage Zone to meet the Central lower crustal block. The Dunnage Zone is allochthonous over these two blocks. The Gander Zone represents the surface expression of the Central lower crustal block. A third crustal block, the Avalon crustal block is marked by a sharp boundary which coincides with the boundary between the Gander and the Avalon zones and extends to the continental edge of the Grand Banks.

Early Ordovician faunal differences divide the oceanic rocks of the Dunnage Zone into the peri-Laurentian Notre Dame Subzone and the peri-Gondwanan Exploits Subzone (Fig.2.1; S.H. Williams et al., 1995), this division is also confirmed by different Pb isotopic signatures (Williams et al., 1988). These subzones are separated by the Red Indian Line and its southern continuation along the Cape Ray Fault (Lin et al., 1994). This suture zone effectively separates the Laurentian margin formed by the Humber Zone and the Notre Dame Subzone from the peri-Gondwanan margin of the Iapetus ocean (Exploits Subzone and Gander and Avalon zones). The profound faunal differences in the Arenig mark the peak of faunal provincialism, suggesting the presence of an ocean tract more than 2000 Km

wide separating both margins (S.H. Williams et al., 1995), which is also supported by paleomagnetic data (Van der Pluijm et al., 1995). This indicates that the peri-Laurentian and the peri-Gondwanan margins of the Newfoundland Appalachians had separate geological evolutions until the Late Ordovician-Early Silurian or early stages of the Silurian Salinic orogeny, which marks the climax in the Newfoundland Appalachians (Dunning et al., 1990). In the following description the different lithotectonic zones and subzones of the Newfoundland Appalachians have been grouped according to their linkage to either margin of the Iapetus Ocean, whereas their common Mid to Late Paleozoic evolution is treated in a separate subsection.

2.1.1.-The Laurentian/peri-Laurentian margin of the Newfoundland Appalachians: The Humber Zone, the Notre Dame Subzone and their equivalents:

The Humber Zone (Williams, 1995b) represents the edge of the Laurentian continent against which the peri-Laurentian oceanic elements of the Dunnage Zone (Williams, 1995e) were accreted during the Middle Ordovician Taconic event, while the Iapetus Ocean was still open (Fig.2.1). These elements are the Notre Dame Subzone and the Dashwoods Subzone or Central Gneiss Terrane. The lower Paleozoic faunas (S.H. Williams et al., 1995) and the paleomagnetic data (Van der Pluijm et al., 1995) from the Notre Dame Subzone indicate its Laurentian affinities. The Twillingate Subzone (Fig.2.1) is included in the peri-Laurentian margin because it lies within the Notre Dame Subzone.

The Humber Zone:

The Humber Zone is the westernmost zone of the Newfoundland Appalachians (Fig.2.1). It has a Grenvillian basement (e.g. Erdmer and Williams, 1995) and a Late Precambrian-Ordovician cover (e.g. Williams et al., 1995d), which can be correlated with other rocks west of the Appalachian deformational front. These features tie the Humber Zone with Laurentia (i.e. North American craton). The main characteristics of this zone reflect a Late Precambrian rifting event, attributed to the opening of the Iapetus Ocean, which was followed by the development of a passive margin during the Cambrian and Early-Middle Ordovician (Williams, 1995b). During the Middle Ordovician Taconic event, the advance of the Taconic nappes transformed the passive margin into a foreland basin which was partially incorporated into the advancing allochthons.

There are four main Taconic allochthons: the Humber Arm, Hare Bay, Old Mans Pond and Southern White Bay allochthons (Fig.2.1; Williams, 1995c). The allochthons contain tectonic slivers from the advancing flysch, from the passive margin carbonate platform (St. George and Table Head groups), as well as Cambro-Ordovician melanges and ophiolite suites with preserved metamorphic soles. Age of ophiolite formation in the Humber Arm allochthon ranges from 505+3/-2 Ma for the Little Port Complex (Jenner et al., 1991) to 485.7 +1.9/-1.2 Ma for the Bay of Islands Complex (Dunning and Krogh, 1985). The Little Port Complex is interpreted as generated in a volcanic arc setting whereas the Bay of Islands is interpreted as produced in a supra-subduction setting (back-arc), indicating the presence of a subduction zone out board of Laurentia. $^{40}Ar/^{39}Ar$ cooling ages of 469±5 Ma to 464±9 Ma from the metamorphic sole of the Bay of Islands Complex (Dallmeyer and Williams, 1975; Archibald and Farrar, 1976) provide a younger age limit for the ophiolite obduction. A Llandeilo cover over the Bay of Islands Complex and a Caradoc

cover over the Humber Arm allochthon indicate that the tectonic imbrication associated with the Taconic event was over by the Middle-Late Ordovician. Final emplacement of the Humber Arm and Hare Bay allocbthons is related to gravity sliding (Cawood, 1989; 1990) after peak orogenesis in the Mid Paleozoic (Salinic orogeny).

The Humber Zone also contains polydeformed and regionally metamorphosed rocks, which locally overlie Grenville basement. They form the Baie Verte or Fleur de Lys block and the Corner Brook Lake block (Fig. 2.1; Cawood et al., 1995; Hibbard et al., 1995) and they are referred to as the internal Humber Zone (Hibbard et al., 1995), since they are located between the external allochthons and the Dunnage Zone. These rocks are mostly siliciclastic with minor metavolcanic rocks and marble (Fleur de Lys Supergroup) intercalated with mafic-ultramafic rocks of ophiolitic affinity. Peak metamorphic conditions in both blocks reached high-pressure amphibolite facies (7-9 Kb and 700-750°C in Baie Verte; Jamieson, 1990; 7-9 Kb and 650°C in the Corner Brook Lake; Cawood et al., 1995), with local peak pressure conditions in the eclogite facies (Baie Verte, 10-12 Kb and 450-500°C; Jamieson, 1990). The available absolute time constraints indicate that regional metamorphism and deformation in these two blocks are Early Silurian , ca. 430-425 Ma (Cawood et al., 1995) and not Taconian as previously thought (Hibbard et al ., 1995).

The peri-Laurentian Dunnage Zone:

The Notre Dame Subzone:

This subzone contains Early Paleozoic thick sequences of marine volcano-sedimentary rocks which contain lower Ordovician Laurentian warm water fauna (S.H.Williams et al., 1995 and ref within) and associated volcanogenic sulphide deposits with non-radiogenic Pb isotopic signatures, together with ophiolitic complexes broadly coeval with the Bay of Islands ophiolite in the Humber Zone (Fig.2.1; Williams, 1995d,e). These rocks are

interpreted as remnants of a peri-Laurentian Tremadocian to Early Llanvirn arc/back arc system.

The ophiolitic complexes include the Birchy, Advocate and Point Rousse complexes in the Baie Verte area (Fig.2.1), which are polydeformed, dismembered and locally metamorphosed (Birchy complex; peak P 9 Kb and 500°C; Jamieson and O'Bierne-Ryan, 1991), as well as other disrupted ophiolites, such as the Pynns Brook and Grand Lake Complexes and the Hungry Mountain tonalite-gabbro complex. The more complete Betts Cove ophiolite (Fig.2.1) has been dated at 488.6 +3.1/-1.8 Ma (Dunning and Krogh, 1985) and is conformably covered by volcanics and sediments of the Arenig Snooks Arm Group (c.f. Williams, 1995e). The most extensive ophiolite is the Annieopsquotch Complex, which has been dated at 477.5 +2.6/-2 Ma and 481+4/-2 Ma (Dunning and Krogh, 1985). This data confines the timing of ophiolite generation to the Late Tremadoc-Arenig.

The volcanic and sedimentary rocks of the Notre Dame Subzone have been divided in two belts: a northern mafic volcanic belt and a southern belt of bimodal volcanics (Williams, 1995e). The northern belt contains thick mafic pillow lavas, associated dykes and sills, clastic sedimentary rocks (greywackes, slates and cherts) and scarce limestone lenses with Late Arenig-Llanvirn fauna. These rocks, like the Snooks Arm Group, locally overlie the Tremadoc-Arenig ophiolitic complexes. To the south, the belt of bimodal volcanics contains abundant basalt and rhyolite intercalated with marine and terrestrial sedimentary rocks. This belt is divided in two major units, the Roberts Arm Group to the north and the Buchans Group to the south (Fig.2.1), both with calc-alkaline igneous rocks which are interpreted as arc-derived (Swinden et al., 1990; cf. Williams, 1995e). Conodonts from the Buchans Group are Late Arenig-Llanvirn which agrees with an age of

473+3/-2 Ma of a rhyolite in this group. A coeval rhyolite from the top of the Roberts Arm Group has also been dated at 473±2 Ma (Dunning et al., 1987).

The Dashwoods Subzone:

This subzone (Fig.2.1), formerly the Central Gneiss Terrane (van Berkel and Currie, 1988), includes psammitic and pelitic schists, migmatitic gneiss and minor marble in tectonic contact with mafic and ultramafic tectonic slivers with ophiolitic affinities; both the metasediments and the ophiolitic rocks are intruded by abundant foliated to massive diorites and granodiorites of arc affinity (c.f. Williams, 1995e). The ages of these plutons range from 488 Ma (Dubé et al., 1996) to 456±3 Ma (zircon+titanite, least deformed tonalite; Dunning et al., 1989) and are interpreted as coeval with the tectonic imbrication of the metasedimentary and ultramafic units. An undeformed Early Silurian gabbroic intrusion cross-cutting the tectonic fabric in Ordovician tonalites (431±2 Ma; Main Gut Gabbro; Dunning et al., 1990) and a K/Ar metamorphic hornblende cooling age of 455±14 Ma in rocks from this subzone (Stevens et al., 1982) confirm the Taconian age of deformation and metamorphism in these rocks. Silurian reactivation within the Dashwoods Subzone is limited to the area around the Cape Ray fault (Dubé et al., 1996). Williams (1995e) correlates this subzone with the Dunnage Zone on the basis of the ophiolite-like mafic and ultramafic rocks and the Ordovician tonalites, whereas Cawood et al. (1995) correlate the paragneisses with the Fleur de Lys Supergroup, placing the subzone in the internal Humber Zone. Because the presence of Grenvillian basement has not been proven, the medium to high grade rocks of the Dashwoods Subzone are more correctly included in the Dunnage Zone as a metamorphic equivalent of the Notre Dame Subzone.

Twillingate Subzone: (Unknown affinity)

This is a small subzone within Notre Dame Subzone at Twillingate and New World Islands at the northern boundary between the Notre Dame and the Exploits subzones (Fig.2.1). It is formed by mafic volcanics, including pillow lavas, and non-fossiliferous silicic pyroclastic rocks locally deformed and metamorphosed in amphibolite facies. These volcanic rocks were intruded by the 507+3/-2 Ma tonalitic Twillingate granite (Elliot et al., 1991). This tonalite was subsequently deformed and intruded by mafic dykes with $^{40}Ar/^{39}Ar$ amphibole ages around 470 Ma (Williams et al., 1976). Even though this subzone is surrounded by Notre Dame Subzone rocks with Silurian deformation (Elliot et al., 1991), the presence of Late Cambrian-Early Ordovician deformation is more typical of the Exploits Subzone (Penobscottian event) and therefore its affinity remains unknown.

2.1.2.- The peri-Gondwanan margin of the Newfoundland Appalachians: the Exploits Subzone and the Gander and Avalon zones:

The peri-Gondwanan margin of the Newfoundland Appalachians is characterized by the cold water Acado-Baltic faunas of the Avalon Zone, the Early Ordovician cold-water Celtic faunas of the Exploits Subzone (S.H.Williams et al., 1995) and more significantly by the Late Precambrian Avalonian rocks. These Avalonian rocks record the evolution of an active margin on the periphery of Neo-Proterozoic Gondwana (O'Brien et al., 1996), which is coeval with the Late Precambrian rifting event in the Laurentian margin. The Late Precambrian Avalonian rocks are not restricted to the Avalon Zone, they also appear in tectonic windows under the Exploits Subzone in central Newfoundland and as basement inliers in southern Newfoundland, where the intense Silurian overprint makes the

distinction between the rocks of the Exploits Subzone and the Gander Zone difficult (Fig.2.2). These southern basement inliers are the objective of this study since they represent some of the most outboard relicts of the Late Precambrian margin of Gondwana.

The Exploits Subzone is interpreted as a peripheral Cambro-Ordovician arc which was accreted to a Cambrian passive margin represented by the Gander Zone during the Arenig Penobscottian event (Neuman and Max, 1989). The Avalon Zone escaped these Early Ordovician events and was juxtaposed against the Gander Zone during the Silurian Salinic orogeny. These relicts of Avalonian basement in southern and central Newfoundland, which might represent basement to the Gander Zone, provide a strong linkage with the Avalon Zone or a similar Avalonian terrane (O'Brien et al., 1996; van Staal et al., 1996a). The presence of late Arenig-Llanvirn trilobites with Gondwanan-Avalonian affinities in the Exploits Subzone (S.H. Williams et al, 1995) also indicates a certain proximity with the Avalon Zone.

The peri-Gondwanan Dunnage Zone: The Exploits Subzone

This subzone contains relicts of ophiolitic suites and volcano-sedimentary rocks which were part of Cambro-Ordovician arc and back-arc systems (Fig.2.2). Although lithologically similar to the peri-Laurentian Notre Dame Subzone, the volcano-sedimentary rocks are dominated by sedimentary members. The volcanogenic massive sulphide deposits of this subzone have a contrasting radiogenic Pb isotopic signature, different from those of the Notre Dame Subzone (Williams et al., 1988). Mélanges are common and are interpreted as accretionary prisms (Carmanville Melange, Lee and Williams, 1995) and as slope/trench deposits (Dunnage Melange; Williams, 1995e). Small Precambrian inliers (563±2 Ma Valentine Lake and 565+4/-2 Ma Cripple Back Lake intrusions; Evans et al., 1990) outcrop in tectonic windows under Exploits Subzone rocks of the Victoria Lake Group in central

Newfoundland, confirming the peri-Gondwanan linkage provided by the distinctive Early Ordovician Celtic faunas of this subzone (S.H. Williams et al., 1995)

The main ophiolitic suites of the Exploits Subzone are the Pipestone Pond (494+3/-2 Ma; Dunning and Krogh, 1985), Coy Pond (489 Ma; Dunning and Krogh, 1985) and Great Bend complexes in central Newfoundland (Fig.2.2; Jenner and Swinden, 1993) and the incomplete ophiolite suite of the South Lake Complex in the Western Arm of the Bay of Exploits in northern Newfoundland. The mafic and ultramafic bodies of the Gander River Complex and their southward continuation along strike into the Baie d'Espoir and Bay du Nord groups are interpreted as disrupted ophiolites (GRUB line; Fig.2.2). The 494 Ma Pipestone Pond ophiolite was obducted over the sedimentary rocks of the Mount Cormack Subzone of the Gander Zone and this tectonic contact was stitched by the 474+6/-3 Ma Partridgeberry Hills granite (Colman-Sadd et al., 1992a). This indicates an Arenig age for the Penobscottian ophiolite obduction, which is consistent with the unconformable deposition of Late Arenig sedimentary rocks over the 489 Ma Coy Pond ophiolite at Mount Cormack and over the GRUB ophiolite at Gander Lake.

The volcanic and sedimentary rocks of the Exploits Subzone have been divided into several groups: the Wild Bight and the Exploits groups to the northwest and its equivalent in central Newfoundland the Victoria Lake Group, the Davidsville and Baie d'Espoir groups to the east and the Bay du Nord Group in the south (Fig.2.2). These groups contain felsic and mafic volcanic rocks, including pillow lava with associated diabase and gabbro intrusions, alternating with siliciclastic rocks. The 513±2 Ma Tally Pond volcanic rocks in the Victoria Lake group may mark the inception of arc magmatism. The extrusion of the 498+6/-4 Ma Tulks Hill volcanics in the Victoria Lake Group and the 486±3 Ma Tea Arm tuff in the Exploits Group indicate that arc magmatism (O'Brien et al., 1997) was contemporaneous with Tremadocian ophiolite formation. The Arenig Penobscottian event is

marked by the pre-477 Ma imbrication of ophiolitic-like gabbro and volcano-sedimentary rocks in the southern Bay du Nord Group (Tucker et al., 1994) but there is no evidence for it in the Exploits Group (O'Brien et al., 1997). The Arenig Penobscottian event was followed by a Late Arenig-Llanvirn major back-arc rifting event. This event is marked by back-arc bimodal volcanism, extensional deformation and siliciclastic sedimentation (462+4/-2 Ma, Victoria Lake Group; 468±2 Ma, Baie d'Espoir Group; 466±3 Ma, Bay du Nord Group; cf.Colman-Sadd et al., 1992a; Late Arenig-Llanvirn graptolite faunas in the Davidsville and Exploits groups, c.f. O'Brien et al., 1997). This is followed by the conformable deposition of Upper Llanvirn-Llandeilo limestones and Caradoc shales and greywackes at the top of the Exploits Group (e.g. Williams, 1995e), marking a Middle-Upper Ordovician period of tectonic inactivity which coincides with the introduction of warm water Laurentian faunas (S.H. Williams et al., 1995).

Indian Bay Subzone:

According to Williams (1995e) the volcanic and sedimentary rocks at Indian Pond form a separate subzone and overlay the low-grade Gander Group of the Gander Zone. These rocks contain Late Arenig Celtic fauna indicative of the peri-Gondwana realm (Wonderley and Neuman, 1984; Williams S.H. et al., 1995) and are lithologically equivalent to the basal strata of the Davidsville Group of the Exploits Subzone. Because the contact is not exposed, it is uncertain if they represent an overlap sequence on to the Gander Group or a tectonic slice of the Exploits Subzone, but local stratigraphic relationships seem to support an overlapping relationship (e.g. Williams, 1995e).

The Gander Zone:

The Gander Zone was classically interpreted as the opposing margin to the Humber Zone (Williams, 1964). This zone is bounded to the west by the Exploits Subzone and to

the east by the Avalon Zone. This zone is characterized by low-grade, quartz-rich siliciclastic rocks and medium- to high-grade micaschists and quartzo-feldspathic gneisses. It has been divided in three separate subzones: the northeastern Gander Lake, the central Mount Cormack and the southwestern Meelpaeg subzones (Fig.2.2). These last two zones are interpreted as tectonic windows of the Gander Zone under the Exploits Subzone (Williams et al., 1988). The Meelpaeg Subzone is interpreted to continue in southern Newfoundland along the Port-aux-Basques area (Fig.2.2), however, this is controversial as demonstrated in chapter IV of this thesis.

Gander Lake Subzone:

This subzone has the type sequences of the Gander Zone (Williams, 1979, 1995f). It is underlain by the low grade rocks of the Gander Group and the medium/high-grade Square Pond and Hare Bay gneisses (Fig.2.2), which are interpreted as metamorphic equivalents of the Gander Group. The Gander Group contains non-fossiliferous greenschist facies psammites, pelites and quartzites. A 569 Ma detrital zircon and a reported overlapping relationship with the Late Arenig Indian Bay Subzone provide the older and younger age limits for the deposition of the group (O'Neill, 1991), which is interpreted as a siliciclastic Cambrian passive margin deposit. The Square Pond Gneiss forms a 12 Km wide and 150 Km long band east of the Gander Group, with increasing Silurian Barrovian type metamorphism from greenschist facies in the west to upper amphibolite in the east (King et al., 1995). East of the Square Pond Gneiss, the Hare Bay Gneiss forms a 10 Km by 140 Km band of paragneisses, amphibolites and orthogneisses, which has been correlated with the Little Passage Gneiss to the south (Fig.2.2; Colman-Sadd, 1980). The orthogneisses in the Hare Bay Gneiss have been dated at 487 Ma (megacrystic granite) and 476 Ma (tonalitic orthogneiss; Dunning, unpublished).

Mount Cormack Subzone:

This subzone outcrops in central Newfoundland and it is interpreted as a tectonic window rimmed by the volcano-sedimentary rocks of the Exploits Subzone and the Pipestone, Coy Pond and Great Bend ophiolitic complexes (Fig.2.2). This subzone is formed by sandstones, shales and siltstones, which are correlated with the Gander Group (Williams et al., 1988). These rocks show a metamorphic gradation from sub-biotite facies up to migmatite in the core of the structure. Migmatization (465±2 Ma; Colman-Sadd et al., 1992a) was coeval with granite intrusion (464+4/-3 Ma Through Hill granite; Colman-Sadd et al., 1992a) and post-dates the intrusion of the Partridgeberry Hills granite (474+6/-3 Ma), which stitches the contact between the low grade rim of this subzone and the Exploits Subzone, cross-cutting the Coy Pond Complex (Colman-Sadd and Swinden, 1984).

The Meelpaeg Subzone:

This subzone contains amphibolite facies psammitic rocks and equivalent high-grade migmatites (Fig.2.2). This subzone is separated from the Mount Cormack Subzone by the Pipestone complex, but interlayered quartzite, psammite and metapelite provide a lithological correlation between the subzones (Williams et al.,1988) which is also supported by the coeval granitic plutonism (464±2 Ma Great Burnt granite; Colman-Sadd et al., 1992a). The abundance of amphibolite in the southern part of the complex forms the basis for the lithological correlation with the Port-Aux-Basques complex (Chapter IV) in southern Newfoundland.

The Avalon Zone:

The Avalon Zone (*sensu stricto*; e.g. O'Brien et al., 1996) contains low-grade volcanic, clastic and plutonic rocks of Late Precambrian to Early Paleozoic age (Fig.2.2).

These rocks were juxtaposed against the high grade Hare Bay and Little Passage gneisses of the Gander Zone during the Silurian (O'Brien et al., 1996). The term Avalon Zone (*sensu lato*; e.g. O'Brien et al., 1996) has been used to include the Late Precambrian basement rocks that outcrop in the southern Hermitage Flexure in southern Newfoundland as part of the Avalon Zone (Fig.2.2). These rocks in the Hermitage Flexure, which are the objective of study in chapter III (Cinq-Cerf gneiss), have been overprinted by the Early-Mid Paleozoic tectonothermal events common to the Exploits Subzone and the Gander Zone. Such Early-Mid Paleozoic overprint is not present in the Avalon Zone.

The oldest rock sequences of the Avalon Zone (*s.s.*) are the basal breccia with limestone blocks and the sequence of pillow basalts, tuffs and mafic breccia of the Burin Group, in the Burin Peninsula (Fig.2.2), which are intercalated with a 763±3 Ma complex of gabbro, quartz-diorite and plagiogranite (Krogh et al., 1988). In the nearby Hermitage Peninsula (Fig.2.2) 682 Ma felsic volcanics intercalated with limestones are intruded by bimodal plutonic complexes (673±3 Ma Furby Cove suite; O'Brien et al., 1996), which were unconformable covered by 630-610 Ma volcanic and siliciclatic rocks, following a deformational event (e.g. O'Brien et al., 1996). These 630-610 volcanic rocks have calc-alkaline and tholeiitic affinities and a wide distribution over the Avalon Zone (Love Cove and Connecting Point groups), and are interpreted as volcanic arc. The 630-620 volcano-sedimentary rocks are intruded by the 621±3 Ma Simmons Brook intrusive suite in the Hermitage Bay area and by the 620 Ma Holyrood calc-alkaline granite in the Avalon Peninsula (e.g. O'Brien et al., 1996). These events are coeval with granite intrusion of 616+5/-4 Ma granite (Dunning et al., 1995) in low P / high T biotite-cordierite micaschists at Miquelon island (France), south of the Burin Peninsula. Following a post-620 Ma tectonic event, there is development of extensional basins with coeval deposition of deep water turbidite, glaciogenic debris flows and tillite, as well as subaerial sedimentation and

bimodal volcanism (570+3/-2 Ma, Musgravetown group; 568±5 and 551±6 Ma, Long Harbour group; 565±3 Ma, St. John's and Signal Hill groups; O'Brien et al.,1996) and intrusion of 572+3/-2 Ma granite into the already deformed 610-620 Ma marine volcanic and siliciclastic rocks of the Bonavista Bay area (Northern Avalon Peninsula). These Late Precambrian rocks were weakly deformed and unconformably covered by Cambrian rocks. The Cambrian sequence has been described in detail by Landing (1996) and consists of basal red sandstones and siliciclastics alternating with red limestones (Lower Cambrian), that are followed by Middle Cambrian-Early Ordovician siliciclastic sedimentation alternating with ash-flow tuffs in the Middle Cambrian. The top of the sequence is Arenig and consists of quartz-rich siliciclastics with oolitic ironstone. This Cambrian-Early Ordovician sequence records several unconformities which are interpreted as eustatic changes related to basin development (Landing, 1996). A 441±3 Ma deformed mafic sill in the Avalon peninsula indicates the presence of Middle Paleozoic deformation. Unconformable Early Devonian basins and plutons dated at 394+6/-4 Ma (Krogh et al., 1988) to 374±2 Ma (Kerr et al., 1993) constrain the younger limit for this Mid Paleozoic deformation.

2.1.3.- Middle and Late Paleozoic evolution of the Newfoundland Appalachians:

Following the Early -Middle Ordovician tectonothermal events, major tectonic activity ceased on both sides of the Iapetus Ocean until the Late Ordovician - Silurian. Middle and Late Ordovician rock sequences in the Exploits Subzone record the introduction of Laurentian faunas, suggesting the movement of the peri-Gondwanan elements of the Dunnage and Gander Zones towards warmer latitudes (S.H. Williams et al., 1995). Final

ocean closure took place in the Late Ordovician -Early Silurian, leading to the Silurian collision between the opposing margin of the Iapetus. The effects of the Silurian Salinic orogeny are most intense in the margins of the Dunnage and Gander zones and the internal parts of the Humber Zone (Fig.2.1). Extensive Silurian volcanic (429-420 Ma) and sedimentary rocks (Llandovery-Wendlock) locally overlie the Precambrian and Early Paleozoic elements of the Humber, Dunnage, Gander zones and Late Precambrian basement of the Hermitage Flexure (Dunning et al., 1990; O'Brien et al., 1991; Williams 1995g-i; Williams et al., 1995a-c,e; Williams and O'Brien, 1995). This sedimentation and volcanism is coeval with metamorphism and deformation at all crustal levels and the generation of extensive I- and S-type plutons in the 431- 415 Ma interval (Dunning et al., 1990). This plutonism is syn-kinematic in most areas, except in the Dashwoods Subzone (431 Ma post-kinematic gabbros). During this period syn-magmatic and subsolidus deformation of the Silurian granites of the northeastern Gander Zone, and their country rock, record lateral movement associated with the final docking of the Avalon Zone along the Dover Fault (Fig.2.2.; Holdsworth et al., 1993; Holdsworth, 1994; Scholfield and D'Lemos, 1995; D'Lemos et al., 1995). Post-kinematic plutons intrude during a final magmatic pulse between 395 and 375 Ma, although most plutons group around 390 Ma; the Ackley granite (378-374 Ma, $^{40}Ar/^{39}Ar$; Kontak et al., 1988) intrudes both the Gander and Avalon Zone stitching the Hermitage-Dover Fault system. This Early Devonian plutonism is coeval with formation of post-collisional basins with terrestrial sediments and volcanics in the Humber, Dunnage and Avalon Zones (Chorlton et al., 1995; Williams 1995g-i; Williams et al., 1995e; Williams and O'Brien, 1995). Therefore, peak orogenesis in the Newfoundland Appalachians took place during the Silurian (Salinic orogeny; Dunning et al., 1990). Devono-Carboniferous transcurrent activity along the Cabot Fault system (Hyde, 1995) lead to the opening of the Deer Lake and Bay St. Georges basins (Fig.2.1; Late Devonian-Middle Carboniferous). Paleontological data indicate the presence

of European forms during this period (European Carboniferous floras; Nowlan and Neuman, 1991, and ref. within).

2.2.- GEOLOGICAL ELEMENTS OF THE SOUTHERN NEWFOUNDLAND APPALACHIANS : THE HERMITAGE FLEXURE

The Hermitage Flexure is the characteristic Z shaped structural trend of the southern Newfoundland Appalachians (Williams et al., 1970; Fig. 2.1 and 2.3). It is in this area that the classic subdivisions of the Newfoundland Appalachians into Humber, Dunnage (Notre Dame and Exploits subzones), Gander and Avalon zones become obscured by intense plutonism, metamorphism and late major faulting (Fig.2.3). These major fault zones bring together blocks with different geological histories, which are from west to east: the Dashwoods Subzone, the gneissic rocks of the Port-aux-Basques area, the Bay du Nord Group, the Silurian La Poile basin with its Late Precambrian-Early Ordovician basement block, the Little Passage gneiss and the Avalon Zone (Fig. 2.3). The Dashwoods Subzone is part of the Laurentian margin of the Iapetus Ocean whereas the other blocks are assigned to the peri-Gondwanan margin. The following is a brief description of these blocks, the main fault systems and the time constraints provided by the abundant syn- and post-collisional plutons. More detailed descriptions of the areas of study are given in chapters III and IV.

The Laurentian Margin:

<u>The Dashwoods Subzone:</u>

This subzone has already been described in section 2.1.1. It consists of extensive tonalitic complexes of Early to Middle Ordovician age (Dunning et al., 1990; Dubé et al.,

1996), mafic-ultramafic complexes (Long Range ultramafic complex) and medium- to high-grade paragneisses (Keepings gneiss; Chorlton, 1984). Time constraints (see section 2.1.1) indicate Middle Ordovician Taconian deformation and metamorphism.

The Cape Ray fault, the Windsor Point Group and the Billiards Brook Formation:

The Cape Ray fault (Fig.2.3) forms the southern extent of the fault lineament defined by the Red Indian Line, which marks the boundary between the relicts of the opposite margins of the Iapetus Ocean. In the central part of the Hermitage Flexure the Cape Ray fault splays into a northern track which forms part of the Red Indian Line and an eastern track, the Gunflap Hills fault splay (Fig.2.4). $^{40}Ar/^{39}Ar$ dating of synkinematic hornblende (407±4 Ma) and biotite (405±4 Ma) indicates that the main movement along the fault, which marks the suturing between the peri-Laurentian Dashwoods Subzone and the rocks of the peri-Gondwanan margin, was Late Silurian-Early Devonian (Dubé et al., 1996). Two groups of deformed low grade rocks are associated with the Cape Ray Fault: the Windsor Point Group (Brown, 1977) and the Billiards Brook Formation (Chorlton, 1980). The Windsor Point Group includes Middle Ordovician volcanics (Dubé et al., 1996), whereas the Billiards Brook formation contains Mid Devonian flora (Cooper, 1954; Chorlton, 1984). Deformation of the Billiards Brook Formation and transcurrent shearing of 386-384 Ma post-tectonic plutons along the southern extent of the fault indicate that the Cape Ray fault remained active past the peak of the Silurian Salinic orogenesis. Further constraints on the timing of deformation along the Cape Ray Fault are given in chapter IV.

The Gondwanan Margin:

The Port-aux-Basques Gneiss (Brown, 1977; *AREA OF STUDY, Chapter IV*):

This gneissic package is bounded to the west by the Cape Ray Fault and to the east by the Bay le Moine shear zone and the 416 Ma La Poile batholith, which separates it from Bay du Nord Group of the Exploits Subzone (Fig.2.4). These are medium- to high-grade metamorphic rocks deformed and metamorphosed during the Silurian Salinic orogeny (Dunning et al., 1990; Burgess et al., 1995). Lithological correlations with the Gander Zone (Meelpaeg Subzone, c.f. Williams, et al., 1995g; Little Passage Gneiss, Brown, 1977) or the Exploits Subzone's Bay du Nord Group (Chorlton, 1984) are hampered by the absence of pre-Silurian absolute ages, but these correlations suggest an affinity with the rocks from the peri-Gondwanan margin of the Newfoundland Appalachians. The Port-aux-Basques Gneiss of Brown (1977) has been recently divided into Grand Bay and Port-aux-Basques complexes and the redefined Harbour Le Cou Group (Fig. 2.4) by van Staal et al. (1996 b, c).

It is the terminology of van Staal et al. (1992; 1996b; 1996c) that is going to be used in the following chapters.

The Bay du Nord Group (Dunnage Zone):

This is a volcano-sedimentary unit locally metamorphosed to amphibolite facies which has had a polycyclic evolution. Tucker et al. (1994) demonstrated that part of the Bay du Nord Group was already deposited and imbricated with ophiolitic-like gabbro prior to the intrusion of the 477.6±1.8 Ma Baggs Hill granite (Chorlton, 1980, Fig.2.3 and 2.4). A Bay du Nord tuff level in the central part of the Hermitage Flexure has been dated at 466±3 Ma (Dunning et al., 1990; Fig.2.3), indicating the composite nature of this group. Clasts of

the Baggs Hill granite were incorporated into conglomerates (Chorlton, 1980) of the younger Dolman Cove belt, but a U-Pb age of a tuff in this belt indicates that at least certain parts of the belt are Silurian (Dunning, pers comm.).

The Bay du Nord Group has been metamorphosed to Barrovian amphibolite facies conditions (Fig.2.4). Polymictic conglomerates with clasts of the Baggs Hill granite (Chorlton, 1980) indicate that the Barrovian metamorphism is post-477 Ma. According to Chorlton (1980), the migmatitic rocks in the Bay du Nord Group were produced by granitic injections associated with the Rose Blanche granite (419 Ma; Dunning unpublished). The Bay du Nord Group is also intruded by the late-kinematic La Poile batholith (416±4 Ma; Chorlton and Dallmeyer, 1986) which, with the Rose Blanche granite, provides the youngest constraints for the Barrovian metamorphic event and the initiation of the post-466 Ma deformation.

The Bay du Nord Group contains massive sulphide deposits with primitive Pb isotopic signatures characteristic of the Exploits Subzone (Swinden and Thorpe, 1984). According to Dunning et al (1990), the Bay du Nord Group can be regionally correlated with the coeval Bay d'Espoir Group (Exploits Subzone) on the basis of lithology, type of mineral deposits and Pb isotopic signatures and geological evolution.

The La Poile Basin:

This is a syn-orogenic basin formed by volcano-sedimentary rocks in greenschist facies conditions (Chorlton, 1980). U-Pb dating of tuff levels at the base and the top of the sequence indicates that it developed between 428 and 420 Ma (O'Brien et al., 1993). Clasts of the Late Precambrian-Early Ordovician basement block were incorporated into conglomeratic levels indicating a basement-cover relationship (Chorlton, 1984; O'Brien et al., 1993). During the subsequent deformation, the basement block was thrust over the

basin along the Cinq-Cerf fault zone, which is sealed by the 390±3 Ma Chetwynd granite (Fig. 2.4; O'Brien et al., 1993). The contact between the La Poile Basin and the Bay du Nord Group is the Bay d' Est fault zone, which Chorlton (1984) interpreted as an extensional fault and O'Brien et al (1991) reinterpreted as thrust fault of the La Poile Basin and its basement over the Bay du Nord Group. This brittle fault zone cuts the 390 Ma Chetwynd granite and the Ironbound pluton (361±5 Ma, $^{40}Ar/^{39}Ar$ hornblende, 350±5 Ma, $^{40}Ar/^{39}Ar$ biotite; Chorlton and Dallmeyer, 1986), indicating a post-390 Ma and a possible post-361 Ma fault movement (Fig.2.4).

The Late Precambrian -Early Ordovician basement block *(AREA OF STUDY, Chapter III)*:

This is a composite block of low grade rocks and gneisses which have recorded Late Precambrian Avalonian, Early Ordovician and Silurian magmatic and deformational events. Late Precambrian rocks have been positively identified in three localities: Cinq-Cerf - Grand Bruit, Grandys Brook and Grey River (Fig.2.3). Undated fragments of this basement are also preserved as mega-enclaves of mica schist and migmatitic gneiss within the Silurian Burgeo batholith (429+5/-3 Ma, 415±2 Ma; Dunning et al., 1990). One of these enclaves, an agmatitic gneiss at Sandbanks, near Burgeo, contains disrupted amphibolite injected by 453±3 Ma leucosome cutting the fabric (Fox Point agmatite; Dunning, unpublished in O'Brien and O'Brien, 1992).

The rocks at Cinq-Cerf - Grand Bruit and Grandys Brook are basement to the La Poile basin (O'Brien et al., 1991). This basement contains both Late Precambrian low grade volcano-sedimentary rocks and the undated gneissic rocks of the Cinq-Cerf gneiss, which are the objective of study in chapter III (Fig. 2.3 and 2.4). The low-grade Late Precambrian rocks were intruded by a 578-566 Ma plutonic suite (Roti suite) and by Early Ordovician

plutons and deformed during the Late Precambrian and the Silurian (O'Brien et al., 1991, 1993).

The Late Precambrian rocks at Grey River (Fig.2.3) are metavolcanics, metasediments, amphibolites and migmatitic gneisses (Blackwood, 1985). A dated migmatitic gneiss with a protolith age of 686+33/-15 Ma and 579±10 Ma metamorphic titanite and unconformable 544±3 Ma tuff confirm the presence of Late Precambrian Avalonian tectonothermal events (Dunning and O'Brien, 1989).

The Little Passage Gneiss (Gander Zone):

This gneiss is formed by sillimanite-bearing mica schists, metapsammites, amphibolites and tonalitic migmatites intruded by leucogranites, including the synkinematic Gaultois granite (421±2 Ma; Dunning et al., 1990). This gneiss is considered as the southern prolongation of the Hare Bay Gneiss of the northeastern Gander Zone (e.g., Williams, Colman-Sadd and O'Neill, 1995), and was correlated with the Port-aux-Basques Gneiss on the basis of lithology and style of deformation by Brown (1975). Most of the deformation is syn-metamorphic (Piasecki, 1988) and is dated at 423+5/-3 Ma (zircon age from a tonalitic migmatite; Dunning et al. ,1990). The gneiss is faulted to the north against the Mid Ordovician Baie D'Espoir Group of the Exploits Subzone along the Day Cove thrust. To the south the gneiss is juxtaposed against the Avalon Zone along the Hermitage Bay Fault.

The Hermitage Bay Fault and the Avalon Zone:

The Hermitge Bay Fault separates the Little Passage gneiss and the Gaultois granite from the rocks of the Avalon Zone (s.s.) in the Hermitage Peninsula (Fig.2.3). This fault zone is interpreted as the southern extent of the Dover fault. These two faults were intruded

by the Ackley granite (378-374 Ma, $^{40}Ar/^{39}Ar$; Kontak et al., 1988). The rocks of the Avalon Zone (Section 2.1.2) have escaped Silurian metamorphism but are locally intruded by Early Devonian granites (e.g., O'Brien et al., 1996). The Avalonian rocks in the Hermitage Peninsula have recorded 685-670 Ma, 630-620 Ma and 580-550 Ma magmatic, deformational and depositional events, some of which are coeval with those in the Late Precambrian basement of the Hermitage Flexure (O'Brien et al., 1996).

2.3.- AVALONIAN EVENTS AND LITHOLOGICAL CORRELATIONS IN THE SOUTHERN NEWFOUNDLAND APPALACHIANS.-

The following two chapters deal with the tectonothermal evolution of two different rock units in the southwest Hermitage Flexure: the Cinq-Cerf gneiss (Chapter III) and the Margaree orthogneiss (Chapter IV). These two rock units were selected with the aim of unravelling the tectonothermal evolution of some of the most outboard elements of the peri-Gondwanan margin of the Iapetus ocean with proven Avalonian affinities, while searching for a pre-Avalonian basement.

The Cinq-Cerf gneiss (Chapter III) is the westernmost gneissic complex of the Late Precambrian basement block of the Hermitage Flexure and according to O'Brien et al (1996) is equivalent to the 686 Ma Grey River gneiss (Fig.2.3). The evidence for Late Precambrian, Early Ordovician and Silurian overprints in the nearby rocks suggested that these could be some of the oldest rocks along the peri-Gondwanan margin of Iapetus, overprinted by Avalonian events and the Paleozoic Penobscottian and Salinic events which are characteristic of the Exploits Subzone and the Gander Zone.

Rocks of the Port-aux-Basques complex form part of the westernmost segment of the peri-Gondwanan margin of the Iapetus ocean in the Newfoundland Appalachians (Fig.2.3). The upper amphibolite facies Margaree orthogneiss (Chapter IV) of the Port-aux-Basques complex resembles the Cinq-Cerf gneiss, whereas the country rock paragneisses resemble the amphibolite-rich rocks in the pre-477 Ma Bay du Nord Group (Fig.2.4; Chorlton, 1984). This would suggest that if there is a Port-aux-Basques complex / Bay du Nord group connection, some of the rocks and the deformation in the Port-aux-Basques complex could be pre-477 Ma or even older. A test of these correlations is provided by the Margaree orthogneiss (Chapter IV), which contains the oldest pre-tectonic intrusive rocks into the metasedimentary members of the Port-Aux-Basques complex (Brown, 1977). The age of these rocks and the tectonothermal events recorded in them will provide the first absolute time constraints on the pre-Silurian tectonothermal evolution of the Port-aux-Basques complex.

CHAPTER III.

THE CINQ-CERF GNEISS (SOUTHWEST Hermitage Flexure):

3.1.- INTRODUCTION:

Some of the strongest evidence for the Gondwanan linkage of the eastern margin of the Iapetus Ocean came from the Late Precambrian rocks of the Hermitage Flexure, Southern Newfoundland. These rocks are Avalonian relicts variably overprinted by the Early Ordovician and Silurian tectonothermal events recorded in the Central Mobile belt of the Newfoundland Appalachians (Fig.3.1; O'Brien et al., 1996). These relicts comprise Late Precambrian low-grade volcano-sedimentary sequences, plutonic suites and gneissic complexes, the Grey-River and Cinq-Cerf gneisses (Dunning and O'Brien, 1989; Chapter 2). These Late Precambrian rocks form two extensive outcrops at Grey River and Grand Bruit-Cinq Cerf, and appear in tectonic windows under Silurian volcanosedimentary rocks (La Poile Basin, O'Brien et al., 1991) and as megaenclaves in the Silurian Burgeo granite (O'Brien et al., 1996), forming the so-called Late Precambrian-Early Paleozoic basement block of the Hermitage Flexure (Fig. 3.1; O'Brien et al., 1991). Late Precambrian plutons also appear in two small basement inliers in the Exploits subzone in central Newfoundland (Fig. 3.1), suggesting that this Late Precambrian basement extends farther north (O'Brien et al., 1996).

These Late Precambrian volcanosedimentary and plutonic rocks are coeval with similar rocks in the Avalon Zone (Fig.3.1; O'Brien et al., 1996). However, the Precambrian gneissic complexes of the Hermitage Flexure, the Grey River and Cinq-Cerf gneisses, do not have lithological equivalents in the Avalon Zone (O'Brien et al., 1996). Prior to this study, Precambrian absolute ages were only available from the Grey River gneiss (686 Ma protolith, 575 Ma metamorphism; Dunning and O'Brien, 1989), whereas the Cinq-Cerf gneiss was inferred to be intruded by 570 Ma plutonic rocks (Dunning and O'Brien, 1989; O'Brien et al., 1993). The Cinq-Cerf gneiss, the westernmost of the two gneissic complexes, was also interpreted to be basement to a nearby, pre-570 Ma, low-grade volcano-sedimentary sequence (O'Brien et al., 1996). This suggested that the Cinq-Cerf gneiss, as defined by B.H. O'Brien (1988, 1989, 1990), could contain some of the oldest, undated, Precambrian peri-Gondwanan rocks in the southwestern Hermitage Flexure. Therefore, making the Cinq-Cerf gneiss an important target to unravel the Precambrian tectonothermal evolution of the westernmost Hermitage Flexure and the subsequent Paleozoic overprints.

The structural lineaments in the southwestern Hermitage Flexure define a convergence of the main zonal divisions of the Newfoundland Appalachians. These zones are difficult to correlate across the Cabot strait with the terrane divisions in Cape Breton Island and the rest of the northern Appalachians (Fig.3.1; Barr and White, 1996). Therefore the data presented in this chapter will be critical to assess these correlations, particularly those between the Avalonian terranes of Cape Breton and the Newfoundland Appalachians (Barr and White, 1996; Van Staal et al., 1996a). Since the Cinq-Cerf gneiss is part of the westernmost proven extent of Avalonian rocks in the Newfoundland Appalachians, this study will provide a unique opportunity to forward the understanding of the geological evolution of the Gondwanan elements along the eastern margin of the Iapetus Ocean. These correlations

and the implications for the Precambrian and Paleozoic evolution of North Atlantic peri-Gondwana will be discussed in Chapter VII of the thesis.

In this study a combination of detailed mapping, petrography, high precision U-Pb geochronology and major and trace element geochemistry has been used to demonstrate the presence of previously unreported Late Precambrian events in the Cinq-Cerf gneiss. These newly reported Precambrian events further strengthen the linkage with the Avalon Zone of the Newfoundland Appalachians. The following data also highlight the intensity of the Silurian overprint in the make-up of the gneissic complex, challenging the previous interpretation of these rocks as high-grade gneisses produced by Precambrian regional metamorphism (O'Brien et al., 1993).

3.2.- LOCATION, LOGISTICS AND OUTCROP

The Cinq Cerf gneiss is located in the southwestern coast of Newfoundland (Canada) 3 Km east of Grand Bruit, 80 Km east of Port-Aux-Basques and 40 Km west of Burgeo. Three sections along the coast were studied: a 2 Km long by 0.5 Km wide section between Sandbank Point and East Diver Head, the largest island in the Three Island group and a 200 m section at Cinq-Cerf Bay (Fig.3.2). Most of the work, however, was concentrated in the largest and most accessible Sandbank-East Diver Head section, which is the one with the best field relationships.

The community of Grand Bruit was used as a field base. Year round access to the community is provided by Marine Atlantic coastal boats. The Sandbank Point - East Diver Head section is easily accessible by foot from Grand Bruit. A boat was used to reach the outcrops at Three Islands and Cinq-Cerf Bay. Boat services can be obtained by hiring a

local fisherman from Grand Bruit. It is recommended that the area be visited during the summer or early in the fall when weather is the best. During this time foggy and wet conditions tend to prevail.

The area is characterized by barren land with extensive rock exposure covered by thin peat bogs and scarce, small "tuckamore" patches. Overall outcrop quality is excellent and the shoreline offers a wide exposure of fresh outcrop.

3.3.- PREVIOUS WORK:

This package of gneisses has been previously mapped as part of 1:63,360 (Cooper, 1954) and 1:50,000 scale regional maps (Chorlton, 1978, 1980; B.H. O'Brien, 1988, 1989). Cooper (1954) was the first to describe these rocks and grouped them with other rock types as part of his "coastal belt". He also mapped several lithological units in the Sandbank area (Cinq-Cerf gneiss of O'Brien, 1988) which have been corroborated in this study. Chorlton (1978; 1980) studied these rocks within a wider regional study of the geology of southwest Newfoundland as part of her Ph.D. thesis at Memorial University (Chorlton, 1984). She made the first detailed description of this set of gneisses which she interpreted as an Early Ordovician igneous complex, the Cinq-Cerf complex (Chorlton, 1980; 1984). Detailed mapping in the La Poile-Grand Bruit area (B.H.O'Brien , 1987; 1988; 1989; 1990) coupled with extensive U-Pb geochronology (Dunning and S.J. O'Brien, 1989; B.H. O'Brien et al., 1991; B.H. O'Brien et al., 1993) demonstrated that the Cinq-Cerf gneiss is part of a polydeformed Late Precambrian-Ordovician basement with Avalonian affinities. B.H. O'Brien (1989; 1990) and B.H. O'Brien et al. (1993) mapped the areal distribution of the gneissic complex, and defined the nature of its boundaries. But due to their scale of work they did not map the complex in detail or define any internal

units. U-Pb geochronology in the complex is limited to the unpublished data of G.R. Dunning and B.H. O'Brien from Three Islands.

3.4.- GEOLOGICAL SETTING:

The Cinq-Cerf gneiss constitutes part of the Late Precambrian-Early Ordovician basement which outcrops south of the Bay d'Est fault in the La Poile-Burgeo area of the Hermitage Flexure (Fig.3.2 ; B.H. O'Brien et al., 1991). This basement and its Silurian volcanosedimentary cover (The La Poile Basin; B.H. O'Brien et al., 1991) are part of a composite block, which is separated by the Bay d'Est fault from the Bay du Nord Group of the Dunnage Zone to the north (Fig.3.2; B.H. O'Brien et al., 1991). Both basement and Silurian cover were deformed during the Silurian Salinic orogeny and intruded by Siluro-Devonian plutonic rocks (Dunning et al, 1990; B.H. O'Brien et al., 1991). This composite block is going to be described following a N-S trend (Fig.3.2), i.e. from the Silurian cover to the Late Precambrian - Early Paleozoic basement, with emphasis on the field and absolute age constraints.

The cover Silurian volcanosedimentary rocks of the La Poile Basin are fault bounded to the north by the Bay d'Est fault and to the south by the Cinq-Cerf fault (Fig.3.2). Late Precambrian rocks also outcrop in tectonic windows within the Silurian La Poile Basin between the Bay d'Est and the Cinq-Cerf faults. These tectonic windows and the presence, in conglomerates of the La Poile Basin, of clasts derived from the nearby Late Precambrian-Early Paleozoic rocks indicate a basement-cover relationship (B.H. O'Brien et al., 1991).

The area south of the Cinq-Cerf fault (Fig. 3.2) is dominated by Late Precambrian, low-grade volcano-sedimentary and intrusive rocks and medium- to high-grade gneisses, the Cinq-Cerf gneiss of O'Brien et al. (1988). Dubé and Dunning (in press) dated a tuff level from the volcanosedimentary sequence, formed by the Whittle Hill sandstone and Third Pond tuff (B.H. O'Brien, 1988; Dunning and O'Brien, 1989), at 585±5 Ma. This sequence hosts the Late Precambrian gold-mineralization at Hope Brook mine (B.H. O'Brien, 1987; Dubé and Dunning, in press) and was intruded by 570 to 563 Ma granitic and gabbroic rocks (Roti suite, Dunning and O'Brien, 1989; B.H.O'Brien et al., 1991; B.H. O'Brien et al., 1993, Dubé and Dunning, in press). Early Ordovician bimodal plutons (499+3/-4 Ma Wild Cove granite, 495±2 Ma Ernie Pond gabbro; Dunning and O'Brien, 1989; B.H. O'Brien et al., 1991) intruded and cross-cut folds in the low-grade Late Precambrian volcanosedimentary sequence, demonstrating the presence of pre-495Ma deformation in the Late Precambrian block (B.H. O'Brien, 1988; B.H. O'Brien, pers comm; B. Dubé, pers comm).

The Cinq-Cerf gneiss of B.H. O'Brien (1988) is defined as composite gneissic complex of migmatite, psammitic paragneiss, schist, amphibolite gneiss and abundant hornblendite and metagabbro. According to the map of B.H. O'Brien (1990), it outcrops as roof pendants in the 390 Ma Chetwynd granite and the 570 Ma Roti granite, and along a strip south of the Grand Bruit fault (Fig.3.2; Cooper, 1954; Chorlton, 1980; B.H. O'Brien et al., 1991). The Grand Bruit fault juxtaposes the 585 Ma low-grade volcanosedimentary rocks and the ca. 570-560 Ma Roti suite with the Cinq-Cerf gneiss (Fig.3.2). According to B.H. O'Brien et al. (1993), this fault is a polycyclic structure which was stitched at. 568 Ma by the Roti granite and variably reworked during the Precambrian and the Silurian.

Silurian deformation resulted in final thrusting of the Late Precambrian basement block over the La Poile Basin along the Cinq-Cerf fault, and tectonic juxtaposition along the

Grand Bruit fault of the Cinq-Cerf gneiss against the Roti granite and the Whittle Hill sandstone. The 422±2 Ma Gallyboy Harbour tuff in the La Poile Basin and the stitching Chetwynd granite (390±3 Ma) provide the older and younger limits for thrusting along the Cinq-Cerf fault (O'Brien et al., 1991). The 429±2 to 430±2 Ma Western Head granite (B.H. O'Brien et al., 1991) was deformed during thrusting along the Grand Bruit fault, indicating that the thrusting was syn- to post-429 Ma. The Western Head granite intruded into the Cinq-Cerf gneiss and was subsequently intruded by the 419±2 Ma Otter Point granite and the 390±2 Ma Chetwynd granite (B.H. O'Brien et al., 1991).

Evidence for the Precambrian age of the Cinq-Cerf gneiss:

The Precambrian age of the Cinq-Cerf gneiss (Dunning and O'Brien, 1989) is based on an unpublished age of 547 Ma from Three Islands (Dunning and B.H. O'Brien, unpublished) and indirect evidence which relies on the interpretation of the gneissic/schistose megaenclaves in 563 Ma Roti granite as roof pendants of the Cinq-Cerf gneiss (Fig.3.2), the presence of gneissic clasts in the low-grade Late Precambrian volcanosedimentary sequence (B.H. O'Brien, pers comm.) and more importantly the timing of movement along the Grand Bruit fault. According to B.H. O'Brien et al. (1993), the Grand Bruit fault (Fig.3.2) is a Late Precambrian structure along which the Cinq-Cerf gneiss was thrust over the low grade volcanosedimentary sequence and was stitched by the 568 Ma Roti granite and reactivated by mylonitic deformation at 566 Ma and in the Silurian. This interpretation is based on the intrusion of a 566±2 Ma aplitic dyke (with 543 Ma monazite and 414±3 Ma titanite ages), which is interpreted to be syn-kinematic, into mylonitic 568±3 Ma Roti granite and a reported undated intrusive contact between the Roti granite and the Cinq-Cerf gneiss. All these relationships are reported from the Grand Bruit fault at the contact between the Roti granite and the Cinq-Cerf gneiss in Cinq-Cerf Bay (Fig.3.2). On the basis of this contact, they interpreted that the 568 Ma Roti granite was

stitching the contact between the Cinq-Cerf gneiss and the Whittle Hill sandstone. The 543 Ma monazite was interpreted as metamorphic and produced by a significant regional thermal event associated with the pre-499 Ma deformation of the Whittle Hill sandstone. O'Brien et al. (1996) also reported a 448+9/-3 Ma metamorphic titanite from the 547+2/-7 Ma Cinq-Cerf gneiss dated at Three Islands (Dunning and B.H. O'Brien, unpublished).

3.5.- PROBLEMS AND OBJECTIVES:

The objective of this study is to search for the oldest members of the Cinq-Cerf gneiss of B.H. O'Brien (1990) in the type localities of Sandbank Point, Three Islands and Cinq-Cerf Bay, and in the process to unravel the tectonothermal events recorded in these sections. Field relationships suggest that this is a polycyclic unit, but it is uncertain how much of the gneissic character is due to Precambrian or to Paleozoic events. The existance of the Precambrian high-grade metamorphic character that B.H. O'Brien (1988) attributed to this gneissic complex remains to be proven, as it is not evident from the work of Chorlton (1984).

The previous work shows several problems such as the reported intrusive field relationship between the 570 Ma Roti granite and the Cinq-cerf gneiss of B.H. O'Brien et al. (1993). Such a direct relationship needs to be dated to demonstrate the Precambrian age of the gneiss, given the strong lithological resemblance between the Late Precambrian, Early Ordovician and Silurian intrusive rocks in the field area. The interpretation of the 540 Ma monazite in the 566 Ma aplitic vein of the Roti suite as a "significant regional thermal event" (B.H. O'Brien et al, 1993), when the country rock to the Roti suite is in the greenschist facies (Whittle Hill sandstone; O'Brien et al., 1993), remains questionable. The reported 448 Ma titanite age from Cinq-Cerf gneiss (Dunning, unpublished in B.H.

O'Brien et al , 1993 and S.J. O'Brien et al, 1996) suggests a Late Ordovician overprint in the Cinq-Cerf gneiss in addition to the Late Precambrian and Silurian tectonothermal overprints in nearby rocks.

Therefore, there is a certain degree of uncertainty about the character and timing of the different overprints in the Cinq-Cerf gneiss and surrounding rocks. This shows the necessity of 1) finding clear field relationships which can be precisely dated to constrain the different tectonothermal events in the Cinq-Cerf gneiss, and 2) making a detailed description of the different lithologies in the complex. Limited major and trace element geochemistry was gathered to test lithological correlations and to help elucidate the Precambrian evolution of the Late Precambrian basement block.

3.6. LITHOLOGICAL UNITS, FIELD RELATIONSHIPS AND ABSOLUTE U-Pb AGES.

As a result of the detailed mapping, several units were differentiated in the Cinq-Cerf gneiss unit of B.H. O'Brien (1988, 1989, 1990). The oldest is a composite gneissic unit, with several gneissic subunits, for which the name Cinq-Cerf gneiss is preserved. A Precambrian granodiorite (Sandbank granodiorite) and a metagabbro unit (Sandbank Point metagabbro) were separated from the Cinq-Cerf gneiss unit of B.H. O'Brien. The areal extent of the ca. 430 Ma Western Head granite was refined, including dykes of mylonitic granite which were previously correlated with the 570-560 Ma Roti suite by B.H. O'Brien (1990, Fig. 3.3). The post-Western Head granite, mafic dyke swarms were also mapped and described as a separate unit. All these units were defined in the Sandbank Point - East Diver Head section, but most of them can also be found at the Three Islands and Cinq-Cerf bay sections.

The lithological units were originally separated on field criteria. These criteria and particularly outcrop relationships are stressed in the following description. This might make the description a bit cumbersome, however, it is necessary given the geological complexity of the area, with rocks and structural fabrics with different ages which resemble each other. Dunning and O'Brien (1989) and O'Brien et al (1993) demonstrated the presence of Late Precambrian, Early Ordovician and Silurian mafic and felsic intrusive rocks in close proximity or in contact with each other. Also the similarity of the style of the Late Precambrian and Paleozoic deformational events (O'Brien et al., 1993) restricts the use of structural criteria to identify these rocks. It is only on the basis of well defined and dated intrusive field-relationships that some of these bodies can be separated. Intrusive and structural overprinting field-relationships were used to define a relative sequence of "older" and "younger" intrusive rocks and structural fabrics, which was tested with U-Pb absolute ages. Both the relative and the U-Pb absolute ages of the different rock types have been included with the unit description. This description goes from older to younger units.

Note: To avoid confusion, the terms "older" and "younger" in the following description refer to the relative ages provided by the field relationships. Details of the U-Pb analytical procedure, including sample preparation, are provided in appendix A.1.

3.6.1.-The composite Cinq-Cerf gneiss: redefinition.

This unit comprises all gneissic rock types that pre-date the 429 Ma Western Head granite (Fig.3.3). They all show a complex deformation involving boudinage and complex refolding which is not present in the Western Head granite. The main characteristics of these rock types will be described in each of the three sections studied, but with particular emphasis in the Sandbank Point-East Diver Head section.

Sandbank Point-East Diver Head section:

This section contains different lithologies which will be described from east to west, from East Diver Head towards Sandbank Point (Fig.3.3). Near East Diver Head, there is an exceptional outcrop of the Cinq-Cerf gneiss with cross-cutting relationships among different mylonitic fabrics and several generations of intrusive rocks (Fig.3.4). In this outcrop the older (composite) mylonitic fabric, which is responsible for the gneissic banding, is cross-cut by several "younger" granitic dykes (U-Pb sample 94-PV-11). These "young" granite dykes are overprinted by a later mylonitic fabric, whose strain the gneiss has escaped (Fig.3.5). Although in the old mylonitic fabric the strain is quite intense, it is possible to recognize slivers of older granitic orthogneisses (U-Pb sample 94-PV-12) intrusive into metapsammitic paragneiss/schist (Fig.3.4), and an earlier set of amphibolite dykes intrusive into both (Fig.3.5). As a result of the overprint by the old mylonitic fabric, these lithologies, including the amphibolite dykes, form a composite banded gneiss. This composite banded gneiss is cross cut by dykes of "younger" mylonitic granite and a latest set of mafic dykes (Fig. 3.5). These mafic dykes also intrude the "younger" mylonitic granite and have been weakly overprinted by the strain associated with the late mylonitization. *Note: The late mafic dyke swarm is quite extensive north of the sampling locality of U-Pb sample 94-PV-11 (Fig.3.4), the swarm was not represented on MAP 3.1 nor Fig.3.4 to simplify the geology.*

To the west, the composite banded paragneiss grades into an *amphibole-rich banded gneiss*, which resembles a metavolcanic rock (Fig.3.6). Layering in this rock is defined by centimetric to millimetric irregular alternations of fine-grained, amphibole-rich green and grey layers and feldspar-rich felsic layers. In the felsic layers, amphibole (green clinoamphibole) porphyroblasts reach 0.5 to 1 cm in length, suggesting a metasomatic origin (i.e. metamorphic differentiation). There are also metric-scale gabbroic pods

intercalated in the gneiss (Fig.3.6), but there are no granitic orthogneisses or early mafic dykes. These gabbroic pods are formed by coarse-grained plagioclase and amphibole. There is no apparent fabric in them and locally they are porphyritic. The compositional banding in the surrounding banded gneiss wraps around these gabbroic pods, which might represent apophyses of metagabbro and seem to have been boudinaged and folded (Fig.3.6). The contacts with the banded gneiss are sharp to diffuse suggesting metasomatic processes during metamorphism. This is consistent with the chaotic porphyritic texture of some of the pods and the same texture was observed in metasomatized areas of the nearby Sandbank metagabbro.

Farther west, in the rocky point west of East Diver Head (Fig.3.7), occurs a veined-gneiss formed by the intrusion of late massive granitic dykes into the paragneiss. Disharmonic folding of the granitic dykes at the fold hinges suggests syn-magmatic deformation (McLellan, 1983, 1984).

The rest of the gneissic outcrops west of this rocky point are relatively similar to one another. They comprise a strained quartzo-feldspathic gneiss (Fig.3.8) of uncertain protolith with deformed boudins of undated granite alternating with metric pods of competent metagabbro (Sandbank metagabbro). This part of the section also contains an outcrop with exceptionally well preserved cross-cutting relationships. In this outcrop a tourmaline-bearing schist/paragneiss with greenschist facies mineral assemblages (Bt+Ms+Chl+Qtz+Kfs+Pl (oligoclase)+Ep+Tur) is intruded by a set of aplitic/pegmatitic veins (mineral assemblage, Qtz+Kfs+Pl) along the planes of the schistosity (Fig.3.9), resembling an anatectic migmatite and forming a composite veined-gneiss. One of these aplitic veins, showing ptygmatic folding, cross-cuts an older granodiorite (Sandbank granodiorite; U-Pb sample) and merges with the aplitic veins in the paragneiss (Fig.3.10 and 3.11). The aplitic veins in the paragneiss merge with a granite with gabbroic xenoliths

which is also intrusive into the paragneiss, suggesting that they represent granite injections. This composite veined-gneiss is intruded by a "younger" granite/granodiorite which is variably mylonitized and intruded by a set of late mafic dykes.

Cinq-Cerf Bay and Three Islands:

The Cinq-Cerf gneiss at the type locality of Cinq-Cerf Bay consists of a polydeformed, green-grey banded gneiss with epidote-rich and locally amphibole-rich layers (Fig.3.12). This rock resembles the amphibole-rich banded gneiss and the tourmaline-bearing schist/paragneiss at Sandbank Point, but no tourmaline was identified in this section. Also, there is no evidence of older granitic orthogneiss.

At the Three Islands, the Cinq-Cerf gneiss comprises a veined-gneiss with abundant refolded granitic dykes, responsible for the veining. The country rock to the dykes is a fine grained mica-bearing grey rock of uncertain protolith (schist / paragneiss ?). The granitic dykes are also intrusive into metagabbro. Althought the metagabbro constitutes a massive unit, there are some deformed centimetre-scale gabbroic pods incorporated into the gneiss. In this section the scale of the mapping did not allow separation of the country rock from the refolded granitic/granitoid dykes, and both are merged together as a single gneissic unit (Map.3.2).

The Cinq-Cerf gneiss is therefore redefined as a composite unit of psammitic paragneiss/schist, amphibole-rich banded paragneiss and quartzo-feldspathic gneiss with slivers of highly strained granitic orthogneiss, deformed amphibolite dykes and gabbroic pods. Locally the metasedimentary lithologies are veined by aplitic and intermediate dykes and deformed, producing a veined-gneiss which resembles anatectic migmatite.

U-Pb geochronology:

The geochronology in this unit has been focused on the two high quality outcrops of the Sandbank Point-East Diver Head section (Fig.3.4 and 3.10). In these two outcrops, the intrusive older granitic orthogneiss and the Sandbank granodiorite (Next section) provide a younger limit for the depositional age of the metasedimentary members of the gneiss.

Details of the U-Pb analytical procedure, including sample preparation, are provided in appendix A.1.

Older granitic orthogneiss: This sample comes from the contact between the older granitic orthogneiss and the younger granitic dykes (Fig.3.5 and 3.13). The granitic orthogneiss has been intruded by a set of mafic dykes which predate the intrusion of the late granite dykes (Fig.3.5 and 3.13). This rock provides a younger limit for the deposition of the country rock paragneiss and an older limit for the gneissic banding and the intrusion of the older mafic dykes.

This rock yielded large amounts of high quality euhedral zircon. All fractions are formed of stubby (1:3 width/length ratio), multifaceted, sharp, clear, inclusion-free prisms. Of seven zircon fractions analyzed, five have error ellipses touching the concordia curve (Fig.3.14; table 3.1). The small euhedral prisms of fraction Z6 were not abraded to constraint the lower intercept of the discordia line. Fractions Z1 to Z6 define a discordia line with a 93% probability of fit and an upper intercept at 676 Ma and a lower intercept at 433 Ma. The lower intercept coincides with the age of the cross-cutting younger granite dykes (Western Head granite), suggesting that these are responsible for the Pb loss. With the lower intercept pinned at 431±2 Ma, the resulting discordia line (97% probability of fit)

has an upper intercept of **675+12/-11 Ma**. This upper intercept is interpreted as the intrusion age. Fraction Z7 suggests the presence of 2.0 Ga inheritance, projected from 675 Ma.

3.6.2.- The 584 Ma Sandbank Granodiorite.

This is a weakly deformed, amphibole-bearing granodiorite (U-Pb sample 94-PV-6) with mafic inclusions, resembling some of the nearby granodiorite facies of the 430 Ma Western Head granite. It forms a small outcrop of about 100 m^2 between Sandbank Point and East Diver Head (Map 3.1; Fig. 3.3). The country rock consists of tourmaline-bearing paragneisses with abundant aplitic veins (Fig.3.9). The strain gradient in the country rock paragneiss increases towards the contact with the granodiorite with the foliation wrapping around the granodiorite. This indicates that the granodiorite predates the development of the main foliation in the paragneiss (Fig.3.10 and 3.11). It is not possible to assess if there was an older pre-intrusive fabric in the country rock paragneiss due to the millimeter-scale of the compositional banding, the high strain following emplacement of the granodiorite and the absence of cross-cutting relationships. An aplitic vein cross-cuts the granodiorite and merges with the aplitic dykes in the country rock paragneisses (Fig.3.10; 3.11), indicating that the veining and the deformation of the veined-gneiss took place after the intrusion of the granodiorite. According to the field relationships (Fig.3.10; 3.11), the protolith age of this rock will provide a younger absolute age limit for the country rock paragneiss and an older limit for the aplitic veining and subsequent deformation of the aplitic veins and the tourmaline-bearing paragneiss.

This rock consists of plagioclase (An20-30), K-feldspar, quartz, biotite, green amphibole (hornblende) and opaques, and secondary actinolite, chlorite, epidote,

zoisite/clinozoisite and titanite. Zircon and apatite are accessory minerals. There is wide preservation of primary igneous features such as concentric zoning in plagioclase, which suggests that the Cinq-Cerf gneiss was not affected by a high grade regional tectonothermal event after the intrusion of this rock. In hand sample the rock has a weak subsolidus fabric with no apparent penetrative cleavages except for late, high angle, discrete (>0.5 mm thick) joints filled with chlorite +epidote+zoisite

U-Pb geochronology:

This rock yielded high quality zircons. Fractions Z1, Z2 and Z3 are formed by stubby euhedral, inclusion-free prisms; fraction Z4 consists of small euhedral elongated (1:5 length/width ratio) prisms. The four zircon fractions analyzed define a discordia line (14.8% probability of fit) with an upper intercept of **584 +7/-6 Ma** and a lower intercept of 326 Ma (Fig.3.15; table 3.1). The upper intercept is interpreted as the crystallization age; whereas the lower intercept apparently does not have a real geological meaning. The large Pb loss in fraction Z4 can be explained by greater radiation damage due to the higher U concentration (205 ppm; twice that of the other fractions) and lead diffusion facilitated by the larger length/width ratio, compared with the other fractions (Table 3.1).

3.6.3.- The 557 Ma Sandbank Point metagabbro.

This rock type is common to all areas, including the Cinq-Cerf Bay section, outcropping as small stocks (Fig.3.3; Map 3.1, 3.2 and 3.3). The largest outcrop is the one at Sandbank Point, which was already mapped by Cooper (1954). Therefore, it is proposed to name this rock type the Sandbank Point metagabbro. This is a mafic rock dominated by amphibole (Ø≈1mm) with about 20-30% felsic phenocrysts (Ø ≈ 2-3 mm),

giving a porphyritic texture. The metagabbro does not show any penetrative fabric, except in retrogressed areas and discrete high strain zones where the amphiboles have a preferred orientation defining the gneissosity. Three main facies were observed in the field:

A) *Mafic metagabbro/meta-diorite (Fig.3.16):* This is the most typical rock type. It dominates the exposures at Sandbank Point, Cinq-Cerf Bay as well as Three Islands. The main mineralogy is 65-70% green clinoamphibole (Hornblende-Actinolite)+ 30% plagioclase (An30-55)+ ≈ 5% opaques ± minor quartz ± K-feldspar? + epidote*+ clinozoisite*±(carbonate*)±titanite *(* secondary minerals)*. Accessory minerals are apatite and zircon. Texturally the rock still preserves some igneous features like weak concentric zoning in some plagioclase crystals and large plagioclase (Ø≈2-3mm) with subhedral tabular shape. The amphibole, however, is metamorphic and the dominant texture is granoblastic. This granoblastic texture has been overprinted by greenschist facies metamorphic/deformational events. At Three Islands low strain areas also show a granoblastic texture with complete recrystallization of most plagioclase and a minimal greenschists facies overprint.

B) *Leuco-metadiorite (Fig.3.16):* This rock type is restricted to Sandbank Point. It appears as irregular dykes intrusive into the mafic metadiorite. These dykes show gradational to sharp contacts, suggesting that the intrusion took place when the host was in a subsolidus/solidus state, and that they probably represent a late differentiate of the mafic intrusion.This rock is formed by ≈60% plagioclase (oligoclase-andesine) + ≈35% green clinoamphibole +≈5% opaques, and minor quartz. Most plagioclases still preserve a weak concentric zoning and a euhedral/subhedral tabular shape. The amphibole and the opaques coexist in interstitial positions between the plagioclase laths. The amphibole accumulations, hornblende-actinolite, show granoblastic textures, indicating a metamorphic origin. Late

retrogression was associated with growth of minor chlorite, epidote and white mica (sericite?).

C) *Coarse hornblendite :* This rock type outcrops in Three Islands where the metagabbro-diorite is generally more amphibole-rich than the equivalent rock types at Sandbank Point, with the hornblendite representing the most extreme case. This rock type contains 65-70% green clinoamphibole (actinolite-tremolite), 5-10% clear orthoamphibole (anthophyllite?), 10-15% biotite and 5-10% opaques with minor relicts of plagioclase (An 50). The clinoamphibole, orthoamphibole and biotite show euhedral-subhedral shapes and appear in contact, suggesting that they grew in equilibrium. Some clinoamphiboles show opaque rich cores which might be relict pyroxene. The rock has a decussate texture with 5mm long clinoamphibole defining the framework.

Field relationships:

Sandbank Point-East Diver Head (Fig.3.3; Map 3.1): The metadiorite/metagabbro forms a relatively large body which is cut by the Grand Bruit fault and intruded by the Silurian Western Head granite-granodiorite and a swarm of late dykes. This metagabbro and other gabbroic apophyses are intrusive into the composite Cinq-Cerf gneiss (Map 3.3).

Three Islands (Fig.3.3; Map 3.2): The metagabbro at Three Islands resembles that at Sandbank Point but it is dominated by mafic rock types, from mafic metadiorite to hornblendite. The metagabbro is intruded by refolded felsic to intermediate pre-Western Head granitoid dykes (Fig.3.17). These felsic dykes and their highly strained country rock form a veined gneiss which was mapped as Cinq-Cerf gneiss (Map 3.2). Dunning and B.H. O'Brien dated one of these intermediate dykes at 547+2/-7 Ma (unpublished), suggesting that the metagabbro at Three Islands is older than 547 Ma. Both the gneiss and

the metagabbro are intruded by the Silurian Western Head granite and a series of late mafic and aplitic dykes.

Cinq-Cerf Bay (Map 3.3) : This section contains two metagabbroic stocks which resemble the mafic metadiorites at Sandbank Point. These rocks were probably intrusive into the highly deformed metasediments. The intrusive contacts have been reworked by brittle deformation, which has wiped out the primary intrusive relationships. These metagabbros are intruded by granitic dykes with mafic enclaves which resemble both the Late Precambrian Roti suite and the Silurian Western Head granite. One of the metagabbros is also cross-cut by a late mafic dyke (post-Western Head granite?).

U-Pb geochronology:

The Sandbank Point mafic metagabbro/metadiorite was chosen for U-Pb dating because it is the most extensive and common facies of the Sandbank metagabbro. It is intrusive into the composite Cinq-Cerf gneiss and is intruded by the Western Head granite. The sampling locality at Sandbank Point (Map 3.1) shows a clear intrusive relationship with the Western Head granite and it coincides with an area of important high-temperature (syn-magmatic?) deformation in the Western Head granite. Texturally, the U-Pb sample has the characteristics described in the mafic metadiorite but all grain contacts have been modified by the D2 deformation (syn-late-Western Head granite), with mafic and feisic elongate patches (0.5 to 1mm long and 1mm thick) defining a weak gneissic banding. This rock is quartz-bearing, which suggests that it might represent a more evolved part of the mafic intrusion and therefore more likely to be zircon-bearing.

Four fractions of gem quality zircon were separated from this rock (Table 3.1). Fraction Z4 was not abraded to help constraint the discordia line. Fractions Z1, Z2, Z3 are between 0.37% and 0.73 % discordant (Fig.3.18) and the discordia line defined by all

fractions (46% probability of fit) has an upper intercept of 557 Ma and a lower intercept of 321 Ma. The upper intercept is interpreted as the crystallization age (**557+14/-5 Ma**). The large positive error of the upper intercept is due to the shallow angle of intersection between the discordia line and the concordia curve. The lower intercept at 321 Ma apparently does not have any geological significance, but it is indicative of an Late Paleozoic disturbance.

3.6.4.- The Silurian Western Head granite (2 Facies):

The later Western Head granite is a 15 km long intrusive body which defines the southern boundary of the Cinq-Cerf gneiss between Cinq-Cerf Bay and Grand Bruit (Fig.3.2; O'Brien et al., 1991). This rock type was originally included in the Cinq-Cerf gneiss unit of B.H. O'Brien (1990) by Cooper (1954) and later reported by Chorlton (1980). But it was only Cooper (1954) who mapped the outcrops of the Western Head granite between Sandbank Point and East Diver Head in detail. During the present study, the rocks mapped by Cooper (1954) were confirmed and two facies of this granite were identified in the Sandbank Point-East Diver Head section. The first one is the "young" mylonitic granite (Fig.3.5) which was previously correlated with the Roti granite by B.H. O'Brien (1990). U-Pb dating however shows that it is coeval with the Western Head granite. The second facies is a granite-granodiorite with mafic and gneissic enclaves (Fig.3.19 and 3.20), which is the lithological equivalent of the Western Head granite of B.H. O'Brien (1990) in Grand Bruit and Three Islands.

Mylonitic granite: This rock type outcrops near East Diver Head (Fig.3.4 and 3.5), very close to outcrops of the Roti granite (B.H. O'Brien, 1990). It consists of several 1 to 3 m wide granite dykes which are emplaced cross-cutting earlier structures in the country rock (banded gneiss and 675 Ma granitic orthogneiss). The local incorporation of angular

blocks of the country rock at the front of some of the dykes is indicative of stoping, althought the dykes were probably emplaced by dilatation (Park, 1983). At the nearest rocky point west of East Diver Head the granite can be traced to granitic injections which are disharmonically folded mimicking a migmatite (Fig.3.7). Later low-grade heterogeneous mylonitic deformation was concentrated in the granite, rather that the country rock (Fig.3.5), and resulted in intense mylonitization and pervasive retrogression of the primary mineral assemblages. The granite is cross-cut by a swarm of late mafic dykes which are also variably overprinted by the low-grade shearing.

Texturally the rock is a mylonite with a well developed S-C fabric around partially to totally sericitized 2 mm (Øav) feldspar porphyroclasts. These porphyroclasts have chlorite and white mica inclusions. The porphyroclasts form around 30-40% of the rock. The mylonitic matrix (Øav≈ 0.05mm) consists of 30% phyllosilicates (Chlorite, white mica) and epidote and 70% quartzo-feldspathic material.

Granite-granodiorite with mafic and gneissic enclaves: In the area of study, this rock type outcrops between Sandbank Point and East Diver Head and at Three Islands. Detail mapping at Three Islands expanded the extent of the Western Head granite unit of B.H. O'Brien (1990). The lithological similarities of this granite in Three Islands and Sandbank Point with the Western Head granite at Grand Bruit are such, that they permit a secure correlation with the 429±2 Ma Western Head granite (O'Brien et al., 1991). It should be noted that Cooper (1954) also mapped the same outcrops in map 3.2 as Western Head granite. The field aspect is that of a felsic granitoid with abundant mafic and gneissic enclaves (Fig.3.19). Locally, these enclaves are isoclinally folded, sheared and stretched, indicating magmatic or high temperature subsolidus deformation. At Sandbank Point there are abundant felsic injections backveining mafic material and mafic dykes showing a complex deformation, which is not present in the country rock metagabbro (Fig.3.20).

This suggests the presence of coeval mafic magmatism and deformation during the intrusion of the Western Head granite. The high temperature deformation is followed by low-grade heterogeneous mylonitization along discrete shear zones.

This rock is composed of plagioclase (An25), quartz, K-feldspar, biotite, ±clinoamphibole, opaques and secondary epidote, chlorite, titanite and white mica, with apatite and zircon as accessory phases. According to the relative modal proportions of plagioclase, feldspar and quartz, the rock can be classified as a granodiorite/granite.

The presence of 1-2 mm wide plagioclase and feldspar crystals suggests that the rock had a primary equigranular texture. Although, the superimposed subsolidus deformation has produced areas with extensive grain reduction (Ø≈ 0.2 mm), most of the strain has been taken by the quartz grains and by the biotite-rich levels. It is in the biotite-rich levels that epidote group minerals, titanite, chlorite and white mica are concentrated, and these are also areas of important quartz grain reduction. Plagioclase shows local primary concentric zoning. Both plagioclase and feldspar have irregular grain boundaries with variable grain reduction and recrystallization and, in the case of the feldspar, some of the recrystallized areas show microcline twins and mantle-like structures around larger crystals.

U-Pb geochronology:

The dated sample of the mylonitic granite was collected from the same outcrop as the sample from the old granitic orthogneiss (Fig.3.4 and 3.5). The granite dyke cross-cuts the gneissosity in the 675 Ma granitic orthogneiss and the surrounding banded gneiss, including the old amphibolite dykes. The granite is overprinted by a later mylonitic event and cross-cut by a swarm of late mafic dykes. Therefore, the protolith age of this rock provides a younger age limit for the deformational event(s) responsible for the gneissic banding, and for the intrusion of old amphibolite dykes. It also provides an older limit for

the late mylonitization, the greenschist facies retrogression and the intrusion of the late mafic dykes, as well as a direct date of the syn-magmatic deformation of the granite injections in figure 3.7.

The five zircon fractions analyzed define an unpinned discordia line (68% probability of fit) with an upper intercept of 431+8/-2 Ma and a lower intercept of -17 Ma. If the lower intercept is pinned at 0±17 Ma, the resultant discordia line has an upper intercept of **431.5 ±1 Ma** (Fig.3.21). This upper intercept reflects the crystallization age, the precision of the age is also consistent with that of the $^{207}Pb/^{206}Pb$ ages. All zircon fractions are U-rich (792 to 489 ppm; table 3.1) which resulted in slightly discordant analyses, even though some fractions were strongly abraded (Table 3.1).

Note: The 321 Ma and 326 Ma lower intercepts of samples 94-PV-4 (557 Ma; metadiorite) and 94-PV-6 (584 Ma; granodiorite) reflect Late Paleozoic disturbance of the Pb systematics. These lower intercepts could be a combined effect of major disturbance during the intrusion of the Western Head granite (431 Ma) and minor Pb loss like that of the Western Head granite (sample 94-PV-11).

3.6.5.- Late dykes.-

These dykes cross-cut the 431-429 Ma Western Head granite and post-date the syn-magmatic / high temperature subsolidus deformation observed in it. They form important swarms at the contact of the Western Head granite, both near East Diver Head and at Three Islands (Map 3.1 and 3.2). All these dykes cross-cut folds in both the Western Head granite and the Cinq-Cerf gneiss. Although they are variably sheared in places, these dykes are not folded. There are four major types of late dykes: felsic-granitic, green-mafic, grey-

intermediate and porphyritic dykes. The porphyritic dykes represent the final intrusive pulse in the area.

Felsic-granitic dykes:

These dykes are intrusive into late mafic dykes as well as the 557 Ma Sandbank metagabbro, but they do not cut the Western Head granite. They are aplitic and although relatively scarce they should not be confused with the pre-Western Head granite folded aplitic dykes at Three Islands.

Grey-intermediate dykes:

These dykes are relatively common in Three Islands, but only intruding into the pre-Western Head portion of the island. These dykes are cross-cut by mafic dykes. They show a well developed fabric (Ø av.≈ 0.2 mm) of oriented green clinoamphibole (Actinolite-Hornblende), plagioclase (oligoclase), brown-green biotite, quartz, K-feldspar (?) and opaques. This fabric is not penetrative, however the plagioclases show tapered twins and undulose extinction, indicating intracrystalline deformation. Grain boundaries are straight to lobate and with triple junctions. Late growth of epidote around opaque-rich areas and chlorite after biotite suggest that the fabric was produced in the amphibolite facies, probably during cooling.

Green-mafic dykes:

These are dark green to grey-green and intrusive in all rock types, including the Western Head granite. They are, however, intruded by the porphyritic dykes and, at Three Islands, by aplitic dykes. Dated field relationships indicate that they are younger than 431 Ma (Fig.3.4 and 3.5). Some of these dykes contain ultramafic and granodioritic enclaves (both in the same dyke) and rounded, centimetric quartz enclaves. These mafic dykes with

quartz enclaves appear both at Sandbank Point and Three Islands. Cross-cutting relationships indicate the presence of at least two generations of post-431 Ma mafic dykes, although they might represent different injections during the same intrusive event. Deformation tends to be concentrated in the thinner dykes and it is associated with formation of a penetrative greenschist-subgreenschist facies foliation.

Amphibole-plagioclase porphyritic dykes:

These dykes intrude the mafic dykes (Fig.3.4) and are the youngest intrusions in the area. They consist of plagioclase (An40-50) phenocrysts (2 to 3 mm long) and glomeroporphyritic accumulations (3 mm long) of green clinoamphibole (Actinolite?) + chlorite + biotite (minor) and an oriented matrix (Ø av ≈ 0.1mm) of plagioclase (oligoclase) + green clinoamphibole + opaques + chlorite* + epidote* + titanite* (**secondary minerals*). Titanite commonly grows late after opaques (ilmenite?). The plagioclase laths are oriented and although variably sericitized they still preserve the primary concentric zoning and the euhedral tabular shapes. Greenschist deformation and retrogression resulted in the transformation of the primary mafic minerals into clinoamphibole accumulations and variable development of a penetrative fabric, including discrete C' shear planes.

Titanite from a mafic porphyritic dyke at Three Islands has provided an age of **420±3 Ma** (Dunning and B.H. O'Brien, unpublished). Since titanite is growing during the final greenschist facies overprint, this age provides a younger limit for dyke emplacement and dates the greenschist facies retrogression.

3.7.- STRUCTURAL EVOLUTION:

Two main phases of deformation can be distinguished in the Cinq-Cerf gneiss. The first one, D1 includes all deformation predating the intrusion of the Silurian Western Head granite. D2 covers the syn-Western Head granite solidus/subsolidus deformation and the following low grade Silurian mylonitization. D2 is bracketed by the intrusion of the 430 Ma Western Head granite and by the 420 Ma greenschist facies titanite in the late porphyritic dykes. However, some late-brittle features could be younger than 420 Ma. These phases of deformation were divided into subphases, to differentiate the overprinting structural elements that occur in each outcrop.

3.7.1.- D1 deformational events (pre-431):

The earliest event recognized in the *Sandbank Point - East Diver Head section* is the D1 deformation which affects the composite Cinq-Cerf gneiss, including the 675 Ma orthogneiss. This event resulted in a composite penetrative fabric with a mylonitic aspect. This fabric also affects the old mafic dykes which intrude the 675 Ma orthogneiss. Later boudinage (D1) affected both the mafic dykes and the fabric in the surrounding rocks. These boudins were subsequently openly folded during D2 (Fig.3.4 and 3.5).

A hand sample -scale and microscopic examination of the composite S1 fabric in the 675 Ma orthogneiss indicates the presence of three cryptic fabric elements: an early $S1^a$ fabric (compositional banding) is cross cut by discrete millimetric polycrystalline quartz veins ($S1^b$?), both of which are folded by $F1^c$ folds with an axial planar $S1^c$ fabric. $F1^c$ folds are millimetric to centrimetric in scale and very cryptic (Fig.3.22). The old mafic dykes, which intrude the 675 Ma orthogneiss, do not show evidence for $F1^c$ folds but have a fabric parallel to $S1^c$ in the orthogneiss, which is interpreted as $S1^c$. This would suggest

that the mafic dykes intruded after the $S1^a$ fabric was produced in the 675 Ma orthogneiss. It is unclear if the D1boudinage observed in the mafic dykes was contemporaneous with the $F1^c$ folding, but these boudins are subparallel with the orientation of the dominant composite $S1^a$-$S1^c$ fabric.

The $S1^a$ fabric is a compositional banding defined by the orientation of the biotite flakes (0.3 mm long), areas with slightly different abundances of oxides, phyllosilicates and epidote and slight differences in the grain size (Ø≈0.1-0.3 mm) of the quartzo-feldspathic load-bearing framework (Handy, 1990). $S1^c$ is a wide cleavage defined by oriented new grown biotite and chlorite. Both quartz and feldspar have a weak preferred orientation parallel to the $S1^c$ micas, undulose extinction, lobate grain boundaries and extensive evidence for subgrain development and recrystallization. Recrystallization apparently took place by subgrain rotation (Passchier and Trouw, 1994). Pre-$S1^c$ aggregates (Ø≈0.9 - 0.7 mm) of plagioclase (Ø≈0.3 mm) and minor quartz and feldspar (Ø≈0.1 mm) probably represent core-and-mantle structures (Passchier and Trouw, 1994). This plagioclase has abundant small quartz inclusions which are not observed elsewhere in the section. This suggests that this plagioclase is the product of a pre-$S1^c$ deformation and, therefore, indicates a tectonic origin for the $S1^a$ fabric. Late joints filled with epidote, zoisite and chlorite are ascribed to the S2 Silurian deformation.

The *amphibole-rich banded gneiss* also shows a tight complex folding of the compositional banding ($S1^{a?}$). Millimetric to centimetric $F1^c$ folds can be identified but they have an intense D2 overprint (Fig.3.7). The character of the D2 overprint is complex due to the rheological contrast between the competent gabbroic pods and the surrounding paragneiss. This has resulted in local incoherent D2 folding due to the deflection of the gneissosity (composite S1fabric) around the competent gabbroic pods (Fig.3.7).

The *country rock to the 584 Ma weakly deformed granodiorite*, the tourmaline bearing paragneiss, shows one well defined composite schistose/gneissose fabric (S1). There are some very cryptic intrafolial folds (F1c folds?), but they can not be positively identified as F1 folds. The D2 reworking of the S1 fabric has deflected it around the more competent 584 Ma granodiorite (Fig.3.11). Because the S1 fabric and the intrusive contact were brought into parallelism, it is not possible to assess a clear cross-cutting relationship between the 584 Ma granodiorite and the S1 fabric in the country rock paragneiss. The post-584 Ma aplitic dykes intruded along the planes of the S1 schistose fabric, locally cross-cutting S1 and, indicating that the S1 schistose fabric pre-dates the aplitic dykes (Fig.3.11). The aplitic dykes were tightly folded and sheared, under greenschist facies conditions. This resulted in the deflection of the resultant composite S1-S2 fabric around the 584 Ma granodiorite. The reworking of the contact between the 430 Ma Western Head granite and the paragneiss (Fig.3.11) indicates that the composite S1-S2 fabric is post-430 Ma, i.e. D2. Therefore, the subsequent small scale open folding, crenulation, of the composite S1-S2 fabric is post-430 Ma (i.e. D2).

The fabric in the tourmaline-bearing paragneisses consists of a compositional banding (S1) of uncertain origin (S0+S1?). The S1 banding is formed by 5 to 1 mm thick irregular phyllosilicate-rich (Biotite+chlorite+white mica) and quartzo-feldspathic layers (Ø ≈ 0.2 - 0.6mm). Some of the quartzo-feldspathic layers define tight intrafolial folds ($F1^c$?), with limbs cut at a shallow angle by the aplitic veins. In the compositional bands (S1) the phyllosilicates were realigned during D2 defining an S1+S2 fabric with chlorite and white mica overgrowing biotite (Fig.3.23). Green tourmaline porphyroblasts (Ø≈ 0.5-2 mm) are concentrated in the phyllosilicate-rich layers and postdate the S1+S2 fabric. The aplitic veins are 1 to 0.5 cm wide, have granitic modal compositions with minor plagioclase and average grain size of 2 mm of diameter (Ø max ≈ 7 mm) and they contain blue tourmaline.

K-feldspar and quartz form a two phase load bearing framework (Fig.3.23; Handy, 1990). Quartz with serrated boundaries, subgrains and parallel deformation bands is the weak phase and shows dynamic recrystallization. K-feldspars show new grains (Ø≈0.3 mm) with microcline twins produced by grain reduction at the borders of the crystal (Fig.3.23). These new grains are partially recrystallized forming core-and-mantle structures. A later event is recorded by the growth of new white mica associated with sericitization of plagioclase, fracturing of tourmaline and deformation of S2 white mica. This is probably related to the late open folding of the composite S1-S2 fabric. The nearby 584 Ma granodiorite (Fig.3.10 and 3.11) still preserves a primary equigranular texture with plagioclase, K-feldspar and quartz (Ø≈ 1-3 mm) forming the main framework and biotite, clinoamphibole, chlorite, epidote and oxides in interstitial positions (Øav ≈ 0.5 mm). Both plagioclase and feldspar have subhedral tabular shapes with irregular grain boundaries and small mantles of a quartzo-feldspathic matrix, plagioclases also show well defined primary concentric zoning (Fig.3.24). The quartz grains with subgrains and parallel deformation bands have anhedral shapes with lobate boundaries, indicating that it is the weak phase of the framework. Biotite, chlorite, epidote, clinoamphibole and opaques are concentrated in intergranular positions in areas of grain reduction defining a weak fabric (S2?, Fig.3.24).

The *quartzo-feldspathic gneiss with granite boudins* also shows an S1 schistosity/compositional banding overprinted by D2 folding. Locally, the quartzo-feldspathic gneiss shows a cryptic dome and basin fold interference (two generations of F1 folds or a fish-hook fold?) of the compositional banding (S1), overprinted by F2 folds (Fig. 3.8). It is uncertain if the granite boudins are Silurian or not. The boudins pre-date the Silurian greenschist facies mylonitization, but they could have been associated with the high temperature Silurian D2 deformation.

At ***Three Islands***, the Late Precambrian granitoid dykes show two apparent phases of folding, also present in some of the metagabbros. The *547 Ma granitoid dykes* have a gneissic compositional banding ($S1^a$, primary ?) defined by the alternation of plagioclase (oligoclase) and green amphibole-rich bands with a granoblastic texture (Øav ≈ 0.2 mm). Biotite flakes define a discontinuous, spaced foliation ($S1^b$) cross-cutting the compositional banding, and axial planar to the $F1^b$ folds affecting the $S1^a$ banding (Fig.3.26). Titanite (448+9/-3 Ma; Dunning and B.H. O'Brien, unpublished) appears as inclusions in both biotite and amphibole, as well as in intergranular positions, and is locally aligned with biotite. This suggests that the fabric defined by the biotite predates recrystallization and is older than 448 Ma. Discrete shear bands cross cutting the $S1^b$ biotites and deformation of quartz that postdates recrystallization indicate a weak brittle overprint (S2).The Silurian D2 shearing is axial planar to the last phase, therefore indicating that this final folding is Silurian. However, the relationship of the pre-F2 fabric and earlier folding with the D1 elements described in the Sandbank Point-East Diver Head section is uncertain. Lack of detailed structural mapping prevents any further interpretation.

The ***metagabbros*** at Sandbank Point and Three Islands generally have granoblastic textures with triple point junctions between plagioclase and green clinoamphibole, some plagioclase laths preserve subhedral tabular shapes and a weak concentric zoning. These textures are variably overprinted by later D2 deformation: lobate grain boundaries, grain reduction with growth of epidote and chlorite, small core-and-mantle structures in plagioclase, brittle displacement of plagioclase twins and dynamic recrystallization of quartz (Fig.3.25). Locally there is a gneissic banding defined by 0.5 to 1 cm elongated plagioclase and amphibole-rich domains with oriented amphiboles (green hornblende, Fig.3.25) which at Sandbank Point is probably related to the intrusion of the Western Head granite (S2 fabric).

At ***Cinq-Cerf Bay*** the contact between the Silurian Western Head granite and the Cinq-Cerf gneiss has been reworked by a late brittle fault zone. The Western Head granite shows some evidence of syn-magmatic deformation but does not show any internal folding or important D2 solidus/subsolidus deformation, as in the other two previous sections. Gneissic enclaves of amphibolitic banded gneiss in the nearby 568 Ma Roti granite suggest the presence of a pre-568 Ma event. It is assumed, however, that the brittle deformation and possibly the latest folding in the Cinq-Cerf gneiss (Fig.3.27) are Silurian. Locally, the compositional banding (S0+S1?=$S1^a$) is folded by 3 phases of folding, $F1^b$, $F1^c$ and F2. Interference patterns are best seen in the hinges of F2 folds (Fig.3.27), although they can also be identified in areas under D2 shearing. F2 folds have steep plunges (50°-70°) which are consistent with the steep dip of the main gneissosity (average 70°). In cross-section, the S1 gneissosity is boudinaged. In plan view, small boudins are locally sheared by D2, but any relationship between these two types of boudins is uncertain. It should be noted that the Cinq-Cerf Bay section presents several problems: a) the compositional banding is cryptic and given the small scale structural complexity, it is very difficult to trace structures even at outcrop scale (Fig.3.12 and 3.27); b) the effect of the strain partitioning created by the three (undated) gabbroic bodies in the section is uncertain (Map 3.3); c) there is an important late brittle overprint.

3.7.2.- Silurian D2 deformation.-

The D2 Silurian deformation is subdivided into $D2^a$ and $D2^b$ subphases. $D2^a$ is the high temperature solidus/subsolidus deformation associated with the emplacement of the 430 Ma Western Head granite. High temperature $F2^a$ folds have an axial planar mylonitic fabric, $S2^b$. The D2 mylonitic fabric was associated with heterogeneous greenschist facies shearing of the Western Head granite and its country rock. This shearing produced $F2^b$ folds which are transected by late mafic dykes. These late mafic dykes are also variably

sheared depending on their degree of retrogression, and they usually follow the trace of the mylonitic foliation. This suggests that the same stress field was present all along during the intrusion and cooling of the Western Head granite and intrusion of the late dykes.

D2^a, high-temperature solidus-subsolidus deformation:

This deformation is associated with the emplacement of the 430 Ma Western Head granite, indicating the syn-tectonic character of this intrusion. This deformation is best expressed in the Western Head granite at Sandbank Point, Three Islands and Grand Bruit, the last area is 2 Km west of the field area.

The high-temperature D2^a deformation is characterized by tight isoclinal asymmetric folding and shearing of the enclaves in the Western Head granite. At Sandbank Point, the Western Head granite and coeval mafic dykes show a complex folding, the mafic dykes are ductily sheared and folded (Fig. 3.28). Well exposed cross sections of these structures at Grand Bruit show a compositional fabric defined by aplitic and mafic dykes and gneissic and mafic enclaves. The trend of the fabric has an anastomosed character typical of ductile deformation, with strain partitioning around stiff granitic domains and ductile shearing and folding of amphibolite enclaves in the less competent surroundings. These features indicate that the granite was already in a solid state and that deformation took place at high temperature (Fig.3.29). Local disharmonic folding of Western Head injections into the Cinq-Cef gneiss (Fig. 3.7) indicate that deformation also took place while the granite was in a magmatic/submagmatic state (McLellan, 1984; Paterson et al., 1989).

The high temperature asymmetric folding is consistent with the intrusion pattern of the Western Head granite into the Cinq-Cerf gneiss, as well as with the local folding of the gneissosity in the country rock gneiss. Outcrop pattern suggests a rough north-south stress

field which is compatible with the one deduced from the overprinting lower grade mylonitization, $D2^b$ deformation (Fig.3.29).

$D2^b$, low-grade retrograde deformation:

This subphase of the D2 deformation is characterized by a heterogeneous mylonitization of both the Western Head granite and the Cinq-Cerf gneiss. The mylonitic foliation (D2) is axial planar to the $F2^a$ high-temperature folds in the Western Head granite. The mineral and stretching lineations (L2) associated with the S2 mylonitic foliation and the associated S-C fabrics indicate a shear sense of top to the north-northeast (Fig.3.30). Also, associated with the mylonitization there is ductile folding of the less competent layers (F2 folds). The plunge of the F2 folds, oblique to L2, and the fold asymmetry are consistent with the shear sense (Fig. 3.30). F2 axial planes are parallel to the S2 mylonitic foliation. This $F2^b$ folding is concentrated in the gneiss where the contrast of competencies is more significant. The plunge of the $F2^b$ folds is consistent with the folding of the S1 gneissosity (Fig.3.30). In the metagabbros this deformation is associated with retrogression and it is restricted to discrete shear zones (Fig. 3.31) and conjugate fracture systems (Fig.3.32).

The map pattern shows that the late mafic dykes are in many cases subparallel to the mylonitic foliation (Map 3.1 and 3.2; Fig.3.7). These dykes also have developed non-coaxial fabrics subparallel to S2, both magmatic and mylonitic. The last ones are associated with important retrogression. Althought some of these dykes have enclaves, there is no evidence for stoping but for emplacement by dilatation. However the orientation of the dykes, subparallel to $S2^b$, is apparently incompatible with dilatational emplacement (Park, 1983). This can be solved if the space for emplacement is created by previous anisotropies such as fractures and shear planes (S2, C-planes). This would require the S2 planes to act

as brittle thrust planes creating a space between the hangingwall and the footwall and the additional hydrostatic pressure from the dyke to favour the propagation of the dyke (Fig.3.30). Cooling of the dyke would stop its propagation, and the associated retrogression would favour the development of ductile shearing with mylonitic fabrics parallel to the mylonitic S2. This process would require that these dykes were emplaced during the late-D2 stages. This is compatible with the fact that the late dykes cross-cut F2 folds. However, further fieldwork is necessary to confirm this hypothesis.

The most characteristic microtextural feature of the $D2^b$ deformation is its mylonitic foliation (Fig.3.29 and 3.33). This mylonitic foliation is well developed in the Silurian intrusions, particularly in the 431 Ma granitic dyke. In this rock the primary granitic framework has collapsed into a boudin-matrix microstructure (Handy, 1990). The quartzo-feldspathic matrix (Ø< 0.05 mm) with white mica and chlorite surrounds winged retrograde feldspar and quartz porphyroclasts, defining S-C structures (Fig.3.33). Chlorite and white mica are both stable in the S-C and C' planes and are associated with extensive grain reduction and subgrain rotation dynamic recrystallization of quartz (Passchier and Trouw, 1996), indicating the greenschist facies character of this fabric. On the late mafic dykes, the $D2^b$ fabrics vary between recrystallized, amphibolite facies, continuous foliations to lower amphibolite-upper greenschist overprint of the magmatic fabrics (Fig.3.34) and greenschist facies mylonitization. This textural variation reflects the heterogeneous character of the $D2^b$ mylonitization and the close relationship between retrogression and mylonitization.

3.7.3.- Discussion and conclusions:

The deformational events within the Cinq-Cerf gneiss have been grouped in two main phases, D1 and D2. D1 is pre-Silurian and can be divided in different subphases, all of

which pre-date the intrusion of the 430 Ma Western Head granite. D2 is Silurian and resulted in the thrusting of the Cinq-Cerf gneiss along the Grand Bruit fault. A $D2^a$ subphase of high-temperature deformation, mostly in the Western Head granite, was separated from a later heterogeneous greenschist facies overprint, the $D2^b$ subphase.

D1 has a polyphase character. It is unclear how individual fabrics relate between outcrops. The pre-584 Ma lithologies have an S1a compositional banding which in the case of the 675 Ma orthogneiss is tectonic. $S1^a$ is locally cut by small polycrystalline quartz veins ($S1^b$) which might represent tension cracks. $S1^a$ and $S1^b$ are tightly folded by $F1^c$ folds and cross cut by an axial planar $S1^c$ foliation. The resultant composite $S1^a$-$S1^c$ fabric forms the dominant fabric in the Precambrian members of the gneissic complex. These fabrics have a small grain size and do not show evidence for coarsening during recrystallization. Chlorite, biotite and green clinoamphibole are stable in the $S1^c$ fabric in the paragneisses. This suggests lower amphibolite conditions which is consistent with the preponderance of grain rotation recrystallization (Passchier and Trouw, 1996). Conditions of formation of $S1^a$ fabric are more difficult to estimate but the extensive grain reduction, the small size of the phyllosilicates and the absence of coarsening after recrystallization suggest that this is not a high-grade fabric.

Timing of the S1 fabrics is unclear (Fig.3.35). $S1^a$ is post-675 Ma, it is bracketed by the undated old mafic dykes and it is not present in the 584 Ma and 557 Ma intrusions. The gabbroic pods in the banded gneiss also seem to postdate the compositional banding. $S1^c$ fabrics are synchronous or postdate the old mafic dykes and are older than 430 Ma. They are not present in the 587 and 557 Ma intrusions. The 547 Ma granitoid dykes at Three Islands were deformed between 547 and 448 Ma under amphibolite facies conditions. However, the relationship between the $S1^c$ fabrics and the 547-448 Ma deformation at Three Islands is unclear. The 587 and 557 Ma intrusions escaped most of the Silurian and

the post-547 Ma D1 deformation. Therefore, they do not provide a valid upper constraint for the D1 deformation but they require reassessment of the 543 Ma major regional tectonothermal event proposed by B.H. O'Brien et al. (1993) to explain their monazite data. In the case of the Sandbank Point-East Diver Head section the younger age limit for the D1 deformation is provided by the dated 430 Ma late granite which cross-cuts the old mafic dykes and the $S1^a$-$S1^c$ fabrics in the 675 Ma orthogneiss. The (pre-Silurian?) metamorphism of the 557 Ma Sandbank metagabbro is problematic. Partially preserved concentric zoning in plagioclase suggests that it took place under static conditions. But it is uncertain if this was due to autometamorphism during cooling, regional amphibolite facies burial metamorphism or if it was induced by a later intrusion. It is also uncertain if the 448 Ma titanite from Three Islands grew in response to a nearby, unidentified 450 Ma intrusion or if it is the product of prolonged cooling and recrystallization after earlier deformation.

The Silurian fabrics have been grouped into a single phase D2 divided into two $D2^a$ and $D2^b$ subphases. The $D2^a$ subphase is associated with the intrusion of the c.430 Ma Western Head granite and includes all syn-magmatic and high temperature subsolidus fabrics. Heterogeneous mylonitization, brittle-ductile deformation and lower amphibolite - greenschist facies retrogression followed the intrusion of the Western Head granite. This $D2^b$ deformation was broadly coeval with the intrusion of various swarms of late dykes. The final stages of the $D2^b$ deformation are constrained by 420 Ma titanite associated with greenschist facies overprint of a late mafic porphyritic dyke. Kinematic indicators and the orientation of the $S2^b$ mylonitic fabric and the L2 lineation indicate that the $D2^b$ heterogeneous deformation was related to thrusting along the Grand Bruit fault.

3.8.- GEOCHEMISTRY OF THE 557 Ma SANDBANK METAGABBRO-METADIORITE:

This geochemical sampling has been carried out to gather information about the tectonic environment at the time of intrusion of the 557 Ma Sandbank metagabbro, as well as to asses the field-based correlations between the dated mafic metagabbros and the felsic metadiorites at Sandbank Point and similar lithologies at Three Islands.

Major element whole rock analyses were performed by XRF on glass pellets. The trace elements were analyzed by XRF on press pellets and by ICP-MS. Details of the analytical techniques, including precision and limits of detections are presented in appendix A.2.

3.8.1.- Geochemistry:

The sample suite (Table 3.2) ranges from basaltic (44.86% SiO2) to basaltic-andesitic compositions (53.32% SiO2; Fig.3.36). The highest MgO concentration (13.96%) corresponds to the hornblendite at Three Islands and the lowest to the leuco-diorites (3.99% to 5.59%), the mafic metagabbros range from 5.52% to 9.34% (Fig. 3.36). Al_2O_3 concentration ranges from tholeiitic (15.20%) to high alumina compositions (19.59%). The highest alumina concentrations are those of the plagioclase-rich metadiorites (Fig.3.36). TiO_2 (0.47-1.65%) is variable although seems to show an increase with decreasing MgO. P_2O_5 shows a well defined trend of enrichment with decreasing MgO, except for the MgO rich samples. K_2O is low (0.18-0.68%), except for the MgO rich samples (1.1%; Fig 3.36). Na_2O varies between alkalic and sub-alkalic values, with highest values for the plagioclase-rich metadiorites (Fig.3.36).

Most trace elements in the suite do not show a well defined trend with major element variation, which could be an effect of a small sample set combined with sampling bias. The

exception is a positive correlation between Ni (355 to 5 ppm) and Cr (755 to 26 ppm) with MgO and a negative correlation between Sr and MgO. The REE patterns show a relatively flat chondrite-normalized pattern with a slight enrichment in LREE (Fig. 3.37). Sample G-CQ-7A (mafic metadiorite, Sandbank) constitutes an exception, showing a LREE depleted and small Eu negative anomaly. The Eu anomaly is absent in most samples or is poorly developed with both negative and a positive characters (Fig. 3.37). The REE rich patterns in both the Sandbank Point and Three Islands samples correspond to the felsic metadiorites. Although parallel to those of Sandbank Point, the patterns from Three Islands are REE depleted regardless of lithology. MORB (Pearce, 1983) - normalized multielement patterns are characterized by a slight depletion in HFSE with respect to MORB and a weak Nb anomaly (Fig.3.37). Mobile elements (Pearce, 1983; Jenner, 1996 and ref. within) were not plotted to avoid any scattering due to partial element mobility during secondary processes. The patterns show a good degree of consistency among the different lithologies. The samples from Three Islands are also slightly depleted in Ti and Y, but this seems to be an effect of the sample bias towards mafic-rich lithologies. The pattern of sample GCQ7A (mafic metagabbro, Sandbank Point) departs from the rest showing a MORB-like pattern (Fig.3.37).

3.8.2.- Discussion: geochemical signatures, tectonic environments and petrogenetic processes.-

There is no significant difference between the samples from Three Islands and Sandbank Point, except for a slight depletion in HFSE and REE, suggesting that they are part of the same suite. This also reinforces the notion that the leuco-diorites are cogenetic with the mafic metagabbros, even though they intruded the former in a solidus/subsolidus state. Given the difference in major element concentrations, the similarity of the geochemical signatures suggests that any effects in the trace element signatures derived

from possible cumulates are minimal. Thus the sample suite as a whole can be safely used for tectonic discrimination purposes.

The major elements point towards a tholeiitic character for the suite (Fig.3.36) but they do not offer a reliable characterization of the suite, due to the metamorphic overprint. Inmobile elements like Zr, Ti, Nb,Y, La and V (Hellman et al., 1979: Merriman et al., 1986) confirm the subalkaline character of the suite (Fig.3.38).

REE element patterns, except for sample G-CQ-7A, are quite similar to those of arc-tholeiites (althought lacking a negative Eu anomaly) and back arc basin basalts (6-30 times chondrite enriched flat patterns with a slight tendency to LREE enrichment and no Eu anomalies; Wilson, 1989). The LREE-depleted pattern of sample GCQ7A (Fig.3.37) is typical of MORB-like tholeiitic magmas, and this is also reflected in the MORB (Pearce, 1983)-normalized multielement patterns (Fig.3.37). The other samples show MORB-normalized multielement patterns which are more characteristic of volcanic arc tholeiites, with a slight negative Nb anomaly, HFSE depletion and a small Th enrichment with respect to MORB. These patterns could also resemble those of back arc basalt (Wilson, 1989).

Bivariate tectonic discrimination diagrams (Fig. 3.38) confirm the tholeiitic character of the suite and indicate a transitional character between volcanic arc and MORB tholeiites. Ternary discrimination plots also indicate a transitional character. Samples plot in tholeiitic fields both of volcanic arc and MORB (Fig.3.39), in most tectonic discrimination diagrams. However, they plot exclusively in the island arc tholeiite field of the TiO_2-MnO-P_2O_5 diagram (Mullen, 1983).

The geochemical characteristics of the whole sample set are typical of a tholeiitic suite with transitional character. Sample G-CQ-7A (44.8% SiO_2, 8.6% MgO) has MORB

characteristics and it could represent a primary magma derived from an asthenospheric MORB source, possibly a spinel lherzolite. The other samples could be explained in terms of interaction between lithosphere/MORB mantle sources (Wilson, 1989), which is characteristic of transitional basalts. It could be argued that the same effect can be achieved by lower crust contamination. SiO_2 and MgO concentrations do not suggest a large degree of crustal contamination, althought isotopic data will be needed to test these hypothesis.

The tholeiitic character of the samples requires a tectonic setting which could produce the shallow asthenospheric melting responsible for the REE patterns of the suite. The most simple one is an ensialic arc/back arc environment, which could explain the weak volcanic-arc signatures of most of the sample set and the MORB-like signatures of sample G-CQ-7A.

3.9.- GEOLOGICAL EVOLUTION OF THE CINQ-CERF GNEISS AND THE LATE PRECAMBRIAN BASEMENT OF THE SOUTHWEST HERMITAGE FLEXURE.-

The metasedimentary members of the Cinq-Cerf gneiss and the intrusive 675 Ma granitic orthogneiss constitute the oldest rocks of this part of the Hermitage Flexure. Foliated clasts resembling the Cinq-Cerf gneiss are present in the basal conglomerates of the Whittle Hill sandstone (B.H. O'Brien, 1988; pers comm). These basal sequences were overlain by 585-584 Ma volcanic tuffs which are coeval with the 584 Ma granodiorite in the Cinq-Cerf gneiss (Table 3.3). These field relationships suggest that the pre-584 Ma Cinq-Cerf gneiss was basement to the Whittle Hill sandstone and that the 584 Ma granodiorite probably represents an intrusive equivalent of the coeval tuffs. This also suggests the presence of an early event(s) between 675 and 584 Ma. Some of the c.585 Ma tuffs are cross-cut by the 576-573 Ma felsic porphyries, which preceded the 573-566 Ma Au-porphyry-Cu mineralization of the Whittle Hill sandstone (Dubé and Dunning, in press). According to B.H. O'Brien et al (1993), the 563-568 Ma Roti granitic suite intruded both the Whittle Hill sandstone and the Cinq-Cerf gneiss, with a fragment of Cinq-Cerf gneiss forming a roof pendant (B.H. O'Brien, 1988). Such relationships of the Roti granite suite require subsidence of the sedimentary basin in which the Whittle Hill sandstone was deposited. This could be accomplished by normal faulting. This would help to bring the Whittle Hill sandstone to the same crustal level as its basement (Fig.3.40), so that both could be contemporaneously intruded by the 568-563 Ma Roti suite. According to Dubé and Dunning (in press), the Whittle Hill sandstone is also intruded by another set of mafic and intermediate dykes at 565-566 Ma. These are maximum $^{207}Pb/^{206}Pb$ ages, the error ellipses of less than 1% discordant fractions intercept the concordia curve at c. 560 Ma. This makes this set of dykes in the Whittle Hill sandstone coeval within error with the

intrusion of the 557 Ma Sandbank metagabbro. This metagabbro is intruded at Three Islands by a 547 Ma granitoid (B.H. O'Brien and Dunning, unpublished). This shows that the Whittle Hill sandstone and its basement, the Cinq-Cerf gneiss, had a protracted history of intrusive activity, from the inception of the sedimentary basin, at c.585 Ma, to 547 Ma.

The extensive 570-560 Ma intrusive activity is interpreted as arc-related (Dubé and Dunning, in press), as is the genetically-related Au-porphyry Cu mineralization at Hope Brook. The geochemical signatures of the Sandbank metagabbro are indicative of shallow asthenospheric melting at c.557 Ma and, therefore, an extensional setting. The weak volcanic arc signatures in the metagabbros suggest a back-arc / arc transitional environment as the most simple hypothesis. If subduction was continuous from 585 Ma to 547 Ma, this could have led to regional extension which would facilitate basin formation, subsidence and sedimentation, as well as volcanism and pluton emplacement during different episodes at 585-584 Ma, 576-573 Ma, 568-563 Ma, 557 Ma and 547 Ma. Although at smaller scale, this tectonic scenario resembles that proposed by Dallmeyer et al (1996) for the Andean Mesozoic evolution of Northern Chile.

Direct dating of Late Precambrian deformation both in the Cinq-Cerf gneiss and the surrounding Late Precambrian rocks has proved to be difficult. B.H. O'Brien et al (1993) interpreted a concordant 566 Ma aplite within a shear zone hosted by 568 Ma Roti granite as syn-kinematic. The same field relationship, however, could be interpreted to result from a contrast of competencies during the Silurian mylonitization. These authors also reported two monazite analysis (0.7 and 1.4% discordant) and a concordant 414 Ma titanite age from the same aplite. The 0.7 % discordant monazite was interpreted as dating a "significant regional metamorphic event". As already discussed there is no geological evidence for such an event. This monazite age could represent a local thermal disturbance created by a c.545 Ma intrusion or it could be an artifact produced by a shallow discordia

line due to the Silurian disturbance. But more analyses from the same mineral separates will be needed to test either hypothesis. There is, however, strong field evidence to infer pre-585 Ma and post-585 Ma Precambrian deformation, particularly if the 568-563 Ma Roti granite intruded the Whittle Hill sandstone with the Cinq-Cerf gneiss forming a roof pendant (Fig. 3.40; B.H. O'Brien, 1988; 1990). Although in an arc environment, this deformation is interpreted as extensional, which is a common feature in such settings (Hamilton, 1994), in order to produce the 585 Ma sedimentary basin and to create the room for the 585-547 Ma intrusions. This is consistent with the extensional environment required for the geochemical signatures of the 557 Ma Sandbank metagabbro. This extension is followed by folding of the Whittle Hill sandstone. These folds are cross-cut by 499-495 Ma intrusions (B.H. O'Brien et al., 1991), indicating a pre-Tremadocian age for the folding event and suggesting an Avalonian compression. It should be noted that there is no well defined lower limit for this deformation. Therefore, the data from the Cinq-Cerf gneiss combined with that of the low grade Late Precambrian volcanoclastics and intrusions provide evidence for three Precambrian deformations: an earlier event(s) between 675 and 585 Ma; an extensional deformation associated with the 585-584 deposition of the volcanosedimentary sequences of the Whittle Hill sandstone and the prolonged intrusive activity; and a final folding of the Whittle Hill sandstone (Fig.3.41). The terms extension and compression are used in a wide sense, the same effects could also be achieved by transtension and transpression. But overall this tectonic activity is viewed to occur along the overriding plate of an active margin.

The 499 Ma granodiorite and 495 Ma gabbro (Dunning and O'Brien, 1989; B.H. O'Brien et al., 1991) intruded the deformed low-grade Whittle Hill sandstone contemporaneously with the generation of Tremadocian ophiolites in suprasubduction environments along the Gondwanan margin of Iapetus (Colman-Sadd et al., 1992; Jenner

and Swinden, 1993). Temporally (Fig.3.41), these intrusions could be ascribed to the Penobscottian event but there is no evidence for Penobscottian deformation, unlike in the nearby composite Bay du Nord Group (Tucker et al., 1994). This agrees with the observations from the northern Exploits Group (B.H. O'Brien et al., 1997) which has also escaped the Penobscottian events, otherwise well preserved in Central Newfoundland (Colman-Sadd et al., 1992).

The 448+9/-3 Ma titanite from the 547 Ma granitoid dyke at Three Islands (Dunning and B.H. O'Brien, unpublished) is difficult to interpret. This is a cooling age after a deformational and metamorphic event of unknown significance. The southwest part of the Hermitage Flexure contains c.450 Ma intrusions and metamorphic rocks (Dunning unpublished in B.H. O'Brien and S.J. O'Brien, 1992; Van Staal et al., 1994; Dunning, unpublished). But no evidence for such a body was found in the Cinq-Cerf gneiss.

The Silurian intrusion of the Western Head granodiorite-granite (431-429 Ma) is contemporaneous with the opening of the La Poile Basin, to which the Late Precambrian block is basement (Fig.3.41; B.H. O'Brien et al., 1991). This took place in a complex tectonic setting during the climax of the Silurian, Salinic, continent-continent collision (Dunning et al., 1989). The opening of the basin continued while the Western Head granite and the Cinq-Cerf gneiss were undergoing deformation associated with thrusting along the Grand Bruit fault. This basin was finally inverted and deformed between 423Ma and 419 Ma contemporaneously with the intrusion of the 419 Ma Otter Point granite into the Western Head granite and final thrusting of the Cinq-Cerf gneiss along the Grand Bruit fault. Finally the 390±3 Ma Chetwynd granite intruded postcollisionally stitching all tectonic and intrusive contacts between the Late Precambrian basement, the La Poile basin and the Silurian intrusions (Fig.3.41).

CHAPTER IV

THE MARGAREE ORTHOGNEISS (Port-aux-Basques complex, southwest Newfoundland Appalachians).

4.1.- INTRODUCTION :

The Port-aux-Basques complex (van Staal et al., 1992) occupies one of the most critical positions in the Newfoundland Appalachians, east of the suture zone defined by the Cape Ray Fault zone (Fig.4.1; Brown,1975; Lin et al., 1994; Dubé et al., 1996), separating the peri-Laurentian Dashwoods Subzone from the peri-Gondwanan Bay du Nord Group and the Avalonian basement of the Hermitage Flexure. The assessment of the age and tectonic linkage of the Port-aux-Basques complex has always been problematic. This gneissic complex and the nearby Grand Bay complex (van Staal et al, 1996b) have been depicted with a question mark on most lithotectonic maps of the Newfoundland Appalachians (Williams et al., 1988), and has been interpreted as a Precambrian basement (Brown, 1975) and as an Ordovician island arc (Chorlton, 1984)

The Port-aux-Basques and the Grand Bay complexes comprise a set of lower to upper amphibolite facies mica schists, paragneisses, amphibolites and orthogneisses with local massive sulphide deposits. These rocks have an anomalous tectonic position, they are situated east of the Cape Ray Fault on the peri-Gondwanan margin of the Iapetus ocean, but on the edge of the seismically-defined Grenvillian crustal block (Keen et al., 1986). Pb

isotopic signatures of the associated massive sulphides are also anomalous, in between those of the Notre Dame and Exploits subzones (Isle-aux-Morts prospect; O'Neill, 1985). These two complexes and the nearby rocks of the Harbour le Cou Group have been correlated with the Little Passage Gneiss in the Hermitage Bay area (Brown, 1975), the Bay du Nord Group and the La Poile Group (Chorlton, 1984), as well as with the Meelpaeg Subzone of the Gander Zone (Colman-Sadd et al. compilers, 1990) and with both the Bay du Nord Group (Exploits Subzone) and the Gander Zone (Lin et al., 1994). The assignment of the Port-aux-Basques complex to any of these zonal divisions is problematic, simply because its age and pre-Silurian geological evolution is unknown.

The following data set constitutes the first constraints on the age and tectonic linkage of the Port-aux-Basques complex. This data is based on regional and detailed mapping coupled with precise U-Pb geochronology of a set of orthogneisses known as the Margaree orthogneiss (van Staal et al., 1996b,c). According to Brown (1977), these rocks pre-date deformation and metamorphism of the Port-aux-Basques complex and, structurally, are the oldest rocks in the area. Reconnaissance geochemistry was carried out to provide a geochemical characterization of the main rocks types and to gather some information about the type of tectonic environment.

General statement:

The nomenclature in the field area is confusing due to the use of the local name of Port-aux-Basques to describe different individual rock types and sets of rocks, particularly gneissic rock types. Van Staal et al. (1992) divided the Port-aux-Basques Gneiss unit of Brown (1973; 1975; 1977) into the three divisions: Grand Bay complex, Port-aux-Basques complex and part of the Harbour le Cou Group; reserving the name Port-aux-Basques gneiss for the metasedimentary paragneisses and schists in the Port-aux-Basques complex.

It is the terminology of van Staal et al. (1992; 1996b; 1996c) that is going to be used in the following sections. Port-aux-Basques gneiss will refer only to the metasedimentary rocks (paragneisses and schists) of the Port-aux-Basques complex and the nearby Grand Bay complex (van Staal et al., 1992).

4.2.- LOCATION, ACCESS AND LOGISTICS:

The area of study is located in southwestern Newfoundland (Canada) in an area between the localities of Port-aux-Basques and Isle-Aux-Morts occupying the SE quadrangle of the 1:50,000 Port-aux-Basques sheet and the NW quadrangle of the neighbouring Rose Blanche sheet.

Coastal sections have been accessed by foot and are characterized by a 5 to 20 meter wide fresh outcrop along the shoreline. River sections also display good quality outcrop, although they are more difficult to access, particularly the one at Grandys Brook. This section was accessed with helicopter support, and to reach the upper third of the gorge it was necessary to use rock climbing skills. The Grandys Brook section is only recommended to be visited when the river is low. In general, the whole area is barren land covered by thin peat bogs, therefore the overall rock exposure is quite good. Excellent outcrops of the Margaree orthogneiss can be found in the quarries along the road to Isle-Aux-Morts, the Dolphin road and near Margaree.

Field work was carried out as part of a Geological Survey of Canada (GSC) project team under the direction of Cees van Staal, which mapped the Port-aux-Basques and Rose Blanche areas at 1:25,000 scale (van Staal et al., 1996 b,c). The opportunity of teaming up with the GSC allowed the author to use their logistics and to integrate his mapping within the regional GSC mapping. Field work was carried out in two field seasons. During the

first season (August 1993) the author mapped and defined the main units of the composite Margaree orthogneiss. During this time, the coastal section around Fox Roost was mapped at 1:5000 scale and the extension of the Margaree orthogneiss up to Grandy's Brook was recognized. In July 1994 the section at Grandys Brook was mapped in detail by the author and the orthogneiss was mapped, in the nearby highlands, during a week and a half fly-camp. The northeastern extent of the complex beyond Grandys Brook was mapped by the GSC (C. van Staal and L. Hall). At the end of August and early September 1994 the author mapped with the GSC outside the field area, both in the Port-aux-Basques and the Rose Blanche sheets, which helped him to realize the regional complexities of the area.

4.3.- THE MARGAREE ORTHOGNEISS : DEFINITION

The Margaree orthogneiss is a composite gneissic unit within the Port-aux-Basques complex. It comprises biotite ± hornblende-bearing felsic and mafic orthogneisses, amphibolite dykes and ultramafic rocks. This gneiss extends from Channel Island, in Port-aux-Basques, westward to the coastline of Margaree and Fox Roost forming a 2 Km wide band that can be traced at least 15 Km inland beyond Grandys Brook (Fig.4.1). The outcrop pattern of the Margaree orthogneiss closely follows the trend of a well defined positive regional magnetic anomaly (Fig.4.2), which is a good indication of the consistency of the field mapping and the lithological contrast with the surrounding paragneiss. A contrasting lithological character with the surrounding, sedimentary-derived, Port-aux-Basques gneiss is the absence of garnet, Al_2SiO_5 polymorphs or muscovite. Also in the Margaree orthogneiss there is no clear evidence for anatexis.

4.4.- PREVIOUS WORK :

Compared with other parts of the Newfoundland Appalachians the southwest coast, in this case the Port-Aux Basques area, has not received much attention until recent times. Gillis (1972) included for the first time the Port-aux-Basques area as part of a 1:250,000 reconnaisance regional map of southwest Newfoundland. Brown (1973) mapped the area around Port-aux-Basques, including part of the field area, at 1:20,000 scale as part of an M.Sc. project at Memorial University. He later expanded the mapping at 1:50,000 scale to cover the area up to Garia Bay as part of his Ph.D. thesis at Memorial University (Brown, 1975). All this mapping is compiled in the work of Brown for the Geological Survey of Newfoundland (1:50.000 Port-aux-Basques and Rose Blanche sheets; Brown, 1977). Chorlton (1984) compiled the geology of southwest Newfoundland as part of a PhD thesis at Memorial University involving extensive fieldwork in the neighbouring Bay du Nord Group and the peri-Laurentian Dashwoods Subzone. She correlated the Port-aux-Basques gneiss of Brown (1977) with her Bunker Hill gneiss in the Bay du Nord Group, and noticed the similarities with the amphibolite-rich gneisses north of the Gunflaps Hill fault splay. Therefore, she assumed that the Port-aux-Basques gneiss was part of the Ordovician arc sequences preserved in the Bay du Nord Group. O'Neill (1985) mapped the area around the Isle-aux-Morts prospect and studied the mineralization and regional metamorphism as part of an M.Sc. at Memorial University. Wilton (1984) and Dubé and Lauziere (1996) mapped the mineral occurrences and structures around the Cape Ray Fault zone. In 1992 Cees van Staal (GSC) began the 1:25,000 remapping of the Port-aux-Basques and Rose Blanche sheets (van Staal et al., 1996b,c). Apart from the present thesis two other theses were done in the Port-aux-Basques area in conjunction with the GSC mapping, cosupervised by van Staal. D. Scholfield's Ph.D thesis at Keele Univ. (U.K.)

deals with the general geochemistry of the area whereas J. Burgess' M.Sc. thesis (Univ. of Maryland, U.S.A.) focused on the metamorphism of the area (Burgess et al., 1993; 1995).

Age determinations in the area are limited to K-Ar data from Gillis (1972), U-Pb titanite dating (Dunning et al., 1990) and the data of Burgess et al. (U-Pb titanite, $^{40}Ar/^{39}Ar$; 1995). Dubé et al. (1996) reported U-Pb and $^{40}Ar/^{39}Ar$ data which constrain the timing of deformation around the Cape Ray Fault zone. Van Staal et al. (1994) reported preliminary U-Pb data of this thesis and other geochronological studies in the surrounding areas.

The composite Margaree orthogneiss was differentiated from the Port-aux-Basques Gneiss of Brown (1977) during the fieldwork carried out by GSC in 1992 (van Staal, pers comm). Even though Brown (1977) merged these rocks with the nearby paragneisses, he recognized the presence of relics of an earlier gneissic banding in "a set of migmatites and granitic slivers" in the Margaree- Fox Roost area.

4.5.-GEOLOGICAL SETTING:

The Margaree orthogneiss forms part of the rocks of the Port-aux-Basques area adscribed to the peri-Gondwanan margin of the Newfoundland Appalachians. According to Brown (1977) these rocks (Grand Bay and Port-aux-Basques complexes of van Staal et al., 1996b,c) were the crystalline basement to eastern continental margin of the Iapetus Ocean and were separated by a cryptic suture, the Cape Ray Fault zone, from the Laurentian basement (Cape Ray Igneous Complex). While this interpretation has changed, it is held that the Cape Ray Fault is a suture separating a block of Early Paleozoic rocks with Laurentian affinities (Dunning et al., 1989) from one with Gondwanan affinities (Lin et al., 1994; Burgess et al, 1995; Williams, 1995; Dubé et al., 1996). These two blocks

were juxtaposed during the Silurian Salinic orogeny (Dunning et al., 1990; Lin et al., 1994; Dubé et al., 1996).

4.5.1.- The Cape Ray Igneous Complex and the Windsor Point Group (Laurentian side; Fig. 4.1.):

The Cape Ray Igneous Complex (CRIC) constitutes part of the Dunnage Zone (Dunning et al., 1989), Dashwoods Subzone (Williams, 1995). The CRIC comprises tonalitic to granitic orthogneisses, which intrude metamorphosed ultramafic-mafic rocks (Long Range Mafic-Ultramafic complex; Chorlton, 1984) and sillimanite-bearing paragneisses with marble layers. The CRIC and its country rock are interpreted as the metamorphic equivalent of the Notre Dame arc (Lin et al., 1994). Dubé et al. (1996) reported a 488±3 Ma age for a megacrystic granite and a 469±2 Ma age for a tonalite within the CRIC near its contact with the Windsor Point Group.

The low grade rocks of the Windsor Point Group (WPG) separate the CRIC from the metasedimantary Port-aux-Basques gneiss. The WPG consists of bimodal volcanics and sediments including conglomerate beds which contain CRIC clasts (Dubé et al., 1996). The WPG rests unconformably on the CRIC (Brown, 1975; Wilton, 1983; Chorlton, 1984). A black rhyolite, interlayered with the conglomerates at the base of the group, has provided an age of 453+5/-4 Ma. The intrusion of pre-kinematic gabbro sills (424+4/-3 Ma) provides a younger age limit for the whole sedimentary package. The pre-kinematic gabbro is intruded by the coeval pre-kinematic Windowglass Hill granite (424±2 Ma; Dubé et al., 1996).

4.5.2.- The Cape Ray Fault Zone (Fig.4.1.):

Deformation along the Cape Ray Fault Zone (CRFZ) affects both the Windsor Point Group and the metasedimentary Port-aux-Basques gneiss and resulted in oblique thrusting of the Port-aux-Basques gneiss over the WPG. $^{40}Ar/^{39}Ar$ ages of synkinematic hornblende (407±4 Ma) and biotite (403±4 Ma), from CRFZ mylonites affecting the Port-aux-Basques gneiss are interpreted to date the thrusting (Dubé et al., 1996). The northern sector of the CRFZ was later reactivated as part of a system of sinistral transcurrent faults (403±6 - 399±6 Ma; K-Ar Ms; Dubé et al., 1996; 385±5 - 384±5 Ma, $^{40}Ar/^{39}Ar$ Hbl, Bt; Chorlton and Dallmeyer, 1986). The post-collisional Isle-Aux-Morts granite (386±3 Ma) and Strawberry Hill granite (384±2 Ma, Dubé et al., 1996) intruded the CRFZ and provide the youngest limit for deformation along the CRFZ (Dubé et al., 1996).

4.5.3.- The gneissic lithologies of the Port-aux-Basques area (Gondwanan side, Fig.4.1.):

These gneissic rocks, originallly grouped under the Port-aux-Basques Gneiss (Brown, 1977), have been divided in three units (Fig.4.1 Van Staal et al., 1992): Grand Bay complex (GBC), Port-aux-Basques complex (PaBC) and Harbour le Cou Group (HlCG). These divisions have tectonic boundaries; the CRFZ separates the GBC from the Windsor Group, the Grand Bay Thrust separates the GBC from the PaBC and the Isle-aux-Morts Fault separates the PaBC from the HlGC. The regional metamorphic grade shows a west to east increase from the lower amphibolite Grand Bay Complex to the upper amphibolite Harbour le Cou Group which sharply ends against the Bay le Moine shear zone (Fig.4.1; Burgess et al., 1993; 1995).

The Grand Bay complex (GBC): This unit comprises gedrite-bearing schists, metapsammites (greywackes and felsic volcanics?), metapelites and coticule beds (metavolcanic?; van Staal et al., 1996b). Pyritiferous zones are common in the complex, the largest one is associated with the Zn-Pb-Cu-Ag massive sulphide deposit of the Isle-Aux-Morts prospect (O'Neill, 1985). Amphibolite and ultramafic bodies are commonly intercalated with the metasediments. This unit also contains abundant mafic and felsic orthogneisses (Grand Bay granodiorite and Kelby Cove orthogneiss, Fig. 4.1 ; van Staal et al., 1996b) as well as intrusions of the Port-aux-Basques granite (Brown, 1973, O'Neill, 1985; van Staal et al., 1996b). Mineral assemblages in Al-rich pelites are Grt+St+Chl+Bt and Grt+Ky+Bt±St (Brown, 1973; 1975; O'Neill, 1985; Burgess et al., 1993), garnet-biotite geothermometry indicates peak temperatures of 580±50°C (Burgess et al., 1995). $^{40}Ar/^{39}Ar$ cooling ages in amphibole range from 401Ma to 393 Ma (Burgess et al., 1995). Dunning et al. (1990) reported a 412±2 Ma $^{206}Pb/^{238}U$ titanite age from the vicinity of the Isle-Aux-Morts prospect. U-Pb monazite dating in this unit suggests that peak metamorphism was reached at 415 Ma (Dunning, unpublished).

The Port-aux-Basques complex (PaBC): This complex contains a metasedimentary unit, Port-aux-Basques gneiss (van Staal et al., 1996b,c) which is intruded by abundant amphibolite dykes, the Port-aux-Basques granite, the Kelby Cove orthogneiss, the ***Margaree orthogneiss*** and late granite sheets and pegmatites. According to Brown (1977) and van Staal et al. (1996b,c), the rocks of the Margaree orthogneiss are the oldest set of intrusions into the metasedimentary Port-aux-Basques gneiss. In the PaBC, the Port-aux-Basques gneiss contains metapelites, metapsammites, amphibole rich layers (para-amphibolites) and local epidote-rich layers; although present, coticules are very scarce. Van Staal et al. (1996b,c) interpreted the gradation from quartz-rich psammites to micaceous and feldspathic psammites as a variation upwards through stratigraphy. There is an increase

in metamorphic grade in the unit from the kyanite zone in the west to the second sillimanite zone in the east. The second sillimanite zone is characterized by anatectic migmatites, produced by Ms-out reactions, which are aligned with the S2 foliation and folded by F3 (Brown, 1975; Burgess et al., 1993; Burgess et al., 1995). Peak metamorphic conditions are of 10-8Kb and approximately 700°C (Owen, 1992; Burgess et al., 1995). $^{40}Ar/^{39}Ar$ cooling ages in this unit range from 407 - 399 Ma (Hornblende) to 394-391 Ma (Muscovite; Burgess et al., 1995). Reported U-Pb monazite data range from 420 to 415 Ma (van Staal et al., 1994).

The Harbour le Cou Group (HlCG): The HlCG (Lin et al., 1993) is an extension of the Harbour le Cou unit of Brown (Brown, 1975). This group is separated from the Port-aux-Basques Complex by the Isle-aux-Morts shear zone (Brown, 1977; van Staal et al., 1993; Piasecki, 1995). The lack of amphibolite dykes and pre-tectonic granitic orthogneisses indicates that this group represents a different geological unit from the GBC and the PaBC and this led Brown (1975) to consider it as a cover sequence to the PaB gneiss. The HlCG has been divided into the Otter Bay formation and the Grandy's formation (van Staal et al., 1996c). The Otter Bay formation comprises garnet-bearing metapsammites, rusty pyrite-rich metapelites, calc-silicate pods and narrow bodies of orthoamphibolites. At the contact with the overlying Grandy's formation there are metamorphosed pillow lavas with tholeiitic basaltic composition (Lin et al., 1993; Scholfield et al., 1993). The Grandy's formation is composed of rusty metapelites, schists, metapsammites and coticule layers. The HlCG has extensive development of anatectic migmatites. Reported peak metamorphic conditions involved temperatures in excess of 700°C and 6.6 to 5.2 Kb pressure (Burgess et al., 1995). $^{40}Ar/^{39}Ar$ cooling ages range from 419 to 404 Ma in amphibole and 391 Ma for muscovite (Burgess et al., 1995). Burgess et al. (1995) also reported a titanite U-Pb age of 418±9 Ma. The eastern HlCG is

intruded by the late-D2, early-D3, garnet-bearing, two mica granite sheets of the Rose Blanche granite (Benn et al., 1993; 419 Ma, Dunning unpublished). The HICG is bounded to the east by the Rose Blanche granite and the Bay Le Moine shear zone (Chorlton and Dallmeyer, 1986; Lin et al., 1993).

The GBC, PaBC and HICG share the same structural history which consists of three main phases of regional deformation (D1, D2 and D3), all of which affected the Margaree orthogneiss. D1 structures are scarce recumbent folds (F1) with associated axial planar schistosity (S1). During D2, S0 and S1 were transposed, leading to the formation of the dominant gneissosity (S0-S1-S2); F2 folds are recumbent. D3 transpression is characterized by upright to steeply inclined periclinal folds (F3), local oblique ductile shear zones and dextral, transcurrent major shear zones; an S3 schistosity is developed locally. D3 is responsible for the dome and basin interference pattern of the regional macrostructures. Locally there is development of a D4 phase which consists of a low grade overprint of D3 structures (Van Staal et al., 1992; Burgess et al., 1995). Peak metamorphism was reached during D2.

4.6.- MARGAREE ORTHOGNEISS, LITHOLOGICAL UNITS: description, internal field relationships and age:

Two type sections of the Margaree orthogneiss, one at Margaree-Fox Roost and another at Grandys Brook, were studied in detail. Part of the Margaree-Fox Roost section (Fig.4.3.) was mapped at 1:6000 scale (Fig.4.4) whereas part of the Grandys Brook section was mapped at 1:15000 scale. The Margaree-Fox Roost section is characterized by variably deformed hornblende-bearing "tonalitic" orthogneisses, granitic orthogneisses, amphibolites, ultramafic rocks and "migmatitic" gneisses. The Grandys Brook section is

similar but mafic dioritic intrusions are common, whereas no ultramafic rocks were observed. The surrounding PaB gneiss is a variably migmatized quartzo-feldspathic paragneiss. Detailed mapping of the Margaree orthogneiss allowed the distinction of a set of lithological units which will be described next. Some of these units were directly dated by U-Pb geochronology. These absolute ages provide a limit for the undated units, on the basis of the relative chronology constrained by the field relationships.

Details of the U-Pb analytical procedure, including sample preparation, are provided in appendix A.1.

4.6.1.- Hornblende-bearing tonalitic orthogneiss:

Several amphibole-bearing rock types have been grouped in this unit; these are granodioritic orthogneisses with mafic enclaves and a mafic unit in the Fox Roost section with an overall tonalitic character. This mafic unit at Fox Roost is different from the relatively homogeneous granodioritic orthogneisses. It consists of mafic sheets of dioritic orthogneisses, amphibolites and small ultramafic pods back veined by partially hybridized felsic centimetre to metre-wide granitic veins (Fig.4.5). These granitic veins merge with granitic orthogneisses suggesting that both are coeval (Fig.4.5).

The granodioritic orthogneisses are well exposed in Margaree at the nearest quarry at the side of the road, along the Dolphin road (Fig.4.3) and in the Grandys Brook section. These gneisses are, in general, fine to medium grained (Ø≈ 1 mm) and they usually contain amphibole-bearing felsic veins, mafic (amphibole + biotite) banding, amphibolite rich enclaves and folded and boudinaged amphibolite dykes. The amphibole in the felsic veins (Fig.4.6) grew as poikiloblasts, this and the diffuse contacts of these veins suggest that they were produced by metamorphic differenciation. The gneissic foliation is defined by mafic layers and thin discontinuous felsic bands of plagioclase, quartz ± hornblende

(Fig.4.6). Amphiboles are preferably oriented in the foliation plane defining a mineral lineation. The modal mineralogy is approximately 35~30% plagioclase (An20-30), 30% green hornblende, 10~15% pale-dark brown biotite, 20% quartz, >10% K-feldspar. Epidote, apatite, zircon and opaques are the main accessory minerals, in some cases titanite occurs as an accessory phase.

Age:

Dioritic sheets of the mafic tonalitic orthogneiss at Fox Roost were unsuccessfully sampled for zircon. The field relationships at Fox Roost suggest that they are older or coeval with the granitic orthogneiss (U-Pb sample 93-PV-5; Fig.4.4 and 4.5.). Therefore, the granitic orthogneiss at Fox Roost provides at least a minimum age for the dioritic sheets. The extensive back-veining of the amphibolite-rich sheets suggests that both mafic and silicic magmas were probably coeval (Fig. 4.5; Fernández and Barbarin, 1991).

Granodioritc orthogneiss (U-Pb sample 93-PV-3): A hornblende-bearing felsic granodioritic orthogneiss was sampled in the quarry on the side of the road outside Margaree (Fig.4.6). The same rock was also sampled for geochemical analysis (sample G-MA-B). It has a well developed foliation and contains tightly folded amphibolite exhibiting straight contacts. The orthogneiss is intruded by an undeformed, late, coarse-grained pink granite and a pink pegmatite.

Four zircon fractions were analyzed (Table 4.1). The fractions were composed of elongated (1:7-1:5; width/length ratio) sharp prisms with no cracks, few inclusions and rounded tips. Fractions Z1, Z2 and Z3 were air abraded (Krogh, 1982); fraction Z4 was not abraded. These four fractions define a discordia line with an upper intercept of 474+14/-4 Ma with a lower intercept of 141 Ma (Fig.4.7). The age **474+14/-4 Ma** is interpreted as the protolith age of the granodioritic orthogneiss.

4.6.2.- Granitic orthogneiss:

This rock type constitutes about 30 to 40% of the gneissic complex exposed in the Margaree-Fox Roost section. In both the Margaree-Fox Roost and the Grandys Brook sections they appear to be injected into both types of tonalitic gneisses earlier described and contain discrete amphibolite enclaves/dykes, which have been boudinaged and folded (Fig.4.8 and 4.9). In many instances the ductile deformation and the contrast of competencies do not allow to assert whether or not some of the amphibolites represent true dykes or enclaves. The pale grey colour, the absence of garnet, muscovite or sillimanite and the apparent higher strain (smaller grain size) differentiate this granitic orthogneiss from the pinkish, 450 Ma, foliated, locally two-mica Port-aux-Basques granite, as well as the fact that the granite is clearly intrusive into the PaB gneiss and generally does not have mafic dykes.

This granitic orthogneiss is medium grained (Ø≈ 1mm) and has a gneissic foliation defined by biotite rich layers and 1 to 3 mm thick granoblastic bands of quartz, plagioclase and K-feldspar. Most outcrops have thin (less than 5cm wide) coarse-grained felsic veins with diffuse contacts (metamorphic differentiation?; Fig.4.5.d, 4.8 and 4.9). The modal composition of these orthogneisses is approximately 40% quartz, 25% plagioclase (An 15-25), 15% K-feldspar and ≈ 20% brown biotite. Epidote, opaques, apatite and zircon are the most common accessory phases, although titanite is in places present

Age:

This lithology has been sampled both in the Margaree-Fox Roost and Grandys Brook sections to test field correlations, and because it provides the youngest relative age within the complex, except for some amphibolite dykes.

Margaree-Fox Roost section (Sample 93-PV-5): This granitic orthogneiss has a felsic composition and contains amphibolite enclaves/dykes which have been boudinaged and folded by F3 (Fig.4.8). The main gneissosity (granoblastic fabric) in the orthogneiss has also been folded by F3. The granitic orthogneiss merges with the felsic veins and dykes, which mingle with the amphibolites in the mafic tonalitic orthogneiss, and with the felsic veins of the "migmatitic gneiss". These two units show minor F2 folds. However, F2 folds have not been recognized in the granitic orthogneiss.

Five zircon fractions were analyzed (Table 4.1). Fractions Z1, Z2, Z3 and Z4 were air abraded; fraction Z5 was unabraded. The zircon morphology of the selected fractions is very similar to the granodioritic orthogneiss. Fractions Z1, Z4 and Z5 define a discordia line with an upper intercept of 473+16/-6 Ma; however because of the low probability of fit the age provided by Z1 is preferred. Fraction Z1 is concordant and provides a best age estimate of 472±2.5 Ma (Fig.4.10). Fractions Z2 and Z3 fall out of the discordia line due to a combination of lead loss and a small degree of inheritance. The age **472±2.5 Ma** is interpreted as the protolith age for the granitic orthogneiss.

Grandys Brook section (Sample 94-PV-2): This is a medium grained biotite-bearing rock with granitic modal composition. It has been clearly intruded by mafic dykes (amphibolites) which have been boudinaged and folded (Fig.4.11 and 4.13).

Three zircon fractions (Z1,Z2 and Z3) and two titanite fractions (T1 and T2) have been analyzed (Table 4.1). The two titanite fractions are concordant and provide an age of **411±2 Ma** which is interpreted as a cooling metamorphic age (Fig.4.12). Zircon fractions Z1, Z2 and Z3 define a discordia line with an upper intercept of 466.8 Ma for a lower intercept pinned at 5±5 Ma. The upper intercept is in agreement with the age of fraction Z1

(465±3 Ma) which is concordant and provides a more reliable age estimate (Fig.4.12). This **465±3 Ma** age is interpreted as the protolith age of the granitic orthogneiss.

4.6.3.- Amphibolite:

The amphibolites outcrop as tighly folded, stretched and boudinaged dykes or enclaves (Fig. 4.5., 4.8., 4.9., 4.11, 4.13 and 4.14). Because they are too many and too small to be mapped alone they have been combined with the tonalitic and granitc orthogneisses (Fig.4.4 and 4.11). Usually they are 30 to 60 cm wide and can be up to several metres long. They have a homogeneous aspect with an L-S fabric defined by recrystallized hornblende (up to 1.7 mm long) and biotite (0.3 mm long). Their modal composition varies from 80%-90% green hornblende + 10%-20% plagioclase (An35) to 50~60% green hornblende + 5~10% brown biotite + ≈ 30% plagioclase (An 30) + quartz. The accessory phases are rutile, apatite and opaques in the hornblende-rich varieties and titanite, apatite and opaques in the biotite (quartz)-rich varieties. Epidote, with allanite cores, in accessory proportion is found after late retrogression of green hornblende and minor chlorite and sericite are also produced during retrogression of biotite and plagioclase, respectively.

Age:

The presence of abundant centimetre-scale amphibolite enclaves in the 474 Ma granodiorite suggests bimodal magmatism at the time, indicating that some amphibolites could be coeval with the granodiorites. Abundant amphibolite enclaves were also observed in pre-466 Ma tonalites at the Grandys Brook section. This would be consistent with field relationships observed in the "tonalitic gneisses" at Fox Roost, such as the 472 Ma felsic granites back-veining amphibolite sheets (Fig4.5) and dispersing them as enclaves and disrupted amphibolite dykes with diffuse contacts (Fig.4.9; partial assimilation, mingling,

hybridization?). These features are commonly displayed in ultramafic/mafic-silicic intrusive complexes (Sutcliffe et al., 1990; Sha, 1995) or in coeval intrusion of mafic magmas in felsic magma chambers (Fernández and Barbarin, 1991; Wiebe, 1991; Bateman, 1995). Field relationships of individual amphibolites are in places difficult to interpret due to the contrast of competencies with the granitic orthogneiss, with most amphibolite bodies in the Margaree orthogneiss occurring as variably sheared and folded boudins (Fig.4.5; 4.8). Although some could be identified as intrusive dykes (Fig.4.9), most of them could represent mafic enclaves. In the Grandys Brook section, amphibolite dykes intrude the 465 Ma granitic orthogneiss and were affected by D3 indicating that this generation of dykes is post-465 Ma and pre-D3. Some of these dykes cut compositional banding in the 465 Ma orthogneiss. Therefore there are, at least, two generations of orthoamphibolite in the Margaree orthogneiss, one probably coeval with the 474-472Ma felsic orthogneisses and another post-465 Ma and pre-D3.

Margaree-Fox Roost (Sample 93PV6): This sample is a quartz-bearing amphibolite dyke intrusive into felsic tonalitic orthogneisses (Fig.4.14). The mineralogical composition of this sample is green hornblende, plagioclase (oligoclase) and brown biotite with quartz, opaques and titanite in minor proportions; apatite is the main accessory mineral. These minerals (except apatite) are recrystallized and the amphibole defines a mineral lineation which is parallel to the plunge of the minor F3 folds. No zircon was extracted from this sample nor from a previous sample collected by G.R. Dunning from a similar lithology.

One fraction of brown titanite was analyzed from this sample (Table 4.1). This fraction provided a concordant age of **410±2 Ma** (Fig.4.15.). This is a metamorphic age. It is uncertain whether it is a cooling age (Tc 600°-550°C; Heaman and Parrish, 1990) or a crystallization age after post-D3 recrystallization (Fig.4.16). But in either case this age provides the youngest age limit for the amphibolite dykes.

4.6.4.- Other lithologies:

Ultramafic rocks:

These rocks are quite common in the Margaree-Fox Roost section but were not observed in the Grandys Brook section. They outcrop as pods (Ø= 5 to 10 metres) of coarse grained (Ø = 0.3 to 1 cm) mafic minerals, which appears to be primarily amphibole in hand sample. They are associated with the most mafic-rich areas of the diorite-amphibolite sheets in the mafic tonalitic orthogneisses, which suggests that they might represent cumulates. In the field, they do not show an internal fabric and they act as stiff material in ductile shear zones, with the granitic orthogneisses wrapping around them. Small pods are usually retrogressed to epidote.

The samples studied have an acicular-decussate texture defined by colourless tremolite and pale-green Mg-rich actinolite (?) crystals (>70%) and partially oriented aggregates of a micaceous (Ø≈ 0.2 mm) mineral tentatively identified as chlorite (*), possibly Mg-rich (<30%). Apatite, rutile and opaques are accessory minerals. Burgess et al. (1992) described another variety of ultramafic pod with actinolite-spinel-clinopyroxene which has not been observed in this study. They also reported clinopyroxene replaced by talk.

(*) Micaceous to fibrous, colourless, non pleocroic, low relief (lower than tremolite), first order white birefrigence, parallel extinction and length-fast.

Age:

The ultramafic pods are associated with the amphibolite rich areas in the Fox Roost section (Fig.4.4). Such a relationship is also found in ultramafic/mafic-silicic intrusive complexes (Snoke et al., 1981; Kelemen and Ghiorso, 1986; Sha, 1995). Therefore if the ultramafic rocks represent an ultrabasic cumulate of the amphibolite, then they are coeval

with the amphibolites. The amphibolites are back-veined by c.472 Ma granitic orthogneisses, suggesting, by field correlation, that the ultramafic rocks are c.472 Ma.

Banded gneiss:

This gneiss coincides with areas of high strain ductile shearing in the Fox Roost section (Fig.4.5d and Fig.4.9). The protolith of the banded gneiss is uncertain, which prompted its definition as a separate unit during the small scale mapping of the Fox Roost section. In the Grandy's Brook section, 1km upstream from the section mapped in detail, banded gneisses like those of Fox Roost were identified in a high strain ductile shear zone and mapped as Margaree orthogneiss (Fig4.1).

This gneiss consists of centimetre-wide leucocratic bands of quartz, plagioclase (An 25-30) and minor K-feldspar alternating with mafic bands of green amphibole and brown-greenish biotite. These bands are metre-long and discontinuous. The mafic bands also contain felsic minerals as well as minor epidote, titanite and opaques. Zircon and apatite are accessory minerals. Average grain size is 1mm. Locally, there are quartz-rich bands and leucocratic bands with small garnets which resemble the quartzo-feldspathic country-rock paragneisses. Small mafic, epidote-rich pods (Ø≈ 30-50 cm) show asymmetric wings produced by ductile flow of the surrounding rock around them. Their stiff rheological behaviour suggest that they might be retrogressed ultramafic rocks.

Age:

These high strain zones are located in the flanks of F3 folds (Fig4.5b,d and 4.9). In the case of the Fox Roost section the banded gneisses are related to apparent oblique, ductile, dextral shear zones (Fig4.9). The presence of stable epidote in the fabric but the absence of chlorite suggests that some of the transposition took place in the amphibolite

facies, possibly in the epidote-amphibolite subfacies. This indicates that the gneissic banding was produced by D3 transposition of the main gneissosity (Fig.4.5d).

"Migmatitic" gneiss:

This rock type is exclusive to the Fox-Roost section. It consists of 1 to 10 cm thick leucocratic bands with subordinate melanocratic bands and mafic rafts resembling diatexitic migmatites (Mehnert, 1968). This rock type appears in areas of relatively low D3 strain. The banding in this rock has been folded and sheared during D2 and D3; it usually shows a complex fold and interference pattern resembling disharmonic folding. The boundaries of this unit with the surrounding granitic and tonalitic orthogneisses are diffuse and felsic veins from the gneiss merge with the granitic orthogneiss. The amount of leucocratic material (70%-80%) however contrasts with a 20%-40% abundance of true anatectic patches in metapelites of the surrounding paragneisses.

The felsic domains contain K-feldspar (40%), quartz (50%), plagioclase (10%). Grain size can be up to 7-4 mm. The melanocratic domains are formed by brown biotite (40%), plagioclase (25%, Oligoclase), K-feldspar (10%) and quartz (15%). Minor epidote overgrew biotite during retrogression. Apatite and zircon are accessory minerals. In amphibole-rich areas titanite is present as an accessory phase. Althought the transition between the felsic and melanocratic domains is relatively sharp at mesoscopic scale. At the microscopic scale, it is gradational and individual quartz and K-feldspar crystals are embedded in both domains. It should be noted that there is no garnet, sillimanite, cordierite or orthopyroxene in the mafic bands. These features suggest that this rock type is not an anatectic migmatite. The textural features coupled with the field evidence of felsic veins merging with the granitic orthogneisses suggest that this rock type represents a set of ductily deformed aplitic granitic dykes and back-veined mafic/tonalitic rock types.

Age:

Structural relationships indicate that this rock is pre-D2. Felsic veins in one locality (around U-Pb sample 92-GD-3) merge with the 472 Ma granitic orthogneiss, indicating an age of 472 Ma. This rock type is locally intruded by 417 Ma late-syn-D3 granitic dykes (chapter 4.5.2.3).

4.7.- THE COUNTRY ROCK PORT-AUX-BASQUES GNEISS AND THE LATE INTRUSIONS: GENERAL DESCRIPTION, FIELD RELATIONSHIPS AND AGE.

What follows is a general description of the paragneisses (Port-aux-Basques gneiss of van Staal et al., 1996b,c) that constitute the country rock to the Margaree orthogneiss and other granitic intrusive types which are younger than the Margaree orthogneiss (Port-aux-Basques granite and late syn-D3 and post-D3 minor intrusions).

4.7.1.- Port-aux-Basques gneiss (paragneiss).

In the area of study the Port-aux-Basques gneiss is in the sillimanite isograd (Burgess et al., 1995). The gneiss is dominated by quartzo-feldspathic lithologies (metapsammites) with subordinate amphibolite and metapelite. Burgess et al. (1995) determined peak metamorphic conditions of ≈700°C and 9 Kb using stable mineral assemblages and thermobarometry in pelitic rock types and amphibolites.

Around Margaree-Fox Roost, the Port-aux-Basques gneiss is dominanted by quartzo-feldspathic paragneisses and amphibolites. The presence of garnet-rich and quartz-rich layers sets apart these gneisses from the Margaree orthogneiss. They are composed of

biotite, plagioclase (An20), K-feldspar, quartz , ± garnet, ± sillimanite (fibrolite) and opaques, modal proportions vary among layers. Sillimanite is scarce and partially retrograded to muscovite and chlorite and epidote grew during retrogression. Chlorite grew after retrogression of biotite and garnet, whereas epidote is associated with amphibole retrogression or associated with biotite and in most places has an allanite core. Zircon, monazite (?) and apatite are present in accessory proportions. Average grain size is 0.9 mm, although varies from 0.1mm to 4 mm. The gneissosity is defined by the alternation of biotite-rich levels, usually less than 1 cm thick, with plagioclase-quartz rich layers. Garnet tends to appear in restricted biotite and plagioclase-bearing layers defining a compositional banding. The fabric in these rocks will be described in detail in section 4.6.

In the outcrops on the Dolphin road near the road to Isle-aux-Morts (Fig4.3), the Port-aux-Basques gneiss is more pelitic, has anatectic patches, 1-2 metre thick garnet-bearing foliated granites and a rusty appearance. The anatectic leucosome patches can be up to 30-40% of the outcrop. The leucosomes have a granitic composition and are bordered by biotite + sillimanite ± garnet selvedges. These leucosomes (1-5 cm thick and up to 25 cm long) are aligned with the gneissosity (S2) with stromatic structure. Migmatite is also abundant in the Grandys Brook section particularly along the more pelitic NW border of the Margaree orthogneiss (Fig4.1).

The amphibolites in the Port-aux-Basques gneiss are hornblende-rich massive mafic boudins and partially boudinaged layers and amphibole-rich quartzo-feldspathic layers. The massive amphibolites are composed of hornblende + plagioclase ± biotite ± clinopyroxene ± garnet + titanite and probably represent mafic dykes. The amphibole-bearing quartzo-feldspathic levels are composed of amphibole + biotite + plagioclase + quartz ± K-feldspar + opaques + epidote and probably are para-derived amphibolites. These two types of amphibolites are variably recrystallized and have an average grain size of 1 to 3 mm. Other

minor lithologies in the Port-aux-Basques gneiss are epidote-rich bands and scarce coticule levels.

Age:

The map pattern of the Margaree orthogneiss (Fig4.3) indicates that the orthogneisses are interleaved with the Port-aux-Basques gneiss. The contacts between the Margaree orthogneiss and the Port-aux-Basques gneiss are tectonically reworked. Locally the contacts coincide with late-brittle ductile shear zones (eastern contact of the Margaree-Fox Roost section, Fig4.4), but in most cases the contacts are straight due to the intensity of D3 (Fig.4.17). True intrusive relationships have only been observed at Grandys Brook (Fig.4.18). Such relationships and the map pattern suggest that the Margaree orthogneiss intruded the Port-aux-Basques gneiss. Therefore the paragneisses and mica schists of the Port-aux-Basques gneiss are pre- 474 Ma (pre-Mid Arenig).

4.7.2.- Port-aux-Basques granite:

This is a foliated, coarse grained, fresh pink granitic gneiss (Brown, 1973) and generally has an equigranular to porphyroblastic texture with 2cm porphyroblasts. According to Brown (1973) the essential mineralogy is quartz + plagioclase + K-feldspar + biotite ± muscovite ± garnet ± (amphibole). In the area of study, this granite can be differentiated from the granitic varieties of the Margaree orthogneiss by its general field appearance and homogeneous aspect, the presence of minor muscovite and garnet and the absence of mafic enclaves.

The Port-aux-Basques granite outcrops as granite sheets usually not exceeding 100 m of thickness. The continuity of some kilometre-long granitic sheets provided a reliable marker level. Outcrop pattern shows that the Port-aux-Basques granite was folded by F2

and F3 folds (Fig. 4.1). In the area of study, minor F3 folds were observed folding and locally crenulating the foliation in the granite, indicating that this foliation is pre-D3. The gneissose solid-state S2 fabric in the Port-aux-Basques granite is parallel to the main gneissosity in the paragneiss (S2), which is also crenulated at the F3 fold hinges. In outcrop, the granite is generally concordant with the regional gneissosity. However in the easternmost part of the Fox Roost section a slightly discordant, undated, strongly foliated, garnet-bearing granitic gneiss intrudes the Margaree orthogneiss and the nearby paragneisses (Fig.4.4). In the vicinity of Isle-aux-Morts and according to outcrop pattern, the eastern border of the Margaree orthogneiss is intruded by a pre-D3 pink foliated granitic gneiss (Fig 4.3). Field relationships in the area of study indicate that the Port-aux-Basques granite is pre-D3 and pre-to syn-D2, and apparently postdates the intrusion of mafic dykes in the Margaree orthogneiss.

According to Brown (1977) and van Staal et al. (1994), west of the area of study, the Port-aux-Basques granite cross-cuts S1 foliations, but the internal foliation in the granite is folded by F2 folds. These authors consider that the Port-aux-Basques granite is inter-D1-D2 or late syn-D1. Van Staal et al (1994) reported an age of 453±3 Ma for a trondhjemitic unit of the Port-aux-Basques granite between Port-aux-Basques and Margaree (Fig.4.1). It should be noted that this particular rock type is atypical of the Port-aux-Basques granite.

It is possible that different generations of granite might have been lumped as Port-aux-Basques granite in the field area, including some Rose Blanche-like pre-D3 granites. In some cases, however, all that can be seen in outcrop is an undated biotite-bearing, pink, fine-medium grain granite folded by minor F3 folds, that is intrusive into the paragneisses (Fig.4.3). The foliation in the biotite-rich enclaves in the granite is axial planar to the folds deforming the granite and in many cases S3 is the dominant foliation. These field relationships are similar to those of anatectic leucomes in the country rock paragneiss,

which are parallel to S2 defining the gneissosity and are folded by F3. According to these field relationships, in the area of study the Port-aux-Basques granite is clearly pre-D3 but it could be syn- to late-D2. This suggests that some granites could have been generated contemporaneously with the peak metamorphism, during D2.

4.7.3.- Late intrusions: granitic and pegmatitic dykes.

The late intrusions in the area of study are constituted by syn-to late-D3 granitic dykes, pegmatites and post-tectonic dioritic dykes.

Late syn-D3 granitic dykes:

White, late syn-D3, granites outcrop in the Grandy's Brook section. The largest of these granites contains abundant rafts of ductily deformed country rocks including quartzo-feldspathic paragneiss, orthogneiss and amphibolite. Generally, they have a syn-magmatic to early solid-state foliation which is variably folded by F3. In apperance the syn-D3 granites of the Grandys Brook section resemble the Rose Blanche granite (ca. 419 Ma; van Staal et al., 1994). Late syn-D3 granitic dykes are also well exposed in the Fox Roost section and the mouth of the Isle-aux-Morts River. In Fox Roost (Fig.4.4, 4.19), a fine-grained late syn-D3 granitic dyke was dated (U-Pb sample 92-GD-11). Brown (1973) reported similar late-D3 aplitic dykes in the vicinity of Port-aux-Basques.

Age (U-Pb):

Late syn-D3 granitic dyke (Sample 92-GD-2): This is a grey fine-medium grained equigranular, biotite-bearing granitic dyke. The dyke cuts the main gneissosity (Fig.4.19, 4.20), including tight F3 folds, it is folded and contains a weakly developed foliation (magmatic fabric?) which has been folded. The dyke is, therefore, interpreted to have intruded during the late stages of D3.

Six zircon and one titanite fraction have been analyzed (Table 4.1). The titanite fraction (T1) is U-poor (64.6 ppm) and 8% discordant due to the effects of the common Pb correction. U-Pb ages of 407 Ma and 412 Ma for this titanite are, however, in good agreement and are consistent with the concordant 410±2 Ma titanite age from the nearby amphibolites (section 4.6.1). Most zircons extracted from this rock are heavily cracked, even the best quality prisms and needles (fractions Z1, Z2, Z3, Z4 and Z5) show cracks. Fraction Z6 consists of prisms and prism fragments. All fractions were strongly air abraded, except fraction Z5 (unabraded). Z6 has the oldest $^{207}Pb/^{206}Pb$ age but it is the most discordant fraction (5%), which suggests the presence of inheritance. Fractions Z1, Z2, Z3, Z4 and Z5 are closely clustered along a discordia line with an upper intercept of 417.3 Ma and a lower intercept of 18.9 Ma. A discordia line (64% probability of fit) traced pinning the lower intercept at 17±30 Ma provides an upper intercept of **417+7/-4 Ma** (Fig.4.21). This upper intercept is in agreement with the $^{207}Pb/^{206}Pb$ ages of the individual fractions (Table 4.1). This age of 417+7/-4 Ma is interpreted as the intrusion age and, therefore, the age of the final stages of the D3 deformation.

Pegmatites:

Two generations of pegmatites are present in the area of study, pre- and post-D3. The mineralogy of these rocks was already described by Brown (1973). They consist of K-feldspar (up to 10 cm Ø), muscovite, biotite, quartz and tourmaline.

The *pre-D3 pegmatites* are concordant with or cut the main gneissosity. They were sheared and boudinaged during D3, but there is no evidence of F2 folding. These pegmatites are well exposed in the road outcrops close to Isle-aux-Morts (Fig.4.17).

Post-D3 pegmatites are common in Fox Roost section. They usually intrude along extensional cracks while the Margaree orthogneiss had a brittle behaviour, and many have an aplitic core (Fig.4.5d).

Aplitic and granitic dykes (post-D3):

The *aplitic dykes* are grey, fine to medium grained, biotite-bearing and locally garnet-bearing. They resemble the late syn-D3 dyke dated at Fox Roost, but they do not have a fabric. They intrude as small bodies, less than 5 metre thick, cutting D3 structures. In the west side of the mouth of the Isle-aux-Morts River one of these dykes stitches the contact between the Margaree orthogneiss and the surrounding paragneiss, but it is reworked within a late brittle-ductile shear zone. This suggests that these dykes are post-D3 and probably pre- local D4.

A *post-D3 granite dyke* outcrops in the quarry outside Margaree, sample locality of sample 93-PV-3 (tonalitic orthogneiss). This is a 2 to 3 metre thick coarse-grained pink granite. Also in the same locality there are some late pink granitic patches in the Margaree orthogneiss. This late granite is probably associated with the post-D3 pegmatites.

Post-tectonic mafic dyke:

This is a fine grained green dioritic dyke (Brown, 1973). It outcrops east of Fox Roost, in the coastal section. It is undeformed, it cross cuts the structures in the complex and has chilled margins.

4.8.-STRUCTURAL EVOLUTION OF THE MARGAREE ORTHOGNEISS AND SURROUNDING PORT-AUX-BASQUES GNEISS:

The Margaree orthogneiss has a compositional banding which defines the main gneissosity. This gneissosity has been stretched, folded and, locally, transposed as a result of a series of deformational events. The following is a description of the structural characteristics of the Margaree orthogneiss and the surrounding paragneiss. This part of the study will attempt to bridge the time constraints and conditions of deformation in the Margaree orthogneiss with those in the PaB gneiss (Burgess et al., 1995).

4.8.1.- Phases of deformation: definition and characteristics:

Brown (1975) and van Staal et al. (1992) recognized four deformational events in the Port-aux-Basques area. The main ones are D2 and D3. D1 is a conspicuous event only recognizable in F2 fold closures in the kyanite zone and as an internal schistosity in syn-D2 garnets in the first sillimanite zone. D4 is a late ductile-brittle episode.

D1-D2 deformation:

In the Margaree orthogneiss, like everywhere in the second sillimanite zone, neither D1 fabrics nor structures are preserved. However, since the gneissosity is being folded by F2 it should be interpreted as a pre-D2 feature, most likely S0-S1 (Fig.4.22).

The gneissosity is folded by minor folds (F2) which are refolded by F3 folds. This interference produces an apparent F2 sheath-fold geometry (Fig.4.22). These F2 folds are the best indicator of a D2 event. Amphibolite boudins are tightly folded by F3 folds suggesting that the boudinage was part of a previous deformation (Fig.4.8), this is consistent with the local D3 shearing of felsic D2 boudins in the nearby paragneiss

(Fig.4.23). The contrast of competencies between the amphibolite and the granitic orthogneiss is quite variable but overall the amphibolite is less competent and develops mullions during the boudinage, indicating high-temperature deformation (Talbot and Sokoutis, 1995). These mullions are probably D2 structures, although some could be primary syn-magmatic features, and were subsequently folded by F3. It should be noted that in one locality, at the mouth of the Isle-aux-Morts River, Fox Roost like "tonalitic" gneisses have developed a pre-F3 foliation in the amphibolite boudins suggesting that the boudins pre-date this foliation. This brings the possibility that some mafic boudin-like features could also be apophyses of mafic dykes propagated by echelon offset of the country rock and deformed by D2 and D3 or that they were produced during a previous event (D1?).

In the surrounding paragneiss, S2 fabrics are well preserved particularly in the pelitic layers, where leucosomes in stromatic migmatites are aligned with the S2 foliation and are folded by F3 (Fig.4.24). As already pointed out by Burgess et al. (1995), this suggests that D2 took place during peak metamorphism. The same authors interpreted the gneissic banding as a product of D2 transposition of original compositional banding (S0) and the S1 fabric. Exceptionally, S0-S2 relationships are preserved in psammitic lithologies. F2 folds are relatively abundant, but due to the intense D3 overprint it is not possible to follow the trace of D2 macrostructures in the field. Some macrostructures like the kilometer-scale refolded ribbon of paragneiss in the easternmost package of Margaree orthogneiss, however, could be interpreted as a D2 structures (Fig.4.1). This interpretation is supported by similar D2-D3 interference patterns defined by the Port-aux-Basques granite west of the area of study (Fig.4.1).

D3 ductile deformation :

D3 is the final major event recorded in the Margaree orthogneiss and the surrounding paragneiss. It is characterized by high temperature ductile deformation (Fig.4.25), followed by amphibolite facies retrogression. D3 produced minor tight asymmetrical isoclinal folds plunging 45° to the NE, on average, which steepened the main gneissosity (Fig.4.5b, 4.26). Mineral lineation (90% amphibole lineations) are parallel to the F3 fold axis (Fig.4.26). The D3 folding produced the main outcrop pattern of the Margaree orthogneiss with minor F3 folds defining the fold closures (Fig.4.3). D3 high-temperature ductile shear zones were developed in areas under shearing during the F3 kilometer-scale folding. This shearing is accommodated by ductile-flow, stretching and thinning of the gneiss without any field evidence for mylonitization, although microstructural evidence indicates the development of a composite fabric. In the Fox Roost area, this shearing generated the banded gneiss, with asymmetrical boudins indicating an overall oblique dextral shear sense. Evidence for boudinage associated with D3 ductile shear zones is also widespread in the section along the road to Isle-aux-Morts, both in the Margaree Complex and the PaB gneiss (Fig.4.27). In these shear zones the boudinage is produced by non-coaxial deformation during oblique ductile shearing (Fig.4.28). Both pegmatitic and mafic dykes developed asymmetric boudins. In the Grandys Brook section, pegmatites were generated in the boudin necks during the D3 boudinage of mafic dykes (Fig.4.13). Associated overprint of F2 folds indicates that the shearing and boudinage is D3 (Fig4.11).

In the paragneiss, F3 folding in pelitic lithologies is usually associated with an axial planar crenulation cleavage (S3; Burgess et al., 1993) affecting S2 but it is generally absent in quartzo-feldspathic gneisses. It is only in one locality that an S3 axial planar crenulation cleavage was observed in the Margaree orthogneiss; this crenulation was produced by cm-

scale F3 microfolding of the gneissosity. The Port-aux-Basques granite has been folded by F3 (Fig.4.3) and contains a well developed S3 axial planar fabric in biotite-rich enclaves. D3 crenulation cleavage of the main solid state fabric in the Port-aux-Basques granite is also found in F3 fold closures.

As it is shown in Fig.4.26 there is no difference in the trend of the gneissosity, F3 fold plunges and mineral lineation between the Margaree orthogneiss and the surrounding paragneiss. D3 folding of leucosomes in the paragneiss indicates that D3 is post-peak metamorphism. The ductile style of D3 deformation is typical of high-grade conditions, suggesting that high temperatures were maintained between D2 and D3.

Late brittle-ductile deformation:

D4 or late-D3 structures can be found along the southern border of the Margaree orthogneiss (Fig.4.3, 4.4). In this area a series of discrete braided brittle-ductile shear zones separate the Margaree orthogneiss from the metasedimentary Port-aux-Basques gneiss. These shear zones could potentially be related to the Isle -aux-Morts fault zone. Late brittle faults are common in the Margaree-Fox Roost section as well as in the Grandys brook section (Fig.4.11).

In the Margaree-Fox Roost section, two metric-scale ultramylonite bands were recognized, developed around pegmatites (Fig.4.3). It is however unclear whether these bands should be assigned to the D3 or D4 phase. The mylonitic bands are characterized by 0.5 to 1 cm K-feldspar and plagioclase porphyroclasts "floating" in a dark micaceous matrix with quartz-rich bands (1mm thick and > 5 cm long quartz ribbons). The rock has a composite fabric. Amphibolite layers in these mylonite bands are boudinaged and folded. The same folding affects the layering defined by the quartz ribbons. The fabric in these

ultramylonites is slightly discordant with the gneissosity in the surrounding granitic orthogneisses.

4.8.2.- Microstructure:

This is a description of the microstructural features of the rock fabric in the main rock types of the Margaree orthogneiss. These microstructural features will be compared with those in the metasedimentary quartzo-feldspathic lithologies of the nearby Port-aux-Basques paragneiss. These lithologies should have had a rheological behaviour comparable to that of the felsic orthogneiss, allowing an assessment of the conditions of fabric development in the Margaree orthogneiss from those of the nearby Port-aux-Basques gneiss (Burgess et al., 1995). The terminology used is that of Shelley (1993) and Passchier and Trouw (1996).

472 Ma granitic orthogneiss:

In hand sample this rock has a gneissic planar fabric defined by oriented biotite, biotite-rich domains separate irregular 1-5 mm thick quartzo-feldspathic layers with a sugary texture. The gneissosity in the rock is defined by the alternation of the biotite-rich and quartzo-feldspathic domains. The aligned biotites (1 mm long), although recrystallized, wrap around plagioclase and feldspar porphyroclasts (Ø ≈ 1.5 to 2.5 mm), suggesting a stage of non-coaxial deformation (Fig.4.29). Large quartz grains (Ø=1.5 mm) have subgrains with parallel deformation bands indicating recovery. In areas of quartz grain reduction (Ø= 0.2 - 0.4 mm), such as contacts with feldspar porphyroclasts, quartz-quartz contacts are ameoboid suggesting dynamic recrystallization. These areas of grain reduction usually coincide with biotite-rich domains and are marked by oriented biotite grains. Plagioclase crystals commonly have deformed twins and contain biotite and quartz inclusions. Locally some plagioclase crystals seem to be "pinning" quartz and biotite

grains, which might be indicative of grain boundary migration recrystallization (Fig.4.29). Overall plagioclase - quartz - K-feldspar contacts are lobate. Locally K-feldspar crystals have undulatory extinction indicating intracrystalline deformation. Anhedral epidote with allanite cores grows late, apparently overgrowing biotite. Accessory titanite is associated with the biotite-rich layers and aligned with the biotite; it is euhedral-subhedral and it is in most places in contact with opaque minerals (ilmenite?).

This fabric has been partially recrystallized after D3 deformation. This recrystallization took place within the stability field of epidote and titanite. There is no growth of chlorite which suggests conditions within the amphibolite facies.

474 Ma granodioritic orthogneiss:

In hand sample this rock type (U-Pb Sample 93-PV-3) has a single gneissic banding. The gneissosity is defined by 1 to 2 cm long and 1-2 mm thick alternations of mafic and felsic agregates with a sugary texture.

The petrography shows the presence of two fabrics. The main gneissic, granoblastic fabric is cut by discrete high strain areas (S3?). These high strain areas are developed around amphibole-rich domains with a granoblastic polygonal texture between green hornblende, plagioclase (An25-30), K-feldspar and quartz (static recrystallization?). The granoblastic domains can be in excess of 5 mm of diameter, with average grain size between 0.5 and 1 mm. Individual amphibole crystals can be up to 3.6 mm long; they are anhedral and in most cases they have a rounded quartz inclusions and oriented biotite inclusions. These granoblastic domains grade into areas where most crystals have lobate to amoeboid contacts, suggesting dynamic recystallization by grain boundary migration. The high strain areas are up to 1.7 mm wide. In the high strain areas there is grain reduction of quartz, feldspar (microcline) and plagioclase (Ø<0.5 mm) and myrmekite (quartz in

microcline). The contacts between these phases are amoeboid (serrated), and there is extensive development of subgrains suggesting dynamic recrystallization. Also in the high strain areas, biotite is recrystallized, preferably oriented and associated with growth of euhedral-subhedral epidote with allanite cores after amphibole. It should be noted that chlorite is absent. Outside the granoblastic domains, plagioclase twins are bent, sheared and have tapering edges, indicating intracrystalline deformation (D3?). Quartz grains with subgrains showing parallel deformation bands are relatively common, indicating recovery. K-feldspar usually has undulatory extinction.

All this suggests that dynamic recrystallization in the late weak fabric took place in the epidote - amphibolite subfacies (approx. 500°-600°C). The granoblastic texture preserved in the amphibole-rich domains could represent a post-peak T (post-D2-early D3) initial stage of recrystallization.

Amphibolite:

This rock type has an L-dominant L-S fabric defined by elongated amphibole and oriented biotite (biotite-bearing amphibolite; Fig.4.16) and plagioclase±quartz-bearing domains (>1mm thick and 3mm long). The mineral lineation is parallel to the plunge of the F3 minor folds. On average the amphibole crystals (green hornblende) are up to 1.7 mm long whereas biotite crystals are 0.5 mm long. Triple point junctions are common at grain boundaries defining a polygonal fabric. Grain boundaries show straight amphibole-amphibole and plagioclase-plagioclase contacts and slightly lobate to straight amphibole-plagioclase contacts (Fig. 4.30). Plagioclase crystals (An20-30) in most places have deformed twins (bent, tapered twins). Subhedral to anhedral titanite in sample 93-PV-6 (410±2 Ma; Fig.4.16) is elongated parallel to amphibole aggregates and has straight contacts with amphibole.

These observations indicate recrystallization, following D3, by grain boundary area reduction in the amphibolite facies. Epidote, chlorite and sericite only appear as late retrograde products, commonly associated with brittle fractures.

Banded gneiss:

The banded gneisses at Fox Roost are the product of D3 ductile shearing. The study has focused on the "tonalitic" lithologies. Samples collected 200m apart show a variable degree of recrystallization. The features of the least recrystallized sample provide the best insight into the conditions and mechanisms of deformation during D3. As in the granodioritic gneisses, this sample shows a composite fabric which is not recognizable in hand specimen. Thin (approximately 0.5 mm wide) high strain zones isolate amphibole- and plagioclase-rich domains, which locally preserve a granoblastic fabric (Fig.4.31). In these high strain zones there is extensive grain reduction of biotite, quartz and locally amphibole (average Ø = 0.2 mm), with associated dynamic recrystallization of quartz and growth of epidote. Epidote grew in association with biotite at the expense of amphibole (Fig.4.31). Outside these high strain areas, quartz (Ø av= 1mm) has lobate contacts with other phases, suggesting recrystallization by grain boundary migration, and has subgrains with parallel deformation bands indicating recovery. Both plagioclase and K-feldspar (Ø≈ 0.8 mm) have lobate boundaries with other phases, except in grain reduction areas where they are ameoboid. Plagioclase shows tapered and bent twins, indicating intracrystalline deformation (Fig.4.31). Amphibole has straight extinction. Euhedral to subhedral titanite is present as inclusions in plagioclase and amphibole as well as in areas with extensive quartz recrystallization; it seems to predate the high strain zones (i.e. pre-D3).

In the recrystallized sample the high strain zones have disappeared, grain boundaries are lobate and quartz is recrystallized into polygonal subgrains with few deformation bands

left. The fabric is defined by elongated agregates of biotite + green amphibole + epidote + minor titanite. There are euhedral titanite grains included in biotite suggesting that they might have recrystallized with biotite.

Port-aux-Basques gneiss (paragneisses):

The quartzo-feldspathic lithologies in the Port-aux-Basques gneiss show similar features to the Margaree orthogneiss. Grain size varies between 0.2 and 1.5 mm.

In lithologies dominated by plagioclase (An 20-30), K-feldspar, quartz and biotite, the latter is recrystallized and shows a preferred dimension orientation defining the fabric. These biotite grains wrap around garnet and plagioclase-rich domains. Plagioclase shows deformed twins and K-feldspar has undulatory extinction, indicating intracrystalline deformation of these phases. Quartz grains show evidence for both recovery and dynamic recrystallization by grain boundary migration. The fabric in amphibole bearing lithologies (Plagioclase (≈An 35) + quartz + hornblende + biotite + K-feldspar + titanite + epidote) resembles that described in the banded gneiss; the fabric is variably recrystallized but shows evidence for grain reduction along discrete high strain zones (D3). Epidote-rich lithologies (quartz + epidote+ (plagioclase) +(hornblende) + titanite) have a polygonal granoblastic texture, with quartz grains showing evidence of recovery. Muscovite-bearing lithologies show muscovite and biotite defining the fabric. Locally, muscovite overgrows sillimanite (fibrolite) probably as part of the retrograde reaction sillimanite + K-feldspar + (H_2O) = muscovite, this muscovite is also recrystallized. In the same muscovite-sillimante-bearing rock, anatectic (?) leucosomes (Qtz + plagioclase (An25) + K-feldspar ± biotite) have a larger grain (Ø=2mm) than the mesosome (Ø≈1mm) with lobate to ameboid grain boundaries, suggesting dynamic recrystallization. The plagioclase in the leucosomes does not show deformed twins but these are common in plagioclase in the mesosome. Chlorite is in most places present in these lithologies as a late retrograde product after biotite and

garnet, and it can be associated with areas with minor quartz-grain reduction. There is also partial sericitization of plagioclase as part of this late retrogression.

These features indicate the amphibolite-facies retrograde character of the final stages of the D3 deformation and the following partial recrystallization. Plagioclase and feldspar intracrystalline deformation suggests amphibolite facies deformation prior to recrystallization. Sillimanite retrogression, widespread epidote, stable muscovite and absence of chlorite suggest that the recrystallization took place in the lower amphibolite facies, below the stability field of sillimanite.

D4 brittle-ductile microstructures: post-D3 ultramylonites:

The fabric is defined by quartz ribbons and a composite fabric (Øav ≈ 0.1 mm) of biotite + quartz + muscovite + epidote/zoisite. This fabric wraps around plagioclase and K-feldspar porphyroclasts (Ø = 1 to 7 mm) which behave as stiff particles (Fig.4.32). Some of these porphyroclasts are composite and indicate a stage of recrystallization prior to the mylonitization. Quartz in the ribbons (1 to 2 mm thick) has ameboid contacts and subgrains with parallel deformation bands. Grain boundary migration seems to be the dominant recrystallization process (Fig.4.32). Chlorite is scarce and usually late as a product of retrogression of biotite flakes.

The preponderance of grain boundary migration recrystallization in the quartz ribbons suggests temperature in excess of 400°C during deformation, whereas the stiff behaviour of plagioclase would indicate low to medium grade conditions (Passchier and Trouw, 1995). Biotite is stable in the main fabric with minimum retrogression into chlorite, this would be consistent with temperatures in excess of 400°C. Chlorite, however, is well developed in other D4 narrow brittle shear zones. Therefore, these ultramylonites were probably

developed in a stage between D3 and D4, coinciding with the recrystallization in the lower amphibolite facies.

4.8.3.- Discussion: Timing and conditions of deformation

In the area of study there is no evidence for deformation which predates the intrusion of the Margaree orthogneiss. Three main phases of deformation can be recognized in the Margaree orthogneiss which are correlated with the main regional D1, D2 and D3 phases (Brown, 1977; Burgess et al., 1995), late brittle-ductile features are ascribed to a D4 phase. Therefore, the 474-465 Ma protolith ages of the Margaree orthogneiss provide the older limit for the deformation in the area (Fig.4.33).

The regional D1 deformation postdates the intrusion of the Margaree orthogneiss and, therefore, it is younger than 465 Ma. According to van Staal et al. (1994), the 453±3 Ma Port-aux-Basques granite, which is syn-D1 and dates the D1 phase, is folded by the D2 and D3 phases. D2 took place during peak metamorphism (Fig.4.33). According to Burgess et al (1995), the D2 deformation was associated with migmatization and intrusion of the anatectic granites like the Rose Blanche granite (Been et al., 1993), which has been dated c. 419 Ma (Dunning, unpublished). In the area of study, monazites from a migmatite near Margaree have been dated at 417±2 Ma (Dunning, unpublished), providing the closest metamorphic age constraint to the time of peak metamorphism and D2 deformation. D3 deformation in the Margaree orthogneiss and surrounding paragneiss was associated with high temperature ductile deformation. The D3 folding of anatectic leucosomes and granite dykes indicate that D3 postdates the peak metamorphism. The final stages of the D3 deformation in the Margaree orthogneiss are dated by the 417+7/-4 Ma protolith age of a late syn-D3 granitic dyke (Fig.4.33). D3 is followed by partial recrystallization; mineral assemblages (Fig.4.34) indicate that the recrystallization took place in the amphibolite

facies. Recrystallized titanite in both amphibolite and granitic orthogneiss has a 410±2 Ma U-Pb age. Therefore, the titanite age could be interpreted as cooling age (Tc ≈ 550°-600°C) or as age of recrystallization. Recrystallization is taking place at conditions close to titanite blocking temperature so either of the two interpretations implies that the D4 brittle-ductile structures are younger than 410 Ma (Fig.4.33; 4.34) and D3 deformation is older than 410 Ma.

The P-T conditions of deformation in the Margaree orthogneiss cannot be estimated. The mineral assemblages are not suitable for thermobarometry (Fig.4.34), but it is possible to infer that temperatures were never above the reaction biotite + plagioclase + quartz = orthopyroxene + K-feldspar + melt (T<750°-800°C; Fig.10-16 of Spear, 1993) during peak metamorphism. The similarities in the style of the D2 and D3 deformations, between the Margaree orthogneiss and the country rock paragneiss, suggest that the P-T-d conditions of Burgess et al. (1995) for the surrounding Port-aux-Basques gneiss could be extrapolated to the Margaree orthogneiss. The lower viscosity of the amphibolite boudins with respect to the granitic orthogneisses during D2 (development of mullion structures) is consistent with the temperatures of 700°-750°C at ≤8 Kbar proposed by Burgess et al. (1994) for peak metamorphism. The conditions for D3 are difficult to estimate, but the preponderance of grain boundary migration recrystallization of plagioclase, K-feldspar and quartz and the bending of plagioclase twins are consistent with upper to middle amphibolite conditions. The absence of chlorite in the mafic lithologies indicates temperatures for recrystallization above the stability of chlorite (≈550°C, chapter 11 of Spear, 1993). Epidote is widespread during recrystallization in the tonalitic orthogneisses and banded gneisses but generally absent in amphibolite; this could indicate temperatures below 650°C (epidote out reaction in mafic rocks; chapter 11 of Spear, 1993). This upper temperature limit would be consistent with the sillimanite = muscovite retrogression in the PaB gneiss, i.e recrystallization within

the muscovite stability field. Therefore, the widespread recrystallization seems to have taken place in the amphibolite facies. Chlorite appears as a retrograde product. In the case of D4 structures chlorite forms part of the microfabric indicating lower amphibolite to greenschist facies conditions.

4.8.4.- Conclusions:

The Margaree orthogneiss records three main phases of deformation which are correlated with the regional D1, D2 and D3 phases (Brown, 1977; Burgess et al., 1994). D1 is represented by the compositional banding which is interpreted as an S0-S1 feature and therefore is younger than 465 Ma. During D2 there is development of sheath-like folds (F2) and boudinage, coinciding with peak metamorphism (c.419-417 Ma). D3 followed peak metamorphism and is responsible for the main outcrop pattern of the Margaree orthogneiss. F3 minor folding and shearing was widespread in the Margaree orthogneiss and the surrounding paragneiss. D3 was characterized by high-temperature ductile deformation which was accommodated by initial grain reduction and grain boundary migration recrystallization of plagioclase and K-feldspar; deformed plagioclase twins also indicate intracrystalline deformation. A late syn-D3 granitic dyke constrains the D3 deformation at 417+7/-4 Ma. D3 deformation took place in amphibolite facies and was followed by partial recrystallization. 410±2 Ma titanite ages could be interpreted to date the recrystallization process and they also provide an older age limit for the D4 brittle-ductile structures. These late mylonitic bands and brittle-ductile shear zones (fault zones) have been grouped within a D4 phase. The D4 structures were generated within lower amphibolite to greenschist facies conditions.

4.9.- GEOCHEMISTRY OF THE MARGAREE ORTHOGNEISS:

This geochemical study was designed to gather a first insight into the geochemical signatures of the most representative rock types of the Margaree orthogneiss. For this purpose ultramafic rocks, amphibolites, granodioritic and granitic orthogneisses of the Margaree orthogneiss were sampled along the Margaree - Fox Roost section. Although the sample set is quite limited it can provide some constraints to allow an evaluation of the tectonic setting and to dismiss certain petrogenetic hypotheses.

Major element whole rock analyses were performed by XRF on glass pellets. The trace elements were analyzed by XRF on press pellets and by ICP-MS. Details of the analytical techniques, including precision and limits of detections are presented in appendix A.2.

4.9.1.- Geochemical signatures:

Ultramafic rocks (Table 4.2):

These rocks are characterized by low SiO_2 compositions (45.6%: Fig.4.35), low TiO_2 (≈0.5%), total alkalis ($Na_2O + K_2O$= 1.62-1.31) and Al_2O_3 (≈ 15%); high MgO (≈ 18.5%) and relatively high Fe_2O_3* (≈10.5%). They are enriched with respect to other lithologies in Ni (452-382 ppm) and Cr (888-846 ppm). Although they are REE poor (La ≈ 2.39; Lu ≈ 0.11); REE elements patterns (Fig.4.36A) are slightly enriched in LREE and show a small positive Eu anomaly. MORB (Pearce, 1973) normalized patterns (Fig4.36B) show a general depletion in high field strength elements (HFSE), a relative enrichment in large ion lithophile elements (LILE) and the presence of a small Nb negative anomaly but no Ti anomaly.

Orthoamphibolites (Table 4.2.)

These rocks have basaltic compositions (47.7 - 50.2% SiO_2; Fig.4.35). This set of amphibolites show low Al_2O_3 (17.63 - 14.02%) and total alkalis, high MgO (11.24 - 5.37%) and TiO_2 between 2.02% - 0.79%. Ni (283 to 24 ppm) and Cr (772 to 62 ppm) are quite variable in the sample set, showing a positive correlation with the MgO concentration. This variation in compatible elements is also reflected in the REE element patterns, the sample set shows REE and LREE enrichment with decreasing MgO (Fig.4.36A). Samples with high MgO, Ni, Cr and low TiO_2 show LREE depleted patterns (Fig.4.36A). MORB (Pearce, 1973) normalized patterns (Fig.4.36B) show an enrichment in LILE, a negative Nb anomaly, an overall depletion in HFSE and a poorly defined Ti negative anomaly. HFSE variations in the sample set are similar to those observed in the REE, i.e. they increase with decreasing MgO.

474 -472 Ma granodioritic and granitic orthogneisses:

The 474 Ma hornblende-bearing tonalitic/granodioritic orthogneisses, have intermediate compositions (62.17 to 64.85% SiO_2) whereas the 472 Ma granites have felsic compositions (71.12 to 74.07% SiO_2). This set shows a decrease in TiO_2 (0.61-0.32%), Al_2O_3 (17.01 - 12.92%), Fe_2O_3* (5.46 - 1.9%), MgO (2.73 - 0.54%), MnO (0.1 - 0.03%), CaO (5.31 - 1.5%) and P_2O_5 (0.2 - 0.05%) with increasing SiO_2. Only the alkalis do not seem to show a systematic variation. REE patterns (Fig4.37A) are enriched in LREE and show a minor Eu anomaly. The granodiorites are more enriched in REE than the granites, have a better defined Eu anomaly and have almost flat HREE. Primitive mantle-normalized (Sun, 1980) multielement patterns (Fig.4.37B) are characterized by enriched LILE, Nb, P and Ti negative anomalies with granodiorites patterns showing an enrichment over granites.

4.9.2.- Tectonic signatures:

Ultramafic rocks, a potential cumulate:

The low REE concentration, with LREE enrichment and positive Eu anomaly in the ultramafic bodies are compatible with the primary mineralogy of a clinopyroxene-plagioclase cumulate. In outcrop, these rocks are associated with the amphibolite-rich areas, suggesting that they might represent a cumulate phase separated from the mafic magma responsible for the amphibolites. Isotopic data would be needed to confirm the hypothetical relationship between the ultramafic rocks and the surrounding amphibolites. Due to their suspected cumulate nature, the geochemistry of the ultramafic rocks will not be used to assess possible tectonic environments.

Amphibolites:

Althought potentially modified by metamorphic processes, the major element characteristics of the amphibolites are indicative of tholeiitic affinities (Fig.4.35; Middlemost, 1975). This is consistent with the LREE-poor patterns of the least evolved samples (Fig4.36A), indicating derivation from a depleted mantle source (likely asthenosphere; Wilson, 1989). Multielement MORB-normalized spidergrams (Fig4.38B) show a slight LILE enrichment with a variably defined Nb negative anomaly and a poorly defined Ti anomaly. This could suggest the presence of minor volcanic arc mantle component or crustal contamination. The high MgO, Cr and Ni concentrations suggest that these geochemical characteristics are from a mantle source, rather than crustal contamination (Pearce, 1983). A battery of tectonic discrimination diagrams (Fig. 4.39) indicate the tholeiitic nature of the amphibolites and the volcanic arc character of the sample set. This is particularly well reflected in the diagrams based on immobile trace elements (Fig 4.39C, Ti-Zr-Y; Pearce and Cann., 1973; Fig4.39D, Zr-Th-Nb; Wood, 1980;

Fig4.39F, Nb-Zr-Y; Mechesde, 1986). These diagrams also show a shift of the samples to the VAB (volcanic arc basalts) field with decreasing MgO content. This shift to VAB is also observed in the shape of the MORB-normalized multielement diagrams (Fig4.36B). These multielement patterns resemble those of volcanic arc tholeiites (Fig4.38B). Secondary element mobility is probably responsible for the relative variations of K_2O, Rb and Ba among samples (Jenner, 1996). However, the relative enrichment in LILE with respect to MORB is likely to be a primary feature, particularly since the variations in Sr and Th concentrations are consistent with the variation of immobile elements, like the HFSE.

Granodioritic and granitic orthogneisses:

Althought the number of samples is quite small and with a wide range of SiO_2 content (62%-74%), the geochemical signatures are strikingly similar. When classified following the schemes of Maniar and Piccoli (1989) and Pearce et al. (1984) they correspond to volcanic arc granitoids (VAG; Fig4.40). Ocean ridge granite (ORG; Pearce et al., 1984)-normalized multielement patterns show a Nb negative anomaly with a Ce peak and LILE enrichment (Fig.4.41). This pattern resembles that of the Chilean volcanic arc granitoids but the LILE side of the pattern has similarities with that of the granitoids from the Skaergaard intrusion (tholeiitic layered intrusion; Hyndman, 1985). The patterns are however quite different from the syn-collisional Variscan granites of southwest England which are derived from mature crustal sources.

4.9.3.- Discussion: Petrogenetic processes and tectonic signatures.

The Mg-rich amphibolites have a geochemical signature typical of tholeiitic basaltic magmas. The high MgO, Ni and Cr and low SiO_2 concentrations suggest that there was little crustal interaction, and the geochemical signatures are a function of the mantle source (Pearce,1983). The LREE depleted patterns (Fig4.36A) are indicative of shallow melting of an Sp-lherzolite mantle source (Wilson, 1989; Ellam, 1992); probably from mantle

asthenosphere slightly affected by a subduction zone component. This is consistent with the LREE-poor and HFSE-poor patterns with respect to MORB, which are typical of primary magmas produced by a high degree of partial melting of a depleted mantle source (Pearce, 1983). The progressive enrichment in LREE with decreasing MgO and the relatively straight variations of the log-log compatible vs. incompatible element diagrams resemble the effects of crystal fractionation (Fig. 4.36A, 4.42). However, crystal fractionation modelling (Fig.4.43) shows that the LREE-enriched and REE-flat amphibolites cannot be generated by fractionation of the Mg-rich and LREE-poor amphibolites. Also the comparison of the MORB-normalized patterns of the felsic orthogneisses with those of the amphibolites indicates the trace element variation was not produced by simple binary mixing between felsic and mafic magmas (Fig.4.44). Therefore, the variation could reflect both a change of mantle sources or the effects of complex petrogenetic processes such as assimilation-crystal fractionation, assuming that all samples are part of the same magma batch. This assumption is unlikely since the presence of syn-472 Ma and post-465 Ma mafic suites is demonstrated. Field relationships indicate that the LREE-poor amphibolites are coeval with the 472 Ma granitic orthogneisses. However, it is not possible to assess if the LREE-enriched amphibolite is part of a post-465 Ma mafic suite. This sample has a Mg number of 29 which indicates that it is evolved, from a source enriched with respect to that of the LREE-poor amphibolites. If there was no crustal interaction, it would indicate melting of a deeper mantle source (garnet-lherzolite?; Ellam, 1992). The Nb-anomaly of this sample and the HFSE enrichment define an attenuated volcanic arc signature (Fig4.38B), which might be indicative of a transitional setting.

The trace element multielement patterns of the granodioritic orthogneisses (60-62% SiO2) indicate that the intermediate compositions are not a product of simple mixing between granitic and basaltic magmas (Fig4.44). These geochemical characteristics are like

those of volcanic arc andesites (Gill, 1981). The trace element depletion of the granites with respect to the granodiorites suggests that the first could have evolved by crystal fractionation from an intermediate melt. On the other hand, if the granites were the product of crustal partial melting, the small enrichment in LILE would suggest that they were generated from an immature crustal source. These hypotheses are impossible to evaluate since the size of sample set prevents any modelling. Also, isotopic data are needed to make the correct petrogenetic assessment, since the concentrations of the most reliable trace elements for granite modelling (Rb, Sr, Ba; Bea, 1996) were probably modified by secondary processes (metamorphism). Even with these limitations, the contemporaneity of tonalitic and granitic melts (474-472 Ma), the consistency of the geochemical signatures, the variability of magma types and the relative abundance of tonalitic intrusions over granitic ones are features consistent with the origin of the suite in a volcanic arc root (Dallmeyer et al., 1996; Hyndman, 1985; Gill, 1981). The intermediate-felsic magmas were coeval with tholeiitic mafic magmas, suggesting that such an arc root was located in an area undergoing important extension and upwelling of asthenospheric material (shallow melting). A volcanic arc / back-arc transitional environment would be consistent with such characteristics (Hamilton, 1994; Clift et al., 1994).

4.10.-INTERPRETATION.

The reported field relationships from the Margaree orthogneiss indicate that intrusion of mafic and felsic magmas was coeval. U-Pb crystallization ages from both the tonalitic (474 Ma) and granitic (472-465 Ma) rock types place the intrusion of the Margaree orthogneiss in the Late Arenig-Early Llanvirn (Time scale of Tucker and McKerrow, 1995). The variety of coeval magma types suggests that the Margaree orthogneiss

represents an ultramafic/mafic-felsic intrusive complex dominated by tonalitic rock types. The abundance of mafic enclaves in the tonalitic rock types suggests coeval injection of basic magmas into the same magma chamber. The granitic orthogneisses generally lack mafic enclaves and back-vein mafic-tonalitic orthogneisses, suggesting that they are apparently intruding into partially solidified mafic magmas. An alternative interpretation is that the mafic-rich bands in Fox Roost represent injections into a partially crystallized felsic magma chamber. The presence of meter-scale ultramafic (cumulate) enclaves indicates crystallization of the mafic magma. This would provide a mechanism to superheat the surrounding granite, so it back-veins the crystallizing mafic magma (Wiebe, 1991; Barbarin and Didier, 1991; Fernández and Barbarin, 1991). Since all textural evidence has been wiped out by overprinting metamorphic and deformational events, it is not possible to reject any of these interpretations. The last interpretation is consistent with certain field relationships which suggests the intrusion of mafic dykes into partially solidified granite. At Grandys Brook, a generation of mafic dykes is intrusive into 465 Ma granitic orthogneisses, indicating that mafic magmatism continued after the intrusion of the Margaree orthogneiss. Therefore, it is possible to speculate that mafic magmatism was coeval during all stages of intrusion and crystallization of the tonalitic and felsic members of the Margaree orthogneiss.

The geochemistry of the main rock types does not support magma mixing. This can be explained by the compositional contrast between mafic and felsic magmas. Such contrast would prevent any important chemical mixing (e.g., Bateman, 1995). Therefore, the mingling observed in the complex is better explained by vigorous free convection and mechanical mixing as a result of mafic injections into the magma chamber. The volcanic arc geochemistry of the tonalites and granites and the volcanic arc tholeiitic character of most mafic magmas can be explained by shallow melting of a spinel-lherzolite mantle

source in a supra-subduction environment. The abundance of basaltic magma could also explain the generation of the intermediate tonalitic magmas by magmatic underplating and partial melting of crustal material, that is assuming that these are crustal-derived melts (Fig.4.45). This hypothesis , however, should be confirmed in the future by gathering a larger geochemical data base, including Nd isotopic data. However, the dominance of tonalitic rock-types, at c. 474 Ma, is consistent with a volcanic arc environment on continental crust. The inferred shallow depths of the coeval tholeiitic basaltic magmas would suggest the presence of a 474-472 Ma transitional continental arc/back-arc environment analogous to that of the Taupo volcanic zone in Northern New Zeland (Gamble et al., 1994). The 465 Ma granitic magmas and the cross-cutting amphibolites indicate that magmatic activity and high geothermal gradients continued, at least, into the Early Llanvirn. How, the LREE-rich amphibolites relate to this magmatism is unknown, it is also uncertain at this stage if they are really derived from an enriched mantle source.

4.10.1.- The Margaree orthogneiss: its relationship with the Early Ordovician Penobscottian events and the Arenig-Early Llanvirn back-arc extension along the peri-Gondwanan margin of the Newfoundland Appalachians.

The geochemistry and field-relationships of the Margaree orthogneiss suggest that it is a Late Arenig-Early Llanvirn arc/back-arc mafic-felsic intrusive complex. The timing of intrusion is contemporaneous with the main back-arc rifting event in the Canadian Appalachians (Swinden et al, 1990; Van Staal et al., 1991) and coincides with coeval magmatic activity in both the Dunnage (Exploits) and the Gander Zone (Chapter II.). The Margaree orthogneiss is coeval within error with the stitching 477 Ma Baggs Hill and 474 Ma Partridgeberry Hill granites that post-date the Penobscottian ophiolite-arc imbrication and ophiolite obduction over the peri-Gondwanan margin of the Iapetus Ocean in the

Newfoundland Appalachians (Fig.4.45; Colman-Sadd et al., 1992a; Tucker et al., 1994). The geological evolution of the Port-aux-Basques area, unravelled from the study of the Margaree orthogneiss, postdates the Penobscottian amalgamation of the Early Ordovician Exploits Subzone with the Gander Zone. Therefore, it is not possible to assign the country rock paragneisses to the Dunnage or Gander Zone, or to reject the hypothesis that their metasedimentary protoliths were deposited during the Penobscottian imbrication.

Ages of volcanism coeval with the intrusion of the 474-465 Ma Margaree orthogneiss are also present in the Exploits Group (O'Brien et al., 1997) and along strike in the composite Bay du Nord Group (466±3 Ma tuff; Dunning et al., 1990) and the Baie d'Espoirs Group (Fig.4.45; 468±2 Ma; Colman-Sadd et al., 1992a). The geochemistry of the syn-472 Ma tholeiitic amphibolites in the Margaree orthogneiss resembles that of coeval basalts in the Lawrence Head Formation, northern Exploits Group (O'Brien et al., 1997). The evolution of this part of the Exploits group is related to back-arc extension after the formation of the Tremadoc-Early Arenig Tea Arm arc. This arc was followed by Mid-Arenig extension and formation of a Late Arenig-Early Llanvirn back arc. Low P / high T anatexis at 465±2 Ma and 464 Ma intrusion of anatectic granites in the Mount Cormack and nearby Meelpaeg Subzone of the Gander Zone (Fig.4.45; Colman-Sadd et al., 1992) indicate the presence of a high geothermal gradient as would be expected in a continental back-arc environment.

If the Bay du Nord Group is the equivalent in southwest Newfoundland of the Exploits Group, the arc/back arc transition must be represented by the post-477 Ma volcano-sedimentary sequences hosting the 466 Ma tuff in the Bay du Nord group (Dunning et al., 1990; Tucker et al., 1994). The western position of the Margaree orthogneiss, near the Silurian suture zone, and the difference in Pb signatures of the associated VMS deposits between the Grand Bay / Port-aux-Basques complexes and the

Bay du Nord Group (O'Neil, 1985) suggest that the Margaree orthogneiss occupied an external position along the peri-Gondwanan margin of Iapetus. Such position could explain the Late Arenig transitional arc/back-arc environment, as the Early Ordovician arc retreated ocean-wards, during the Arenig back-arc extension (Fig.4.46).

CHAPTER V

THE IBERIAN MASSIF: geological setting and general objectives.

5.1.INTRODUCTION:

The aim of this chapter is to provide a concise overview of the geology of the commonly accepted lithotectonic zones of the Iberian Massif to those readers who are not familiar with its geology. The emphasis of this review is on the currently available age constraints on the timing of the pre-Variscan and Variscan tectonothermal events. This overview also serves to introduce the area of study in the Central Iberian Zone (Sierra de Guadarrama, Chapter VI) in the wider regional geological context of the Iberian Massif. The rationale behind selecting the Central Iberian Zone for this kind of comparative study between the Iberian Massif and the Gondwanan side of the Newfoundland Appalachians, is also explained.

5.2.- LITHOTECTONIC ZONES OF THE IBERIAN MASSIF: general overview.

The Iberian Massif constitutes the southern portion of the European Variscides. It has been divided in several tectono-stratigraphic zones (e.g., Quesada, 1991), which are from north to south and east to west (Fig. 5.1.): Cantabrian Zone (CZ), West-Asturian Leonese Zone (WALZ), Central Iberian Zone (CIZ), Galicia-Trás-os-Montes Zone (GTMZ), Ossa-Morena Zone (OMZ), Pulo do Lobo Zone (PLZ) and South Portuguese Zone (SPZ). Quesada (1991) considered the Galicia-Trás-os-Montes, Pulo do Lobo and South Portuguese Zones as exotic terranes accreted to an Iberian Autochthon terrane (OMZ+CIZ+WALZ+CZ) during the Variscan orogeny. This view is disputed by some authors, who consider that the border between the OMZ and the CIZ is an "Early Variscan suture" (Matte, 1986; Azor et al., 1994). This is supported by the Morrocan affinities of the Ordovician fauna in the OMZ and a different Paleozoic lithostratigraphy from that of the CIZ. The Paleozoic lithostratigraphic and faunal similarities between the CIZ, WALZ and CZ, are so strong that they effectively indicate that these three zones formed the single most extensive Paleozoic terrane of the Variscan belt. According to Paris and Robardet (1991), the Ordovician faunas of the CIZ define the Central Iberian faunal domain of the Southern Variscides, which extends into the central Armorican Massif; whereas the Ordovician faunas of the WALZ and the CZ have more affinities with the Ebro-Aquitanian faunal domain, which occupies most of the southern Variscides (Fig.5.1). This shows that the Iberian terrane defined by the CIZ, WALZ and CZ has significant and reliable paleogeographic links with the rest of the Southern Variscides.

The following is a description of these zones with a particular emphasis on the pre-Variscan evolution and the available constraints on the timing of the Variscan events (Fig.5.2). It will start with a description of the so-called exotic terranes (SPZ, PLZ and

GTMZ) followed by a description of the zones that form the Iberian Autochthon terrane of Quesada (1991; OMZ, CIZ, WALZ and CZ), but treating the OMZ as a potential independent terrane.

5.2.1- The South Portuguese Zone (SPZ) and the Pulo do Lobo Zone (PLZ)

These two zones are located in the southwesternmost extent of the Iberian Massif and represent exotic elements accreted against Iberia (OMZ) during the Variscan orogeny (Fig. 5.1 and 5.3). Previously grouped in the classic South Portuguese Zone of Lotze (1945) and Julivert et al. (1979), the oceanic affinities of the PLZ have prompted this separation (c.f. Oliveira, 1990). The vergence of the Variscan structures indicates a southwest tectonic transport, i.e. towards the more external South Portuguese zone (Silva et al., 1990). The contact between these two zones and the OMZ is a suture zone defined by the trace of the Beja-Acebuches ophiolite (Fig.5.1).

The South Portuguese Zone (Fig.5.1; e.g., Oliveira, 1990) has an unknown basement. The oldest rocks that outcrop in this zone are pre-orogenic sedimentary rocks with Famenian (U.Devonian) fauna. Syn-orogenic sequences in this zone range from the Late Famenian to the Early Visean (L. Carboniferous; Fig. 5.2). As a result of the Variscan collision a foreland basin was developed from the Late Visean to the Early Westphalian (Mid Carboniferous; Fig. 5.2).

The Pulo do Lobo Zone (Fig.5.1; e.g., Oliveira, 1990) is formed by sedimentary rocks intercalated with bimodal volcanic rocks (N-MORB tholeiites) that host the massive sulphide deposits of the Iberian Pyrite belt. Blocks in melanges of this zone have provided Upper Devonian fossils. Overstepping sequences, according to Quesada (1991), have Famenian fauna (Fig.5.2). These rocks were intruded at 330 Ma by the syn-kinematic Gil Márquez composite pluton (Rb-Sr; Giese et al., 1993). The back-arc Beja-Acebuches

ophiolite separates the volcano-sedimentary PLZ from the OMZ along a narrow band in which the ophiolitic sequence has been condensed (e.g., Oliveira, 1990; Silva et al., 1990). This ophiolitic sequence has been affected by deformation and a low P / high T metamorphic event ranging from greenschist to granulite facies, with local relicts of garnet-clinopyroxene assemblages (e.g., Munha, 1990). Dallmeyer et al. (1993) reported an $^{40}Ar/^{39}Ar$ hornblende metamorphic cooling age of 340 Ma from the ophiolite, which provides a minimum age for the ophiolitic protoliths and the metamorphic event (Fig.5.2 and 5.3).

5.2.2.- The Galicia Trás-os-Montes Zone (GTMZ):

The GTMZ is located in the northwest corner of the Iberian Massif (Fig.5.1 and 5.3). This zone is interpreted as a composite allochthonous unit emplaced over the Central Iberian Zone (Farias et al., 1986). The zone has been divided in two domains characterized by different lithologies and tectonothermal events: the Schistose Domain and the Domain of the Complexes. The Schistose Domain is interpreted as the western extent of the Central Iberian Zone (Farias, 1992), whereas the Domain of the Complexes is interpreted as a mixture of Iberian and exotic units (Arenas et al., 1986).

The Schistose Domain

This domain (Fig.5.3) is formed by variably metamorphosed siliciclastic rocks with abundant volcanic rocks, ranging from tholeiitic and alkaline basalt to peralkaline rhyolite (e.g. Northeastern Portugal; Riberiro, 1987). According to Farias (1992), the basal volcano-sedimentary units could be Late Ordovician. Llandovery to Wenlock graptolites indicate a Silurian age for most of the rock sequence (Matte, 1968; Romariz, 1969; Fernández Tomas, 1981). The top of the sequence is considered to be Early Devonian on the basis of the 387±16 Ma age of the volcaniclastic Mamoa orthogneiss (Rb-Sr;

Marquinez, 1984). Locally, these Middle Paleozoic rocks rest on orthogneisses, but the nature of the contact is unknown (Farias et al., 1986, 1992). Orthogneisses in this domain (Fig.5.3) are poorly dated and ages range from 378 Ma (Noya migmatitic augen gneiss lower intercept U-Pb Zrn; Kuijper et al., 1982) to 570±14 Ma (Sisargas orthogneiss upper intercept U-Pb Zrn; Allegret and Iglesias Ponce de Leon, 1987).

Most of the rocks of the Schistose Domain were variably metamorphosed from greenschist to upper amphibolite facies under low pressure conditions, but there are some local blueschist facies occurences under the Morais complex (e.g., Farias, 1992). The minimum age for metamorphism is constrained by 316 to 307 Ma $^{40}Ar/^{39}Ar$ whole rock and muscovite metamorphic cooling ages (Martínez Catalan et al., 1993). The two-mica S-type granites in this domain are also Late Carboniferous (318±21 Ma La Guardia granite, Rb-Sr; Van Calsteren et al., 1979). The blueschist facies (420°C, 11 Kb) volcanosedimentary correlatives of the Schistose Domain, underlying the Morais Complex (Fig.5.3; NE Portugal), have provided a controversial $^{40}Ar/^{39}Ar$ white mica age of 336±2 Ma (Gil Ibarguchi and Dallmeyer, 1991; c.f. Martínez Catalan et al., 1996)

According to Farias (1992), the Mid Paleozoic rocks of the Schistose Domain correlate with similar Upper Ordovician - Silurian volcanosedimentary rocks in the Central Iberian Zone. These blueschists although ascribed to the Schistose Domain are considered by Farias (1992) as an allochthonous unit.

The Domain of the Complexes

This domain (Fig.5.3) comprises the allochthonous complexes of NW Iberia: Cabo Ortegal, Ordenes, Morais, Braganza complexes and the rocks of the Malpica-Tuy band (Arenas et al., 1986). According to Arenas et al. (1986) these complexes represent klippen of the same tectonic stack. The stack consists of a basal high P/low T unit, locallly reaching

eclogite facies, overlain by a low-medium grade ophiolitic unit and a high P/high T upper allochthonous unit. The Malpica-Tuy band contains only the basal part of this stack. By contrast, the Ordenes and Morais complexes have an extra unit overlaying the upper high P/high T unit. This uppermost unit is interpreted as a fragment of the continental land-mass which collided against the Iberian Autocthon terrane.

Following Arenas et al (1986) the base of the tectonic stack is formed by per-alkaline, alkaline and calc-alkaline (480 Ma, U-Pb; Santos Zalduegui et al., 1995) orthogneiss, metasedimentary rocks and partially retrogressed eclogite and high P / low T rocks. White mica ages from eclogite lenses in the Malpica-Tuy band (Fig.5.3) range from 324 to 358 Ma (K-Ar) and 370 to 378 Ma (Rb-Sr; Van Calsteren et al., 1979). According to Arenas et al. (1986), these two units were part of the Iberian margin.

Tectonically on top of these "Iberian" units, there is a series of tectonic slices of greenschist to amphibolite facies rocks with ophiolitic affinities. $^{40}Ar/^{39}Ar$ amphibole cooling ages from this unit range from 397 to 380 Ma and are interpreted to date ophiolite obduction (v. Cabo Ortegal, Peucat et al., 1990; Morais, Dallmeyer and Gil Ibarguchi, 1991; Braganza, Dallmeyer et al., 1991). Santos Zalduegui et al. (1996) dated a meta-plagiogranite from the ophiolite unit of the Cabo Ortegal Complex at 472±3 Ma (Fig.5.3; U-Pb, Zrn); this rock was metamorphosed up to 700°C and 11 Kb. This age contrasts with an Early Devonian protolith age from a greenschist facies ophiolitic gabbro in the ophiolitic unit of the Ordenes Complex (Fig.5.3; 395±2 Ma, U-Pb zircon; Dunning et al., 1997).

The ophiolitic unit is overlain by a composite upper allochthon made of high P/ high T gneisses, mafic eclogite and peridotite, the granulite unit. This unit contains high P / high T fabrics overprinted by amphibolite facies assemblages during the imbrication of the unit (Fernández, 1994). In Cabo Ortegal (Fig.5.3), the protoliths of the mafic eclogites are

interpreted as arc or back-arc products (Peucat et al., 1990). Peucat et al. (1990) reported 480-490 Ma U-Pb zircon ages from the mafic eclogites. SHRIMP U-Pb analysis of the same zircon separates indicated an Early Ordovician protolith age and an Early Devonian (390 Ma) age for the metamorphic event (Schafer et al., 1993). This high P/ high T event is constrainted by precise U-Pb dating of zircon (406±4 Ma ; 388±3 Ma) and titanite (389±2 to 383±3 Ma) from the high P mafic granulites (Santos Zalduegui et al., 1996). A garnet pyroxenite from the Cabo Ortegal peridotite dated at 392±4 Ma (Peucat et al., 1990) provides an older limit for the imbrication of this complex; the tectonic fabric in this peridotite is cross-cut by a 388±2 Ma pegmatite (zircon and monazite; Santos Zalduegui, 1996). Rutile U-Pb ages at 383±1 and 382±3 Ma (Santos Zalduegui et al., 1996; Valverde Vaquero and Fernández, 1996) and 375 Ma $^{40}Ar/^{39}Ar$ muscovite (Peucat et al., 1990) provide greenschist facies cooling ages and the youngest age limit for the imbrication of the Cabo Ortegal Complex.

The uppermost unit in the Ordenes and Morais Complexes (Fig.5.3) is an exotic slice composed of metabasites, metasedimentary rocks and orthogneiss (augen-gneisses), which is interpreted as the opposing margin of the Iberian Massif (Arenas et al., 1986). These orthogneisses have Early Ordovician protolith ages (ca. 490 Ma; Kuijper et al., 1982; Dallmeyer and Tucker, 1993; Dunning, pers comm.). Muscovite 370-373 Ma $^{40}Ar/^{39}Ar$ cooling ages from these orthogneisses and the underlying ophiolitic unit in the Morais complex (Dallmeyer et al., 1991) provide a younger limit for the imbrication of this exotic unit.

Dallmeyer et al. (1993) interpreted the 365 Ma whole rock $^{40}Ar/^{39}Ar$ age from a phyllonite at the base of the Cabo Ortegal Complex, as the age of the final emplacement of the allochthonous complexes. The peraluminous 310 Ma Espenuca granite (U-Pb monazite; Kuijper et al., 1982) stitches the contact between the Ordenes Complexes and the CIZ

(Fig.5.3) and provides the more reliable younger limit for final emplacement of the complexes over the CIZ.

5.2.3.- The Ossa-Morena Zone (OMZ):

According to Quesada (1991), the OMZ was accreted to Iberia (CIZ+WALZ+CZ) along the Badajoz-Córdoba shear zone (BCSZ) during the Late Precambrian Cadomian orogeny (Fig.5.1). However the complex and distinctive Late Precambrian and Cambrian tectonothermal events, the Morrocan affinities of the Paleozoic faunas and the different Paleozoic lithostratigraphy of the OMZ reflects a separate Paleozoic paleogeographic position from that of Iberia (CIZ, WALZ and CZ).

The OMZ is bounded to the south by the Pulo do Lobo Zone along a transpressional zone (Fig.5.3; Quesada, 1991). The Badajoz-Cordoba shear zone (Fig.5.3; BCSZ; v. Quesada,1991) forms the northern boundary with the CIZ. The BCSZ is tens of kilometres wide and 400 Km long and is bounded to the north by the Peraleda fault (Fig.5.3; Abalos, 1992). This macrostructure has conjugate thrusts and a core of ductile deformation (BCSZ in Fig.5.3.), all overprinted by Variscan transcurrent faults, and hosts variably retrogressed eclogite and granulite (Abalos, 1992). These features have lead some workers to interpret the BCSZ as a reworked suture zone (Burg et al., 1981; Matte, 1986; Quesada, 1991), but it is disputed whether it represents a reworked Cadomian (Abalos, 1992) or Variscan suture (Azor et al., 1994). This shear zone had an estimated, Variscan, minimum sinistral movement of 400 Km (Abalos, 1992) to 200 Km (Azor et al., 1994), but it should be noted that there are no markers to make a proper estimation.

The gneisses of the Azuaga group are the oldest rocks in the OMZ and are interpreted by Quesada (1990a,b) as basement to the OMZ. These gneisses, which outcrop in the BCSZ (Fig.5.3), have been metamorphosed to eclogite/granulite facies and retrograded to

amphibolite facies (Abalos, 1992). The Azuaga group consists of orthogneiss (Azuaga gneiss), amphibolite, paragneiss and minor calc-silicate rocks, black chert and marble. An amphibolite from this unit has provided the oldest protolith age in the OMZ (611+17/-11 Ma , U-Pb Zrn; Schäfer, 1990; Schäfer et al., 1993). The variably metamorphosed siliciclastic rocks of the Serie Negra (tectonically ?) overlay the Azuaga group. The Serie Negra is a siliciclastic rock sequence with abundant black chert and amphibolite dykes in its lower member and siliciclastic with volcaniclastic rocks in its upper member (v. Quesada, 1990a,b). In the BCSZ (Fig.5.3), the amphibolite grade rocks of the Lower Serie Negra have provided $^{40}Ar/^{39}Ar$ amphibole and muscovite metamorphic cooling ages of 560-550 Ma (Dallmeyer and Quesada, 1992). South of the BCSZ, the Upper Serie Negra contains 565 Ma detrital zircon (U-Pb SHRIMP; Schäfer et al., 1993), indicating that the Serie Negra is a composite rock sequence. Reliable protolith ages of Late Precambrian Cadomian magmatism are scarce (585±5 Ma and 544+6/-5 Ma, U-Pb Zrn; Schäfer, 1990; Ochsner, 1993). According to Ochsner (1993), this magmatism has a calc-alkaline character.

South of the BCSZ, the presence of clasts of deformed Serie Negra black chert in the basal lower Cambrian conglomerates indicate the presence of a Late Precambrian/Cambrian unconformity and a deformed Precambrian basement underlying the OMZ. Lower Cambrian carbonates overlie the basal polymictic conglomerate, sandstone and interleaved acid volcanic rocks of the Torreárboles formation (Liñán and Quesada, 1990). These carbonates are overlain by the Mid Cambrian volcano-sedimentary Complex (Oliveira et al., 1992). These Mid Cambrian volcanic rocks range from basalt to rhyolite and have tholeiitic to alkaline-peralkaline character. Their eruption coincides with the intrusion of syn-kinematic anatectic granites associated with low P / high T metamorphism and deformation in the central OMZ, south of the BCSZ (527+10/-7 Ma, U-Pb, Monesterio anatectic granodiorite; Ochsner, 1993; Eguíluz and Abalos, 1992). The intrusion of 525-

510 Ma calc-alkaline plutons and the coeval andesitic volcanism of the syn-orogenic Malcocinado formation (Ochsner, 1993) follows the low P / high T metamorphic event. South of the BCSZ and within the Malcocinado formation there are olistoliths of serpentinite which might represent a dismembered ophiolite (Quesada, 1990a, b). Mid-Upper Cambrian Barrovian metamorphism is locally preserved in the BCSZ (Fig.5.3), including the migmatization of the basal levels of the Serie Negra in the Mina Afortunada gneissic dome (650°C, 6-7 Kb; Abalos, 1992; 520 Ma, U-Pb, Zrn; Dunning, unpublished; 507+9/-6 Ma, U-Pb, Mnz, Ochsner, 1993). This would indicate the effects of a poorly understood Mid Cambrian orogenic event, which is interpreted to have occurred in a continental arc (Ochsner, 1993). The Mid Cambrian calc-alkaline magmatism in the OMZ is followed by Cambro-Ordovician alkaline plutonism along the southern border of the BCSZ (Fig.5.3; A-type granitoids, 503+4/-2 Ma to 498+10/-7 Ma; Ochsner, 1993). A final pulse of pre-Variscan peralkaline (riebekite-clinopyroxene orthogneiss) to meta/peraluminous plutonism is restricted to the BCSZ (Fig.5.3; 470-480 Ma, U-Pb Zr; Ochsner, 1993), and is coeval with Early Ordovician acid volcanism south of the BCSZ (Oliveira et al., 1992).

The Paleozoic sequences in the OMZ have a very distinct character north and south of the BCSZ (Fig.5.3; Robardet and Gutiérrez Marco, 1990). To the north, between the BCSZ and the Pedroches batholith, the Paleozoic sequence is similar to that of the neighbouring CIZ, containing the Arenig Armorican quartzite and Llanvirn to Caradoc black shales and siliciclastic rocks with faunal affinities with the CIZ (e.g. Perejón and Moreno-Eiris, 1992). This suggests that these rocks might represent slices of an outboard part of the CIZ incorporated into the BCSZ. The Ordovician sedimentary sequences south of the BCSZ (Fig.5.3) contain distinctive Ordovician faunas with Morrocan rather than Central Iberian affinities, which define the Ordovician South Iberian faunal domain (e.g. Robardet and Gutiérrez Marco, 1990). This Early Paleozoic sequence rests unconformably

on the Mid Cambrian and contains Arenig grey-green shales instead of the Arenig Armorican quartzite characteristic of the CIZ, WALZ and the CZ; faunal and sedimentological differences with the CIZ persisted during the Silurian and Devonian indicating the distinct character of the OMZ (Paris and Robardet, 1990; Robardet and Gutiérrez Marco, 1990; Perejón and Moreno-Eiris, 1992).

The onset of the Variscan orogeny is marked by syn-orogenic deposits with local volcanic intercalations (Quesada et al., 1990). The basal age of these deposits varies between Frasnian (Upper Devonian) and Lower Visean (Lower Carboniferous). Local $^{40}Ar/^{39}Ar$ metamorphic cooling ages at 360-368 Ma in hornblendes and 331-340 Ma in muscovites of the BCSZ (Dallmeyer and Quesada, 1989) indicate Famenian to Visean (scale of Odin, 1990) Variscan movement along the BCSZ (Fig.5.3). The BCSZ is stitched with the CIZ by an Upper Tournasian (Lower Carboniferous) to Namurian (Middle Carboniferous) syn-orogenic basin (Fig.5.2 and 5.3). Earliest Variscan magmatism in the OMZ is Upper Tournasian but most plutonism seems to be Upper Visean-Namurian to Middle Westphalian (Sánchez Carretero et al., 1990).

5.2.4.- The Central Iberian (CIZ), West Asturian-Leonese (WALZ) and the Cantabrian (CZ) Zones:

These three zones (Fig.5.1) are characterized by a Precambrian/Cambrian unconformity, a Cambrian miogeocline with Lower Cambrian siliciclastic rocks overlain by Lower-Middle Cambrian limestones, an Early Ordovician transgression with deposition of the Arenig Armorican quartzite and Llanvirn black shales (Fig.5.4). As well, these zones have significant Paleozoic faunal similarities which indicate that the CIZ, WALZ and CZ were part of the same pre-Variscan terrane (Fig.5.1). The Central Iberian Zone (CIZ) represents the most outboard part of this terrane. The intensity of the Variscan

tectonothermal events (metamorphism and plutonism) decreases from the CIZ towards the Cantabrian Zone. The thickness of the Paleozoic sedimentary sequences indicate that the WALZ was a Cambro-Ordovician sedimentary trough between the CIZ and CZ. The tapering of the Paleozoic sedimentary wedge towards the CZ indicates its foreland position (e.g., Pérez Estaún et al., 1990). Therefore, these three zones can be interpreted in terms of a hinterland (CIZ), intermediate zone (WALZ) and foreland (CZ) against which terranes were accreted during the Variscan orogeny.

Archean 2.7 Ga granulites overprinted by 1.8 Ga and 0.6 Ga events have been sampled off-shore of these three zones in the Cantabrian sea (Fig.5.5 ; Guerrot et al., 1989). Such basement has never been directly identified on the mainland, but it could be present in some of the high grade metamorphic complexes of the CIZ. The oldest mainland rocks in the CIZ, WALZ and CZ are Late Precambrian low-grade siliciclastic rocks, penetratively deformed during the Precambrian Cadomian orogeny (e.g., Quesada, 1991), with minor volcaniclastic and plutonic rocks (Fig.5.5; e.g., ca. 610 Ma diorite in the WALZ-CZ boundary; J. Fernández Suárez per. comm.) and high-grade Precambrian orthogneisses in the CIZ (Fig.5.5; 617±10 Ma Miranda do Douro orthogneiss; Lancelot et al., 1985). In the northern half of the CIZ there are large outcrops of pre-Variscan augen-gneiss which, although containing dated Early Ordovician intrusions (Fig.5.3; Lancelot et al., 1985; Gebauer et al., 1993), have been assigned a Proterozoic age (e.g., Azor et al., 1992). The volcanic rocks intercalated in the Paleozoic sequence indicate local Cambrian, Cambro-Ordovician, Arenig, Llanvirn and Late Ordovician-Early Silurian pre-Variscan magmatic pulses, which had been generally considered as rift-related minor pulses (e.g., Quesada, 1991). However, some of these views will have to be reassessed as a result of the new data gathered from the pre-Variscan gneisses of the Sierra de Guadarrama (CIZ; Fig. 5.1) in chapter VI of this thesis.

The Central Iberian Zone (CIZ)

This zone is characterized by the abundant Variscan plutonism (poorly constrained between 344-287 Ma, Serrano-Pinto et al., 1987), the local preservation of a Barrovian metamorphic sequence, areas of high-grade metamorphism (low P / high T) alternating with low-grade areas and a widespread Early Ordovician "Sardic" unconformity and deformation, which are exclusive to the CIZ (v. Julivert and Martínez, 1987). The CIZ is bounded to the south by the Badajoz-Cordoba shear zone against the OMZ, to the NW by the allochthonous units of the Galicia -Tras-os-Montes Zone and to the east by the WALZ (Fig.5.5). This zone has been divided according to the style of the Variscan deformation into a northern Domain of Recumbent Folds, also known as Ollo de Sapo Domain, and a southern Domain of Vertical Folds (Fig.5.5; Díez Balda et al., 1990), this division also reflects significant differences in the pre-Ordovician stratigraphy (de San Jose et al., 1992). Low-grade Precambrian rocks occupy extensive areas in the southern Domain of Vertical Folds. By constrast in the northern Domain of Recumbent Folds or Ollo de Sapo Domain, Ordovician rocks rest unconformably on low grade augen-gneisses (Ollo de Sapo gneisses) or tectonically on top of medium-, high-grade metamorphic complexes with abundant orthogneisses (Fig.5.4 and 5.5; e.g., Julivert and Martínez, 1987).

The Precambrian rocks in the southern Domain of Vertical Folds consist of basal slumps and turbidites with abundant greywackes, known as the Schist-Greywacke complex (Fig.5.4; de San Jose et al., 1992). Their age ranges from Late Precambrian to, possibly, Early Cambrian in NE Portugal (Oliveira et al., 1992). López Díaz (1995) has demonstrated the presence of two low-grade Late Precambrian Cadomian (?), penetrative, compressional deformations, the latest of which is pre-Late Vendian (pre-540 Ma; time scale of Odin, 1990). An unconformable Lower Cambrian miogeocline sequence of siliciclastic and carbonate rocks covers the deformed Late Precambrian (Fig.5.4). In the

Montes de Toledo (Fig.5.5), a non-fossiliferous, calc-alkaline volcano-sedimentary complex unconformably overlies the Cambrian (Martín Escorza, 1977a; Muñoz et al., 1985).

In the northern Ollo de Sapo Domain (Fig.5.5), the gneissic rocks of the Ollo de Sapo formation were traditionally considered as Precambrian (Parga Pondal et al., 1964; e.g., Azor et al., 1992), althought some authors considered them Cambrian or Ordovician in age (c.f. Martínez García, 1973). These rocks were originally defined as greenschist facies mylonitic volcaniclastic rocks (Parga Pondal et al., 1964), but most authors correlate them with the rest of the medium and high-grade pre-Variscan augen-gneisses in this domain (Fig.5.5; e.g., Azor et al., 1992; Navidad et al., 1992). These pre-Variscan gneissic formations are particularly extensive in the selected field area of the Sierra de Guadarrama, where they are basement to the Paleozoic sequence. The absolute ages for these pre-Variscan augen-gneisses varies from Late Precambrian to Early Ordovician (Fig.5.5; Lancelot et al., 1985; Vialette et al, 1986; 1987; Wildberg et al., 1989; Gebauer et al., 1993), but the relative importance of the Precambrian versus the Early Ordovician magmatic pulses remains controversial (c.f. Azor et al, 1992; Gebauer et al., 1993).

An Early Ordovician unconformity associated with weak extensional Cambro-Ordovician deformation is widespread throughout the CIZ (Fig.5.4; e.g., Díez Balda et al., 1990; Gutiérrez Marco et al., 1990; López Díaz, 1995). This event is refered as "Sardic" by comparison with similar Ordovician events in Sardinia (Italy; Sardic event of Stille, 1927). Lower Ordovician siliclastic rocks above the Sardic unconformity overlie the augen-gneisses of the Ollo de Sapo Domain, as well as, deformed Precambrian, tilted Cambrian rocks and the Cambro-Ordovician volcano-sedimentary complex of the Montes de Toledo in the southern domain of Vertical Folds (Fig.5.4). This widespread angular unconformity is hidden by the Arenig Armorican Quartzite (e.g., Gutiérrez Marco et al., 1990) which

blankets the entire CIZ, as well as the WALZ and the CZ (Fig.5.4). The overlying Middle to Upper Ordovician stratigraphic sequence of the CIZ also resembles those of the WALZ and CZ (Fig.5.4.; e.g., Gutiérrez Marco et al., 1990) and has equivalents in the Central Armorican Massif (Fig.5.1; France; Young, 1990). A discrete but areally extensive Llanvirn tuff level in the southern Domain of Vertical Folds indicates a local pre-variscan magmatic event (Martín Escorza, 1977). The Upper Ordovician and Silurian rocks of the Western CIZ also record several stratigraphic discontinuities, associated with volcanic and volcaniclastic rocks (e.g., Almadén, Buçao; Gutiérrez Marco et al., 1990), indicating important local pre-Variscan tectonothermal events which eventually lead to the breakdown of the Ordovician Central Iberian faunal/paleogeographic domain between the Central Iberian Zone and the Central Armorican Massif (Paris and Robardet, 1990; Robardet et al., 1990; Robardet and Gutiérrez Marco, 1990). The top of the pre-Variscan Paleozoic stratigraphic sequence in the CIZ locally reaches the Mid Devonian (v. Gutiérrez Marco et al., 1990).

Variscan deformation is marked by syn-orogenic Upper Famenian -Visean deposits and Visean - Lower Namurian flysch sequences. The Variscan deformation has been grouped in three main phases (D1, D2 and D3) followed by a late extensional event. There are also numerous, apparently late, wrench shear zones; but their interplay with the deformational phases remains obscure (Fig.5.6; e.g., Díez Balda et al., 1990). Early Variscan metamorphism in the CIZ is of Barrovian type. It is particularly well preserved in the selected field area in the Sierra de Guadarrama (Chapter VI), and was developed after the initial D1 deformation (Fig.5.5). A second low P / high T metamorphic episode overprinted the initial Barrovian metamorphism. This low P / high T event was associated with anatexis and intrusion of S-type granites (Martínez and Rolet, 1988), gneissic doming and extension during the D2 Variscan deformational episode (Fig.5.6; e.g., Mirando do

Douro/Tormes antiform: Escuder Viruete et al., 1994; Salamanca area, Díez Balda et al., 1995; Toledo anatectic complex, Barbero, 1995).

The earliest Variscan magmatism is marked by local bimodal Frasnian and Tournasian andesites and tuffs in the western CIZ (Fig.5.2; Gutiérrez Marco, 1990). This is consistent with reported Late Devonian plutonism from the western CIZ in Portugal (379±12 Ma to 358±20 Ma, Rb-Sr; e.g., Serrano Pinto et al., 1987). However, the main pulses of Variscan plutonism are restricted to the 344 Ma - 278 Ma interval (e.g., Serrano Pinto et al., 1987). Syn-kinematic, S-type two mica anatectic granites usually range from 327-320 Ma (Rb-Sr) whereas late post-collisional granites and granodiorites group around 310-270 Ma (Rb-Sr, K-Ar; e.g., Serrano Pinto et al., 1987; Yenes et al., 1996). The post-collisional volcanism is restricted to high-K andesites locally associated with the Permo-Carboniferous post-orogenic deposits in the eastern Sierra de Guadarrama (Ancochea et al., 1981).

The West-Asturian Leonese Zone (WALZ)

The WALZ (Lotze, 1945; Julivert et al., 1972) is located between the Central Iberian Zone and the external Cantabrian Zone (Fig.5.1). The oldest rocks in this zone are the Precambrian schists and psammites with minor volcaniclastic levels of the Villalba series (Fig. 5.4). An unconformable Lower Cambrian miogeocline sequence marks the base of the Paleozoic stratigraphic sequence, and it is overlain by a thick Upper Cambrian to Arenig siliciclastic sedimentary package (Serie de los Cabos) and Llanvirn black shales like those of the CIZ (Fig.5.4). This Paleozoic pre-orogenic sequence is topped by Upper Devonian sedimentary rocks (Fig.5.2; Perez-Estaun et al., 1990).

The Variscan deformation in the WALZ is characterized by east vergent D1 recumbent folds, local D2 east vergent ductile shearing (e.g., basal thrust of the Mondoñedo nappe)

and D3 steep open folding (e.g., Martínez Catalan et al., 1990). These three phases of deformation constitute the classic model for the Variscan deformation in the northern Iberian Massif (Perez Estaun et al., 1991), which has beeen extrapolated into areas of the CIZ (e.g., Sierra de Guadarrama; Gonzalez Lodeiro, 1981). Variscan greenschist to sub-greenschists facies regional metamorphism dominates the WALZ, but along the western border with the CIZ it reaches amphibolite facies with relicts of a prograde Barrovian zonation (Fig. 5.6; Martínez et al., 1990). Discrete Variscan granites appear associated with local belts of LP/HT contact metamorphism but most granites are concentrated along the amphibolite facies border with the CIZ (Fig. 5.6). The plutonism is constrained by the main phases of Variscan deformation, post-D1 ~ syn-D2 and post-D3, but there is no reliable absolute age control for the plutonism (317-274 Ma, Rb-Sr, K-Ar; e.g., Serrano Pinto et al., 1987). The timing of Variscan deformation is constrained by the syn-orogenic deposits of the San Clodio fm. (Lower Carboniferous) which have been affected by all main phases of deformation and by the Upper Westphalian B deposits post-dating D3 structures in the Sierra de la Demanda (Fig.5.2; Perez Estaun et al., 1990). Post-orogenic basins are Stephanian B-C. These age constraints are consistent with reported 300 to 275 Ma $^{40}Ar/^{39}Ar$, whole rock and muscovite metamorphic cooling ages (Martínez Catalan et al., 1993). A whole rock $^{40}Ar/^{39}Ar$ age of 321 Ma from a phyllonite in a shear zone is considered to date deformation at the border between the WALZ and the Cantabrian Zone (Fig.5.6; Narcea antiform; Martínez Catalan et al., 1993).

The Cantabrian Zone (CZ)

The CZ constitutes the foreland of the Variscan orogen in the northern Iberian Massif (Fig.5.1). It lacks Variscan metamorphism, and Variscan plutonism is restricted to discrete post-collisional plutons associated with Permo-Carboniferous volcanism (Valverde-Vaquero, 1993). The Paleozoic pre-orogenic sequence is the most complete of the Iberian

Massif and was deposited unconformably over deformed Precambrian strata (Fig.5.4). The Precambrian rocks outcrop in the Narcea antiform along the border with the WALZ (Fig.5.6), and contain volcaniclastic intercalations and discrete plutonic stocks (ca.610 Ma; J. Fernández Suárez, per comm.) indicative of a discrete Cadomian/Avalonian magmatic event. The volcanic intercalations in the Paleozoic sequence also indicate a series of pre-Variscan magmatic pulses: very minor Cambrian volcanism (eg., Corretge and Suárez, 1990), discrete Cambro-Ordovician and Arenig alkaline bimodal magmatism (Gallastegui et al., 1992), local Upper Ordovician-Lower Silurian alkaline basalts (Valverde Vaquero and Hepburn, 1995) and very restricted Devonian tholeiitic volcanism (e.g., Corretge and Suárez, 1990). The top of the pre-orogenic sequence is Lower Carboniferous (Fig.5.4), although the Upper Devonian-Lower Carboniferous change in sedimentary environment and direction of sediment transport might be associated with the onset of the Variscan orogeny. The first Late Visean - Early Namurian syn-orogenic sequences (Fig.5.2) mark the onset of the Variscan deformation, but thrust-related sedimentary wedges did not developed until the Westphalian B. Final thrusting took place in the Stephanian B (Perez-Estaun and Bastida, 1990).

5.3.- THE CENTRAL IBERIAN ZONE, A CRITICAL AREA OF THE IBERIAN MASSIF: GENERAL OBJECTIVES.

The Central Iberian Zone (CIZ) is part, with the WALZ and the CZ, of the largest single terrane in the Southern Variscides. This terrane contains evidence of Late Precambrian Cadomian deformation and an unconformable Lower Cambrian miogeocline (Fig.5.4); which is common to the circum-Atlantic Avalonian/Cadomian belt (v. Chapter I).

Unlike the peri-Gondwanan elements of the Appalachians, this Iberian terrane has remained in the peri-Gondwanan realm during the Paleozoic (e.g., Paris and Robardet, 1990).

Recent geochronological research in the Iberian Massif has generally overlooked the Central Iberian Zone, even though this zone contains large outcrops of pre-Variscan orthogneisses (Fig.5.5) with Variscan metamorphic and deformational overprints (Fig.5.6). The study undertaken (chapter VI) of the Sierra de Guadarrama was designed to unravel some of the controversies surrounding the pre-Variscan and Variscan evolution of the Central Iberian zone, which are outlined below.

Pre-Variscan basement and pre-Variscan tectonothermal events:

Extensive pre-Variscan augen-gneisses outcrop in the cores of the antiforms of the northern Central Iberian Zone, in the Ollo de Sapo Domain (Fig.5.5), with no trace of the Cambrian miogeocline sequences of the southern CIZ, WALZ and CZ. These augen-gneisses are generally interpreted as a Precambrian basement upon which the unconformable Ordovician sequences were deposited (Parga et al., 1964; Julivert et al., 1972; Azor et al., 1992). This view is, however, disputed by Ferragne (1968) and Martínez García (1972), who suggested a Cambro-Ordovician age for these rocks. The available geochronological data is scarce and contradictory, indicating both Precambrian and Early Ordovician ages for these rocks (Fig.5.5). Part of this dispute comes from the fact that megacrystic granites, granitic orthogneisses and felsic volcaniclastic rocks have been merged together under the name "Ollo de Sapo" gneisses and given the status of a stratigraphical formation (Parga et al., 1964; Gutiérrez Marco et al., 1990). To complicate matters, low and high grade augen-gneisses have been correlated in many instances. Some of these pre-Variscan orthogneisses are the deepest rocks in the Central Iberian Zone, outcropping in the core of the metamorphic complexes of the Ollo de Sapo antiform,

Miranda do Douro antiform, the Spanish Central System and the Toledo anatectic complex (Capote et al., 1982; Díez Balda et al., 1990; Barbero, 1995). Therefore, it is possible that some of these rocks might be part of a Proterozoic, 2.0-1.8 Ga crystalline basement like that sampled in the off-shore Cantabrian Zone (Fig.5.5; Guerrot et al., 1989). However, the intense Variscan overprint seems to have obliterated the trace of any earlier structures.

Variscan tectonothermal events:

The absolute timing of the deformational and metamorphic events in the Central Iberian Zone is poorly constrained. It is generally based on relative relationships between deformation / metamorphism (Fig.5.6) and dated plutons with K-Ar and Rb-Sr ages (e.g., Martínez et al, 1990). So far there are no reliable direct ages on fabrics or metamorphism. However, reliable and precise ages are critical to understand when and how the Variscan deformation was transferred from the hinterland of the orogen towards the foreland. The Variscan deformation along the northern branch of the Iberian Massif has been generally viewed as a continum, from the Late Silurian -Early Devonian to the Late Carboniferous (Perez Estaun et al., 1991; Doblas et al., 1994; Martínez Catalan et al., 1996). According to this interpretation, it is the overthickening produced by the emplacement of the allochthonous units of the Galicia Tras-os-Montes Zone that led to the Barrovian metamorphism of the Central Iberian Zone. This seems contradictory, since the 385-375 Ma, Mid Devonian cooling ages from the allochthonous complexes are coeval with the final deposition of the pre-orogenic sequence in the Central Iberian Zone, and the pre-D1 syn-orogenic deposits were not deposited until the Late Devonian-Early Carboniferous (Fig.5.2). Despite this, poorly defined ca. 380 Ma U-Pb zircon lower intercepts from the Sierra de Guadarrama have been interpreted to date the Barrovian metamorphism on the basis of this model-driven scheme (Wildberg et al., 1989).

Timing of the low P / high T metamorphism in the CIZ is also uncertain, as it has never been directly dated. This metamorphism is seen as the cause of the ca. 320 Ma S-type anatectic granites (Martínez et al., 1990; Escuder Viruete et al., 1994; Barbero, 1995). However, according to Wildberg et al. (1989) and Doblas et al. (1994) the low P / high T metamorphism is related to the intrusion of the voluminous 300-290 Ma post-collisional plutons. The first interpretation suggests a single metamorphic cycle of Barrovian peak pressure conditions and decompression to low-P/ high-T conditions (e.g., Tormes dome; Escuder Viruete et al., 1994). The second interpretation however implies that there are two metamorphic cycles, a syn-collisional Barrovian metamorphism and a separate late-orogenic low P / high T one closely associated with the voluminous post-collisional plutonism and late extension (Doblas et al., 1994a,b).

CHAPTER VI

GEOLOGICAL EVOLUTION OF THE EASTERN SIERRA DE GUADARRAMA (Central Iberian Zone).

6.1.- INTRODUCTION:

The Sierra de Guadarrama contains some of the most extensive and best exposed outcrops of pre-Variscan orthogneisses of the entire Iberian Massif (Chapter V). The age of these gneisses has remained controversial and unresolved (Wildberg et al., 1989 vs. Vialette et al., 1986; 1987). Two metamorphic overprints and a complex deformational pattern suggest that these gneisses could be a potential crystalline basement to the Central Iberian Zone (Quesada, 1992). Timing of deformation and metamorphism in the area and the true extent of the Variscan overprint are also unknown (Bellido et al., 1980; Doblas et al., 1994).

The gneisses of the Sierra de Guadarrama have been correlated with lithologically similar gneisses in the Ollo de Sapo and the Miranda do Douro Antiforms (Azor et al., 1992 and ref. within; Gebauer et al., 1993), suggesting that they are part of a 600 Km long belt of pre-Variscan orthogneisses which extends from central to NW Spain (Fig. 6.1). The most important structure of the eastern Sierra de Guadarrama is the Berzosa-Riaza shear zone (Fig.6.2 ; Fernández Casals, 1979). This major, ductile shear zone puts in contact a high grade gneissic infrastructure with abundant pre-Variscan orthogneisses (Guadarrama

Complex, Capote et al., 1982; Western Guadarrama Domain; Macaya et al., 1991) against an overlying medium-low grade suprastructural cover, also with pre-variscan orthogneisses (Somosierra-Ayllon Complex, Capote et al., 1982; Eastern Guadarrama Domain; Macaya et al., 1991). The shear zone preserves a condensed undated Barrovian metamorphic sequence (M1) partially overprinted by low-P / high-T metamorphism (M2). The shear zone is sealed by the La Cabrera post-collisional granite. Therefore, the area around the BRSZ offers an excellent opportunity to tackle both the timing of pre-Variscan and Variscan events as part of a single study using a variety of U-Pb thermochronometers in combination with detailed fieldwork and petrography.

The research in the Sierra de Guadarrama had two clear and different objectives: (A) to obtain the protolith ages of the pre-Variscan orthogneisses and (B) to constrain the time of deformation and metamorphism in the Somosierra sector. The results obtained on the pre-Variscan and Variscan events form two independent data sets, which for the sake of clarity will be presented separately. The information in the following sections (6.3, 6.4 and 6.5) is aimed to provide a clear understanding of the main geological elements of the area of study.

Note: The area of study covers the contact between the Western and Eastern Guadarrama Domains (Macaya et al., 1991), also known as the Guadarrama and Somosierra-Ayllón Complexes of the Spanish Central System (Capote et al., 1982). In order to avoid confusion the term ***Somosierra sector*** *will be used with a geographical connotation and the terminology of Macaya et al. (1991) will be followed.*

6.2.- LOCATION, LOGISTICS.-

The area of study is located in Central Spain approximately 90 Km north of Madrid at the border between the provinces of Segovia, Guadalajara and Madrid. This area is the border between the Sierra de Guadarrama and the Sierra de Ayllon of the Spanish Central System mountain chain. It is also known as the Somosierra, which is the most significant mountain pass of the area. The field area covers approximately a north-south rectangle defined by Riaza to the NE and Buitrago del Lozoya to the southwest (Fig. 6.2), with altitudes between 1000 and 2000 meters above sea-level.

The area of study covers part of the 1: 50,000 geological map sheets of Riaza, Tamajon (Hernaiz Huerta et al., in press), Pradena (Azor et al., 1991) and Buitrago (Bellido et al., 1991). The 1: 50,000 sheets of Riaza and Tamajon (Hernaiz-Huerta et al., in press) were mapped as part of an ITGE (Spanish geological survey) mapping project during 1993-1995. Close collaborative work with the mapping crew allowed the author to cover a large portion of ground with reliable field control during the rock sampling for the U-Pb dating. Some of the following geochronological data was incorporated in the memoirs of these 1: 50,000 map sheets (Hernaiz Huerta et al., in press a,b). This close collaboration was also reflected in joint publications (Hernaiz Huerta et al., 1996; Escuder Viruete et al., 1996; Valverde Vaquero et al., 1996).

The author's field mapping was concentrated in the Buitrago map sheet, outside the area covered by the ITGE team, and particularly in the vicinity of the Rio Sequillo, Puentes Viejas, el Tenebroso and El Villar dams, which offer excellent outcrops. Outcrop quality is generally good, although in the southern part of the area the lack of exposure makes it difficult to trace certain structures. Fieldwork was carried out in two field seasons during spring of 1994 and 1995 with Montejo de la Sierra as field base. Most mapping was done

using the 1:10,000 topographic maps and the 1991, 1:18,000 aerial photographs of the Community of Madrid (Community of Madrid cartographic services).

6.3.- PREVIOUS WORK.-

Early work in the Sierra de Guadarrama started in the last century with the work of del Prado (1884) and MacPherson (1883; 1901). Work up to the early 1980's has been reviewed in a compilation by Bellido et al. (1981). It should be noted that this area has been studied by different groups from the Universidad Complutense of Madrid for several decades. A great part of this work is, however, in the form of unpublished theses. Therefore, it is only the most significant and accessible work which is going to be reviewed below.

The stratigraphy of the Sierra de Guadarrama, including other parts of the Spanish Central system has been described in the works of Lotze (1929), Schroeder (1930), Sommer (1965), Schafer (1969), Hamman and Schmidt (1972), Soers (1972), Bischoff et al. (1973), Capote and Fernández Casals (1975), Bellido et al. (1981), Gonzalez Loderiro (1981) and the compilation of Gutiérrez Marco et al. (1990).

The pre-Variscan gneisses of the Sierra de Guadarrama and the Central System have been studied by De Waard (1950), Febrel et al. (1958), Bischoff et al (1973, 1978), Fernández Casals (1974), Capote and Fernández Casals (1975), Navidad and Peinado (1976; 1981), Navidad (1975, 1979), Peinado and Alvaro (1981), Fuster et al (1981), Navidad and López Ramos (1981). The compilation work of Navidad et al (1992) includes major and trace element geochemistry of the main types of orthogneisses. *Geochronological studies* of these rocks are limited to the data of Bischoff et al (K-Ar and

Rb-Sr, 1973; Rb-Sr, 1978), Vialette et al (Rb-Sr; 1986; 1987) and Wildberg et al (U-Pb; 1989).

The metamorphism of the Somosierra sector of the Sierra de Guadarrama was studied by Heim (1952), Fuster et al. (1974), López Ruiz et al. (1975), Casquet and Fernández Casals (1981), Arenas et al. (1980; 1982), Gonzalez Casado (1987a,b), Gonzalez Casado and Casquet (1987), Azor et al. (1991), Bellido et al. (1991) and Escuder Viruete (in Hernaiz Huerta et al., in press. a, b). Quantitative P-T estimations are limited to garnet-biotite thermometry (Casquet and Navidad, 1985) and fluid inclusion data (Casquet, 1986). It is worth mentioning the description of relicts of eclogite/granulite assemblages in the Sierra de Guadarrama east of the area of study (Fig. 6.2) by Villaseca (1983, in Casquet and Navidad, 1985) and the work of Casquet and Tornos (1981) in the Sierra de Guadarrama near the eastern side of the area of study.

The structure of the Sierra de Guadarrama has been described by Bard et al. (1970), Fernández Casals and Capote (1970), Soers (1972), Capote et al. (1977), Fernández Casals (1979), Alvaro et al. (1981), Bellido et al. (1981), Capote et al. (1981), Gonzalez Lodeiro (1981), Arenas et al. (1982), Capote et al. (1982), Gonzalez Casado (1986), Gonzalez Casado and Casquet (1987a, 1987b), Gonzalez Lodeiro et al. (1988), Martín Escorza (1988), Azor et al. (1991a, 1991b), Macaya et al. (1991), Bellido et al. (1991), Fernández Rodriguez (1992) and Hernaiz Huerta et al. (1996). It is also worth mentioning the description of extensional structures by Martín Escorza (1977 and 1981) in the El Escorial Massif (Fig. 6.2). *Tectonic models* for the Sierra de Guadarrama and the Spanish Central System have been proposed by Capote et al (1982), Macaya et al. (1991), Doblas (1991), Azor et al. (1992) and Doblas et al. (1994 a, b).

The main characteristics of the *La Cabrera granite* and the *Variscan plutonism* in other parts of the Spanish Central System are summarized in Alvaro et al. (1981), Bellido et al. (1981, 1991) and Ugidos (1990). The only *geochronological data* on La Cabrera granite is that of Vialette et al. (Rb-Sr; 1981). Serrano Pinto et al. (1987) and Yenes et al. (1996) have summarized the available geochronological data on the granitoids of the Spanish Central System (Rb-Sr, K-Ar). Hernando et al. (K-Ar; 1980) dated the post-collisional volcanism of Atienza, east of the area of study (Fig. 6.2).

6.4.- GEOLOGICAL SETTING.-

The Sierra de Guadarrama forms the easternmost part of the Spanish Central System (Fig. 6.2). This is an alpine horst which exposes the basement of the Mesozoic cover sequences of the Spanish Meseta. This pre-Mesozoic basement is formed by voluminous Variscan granites and gneissic massifs to the west (Ojos Albos-La Cañada, El Escorial, El Caloco, Sierra de Guadarrama) and Paleozoic strata (Sierra de Guadarrama) to the east (Bellido et al., 1981). All these rocks are part of the already discussed Central Iberian Zone (Section 5.2.4.).

The geology of the Sierra de Guadarrama is best described in terms of a gneissic infrastructure (Western Guadarrama Domain) and a low-medium grade suprastructure (Eastern Guadarrama Domain), separated by a major ductile shear zone (Berzosa-Riaza shear zone; Fernández Casals, 1979, Macaya et al., 1991). Apart from this shear zone, the most significant macrostructures are: the Majalrayo syncline and the Cardoso and Hiendelaencina antiforms in the Eastern Domain, and the Cervunal detachment and the Robregordo fault in the Western Domain (Fig. 6.2). The Cervunal detachment (Berzosa Fault of Gonzalez Lodeiro et al., 1988) is a late extensional fault along the trace of the

Berzosa-Riaza shear zone, and it is taken as the boundary line between the two domains (Bellido et al., 1981; Macaya et al., 1991). The area of study is located between the Western flank of the Majalrayo syncline and the Robregordo fault. It covers the Berzosa-Riaza shear zone, the Cardoso antiform and upper levels of the Western Guadarrama Domain (Fig. 6.2 and 6.3).

According to most authors the Variscan macrostructures were produced by three main phases of Variscan deformation and late extensional faulting (Capote et al., 1982; Macaya et al., 1991; Doblas et al., 1994). D1 affects both domains, but it is more evident in the suprastructure. It is west vergent and has a compressional character. During D2 major shear zones were produced in the Western Domain and the lower structural levels of the Eastern Domain, including the Berzosa-Riaza shear zone. D3 is interpreted as a stage of backfolding, producing retrovergence of the D2 structures and overprinting the D1 macrostructure of the suprastructural Eastern Domain. D3 is followed by late brittle-ductile extension and is responsible for late structures like the Robregordo fault and the Cervunal detachments. A polyphase metamorphism was developed in association with these phases of deformation. It consists of an inter-D1/D2 Barrovian stage (M1) and a syn-D2/late-D3 stage of low pressure/high temperature metamorphism (M2). The Barrovian metamorphic zonation is best preserved in a band along the Berzosa-Riaza shear zone and the lower structural levels of the Eastern Domain, Cardoso and Hiendelaencina antiforms. In the Western Domain, the low pressure / high temperature M2 stage reached temperatures in excess of 700°C (Tornos and Casquet, 1981; Casquet and Navidad, 1985), leaving only relicts of the Barrovian assemblages.

The Eastern Guadarrama Domain lacks Variscan plutonism and has a well defined Early Ordovician to Lower Devonian, fossil-bearing, stratigraphic sequence underlain by pre-Variscan orthogneisses, mostly volcanic-derived (Fig. 6.2; Navidad et al., 1992). This

Paleozoic sequence rests unconformably on the pre-Variscan gneissic sequences of the Cardoso and Hiendelaencina antiforms (e.g., Bellido et al., 1981). This unconformity is defined by the Bornova microconglomerate in the Hiendelaencina antiform (Soers, 1972), which has been correlated with discrete microconglomerate levels between the Armorican quartzite (Arenig) and the underlying Cardoso gneiss in the Cardoso antiform (Gonzalez Casado, 1981). According to Bellido et al (1981), this unconformity is equivalent to the Sardic unconformity of the rest of the Central Iberian Zone.

Metamorphism in this domain varies from lower greenschist facies, pyrophyllite-bearing assemblages in the upper structural levels of the Majalrayo synform, to the staurolite zone in the core of the Cardoso and Hiendelaencina antiforms (Bellido et al., 1981). In the core of the Hiendelaencina antiform a D2 shear zone exposes augen-gneisses of the kyanite zone in its footwall (Fig.6.2; Hiendelaencina thrust of Gonzalez Lodeiro, 1981; Navidad and Peinado, 1981). Bellido et al (1981) correlated these gneisses with the pre-Variscan mylonitic granites that outcrop in the Berzosa-Riaza shear zone.

The Berzosa-Riaza shear zone is a Variscan D2 structure with a present day east vergence and a top down to the SE shear sense (Fernández Casals, 1979; Macaya et al., 1991). This shear zone contains a condensed Barrovian metamorphic sequence partially overprinted by low pressure assemblages during D2 deformation. This shear zone includes the kyanite-sillimanite bearing metasedimentary rocks and orthogneisses of the upper levels of the Western Guadarrama domain and the staurolite and garnet-chloritoid zone metasedimentary rocks and orthogneisses of the lower part of the Eastern Guadarrama Domain (Fig. 6.3). The late brittle -ductile Cervunal detachment marks the only significant metamorphic break, that is between the sillimanite zone with relict kyanite to the west and staurolite zone to the east. To the south the intrusion of the post-kinematic La Cabrera

pluton seals the shear zone and stitches the contact between the two domains of the Sierra de Guadarrama, but with no clear evidence that it cross-cuts the Cervunal detachment.

The Western Guadarrama Domain (Fig.6.2 and 6.3) is formed by extensive massifs of pre-Variscan orthogneisses (augen-gneisses, foliated megacrystic granites and foliated leucogranites) and quartzo-feldspathic paragneisses, mica schists and minor calc-silicates and marbles. These rocks are intruded by Variscan granites, particularly along the western border (Fig.6.2), most of which are post-kinematic (Bellido et al., 1981). Metamorphic grade increases towards the west with increasing anatexis, from the first sillimanite to the second sillimanite zone and a western zone with cordierite + sillimanite paragenesis (Bellido et al., 1981; Tornos and Casquet, 1981; Casquet and Navidad, 1985).

Lithologically the Western domain has been divided into a Lower and Upper Series (Bellido et al., 1991). This division roughly coincides with the trace of the Robregordo fault and the trace of the cordierite-in isograd. The Lower Series, to the west, consists of extensive massifs of augen-gneisses (granitic orthogneisses) with minor paragneisses, and corresponds to the deepest structural levels. The Upper Series is dominated by metasedimentary rocks, although there are abundant orthogneisses. These orthogneisses are, however, comparable with those in the Lower Series. The Upper Series forms the eastern border of this domain and is covered in this study.

6.4.1.- Macrostructure of the Somosierra sector of the Sierra de Guadarrama.-

This section provides a frame of reference for the main macrostructures within the area of study. These elements will be described from east to west, i.e. from the upper structural levels towards the lower ones (Fig. 6.3).

The upper levels of the area of study are occupied by a *crenulation band* (Hernaiz Huerta et al., 1996) which overprints the D1 fabrics of the Majalrayo syncline and can reach up to 10 Km in width (Gonzalez Casado and Casquet, 1987; Hernaiz Huerta et al., 1996). This band roughly coincides with the trace of the Armorican Quartzite, which defines the outline of the Cardoso antiform and the southwest extent of the Majalrayo syncline (Fig. 6.3). As the intensity of the D2 deformation increases the crenulation band gradually passes into the *Berzosa-Riaza shear zone*. This transition into mylonitic fabrics takes place over 2 to 4 Km in the wider parts of the Cardoso antiform but over a narrow and sharp band of tens of meters in the northern part of the antiform and the southwest flank of the Majalrayo syncline. This shear zone dips approximately 45° to the east and has a width between 8 and 3 Km over a continuous, 50 Km long, N-S outcrop. The eastern part of the shear zone was reactivated by a N-S extensional detachment, *the Cervunal detachment*. (Hernaiz Huerta et al., 1996). This detachment cuts the mylonitic fabrics in the shear zone at a higher angle, apparently along the whole length of the Berzosa-Riaza shear zone (Gonzalez Casado et al., 1988). The western border of the Berzosa-Riaza shear zone is marked by a high strain zone with fabrics in the 1st. sillimanite isograd. This western boundary has been locally reactivated, particularly along its northern extent, by a discontinuous extensional detachment, *the Montejo detachment*. (Hernaiz Huerta et al., 1996).

In the Buitrago-Manjirón area, structurally underneath the Berzosa-Riaza shear zone, the gneissic rocks of the Western Guadarrama Domain form a domal structure, *the Manjirón antiform* (Fig. 6.3; Fernández Casals, 1979). A complex shear zone, about 1 Km wide, separates these gneisses from the gneisses of the Buitrago area to the west. It will be referred to as the *Madarquillos shear zone* (Fig. 6.3), but it is also known as the Madarquillos synform (Fernández Casals, 1979) or the Madarcos antiform (Azor et al.,

1991). The Madarquillos shear zone has a complex northern extent, as it apparently merges with the Berzosa-Riaza shear zone. West of this shear zone, the gneisses of the Buitrago area exposed along the Puentes Viejas dam show a complex deformational pattern, with megaboudins and structures produced in the stability field of the 2nd Sillimanite zone.

6.4.2.- Metamorphic zonation.-

The distribution of the metamorphic isograds shows a normal metamorphic sequence of increasing metamorphic gradient towards the lower structural levels of the Eastern Domain and the upper ones of the Western Domain (Fig.6.3). These isograds mark the first appearance, or disappearance, of the index mineral. The ones in the upper structural levels, the chloritoid and garnet isograds were produced syn- to late-D1 and are folded following the trace of the Cardoso Antiform. The staurolite-isograd is also partially folded. Staurolite and chloritoid coexist along a 500 to 700 m wide band (Gonzalez Casado, 1987) which corresponds to the trace of the isograd. Final growth of staurolite took place after D2. Sillimanite and andalusite coexist as late-D2 minerals along a narrow band east of the Cervunal detachment (Gonzalez Casado, 1987; Escuder Viruete in Hernaiz Huerta et al., in press). Within the Berzosa-Riaza shear zone in the sillimanite zone, there is a 3 to 5 Km wide band with abundant kyanite produced during the interval between the D1-D2 deformational phases. This kyanite was partially transformed into sillimanite (fibrolite) during D2 (Gonzalez Casado, 1987). The western border of the Madarquillos shear zone marks the disappearance of muscovite and the presence of sillimanite + K-feldspar paragenesis. It should be noted that the Manjirón antiform contains abundant migmatites and other lithologies apparently retrogressed in the sillimanite + muscovite zone during D2. Cordierite assemblages are limited to the westernmost part of the area of study, and they are late-kinematic to post-kinematic. These late low pressure / high temperature mineral assemblages are consistent with local evidence for minor post-kinematic anatexis and

migmatization (Bellido et al., 1991). The regional cordierite-in and muscovite-out isograds and the sillimanite (kyanite) zone are cut by the post-kinematic La Cabrera granite and overprinted by its contact metamorphic aureole (650°C, 1-2 Kb; Bellido, 1980).

The final metamorphic zonation is the product of the partial overprint by low-pressure assemblages of the initial Barrovian paragenesis during the D2 deformational event, and the subsequent deformation. As already mentioned the D2 event was responsible for the Berzosa-Riaza shear zone and the condensation of the metamorphic isograds. The relationships between metamorphism and deformation, however, will be discussed later in the section dedicated to the Variscan tectonothermal processes.

6.5.-LITHOLOGICAL UNITS OF THE SOMOSIERRA SECTOR OF THE SIERRA DE GUADARRAMA.-

The different lithological units of the area of study are going to be presented from east to west, i.e. structurally downwards (Fig.6.4). This description will be concentrated mainly on the rocks that were studied in detail as part of this study.

6.5.1.- Eastern Guadarrama Domain (Fig. 6.4 and 6.5).-

All rocks studied are structurally below the Armorican quartzite, and they form the stratigraphy of the Cardoso antiform. These rocks are in the garnet and staurolite zones. In the Cardoso antiform, below the Armorican quartzite there is a non fossiliferous siliclastic rock sequence with a characteristic felsic mylonitic volcaniclastic/volcanic level, the Cardoso gneiss. An Ordovician "Sardic" unconformity has been inferred between the Cardoso gneiss and the overlying sedimentary rocks (Gonzalez Lodeiro, 1981). These rocks will be described from top to bottom.

The Armorican quartzite:

It is also known as the Alto Rey Formation (Schäfer, 1969). This is a massive unit of white quartzite with beds of meter scale showing cross-lamination. It has a thickness of approximately 80 meters, but locally it has been duplicated by tight isoclinal folds (Fernández Casals, 1979). It is inferred to be Arenig in age by lithological correlation with similar levels on the opposite limb of the Majalrayo syncline which contain Early Ordovician trace fossils. The Arenig age of these trace fossils is also based on correlation with other areas of the northern Iberian Massif where the Armorican quartzite contains Upper Arenig graptolites (Gutiérrez Marco et al., 1990).

The Constante Formation and the problem of the "Sardic" unconformity:

The Constante Formation (Schäfer, 1969; Gonzalez Lodeiro, 1981) is the stratigraphic equivalent of the Bornova Formation (Soers, 1972) in the opposite limb of the Majalrayo syncline (Fig.6.2 and 6.5). This is a sequence of light and dark grey mica schists with brown and black slates, alternating with quartzites and minor microconglomerate beds. Gonzalez Casado (1987) also included in this formation the mica schists, metapsammites, quartzites and minor para-amphibolites inmediately above the Cardoso gneiss. The quartzite levels increase in abundance towards the upper part of the formation, which seems to have a gradual transition to the overlying Armorican quartzite. These quartzite levels have individual thickness between 1 and 2 meters. The age of the formation is believed to be Tremadoc, based on *cruziana* from the Bornova Formation. It should be noted, however, that clear paleontological evidence of Tremadocian faunas have not been found in the Central Iberian Zone nor the West Asturian-Leonese and Cantabrian Zones (G. García Alcalde, pers comm.).

The base of the Constante Formation is problematic. Gonzalez Lodeiro (1981) puts it in the microconglomerate beds above the mica schists which overlay the Cardoso gneiss. Gonzalez Casado (1987), however, prefers the contact with the Cardoso gneiss. These two interpretations are based on the supposedly Precambrian age of the Cardoso gneiss, and extrapolations of the relationships between the Bornova Formation and the underlying gneissic porphyroids in the Hiendelaencina antiform (Fig. 6.5.). This illustrates the problem of the lack of substantial field evidence to support the presence of an unconformity in the rock sequence between the Cardoso gneiss and the overlying Armorican Quartzite. During this study and those of Hernaiz Huerta et al (in press a , b), no field relationships were found with which to substantiate the presence of the Sardic unconformity. This, however, might be explained by the intensity of the mylonitic Variscan D2 deformation which could have obliterated any evidence of an angular or erosive unconformity.

The "pre-Ordovician" rock sequence (El Cardoso gneiss):

This rock sequence constitutes the core of the Cardoso antiform (Fig. 6.4). It is composed of mica schists, metapsammites, quartzites, para-amphibolites and a distinct porphyroid unit known as the Cardoso gneiss. The sequences above and below the Cardoso gneiss are relatively similar, although, para-amphibolites are relatively more abundant as intercalations in the Cardoso gneiss and the strata below. These para - amphibolites form small lenses with an average thickness of 10 to 20 cm, and are composed of plagioclase + quartz + green amphibole + (titanite) ± epidote.

The Cardoso gneiss (Schäfer, 1969) is a variably sheared, leucocratic, porphyritic rock formed mostly by plagioclase + quartz + biotite + muscovite ± (K-feldspar). Porphyroclasts form 30 - 40% of the rock, ranging in size from 0.1 to 5 cm and are mostly rounded blue quartz and fragments of plagioclase, microgranite and fiamme-like dark

micaceous fragments. In the fine-grained facies, the porphyroclasts range from 5 to 7 mm in diameter and are only 5 to 10% of the rock. The porphyroclasts show an unsorted granulometric distribution "floating" in a micaceous leucocratic matrix. All these characterisitics, and the intercalations of lenses of mica schists and para-amphibolites, indicate that the Cardoso gneiss was originally a felsic pyroclastic rock, as proposed by Schäfer (1969). The heterogeneous D2 deformation has transformed the rocks into a mylonitic augen-gneiss, but the character previously described is well preserved in low strain areas. Wildberg et al. (1989) reported a lower intercept age of 540±30 Ma (U-Pb zircon), which they interpreted as the protolith age of the Cardoso gneiss. This age is based on a poorly fitted discordia line defined by highly discordant zircon fractions. However, their best quality zircon (ie. the more concordant fractions) suggested an Early Ordovician age, which questions the validity of their interpretation.

6.5.2.- The Berzosa-Riaza shear zone, upper levels of the Western Guadarrama Domain.-

The lithologies described next are part of the N-S trending band defined by the El Cervunal and Montejo detachments (Fig.6.4 and 6.6). This band is 3 to 5 Km wide and has an estimated thickness of 1500 m, based on the dip of the main foliation. All these rocks are in the sillimanite zone and the relict M1 kyanite Subzone. These metasedimentary and plutonic rocks have been strongly deformed during the development of the Berzosa-Riaza shear zone. Three intrusive types can be differentiated in the field: foliated megacrystic granites (augen gneisses), foliated S-type leucogranites and pegmatites.

Metasedimentary rocks:

The main lithologies are mica schists and quartz-rich psammites with minor amphibolite (Casquet and Fernández Casal, 1981). The psammites, in 30 cm thick bands,

usually alternate with 5 to 10 cm thick layers of mica schists forming a relatively homogeneous sequence and tend to dominate towards the lower structural levels (Fig.6.7). The amphibolites outcrop as meter-scale boudins but they were only identified in the northern extreme of the shear zone (Hernaiz Huerta et al., in press a,b).

Foliated megacrystic granites (augen-gneisses):

These are mylonitic two mica granites dominated by a megacrystic facies with 2 to 4 cm long K-feldspar/plagioclase crystals, and minor foliated leucogranite. They are composed of K-feldspar + plagioclase + biotite + muscovite + quartz, with apatite, zircon and opaques as accessory phases. They outcrop as elongate kilometer-scale bodies along the footwall of the Cervunal detachment. Three of these bodies have been studied in detail, the Riaza, Nazaret and Berzosa gneisses (Fig. 6.4). The *Nazaret and Berzosa gneisses* outcrop in the southern part of the Berzosa-Riaza shear zone, within the sillimanite zone (Fig.6.6). They show heterogeneous deformation with a penetrative S-fabric isolating K-feldspar and plagioclase augen, some of which are ductily deformed. Locally there are high strain areas with well developed L-fabrics (leucogranites in the Berzosa gneiss) and low strain areas showing a crenulation of the main foliation (Nazaret gneiss). The *Riaza gneiss* is located in the northern part of the shear zone between the sillimanite and the staurolite zones. It has been strongly mylonitized, particularly along its eastern side where it is tranformed into a mylonitic gneiss. Otherwise it shows megacrystic facies alternating with minor leucogranite (Arenas et al., 1982). Due to the high strain in the area it is not possible to be certain whether the Riaza gneiss belongs to the sillimanite or the staurolite zone. The problem of the obliteration of the original intrusive relationships is common to all these orthogneisses. Overall they are considered pre-Variscan, however there are no published absolute ages to confirm this view (Bellido et al., 1981; Navidad et al., 1992).

Foliated leucogranites (S-type granites):

These are medium-grained, garnet-bearing, two mica leucocratic granites, with quartz + K-feldspar + plagioclase + muscovite + biotite and garnet, tourmaline, apatite and opaques as minor phases. They are weakly to strongly foliated and have clear intrusive relationships with the surrounding metasedimentary rocks. They usually outcrop as discrete bodies, 10 to 20 meters thick on average, with a well defined planar fabric and parallel contacts with the surrounding country rock. These field characters make them different from the, otherwise lithologically similar, leucogranites in the foliated megacrystic granites. Discrete bodies of garnet-bearing leucogranites have been described, west of the Cervunal detachment, all along the Berzosa-Riaza shear zone as leucogneisses and interpreted as pre-Variscan (Arenas et al., 1982; Azor et al., 1991; Bellido et al., 1991; Hernaiz Huerta et al., in press a, b).

Two of these discrete bodies of leucogranite are well exposed along the road from Paredes to Berzosa (Fig.6.6). The first one, the Paredes S-type granite, is close to the western border of the Berzosa-Riaza shear zone, and it is a representative example of these bodies. It has been boudinaged and shows a well defined foliation with flattened and stretched 5 cm thick pegmatitic veins. These pegmatite veins do not show a subsolidus fabric, but it is uncertain if this is a syn-kinematic leucogranite. This is not the case of the Serrada S-type granite which has an aplitic to pegmatitic texture with a weak subsolidus fabric. It cross-cuts fabric in the country rock metasedimentary rocks, suggesting a syn-kinematic (D2) emplacement. There are no absolute ages for these bodies but it is possible that they might represent both pre-Variscan and Variscan magmatic pulses.

Pegmatites:

West of the Cervunal detachment, there are widespread pegmatitic dykes with a syn / late-kinematic character with respect to the Berzosa-Riaza shear zone. They have modal granitic compositions with K-feldspar + quartz + plagioclase + muscovite + biotite + tourmaline ± sillimanite ± andalusite. These pegmatitic dykes cross-cut the main fabric in the metasedimentary rocks and are variably deformed with and without a penetrative subsolidus fabric. The late-kinematic character indicates that they are Variscan.

6.5.3.- The Western Guadarrama Domain (Buitrago-Manjirón area):

The complexity of the area and the contradictions found in recent geological maps (Azor et al., 1991; Bellido et al., 1991) forced the creation of a new set of lithological units by the author. The criteria, upon which the units were defined, were developed exclusively on field basis and emphasize the separation between igneous and sedimentary (i.e. supracrustal) protoliths. After field work it was found that these criteria closely resemble those of Fernández Casals (1979), and in addition acknowledges the presence of unusual biotite-bearing migmatites, which might be non-anatectic in origin and derived from an igneous protolith (Bellido et al., 1991).

Lithological units (Fig.6.6):
Madarquillos shear zone:
* Garnet mica schists and black quartzites:
* Muscovite-sillimanite metapsammites:
Manjirón antiform and Buitrago area (gneissic areas)
Metasedimentary rocks
* Migmatitic paragneisses (Fig.6.7d)
- Quartzo-feldspathic paragneisses:
- Anatectic migmatites:
* Calc-silicates:
* Marble:

Unknown origin:
* El Villar biotitic migmatitic gneiss (non-anatectic migmatites)
Orthogneisses:
* Granitic augen-gneisses / foliated megacrystic granites
* Gneissic garnet-bearing leucogranites (Two types)
Intrusive rocks:
* Pegmatites

These lithological units have been divided along lithological and metamorphic criteria into metasedimentary units with stable muscovite (1st sillimanite-zone, i.e. those in the Madarquillos shear zone) and gneissic units (Manjirón antiform and the rocks in the 2nd sillimanite-zone west of the Madarquillos shear zone). It should be noted that, in the Manjirón antiform, muscovite and sillimanite are stable in the deformational fabrics that post-date migmatization .

METASEDIMENTARY ROCKS:

Garnet mica schists with black quartzites (Madarquillos shear zone; Fig.6.6):

This unit is well exposed on the eastern side of the Puentes Viejas dam, forming a narrow, 500 meter wide band separating the muscovite-sillimanite metapsammites from the gneisses of the Manjirón antiform. This unit is characterized by abundant garnet porphyroblasts up to 1 cm in diameter and centimetric sillimanite (fibrolite) patches growing in a biotite-muscovite mica schist (Fig. 6.8). The mica schist is dominated by Bt-Ms rich domains with refolded fibrolite patches and minor, discontinuous, 2 mm thick, quartzo-feldspathic layers. These mica schists alternate with minor mica-rich psammitic levels (>10 cm thick). These lithologies are cross cut by refolded quartz-veins and by deformed pegmatitic veins. Some of the centrimeter-scale pegmatites might represent anatectic melts generated in situ. A well developed crenulation cleavage overprinting the schistosity is characteristic of this unit. Black quartzite beds are locally intercalated with the

mica schists. The most distinctive ones are those that outcrop in the northern closure of the Manjirón antiform (Bischoff et al., 1973). Other good examples are also found near the Puentes Viejas dam. These are bands of meter-scale thickness with 3 to 10 cm thick layers of fine-grained quartz, minor white mica and opaque minerals (graphite?).

This whole unit, although very distinctive in field appearance, is difficult to map because of its apparent discontinuous nature and the lack of continuous outcrop. The outcrops along the N-NE border of the Manjirón antiform (Fig.6.4.) can be correlated with those along the eastern Puentes Viejas dam, confirming that these rocks are along the contact between the Madarquillos shear zone and the gneisses of the Manjirón antiform.

Muscovite-sillimanite metapsammites:

These rocks form a well defined band about 800 m wide which runs north-south along the Madarquillos shear zone (Fernández Casals, 1979). This metapsammites are dominated by quartzo-feldspathic lithologies composed of quartz + K-feldspar + plagioclase + muscovite + biotite + sillimanite (fibrolite) ± garnet, including quartzitic layers, and have minor intercalations of mica schists and discrete levels of black quartzite. At the Puentes Viejas dam, there is a normal contact with the garnet mica schists. To the west there is a gradual appearance of leucosomes and migmatization.

Migmatitic paragneisses (Fig 6.7d):

This unit groups felsic quartzo-feldspathic paragneisses and metapsammites, alternating with migmatite-rich areas. Also common is the presence of minor intercalations of calc-silicate, metaquartzite and rare marble.

* *Quartzo-feldspathic paragneisses (Fig.6.8; 6.9):* These gneisses are formed by layers of variable thickness consisting of quartz + K-feldspar + plagioclase + biotite +

sillimanite ± garnet ± muscovite in different modal proportions, but generally biotite-poor, which alternate with bands of stromatic migmatites. These paragneisses are well exposed on the western side of the Puentes Viejas dam, in general they have granitic composition with the most massive layers resembling granite sills. In the Manjirón antiform side of the Puentes Viejas dam (sillimanite+muscovite zone), muscovite-bearing quartzo-feldspathic gneisses alternate with migmatites. There is also a homogeneous, medium-grained quartzo-feldspathic gneiss of uncertain protolith, but the rheological behaviour and the presence of abundant quartz-veins contrast with the nearby gneissic leucogranites, suggesting that it might be a highly strained paragneiss.

* *Anatectic migmatites* (Fig.6.10; 6.11) are well exposed along the southern shore of the head of the Puentes Viejas dam, in the Manjirón antiform (sillimanite + muscovite zone). These are stromatic types with 20% to >60% leucosome of granitic composition (quartz + K-feldspar + plagioclase ± garnet) in a paragneissic neosome. Most leucosomes are about 1 cm thick and <10 cm long and they are interconnected in the diatexitic types. The melanosomes are formed by biotite + sillimanite (fibrolite) + muscovite ± tourmaline, with sillimanite overgrowing muscovite. In the Manjirón antiform, north of the Puentes Viejas dam, some of these migmatitic areas are associated with large bodies of gneissic leucogranites.

In the Buitrago area (Sill+Kfs zone), there is also a variable degree of migmatization with local areas with 40% to >60% melt (i.e. leucosome). Most of these migmatites correspond to stromatic types but there are nebulitic facies in low strain areas. These leucosomes are also of granitic composition and in general are garnet-bearing. Most leucosomes are medium-grained and have centimetric proportions. The melanosomes are formed by biotite + sillimanite (fibrolite) ± garnet. Even though melting was relatively extensive, there are very few anatectic granitic dykes associated with the migmatites. The

leucosomes, although in places contorted, are generally concordant with the compositional banding in the host neosome, defining the gneissosity. In this area the gneissosity is in cases cut by late tourmaline-bearing aplitic to pegmatitic patches, located along shear bands, boudin necks and tension cracks (Fig.6.10).

Calc-silicates and amphibolites (Fig. 6.12.):

Most amphibole-bearing lithologies are partially amphibolitizated garnet-pyroxenites with centimeter to millimeter-scale garnet- and clinopyroxene-rich bands. These rocks generally outcrop as boudins, some up to 15 meters long, associated with the migmatitic paragneisses. They are relatively scarce but common to both the sillimanite + muscovite and the sillimanite + K-feldspar zones. These calc-silicates are best exposed at the base of the wall of the Puentes Viejas dam and correspond to the "Paredes-type para-amphibolites" of Casquet and Fernández-Casals (1981). Their mineralogy is clinopyroxene + garnet + plagioclase + titanite ± quartz ± calcite ± zoisite ± (rutile) ± green amphibole. In the sillimanite + K-feldspar zone some of the calc-silicates preserve mineral associations of quartz + clinopyroxene + garnet. Amphibole grew during retrogression coevally with the boudinage. Some of the lenses have internal boudins with the quartz + plagioclase + amphibole in the necks and tension cracks. Locally some of the calc-silicates are retrogressed by a skarn type of alteration.

The Braojos dyke (Azor et al., 1991) is located north of the area of study along the eastern border of the Robregordo fault, this is a 2 Km long, deformed dyke which is interpreted as an orthoamphibolite (Azor et al., 1991). It is composed of clinopyroxene + plagioclase + green amphibole + titanite + (chlorite) + (epidote) + apatite ± rutile. Green amphibole was formed after retrogression of clinopyroxene during deformation. Chlorite and epidote are also retrograde products.

Marbles:

They have only been found at the base of the Puentes Viejas dam (white diopside + zoisite + calcite + tremolite?) in association with calc-silicate layers, and near Pinilla de Buitrago at the mouth of the stream Arroyo de Pinilla. In the last case they are associated with migmatites. Small wollastonite-bearing marble layers have also been reported to the north, near Piñuecar (Casquet and Fernández Casals, 1981) and Somosierra (Azor et al., 1991).

UNCERTAIN PROTOLITH:

El Villar biotite-bearing migmatite (non-anatectic migmatite):

These gneisses were previously known as leucogneisses / diatexites (Fernández Casals, 1979) or banded gneisses (Bellido et al., 1991). In the first case they were grouped with the foliated leucogranites and in the second they were merged with the paragneisses. However, as noticed by Bellido et al (1991) they have a distinctive character and could be derived from an igneous protolith. These rocks are well exposed in the Manjirón Antiform (Sill+Ms zone), as well as in the Buitrago area (Sill+Kfs zone) between el Cuadrón and Cincovillas (Fig.6.6; 6.13). In the Manjirón antiform they outcrop in El Villar dam and at the tail of the Tenebroso dam. In the latter location these gneisses form a single massive megaboudin (100's of meters long) surrounded by an envelope of less competent migmatitic paragneisses, within the same structural level as the boudins of garnet-clinopyroxene calc-silicate.

These rocks are massive, highly strained, biotite-bearing, quartzo-feldspathic gneisses of granitic modal composition, with highly strained felsic aplitic to pegmatitic dykes. The mineralogy is relatively simple with plagioclase + quartz + K-feldspar + biotite ± muscovite

as major phases and minor sillimanite and garnet. The gneissosity is defined by discontinuous, medium-grained, felsic layers alternating with fine-grained granitic, biotite-rich domains with aligned micas defining the fabric. As a result, the rock resembles a flattened stromatic migmatite. However, the biotite-rich levels around the felsic domains are no different in terms of mineral assemblages and grain size from the ones defining the fabric in the more homogeneous granitic domains, except for the abundance of biotite, calling into question the presence of a restitic melanosome. Also, in contrast with the nearby anatectic migmatites there is no significant sillimanite or garnet in the rock, not even associated with the biotite-rich layers. In many instances, such as around el Cuadrón, the felsic domains resemble strained pegmatitic veins or flattened and strained feldspar megacrysts; or, such as at the El Villar dam, they have a medium-, coarse-grained texture which does not differ from that of the nearby aplitic dykes (Fig.6.13). Therefore it is difficult to interpret these gneisses as diatexites or anatectic migmatites. The relatively homogeneous aspect in all outcrops, with no evidence of metasedimentary layers, and the local presence of feldspar megacrysts (El Tenebroso), suggest that this gneiss type might be a highly strained granitic orthogneiss.

GRANITIC ORTHOGNEISSES:

Granitic augen gneisses / foliated megacrystic granites (Fig.6.14):

These rocks show a variation from augen gneisses to foliated megacrystic granites depending on the amount of strain. They have a simple mineralogy with quartz, K-feldspar and plagioclase (An10-15) in granitic modal proportions and a variable proportion of biotite. Also common is the presence of metamorphic sillimanite (fibrolite), garnet and cordierite and retrograde muscovite. The megacrysts and augen are formed by tabular primary K-feldspars with Carlsbald twinning. Bellido et al (1991) also reported plagioclase

megacrysts in some of these rock types. The size of the megacrysts varies between 2 and 8 cm, with exceptional individuals in excess of 10 cm. The density (20% to 5%) of megacrysts, their size and the variable content of biotite in the matrix have prompted a complex classification scheme for these rocks (Azor et al., 1991; Bellido et al., 1991). This classification was not used because it is biased by the local amount of strain. However, there is a variation from biotite-rich facies to biotite-poor leucogranitic facies, which in the case of the Buitrago gneiss is observed within the same body.

These gneisses form distinct bodies (massifs) in the Sill+Kfs zone and outcrop over extensive areas all over the Western Domain of the Sierra de Guadarrama. Outcrops of similar looking augen-gneiss have also been found in the southwest corner of the Manjirón antiform. Three of these bodies have been studied in detail in the Buitrago area: the Buitrago, Cincovillas and Lozoya gneisses (Fig.6.6). The first one is a composite body of leucogranite and megacrystic granite whereas the other two are megacrystic granites.

Gneissic leucogranites (Fig.6.15):

These are garnet-bearing foliated granites, similar to the foliated leucogranites described in the Berzosa-Riaza shear zone. They have a widespread distribution both in the Manjiiron antiform (Sill+Ms zone) and in the Buitrago area (Sill+Kfs zone). They range from 50 cm thick dykes to kilometric bodies. They in most places appear in two different situations: as dykes or late intrusions in granitic augen-gneisses; as independent bodies intruding into the migmatitic paragneisses. The mineralogy in both cases is very similar with quartz + K-feldspar + plagioclase in granitic modal proportions, minor biotite and garnet, and scarce muscovite and sillimanite (fibrolite). In the largest bodies, variably strained feldspar megacrysts, 2 cm long on average, are commonly present. The fabric is defined by the orientation of the mica flakes and a gneissosity defined by feldspar-rich

domains. In constrast with the augen gneisses, there is no clear evidence of migmatization in these rocks.

The gneissic leucogranites associated with the augen gneisses are very common in the Buitrago gneiss, where they make up to >30% of the exposure (Fig.6.6). In general they have aplitic to equigranular facies and in most cases contain garnet porphyroblasts. They range from small metric aplitic dykes, clearly intrusive into country rock augen-gneiss, to kilometer scale leucogranite. These leucogranites have been interpreted as pre-Variscan late stage differenciates of the augen gneisses (Bellido et al., 1981; 1991).

The second type appears as individual decameter to kilometer-scale intrusions. The largest one is the Horcajuelo orthogneiss (Fig. 6.6), which occupies the northern half of the Manjirón antiform (Sill+Ms zone), from Paredes to Horcajuelo. This is a 7 Km long leucogranite with a well defined gneissosity and a migmatitic envelope, locally resembling a diatexite. South of Gandullas, along the Puentes Viejas dam, there is a similar body of smaller scale but also with a migmatitic envelope (Sill+Ms zone). In this case the migmatites merge with the leucogranite, both of which are deformed by the D2 phase. Therefore, it is possible that some of the migmatites around these bodies might have been generated during the intrusion of the leucogranites, either by local anatexis or by granitic injections. Although generally considered pre-Variscan, it is possible that some of these leucogranites might be granitic mobilizates produced during Variscan peak metamorphism.

6.5.4.- La Cabrera granite (Late Variscan pluton) and late intrusions:

The La Cabrera granite (Bellido et al., 1981; 1991) outcrops in the southern part of the area of study over a 20 Km long and 10 Km wide area. It is undeformed and has a post-

tectonic character, sealing the Berzosa-Riaza shear zone and cross cutting the structures and metamorphic isograds of the Western Guadarrama domain (Fig. 6.3). Conditions of 1 Kb and 660°C for its contact metamorphism indicate that it was emplaced when both the Eastern and Western Guadarrama domains were at the same crustal level.

This felsic pluton has two main facies: a coarse-medium grained granite and a fine-grained leucogranite. The dominant coarse - medium-grained granitic facies is composed of quartz, K-feldspar, plagioclase (An20-30) and biotite, and has an equigranular texture with local heterogranular and megacrystic facies, as well as minor granodioritic end members. This facies has a Rb-Sr whole rock isochron age of 315±14 Ma (Vialette et al., 1981). The fine-grained leucogranite outcrops in the core of the intrusion, and has an equigranular texture composed of quartz, K-feldspar, plagioclase (An13-17) and biotite. It has a Rb-Sr whole rock isochron age of 288±5 Ma (Vialette et al., 1981).

Other late intrusions:

* *Porphyritic dykes:* These are brown / green porphyritic dykes with K-feldspar and plagioclase phenocrysts and chilled margins. They contain quartz, K-feldspar, plagioclase (An 12-33) and biotite in granodioritic modal proportions (Bellido et al., 1991). Locally they also have minor amphibole and orthopyroxene. These dykes form a NW-SE swarm which cross-cuts the La Cabrera granite and its gneissic country rock; there are also minor antithetic dykes with a NE-SW trend. According to Bellido et al. (1991) they are not genetically related with the La Cabrera granite.

* *Quartz veins:* Late large-scale quartz veins have been only found in the Buitrago gneiss. These are 2 to 3 meters wide and less than 500 meters long veins with a NW-SE trend. Bellido et al (1991) also reported similar veins with a NE-SW trend and considered these two set of meter-scale veins to be associated with late fracturing.

6.6.-PRE-VARISCAN EVOLUTION: U-Pb evidence for a major Early Ordovician felsic magmatic event in the Sierra de Guadarrama.-

6.6.1.- Introduction.-

The Sierra de Guadarrama has a wide variety of pre-Variscan orthogneisses, which have been correlated with similar rock types along the Ollo de Sapo Domain of the Central Iberian Zone (Azor et al., 1992). The Precambrian (Cadomian) versus the Early Ordovician protolith age of these rocks is controversial in the Sierra de Guadarrama (Wildberg et al, 1989 vs. Vialette et al., 1986, 1987) and the rest of the Ollo de Sapo domain (Gebauer et al., 1993 vs. Azor et al., 1992). Given the variety of rock types, it was important not only to resolve the protolith ages but to clarify the potential problems derived from speculative correlations between rocks from different crustal levels with different volcanic and plutonic protoliths (e.g., Azor et al., 1992; Navidad et al., 1992). For this reason the area around the Berzosa-Riaza shear zone (BRSZ) was selected for this kind of study.

The BRSZ exposes an attenuated mid-crustal section (Sill-Ky zone) separating the suprastructural Eastern Domain (Chl to St zones) from the high-grade infrastructure of the Western Guadarrama Domain (Sill+Kfs zone). Therefore, this area offers an exceptional opportunity to sample, in a single cross-section, pre-Variscan gneisses from different crustal levels. The rocks selected for this study are representative of the main types of pre-Variscan orthogneisses of the Sierra de Guadarrama (Bellido et al., 1981; Navidad et al., 1992): the volcaniclastic Cardoso gneiss is the equivalent of the upper crustal Ollo de Sapo formation and Hiendelaencina gneiss; the Riaza gneiss is a lithological and structural correlative of the medium grade Nazaret-Berzosa-Pedrezuela orthogneisses in the BRSZ and similar gneisses in the Hiendelaencina antiform; the Buitrago gneiss clearly shows the complex relationships in the so-called "leucogneisses" of the Sill+Kfs zone; and the Lozoya

gneiss is also a classic example of the so-called "glandular gneisses " or "Morcuera gneisses" of the deeper structural levels of the Sierra de Guadarrama.

Regarding zircon morphology, the previous work of Wildberg et al (1989) in the Sierra de Guadarrama showed the presence of significant amounts of older zircon inheritance in these rocks. Therefore, only the best euhedral zircons were hand-picked under the microscope for analysis. To minimize the problems arising from zircon inheritance, the zircon selection was restricted to the best quality, four-sided, needle-like, euhedral prisms with a length/width ratio of 1:7 to 1:10. This type of zircon morphology is unlikely to grow over an inherited core (Gneiss type IV zircon of Vavra, 1990). However, their large surface to volume ratio makes them more susceptible to diffusive Pb-loss. This was minimized with extensive use of the air abrasion technique of Krogh (1982), by mechanically removing the outer surface of the crystals. Unabraded fractions were analyzed to assure the definition and trace of the discordia lines.

Details of the U-Pb analytical procedure, including sample preparation, are provided in appendix A.1.

6.6.2.- U-Pb geochronological results (Table 6.1):

EASTERN GUADARRAMA DOMAIN:

Cardoso Gneiss:

This rock has been heterogeneously sheared and metamorphosed to staurolite grade. Porphyroclasts consisting of 10 to 2 mm fragments of plagioclase, K-feldspar, microgranite and subrounded primary blue quartz are distributed in a micaceous matrix (Fig. 6.16). This, plus the gradual transition into the overlying and underlying

metasedimentary rocks, coupled with the intercalations of mica schists and para-amphibolites, indicate a volcanogenic origin, possibly as a felsic tuff.

Of eight zircon fractions analysed, Z1 is concordant anchoring the Z1-Z4 discordia line at **480±2 Ma**, the interpreted age of extrusion (Fig. 6.16). The upper intercept at 2645 Ma and intercepts of Z1-Z7 and Z1-Z8 (not shown) suggest the presence of 2.0-2.6 Ga inheritance.

Riaza Gneiss:

This is a heterogeneously mylonitized megacrystic granitic orthogneiss (Fig. 6.17) with minor leucogranitic facies (Arenas et al., 1982). This gneiss is in contact with both the metasedimentary rocks of the staurolite and sillimanite (kyanite) zones along a high strain zone which has transposed any primary relationships. The U-Pb sample is a mylonitic two-mica megacrystic granite with 2 cm long K-feldspar megacrysts.

Fractions Z1, Z2, Z3, Z5 and Z6 have been intensively abraded and define two independent discordia lines, line Z1-Z4 and line Z1-Z6. The line Z1 to Z4 provides an upper intercept of **468+16/-8 Ma** which is interpreted as the best estimate for the protolith age. The line Z1 to Z6 suggests the presence of Archean (2.6 Ga) inheritance (Fig.6.17). Analyses Z7 and Z8 are interpreted to contain a minor inherited component and have undergone Pb loss.

WESTERN GUADARRAMA DOMAIN:

Buitrago gneiss:

This rock has been interpreted both as a pre-Variscan orthogneiss (Bellido et al., 1991) and a Variscan anatexite (Fernández Casals, 1979). Traditionally called a "leucogneiss"

(Bellido et al., 1981; Azor et al., 1990), the Buitrago gneiss is composed of two rock types, a biotite-bearing augen-gneiss (Sample BU-1) and a garnet-bearing foliated leucogranite (Samples BU-2 and PIB-1). The augen gneiss has a composite solid-state fabric defined by stiff primary K-feldspar porphyroclasts (Ø = 2-4 cm) and ductily deformed quartzo-feldspathic domains. Sample BU-2 is an aplitic vein intrusive in sample BU-1 which mimics an anatectic vein (Fig.6.18). Sample PIB-1 is a foliated leucogranite dyke intrusive into the augen-gneiss. Although samples BU-2 and PIB-1 have clear intrusive relationships, cross-cutting relationships with the tectonic fabric in the augen gneiss are not seen.

Sample BU-1 (Fig 6.18; 6.19): foliated megacrystic granite (Buitrago de Lozoya)

The discordia line Z1-Z6 (25% probability of fit; v. Davis, 1982) has an upper intercept of **488+10/-8 Ma** which is the best estimate for the protolith age (Fig.6.19). Analysis Z3 was not included in the regression of the discordia line as it is interpreted to show the combined effect of Pb loss and minor inheritance.

Sample BU-2 (Fig.6.18; 6.20): foliated aplitic vein intrusive into BU-1 (Buitrago de Lozoya)

With error expansion all five fractions define a discordia line (58% probability of fit) with an upper intercept of 482+16/-12 Ma. However, a Z1-Z2-Z5 discordia line with a higher probability of fit (76%) and an upper intercept of **482+8/-7 Ma** is preferred for the protolith age (Fig.6.20).

Sample PIB-1: Foliated leucogranite (Pinilla de Buitrago; Fig. 6.21)

Five fractions of abraded needle-like zircon (Table 1), define a discordia line with an upper intercept of **482+9/-8 Ma** for igneous crystallization (Fig.6.21). This protolith age

is coeval with samples BU-1 and BU-2 suggesting that the foliated leucogranites are a late magmatic phase differentiate. This is also consistent with the high U content of the zircons compared to those of sample BU-1 (Table 6.1)

Lozoya gneiss (LO-1): Augen gneiss / granitic orthogneiss (Fig. 6.22).

This is a ductily-deformed biotite-bearing augen gneiss containing primary feldspar augen up to 7cm in diameter. This rock type covers most of the Western Guadarrama Domain with an approximate areal extent of 1000 km^2. It is also locally known as "Morcuera gneiss" (Fernández Casals, 1974) or "feldspathic glandular gneiss" (Navidad et al., 1992) and "meso-melanocratic orthogneiss", where strongly deformed (Navidad et al., 1992). The dated sample was collected from the type locality proposed for the Morcuera gneiss by Casquet et al. (stop 3.1. and figure 16 of Alvaro et al., 1981). The sample has metamorphic cordierite and sillimanite (2nd sillimanite / cordierite zone).

Of five zircon fractions analyzed, Z1 is concordant providing a protolith age of **477±4 Ma** (Fig. 6.22a). Three monazite and one xenotime fraction define an independent discordia line with an upper intercept of 480±40 Ma confirming the protolith age (Fig. 6.22b). The concordant monazite and xenotime pin the lower intercept at **322±2 Ma**, which represents the age of Variscan LP/HT metamorphism. The large grain size of the concordant monazite (M1, Table 6.1) suggests that the monazite-xenotime discordia line is a mixing line between igneous and metamorphic monazite, rather than variable resetting of igneous monazite. The Z1-Z2-Z3 discordia line has a lower intercept of 221 Ma with no apparent geological meaning, possibly due to a combination of Variscan partial resetting and Mesozoic Pb-loss (Fig.6.22b). Analysis Z4 reflects combined Pb loss and inheritance; a line Z1-Z5 (Fig.6.22c) suggests the presence of 2.6 Ga inheritance.

6.6.3.- Discussion: Geological significance of the new U-Pb ages:

The U-Pb zircon ages for the Riaza gneiss (468+16/-8 Ma), the Buitrago gneiss (488+10/-8 Ma, megacrystic facies; 482+8/-7 Ma and 482+9/-8 Ma, aplitic and leucogranitic facies) and the Lozoya gneiss (477±4 Ma) are representative of the main types of pre-Variscan orthogneisses of the Sierra de Guadarrama (Fig.6.23), indicating the presence of an important granitic intrusive event in the Arenig (485-470 Ma; time scale of Tucker and McKerrow, 1995). The concordant 480±2 Ma U-Pb zircon age of the volcaniclastic Cardoso gneiss invalidates the previously accepted age of 540±30 Ma (Wildberg et al., 1989). This new age indicates that volcanism and plutonism were coeval and constrains the lower limit of the Arenig "Sardic" unconformity in the Sierra de Guadarrama (Soers, 1972; Gonzalez Lodeiro, 1981), indicating a close relationship between the Sardic deformation and the Arenig felsic magmatism. It also indicates that the overlying Constante formation is not Tremadocian but Arenig in age. The mixing line between igneous and metamorphic monazite and xenotime of the Lozoya gneiss not only confirms the Arenig protolith age, but provides the first reliable age, 322±2 Ma, for the Variscan low P / high T metamorphic overprint of the gneisses of the Western Guadarrama Domain. This last point will be further discussed in the Variscan section.

These U-Pb ages support the Rb-Sr data of Vialette et al (1986; 1987), suggesting that most of the pre-Variscan orthogneisses of the Sierra de Guadarrama are Early Ordovician. This, however, does not exclude the presence of unidentified, older orthogneisses.

6.7.- VARISCAN TECTONOTHERMAL EVOLUTION OF THE SOMOSIERRA SECTOR OF THE SIERRA DE GUADARRAMA: Structural, metamorphic and U-Pb geochronological constraints.

6.7.1.- Introduction

This section presents the structural, metamorphic and geochronological data used to constrain the Variscan tectonothermal evolution of the Somosierra area of the Sierra de Guadarrama. The data are presented in the order outlined before and will be followed by a discussion focusing on the timing and character of the Variscan metamorphic and deformational events.

6.7.2.- Structural evolution:

The structural evolution of the Somosierra sector of the Sierra de Guadarrama can be described in terms of two major deformational events, D1 and D2. D1 had a compressional character and was responsible for the regional crustal overthickening (Fernández Casals, 1979; Macaya et al., 1991). In the area of study, the D1 macrostructure has been completely obliterated by the D2 event. D2 is a major ductile shearing event, during which the Berzosa-Riaza shear zone was produced. This event is widespread in the gneissic infrastructure, Western Domain, and in the lower structural levels of the Eastern Guadarrama domain. D2 is coeval with a low pressure /high temperature overprint of the inter D1-D2 Barrovian metamorphic mineral assemblages (Fernández Casals, 1979; Bellido et al., 1981; Casquet et al., 1983; Macaya et al., 1991; Hernaiz Huerta et al., 1996).

Historically, the first detailed structural analysis of this area of the Sierra de Guadarrama (Fernández Casals, 1979) considered only two main phases of deformation (D1 and D2), followed by minor late deformation (D3). Gonzalez Lodeiro (1981)

incorporated the model from the West Asturian Leonese Zone (WALZ) of three main phases of Variscan deformation, interpreting the D3 phase, as in the WALZ, as backfolding. It should be noted that in the Sierra de Guadarrama, like in the WALZ, only F1-F3 fold interference patterns were recognized in the low grade rocks (Gonzalez Casado, 1988). The D2 phase was, as in the WALZ (Basal shear zone of the Mondoñedo nappe, Martínez Catalán et al., 1990), restricted to major shear zones such as the Berzosa-Riaza shear zone. Subsequent workers extended the D3 backfolding to the gneissic infrastructure (Capote et al., 1983; Macaya et al., 1991; Azor et al., 1991 a,b; Bellido et al., 1991). This scheme however, was questioned by Hernaiz Huerta et al. (1996) who interpreted the Berzosa-Riaza shear zone as a major ductile extensional shear zone. Such a possibility was timidly advanced by Gonzalez Casado and Casquet (1987). This new interpretation eliminates the necessity of D3 backfolding to explain the west vergence of the regional macrostructures.

In the following description, the so-called high temperature D3 structures (Casquet et al., 1983; Macaya et al., 1991; Azor et al., 1991; Bellido et al., 1991) are interpreted to be formed by progressive deformation during D2. The term D3 is used to described late, low grade deformational features. This scheme coincides with the one independently developed by Hernaiz Huerta et al. (in press,a and b) in the Cardoso antiform (Fig. 6.24), and it is similar to the one initially proposed by Fernández Casals (1979). Most of the author's structural work was concentrated in the area between the Hiruela mountain pass, upper levels of the BRSZ, and the Rio Sequillo dam, west of Buitrago (Fig.6.25).

D1 deformation:

The D1 event is well defined in the supracrustal Eastern Guadarrama Domain, where it deforms the Mid Paleozoic sedimentary sequence. In the gneissic Western Guadarrama

domain, this deformation preceded the Barrovian metamorphism and the low pressure / high temperature metamorphic overprint. Therefore, all fabrics preceding peak metamorphic conditions are considered to be D1. This might include several subphases of deformation which could not be properly defined due to the intense D2 overprint.

D1 in the gneissic infrastructure is considered Variscan in age. Pre-Variscan fabrics could not be identified during this study or in previous studies (eg. Macaya et al., 1991). But as a cautionary note, this does not mean that relicts of them might not be present in certain parts of the Sierra de Guadarrama or in other gneissic complexes of the Spanish Central System (Macaya et al., 1991).

Eastern Guadarrama Domain:

This domain contains two well defined D1 macrostructures, the Majalrayo syncline and the Galbe de Sobre anticline (Fig.6.2; Macaya et al., 1991; Hernaiz Huerta et al., 1996). Both structures are east of the area of study and have an axial planar, S1, slaty cleavage and associated minor F1 folds indicating an east vergence during the D1 Variscan compression.

In the area of study, the D1 structures are overprinted by the D2 deformation. In the upper structural levels of the eastern flank of the El Cardoso antiform, the S1 fabrics are crenulated by D2 (Fig. 6.24; crenulation band of Hernaiz Huerta et al., 1996). Towards the lower structural levels of the Eastern domain, in the Cardoso antiform, the S1 fabrics are completely transposed by the D2 deformation. Relicts of the S1 fabric are only preserved as a partially transposed fabric in low strain areas, fold hinges in F1-F2 interference folds and as internal inclusion trails (Si) in pre-D2 porphyroblasts. Therefore, the resultant main fabric (Sp) is an S0-S1-S2 composite fabric (Fig. 6.7a).

Western Guadarrama Domain:

West of the area of study, Macaya et al (1991) described discrete D1 shear zones, affecting mostly metasedimentary rocks, separating kilometer-scale wedges of augen-gneisses. They inferred that these east-vergent wedges of augen-gneisses and the associated D1 shear zones formed the D1 macrostructure of this domain.

In the area of study, Azor et al. (1991b) suggested the presence of an F1 recumbent syncline in the Buitrago area. However, such structure was inferred on the assumption of an oversimplified stratigraphy formed by orthogneisses overlain by metasedimentary rocks, without taking into account the constraints imposed by the metamorphic zonation. During this study no major F1 macrostructures were recognized in the field due to the intense D2 overprint, this also coincides with the observations of Fernández Casals (1979).

Although D1 macrostructures could not be reconstructed, there is abundant evidence for D1 structures in all structural levels of the Western Guadarrama Domain. In the following description the main gneissosity (Gn), or compositional banding, is considered as a composite S0-S1 fabric (Fig.6.8).

In the sillimanite-kyanite-bearing metasedimentary rocks of the Berzosa-Riaza shear zone, D1 structural features are preserved as intrafolial folds in the main foliation (S2; Fig. 6.7c). Inclusion trails (Si) in garnet and kyanite porphyroblasts also indicate the presence of an earlier S1 fabric.

Relicts of D1 structures are best preserved in discrete levels of the Sill+Ms metapsammites of the Madarquillos shear zone. Locally, it is possible to observe a penetrative S1 fabric cross cutting S0, both being overprinted by F2 asymmetric folds with an axial planar S2 fabric. However, there is not enough high quality outcrop to

convincingly trace the D1 structure. In this lithological band there are also abundant F1-F2 interference figures.

In the sillimanite-mica schists and the sillimanite+muscovite metasedimentary rocks of the Manjirón antiform, the presence of variably refolded quartz veins is also common. Some of these veins cross-cut S0 forming part of a composite S0-S1-S2 fabric, and are variably refolded by three local phases of folding. The structural significance of these veins is uncertain, i.e: dilatational veins or quartz segregations along a preexisting foliation. It should be noted that such veins were not observed in the migmatitic lithologies.

In the gneissic and migmatitic lithologies of the Manjirón antiform and the Buitrago area, the D1 structural features are best preserved inside the metric-scale calc-silicate boudins. They consist of a gneissosity (S0-S1?) defined by compositional alternations of garnet-rich and clinopyroxene-rich layers with granoblastic texture, which has also been folded (F1) under the same high grade conditions (Fig. 6.12). In the quartzo-feldspathic lithologies there are F1-F2 interference patterns with centrimetric scale, F1, isoclinal folds (Fig.6.7; 6.8). In many cases, these are intrafolial folds which evidence the composite (S0-S1) character of the main gneissosity. Also the main gneissic fabric in the El Villar type biotite-bearing migmatites (subsolidus migmatites?; section 6.5.3) is overprinted and partially transposed by the D2 event, suggesting that the gneissosity is partially D1.

The leucosomes of the anatectic migmatites of the Buitrago area (Fig. 6.11, Sill+Kfs zone) form stromatic migmatites which are aligned with the compositional banding in the nearby quartzo-feldspathic lithologies, and have been folded and sheared during D2. Most of them, as already recognized by Fernández Casals (1979), appear to be late- to post-D1 and some show refolding suggesting that they might have already formed during D1.

However, as pointed out by McLellan (1984), such refolding is common during syn-magmatic deformation of migmatites with more than 30% melt.

D2 deformation:

This major ductile shearing event affected the gneissic Western Guadarrama Domain and the deeper structural levels of the Eastern Guadarrama Domain. All previous authors agree that the juxtaposition of the Eastern and Western Guadarrama Domains took place along the Berzosa-Riaza shear zone during this event (i.e. Fernández Casals, 1979; Bellido et al., 1981; Macaya et al., 1991; Hernaiz Huerta et al., 1996). Other structures developed during D2 are the Cardoso antiform in the Eastern Domain (Hernaiz Huerta et al., 1996) and the Manjirón antiform and the Madarquillos shear zone in the Western Domain (Fernández Casals, 1979).

El Cardoso antiform and the D2 crenulation band (Eastern Guadarrama Domain):

The Cardoso antiform is the result of the overprint of the D2 deformation on the suprastructural Eastern Guadarrama Domain, whereas the crenulation band (Hernaiz Huerta et al., 1996) is the uppermost part of the D2 deformational front. The elements of the crenulation band have been described in detail by Fernández Casal (1979), Gonzalez Casado and Casquet (1987) and Hernaiz Huerta et al. (1996), all of which considered to be a D2 structure. Gonzalez Lodeiro et al. (1988), however, suggested that the crenulation band was a D3 structure and interpreted the Cardoso antiform as D3, but indicated the D2 character of the shear zone in the core and western limb of the antiform.

Across the crenulation band, the strain of the D2 deformation increases structurally downwards, where the D2 crenulation cleavage (Fig. 6.26) passes into a D2 ductile

mylonitic fabric (S2; Fig.6.7a,b; 6.26). The S2 mylonitic fabric transposes the SO and the S1 fabrics, defining the Berzosa-Riaza shear zone. The S2 mylonitic foliation is axial planar to the Cardoso antiform, indicating its D2 character (Fig.6.24; Hernaiz Huerta et al., 1996) and it is not folded by a later D3 event as proposed by Gonzalez Lodeiro et al. (1988). This last point was confirmed during an east-west reconnaissance traverse passing through the core of the antiform, north of El Cardoso.

The Berzosa-Riaza shear zone (Eastern and Western Guadarrama domains):

The Berzosa-Riaza shear zone is characterized by a well developed ductile mylonitic foliation (S2), which transposes the previous structures into parallelism. This foliation trends 17° to 18° N in both the Eastern (St-zone) and the Western Domains (Sill-Ky zone). In the Cardoso antiform and the Eastern Domain, S2 plunges 54°E on average (Hernaiz Huerta et al., 1996); whereas in the Sill (Ky) zone it is shallower, plunging 30°E on average (Fig.6.27 and 6.28).

In the St-zone (Eastern Guadarrama domain) the S2 foliation is defined by the orientation of biotite and muscovite (Fig.6.26). This fabric is coeval with the growth of staurolite, indicating amphibolite facies conditions. The mineral lineation and stretching lineation (L2) are defined by quartz-rich pressure shadows with a mica-rich envelope around garnet, staurolite and chloritoid porphyroblasts (Fig.6.7b). The staurolite porphyroblasts are in most cases subparallel to the lineation. This lineation is oblique to the dip of the S2 foliation and has an average orientation and dip of 150/47. There is extensive development of asymmetric pressure shadows around porphyroblasts in the metasedimentary rocks and the porphyroclasts of the Cardoso gneiss. They all indicate a shear sense of top down to the SE which is also consistent with S-C and micafish structures. Towards the top of the shear zone there are abundant trails of sheath folds in the

more competent quartzitic lithologies, with the same shear sense (Hernaiz Huerta et al., 1996). Boudinage is also parallel to the lineation.

In the Sill-Ky zone, the S2 fabric is defined by oriented fibrolite and biotite which are growing at the expense of the inter D1-D2 kyanite. Muscovite is stable and also defines the S2 foliation in association with sillimanite + biotite. Therefore, in this zone the S2 is a 1st - Sill zone fabric (Fig.6.26). The mineral lineation in the metasedimentary rocks is defined by elongated fibrolite, quartz-rich pressure shadows, reoriented kyanite porphyroblasts and quartz ribbons and striations in sheared quartz-veins. In the orthogneisses, particularly the augen-gneisses, the lineation is defined by quartzo-feldspathic ribbons around feldspar porphyroclasts. In this zone boudinage parallel to the mineral lineation (Lmin) is widespread, indicating that this is a stretching lineation. This lineation is oblique to the dip of the S2 foliation and has an average orientation and dip of 151/26 (Fig.6.27 and 6.28). Kinematic indicators such as asymmetric pressure shadows, winged porphyoclasts, asymmetric boudinaged, S/C structures and shear bands (C' planes; Hanmer and Passchier, 1991), indicate a shear sense of top down to the SE.

The Manjirón antiform, Western Guadarrama Domain.

The Manjirón antiform is a dome-like structure whose northern half is formed by the Horcajuelo gneissic leucogranite and its migmatitic envelope. The southern half is formed by migmatitic paragneisses, minor calc-silicate rocks and leucogranites, and the El Villar type biotite-bearing migmatites (subsolidus migmatites?, section 6.5.3). This structure, like the BRSZ, is cross-cut to the south by the La Cabrera granite (Fig.6.3; 6.25).

In the northern closure of the Manjirón antiform, the structural data from the metasedimentary rocks in the limbs and the orthogneisses and migmatites in the core indicate that the main foliation (S1) defines a theoretical fold with a fold axis (144/37)

parallel to that of the minor F2 folds (Fig.6.27). These minor F2 folds crenulate S1 in the mica schist lithologies and overprint F1 folds in the psammitic lithologies. The plunge of the F2 folds is also parallel to the mineral lineations (L min av., 139/33; Fig.6.27). The same relationships are also found in the cross section along the Cocinillas river (Fig.6.28). In this case the gneissosity in the migmatites (Gn) is folded with a good agreement between the F2 fold axis and the theoretical fold. This is also confirmed by the distribution of the foliation in the Horcajuelo orthogneiss (Fig.6.28). To the south, in the area around the head of the Puentes Viejas dam, gneissosity and F2 folds display the same relationships, with parallelism between the F2 fold axis and the mineral lineation defined by sillimanite and quartz (Fig.6.28). It should be noted that south of Paredes the contact between the BRSZ and the migmatitic gneisses is a high strain zone with an intense D2 transposition of the migmatites into a straight gneiss. Planar fabrics are also dominant south of Manjirón in the El Villar type biotite-bearing migmatites and the associated lithologies (Fig.6.29).

Most of the asymmetric folds in the Manjirón antiform are Z-shaped (Fig.6.8), suggesting a shear sense of top to the S-SE. These folds have muscovite and sillimanite stable and folded anatectic leucosomes (Fig.6.11). This shear sense is also confirmed by shear bands (C' planes) with sillimanite. This indicates that movement took place in metamorphic conditions between the 1st and the 2nd sillimanite isograds. But the best kinematic indicators for the D2 deformation are provided by the asymmetric calc-silicate boudins at the base of the Puentes Viejas dam. The retrogression of the garnet-clinopyroxene mineral assemblages to plagioclase-amphibole confirms the amphibolite facies metamorphic conditions of the D2 deformation. Boudin asymmetry and amphibole mineral lineations indicate a shear sense of top to the south. The D2 mylonitic foliation in the migmatites surrounds these boudins and is parallel to the large limbs of the asymmetric F2 folds. Trails of asymmetric folds develop around the largest boudins , which partially

control the plunge of the fold axis. It should be noted that the D2 foliation also surrounds a large megaboudin of El Villar type biotite-bearing migmatite associated with the calc-silicate boudins.

The Madarquillos shear zone, Western Guadarrama Domain:

The Madarquillos shear zone is a structure originally defined by Fernández Casals (1979) as a D2 shear zone, even though she called it a synform. This structure is presently defined by the trace of the sillimanite + muscovite metapsammites and mica schists. It extends from south of Manjirón, where it is poorly exposed, to the northern closure of the Manjirón antiform (Fig. 6.3 and 6.25). At the Puentes Viejas dam the structure is bordered to the east by a high-temperature (sillimanite -bearing fabric), subvertical, strike-slip shear zone (Fig.6.25), and to the west it presents a gradual transition to migmatitic lithologies which are sharply separated from the gneisses of the Buitrago area by a 10 to 30 meter wide band dominated by L-fabrics and quartz-rods (the L-fabric band, Fig.6.25). In the Madarquillos river section and farther north, the western border of the Madarquillos shear zone is a high-strain D2 shear zone overprinting the Sill+Kfs zone gneissic and migmatitic lithologies of the Buitrago area (Fig. 6.25).

The main foliation in this shear zone is an S2 schistosity / compositional banding produced by the transposition and crenulation of S0 and S1(Fig.6.30). The S2 fabric is axial planar to the F2 folds in the metapsammites (Fig.6.31). In the sillimanite + muscovite mica schists there are clear relationships between the D2 boudins and the F2 folds, suggesting that both were coeval (Fig.6.32 and 6.33). The F2 folds are tight to isoclinal folds with S0 generally parallel to S2 along the fold limbs (Fig. 6.31). The main foliation (S0-S2) has an average trend and dip of 17/38E to 8/35E (Fig.6.34). The mineral lineation is defined by centimetric elongated patches of fibrolitic sillimanite and quartz oblique to the

dip of the main foliation (150/24 to 138/32 on average; Fig.6.34). The axis of the F2 folds are subparallel to the mineral lineation (154/28 to 135/30 on average; Fig.6.34). Shear bands with stable sillimanite (C' planes; Fig.6.35) are also commonly developed with an average trend and dip of 22/57E (Fig. 6.34). In the "L-fabric band" the linear fabric plunges 151/26 (Fig.6.34; 6.36), the shear sense is poorly defined but seems to be top up to the NW. It is, however, unclear if this is a D2 structure or a later reworking.

In the Mardarquillos synform there are abundant kinematic indicators such as S/C structures with a very small angle between S and C planes, shear bands (C' planes), asymmetric boudinage and asymmetric folding of variably oriented quartz and pegmatitic veins (Fig.6.32). This variety of kinematic indicators permitted the independent confirmation of the shear sense. In the eastern side and center of the Madarquillos shear zone the shear sense is top down to the SE (Fig.6.32; 6.35). In the Madarquillos river section, although locally there are a few kinematic indicators suggesting top up to the NW (Fig.6.37), most of them are consistent with top down to the SE tectonic transport (Fig.6.35). There is, however, a significant area with D2 shear sense top-up to the NW in the Puentes Viejas dam between the metapsammites and the L-fabric band (Fig. 6.25; 6.37). Structurally below, in the Rio Madarquillos section, the migmatites and gneisses of the Buitrago area were transposed into straight gneisses during a top down to the SE shearing (Fig. 6.33). This shearing, like the one in the Madarquillos shear zone took place in metamorphic conditions of the Sill+Ms zone.

Buitrago area, Western Domain:

This area corresponds to the sillimanite + K-feldspar gneisses west of the Madarquillos shear zone. The D2 deformation in this area has a heterogeneous character. The deformation in the migmatitic paragneisses produced complex shear zones such as the

"high temperature deformation band" exposed along the Puentes Viejas dam, between Buitrago and the L- fabric band (Fig.6.25). This is a band with a complex ductile deformation and fabrics developed under metamorphic conditions of the Sill+Kfs zone. The granitic orthogneisses in the Buitrago area, although heterogeneously deformed, do not show the complex folding observed in the surrounding paragneisses.

The migmatites and quartzo-feldspathic paragneisses in the "high temperature deformation band" form metric-to decametric-scale, boudin-like, lenses separated by ductile shear zones (Fig.6.38). Inside these lenses the gneissosity is folded whereas to the outside it is transposed by D2 shear zones, indicating an important flattening component associated with the D2 non-coaxial shearing (Fig. 6.39). Some of these lenses show complex fold interference patterns and disharmonic folding but most anatectic migmatites are harmonically folded and sheared. Muscovite is not present in the fabric indicating conditions for the D2 deformation in the Sill+Kfs zone (Fig.6.30). In the shear zones the gneissosity (S2 mylonitic fabrics plus transposed S0-S1) has a NE trend and a shallow plunge to the SE (Fig.6.34). The mineral lineations, defined by fibrolite, are almost parallel to the dip of the S2 ductile fabrics, plunging 147/22 on average (Fig.6.34). The distribution of the poles to the gneissosity suggests folding along a 145/23 theoretical fold axis. This theoretical fold axis is parallel to the orientation of the F2 folds (151/27; Fig.6.34). These F2 folds were produced inside the more competent lenses, and are also parallel to the mineral/stretching lineation in the shear zones (Fig.6.39). Shear bands (C'planes) are common particularly in the more competent quartzo-feldspathic lithologies (Fig.6.38; 6.40). They have an average trend and dip of 46/44S, almost normal to the mineral lineations (Fig.6.34). These shear bands or C' planes have sillimanite stable in the shear planes, and locally are filled by late pegmatites (Fig.6.40). These late pegmatites are

relatively common and cross-cut the S2 foliation (Fig. 6.41), confirming the high temperature conditions.

The granitic orthogneisses are characterized by a composite planar fabric which formed around the more competent feldspar porphyroclasts, and an associated mineral/stretching lineation defined by fibrolite and quartzo-feldspathic aggregates (Fig. 6.14). Metric boudins, parallel to the Lmin, were formed during the heterogeneous D2 deformation. Antithetic shear bands are common near the boudin necks; the dominant shear bands have an average trend and plunge of 37/50E (Fig.6.34). Folding is restricted to the nearby migmatitic lithologies (Fig.6.11). In general the stretching lineation in both the Buitrago and Cincovillas gneisses shows a remarkable similarity plunging 160/26 on average. This is slightly oblique to the dip of the average gneissosity in the Buitrago gneiss, 20/32E, which is similar to that in the high strain zone in the Cincovillas gneiss, whereas the low strain zones of the Cincovillas gneiss have a flat lying foliation (Fig.6.34). The F2 fold axis in the nearby migmatitic gneisses are subparallel to the Lmin in the orthogneisses (153/32; Fig.6.34). This is consistent with the D2 character of the deformation in the orthogneisses, as already stated by Fernández Casals (1979). In the area around El Cuadrón (Fig.6.33), the scatter of the structural data has been attributed to the intrusion of the La Cabrera granite (Fernández Casals, 1979).

Late deformations (D3):

The later deformational events have been grouped under a D3 deformational phase. This phase has a greenschist facies retrograde character and a minor importance compared to the main D1 and D2 phases.

The most common structures are kink-folds, upright crenulations and discrete brittle faults (Fig.6.42). The most significant macrostructures are the greenschist facies Montejo

and El Cervunal detachments. The Montejo detachment is a minor reactivation of the western border of the Berzosa-Riaza shear zone. Most of this reworking took place along a phyllonite band in the northern extreme of the BRSZ, in the Arroyo de la Garganta (Hernaiz Huerta and Escuder Viruete, pers comm.). In the area of study, only small discrete reactivations were recognized (Fig.6.42). The Cervunal detachment however, is a continuous greenschist facies brittle-ductile fault zone which can be traced from Riaza to Berzosa (Fig.6.3). It has a band of elongated augen-gneisses (Riaza, Nazaret and Berzosa gneisses) in its footwall, whereas the hangingwall is formed by the staurolite-mica schists of the Eastern Guadarrama Domain. This fault zone is well exposed west of El Cardoso, where an east-dipping high angle foliation cross-cuts the S2 fabric. Also near the Hermita de Nazaret a metric mylonite zone can be recognized separating the Nazaret gneiss from the staurolite-mica schists. Gonzalez Casado and Casquet (1987; 1988) reported greenschist facies shear bands along the trace of the detachment, but their relationship with the detachment is uncertain.

Structural evolution, discussion.-

The proposed sequence of deformational events is very similar to the one originally proposed by Fernández Casals (1979). The D1, responsible for the crustal overthickening, has been obliterated by the later D2 event, and it is only well preserved in the suprastructural Eastern Domain, east of the area of study. The D2 event in the area of study was associated with large scale ductile shearing. This shearing was concentrated along the Berzosa-Riaza shear zone but it is also widespread in the gneissic infrastructure, as recognized by other workers (i.e. Macaya et al., 1991; Azor et al., 1991). The field area covers staurolite-chloritoid mica schists in the Eastern Domain to sillimanite + K-feldspar migmatitic gneisses in the Western Domain. The D2 foliation, L2 lineation and F2 fold axes in all these rocks have a similar trend with a consistent shear sense of top to the SE

(Fig.6.25, 6.27, 6.28, 6.34). This suggests that the D2 deformation was associated with an oblique extensional event.

An interpretative E-W cross section along the area of study (Fig.6.43) shows that the structural features can be explained considering D2 as a progressive extensional event. This could account for the metric-scale, east vergent F2 folds in the gneisses of the Western Domain without requiring the D3 back-folding event proposed by Capote et al. (1982), Macaya et al. (1991) and Azor et al. (1991a). These authors have indicated the parallelism between their L2 lineations and F3 folds and the consistent top to the SE tectonic transport of the D2 shearing. Such observations, however, are inconsistent with the D3 backfolding along N-S axis proposed by Azor et al. (1991a), since there is only a single set of SE trending L2 lineations and not two sets as expected (Fig. 6.28, 6.27, 6.34). The cross-section proposed here also accounts for the observations of important strain partitioning, with anastomosed shear zones separating competent lenses of quartzo-feldspathic gneisses, and resolves the thickness and extent of the lenses of augen-gneisses without large recumbent folds (Azor et al., 1991; Fig.6.43).

The interpretation of the D2 event as a progressive extensional shearing also explains the parallelism between L2 lineation and the F2 fold axes in the gneissic infrastructure by flattening combined with rotation and shearing of layers oblique to the shear plane. The similarity of trends between different structural levels implies that while extension took place, the deformation migrated to deeper and hotter structural levels under the same oblique extensional regime. This explains the common refolding of anatectic leucosomes and migmatites in both the Manjirón antiform and the Buitrago area. Some of these migmatites show disharmonic folding, suggesting that deformation took place in a magmatic state (McLellan, 1984). Given the post-D1 character of the anatexis, it is likely that anatexis took place during early stages of the D2 deformation and as the leucosomes

crystallized the migmatites began to behave like a Newtonian solid, developing harmonic folds.

D3 and late deformations are downplayed as minor reactivations and modifications of the D2 macrostructure, such as the late extensional reactivations along the Montejo and Cervunal detachments.

6.7.3.- Microfabric development and metamorphism.-

The relationships between metamorphic mineral growth and deformation are presented in this section. These relationships in the Buitrago-Riaza area have been described by López Ruiz et al (1975), Arenas et al. (1980), Casquet and Navidad (1985), Gonzalez Casado (1987), Bellido et al. (1991), Azor et al. (1991), Escuder Viruete et al. (1996) and Hernaiz Huerta et al (in press). It should be noted that the emphasis in this section is being put on the area mapped in detail (Fig. 6.25), i.e. from the chloritoid-staurolite transition to the Sill+Kfs zone.

Chlorite, biotite and garnet zones:

These three zones are located at the upper structural levels of the Somosierra sector of the Sierra de Guadarrama, outside the Berzosa-Riaza shear zone. The trace of the mineral isograds is deformed by the D2 event (Fig.6.44), confirming the syn-D1 or inter D1-D2 character of the mineral assemblages (Gonzalez Casado , 1987; Escuder Viruete et al., 1996). García Cacho (1973; in López Ruiz et al., 1975) described a rare ocurrence of kyanite within the biotite zone, which suggests pressures above 2.5 Kb (Chapter 10 of Spear, 1993).

Staurolite zone:

The staurolite-in isograd follows the trend of the mylonitic front of the Berzosa-Riaza shear zone. The staurolite zone outcrops between the mylonitic front and the Cervunal detachment (Fig.6.44). South of the Cardoso antiform the transition in to the staurolite zone is very sharp but within the antiform there is a wider zone (500 meter, approx.) with coexisting chloritoid and staurolite (Gonzaiez Casado et al., 1987). This transition is well exposed in the Hiruela mountain pass, where chloritoid porphyroblasts up to 3 cm long are partially transformed into Fe-chlorite, garnet and staurolite. There are also biotite porphyroblasts. Both biotite and chloritoid have an internal schistosity (S1?) defined by trails of quartz and opaque inclusions. In the case of chloritoid the internal schistosity is only partially transposed by the external schistosity (S2), indicating an inter D1-D2 and possibly an early D2 character (Fig.6.45). The garnet porphyroblasts also have an internal schistosity which is early- to syn-D2, there also are small euhedral garnets overgrowing chloritoid. These garnets are usually rimmed by chlorite, but they can be in direct contact with chloritoid. Staurolite is usually associated with chlorite and biotite, although locally it can be in direct contact with chloritoid (Fig.6.46). It should be noted that there is no new growth of biotite. The coexistance of biotite and chloritoid is perplexing because one of them should have been removed by reaction:

$$\text{Chloritoid} + \text{biotite} = \text{garnet} + \text{chlorite}$$

This suggests that this reaction has been overstepped but the effect of any extra components such as Mn (Droop and Harte, 1995; Mahar et al., 1997) is uncertain on the stability of biotite in this area. The new growth of staurolite, chlorite and garnet suggests removal of chloritoid by the discontinuous reaction:

$$\text{Chloritoid} = \text{garnet} + \text{chlorite} + \text{staurolite} + H_2O$$

This reaction takes place between 510° and 560°C for pressures in the range between 3 and 8 Kb (Fig.6.47); these are minimum temperature estimates according to the KFASH system. Casquet and Navidad (1985) reported biotite-garnet Fe/Mg exchange temperatures between 574°C and 588°C for this transition. The newly formed staurolite overgrowths the S2 foliation. This D2 foliation transposes the previous D1 foliation, which was defined by quartz and muscovite recrystallized following peak temperature conditions. This indicates that peak temperature conditions in the staurolite-chloritoid transition were late-D2.

In the structurally higher parts of the staurolite zone, chlorite and staurolite are stable suggesting temperatures between 510°-550°C (3 Kb) and 560°-590°C (8 Kb; Fig. 6.47) during D2. In the lower parts of the staurolite zone, the garnets have irregular shapes and a pre-D2 character, chlorite has been removed and there is new growth of syn- to late-D2 biotite and staurolite. The new-grown biotite defines the S2 foliation, in association with quartz and muscovite, whereas the new staurolite partially overgrows the S2. There is also a previous generation of staurolite with an internal schistosity (early-syn D2?) which predates the external S2 (Fig.6.45). This suggests new growth of staurolite and biotite during D2 after reaction:

$$\text{garnet} + \text{chlorite} = \text{staurolite} + \text{biotite} + H_2O$$

According to Spear (Chapter 10, 1993) this reaction takes place at around 580°C (Fig.6.47). This minimum temperature estimate in the KFASH system is consistent with reported Bt-Grt (Fe/Mg) exchange temperatures of 596°C and 616°C for the staurolite zone (Casquet and Navidad, 1985).

Casquet and Navidad (1985) and Gonzalez Casado (1987) reported the presence of late-D2 sillimanite growing in the staurolite zone, as well as post-D2 growth of andalusite (Fig.6.44). The presence of sillimanite could not be confirmed. Andalusite however, was

identified in metasomatic veins cross-cutting the S2 foliation and overprinted by the D3 deformation associated with the Cervunal detachment. This indicates that low pressure conditions were reached after D2 and before D3, and suggests a qualitative clockwise P-T path for the St-zone (Path 1, Fig. 6.47). It is uncertain if the sillimanite formed after staurolite and chlorite, in which case the higher temperatures would have been achieved, as well as if peak pressures were in the kyanite or the sillimanite stability field.

Sillimanite (kyanite) zone:

This zone contains pre-D2 kyanite partially replaced by syn-D2 fibrolitic sillimanite. It covers the whole extent of the BRSZ west of the Cervunal detachment, forming a 3 Km wide band (Fig.6.44). The main foliation in this zone is an S2 resulting from the complete transposition of S1 and S0. S2 is defined by biotite, fibrolitic sillimanite and muscovite (Fig.6.45). The sillimanite post-dates porphyroblasts of kyanite, garnet and staurolite, which are inter D1-D2 (Gonzalez Casado, 1987).

Staurolite is common in the center and eastern part of the band, where it appears in the matrix in contact with kyanite and quartz as part of a Ky+St+Bt±Grt+Pl paragenesis (Fig.6.48). Both kyanite and staurolite have inclusions of rutile and quartz defining an internal schistosity (S1). Garnet mainly contains inclusions of ilmenite and quartz that also define an internal schistosity and only rarely contains rutile inclusions. The kyanite and staurolite relicts are partially corroded and surrounded by syn-D2 muscovite. The kyanite porphyroblasts are locally bent and boudinaged and in places show undulose extinction. Intracrystalline deformation is also common in the plagioclase, indicating a pre-D2 growth. The presence of staurolite, kyanite and quartz in contact, in the pre-D2 matrix, and the absence of chlorite, suggest formation of kyanite by the reaction:

staurolite + chlorite = biotite + kyanite

This reaction indicates temperatures in excess of 600°C and pressures above 6.2 Kb (Fig.6.47; Chapter 10 of Spear, 1993) during the inter D1-D2 interval. It is only in the deeper parts of the shear zone, with no kyanite, that there are staurolite inclusions in garnet (Fig.6.49), indicative of the reaction:

staurolite = garnet + biotite + Al-silicate

This reaction was observed in a rock with the paragenesis Sill+Grt+Bt±St+Ms+Qtz. In the lower parts of the shear zone the pre-D2 assemblage Ky+Grt+Bt is common, but it is uncertain if it is a result of staurolite consumption. Therefore, the only constraint on the demise of staurolite is that it took place during D2 in the sillimanite stability field at conditions below 8 Kb and 680°C, as indicated by the previous reaction (Chapter 10 of Spear, 1993; Fig.6.47). This is consistent with transformation of kyanite into sillimanite during D2, indicating the decompressional character of this deformation. The exact trajectory of the P-T path during the decompression is uncertain (Path 2, Fig.6.47), but the presence of late- to post-D2 metasomatic veins with andalusite and reported Ky=And and Sill=And replacements (Arenas et al., 1980; Gonzalez Casado, 1987; Escuder Viruete in Hernaiz Huerta et al., in press) indicate the andalusite stability field was reached after D2. Even though pegmatite veins are common in this zone, the lack of evidence of melting further restricts the trajectory of the P-T path.

Sillimanite + muscovite zone:

This zone occupies the Madarquillos shear zone and the Manjirón antiform (Fig.6.44). In the Madarquillos shear zone both the metapsammites and the mica schists have the same mineral assemblage with Sill+Bt+Grt+Ms+Qtz±Pl, although in different modal proportions. The sillimanite is fibrolite and defines both gneissosity and the S2 fabric in association with biotite and muscovite. The fibrolite in the gneissosity is folded (F2),

recrystallized biotite and muscovite have a decussate texture defining the hinges of the F2 folds, quartz is also recrystallized and annealed containing muscovite. These textural relationships indicate that both muscovite and sillimanite, as well as garnet, were stable during the recrystallization that followed the D2 event. This suggests conditions in the stability field of sillimanite and probably above the breakdown of staurolite (620° to 680°C; Fig. 6.47). Pegmatitic veins are common in the sillimanite + muscovite psammites and mica schists but it is uncertain if they represent minor anatexis. These veins, however, differ from the anatectic migmatites in the nearby Manjirón antiform.

The migmatites of the Manjirón antiform are well exposed at the head of the Puentes Viejas dam (Fig.6.11). They contain 20% to more than 60% leucosome with the mineral assemblage Pl (An 15)+Kfs+Qtz±Grt. These leucosomes still preserve magmatic textures such as concentric zoning of plagioclase and late interstitial crystallization of quartz among euhedral-subhedral plagioclase laths (Fig.6.50). The melanosome consists of the assemblage Bt + Ms + Sill. It should be noted that there is abundant tourmaline associated with the melanosomes but not in the leucosomes. Garnet is growing in both the leucosome and the melanosome. Nearby paragneisses consist of the assemblage Ms+Bt+Sill+Grt+Pl+Qtz+(Kfs?). In these paragneisses, muscovite is stable in the matrix and it is also present as inclusions in plagioclase poikiloblasts. This suggests that anhydrous melting of muscovite (Ms+Pl+Qtz = Kfs+Al_2SiO_5+ melt; Chapter 10 of Spear, 1993) did not take place in these rocks.

The presence of garnet in the anatectic migmatites and the large volumes of anatectic melt would suggest that anatexis, if anhydrous, took place by melting of biotite (Bt+Al_2SiO_5+Pl+Qtz = Grt+Kfs+melt; Le Breton and Thompson, 1987) at temperatures in excess of 720°C (Fig.10-16 of Spear, 1993). The presence of tourmaline restricted to the melanosome questions the effect of any boron solubility in the melt, which could have

lowered the granite solidus (Johannes, 1985). There is a problem explaining the large relative volumes of anatectic melt in the migmatites when nearby rocks do not have clear evidence for biotite melting or breakdown and melting of muscovite. This field relationship could be explained if, during the D2 extensional shearing, there was juxtaposition of lenses of hotter/deeper rocks undergoing anatexis against rocks in the Sill+Ms stability zone. In the Sill+Ms zone during D2, the replacement of garnet by intergrowths of fibrolitic sillimanite and biotite and the formation of sillimanite clusters pseudomorphing garnet is common. This indicates the presence of mass transfer at mineral scale during D2. Therefore significant amphibolite facies retrogression of the migmatites in the Manjirón antiform may have occurred after fluid release from the crystallizing anatectic melts, followed by recrystallization in the Sill+Ms stability field (Fig.6.45; 6.47). This hypothesis, however, has to be evaluated with quantitative thermobarometry. It could also be speculated that these migmatites were part of a pre-variscan orogenic event, but such possibility is invalidated by U-Pb dating (Section 6.7.4).

In the Manjirón antiform, calc-silicate rocks are particularly well exposed at the base of the Puentes Viejas dam (Fig.6.12). They consist of the inter D1-D2 assemblage Grt + Cpx + Qtz ± Cal ± Zo+Ttn± Rt, with plagioclase and amphibole growing after D2 retrogression of clinopyroxene and garnet. According to Casquet and Fernández Casals (1981) these inter-D1-D2 Grt-Cpx parageneses might represent a high grade, eclogite or granulite facies, event followed by syn-D2 amphibolitization. This corroborates the presence in the Manjirón antiform of an earlier (inter D1-D2) high grade event followed by syn-D2 mid amphibolite facies retrogression in the Sill+Ms zone.

Sillimanite + K-feldspar zone (Fig.6.44):

West of the Madarquillos shear zone the gneissic infrastructure of the Western Guadarrama Domain is all in the Sill+Kfs zone. In this area relicts of inter D1-D2 kyanite and staurolite have been described by other workers (Bellido et al., 1991; Azor et al., 1991b) but were not observed in this study. The mineral assemblage in the metapelites of this zone is Sill (fibrolite)+Bt+Kfs+Grt±Pl in association with granitic leucosomes, which previous workers considered to be syn-D2. This indicates the breakdown of muscovite following the vapor absent melting reaction:

$$\text{muscovite} + \text{quartz} = \text{K-feldspar} + Al_2SiO_5 + \text{melt}$$

This indicates temperatures above 650°-750°C in the pressure range between 3.5 and 10 Kb for the anatexis (Chapter 10 of Spear, 1993). In some of the migmatitic rock types the percentage of melt is 40% to 60% of the rock. If this melting took place under vapor absent conditions, such volumes of melt would require additional partial melting by biotite breakdown (Clemens and Vielzeuf, 1987), possibly after the reaction (Le Breton and Thompson, 1988):

$$\text{biotite} + Al_2SiO_5 + \text{plagioclase} + \text{quartz} = \text{garnet} + \text{K-feldspar} + \text{melt}$$

Such a reaction would require temperatures in excess of 720°C (Fig.10-16 of Spear, 1993). The absence of orthopyroxene in the mineral assemblage places a limit of approximately 800°C for the peak temperature conditions (Fig.10-16 of chapter 10 of Spear, 1993).

The relationships between migmatization and deformation, as already described, are not simple. The leucosomes are post-D1 and are folded and locally sheared by the D2 event. The sillimanite is stable in the D2 mylonitic fabric and is part of the stable

paragenesis Sill + Kfs +Bt. Garnet is in places deformed confirming the high-temperature character of the final D2 deformation. The leucosomes are folded, some with disarmonic folds, suggesting that they were generated at high temperature during anatexis. This would imply that migmatization took place during D2, and deformation continued to progress while the leucosomes crystallized in the Sill+Kfs zone stability field and underwent subsolidus deformation. The presence of late melts cross-cutting the D2 fabrics is common in this area. These are tourmaline-bearing granitic/pegmatitic melts, indicating that boron was dissolved in the melt. Johannes (1985) indicated that boron can significantly lower the granite solidus, but these melts suggest that temperatures above 600°C were mantained after D2.

Cordierite-bearing assemblages (Crd-Bt-Sill-Ms-Kfs-Pl-Qtz) were identified in the Lozoya orthogneiss (Fig.6.6 and 6.44), west of the area mapped in detail. López Ruiz et al. (1975) and Bellido et al. (1991) reported the occurrence of cordierite in the surrounding paragneisses. According to Bellido et al (1991), cordierite grew during the final stages of the D2 deformation (as defined in this study). This indicates that low pressure conditions were achieved in the final stages of D2 while still maintaning high temperature conditions. It is also during these final stages of D2 that there is significant amphibolitization of the, scarce, Cpx-rich mafic dykes such as the Braojos dyke (NW of the area map in detail). Reports of wollastonite in marble (Bellido et al., 1991) also confirm the low-P / high-T conditions achieved during the final stages of the D2 deformation. There is also significant late/post-D2 growth of muscovite indicating that fluids were available during the final stages of the D2 deformation.

6.7.4.- U-Pb geochronology to constrain the timing of Variscan metamorphism and deformation:

The D2 extensional deformation in the Berzosa-Riaza shear zone (BRSZ) coincided with peak metamorphic conditions in the amphibolite facies. Under these circumstances, it is possible to constrain the timing of both metamorphism and deformation by combining U-Pb thermochronometers with different closure temperatures (Tc), such as monazite (Tc ≈ 700°C; Heaman and Parrish, 1991) and titanite (Tc ≈550°-600°C; Heaman and Parrish, 1991), with detailed petrography (Fig.6.51). Smith and Barreiro (1990) and Kingsbury et al. (1993) have shown that monazite grows as a metamorphic mineral after soft phosphates during regional metamorphism at the chloritoid-staurolite transition.

Mica schists were sampled from several localities in the Eastern Domain and the BRSZ, where peak temperatures were below 650°C, to use monazite as a prograde thermochronometer (Fig.6.51, 6.52). Additionally, amphibolites, showing static amphibole growth, were sampled for titanite to bracket the D2 deformation. In the Western Domain, rocks were sampled for monazite in both the Sill+Ms and the Sill+Kfs zone to obtain the age of peak metamorphism and/or cooling ages, including an anatectic leucosome in the Sill+Ms zone to date the migmatization in the Manjirón antiform. An amphibolite in the Sill+Kfs zone was sampled to obtain a titanite cooling age with which to provide a younger limit for the peak metamorphism and the high temperature deformation. Finally , the post-collisional La Cabrera granite was sampled to provide a younger age limit for the Variscan metamorphism and deformation and to assess any relationship between the Late Variscan plutonism and the late-D2 low pressure/high temperature mineral metamorphic growth.

Details of the U-Pb analytical procedure, including sample preparation, are provided in appendix A.1.

EASTERN GUADARRAMA DOMAIN (Cardoso antiform):

Sample Hi-1 (St in / Cld out transition): St-Grt-(Cld) mica schist:

This sample was collected above the Cervunal detachment, in the Puerto de La Hiruela, at the Cld-St transition (Fig.6.26; 6.52). The mineral assemblage is St+Grt+Bt±(Cld)+Ms+Qtz which indicates peak temperatures between 530°-550°C (Fig.6.47). Staurolite in this sample grew during D2 transposition of the S1 fabric and final growth overprinted the S2 fabric. Monazite has been identified as inclusions within S2 biotite.

The two monazite fractions analyzed are slightly discordant above and below concordia, invalidating a preliminary 334±3 Ma $^{207}Pb/^{206}Pb$ age for this rock (Valverde-Vaquero *et al.*, 1995). However, $^{206}Pb/^{238}U$ and $^{207}Pb/^{235}U$ ages from both fractions are in good agreement and provide a growth age for the monazite of **327±3 Ma** (Fig. 6.53; Table 6.2)

Sample Pi-1 (St-zone): St-Grt mica schist

This sample was collected in the St zone, above the Cervunal detachment, along the road to the ski resort of La Pinilla (Fig.6.52). The mineral assemblage is St + Grt + Bt + Ms + Qtz (Fig.6.55). The S2 fabric (biotite+ muscovite + quartz) wraps around the garnet. Garnet contains an internal schistosity (S1) and has corroded rims. Staurolite grew in two stages, pre-D2 and syn- to post-D2. The last stage was probably associated with the reaction Grt + Chl = St + Bt (570° - 610° C ; Chapter 10 of Spear, 1993). Monazite inclusions have been observed in S2 biotite (Fig.6.55) and syn- post-D2 staurolite. Two

analyzed monazite fractions (Fig.6.55) have provided a growth age of **330±2 Ma** (Fig. 6.54: 6.52; Table 6.2).

Sample CA-1 (Core of the Cardoso antiform, St -zone): plagioclase-rich para-amphibolite:

This rock was collected in the core of the Cardoso antiform, within the St-zone (Fig.6.52). This a felsic amphibolite, which outcrops as small boudins. The texture is formed by a granoblastic matrix of plagioclase (An30) and quartz with, up 1cm long, porphyroblasts of post-D2 green clinoamphibole (hornblende) growing with an acicular random orientation. Titanite grew in association with the amphibole, both as euhedral inclusions in the amphibole and as individual crystals in the matrix (Fig.6.56). There is also very minor chlorite (retrogression?). The random orientation of the amphiboles suggest a post-D2 static growth which is consistent with the final, post-D2, growth of staurolite in the surrounding mica schists.

Four titanite fractions were separated for analysis. Two fractions of colourless titanite produced meaningless results due to the low concentrations of U (10 to 17 ppm) and radiogenic Pb (0.5 to 0.8 ppm). The results of fraction T1 (colourless) were confirmed with a fraction of pale brown titanite (T2). Both fractions show a reproducible $^{206}Pb/^{238}U$ isotopic age of **322±2 Ma** (Fig.6.56). This age can be interpreted as the growth age of titanite or as a cooling age, althought the Tc for titanite (550°-600°C) is very close to peak temperature conditions in the St-zone (575°-610°C). Either of these interpretations indicates that 322±2 Ma is the younger absolute age limit for the D2 mylonitic deformation in the Cardoso antiform (Fig.6.52), and for the amphibolite facies metamorphism.

THE BERZOSA-RIAZA SHEAR ZONE (SILL+KY ZONE):

Sample J2-9: Kyanite -staurolite-garnet-sillimanite mica schist:

This sample was collected from the sillimanite-zone with kyanite relicts in between the Montejo and Cervunal detachments (Fig.6.52). The mineral assemblage contains Grt + Ky + Sill(fibrolite) ± St +Bt + Ms + Pl + Qtz (Fig. 6.26). Kyanite and staurolite are pre-D2. The S2 fabric is defined by fibrolite and biotite. Gt-Bt exchange geothermometry indicates a peak temperature of 630±10°C (Valverde-Vaquero, unpublished). Monazite has been recognized as inclusions in S2 biotites (Fig.6.57).

Monazite and rutile were extracted for analysis. Two fractions of brown rutile yielded meaningless results due to the low U concentration and the small percentage of radiogenic Pb.

The two monazite fractions consisted of pale yellow euhedral to subhedral parallelogram-like crystals. The purity of these fractions was checked by EDS analysis with the electron microprobe at Memorial University prior to analysis. Although the fractions are slightly discordant, the $^{206}Pb/^{238}U$ and $^{207}Pb/^{235}U$ isotopic ages of these two monazite fractions are in agreement, providing a growth age of **326±3 Ma** (Fig. 6.57; Table 6.2)

THE WESTERN GUADARRAMA DOMAIN (Sill+Ms and Sill+Kfs zones)

Sample M26-2 (Sill+Ms zone): Folded migmatite, Manjirón antiform (Fig.6.52; 6.58):

Two monazite and six zircon fractions were selected from this sample. The two fractions of clear, inclusion free, yellow monazite resulted in concordant analyses. These two monazite fractions plot slightly above concordia, resulting in younger $^{206}Pb/^{207}Pb$

ages. The U/Pb ages are, however, in agreement and provide a reliable isotopic age of 325±2 Ma for the closure of the U-Pb system. The least discordant zircon fractions (Z1, Z2, Z4 and Z5) are formed by small, clear, euhedral, sharp, zircon needles and elongated prisms. These fractions and the concordant monazites define a discordia line with a 36% probability of fit. The lower intercept of the discordia line is fixed by the concordant monazites at **325.6±2 Ma** (Fig.6.58). The upper intercept at 627+14/-10 Ma has a dubious geological meaning but suggests that presence of Late Precambrian, Cadomian, inheritance. Zircon fractions Z3 and Z6 (not plotted) also indicate older inheritance.

These migmatites are garnet-bearing and contain more than 40% melt, which suggests that they were produced at temperatures above the anhydrous muscovite-out melting reaction probably in part by anhydrous biotite-out melting at temperatures possibly in excess of 720°C (section 6.7.3). Most of the monazites appear in the melanosomes as inclusions in the biotites (Fig. 6.58). The high closure temperature of monazite (Tc≈700°C) and the high quality of the crystals analyzed suggest that the monazite ages date mineral growth. This interpretation is supported by the discordia line defined by the zircon fractions Z1, Z2, Z4 and Z5. Therefore, the lower intercept age at **325.6 ± 2 Ma** probably reflects the age of crystallization of the migmatitic melt, although this needs further confirmation with concordant zircon analyses.

Sample BU-2 (Sill + Kfs zone): 482 Ma aplitic vein, Buitrago gneiss:

Four monazite fractions of different size have been processed from a 482 Ma aplitic vein in the Buitrago gneiss (Fig.6.18; 6.52). Large (M1; 70-200 mesh size) rounded, air abraded, monazites have a concordant age of **337±3 Ma**. This age however could not be reproduced by a second fraction of similar monazites (M2) which have a concordant age of

332±2 Ma. The small platy monazites, without air abrasion (M3 and M4; >200 mesh) have provided ages of **331±3 Ma** and **329±2 Ma**, respectively (Fig.6. 59; Table 6.2).

These ages suggest possible multiple growth of monazite at ca. 337 Ma and ca. 332-329 Ma, but the first age needs further confirmation. These ages represent a minimum age for metamorphism. With the current age data base, it is difficult to interpret them in terms of growth or cooling ages. However, the relative good agreement of fractions M2, M3 and M4 suggests that the age of 332 Ma does not represent cooling. Given the high closure temperature of monazite (Tc=700°C; Heamann and Parrish, 1991), it is likely that these monazite ages indicate the timing of peak metamorphism.

Sample PiB-1 (Sill + Kfs zone): 482 Ma foliated leucogranite, Pinilla de Buitrago, Buitrago gneiss (Fig.6.21; 6.52)

Two fractions of monazite and one fraction of metamict xenotime define a discordia line with an upper intercept of **322±3 Ma** (Fig.6.60). This age could be conservatively interpreted as a cooling age reflecting temperatures below 650-700°C. This temperature range is, however, consistent with an alternative interpretation as a metamorphic growth age associated with the small late anatectic melts which cut the main gneissosity in the surrounding augen-gneisses.

Sample LO-1 (Sill+ Kfs zone): Cordierite-bearing 477 Ma augen-gneiss (Lozoyuela gneiss; Fig. 6.22, 6.52).

Both monazite and xenotime have been separated from this granitic orthogneiss. Monazite can be easily identified in biotite-rich areas associated with biotite + fibrolite + muscovite +cordierite. Muscovite shows signs of instability.

Three monazite and one xenotime fraction define a discordia line (74% probability of fit) with a lower intercept anchored at **322±2 Ma** by a concordant analysis of euhedral xenotime (X1) and two large monazite crystals (M1), (Fig. 6.61; Table 6.2). The upper intercept at 480+42/-41 coincides with the protolith age of the rock (477±4 Ma; Fig.6.22). This suggests that the discordia line represents a mixing line between primary igneous and metamorphic monazite, which is consistent with the lower U concentrations in fraction M3(*). Therefore, **322±2 Ma** probably represents the age of monazite and xenotime growth associated with the cordierite-bearing low P / high T paragenesis, effectively dating the low P / high T metamorphic overprint.

(*) Igneous monazite typically has lower U concentrations than metamorphic monazite. Please compare the U concentrations of the igneous monazites from La Cabrera granite with those of the metamorphic monazites (table 6.2).

Braojos dyke (Deeper levels of the Sill + Kfs zone): Amphibolite (Fig.6.52)

This dyke is formed mostly by plagioclase and green amphibole growing at the expense of clinopyroxene during retrogression and D2 deformation (Fig.6.62). Titanite is common in association with the green amphibole and as inclusions in the clinopyroxene. There is scarce rutile preserved as inclusions in titanite, suggesting that titanite grew partially after rutile possibly during retrogression.

Two titanite fractions, pale brown and colourless, were analyzed. They both had similar low U concentrations. The resultant analyses are slightly discordant, T2 overlaps concordia within uncertainties. As already discussed this is an effect of the model common Pb correction used (Stacey and Kramers, 1975). In rocks of this age, however, this effect is minimal for the case of the $^{206}Pb/^{238}U$ isotopic ages. This is confirmed by the duplication of the $^{206}Pb/^{238}U$ ages in fractions T1 and T2, which provide an age of

321±3 Ma (Fig.6.62). This age is taken as the age of closure of the U-Pb system in these titanites. It is interpreted as a cooling age (Tc≈ 600°-550°C) reflecting the amphibolitization associated with the D2 deformation in the vicinity of the Robregordo fault.

THE POST-TECTONIC LA CABRERA GRANITE:

This is a composite pluton formed by granitic and granodioritic facies which are thought to be coeval (Bellido et al., 1981). Published whole rock Rb-Sr isochrons provided an age of 310±14 Ma for the granodioritic facies and 287±5 Ma for the leucogranites (Vialette et al., 1981). It is the external granodioritic facies that was sampled for U-Pb dating (Fig.6.52, 6.63).

Four zircon fractions and three monazite fractions were separated for analysis. The zircon fractions consisted of euhedral multifaceted, clear, prims separated by size (Table 6.2). Although intensively abraded, they all show between 4% and 10% discordance. This discordance could be attributed to a combined effect of minor Pb loss and inheritance. Fraction Z4, zircon prisms with inclusions, is not reported since this analysis was contaminated with common Pb from the fluid inclusions in the zircons.

All three monazite fractions are concordant (Fig.6.63). Fractions M1 and M2 have the smallest error ellipses and provide a combined age of 292±2 Ma, which agrees with the isotopic ages from all three fractions (Fig.6.63). This age of **292±2 Ma** is interpreted as the age of intrusion of the granodioritic facies of the La Cabrera granite

6.7.5.- Timing and character of the Variscan tectonothermal events in the Somosierra area of the Sierra de Guadarrama: conclusions and discussion.

The structural and metamorphic data presented indicate that the earlier Variscan deformation (D1) was responsible for the crustal thickening and the Barrovian metamorphism in the inter D1-D2 interval (Fig.6.64). In the area of study, the D1 macrostructures have been obliterated by the D2 deformation. However, to the east in the Majalrayo syncline and the Galbe de Sorbe anticline, the D1 deformation produced east vergent structures (Gonzalez Lodeiro, 1988; Hernaiz Huerta et al., 1996). East of the area of study, in the Hiendelaencina area, Lower Devonian sedimentary rocks are deformed by the D1 event, therefore providing an older limit for the D1 deformation in the suprastructural Eastern Guadarrama Domain. This deformation is also responsible for the greenschist facies metamorphic zonation observed in the upper structural levels of the area of study (Chl, Bt and Grt zones). The unconfirmed occurrence of kyanite in the Bt-zone (García Cacho, 1973; in López Ruiz et al., 1975) suggests that a Barrovian metamorphic gradient was achieved after D1. Therefore the U-Pb monazite growth ages of 330±2 Ma and 327±3 Ma from the upper and lower staurolite zone could be taken as a younger age limit for the D1 deformation in the suprastructural Eastern Guadarrama Domain (Fig. 6.64).

The inter D1-D2 Barrovian kyanite-staurolite-bearing mineral assemblages preserved in the Berzosa-Riaza shear zone (BRSZ) indicate pressures above 6.2 Kb and temperatures between 600° and 650°C (Fig.6.47) during the D1-D2 interval, confirming the compressional character of the D1 deformation (Fig.6.64). In the gneissic infrastructure of the Western Guadarrama Domain there are only relicts of the D1 structures. The Qtz-Cpx-Grt-(Zo)-(Rt) assemblages preserved in calc-silicate boudins could suggest high pressure

metamorphic conditions after D1 (Casquet and Fernández Casals, 1981), but it is uncertain if they represent peak metamorphic conditions.

The D2 deformational event produced the juxtapositon of the Eastern and Western Guadarrama Domains along the Berzosa-Riaza shear zone (BRSZ) forming a set of associated macrostructures in the Eastern (Cardoso antiform) and Western domains (Manjirón antiform and Madarquillos shear zone). In the upper structural levels of the area of study, the D2 deformation crenulated the D1 structures (D2 crenulation band of Hernaiz Huerta et al., 1996) and folded the Chl, Bt , Cld and Grt isograds. The strain of the D2 deformation increases structurally downwards, leading to a complete transposition of the D1 structures and fabrics by the D2 ductile shearing. The D2 ductile shearing was concentrated along the BRSZ. Peak metamorphism in the lower structural level of the suprastructural Eastern Domain, uppermost part of the BRSZ, coincides with the final stages of the D2 deformation. In the central parts of the BRSZ, relict inter D1-D2 kyanite is transformed into syn-D2 sillimanite, and in the lower parts of the shear zone staurolite is consumed to produce syn-D2 sillimanite and garnet. Post-D2 growth of sillimanite in the lowermost St-zone, Eastern Guadarrama domain, was followed by growth of andalusite. Post-D2 andalusite also grew after kyanite and sillimanite in the central parts of the BRSZ. This indicates that all levels of the Berzosa-Riaza shear zone reached the andalusite stability field after the D2 deformation. The kinematic indicators in the Berzosa-Riaza shear zone show a consistent shear sense of top down to the SE. A single population of L2 mineral and stretching lineations was produced under different P-T conditions, indicating that the BRSZ was a west vergent, oblique, extensional shear zone.

The 330±2 Ma and 327±3 Ma U-Pb monazite ages from the St -zone provide an older age limit for the D2 deformation and peak of metamorphism in the upper parts of the shear zone, whereas the 322±2 Ma titanite age, associated with the post-D2 static growth of

amphibole, provides the younger age constraint. The 326±3 Ma age from the monazite in the Sill (Ky) zone probably represents the age of peak metamorphism and the D2 deformation in the central parts of the BRSZ (Fig.6.52, 6.57, 6.64).

In the gneissic infrastructure of the Western Guadarrama Domain, rocks in the Ms+Sill zone stability field form the footwall of the BRSZ. These rocks were sheared and folded during the D2 event and are characterized by the parallelism of the L2 mineral lineation and the F2 fold axis. Migmatites in this area (325.6 Ma) and relicts of high grade assemblages in calc-silicates boudins indicate that some rocks were at higher grade and subsequently deformed in the Sill+Ms field during the D2 extensional event (Fig.6.64). In the deeper level of the Western Domain, within the Sill+Kfs zone, anatexis was probably reached during the early stages of the D2 deformation and as the D2 deformation progressed the migmatites were folded and sheared in a subsolidus state at high temperature in the Sill+Kfs stability field. A 337 Ma monazite age from the Buitrago gneiss provides the best estimate for peak metamorphism, 332 to 329 Ma monazite ages from the same rock also provide a younger limit for peak metamorphism (Fig.6.64). The late D2 deformation was associated with growth of low P / high T mineral assemblages (322 Ma monazite, xenotime) and amphibolitization of the scarce mafic lithologies (321 Ma titanite, Braojos dyke; Fig. 6.64).

The 322 Ma monazite ages characterize the westernmost part of the area of study, suggesting a transfer of the extensional deformation towards deeper and hotter levels with time. This implies a progressive extensional deformation during the D2 event, which is consistent with the parallelism of the structural trends observed between all levels of the Berzosa-Riaza shear zone and its gneissic footwall. These ages also indicate that high temperatures were still maintained during the final stages of the D2 extensional deformation, while there was the new growth of low pressure/high temperature mineral

assemblages (Bellido et al., 1991). The 321 Ma titanite age from the Braojos dyke also indicates the retrograde character of these assemblages. Therefore, the D2 extensional deformation in the gneissic Western Guadarrama Domain is bracketed between 337 Ma and 321 Ma (Fig.6.64).

The late growth of post-D2 /pre-D3 andalusite in the lower levels of the Eastern Guadarrama domain (Gonzalez Casado, 1987) and the Sill -Ky zone (Arenas, 1980; Gonzalez Casado, 1987) indicates that low pressure conditions were achieved after the D2 extensional deformation. The D3 deformation includes all post-D2 greenschist facies deformations, including the formation of late brittle/ductile extensional detachments (Montejo and Cervunal detachments). The Cervunal detachment separates the Sill(Ky) zone from the lower levels of the Eastern Guadarrama domain (St-zone), the presence of pre-detachement andalusite on both sides of the fault suggests that this could be a minor reactivation nucleated around the elongated bodies of pre-Variscan augen-gneisses of the Sill (Ky) zone.

The 292 Ma post-tectonic La Cabrera granite sealed the Berzosa-Riaza shear zone, cross cutting the D2 macrostructures and the regional metamorphic isograds. This indicates the presence of a 30 Ma gap separating the 322 Ma low P / high T metamorphism from the Late Variscan post-collisional plutonism (Fig.6.52; 6.64). According to Fernández Casals (1979), the La Cabrera granite provides a younger limit for the greenschist facies D3 Variscan deformation (Fig.6.64). It should be noted that there is no reported evidence that the La Cabrera granite intruded into mica schists of the St-zone, therefore it does not provide a real time constraint on the timing of the Cervunal detachment.

6.8.- PALEOZOIC TECTONOTHERMAL EVOLUTION OF THE SOMOSIERRA SECTOR OF THE SIERRA DE GUADARRAMA: DISCUSSION.

This section discusses the tectonic and regional significance of the different tectonothermal events unravelled in the Somosierra sector of the Sierra de Guadarrama (Fig.6.65). First the tectonic significance of the pre-Variscan events will be discussed, including contemporaneous events elsewhere in the Iberian Massif and potential correlatives along the Southern Variscides. This will be followed by a discussion of the significance of the Variscan events both at regional and orogen scale.

6.8.1.- Arenig felsic magmatism in the Sierra de Guadarrama and the nature of the "Sardic" events in the Central Iberian Zone: An Arenig continental magmatic arc.

The "Sardic" deformation in the Central Iberian Zone consists mainly of tilting of blocks and has an overall extensional character (e.g., López Díaz, 1995; Díez Balda et al., 1990). This has led most authors to consider that the Sardic unconformity represents a break-up unconformity associated with a passive margin and the Early Ordovician magmatism as rift-related (e.g., Quesada, 1991). Gebauer et al. (1993), however, interpreted this magmatism as a post-collisional episode related to a hypothetical Late Cambrian collisional event.

The new U-Pb data validates regional correlations between the gneisses of the Sierra de Guadarrama and those in the Ollo de Sapo antiform (465±10 Ma Viana de Bollo orthogneiss, U-Pb zircon ; Lancelot et al., 1985; 488 Ma Ollo de Sapo augen-gneiss, U-Pb SHRIMP; Gebauer et al, 1993), as suggested by previous authors (Parga et al., 1964; Díez Balda et al., 1990; Azor et al., 1992; Gebauer et al., 1993). According to these correlations

the Early Ordovician orthogneisses of the Sierra de Guadarrama are part of a 600 Km long and 5 to 100 Km wide felsic magmatic arc of batholithic proportions, which extends from Central Spain to its NW coast. Additional possible correlatives are the undated calc-alkaline Cambro-Ordovician volcanosedimentary complex of the Montes de Toledo in the southern half of the CIZ (Martín Escorza, 1976; 1977; Muñoz et al., 1985) and the porphyroid levels of the Portuguese side of the CIZ (Gutiérrez Marco et al., 1990; Oliveira et al., 1992), all of which outcrop below the Sardic unconformity.

The available geochemistry on these rocks both in the Sierra de Guadarrama and in Zamora (NW Spain) is relatively limited but includes dioritic to granitic compositions (57-73% SiO2) with volcanic-arc/post-collisional trace element characteristics (Navidad et al., 1992; Gebauer et al., 1993). They are predominantly of dacitic/granodioritic composition. The significant 2.0 to 2.6 Ga zircon inheritance in some samples confirms the involvement of a Proterozoic crustal source in the genesis of these magmas (Lancelot et al., 1985; Wilberg et al., 1989).

The batholithic proportions of the felsic magmatism, the scarcity of associated basic magmas, and a minimum 60 Ma age difference from any previous orogenic event in the CIZ (Late Vendian Cadomian compression; López Díaz, 1995) suggest that this Arenig magmatism represents a short-lived continental magmatic arc. In such a model, the weak extensional deformation associated with the Sardic phase would be related to extension during batholith emplacement (Hamilton, 1995; Cordillera: Tobisch et al., 1995; Chilean Andes: Dallmeyer et al., 1996).

Coeval events in the Iberian Massif and speculative correlatives along the Southern Variscides:

Coeval magmatism is also found in the Ossa Morena Zone (OMZ) and the Allochthonous Complexes of Galicia Tras-os-Montes (GTMZ; Fig. 6.66). This includes alkaline and peraluminous plutonism in the OMZ (U-Pb data; Lancelot and Allegret, 1982; Ochsner, 1993), and mafic and felsic igneous rocks, some with ophiolitic affinities, in the allochthonous units of the GTMZ (U-Pb data; Kuijper et al., 1982; Peucat et al., 1990; Dallmeyer and Tucker, 1993; Santos Zalduegui et al., 1995; 1996). The Early Ordovician magmatism is not an exclusive characteristic of the CIZ. Arenig volcanism associated with deposition of the Armorican Quartzite as well as a weak Sardic unconformity are also present in the CZ (Aramburu and García Ramos, 1993; Gallastegui et al., 1992), but with no signs of Sardic deformation. Contemporaneously, the WALZ formed a deep, graben-like, sedimentary trough separating the CIZ from the CZ. This zone underwent active subsidence resulting in the deposition of a thick siliciclastic sequence (Series de los Cabos; Marcos, 1973) with no evidence for Sardic deformation or unconformities

The well defined, Arenig to Ashgill, faunal and lithostratigraphic similarities between the Central Armorican Massif and the Central Iberian Zone (Young, 1990; Paris and Robardet, 1990; Robardet and Gutiérrez Marco, 1990) suggest a linkage between the coeval felsic magmatism in both areas. In that sense the similarity of the Tremadoc / Lower Arenig syndepositional acid volcanism of the Cap de la Chévre formation in Central Brittany (Fig.6.66; Bonjour and Chauvel, 1988) with the volcaniclastic Cardoso gneiss, both of which predate the Armorican quartzite, is noteworthy. However, the U-Pb age data on the Early Ordovician calc-alkaline and alkaline granitic orthogneisses of Central Brittany (Jegouzo et al., 1986 and ref. within; Thiéblemont et al., 1989; Le Corre et al., 1989) are too limited to establish correlations. Pre-Caradocian felsic magmatism is also abundant

along the southern Variscides (Fig. 6.66; Eastern Pyrenees, Navidad and Carreras, 1995; Sardinia, Carmigniani et al., 1994; northern Apennines, Conti et al., 1993; Ligurian Alps, Cortesogno et al., 1993) but there are no reliable age data to establish a contemporaneity of events.

6.8.2- Timing of Variscan tectonothermal events in the Sierra de Guadarrama: tectonic significance for the evolution of the Central Iberian Zone and the Iberian Massif.

According to Martínez et al. (1990) the metamorphism of the Central Iberian Zone is characterized by an initial Barrovian mineral growth overprinted by low P / high T mineral assemblages and associated S-type plutonism. These relationships between deformation and the Barrovian and low P / high T metamorphism in the CIZ are best preserved in the Sierra de Guadarrama (Julivert and Martínez; 1987; Martínez et al., 1990; Ugidos, 1990; Doblas et al., 1994 a,b), which highlights the major significance of the data obtained during this study (Fig.6.64; 6.65).

Timing of metamorphism and plutonism:

The monazite U-Pb ages indicate that the peak metamorphism associated with the Barrovian event took place between 337-329 Ma in the Western domain and 330-326 Ma in the lower parts of the Eastern domain and the Berzosa-Riaza shear zone (Fig.6.60). This was followed by growth of low P / high T assemblages in the deepest levels of the Western domain at 322 Ma. The 322-321 Ma titanite cooling ages from the Eastern and Western domain indicate that the metamorphism in the Sierra de Guadarrama was part of a single Lower to Middle Carboniferous metamorphic cycle involving two stages of mineral

growth. This was advanced as a hypothesis by Martínez et al (1990), who proposed an age of 330-315 Ma for the low pressure metamorphic growth on the basis of the field relationships with the S-type granites of the CIZ (Rb-Sr ages; Serrano Pinto et al., 1987).

The pre-Variscan protolith and the Variscan metamorphic ages obtained in this study demonstrate that the c.a. 380 Ma lower intercepts of Wildberg et al (1989) in the Sierra de Guadarrama are geologically meaningless. These authors interpreted these intercepts as the age of Barrovian metamorphism, even though this was unlikely given the presence of Emsian (390-385 Ma, Odin et al., 1990) sedimentary rocks in the pre-orogenic sequence of the Eastern Sierra de Guadarrama Domain (Gutiérrez Marco et al., 1990). Wilberg et al (1989) also wrongly interpreted their unpublished 300-280 Ma monazite and zircon ages from the Variscan granites of the Sierra de Guadarrama as the age of the low P / high T overprint. This also invalidates the tectonic models of Doblas et al (1994, a ,b) which relied heavily on the data of Wildberg et al (1989).

To the knowledge of the author, the 292±2 Ma age of the post-tectonic La Cabrera granite is the first precise U-Pb age available for the Late Variscan plutonism in the Central Iberian Zone. This age is coeval within error with the 287±12 Ma high-K calc-alkaline andesitic volcanism in Atienza (easternmost Sierra de Guadarrama; K-Ar; Hernando et al., 1980). This indicates that extensive Late-Variscan post-tectonic plutonism was coeval with the post-tectonic Permo-Carboniferous volcanism, however a larger number of reliable and precise U-Pb ages would be needed to confirm this hypothesis. Such a U-Pb data base would also allow to test if the current scatter of protolith ages (310-270 Ma, Rb-Sr; K-Ar; Yenes et al., 1996) for the post-tectonic plutonism in the CIZ is real or a result of a mixture of imprecise protolith and cooling ages.

The 30 Ma gap between the post-tectonic plutonism and the low pressure/high temperature overprint in the Sierra de Guadarrama indicates a dissociation between the processes of synkinematic migmatization and post-kinematic plutonism. This would suggest that the post-tectonic plutonism in the Sierra de Guadarrama and Spanish Central System could have been produced by melting reactions induced by magmatic heat from mantle-derived magmas. Due to the large volumes of post-tectonic magmas, one can not dismiss the possibility of a local low P / high T overprint in certain parts of the CIZ.

Timing of deformation: Early-Mid Carboniferous syn-collisional extension:

Structural and metamorphic evidence for Variscan syn-collisional extension has been recently reported from several parts of the CIZ (Fig. 6.67; Miranda Douro antiform, Escuder Viruete et al., 1994; the Salamanca detachment zone, Díaz Balda et al., 1995; the Toledo anatectic complex, Barbero, 1995). This study also confirms the extensional character of the D2 deformation, providing for the first time, direct constraints on the timing of extension in the Central Iberian Zone (Fig.6.64). The 337-321 Ma extension is Visean to Namurian (Fig.6.65). This coincides with the first thrusting in the forelands of the Iberian Massif (Cantabrian and South Portuguese zone; Fig.6.67), confirming the syn-collisional character of the extensional process. This is also contemporaneous with the final movement along the Badajoz-Cordoba shear zone (OMZ-CIZ boundary; Fig.6.67), indicating the presence of coeval wrenching and extension, coupled with early thrusting in the opposing forelands, at the scale of the orogen. There are major wrench post-D1 shear zones in the Central Iberian Zone (Central Extremadura and Juzbado-Penalva do Castelo shear zones, Fig.6.64; e.g., Díez Balda et al., 1990). However, there are no reliable constraints on the timing of movement to make a correlation with the oblique extension along the Berzosa-Riaza shear zone.

The D3 folding is Upper Carboniferous (section 6.7.5). The late brittle-ductile extensional detachment reactivation in the Somosierra could be Upper Carboniferous or even Permian. Similar discrete brittle-ductile detachment in other parts of the Central Iberian Zone cross-cut post-collisional plutons (Hernandez Henrile, 1991; Doblas, 1991). On the basis of these observations, and analogies with the metamorphic core-complexes of the Basin and Range (USA), Doblas et al. (1988), Doblas (1991) and Doblas et al (1994 a, b) suggested a process of late-orogenic extensional collapse with coeval low pressure metamorphism and plutonism to explain the late extensional detachments cross-cutting the post-collisional plutons intrusive into the low P / high T metamorphic complexes of the CIZ. The new time constraints from the Somosierra invalidate this hypothesis for the Sierra de Guadarrama.

The time constraints from the Sierra de Guadarrama demonstrate, for the first time, that peak metamorphism and syncollisional extension in the Central Iberian Zone were broadly coeval with ca 340 Ma high P / high T (Vosges; Bohemian Massif) and Barrovian (Massif Central) metamorphism, Visean to Namurian extension and exhumation of metamorphic complexes along the Variscan Belt (Fig. 6.68). It is uncertain if the Visean-early Namurian syncollisional extension in the Central Iberian zone is a simple case of collapse of a thickened orogenic wedge (Platt, 1986; Dewey, 1988) or part of a complex setting involving collision and transpression and/or lateral extrusion with associated extension (Ratschbacher et al., 1989; Mancktelow and Pavlis, 1994). But this study in the Iberian Massif confirms the presence of major, orogenic-scale, Late-Middle Carboniferous syncollisional extension all along the hinterlands of the Variscan belt (Fig. 6.68).

CHAPTER VII

DISCUSSION AND TECTONIC IMPLICATIONS: PRECAMBRIAN AND PALEOZOIC EVOLUTION OF PERI-GONDWANA FROM A COMBINED APPALACHIAN-VARISCAN PERSPECTIVE.

This chapter outlines the major contributions of this study to the understanding of the evolution of North Atlantic peri-Gondwana. The following discussion begins with an assessment of the tectonothermal evolution of the Hermitage Flexure (Fig.7.1 and 7.2) which integrates the results from the Cinq-Cerf gneiss (Chapter III) and the Margaree orthogneiss (Chapter IV) within the wider regional context of the Newfoundland Appalachians. Then the contemporaneity and major importance of the Early Ordovician (Arenig), **ca. 480-470 Ma** magmatic events in the Appalachian Hermitage Flexure and the Variscan Central Iberian Zone, is discussed. This new data highlights the magnitude and hitherto unrecognized parallelism of the Early Ordovician events along the Gondwanan margin of the Iapetus Ocean in the Newfoundland Appalachians with those in the Southern Variscides.

7.1.-TECTONOTHERMAL EVENTS IN THE HERMITAGE FLEXURE (SOUTHERN NEWFOUNDLAND APPALACHIANS): THE EVOLUTION OF WESTERNMOST PERI-GONDWANA.

The Avalonian basement in the Hermitage Flexure (Chapter II & III) is one of the westernmost, inboard, proven, Avalonian/Cadomian terranes in the Appalachians. The Hermitage Flexure (Chapter III; Fig. 7.1 and 7.2) is one of the few areas in the Cadomian/Avalonian belt with well recorded 680 Ma magmatism (Fig. 7.3 and 7.4). Coeval U-Pb, protolith ages have only been reported from the Connaigre Peninsula of the Avalon Zone (685-670 Ma, e.g. O'Brien et al., 1996), the Mira terrane (682 Ma, Cape Breton; Bevier et al., 1993) and the Malvern Complex (677 Ma, southern England; Tucker and Pharaoh, 1991). The characteristic 635-600 Ma Avalonian magmatism has not been reported from the Hermitage Flexure, but the 590-540 Ma magmatic and deformational episodes have equivalents in the post-590 Ma calc-alkaline magmatism and 570-550 bimodal volcanism in Connaigre and Burin Peninsulas (Avalon Zone; O'Brien et al., 1996), the 570-560 Ma late arc magmatism of the British Avalon (Gibbons and Horák, 1996) and the 575-560 Ma calc-alkaline and tholeiitic bimodal magmatism in the Mira Terrane (Fig. 7.3 and 7.4; Barr and White, 1996). This reinforces the correlation between the Late Precambrian basement of the Hermitage Flexure and the Avalon Zone and its equivalents, the British Avalon (Gibbons and Horák, 1996) and the Mira/Caledonia terranes of the Maritime Provinces of Canada (Barr and White, 1996). The combined data from the Hermitage Flexure refutes the hypothetical correlation of Barr and White (1996) between the Late Precambrian basement block of the Hermitage Flexure and the 550-530 Ma volcanic arc magmatism and early Cambrian deformation and metamorphism of the Bras d'Or and Brookville terranes of Cape Breton and Nova Scotia (Fig.7.3 and 7.4).

Small Precambrian inliers of ca. 565 Ma intrusive rocks (Evans et al., 1990) in central Newfoundland suggest that the Late Precambrian basement of the Hermitage Flexure extends farther north. The presence of 569 Ma detrital zircon and 545 Ma detrital titanite in the Gander Group (O'Neill, 1991) indicates an Early Cambrian older limit for the deposition of this siliciclastic sequence. The Gander Group is classically interpreted as a passive margin sedimentary prism formed along the eastern margin of the Iapetus Ocean (Williams, 1979). The presence of a basement to the Gander Group remains to be proven, but the ages of the detrital minerals allow one to suggest that there may be an Avalonian basement like the one of the Hermitage Flexure.

Magmatic activity in the Hermitage Flexure (Fig.7.1) was renewed in the Tremadocian, with the intrusion of 499±2 Ma granodiorite and 496±3 Ma gabbro (B.H. O'Brien et al., 1991) into the previously deformed Late Precambrian low grade volcanosedimentary cover to the Cinq-Cerf gneiss (Fig.7.2; chapter III). This magmatic pulse coincided with the formation of Tremadocian ophiolites (Dunning and Krogh, 1985) in an outboard suprasubduction environment along the eastern margin of the Iapetus Ocean in conjunction with the formation of the Late Cambrian-Early Ordovician volcanic arcs of the Exploits Subzone (see chapter II). The Early Ordovician Penobscottian event (Neuman and Max, 1989) resulted in ophiolite obduction (Central Newfoundland; Colman-Sadd et al., 1992) and passive margin (peri-Gondwanan margin) / arc (Exploits Subzone) juxtaposition. In the Hermitage Flexure the Penobscottian event is marked by the pre-477 Ma imbrication of "ophiolitic" gabbros and volcanosedimentary rocks in the Bay du Nord Group (Fig.7.1; Tucker et al., 1994). This event, however, was not recorded in the nearby Cinq-Cerf block.

Ophiolite obduction was followed by Arenig arc plutonism, volcanism and sedimentation along the peri-Gondwanan margin of the Newfoundland Appalachians and

by a major Late Arenig-Early Llanvirn back arc rifting event which marked the separation of Avalonia from Gondwana (van Staal, 1994; S.H. Williams et al., 1995; O'Brien et al., 1997). The back arc rifting event coincided with the 474-465 Ma intrusion of the bimodal arc / back arc Margaree orthogneiss (Fig.7.1) into the sedimentary protoliths of the Port-aux-Basques paragneiss (Chapter IV). The 474+14/-5 Ma and 472±2.5 Ma members of the Margaree orthogneiss are broadly coeval with the intrusion of the 477±1 Ma Baggs Hill granite (Tucker et al., 1994) in the nearby Bay du Nord Group (Fig.7.2) and the intrusion of the 474+6/-4 Ma Partridgeberry Hills granite in central Newfoundland (Colman-Sadd et al., 1992), which mark the end of the Penobscottian imbrication. The intrusion of the 465±3 Ma member of the Margaree orthogneiss was coeval with widespread bimodal back arc volcanism in the Exploits Subzone, including the Bay du Nord Group (Fig.7.2), and local low pressure / high temperature metamorphism and anatexis of the Gander Zone in central Newfoundland (see Chapter IV).

The intrusion of the 450 Ma Port-aux-Basques granite (van Staal et al., 1994) indicates the presence of a major magmatic pulse which seems to be exclusive to the southwestern Hermitage Flexure (Fig.7.1 and 7.2). This coincides with the enigmatic titanite age of 448+9/-3 Ma in the Cinq-Cerf gneiss (Dunning and O'Brien, unpublished; see chapter III). Whether or not the intrusion of the Port-aux-Basques granite marks the inception of deformation in the Port-aux-Basques Complex (van Staal et al., 1994) is uncertain to this author (see chapter IV). If that was the case it would indicate a local Caradocian collision between certain elements of the Laurentian and peri-Gondwanan margins of the Iapetus Ocean. The notion of a local event is reinforced by the tectonic inactivity and the conformable deposition of Caradocian shales and greywackes in the central and northern parts of the Exploits Subzone (see chapter II).

The Early Silurian syn-kinematic intrusion of the Western Head granite into the Cinq-Cerf gneiss at 431.5±1 Ma is the first reliable record of the Salinic orogeny in the southwest Hermitage Flexure (Fig.7.1 and 7.2). The thrusting of the Cinq-Cerf gneiss over its Late Precambrian cover (chapter III) at 430 to 420 Ma coincided with the opening of the Silurian La Poile Basin, indicating local transtension with abundant mafic and felsic magmatism in this part of the Hermitage Flexure. The ca. 418 Ma inversion of the Silurian La Poile Basin is coeval with 420-418 Ma D2 deformation and peak metamorphism in the Port-aux-Basques complex (Fig.7.1; chapter IV). The intrusion of the 417+7/-4 Ma late-syn-D3 dyke in Margaree orthogneiss and the 410±2 Ma titanite cooling ages from the Margaree orthogneiss record the cooling and exhumation of the Port-aux-Basques complex (see chapter IV). The suturing of the peri-Laurentian Dashwoods Subzone and the Grand Bay/Port-aux-Basques complexes at 415 to 390 Ma along the Cape Ray Fault (Dubé et al., 1996) was followed by widespread Early Devonian at 390-384 Ma post-collisional plutonism in the Hermitage Flexure (see chapter II). Early Devonian deformation appears to be restricted to movement along brittle-ductile wrench faults (Fig.7.1 and 7.2).

The Silurian metamorphism and synmetamorphic deformation reflect the climax of the collision between Laurentia and Avalonia (Salinic orogeny of Dunning et al., 1990). Timing of metamorphism and deformation in the Port-aux-Basques Complex (chapter IV) parallels that of the Little Passage gneiss (Fig.7.2) on the southeastern side of the Hermitage Flexure (ca. 423 Ma migmatization; see chapter II). This indicates that Hermitage Flexure was undergoing crustal thickening, metamorphism and deformation while syn-orogenic sedimentary basins (Silurian La Poile basin) were formed in its upper crustal levels (Fig.7.2; Cinq-Cerf block; chapter III). According to the available age data (see chapter II), the Dashwood Subzone escaped the Silurian tectonothermal events in the opposing Grand Bay/Port-aux-Basques Complex (Fig.7.2). Upper amphibolite facies

Silurian Barrovian metamorphism however overprinted the Laurentian rocks of the Corner Brook lake block at 430-425 Ma (see chapter II), north of the Dashwoods Subzone. These tectonothermal events in the Hermitage Flexure coincided with the docking of the Avalon Zone along the Hermitage-Dover fault (see chapter II) and Silurian metamorphism and intrusion of syn-kinematic anatectic granites along the eastern side of the Gander Zone. This revives the question of a possible Late Ordovician inception of the continent-continent collision. The ca. 430 Ma synkinematic bimodal magmatism observed in the Hermitage Flexure suggests the presence of an abnormal high geothermal gradient with possible mantle involvement, which might be consistent with a 30 Ma gap (England and Thompson, 1984) separating peak metamorphism (ca. 420 Ma) and the possible inception of deformation in the Port-aux-Basques Complex at 450 Ma as proposed by van Staal et al (1994). Whalen, et al. (1987), Whalen et al. (1994) and Kerr et al. (1995) have argued for extensive crustal melting at ca. 430-400 Ma due to lithospheric delamination and lower crustal underplating by mantle-derived mafic magmas. If this was the case the time gap for the onset of the collision might be shorter than 30 Ma. However, magmatic heat transfer from the 430 Ma bimodal magmas on the Silurian (ca.420 Ma) Barrovian geothermal gradient of areas like the Port-aux-Basques complex remains to be proven.

It is worth mentioning that the Avalon Zone (Fig.7.4) does not record any of the Paleozoic events discussed above and that Siluro-Devonian plutonism is restricted to the border with the Gander Zone. Although the Precambrian evolution of the Hermitage Flexure suggests a close link with the Avalon Zone, the subsequent Paleozoic evolution indicates that the Avalon Zone escaped the events (Fig.7.1) that shaped the evolution of the peri-Gondwanan margin of the Iapetus Ocean. It is uncertain if the relative position of the Avalon Zone with respect to the Hermitage Flexure and the Gander Zone might be analogous to that of the Midlands microcraton in the British Avalon (Fig.7.4; Soper,

1988), which escaped Paleozoic overprint. But the new data on the Late Precambrian and Paleozoic polycyclic evolution of the Hermitage Flexure (Fig. 7.1) effectively demonstrates the involvement of Avalonian crust in the Early Ordovician and Silurian evolution of the Gondwanan margin of the central mobile belt of the Newfoundland Appalachians.

7.2.- THE EARLY-MID ORDOVICIAN BREAK-UP OF PERI-GONDWANA: IS THERE A CONNECTION BETWEEN THE SARDIC EVENT IN THE SOUTHERN VARISCIDES AND THE PENOBSCOTTIAN EVENT IN THE NORTHERN APPALACHIANS ?

The Sardic event in the southern Variscides is generally interpreted as Early Ordovician continental rifting (Weber, 1984). This hypothesis is difficult to reconcile with the magnitude of the felsic magmatism in the Sierra de Guadarrama (chapter VI). The striking contemporaneity between the Sardic event in the Central Iberian Zone (chapter VI) and the southern Variscides (Stille, 1927) with the Penobscottian event (Neuman and Max, 1989) on the Iapetus side of the Gondwanan margin of the Northern Appalachians and the similarity of the Early Ordovician events in both areas suggests an alternative hypothesis.

The Penobscottian event, as already discussed, involved an Arenig arc-passive margin collision with obduction of 497 Ma ophiolites, arc magmatism and local metamorphism and deformation followed by a major Late Arenig - Early Llanvirn back arc rifting event (Fig. 7.5 ; Dunning and Krogh, 1985; Colman-Sadd et al., 1992; Tucker et al., 1994; van Staal, 1994; van Staal and de Roo, 1995; Winchester and van Staal, 1995; O'Brien et al., 1997).These events in the northern Appalachians are broadly coeval with formation of the Tremadocian

Belledone ophiolite (Fig.7.5 and 7.6; 496 Ma, Ménot et al., 1988; Pin, 1990; Ménot and Paquette, 1993), the weak Arenig Sardic deformation in the Central Iberian Zone (chapter VI) and local high-P metamorphism and bimodal (leptino-amphibolitic group), alkaline and calc-alkaline magmatism in Iberia and the Southern Variscides (Fig.7.6; Weber, 1984; Matte, 1986; Ziegler, 1986; Gebauer et al., 1981; Pin and Lancelot, 1982; Santallier et al., 1988; Gebauer, 1990, 1993; Neubauer and von Raumer, 1993; Carmignani et al., 1994; Biino et al., 1994). These events in the southern Variscides are similar to the Early Paleozoic events described in the Polish Variscides by Oliver et al. (1993) and suggestive of an active margin. Such an active margin could be an extension along the southern Variscides of the peri-Gondwanan margin of the Iapetus Ocean.

This hypothesis is consistent with Early Ordovician faunal (Paris and Robardet, 1990; Neuman and Harper, 1992; Cocks, 1993; S.H. Williams et al., 1995), paleomagnetic (e.g.,van der Pluijm et al., 1995) and sedimentological (Noblet and Lefort, 1990; Prigmore et al., 1997) data, which indicate close proximity between the peri-Gondwanan elements of the Appalachian-Caledonides and the Variscides. These faunal similarities disappear after the major back-arc rifting event in the Late Arenig-Early Llanvirn in the northern Appalachians (Fig.7.5 and 7.7 ; van Staal, 1994; O'Brien et al., 1997). This event marks the drifting of Avalonia from Gondwana and the opening (or widening) of the Rheic Ocean separating Avalonia, including part of the northern Variscides (Fig.7.7 and 7.8; Paris and Robardet, 1990; Scotese and McKerrow, 1990), from Gondwana (Cocks and Fortey, 1982; Paris and Robardet, 1990; Scotese and McKerrow; 1990; van der Pluijm et al., 1995; Torsvik et al., 1996).

7.2.1.- The subduction-related Jurassic break-up of Southern Gondwana during the opening of the South Atlantic: An analog for the Early Ordovician events in the Southern Variscides and Northern Appalachians ?

The proposed Early Ordovician tectonic scenario for the southern Variscides may be similar to the subduction-related Jurassic extension and break up of the Pacific side of Southern Gondwana in Patagonia and Antarctica during opening of the South Atlantic (Storey et al., 1992). Such a setting (Hamilton, 1994) could account for the Early Ordovician arc magmatism, back-arc spreading leading to ophiolite generation, local extensive felsic magmatism, weak extensional deformation (Sardic phase) and the coexistence of alkaline, bimodal and arc magmatism without invoking far-travelled suspect-terranes. Although at a smaller scale, the proposed Arenig magmatic arc in the Sierra de Guadarrama and NW Iberia could be an analog of the Jurassic Marifil felsic volcanism and the associated batholith of Central Patagonia which was associated with transtension and graben formation along the overiding plate of an active margin (Rapela and Pankhurst, 1992). According to this "South Atlantic" back arc rifting model, the rifting of New Zeland from Antartica is a potential analog for the rifting of Avalonia from Gondwana (Fig. 7.8). This hypothesis implies that Avalonia and the Southern Variscides lay along a single margin facing the same ocean (Iapetus?; Fig. 7.8).

7.3.- FINAL REMARKS

The Variscan collision resulted in the closure of the Rheic ocean and the reamalgamation of the peri-Gondwanan terranes of the circum-North Atlantic to their present day relative position (Fig.7.4 and 7.7). These terranes experienced protracted and complex Paleozoic evolutions, as is demonstrated in this thesis in the case of the Hermitage Flexure and the Sierra de Guadarrama. While this thesis has answered some questions it has also posed others. Testing the hypotheses outlined above would require reliable pin-pointing of the different pre-Variscan magmatic pulses along the Variscan belt, and comparative faunal studies between the Iberian Massif and the Northern Appalachians. It is particularly important to differentiate between Early and Late Ordovician magmatism along the Southern Variscides, the latter being apparently unrelated to the Iapetus cycle (Fig.7.7 and 7.8). In this sense, it is the view of this author that the term "Caledonian" should be avoided when describing Ordovician events in the Variscides, since most of the Scottish Caledonides were on the Laurentian side of the Iapetus Ocean. From a Variscan perspective a term like "Sardic" should be more appropiate to define these Early Ordovician events, which are different from the earlier Avalonian/Cadomian events.

I would like to finish on a different note, I was wondering about the common 20 to 30 Ma gap between the time of peak metamorphism and the onset of the voluminous post-tectonic plutonism in both the Hermitage Flexure and the Sierra de Guadarrama. It is not my intention to speculate about why this is, but to point to the wealth and detail of data to be gained about the timing of orogenic processes in medium and high grade terranes from the detailed integration of field observations and petrography with precise and reliable geochronology, where one is lucky to find good field relationships!!

7.4.- SUMMARY.-

The following is a summary of the main conclusions from each of the three study areas. The suggested connection between these areas is not addressed since it has been discussed in chapter VII.

The Cinq-Cerf gneiss (southwest Hermitage Flexure, Newfoundland Appalachians):

The youngest dated unit in the Cinq-Cerf complex is the variably deformed 431.5±1 Ma Western Head granite, which contains amphibolite and gneissic enclaves and is cross-cut by mafic dykes deformed in upper greenschist facies at 420 Ma (titanite). Syn-magmatic deformation ($D2^a$) of the ca. 430 Ma Western Head granite followed by variable greenschist facies mylonitization ($D2^b$) gives the complex its high-grade gneissic appearance.

The 431 Ma granite intruded into older rocks, including the weakly deformed, hornblende-bearing Sandbank granodiorite (584+7/-6 Ma) and the Sandbank Point metagabbro (557+14/-5 Ma). Both the 584 Ma granodiorite and the 557 metagabbros are intrusive into the redefined composite Cinq-Cerf gneiss; which includes amphibole-rich and quartz-rich metasedimentary rocks locally intruded by highly strained 675+12/-11 Ma granitic orthogneiss.

A dated field relationship demonstrates that the 431 Ma granite cross-cuts the gneissic fabric (D1) in the strongly deformed 675 Ma granitic orthogneiss. The preservation of primary magmatic features and the weak deformation of the 584 Ma Sandbank granodiorite indicate the absence of a high-grade regional tectonothermal overprint in the immediate area of this intrusion, and suggest that the D1 composite gneissic fabric, or some of its elements, could be 584-675 Ma in age. The 584 Ma Sandbank granodiorite is coeval with the 584±5 basal volcanic tuffs in the nearby low-grade Late Precambrian

volcanosedimentary rock sequence, which contains gneissic clasts in the basal conglomerates, thus confirming a pre-584 Ma deformational episode and indicating a basement-cover relationship between the Cinq-Cerf gneiss and the low-grade Late Precambrian volcanosedimentary rocks.

The unpublished data of Dunning and O'Brien from Three Islands, a 447 Ma titanite age from a 547 Ma deformed granitoid dyke, remains difficult to explain, but it is consistent with the amphibolite facies granoblastic textures observed in the 557 Ma Sandbank Point metagabbro and the post-584 and pre-499 Ma deformation of the nearby low-grade Late Precambrian volcanosedimentary rocks.

The major and trace element geochemistry of the 557 Ma Sandbank Point metagabbro is characteristic of mantle-derived volcanic arc/transitional tholeiitic magmas. This metagabbro is broadly coeval with the intrusion of 560-565 Ma mafic dykes and 560-570 granites (Roti suite) in the nearby low-grade volcanosedimentary rocks, which are interpreted as volcanic arc-derived.

It is suggested that the Cinq-Cerf gneiss and the nearby Late Precambrian rocks record the evolution of a 585-550 Ma Avalonian volcanic arc. These Precambrian rocks can be correlated with those in the Avalonian and Cadomian belts of North America and Europe, effectively demonstrating the involvement of Avalonian crust in the early Ordovician Penobscottian events of the Northern Appalachians.

The Margaree orthogneiss (Port-aux-Basques complex, southwest Hermitage Flexure, Newfoundland Appalachians)

Detailed fieldwork, U/Pb geochronology and major and trace element geochemistry indicate that the Margaree orthogneiss represents an Early Ordovician mafic-felsic intrusive

complex. This composite orthogneiss, which has been traced inland from Margaree for more than 20 Km, is formed by amphibolites, mafic dioritic orthogneisses, 474+14/-4 Ma hornblende-bearing tonalitic orthogneiss with mafic enclaves, 472±2.5 Ma and 465±3 Ma biotite-bearing granitic orthogneisses and minor ultramafic rocks.

Despite the Silurian upper amphibolite facies overprint, the field relationships suggest that the 472 Ma granites are coeval with extensive mafic magmas. A second generation of amphibolite dykes intruded the 465 Ma granites.

Most of the amphibolites have basaltic compositions and the trace element signature of volcanic arc tholeiites. The 474 Ma tonalites (60-62% SiO2) and the 472 Ma granites (70-72% SiO2) have identical geochemical signatures which correspond to volcanic arc granitoids.

Timing of the Salinic Silurian overprint of the Margaree orthogneiss is constrained by a 417+4/-7 Ma late syn-D3 granitic dyke and 411±2 and 410±2 Ma titanite. The titanite ages are interpreted as amphibolite facies recrystallization ages following the D3 event. These time constraints indicate that the D1, and the syn-peak metamorphism D2 deformational events took place between 465 and 417 Ma. This is consistent with nearby data which suggest a syn- to post-450 Ma age for D1 and ca. 420 Ma for D2.

The Margaree orthogneiss intruded the sedimentary rocks of the Port-aux-Basques complex coevally, within error, with the stitching plutons that postdate the Penobscottian Early Ordovician ophiolite obduction (477±1 Ma Baggs Hill granite; Tucker et al., 1994; 474+6/-4 Ma Partridgeberry Hills granite; Colman-Sadd et al., 1992), Arenig-Early Llanvirn volcanism in the Exploits, Baie d'Espoir (468±2 Ma; Colman-Sadd et al., 1992) and Bay du Nord (466±3 Ma; Dunning et al., 1990) groups and with anatexis and granite intrusion in the Mt. Cormack (465±2 and 464+4/-3 Ma; Colman-Sadd et al., 1992) and Meelpaeg subzones (464±2 Ma; Colman-Sadd et al., 1992). It is suggested that the

Margaree orthogneiss was in an arc/back-arc transitional setting at the time of the major back-arc rifting event on the peri-Gondwanan margin of the Northern Appalachians, following the Penobscottian arc-continent collision.

The Sierra de Guadarrama, Central Iberian Zone (Iberian Massif).

Pre-Variscan evolution: Early Ordovician "Sardic" magmatism.

U-Pb protolith ages of the main types of pre-Variscan orthogneisses of the Somosierra area of the Sierra de Guadarrama demonstrate the presence of an important Early Ordovician felsic magmatic event recorded in the high-grade Western Domain, the overlying low - medium-grade Eastern Domain of the Sierra de Guadarrama and the boundary zone defined by the Variscan, extensional Berzosa-Riaza shear zone (BRSZ).

U-Pb zircon dating of the orthogneisses of the high-grade Western Domain has provided an age of 477±4 Ma (Lozoya gneiss) for the augen gneisses / foliated megacrystic granites, which form the extensive batholithic Morcuera (Glandular) gneiss; it also indicates that the so-called leucogneisses of this domain consist of 488+10/-8 Ma megacrystic granite intruded by 482+8/-7 Ma aplitic veins and 482+9/-8 Ma leucogranitic dykes (Buitrago gneiss). These granitic orthogneisses are contemporaneous with the 480±2 Ma volcaniclastic Cardoso gneiss, which outcrops below the Ordovician "Sardic" unconformity in the Eastern Guadarrama Domain. The pre-Variscan granitic orthogneisses within the BRSZ have a slightly younger age of 468+16/-8 Ma (Riaza gneiss).

In the Sierra de Guadarrama and the rest of the CIZ the Arenig Armorican Quartzite was deposited on top of the Sardic unconformity; therefore, the 480±2 Ma age of the Cardoso gneiss limits the age of the unconformity and the associated Sardic deformation to the Mid-Late Arenig, suggesting a strong linkage with the Arenig felsic magmatism.

The new U-Pb ages corroborate the previous 492-470 Ma whole rock Rb-Sr ages for similar gneisses in other parts of the Sierra de Guadarrama (Vialette et al., 1986;1987), suggesting that most of the pre-Variscan orthogneisses of the Sierra de Guadarrama were generated during the Early Ordovician. These orthogneisses are interpreted as the relicts of a short-lived Early Ordovician continental magmatic arc. The new U-Pb ages also validate regional correlations along strike with the pre-Variscan orthogneisses in the Ollo de Sapo antiform, suggesting that they are part of a 600 Km long relict Early Ordovician felsic magmatic belt which extents from the Sierra de Guadarrama to the northwest coast of Spain.

Variscan evolution of the Sierra de Guadarrama: Early-Middle Carboniferous peak metamorphism and syn-collisional extension and Permo-Carboniferous post-collisional plutonism.

In the area of study the low-medium grade Eastern Guadarrama Domain (St, Cld, Grt and Bt zones) is juxtaposed against the high grade Western Guadarrama Domain (1st Sill - 2nd Sill zones) along the BRSZ (Ky-1st Sill and St zones). In the field area there is no evidence of large-scale D1 compressional structures but an inter-D1-D2 Barrovian metamorphic sequence is well preserved within the BRSZ, with relicts of Ky-St-Qtz mineral assemblages indicating metamorphic conditions in excess of 6.5 Kb and 600°C.

The D1 deformation was followed by a major D2 extensional event with generalized ductile shearing and formation of the BRSZ. The D2 deformation took place during the thermal peak of the Barrovian event in the lower level of the Eastern Domain, and during peak metamorphism, anatexis and growth of low-pressure assemblages in the high-grade Western Domain.

The close relationship between deformation and metamorphic mineral growth allowed the use of U-Pb monazite, xenotime and titanite dating in combination with textural relationships to obtain prograde and cooling ages. These ages constrain peak metamorphism at 337±3 to 329±3 Ma (U-Pb monazite) and the D2 extensional deformation between 337±3 Ma (U-Pb monazite) and 321±3 Ma (U-Pb titanite) in the Sill+Kfs zone of the Western Domain, at 325.6±2 Ma (U-Pb monazite, zircon) in the Sill+Ms zone, at 326±3 Ma (U-Pb monazite) in the relict kyanite Subzone of the BRSZ and between 330±2 - 327±3Ma (U-Pb monazite) and 322±2 Ma (U-Pb titanite) in the St zone and the chloritoid-staurolite transition of the Eastern Domain. The growth of low P/high T cordierite-bearing mineral assemblages during the late stages of the D2 deformation in the Western Domain has been dated at 322±2 Ma (U-Pb monazite and xenotime).

Following the main D2 extensional event the area was reworked by greenschist facies D3 deformation and late extensional detachments. The shallow level intrusion of the post-collisional 292±3 Ma (U-Pb monazite) La Cabrera granite stitches the BRSZ, providing an upper limit for the D3 deformation and, possibly, for the late extensional detachments.

This new data demonstrates for the first time the syn-collisional character of the Late Visean - Early Namurian extension in the Central Iberian Zone, which is also common to other parts of the Variscan belt, and provides the first reliable constraints for the time of peak metamorphism (337-326 Ma). It also shows the presence of a 30 Ma interval between the low P / high T mineral growth and the post-collisional plutonism, indicating that there is no relationship between these two processes in the Sierra de Guadarrama.

REFERENCES CITED:

Abalos, B., 1992, Variscan shear-zone deformation of late Precambrian basement in southwest Iberia: implications for circum-Atlantic pre-Mesozoic tectonics: J. Struct. Geol., v. 14, p. 807-823.

Aftalion, M.; Bowes, D.R. and Vrána, S., 1989, Early Carboniferous U-Pb zircon age for garnetiferous perpotassic granulites, Blansky les massif, Czechoslovakia: Neues Jab. Min. Abh., v. 4, p. 145-152.

Allegret, A. and Iglesias Ponce de Leon, M., 1987, U-Pb dating of Sisargas orthogneiss (Galicia, NW Spain): New evidence of a Precambrian basement in the northwestern part of the Iberian Massif: N. Jb. Miner. Mh., v. 8, p. 355-368.

Alvaro, M.; Bellido, F.; Capote, R.; Casquet, C.; Fernández Casals, M.J.; Fuster, J.M.; Gonzalez Lodeiro, F.; Navidad, M.; Peinado, M. and Villaseca, C., 1981, Excursion sobre el metamorfismo y estructura del Sistema Central y plutonismo asociado 7-10 septiembre de 1981: Cuad. Geol. Iberica, v. 7, p. 53-97.

Ancochea, E.; Hernán, F.; Vegas, R., 1981, Un marco tectonico para el vulcanismo de Atienza (Provincia de Guadalajara).: Cuad. Geol. Iberica, v. 7, p. 421-430.

Andréasson, A., 1994, The Baltoscandian margin in the Neoproterozoic-early Palaezoic times. Some constraints on terrane derivation and accretion in the Artic Scandinavian Caledonides: Tectonophysics, v. 231, p. 1-32.

Aramburu, C. and García-Ramos, J.C., 1993, La sedimentación cambro-ordovícica en la Zona Cantabrica (NO de España): Trab. Geol., Univ. Oviedo, v. 19, p. 45-73.

Archibald, D.A. and Farrar, E., 1976, K-Ar ages of amphibolites from the Bay of Islands ophiolite and the Little Port Complex, western Newfoundland, and their geological implications: Can. J. Earth Sci., v. 13, p. 520-529.

Arenas, R.; Casquet, C. and Peinado, M., 1980, El metamorfismo del sector de Riaza (Somosierra, Sistema Central Español). Implicaciones geoquimicas y petrologicas: Cuad. Lab. Geol. Laxe, v. 1, p. 117-146.

Arenas, R.; González-Lodeiro, F. and Peinado, M., 1982, La zona de cizalla de Berzosa-Riaza en el sector septentrional . Influencia sobre la configuración de la zonas metamórficas: Cuad. Lab. Xeol. Laxe, v.3, p. 123-161.

Arenas, R.; Gil-Ibarguchi, J.I.; Gonzalez Lodeiro, F.; Klein, E.; Martínez-Catalan, J.R.; Ortega Girones, E.; de Pablo Macia, J.G. and Peinado, M., 1986, Tectonostratigraphic units in the complexes with mafic and related rocks of the NW Iberian Massif: Hercynica, II, p.87-110.

Auvray, B.; Charlot, R. and Vidal, P., 1980, Données nouvelles sur le proterozoïque inférieur du domaine nord-armoricain (France): age et signification: Can. J. Earth Sci., v. 17, p. 532-538.

Azor, A.; Gonzalez Lodeiro, G.; Martín Parra, L.M. and Villar Alonso, P., 1991a, Superposición de estructuras hercinianas en el sector de Buitrago-Somosierra (Sierra de Guadarrama, Sistema Central): Geogaceta, v.10, p.116-118.

Azor, A.; Bardaji, T.; Capote, R.; Casquet, C.; Centeno, J.D.; Escuder, J.; Fernández, P.; Gonzalez Casado, J.M.; Martín Parra, L.M.; Merlo, A.; Navidad, M.; Olmo, A; Peinado, M.; Pineda, A.; Sanz, M.A.; Vicente, G.; Villar Alonso, P. and Villaseca, C., 1991b, Mapa y memoria explicativa del a Hoja # 458 (Prádena) del Mapa Geológico Nacional a escala 1: 50.000, ITGE (Spanish Geol. Survey), pp.103.

Azor, A.; Gonzalez Lodeiro, F.; Hacar Rodriguez, M.; Martín Parra, L.M.; Martínez Catalan, J.R. and Perez Estaun, A., 1992, Estratigrafia y estructura del Paleozoico en el Dominio del Ollo de Sapo: in Gutiérrez Marco, J.; Saavedra, J. and Rabano, I. (Eds.): Paleozoico Inferior de Ibero-America, Univ. Extremadura,pp. 469-483

Azor, A.; Gonzalez Lodeiro, F. and Simancas, J.F., 1994, Tectonic evolution of the boundary between the Central Iberian and Ossa-Morena zones (Variscan belt, southwest Spain): Tectonics, v. 13, p. 45-61.

Bailey, E.B., 1935, Tectonic Essays, Mainly Alpine: Clarendon Press, Oxford, pp. 200.

Bateman, R., 1995, The interplay between crystallization, replenishment and hybridization in large felsic magma chambers: Earth Science Reviews, p. 91-106.

Barbarin, B. and Didier, J., 1991, Macroscopic features of mafic microgranular enclaves: in Didier, J. and Barbarin, B. (Eds.). Enclaves and Granite petrology. Developments in Petrology, 13, Elsevier, Amsterdam, p.253-262.

Barbero, L., 1995, Granulite-facies metamorphism in the Anatectic Complex of Toledo, Spain: late Hercynian tectonic evolution by crustal extension: J. Geol. Soc. London, v. 152, p. 365-382.

Barnes, R.P.; Lintern, B.C. and Stone, P., 1989, Timing and regional implications of deformation in the Southern Uplands of Scotland: J. Geol. Soc. London., v. 146, p. 905-908.

Barr, S.M. and White, C.E., 1996, Contrasts in the late Precambrian-early Paleozoic tectonothermal history between Avalon composite terrane sensu stricto and other possible peri-Gondwanan terranes in southern New Brunwsick and Cape Breton Island, Canada: in Nance, R.D. and Thompson, M.D. (Eds.). Avalonian and Related Peri-Gondwanan Terranes of the Circum-North Atlantic. Geological Society of America Spec. Paper 304, Boulder, p. 95-108.

Bea, F., 1996, Residence of REE, Y, Th and U in granites and crustal protoliths: implications for the chemistry of crustal melts: J. Petrol., v. 37, p. 521-552.

Bellido, F., 1980, Estudio del metamorfismo de contacto producido por la intrusion del pluton granitico de La Cabrera (Sistema Central Español): Est. Geol., v. 36, p. 85-92.

Bellido, F.; Capote, C.; Casquet, C.; Fúster, J.M.; Navidad, M.; Peinado, M. and Villaseca, C., 1981, Caracteres generales del cinturón hercínico en el sector oriental del Sistema Central Español: Cuad. Geol. Ibérica, v.7, p. 15-51.

Bellido, F.; Casquet, C.; Escuder, J.; Klein, E.; Navidad, M.; Peinado, M. and del Olmo, A., 1991, Hoja geológica a escala 1:50.000 y memoria, 2- serie, Buitrago del Lozoya, Mapa geológico de España, ITGE (Spanish Geol. Survey), # 484, pp. 105.

Benn, K.; Genkin, M.; van Staal, C.R. and Lin, S., 1993, Structure and anisotropy of magnetic susceptibility of the Rose Blanche granite, southwestern Newfoundland: kinematics and relative timing of emplacement: Current Research, part D, Geological Survey of Canada, paper 93-1D, p. 73-82.

Bevier, M.L.; Barr, S.M.; White, C.E. and Macdonald, A.S., 1993, U-Pb geochronologic constraints on the volcanic evolution of the Mira (Avalon) terrane, southeastern Cape Breton Island, Nova Scotia: Can. J. Earth Sci., v.30, p. 1-10.

Biino, G.G.; Oberli, F. and Meier, M., 1994, Rates of metamorphic processes constrained by petrology and single zircon U-Pb chronology: a case study on former HP-HT mafic rocks from the central Alps: Mineralogical Magazine, v. 58A, p. 92-93.

Bischoff, L.; Schafer, G.; Schmidt; K. and Walter, R., 1973, Zur Geologie der mittleren Sierra de Guadarrama (Zentralspanien): Forch. Geol. Paläont. Münster, v. 28, p. 27-30.

Bischoff, L.; Lenz, H.; Müller, P. and Schmidt, K., 1978, geochemische und geochronologische Untersuchungen an Metavulkaniten und Orthogneisen der öslichen Sierra de Guadarrama (Spanien): Neues Jb. Mineral Montash, v. 410, p. 470-478.

Blackwood, R.F., 1985, Geology of the Grey River area, southwest coast of Newfoundland: Current research. Newfoundland Department of Mines, Mineral development division report 85-1, p. 153-164.

Bonjour, J.L. and Chauvel, J.J., 1988, Un example de sédimentation initiale dans un basin paléozoïque: étude pétrographique et geochimique de l'Ordovicien Inférier dela presqüîle de Crozon (Finistere): Bull. Soc. Géol. France, p. 81-91.

Brenchley, P.J.; Romano, M.; Young, T.P. and Storch, P., 1991, Hirnantian glaciomarine diamictites-evidence for the spread of glaciation and its effect on Upper Ordovician faunas: in Barnes, C.R. and Williams, S.H. (Eds.) Advances in Ordovician geology, Geological Survey of Canada, paper 90-9, p.325-336.

Brown, P.A., 1973, Structural and metamorphic history of the gneisses of the Port-aux-Basques region, Newfoundland. MSc thesis, Memorial University of Newfoundland, 113 pp.

Brown, P.A., 1975, Basement-cover relationships in Southeast Newfoundland. Ph.D. thesis, Memorial University of Newfoundland, 220 pp.

Brown, P.A., 1977, Geology of the Port-aux-Basques area (11o/11) Newfoundland: Report 77-2, Dept. of Mines and Energy, Government of Newfoundland and Labrador, 1:50000 map, 11 pp.

Brown, M.; Power, G.M.; Topley, C.G. and D'Lemos, R.S., 1990, Cadomian magmatism in the North Armorican Massif: in D'Lemos, R.S.; Strachan, R.A. and Topley, C.G. (editors), 1990, The Cadomian Orogeny: Geol. Soc. London, Spec. Pub. 51, p 181-213.

Bucher, K. and Frey, M., 1994, Petrogenesis of metamorphic rocks: Springer-Verlag, Berlin, pp.318.

Burg, J.P.; Iglesias, M.; Laurent, P.; Matte, P. and Ribeiro, A., 1981, Variscan intracontinental deformation: the Coimbra-Cordoba shear zone (southwest Iberian Peninsula): Tectonophysics, v.78, p.161-177.

Burg, J.P.; van den Driessche; Brun, J.P., 1994, Syn- to post-thickening extension in the Variscan belt of Western Europe: Modes and strcutural consequences: Géol. de la France, v. 3, p. 33-51.

Burgess, J.L.; Brown, M. and van Staal, C.R., 1992, Preliminary report on the metamorphic geology of the Port aux Basques Complex, southwestern Newfoundland: Current Research, Part D, Geological Survey of Canada, paper 92-1D, p. 145-154.

Burgess, J.L.; Brown, M. and van Staal, C.R., 1993, Pressure-temperature conditions and a P-T path for the Port aux Basques area, southwest Newfoundland: Current research, part D, Geological Survey of Canada, paper 93-1D, p. 47-55.

Burgess, J.L.; Brown, M.; Dallmeyer, R.D. and van Staal, C.R., 1995, Microstructure, metamorphism, thermochronology and P-T-t-deformation history of the Port aux Basques gneisses, south-west Newfoundland, Canada: J. Metamorphic Geol., v.13, p.751-776.

Cabanis, B. and Lecolle, M., 1989, Le diagramme La/10-Y/15-Nb/8: un outil pour la discrimination des series volcaniques et la mise en evidence des processus de mélange et/ou de contamination crustale: Compt. Ren. Acad. Sciences, Series II, v.309, p. 2023-2029.

Capote, R. and Fernández Casals, M.J., 1975, Las series anteordovícicas del Sistema Central: Bol. Geol. Min., v. 86, p. 581-596.

Capote, R.; Casquet, C.; Fernández Casals, M.J.; Moreno, F.; Navidad, M.; Peinado, M. and Vegas, R., 1977, The Precambrian in the Central part of the Iberian Massif: Estud. Geol., v. 33, p. 343-355.

Capote, R.; Casquet, C. and González Casado, J.M., 1981, Tectónica y metamorfismo del macizo hercínico de Honrubia (Provincia de Segovia): Cuad. Geol. Ibérica, v. 7, p. 441-454.

Capote, R.; Casquet, C. and Fernández Casals, M.J., 1981, La tectónica de cabalgamientos en el Sistema Central Español: Cuad. Geol. Ibérica, v. 7, p. 455-469.

Capote, R.; Casquet, C. and Fernández Casals, M.J., 1982, Los grandes complejos estructurales del Sistema Central: modelo de evolución tectonometamórfica: Rev. Real Acad. C. Exac., Fis.y Nat., v. 76-2, p. 313-331.

Carmignani, L.; Carosi, R.; Di Pisa, A.; Gattiglio, M.; Musumeci, G.; Oggiano, G. and Pertusati, P.C., 1994, The hercynian chain in Sardinia (Italy): Geodynamica Acta, v. 7, p. 31-47.

Casquet, C., 1986, C-O-H-N fluids in quartz segregations from a major ductile shear zone: The Berzosa Fault, Spanish Central System: Jour. Met. Geol. , v. 4, p. 117-130.

Casquet, C. and Fernández Casals, M.J., 1981, Las anfibolitas de la región de Buitrago del Lozoya (Sistema Central Español): Cuad. Geol. Ibérica, v. 7, p. 121-134.

Casquet, C. and Tornos, F., 1981, Metamorfismo regional e implicaciones geotermométricas en el Alto valle del Lozoya (Sistema Central Español): Cuad. Geol. Ibérica, v.7, p. 135-150.

Casquet, C. and Navidad, M., 1985, El metamorfismo en el Sistema Central Español. Comparacion entre el sector central y el oriental en base al zonado del granate: Rev. Real Acad. C. Exac., Fis. y Nat., v. 79-4, p. 523-548.

Cawood, P.A., 1989, Acadian remobilization of a Taconian ophiolite, Hare Bay allochthon, northwestern Newfoundland: Geology, v.17, p.257-260.

Cawood, P.A., 1990, Late-stage sliding of ophiolite thrust sheets in Oman and Western Newfoundland: in Malpas, J.; Moores, E.M.; Panayioutou, A. and Xenophontos, C., (Eds.) Ophiolites, Oceanic Crustal Analogues. Proceedings of the Symposium "TROODOS 87", Geological Survey Department, Ministry of Agriculture and Natural Resources, Nicosia, Cyprus, p. 433-455.

Cawood, P.A.; Williams, H.; O'Brien, S.J. and O'Neill, P.P., 1988, Trip A1. A geological cross-section of the Appalachian orogen: Field trip guidebook, Geol. Assoc. Can., Mineralogical Association of Canada., Can. Soc. Petroleum Geol. , St. John's (Nfld.) 1988 meeting, pp.159

Cawood, P.A.; van Gool, J.A.M. and Dunning, G.R., 1995, Collisional tectonics along the Laurentian margin of the Newfoundland Appalachians: in Hibbard, J.P.; van Staal, C.R. and Cawood, P.A. (Eds.) Current Perspectives in the Appalachian-Caledonian Orogen: Geol. Assoc. Can. Spec. paper 41, p. 283-302.

Chaloupsky, J., 1990, Precambrian of the Bohemian Massif, Central Europe: in Strachan, R.A. and Taylor, G.K. (Eds.) Avalonian and Cadomian Geology of the North Atlantic, Blackie & Son Ltd., Glasgow-London, p. 93-108.

Chandler, F.W.; Sullivan, R.W. and Currie, K.L., 1987, The age of the Springdale Group, western Newfoundland and correlative rocks - evidence for a Llandovery overlap assemblage in the Canadian Appalachians: Trans. R. Soc. Edin., Earth Sci, v. 78, p. 41-49.

Chorlton, L.B., 1978, Geology of the La Poile area (110/9), Newfoundland: Newfoundland Dept. Mines and Energy Rept. 78-5, 13 pp.

Chorlton, L.B., 1980, Geology of the La Poile River area (110/16) , Newfoundland Dept. Mines and Energy Rept. 80-3, 86 pp.

Chorlton, L.B., 1984, Geological development of the southern Long Range Mountains, southwest Newfoundland: a regional synopsis. Ph.D. thesis, Memorial University of Newfoundland, St. John's, Newfoundland, 580 pp.

Chorlton, L.B. and Dallmeyer, R.D., 1986, Geochronology of early to middle Paleozoic tectonic development in the southwest Newfoundland Gander Zone: J. Geol., v. 94, p. 67-89.

Chorlton, L.B.; Williams, H. and Wilton, D.H.C., 1995, Cape Ray Belt, Chapter 4: in Williams, H. ed., Geology of the Appalachian-Caledonian orogen in Canada and Greenland: Geological Survey of Canada, Geology of Canada, # 6, (*also*, Geological Society of America, The Geology of North America, v. F-1), p.397-403.

Clavez, J.Y. and Vidal, P., 1978, Two billion years old relicts in the Hercyinian belt of Western Europe: Contrib. Min. Petrol., v.65, p. 395-399.

Clemens, J.D. and Vielzeuf, D., 1987, Constraints on melting and magma production in the crust: Earth Planet. Sci. Lett., v. 86, p. 287-306.

Clift, P.D. and leg 135 SCIENTIFIC PARTY, 1994, Volcanism and sedimentation in a rifting island arc terrain; an example from Tonga, southwest Pacific: in Smellie, J.L. (Ed.). Volcanism associated with extension at consuming plate margins. Geol Soc. Spec. Pub. XX, Geol. Soc. London, p. 29-52.

Cocks, I.R.M. and Fortey, R.A., 1982, Faunal evidence for ocean separation in the Paleozoic of Britain: J. Geol. Soc. London, v. 139, p.465-478.

Cocks, I.R.M. anf Fortey, R.A., 1990, Biogeography of Ordovician and Silurian faunas: in McKerrow, W.S. and Scotese, C.R. (Eds.) Palaeozoic palaeogeography and biogeography. Geol Soc. London Memoir 12, p. 97-104.

Cocks, L.R.M., 1993, Triassic pebbles, derived fossils and the Ordovician to Devonian palaeogeography of Europe: J. Geol. Soc. Lon, v. 150, p. 219-226

Cocks, L.R.M. and McKerrow, W.S., 1993, A reassesment of the early Ordovician "Celtic" brachiopod province: J. Geol. Soc. London, v. 150, p. 1039-1042.

Colman-Sad, S.P., 1980, Geology of south central Newfoundland and evolution of the eastern margin of Iapetus: Am. J. Sci., v. 280, p. 991-1017.

Colman-Sadd, S.P. and Swinden, H.S., 1984, A tectonic window in central Newfoundland? Geological evidence that the Appalachian Dunnage Zone is allochthonous: Can. J. Earth Sci., v. 21, p. 1349-1367.

Colman-Sadd, S.P.; Hayes, J.P. and Knight (compilers), I., 1990, Geology of the Island of Newfoundland (Map 90-01; 1:1000000 scale). Geological Survey branch, Dept. of Mines and Energy. Government of Newfoundland and Labrador.

Colman-Sadd, S.P.; Dunning, G.R.; Dec, T., 1992a, Dunnage-Gander relationships and Ordovician orogeny in central Newfoundland: a sediment provenance and U/Pb age study: Am.J. Sci. v.292, p.317-355.

Colman-Sadd, S.P.; Stone, P.; Swinden, H.S. and Barnes, R.P., 1992b, Parallel geological development in the Dunnage Zone of Newfoundland and the Lower Paleozoic terranes of southern Scotland: an assesment: Trans. R. Soc.Edin: Earth Sci. v. 83, p. 571-594.

Conti, P., Di Pisa, M., Gattiglio, M. & Meccheri, M. 1993. The Pre-Alpine basement in the Alpi Apuane (Northern Apennines, Italy): in von Raumer, J.F. and Neubauer, F. (Eds). Pre-Mesozoic geology in the Alps. Springer-Verlag, Berlin. p.610-621.

Cooper, J.R., 1954, The La Poile-Cinq Cerf map area, Newfoundland (1: 63,360 map): Geological Survey of Canada, Memoir 276, pp.62.

Corretge, L.G and Suárez, O., 1990, Igneous rocks (Cantabrian zone): in Dallmeyer, R.D. and Martínez García, E., (Eds). Pre-Mesozoic geology of Iberia, Springer-Verlag, Berlin, p. 72-79.

Cortesogno, L.; Dallagiovanna, G.; Gaggero, L. and Vanossi, M, 1993, Elements of the Palaeozoic history of the Ligurian Alps: in von Raumer, J.F. and Neubauer, F. eds, Pre-Mesozoic Geology in the Alps, Springer-Verlag, Berlin Heidelberg, p.257-277.

Costa, S., 1991, East-west diachronism of collisional stage in the French massif Central: implications for the European Variscan Orogen: Geodin. Acta, v. 5, p. 51-68.

Courjault-Radé, P.; Debrenne, F. and Gandin, A., 1992, Palaegeographic and geodynamic evolution of the Gondwana continental margins during the Cambrian: Terra Nova, v.4, p. 657-667

Dallmeyer, R.D. and Williams, H., 1975, $^{40}Ar/^{39}Ar$ ages from the Bay of Islands metamorphic aureole: their bearing on the timing of Ordovician ophiolite obduction: Can. J. Earth Sci., v.12, p. 1685-1690.

Dallmeyer, R.D., 1988, Polyphase tectonothermal evolution of the Scandinavian Caledonides: in Harris, A.L. and Fettes, D.J. (Eds.), The Caledonian-Appalachian Orogen, Geol. Soc. Spec. Pub. 38, p.365-379.

Dallmeyer, R.D. and Martínez-García, E., 1990, Pre-Mesozoic geology of Iberia: Springer-Verlag, Berlin-Heidelberg, pp.416

Dallmeyer, R.D. and Gil Ibarguchi, J.I., 1990, Age of amphibolitic metamorphism in the ophiolitic unit of the Morais allochthon (Portugal): implications for early Hercynian orogenesis in the Iberian Massif: J. Geol. Soc. London, v. 147, p.873-878.

Dallmeyer, R.D.; Ribeiro, A. and Marques, F., 1991, Polyphase Variscan emplacement of exotic terranes (Morais and Braganza Massifs) onto Iberian sucessions: evidence from $^{40}Ar/^{39}Ar$ mineral ages: Lithos, v.27, p. 133-144.

Dallmeyer, R.D. and Quesada, C., 1992, Cadomian vs. Variscan evolution of the Ossa-Morena zone (southwest Iberia): field and $^{40}Ar/^{39}Ar$ mineral age constraints: Tectonophysics, v. 216, p. 339-364.

Dallmeyer, R.D. and Tucker, R.B., 1993, U-Pb zircon age for the Lagoa augen gneiss, Morais Complex, Portugal: Tectonic implications. J. Geol. Soc. London, v. 150, p.405-410.

Dallmeyer, R.D.; Giese, U.; Hoymann, K.H.; Kramm, U.; Winterfeld, C.; Walter, R., 1993a, The boundary of Ossa-Morena Zone and South-Portuguese Zone in southwest Spain: geodynamic evolution of a Variscan suture during oblique convergence: 1993 Geological Society of America annual meeting, Boston, abstracts with programs, p. A-342.

Dallmeyer, R.D.; Martínez Catalán, J.R.; Arenas, R.; Gil Ibarguchi, J.I.; Gervas, P.; Farias, P.; Aller, J.; Bastida, F. and Gutiérrez Alonso, G., 1993b, $^{40}Ar/^{39}Ar$ dating of mylonites in the allochthonous complexes of NW Spain: TERRA abstracts, EUG meeting VII, Strasbourg, v.5 (1), p.384.

Dallmeyer, R.D.; Brown, M.; Grocott, J.; Taylor, G.K. and Treolar, P. J., 1996, Mesozoic magmatic and tectonic events within the Andean plate boundary zone, 26°-27°30', North Chile: constraints from $^{40}Ar/^{39}Ar$ mineral ages: Journal of Geology, v. 104, p. 19-40.

Davis, D.W., 1982, Optimum linear regression and error estimation applied to U-Pb data: Canadian Journal of Earth Sciences, v. 19, p.2141-2149.

Dewey, J.F., 1969, Evolution of the Appalachian/Caledonian orogen: Nature, v.222, p.124-129.

Díez Balda, M.; Vegas, R. and Gonzalez Lodeiro, F., 1990, Structure (Central Iberian Zone): in Dallmeyer, R.D. and Martínez García Eds, Pre-Mesozoic Geology of Iberia, Springer-Verlag, Berlin Heidelberg, p. 172-188.

Díez Balda, M.A.; Martínez Catalan, J.R. and Ayarza Arribas, P., 1995, Syn-collisional extensional collapse parallel to the orogenic trend in a domain of steep tectonics: the Salamanca Detachment Zone (Central Iberian Zone, Spain): J. Struct. Geol., v. 17, p. 163-182.

D'Lemos, R.S.; Strachan, R.A. and Topley, C.G. (editors), 1990, The Cadomian Orogeny: Geol. Soc. London, Spec. Pub. 51, pp.423.

D'Lemos, R.; Scholfield, D. and King, T., 1995, Deciphering pre-, syn- and post-emplacement structures associated with syn-tectonic plutons: a case study from NE Newfoundland: Abstracts, Tectonic Studies Group, 26th meeting, Cardiff.

Doblas, M.; Oyarzun, R.; Lunar, R.; Mayor, N. and Martínez, J., 1988, Detachment faulting and late Paleozoic epithermal Ag-base-metal mineralization in the Spanish Central System: Geology, v. 16, p. 800-803.

Doblas, M., 1991, Late Hercynian extensional and transcurrent tectonics in Central Iberia: Tectonophysics, v. 191, p. 325-334.

Doblas, M.; López-Ruiz, J.; Oyarzun, R.; Mahecha, V.; Sánchez Moya, Y.; Hoyos, M.; Cebriá, J.M.; Capote, R.; Hernández Henrile, J.L.; Lillo, J.; Lunar, R.; Ramos, A. and Sopeña, A., 1994a, Extensional tectonics in the central Iberian Peninsula during the Variscan to Alpine transition: Tectonophysics, v. 238, p. 95-116.

Doblas, M.; Oyarzun, R.; Sopeña, A.; López-Ruiz, J.; Capote, R.; Hernandez Enrile, M.; Hoyos, M.; Lunar, R. and Sánchez Moya, Y., 1994b, Variscan-late Variscan-early Alpine progressive extensional collapse of central Spain: Geodinamica Acta, v. 7, p. 1-14.

Droop, G.T.R. and Harte, B., 1995, The effect of Mn on the phase relations of medium-grade pelites: constraints from natural assemblages on petrogenetic grid topology: J. Petrol., v. 36, p. 1549-1578.

Dubé, B.; Dunning, G.R.; Lauziére, K. and Roddick, J.C., 1996, New insights into the Appalachian Orogen from geology and geochronology along the Cape Ray Fault zone, southwest Newfoundland: Geological Society of America Bulletin, v. 108, n.1, p. 101-116

Dubé, B. and Lauzière, K., 1996, Structural evolution of a major fault zone: the Cape Ray Fault Zone, southwestern Newfoundland, Canada: Can. J. Earth. Sci., v.33, p. 199-215.

Dubé, B. and Dunning, G.R. (Submitted/Accepted), A Late Proterozoic high-sulfidation epithermal gold deposit: Hope Brook, Newfoundland Canda: Economic Geology.

Dunning, G.R. and Krogh, T.E., 1985, Geochronology of ophiolites of the Newfoundland Appalachians: Can. J. Earth Sci., v. 22, 1659-1670.

Dunning, G.R.; Kean, B.F.; Thurlow, J.G. and Swinden, H.S., 1987, Geochronology of the Buchans, Roberts Arm and Victoria Lake Groups and the Mansfield Cove Complex, Newfoundland: Can. J. Earth Sci., v. 24, p. 1175-1184

Dunning, G.R.; Wilton, D.H.C. and Herd, R.K., 1989, Geology and geochronology of a Taconic batholith, southwestern Newfoundland: Trans. R. Soc. Edin. Earth Sci., v. 80, p. 159-168.

Dunning, G.R. and O'Brien, S.J., 1989, Late Proterozoic-early Paleozoic crust in the Hermitage Flexure, Newfoundland Appalachians: U/Pb ages and tectonic significance: Geology, v. 17, p. 548-551.

Dunning, G.R.; O'Brien, S.J.; Colman-Sadd, S.P.; Blackwood, R.F.; Dickson, W.L.; O'Neill, P.P. and Krogh, T.E., 1990, Silurian orogeny in the Newfoundland Appalachians: J. Geol., v.98, p.895-913.

Dunning, G.R.; Swinden, H.S.; Kean, B.F.; Evans, D.T.W. and Jenner, G.A., 1991, A Cambrian island arc in the Iapetus: geochronology and geochemistry of the Lake Ambrose volcanic belt, Newfoundland Appalachians: Geol. Mag., v.128 (1), p. 1-17.

Dunning, G.R.; Lepvrier, C.; O'Brien, S.J.; Colman-Sadd, S.P. and Maluski, H., 1995, U-Pb and $^{40}Ar/^{39}Ar$ chronology of Avalonian events on Presquíle du Cap Miquelon (le Cap), Saint Pierre et Miquelon (France): Can. J. Earth Sci., v. 32, p.952-958.

Dunning, G.R.; Díaz García, F.; Arenas, R. and Martínez Catalan, J.R., 1997, A Lower Devonian ophiolite in the Allochthonous Complexes of the Iberian Massif (Variscan Belt): U-Pb zircon protolith age from the Careón ophiolite: Terra Abstracts, v. 91, p. 100

du Toit, A.A., 1937, Our wandering continents, a hypothesis of continental drifting: Oliver and Boyd, Edinburgh.

Durling, P.W.; Bell, J.S. and Fader, G.B.J., 1987, The geological structure and distribution of Paleozoic rocks on the Avalon platform offshore Newfoundland: Can. J. Earth Sci., v. 24, p. 1412-1420.

Egal, E.; Guerrot, C.; Le Goff, E.; Thiéblemont, D. and Chantraine, J., 1996, The Cadomian orogeny revisited in Northern Brittany (France): in Nance, R.D. and Thompson, M.D. (Eds.) Avalonian and related peri-Gondwanan terranes of the circum-North Atlantic. Geological Society of America Spec. paper 304, p. 282-318.

Eguíluz, L. and Abalos, B., 1992, Tectonic setting of Cadomian low-pressure metamorphism in the central Ossa-Morena Zone (Iberian Massif, southwest Spain): Precambrian Research, v. 56, p. 113-137.

Ellam, R.M., Lithospheric thickness as a control on basalt geochemistry: Geology, v.20, p.153-156.

Elliott, C.G.; Dunning, G.R. and Williams, P.F., 1991, New U/Pb zircon age constraints on the timing of deformation in north-central Newfoundland and implications for early Paleozoic Appalachian orogenesis: Geological Society of America Bull., v. 103 (1), p. 125-135.

England, P.C. and Thompson, A.B., 1984, Pressure-Temperature-TIme paths of regional metamorphism I. Heat transfer during the evolution of regions of thickened continental crust.: Journal of Petrology, v.25, p. 894-928.

Erdmer, P. and Williams, H., 1995, Grenville basement rocks (Humber Zone), Chapter 3: in Williams, H. ed., Geology of the Appalachian-Caledonian orogen in Canada and Greenland: Geological Survey of Canada, Geology of Canada, # 6, (*also*, Geological Society of America, The Geology of North America, v. F-1), p. 50-61.

Escuder Viruete, J.; Arenas, R.; Martínez Catalán, J.R., 1994, Tectonothermal evolution associated with Variscan crustal extension in the Tormes Gneiss Dome (NW Salamanca, Iberian Massif, Spain): Tectonophysics, v. 238, p. 117-138.

Escuder Viruete, J.; Hernaiz Huerta, P.P.; Valverde Vaquero, P.; Rodriguez Fernández, L.R. and Dunning, G.R., 1996, Evolución microestructural y metamórfica de la zona de cizalla extensional de Berzosa-Riaza: la superposición de asociaciones minerales de Baja-P/Alta-T sobre una secuencia Barroviense: Geogaceta, v. 20(4), p. 879-882.

Eusden, J.D. and Lyons, J.B., 1993, The sequence of Acadian deformations in central New Hampshire: in Roy, D.C. and Skehan, J.W. (Eds.) The Acadian orogeny: recent studies in New England, Maritime Canada and the Autochthonus foreland : Geological Society of America Spec. Pub. 275, p. 51-65

Evans, D.T.W.; Kean, B.F. and Dunning, G.R., 1990, Geological studies, Victoria Lake Group, Central Newfoundland: in Current Research, Newfoundland Department of Mines and Energy, Geological Survey Branch, report 90-1, p. 131-144.

Farias, P.; Gallastegui, G.; Gonzalez Lodeiro, F.; Marquinez, J.; Martín Parra, L.M.; Martínez Catalan, J.R.; Pablo Macia, J.G. and Rodriguez Fernández, L.R., 1987, Aportaciones al conocimiento de la litoestratigrafia y estructura de Galicia Central. IX Reun. Geol. Oeste Peninsular, Oporto.

Farias, P., 1992, El Paleozoico Inferior de la zona de Galicia-Trás-os-Montes (Cordillera Herciniana, NW de España): in Gutiérrez Marco, J.G., Saavedra, J. and Rabano, I. eds: El Paleozoico Inferior de Ibero-America, Univ. de Extremadura, p.496-504.

Faure, M., 1995, Late orogenic carboniferous extensions in the Variscan French Massif Central: Tectonics, v. 14, p. 132-153.

Febrel., T; fuster, J.M. and de Pedro, F., 1958, Explicacion de la hoja 484 (Buitrago de Lozoya): Inst. Geol. Min. de España: pp. 103.

Fernández, A.N. and Barbarin, B., 1991, Relative rheology of coeval mafic and felsic magmas: Nature of resulting interaction processes and shape and mineral fabrics of mafic microgranular enclaves: in Didier, J. and Barbarin, B. (Eds.). Enclaves and Granite petrology. Developments in Petrology, 13, Elsevier, Amsterdam, p. 263-275.

Fernández Casals, M.J., 1974, Significado geotectonico de la formacion Gneises de la Morcuera: Stud. Geol. , v. 7, p. 87-106.

Fernández Casals, M.J., 1979, Las deformaciones hercinicas del limite Somosierra-Guadarrama (Sistema Central): Estud. Geol., v. 35, p. 169-191.

Fernández Casals, M.J. and Capote, R., 1970, La tectónica paleozoica del Guadarrama en la región de buitrago del Lozoya: Bol. Geol. Min., v. 81, p. 562-568.

Fernández Tomas, J., 1981, Mapa y memoria de la hoja # 304 (Hermisende) del mapa geologico de España, E. 1:50.000 (MAGNA). ITGE (Spanish Geol. Survey).

Fernández Rodriguez, C., 1992, La zona de cizalla de Hiendelaencina (Sistema Central Español): analisis de la deformación interna y de la microfábrica: Simposios tomo 2, III Congreso geológico de España, p. 375-384.

Ferragne, A., 1972, Le Precambrien et le Paléozoique de la province d'Orense (N-W de l'Espagne): stratigraphie, tectonique, metamorphisme, Thesis Univ. de Bordeaux, pp. 249.

Fortey, R.A. and Cocks, I.R.M., 1986, Marginal faunal belts and their structural implications, with examples from the Lower Palaeozoic: J. Geol. Soc. London, v.143, p.151-160.

Franke, W., 1989, Tectonostratigraphic units in the Variscan belt of central Europe: in Dallmeyer, R.D. (Eds.), Terranes in the Circum-Atlantic Paleozoic Orogens, Geological Society of America Spec. Paper 230, p. 67-90.

Frisch, W. and Neubauer, F., 1989, Pre-Alpine terranes and tectonic zoning in the Eastern Alps: Dallmeyer, R.D. (Eds.) Terranes in the Circum-Atlantic Paleozoic orogens: Geological Society of America Spec. Paper 230, p. 91-100.

Fuster, J.M.; Aparicio, A.; Casquet, C.; García Cacho, L.; Mora, A. and Peinado, M., 1974, Interacciones entre los metamorfismos plurifaciales y polifásicos del Sistema Central Español: Bol. Geol. Min., v. 85, p. 595-600.

Fuster, J.M.; Navidad, M. and Villaseca, C., 1981, Relaciones entre ortogneises y series volcanosedimentarias en el macizo de el Caloco (Guadarrama Central): Cuad. Geol Ibérica, v. 7, p. 161-171.

Gallastegui, G.; Aramburu, C.; Barba, P.; Fernández, L.P. and Cuesta, A., 1992, Vulcanismo del Paleozoico Inferior en la Zona Cantábrica (NO de España): Gutiérrez-Marco, J.G.; Saavedra, J. and Rábano, I. (Eds.), El Paleozoico Inferior de Ibero-América, Univ. Extremadura (Spain), p.435-451.

Gamble, J.A.; Wright, I.C.; Woodhead, J.D. and McCulloch, M.T., 1994, Arc and back-arc geochemistry in the southern Kermadec arc-Ngatoro basin and offshore Taupo volcanic zone, southwest Pacific: in Smellie, J.L. (Ed.). Volcanism associated with extension at consuming plate margins. Geol. Soc. Spec. Pub. XX, Geol Soc. London, p. 193-213.

Gebauer, D.; Bernard-Griffiths, J and Grünenfelder, 1981, U-Pb zircon and monazite dating of a mafic-ultramafic complex and its country rocks - example: Sauviat-sur-Vige, French Central Massif-: Contrib. Mineral. Petrol., v.76, p. 292-300.

Gebauer, D., 1993, The pre-Alpine evolution of the continental crust of the Central Alps - an overview: in von Raumer, J.F. and Neubauer, F. eds, Pre-Mesozoic Geology in the Alps, Springer-Verlag, Berlin Heidelberg, p. 93-118

Gebauer, D.; Martínez-García, E. and Hepburn, J.C., 1993, Geodynamic significance, age and origin of the Ollo de Sapo augengneiss (NW Iberian Massif, Spain): 1993 Geological Society of America annual meeting, Boston, abstracts with programs, p. A-342.

Gee, D.G., 1975, A tectonic model for the central part of the Scandinavian Caledonides: Am.J.Sci., v. 275A, p. 468-515.

Gibbons, W., 1990, Pre-Arenig terranes of northwest Wales: in Strachan, R.A. and Taylor, G.K. (Eds.) Avalonian and Cadomian Geology of the North Atlantic, Blackie & Son Ltd., Glasgow-London, p.28-48.

Gibbons, W. and Horák, J., 1990, Contrasting metamorphic terranes in northwest Wales: in D'Lemos, R.S.; Strachan, R.A. and Topley, C.G. (editors), 1990, The Cadomian Orogeny: Geol. Soc. London, Spec. Pub. 51, p. 315-328.

Gibbons, W. and Horák, J.M., 1996, The evolution of the Neoproterozoic Avalonian Subduction System: Evidence from the British Isles: in Nance, R.D. and Thompson, M.D. (Eds.) Avalonian and related peri-Gondwanan terranes of the circum-North Atlantic. Geological Society of America Spec. paper 304, p. 269-280.

Giese, U.; Glodny, J. and Kramm, U., 1993, The Gil Marquez intrusion, southwest Spain: syntectonic intrusion, magma-mixing and deformation in a transpressive regime: 1993 Geological Society of America annual meeting, Boston, abstracts with programs, p. A-342.

Gil Ibarguchi, J.I. and Dallmeyer, R.D., 1991, Hercynian blueschist metamorphism in North Portugal: tectonothermal implications: J. Metamorphic Geol., v.9, p.539-549.

Gill, J.B., 1981, Orogenic andesites and plate tectonics. Springer-Verlag, Berlin, pp. 358.

Gillis, J.W., 1972, Geology of the Port aux Basques map area, Newfoundland: G.S.C., paper 71-42.

Gonzalez Casado, J.M., 1986, Estudio geológico de la zona de cizalla de Berzosa-Honrubia (Ph.D. thesis): Coll. Pub. Thesis Univ. Complutense Madrid, 87-2, pp. 295.

Gonzalez Casado, J.M., 1987, Revisión de la zonación metamórfica y los procesos de blastesis-deformación de la región de Somosierra (Sistema Central Español): Estud. Geol., v. 42, p. 209-216.

Gonzalez Casado, J.M. and Casquet, C., 1987, Significado de las estructuras tardías, S-C, de la región de Berzosa-Honrubia (Sistema Central Español): Cuad. Lab. Xeol. Laxe, v.12, p.243-250.

González Casado, J.M. and Casquet, C., 1988, Estructuras distensivas y procesos metamórficos asociados en la Zona de Cizalla de Berzosa: Geogaceta, v. 4, p. 5-6.

Gonzalez Lodeiro, F., 1981, Estudio geologico-estrcutural de la terminacion oriental de la Sierra de Guadarrama (Sistema Central Español): Ph.D. thesis, Univ. de Salamanca.

González Lodeiro, F., 1981, La estructura del anticlinorio del Ollo de Sapo en la región de Hiendelaencina (extremo oriental del Sistema Central Español): Cuad. Geol. Ibérica, v.7, p. 535-545.

González Lodeiro, F.; Martínez Catalán, J.R.; Macaya, J. and Alvarez, F., 1988, Sobre la estructura del Antiforme de El Cardoso y el Sinforme de Majaelrayo y su relación con la Falla de Berzosa: Geogaceta, v.4, p. 11-14.

Guerrot, C.; Peucat, J.J.; Capdevila, R. and Dosso, L., 1989, Archean protoliths within early Proterozoic granulitic crust of the west European Hercynian Belt: possible relicts of the west African craton: Geology, v. 17, p. 241-244.

Guerrot, C. and Peucat, J.J., 1990, U-Pb geochronology of the Late Proterozoic Cadomian orogeny in the northern Armorican Massif, France: in D'Lemos, R.S.; Strachan, R.A. and Topley, C.G. (Eds.). The Cadomian Orogeny. Geol Soc. Spec. Pub. 51, p. 13-26.

Gutiérrez Marco, J.C.; De San Jose, M.A. and Pieren, A.P., 1990, Post-Cambrian Palaeozoic stratigraphy (Central Iberian Zone): in Dallmeyer, R.D. and Martínez García Eds, Pre-Mesozoic Geology of Iberia, Springer-Verlag, Berlin Heidelberg, p. 160-171.

Hamilton, W.B., 1994, Subduction systems and magmatism: in Smellie, J.L. Ed., Volcanism Associated with Extension at Consuming Plate Margins, Geol. Soc. Spec. Pub. 81, p. 3-28.

Hammann, W. and Schmidt, K., 1972, Eine Llandeile-fauna aus der östlichen, Sierra de Guadarrama (Spanien): Meu. Jb. Geol. Paläont. Mh. Jg. M., v. 5, p.294-299.

Handy, M.R., 1990, The solid -state flow of polymineralic rocks: J. Geophys. Res., v. 95, B6, p. 8647-8661.

Hanmer, S. and Passchier, C., 1991, Shear sense indicators: a review: Geological Survey of Canada paper 90-17, pp.71

Hanson, G.N., 1989, An approach to trace element modeling using a simple igneous system as an example: in Lipin, B.R. and McKay, G.A. (Eds.). Reviews in mineralogy, Min. Soc. Am., v.21, p.79-97.

Harland, W.B. and Gayer, R.A., 1972, The Artic Caledonides and earlier oceans: Geol. Mag., v. 109, p. 289-314.

Hatcher, R.D., 1988, The third synthesis: Wenlock to mid-Devonian (end of the Acadian orogeny): in Harris, A.L. and Fettes, D.J. (Eds.). The Caledonian-Appalachian orogen, Geol. Soc. London Spec. Pub. 38, p.499-504.

Heaman, L. and Parrish, R., 1991, U-Pb geochronology of accessory minerals: in Heaman, L. and Ludden, J.N. (Eds.) Short course handbook on application of radiogenic isotope systems to problems in geology, Mineralogical Association of Canada., Toronto, p. 59-100.

Heim, R.C., 1952, Metamorphism in the Sierra de Guadarrama: Ph.D. thesis, Utrech Univ. (Holand).

Hellman, P.L.; Smith, R.E. and Henderson, P., 1979, The mobility of the rare earth elements; evidence and implications from selected terrains affected by burial metamorphism: Contrib. Min. Petrol., v. 71, p. 23-44.

Henderson, P., 1984, Inorganic geochemistry. Pergamon Press, Oxford, pp.353.

Hernaiz Huerta, P.P.; Escuder Viruete, J.; Rodriguez Fernández, L.R.; Valverde Vaquero, P. and Dunning, G.R., 1996, Evolución estructural de la zona de cizalla extensional de Berzosa-Riaza, sector de Somosierra, Sistema Central Español: Geogaceta, v. 20 (4), p. 875-878.

Hernaiz Huerta, P.P. and eight others, in press a, Mapa y memoria explicativa de la hoja a escala 1:50.000 # 432 (Riaza), 2-serie (MAGNA), ITGE (Spanish Geol. Survey).

Hernaiz Huerta, P.P. and eight others, in press b, Mapa y memoria explicativa de la hoja a escala 1:50.000 # 459 (Tamajón), 2- serie (MAGNA). ITGE (Spanish Geol. Survey).

Hernández Enrile, J.L., 1991, Extensional tectonics of the Toledo ductile-brittle shear zone, central Iberian Massif: Tectonophysics, v. 191, p. 311-324.

Hernando, S.; Schott, J.J.; Thuizat, R. and Montigny, R., 1980, Age des andesites et des sediments interstratiphies de la region d'Atienza (Espagne): etude stratigraphique, geochronologique et paleomagnetique: Sc. Geol. Bull., v. 32, p. 119-128.

Hepburn, J.C.; Dunning, G.R. and Hon, R., 1995, Geochronology and regional tectonic implications of Silurian deformation in the Nashoba terrane, southeastern New England, USA : in Hibbard, J.P.; van Staal, C.R. and Cawood, P.A. (Eds.) Current Perspectives in the Appalachian-Caledonian Orogen: Geol. Assoc. Can. Spec. Paper 41, p. 349-366.

Hibbard, J.P. and Samson, S.D., 1995, Orogenesis exotic to the Iapetan cycle in the southern Appalachians: in Hibbard, J.P.; van Staal, C.R. and Cawood, P.A. (Eds.) Current Perspectives in the Appalachian-Caledonian Orogen. Geol. Assoc. Can., Spec. Paper, 41, p. 191-205.

Hibbard, J.P.; St-Julien, P. and Trzcienski, W.E., Jr., 1995, Humber Zone internal: in Williams, H. ed., Geology of the Appalachian-Caledonian orogen in Canada and Greenland: Geological Survey of Canada, Geology of Canada, # 6, (*also*, Geological Society of America, The Geology of North America, v. F-1), p.114-139.

Hoffman, P.F., 1991, Did the breakout of Laurentia turn Gondwana inside out ?: Science, v. 252, p. 1409-1412.

Holdsworth, R.E.; D'Lemos, R.S.; McErlean, M.A. and O'Brien, S.J., 1993, Deformation of the Cape Freels granite related to dextral displacements along the Dover Fault, northeast Newfoundland: Current Research, Nfld. Dept. of Mines and Energy, Geol. Survey branch, report 93-1, p. 221-228

Holdsworth, R.E., 1994, Structural evolution of the Gander-Avalon terrane boundary: a reactivated transpression zone in the NE Newfoundland Appalachians: J. Geol. Soc. London, v. 151, p. 629-646

Hutchinson, R.D., 1962, Cambrian stratigraphy and trilobite faunas of southeastern Newfoundland: Geological Survey of Canada, Bull. 88, pp.156.

Hyde, R.S., 1995, Upper Paleozoic rocks, Newfoundland: in Williams, H. ed., Geology of the Appalachian-Caledonian orogen in Canada and Greenland: Geological Survey of

Canada, Geology of Canada, # 6, (*also*, Geological Society of America, The Geology of North America, v. F-1), p. 523-552.

Hyndman, D.W., 1985, Petrology of igneous and metamorphic rocks. McGraw Hill, New York, pp.786.

Jaffey, A.H.: Flynn, K.F.; Glendenin, L.E.; Bentley, W.C. and Essling, A.M., 1971, Precision measurement of half -lives and specific activities of ^{235}U and ^{238}U: Physical Review, section C: Nuclear Physics, v.4, p. 1889-1906.

Jamieson, R.A., 1990, Metamorphism of an early Paleozoic continental margin, western Baie Verte Peninsula, Newfoundland: J. Met. Geol., v. 8, p. 269-288.

Jamieson, R.A. and O'Bierne-Ryan, A.M., 1991, Decompression-induced growth of albite porphyroblasts, Fleur de Lys Supergroup, Newfoundland: J. Met. Geol., v. 5, p. 272-288.

Jegouzo, P; Peucat, J.J.; Audren, C., 1986, Caractérisation et signification géodynamique des orthogneiss calco-alcalins d'âge Ordovicien de Bretagne méridionale: Bull. Soc. Géol. France, v. 8, II, p. 839-848.

Jenner, G.A.; Longerich, H.P.; Jackson, S.E. and Fryer, B.J., 1990, ICP-MS - A powerful tool for high-precision trace-element analysis in Earth sciences: Evidence from analysis of selected U.S.G.S. reference samples: Chemical Geology, v. 83, p.133-148.

Jenner, G.A.; Dunning, G.R.; Malpas, J.; Brown, M. and Brace, T., 1991, Bay of Islands and Little Port complexes, revisited: age, geochemical and isotopic evidence confirm suprasubduction-zone origin: Can. J. Earth Sci., v. 28, p.1635-1652.

Jenner, G.A.; Swinden, H.S., 1993, The Pipestone Pond Complex, central Newfoundland: complex magmatism in an eastern Dunnage Zone ophiolite: Can. J. Earth Sci., v. 30, p. 434-448.

Jenner, G.A., 1996, Trace element geochemistry of igneous rocks: geochemical nomenclature and analytical geochemistry: in Wyman, D.A. (Ed.). Trace element geochemistry of volcanic rcocks: applications for massive sulphide exploration. Geol. Assoc. Can. short course, v. 12, p.51-77.

Johannes, W., 1985, The significance of experimental studies for the formation of migmatites: in Ashworth, J.R. (Ed.). Migmatites. Blackie, Glasgow, p. 36-85.

Julivert, M.; Fontboté, J.M.; Ribeiro, A. and Conde, L.N., 1972, Mapa tectónico de la Peninsula Ibérica y Baleares: Madrid, ITGE (Spanish Geol. Survey).

Julivert, M. and Martínez, F.J. 1987, The structure and evolution of the Hercynian Fold Belt in the Iberian Peninsula: in Schaer, J.P. and Rodgers, J. (Eds). The Anatomy of Mountain Belts. Princeton University Press, Princeton. p. 65-103.

Kalt, A.; Hanel, M.; Schleicher, H. and Kramm, U., 1994, Petrology and geochronology of eclogites from the Variscan Schwarzwald (F.R.G.): Contrib. Min. Petrol., v. 115, p. 287-302.

Keen, C.E.; Keen, M.J.; Nichols, B.; Ried, I.; Stockmal, G.S.; Colman-Sadd, S.P.; O'Brien, S.J.; Miller, H.; Quinlan, G.; Williams, H. and Wright, J., 1986, Deep seismic reflection profile across the northern Appalachians: Geology, v. 15, p. 182-183.

Kelemen, P.B. and Ghiorso, M.S., 1986, Assimilation of peridotite in zoned calc-alkaline plutonic complexes: evidence from the Big Jim complex, Washington Cascades: Contrib. Mineral. Petrol., v. 94, p. 12-28.

Kerr, A.; Dunning, G.R. and Tucker, R.D., 1993, The youngest Paleozoic plutonism of the Newfoundland Appalachians: U-Pb ages from the St. Lawrence and François granites: Can. J. Earth Sci., p. 2328-2333.

Kerr, A.; Jenner, G.A. and Fryer, B., 1995, Sm-Nd isotopic geochemistry of Precambrian to Paleozoic granitoid suites and the deep-crustal structure of the southeast margin of the Newfoundland Appalachians: Can. J. Earth Sci., v. 32, p. 224-245.

Kilfoil, G.J., 1993, Colour, shaded-relief aeromagnetic map of the Port-aux-Basques area (NTS110). Nfld. Dept. of Mines and Energy, Geol. Survey branch, Map 93-103a (shading from the NW), Open file 110/312, scale 1:250.000.

King, T.; D'Lemos, R.; Holdsworth, B. and Jones, K., 1995, Contrasting P-T-t-d paths for two major shear zones within the Gander Lake Subzone, N.E., Newfoundland: Abstracts, Tectonic Studies Group, 26th meeting, Cardiff.

Kingsbury, J.A.; Miller, C.F.; Wooden, J.L. and Harrison, T.M., 1993, Monazite paragenesis and U-Pb systematics in rocks of the eastern Mojave Desert, California, USA: implications for thermochronometry: Chem. Geol., v. 110, p. 147-167.

Knight, I; James, N.P. and Williams, H., 1995, Cambrian-Ordovician carbonate sequences (Humber Zone), Chapter 3, in Williams, H. ed., Geology of the Appalachian-Caledonian orogen in Canada and Greenland: Geological Survey of Canada, Geology of Canada, # 6, (*also*, Geological Society of America, The Geology of North America, v. F-1), p.67-87.

Kontak, D.J.; Tuach, J.; Strong, D.F.; Archibald, D.A. and Farrar, E., 1988, Plutonic and hydrothermal events in the Ackley granite, southeast Newfoundland, as indicated by total-fusion $^{40}Ar/^{39}Ar$ geochronology: Can. J. Earth Sci., v. 25, p. 1151-1160.

Krogh, T.E., 1973, A low-contamination method for hydrothermal decomposition of zircon and extraction of U and Pb for isotopic age determinations: Geochim. Cosmochim. Acta, v. 37, p. 485-494.

Krogh, T.E., 1982, Improved accuracy of U-Pb zircon ages by the creation of more concordant systems using an air abrasion technique: Geochim. Cosmochim. Acta, v. 37, p.637-649.

Krogh, T.E.; Strong, D.F.; O'Brien, S.J. and Papezik, V.S., 1988, Precise U-Pb zircon dates from the Avalon Terrane in Newfoundland: Can. J. Earth Sci., v. 25, p. 442-453.

Krohe, A., 1996, Variscan tectonics of Central Europe: Postaccretionary intraplate deformation of weak continental lithosphere: Tectonics, v. 15, p. 1364-1388.

Kossmat, F., 1927, Gliederung des varistischen Gebirgsbaues: Abhandlungen des sächsischen geologischen Landesamtes, v.1, pp.39.

Kuijper, R.P.; Priem, H.N.A. and Den Tex, E., 1982, Late Archean-Early Proterozoic source ages of zircons in rocks from the Paleozoic orogen of Western Galicia, NW Spain: Precambrian Res., v. 19, p. 1-29.

Lancelot, J.R. and Allegret, A., 1982, Radiochronologie U/Pb de l'orthogneiss alcalin de Pedroso (Alto Alentejo, Portugal) et évolution anté-hercynienne de l'Europe occidentale: N. Jb. Min. Mth., v.9, p. 385-394.

Lancelot, J.R.; Allegret, A. and Iglesias Ponce de Leon, M., 1985, Outline of Upper Precambrian and Lower Paleozoic evolution of the Iberian Peninsula according to U-Pb dating of zircons: Earth and Planetary Science Letters, v. 74, p. 325-337.

Landing, E., 1996, Avalon: insular continent by the latest Precambrian: in Nance, R.D. and Thompson, M.D. Avalonian and related peri-Gondwanan terranes of the circum-North Atlantic: Geological Society of America Spec. paper 304, p. 29-64.

Le Breton, N. and Thompson , A.B., 1988, Fluid-absent (dehydration) melting of biotite in metapelites in the early stages of crustal anatexis: Contrib. Mineral. Petrol., v. 99, p. 226-237.

Lee, C.B. and Williams, H., 1995, The Teakttle and Carmanville mélanges in the Exploits Subzone of northeastern Newfoundland: Recycling and diapiric emplacement in an accretionary prism: in Hibbard, J.P.; van Staal, C.R. and Cawood, P.A. (Eds.) Current Perspectives in the Appalachian-Caledonian Orogen: Geol. Assoc. Can. Spec. paper 41, p. 147-160.

Le Corre, C.; Bale, P. and Georget, Y., 1989, Le Léon: un domaine exotique au nord-ouest de la chaine varisque armoricaine (France): Geodinamica Acta, v. 3 (2), p. 57-71.

Lefort, J.P., 1989, Basement correlation across the North Atlantic: Springer-Verlag, Berlin, Heidelberg, pp.148.

Lin, S.; van Staal, C.R. and Lee, C., 1993, The Harbour le Cou Group and its correlation with the Bay du Nord Group, southwestern Newfoundland: Current Research, part D, Geological Survey of Canada, paper 93-1D, p. 57-64.

Lin, S.; van Staal, C.R. and Dubé, B., 1994, Promontory-promontory collision in the Canadian Appalachians: Geology, v. 22, p. 897-900.

Liñán, E. and Quesada, C., 1990, Rift phase (Cambrian, *Ossa Morena zone, Stratigraphy*): in Dallmeyer, R.D. and Martínez García, E. (Eds.) Pre-Mesozoic geology of Iberia, p. 259-266.

Longerich, H.P., 1995, Analysis of pressed pellets of geological samples using wavelength-dispersive X-ray fluorescence spectrometry: X-ray spectrometry, v. 24, p. 123-136.

López Díaz, F., 1993, La estructura del anticlinal de Navalpino (Zona Centroibérica): Rev. Soc. Geol. España, v. 6 (3-4), p. 145-163.

López Díaz, F., 1995, Late Precambrian series and structures in the Navalpino Variscan Anticline (Central Iberian Peninsula): Geol. Rundsch, v. 84, p. 151- 163.

López Ruiz, J.; Aparicio, A. and García Cacho, L., 1975, El metamorfismo de la Sierra de Guadarrama. Sistema Central Español: Mem. Inst. Geol. Min. de España, v. 86, pp.127.

Lotze, F., 1929, Stratigraphie und tektonik des Keltiberischen Grundgebirges: Abh. Ges. Wiss. Gottingen Math. Phys., K-1, Neue Folge, v.14 (2), pp.317

Lotze, F., 1945, Zur gliederung der Varisziden der Iberischen Meseta: Geotekt. Forsch., v.6, p.78-92.

Ludwig, K.R., 1980, Calculation of uncertainties of U-Pb isotopic data: Earth Planet. Sci. Lett., v. 46, p. 212-220

Macaya, J.; Gonzalez Lodeiro, F.; Martínez Catalan, J.R. and Alvarez, F., 1991, Continuous deformation, ductile thrusting and backfolding of cover and basement in the Sierra de Guadarrama, Hercynian orogen of central Spain: Tectonophysics, v.191, pp.291-309.

MacPherson, J., 1883, Sucesión estratigrafica de los terrenos arcaicos en España: Anal. R. Soc. Esp. Hist.Nat., v. 10, p.341-378.

MacPherson, J., 1901, Ensayo de la historia evolutiva de la Peninsula Ibérica: Anal. R. Soc. Esp. Hist. Nat., v. 12, p. 123-165.

Mahar, E.M.; Baker, J.M.; Powell, R.; Holland, T.J.B. and Howell, N., 1997, The effect of Mn on mineral stability in metapelites: J. metamorphic Geol., v. 15, p. 223-238.

Mancktelow, N.S. and Pavlis, T.L., 1994, Fold-fault relationships in low angle detachment systems: Tectonics, v. 13, p. 668-685.

Manhès, G.; Allègre, C.J.; Dupré, B. and Hamelin, B., 1979, Lead-lead systematics, the "age of the Earth" and the chemical evolution of our planet in a new representation space: Earth Planet. Sci. Lett., v. 44, p. 91-104.

Maniar, P.D. and Piccoli, P.M., 1989, Tectonic discrimination of granitoids: Geological Society of America Bull., v.101, p. 635-643.

Marcos, A., 1973, Las series paleozoico inferior y la estrcutura herciniana del occidente de Asturias (NW de España): Trab. Geol., Univ. Oviedo, v.6, pp. 113.

Marquinez, J.L., 1984, La geologia del Area Esquistosa de Galicia Central (Cordillera Herciniana, NW de España): Mem. Inst. Geol. Min. España, v. 100, pp.231.

Martín Escorza, C., 1976, Las "Capas de Transicion" y otras series preordovicicas (Cambrico Superior?) en los Montes de Toledo surorientales: sus implicaciones geotectonicas: Estud. Geol. , v.32, p. 591-613.

Martín Escorza, C., 1977a, Nuevos datos sobre el Ordovícico inferior: el límite Cámbrico-Ordovícico y las fases sárdicas en los Montes de Toledo: consecuencias geotectónicas: Estud. Geol., v. 33, p. 57-80.

Martín Escorza, C., 1977b, Estudio preliminar de algunos procesos de deformación y cataclasis en la zona de Robledo de Chavela (Sistema Central): Bol. Geol. y Min., v. 88-6, p.471-493.

Martín Escorza, C., 1981, Un proceso de milonitización con extensión cortical en el macizo metamórfico del Escorial (Cordillera Central): Cuad. Geol. Ibérica, v.7, p. 577-590.

Martín Escorza, C., 1988, Fase Robledo: una etapa distensiva dúctil en la Cordillera Central: Geogaceta, v. 5, p. 44-46.

Martínez, F.J. and Rolet, J., 1988, Late Palaeozoic metamorphism in the northwestern Iberian Peninsula, Brittany and related areas in southwest Europe: in Harris, A.L. and Fettes, D.J. (Eds.). The Caledonian-Appalachian orogen. Geol. Soc. Spec. Pub. 38, p. 611-620.

Martínez, F.J.; Corretge, L.G. and Suárez, O., 1990, Distribution, characteristics and evolution of metamorphism (Central Iberian Zone): in Dallmeyer, R.D. and Martínez García, E. (Eds.). Pre-Mesozoic geology of Iberia. Springer Verlag, Berlin, p. 207-211.

Martínez Catalán, J.R., 1990, Structure (West Asturian-Leonese Zone): in Dallmeyer, R.D. and Martínez García, E. (Eds.). Pre-Mesozoic geology of Iberia. Springer Verlag, Berlin, p. 103-114.

Martínez Catalán, J.R.; Dallmeyer, R.D.; Gil-Ibarguchi, J.I.; Arenas, R.; Gervas, P.; Farias, P.; Aller, J.; Bastida, F. and Gutiérrez Alonso, G., 1993, $^{40}Ar/^{39}Ar$ dating of deformation fabrics in the relative autochton in NW Spain: TERRA abstracts, EUG VII meeting, Strasbourg (1993), v. 5, p.390.

Martínez Catalán, J.R.; Arenas, R.; Díaz García, F.; Rubio Pascual, F.J.; Abati, J. and Marquínez, J., 1996, Variscan exhumation of a subducted Paleozoic continental margin: The basal units of the Ordenes Complex, Galicia, NW Spain: Tectonics, v. 15, p. 106-121.

Martínez García, E., 1973, Deformacion y metamorfismo en la zona de Sanabria, Stud.Geol., v.5, p.7 - 106.

Matte, Ph., 1968, La structure de la virgation hercynienne de Galicie (Espagne): Rev. Geol. Alpine, v. 44, p. 1-127.

Matte, P., 1986, Tectonics and plate tectonics models for the Variscan belt of Europe: Tectonophysics, v. 126, p. 329-374

Matte, Ph., 1995, Southern Uralides and Variscides: comparison of their anatomies and evolutions: Geologie en Mijnbouw, v. 74, p. 151-166.

McKerrow, W.S. and Cocks, L.R.M., 1977, The location of the Iapetus Ocean suture in Newfoundland: Can. J. Earth Sci., v. 14, p.488-495.

McKerrow, W.S. and Scotese, C.R. ((Eds.)), 1990, Palaeozoic Palaeogeography and Biogeography: Geol. Soc. London Memoir # 12, pp. 435.

McLellan, E., 1984, Deformational behaviour of migmatites and problems of structural analysis in migmatite terrains: Geol. Mag., v. 121, p. 339-345.

Meléndez, B.; Talens, J.; Fonollá, F. and Alvares-Ramis, C., 1983, Las cuencas carboníferas del sector central de la Cordillera Ibérica (Henarejos y Montalban). in Martínez Díaz, C. (Ed.). Carbonífero y Pérmico de España. X Congreso Internacional de Estratigrafia y geologia del Carbonífero. ITGE (Spanish Geol. Survey), Madrid, p. 207-220.

Ménot, R.P.; Peucat, J.J.; Scarenzi, D.; Piboule, M., 1988, 496 Ma age of plagiogranites in the Chamrousse ophiolite complex (external crystalline massifs in the French Alps): evidence of a Lower Paleozoic oceanization: Earth Planet. Sci. Lett., v.88, p.82-92.

Ménot, R.P. and Paquette, J.L., 1993, Geodynamic significance of basic and bimodal magmatism in the External Domain (Helvetic realm): in von Raumer, J.F. and Neubauer, F. eds, Pre-Mesozoic Geology in the Alps, Springer-Verlag, Berlin Heidelberg, p.241-254.

Merriman, R.J.; Bevins, R.E. and Ball, T.K., 1986, Petrological and geochemical variations within the Tal y Fan intrusion: a study of element mobility during low-grade metamorphism with implicaitons for petrotectonic modelling: J. Petrol., v. 27, p. 1409-1436.

Meschede, M., 1986, A method of discriminating between different types of mid-ocean ridge basalts and continental tholeiites with the Nb-Zr-Y diagram: Chem. Geol., v.56, p.207-218.

Middlemost, E.A.K., 1975, The basalt clan. Earth Science Reviews, v. 11, p. 51-57.

Miyashiro, A., 1978, Nature of alkalic volcanic rock series: Contrib. Mineral. Petrol., v. 66, p.91-104.

Mullen, E.D., 1983, $MnO/TiO_2/P_2O_5$: a minor element discriminant for basaltic rocks of oceanic environments and its implications for petrogenesis: Earth Planet. Sci. Lett. v. 62, p. 53-62.

Munha, J., 1990, Metamorphic evolution of the South Portuguese/Pulo Do Lobo Zone: in Dallmeyer, R.D. and Martínez García, E. (Eds.). Pre-Mesozoic geology of Iberia. Springer Verlag, Berlin. p. 363-368.

Muñoz, M., Vegas, R. and Roiz, J.M., 1985, El vulcanismo cámbrico del centro de España: programas e resumos 9 reuniao de geologia oeste peninsular, Porto.

Murphy, J.B. and Nance, R.D., 1991, Supercontinent model for the contrasting character of Late Proterozoic orogenic belts: Geology, v. 19, p. 469-472.

Nakamura, N., 1974, Determination of REE, Ba, Fe, Mg, Na and K in carbonaceous and ordinary chondrites: Geochim. Cosmochim. Acta., v. 38, p. 757-773.

Nance, R.D. and Thompson, M.D. (editors), 1996, Avalonian and related peri-Gondwanan terranes of the circum-North Atlantic: Geological Society of America Spec. Paper 304, pp.390.

Navidad, M., 1975, Caracterizacion petrologica de los gneises glandulares del macizo de Hiendelaencina (Guadarrama Oriental): Estud. Geol., v. 31, p. 343-350.

Navidad, M., 1979, Las series glandulares del sector central del macizo Ibérico (Guadarrama centro-occidental): Estud. Geol., v. 35, p.31-48.

Navidad, M. and Peinado, M., 1977, Facies volcanosedimentarias en el Guadarrama Central (Sistema Central Español): Stud. Geol., v. 12, p. 137-159.

Navidad, M. and Peinado, M., 1981, Ortogneises y metasedimentos de la formación infrabasal al Ollo de Sapo (Macizo de Hiendelaencina, Guadarrama Oriental): Cuad. Geol. Ibérica, v. 7, p.183-199.

Navidad, M. and López Ramos, C., 1981, Los ortogneises del sector metamórfico El Vellón-Pedrezuela (Sistema Central): Estud. Geol., v. 37, p. 97-107.

Navidad, M; Peinado, M. and Casillas, R., 1992, El magmatismo pre-Hercinico del Centro Peninsular (Sistema Central Español): in Gutiérrez Marco, J.: Saavedra, J. and Rabano, I. (Eds.): Paleozoico Inferior de Ibero-America, Univ. de Extremadura, p. 485-494.

Navidad, M. and Carreras, C., 1995, Pre-Hercynian magmatism inthe Eastern Pyrenees (Cap de Creus and Albera Massifs) and its geodynamical setting: Geol. en Mijnbouw, p. 65-77.

Neubauer, F. and von Raumer, J.F., 1993, The Alpine basement - linkage between Variscides and East-Mediterranean mountain belts: in von Raumer, J.F. and Neubauer, F. eds, Pre-Mesozoic Geology in the Alps, Springer-Verlag, Berlin Heidelberg, p.641-664

Neuman, R.B., 1967, Bedrock geology of the Shin Pond and Stacyville Quadrangles, Penobscot County, Maine: US Geological Survey Professional Paper 524-I, p. 121-137.

Neuman, R.B. and Max, M., 1989, Penobscottian-Grampian-Finnmarkian orogenies as indicators of terrane linkages: in Dallmeyer ed. Terranes in the circum-Atlantic Paleozoic orogens: Geological Society of America Spec. Paper 230, p. 31-46.

Neuman, R.B. and Harper, D.A.T., 1992, Paleogeographic significance of Arenig-Llanvirn Toquima-Table Head and Celtic brachiopod assemblages: Webby and Laurie (Eds.): Global perspectives on Ordovician geology, Balkema, Rotterdam, p. 241-254.

Noblet, Ch. and Lefort, J.P., 1990, Sedimentological evidence for a limited separation between Armorica and Gondwana during the Early Ordovician: Geology, v.18, p. 303-306.

Nowlan, G.S. and Neuman, R.B., 1991, Paleontological contributions to Paleozoic paleogeographic and tectonic reconstructions, Chapter 10: in Williams, H. ed., Geology of the Appalachian-Caledonian orogen in Canada and Greenland (1995): Geological Survey of Canada, Geology of Canada, # 6, (*also*, Geological Society of America, The Geology of North America, v. F-1), p. 815-842.

O'Brien, B.H., 1987, The lithostratigraphy and strcuture of the Grand Bruit - Cinq Cerf area (parts of NTS areas 110/9 and 110/16), southwestern Newfoundland: Current Research, Nfld. Dept. of Mines and Energy, report 87-1, p. 311-334.

O'Brien, B.H., 1988, Relationships of phyllite, schist and gneiss in the La Poile Bay-Roti Bay area (parts of 110/9 and 110/16), southwestern Newfoundland: Current Research, Nfld. Dept. of Mines, report 88-1, p. 109-125.

O'Brien, B.H., 1989, Summary of the geology between La Poile Bay and Couteau Bay (110/9 and 110/16), southwestern Newfoundland: Current Research, Nfld. Dept. of Mines, report 89-1, p. 105-119.

O'Brien, B.H., 1990, Geology of the La Poile Bay - Couteau Bay region (parts of 110/9 and 110/19) southwest Newfoundland: 1:50.000 scale map. Nfld. Dept. of Mines and Energy. Map 90-07.

O'Brien, B.H. and O'Brien, S.J., 1990, Re-investigation and re-interpretation of the Silurian La Poile Group of southwestern Newfoundland: Current Research, Nfld. Dept. of Mines and Energy, report 90-1, p. 305-316.

O'Brien, B.H.; O'Brien, S.J. and Dunning, G.R., 1991, Silurian cover, Late Precambrian-Early Ordovician basement and the chronology of Silurian orogenesis in the Hermitage Flexure (Newfoundland Appalachians):Am.J. of Sci., v. 291, p. 760-799.

O'Brien, B.H. and O'Brien S.J., 1992, Day 3: Burgeo road (south end), Burgeo to Buck Lake: in Colman-Sadd, S.P.; Cawood, P.A.; Dunning, G.R.; Hall, J.M.; Kean, B.F.; O'Brien, B.H. and O'Brien, S.J. Lithoprobe East in Newfoundland (Burgeo transect): a cross-section through the southwest Newfoundland Appalachians, field excursion A-7 guide book. 92 Geol. Assoc. Can. annual meeting, Wolfville. p.72-84.

O'Brien, B.H.; O'Brien, S.J., Dunning, G.R. and Tucker, R.E., 1993, Episodic reactivation of a Late Precambrian mylonite zone on the Gondwanan margin of the Appalachians, southern Newfoundland: Tectonics, v. 12, p. 1043-1055.

O'Brien, B.H.; Swinden, H.S.; Dunning, G.R.; Williams, S.H. anb O'Brien, F.H.C., 1997, A peri-Gondwanan arc-back arc complex in Iapetus: Early -Mid Ordovician evolution of the Exploits Group, Newfoundland: Am. J. Science, v. 297, p. 220-272.

O'Brien, S.J.; Wardle, R.J. and King, A.F., 1983, The Avalon Zone: a Pan-African terrane in the Appalachian orogen of Canada: Geological Journal, v.18, p.195-222.

O'Brien, S.J.; Strong, D.F. and King, A.F., 1990, The Avalon Zone type area: southeastern Newfoundland Appalachians: in Strachan, R.A. and Taylor, G.K. (Eds.) Avalonian and Cadomian Geology of the North Atlantic, Blackie & Son Ltd., Glasgow-London, p. 166-194.

O'Brien, S.J.; O'Brien, B.H.; Dunning, G.R. and Tucker, R.D., 1996, Late Neoproterozoic Avalonian and related peri-Gondwanan rocks of the Newfoundland Appalachians: in Nance, R.D. and Thompson, M.D. Avalonian and related peri-Gondwanan terranes of the circum-North Atlantic: Geological Society of America Spec. paper 304, p. 9-28

Ochsner, A., 1993, U-Pb geochronology of Upper Proterozoic - Lower Paleozoic geodynamic evolution in the Ossa-Morena Zone (southwest Iberia): constraints on the timing of the Cadomian orogeny: Ph.D. Diss.# 10392, E.T.H. (Zürich), pp. 247.

Odin, G.S. (Ed.), 1990, Phanerozoic time scale: Bull. Liais. IUGS Subcom. Geochronol., 9, Paris.

Oliveira, J.T., 1990, Stratigraphy and synsedimentary tectonism (South Portuguese Zone): in Dallmeyer, R.D. and Martínez García, E. (Eds.). Pre-Mesozoic geology of Iberia. Springer Verlag, Berlin, p.334-347.

Oliveira, J.T.; Pereira, E.; Piçarra, J.M.; Young, T. and Romano, M., 1992, O Paleozóico Inferior de Portugal: Síntese da estratigrafia e da evolução paleogeográfica: in Gutíerrez Marco, J.G.; Saavedra, J. and Rábano, I. (Eds.). Paleozoico Inferior de Ibero-America, Univ. de Extremadura, p. 359-375.

Oliver, G.J.H.; Corfu, F. and Krogh, T.E., 1993, U-Pb ages from southwest Poland: evidence for a Caledonian suture zone between Baltica and Gondwana: J.Geol. Soc. London, v.150, p.355-369.

O'Neill, P.P., 1985, An economic, metamorphic, structural and geochemical study of the Isle-aux-Morts prospect, Southwest Newfoundland. M.Sc. thesis, Memorial University of Newfoundland. 263 pp.

O'Neill, P.P.,1991, Geology of the Weir's Pond area: Nfld. Geol. Survey Report 91-3, pp.144.

Osberg, P.H.; Tucker, R.D. and Berry, H.N., 1995, Is the Acadian suture lost?: in Hussey, A.M. and Johnston, R.A. (Eds.) Guidebook to the field trips in southern

Maine and adjacent New Hampshire, 87th annual meeting NEIGC, Maine Geol. Survey - Dept. of Geology Bowdoin College, Brunswick (Maine, USA), p. 145-172.

Owen, J.V., 1992, Comparative petrology of gneissic rocks in southwestern Newfoundland: Can. J. Earth Sci., v.29, p.2663-2676.

Parga Pondal, I.; Matte, P. and Capdevila, R., 1964, Introduction à la géologie de l'"Ollo de Sapo", Formation porphyroide antesilurienne du Nord Ouest de l'Espagne: Not. Com. Inst. Geol. Min. Esp., v. 76, p. 119-153.

Parga Pondal, I.; Vegas, R. and Marcos, A. (coordinators), 1983, Mapa Geologico del Macizo Hesperico - escala 1:500.000 (Map and memoir): Publicacións da Area de Xeoloxía e Minería do Seminario do Estudos Galegos, Edicións do Castro, Sada -A Coruña, Spain.

Paris, F. and Robardet, M., 1990, Early Palaeozoic palaeobiogeography of the Variscan regions: Tectonophysics, v. 144, p. 193-214.

Park, R.G., 1983, Foundations of structural geology. Blackie, Glasgow, pp.135.

Parrish, R.R. and Krogh, T.E., 1987, Synthesis and purification of ^{205}Pb for U-Pb geochronology: Chem. Geol., v. 66, p. 103-110.

Passchier, C.W. and Trouw, R.A.J., 1996, Microtectonics. Springer-Verlag, Berlin, pp.289.

Paterson, S.R.; Vernon, R.H. and Tobisch, O.T., 1989, A review of criteria for the identification of magmatic and tectonic foliations in granitoids: J. Struct. Geol., v. 11, p. 349-363.

Payne, J.G. and Strong, D.F., 1979, Origin of the Twillingate trondhjemite, North Central Newfoundland: Partial melting in the roots of an island arc: in Barker, F., ed. Trondhjemites, dacites and related rocks: New York, Elsevier, p. 489-519.

Pearce, J.A., 1983, The role of subcontinental lithosphere in magma genesis at destructive plate margins: in Hawkesworth, C.J. and Norry, M.J. (Eds.). Continental basalts and mantle xenoliths, Shiva, Nantwich, p. 230-249.

Pearce, J.A., 1996, A user's guide to basalt discrimination diagrams: in Wyman, D.A. (Ed.). Trace element geochemistry of volcanic rocks : applications for massive sulphide exploration. Geol. Assoc. Can. short course, v. 12, p. 79-113.

Pearce, J.A. and Cann, J.R., 1973, Tectonic setting of basic volcanic rocks determined using trace element analysis: Earth Planet. Sci. Lett., v.19, p. 290-300.

Pearce, J.A.; Harris, N. B.W. and Tindle, A.G., 1984, Trace element discrimination diagrams for the tectonic interpretation of granitic rocks: J. Petrol. , v. 25, p. 956-983.

Pedersen, R.B. and Dunning, G.R., 1997, Evolution of arc crust and relations between contrasting sources: U-Pb (age), Nd and Sr isotope systematics of the ophiolitic terrain of southwest Norway: Contrib. Min. Petrol., v. 128, p. 1-15.

Peinado, M. and Alvaro, M., 1981, Magmatismo pre e intra-hercinico del sector metamorfico de El Escorial (Sistema Central Español): Cuad. Geol. Ibérica, v. 81, p. 201-215.

Perejón, A. and Moreno-Eiris, E., 1992, Paleozoico Inferior de Ossa Morena: in Gutíerrez Marco, J.G.; Saavedra, J.; Rábano, I. (Eds.). Paleozoico Inferior de Ibero-América. Universidad de Extremadura, p. 557-565.

Perez Estaún, A. and Bastida, F., 1990, Cantabrian Zone (Structure): in Dallmeyer, R.D. and Martínez García, E., (Eds.). Pre-Mesozoic geology of Iberia, Springer Verlag, Berlin, p. 55-68.

Perez Estaún, A.; Bastida, F.; Martínez Catalan, J.R.; Gutiérrez Marco, J.C.; Marcos, A. and Pulgar, J.A., 1990, Stratigraphy (West Asturian-Leonese Zone): in Dallmeyer, R.D. and Martínez García, E., (Eds.). Pre-Mesozoic geology of Iberia, Springer Verlag, Berlin, p. 92-102.

Perez Estaún, A.; Martínez Catalán, J.R. and Bastida, J., 1991, Crustal thickening and deformation sequence in the footwall to the suture of the Variscan belt of northwest Spain: Tectonophysics, v. 191, p. 243-253.

Peucat, J.J.; Bernard-Griffiths, J.; Gil Ibarguchi, I; Dallmeyer, R.D.; Ménot, R.P.; Cornichet, J. and Iglesias Ponce de Leon, M., 1990, Geochemical and geochronological cross section of the deep Variscan crust: the Cabo Ortegal high pressure nappe: Tectonophysics, v. 177, p.263-292.

Piasecki, M.A.J., 1988, A major ductile shear zone in the Baie d'Espoir area, Gander Terrane, southeastern Newfoundland: Current research, Newfoundland Dept. Mines and Energy, report 88-1, p. 135-145.

Piasecki, M.A.J., 1995, Dunnage zone boundaries and some aspects of terrane development in Newfoundland: in Hibbard, J.P.; van Staal, C.R. and Cawood, P.A. ((Eds.)), Current Perspctives in the Appalachian-Caledonian Orogen: Geological Association of Canada, Special Paper 41, p. 323-347.

Pin, C. and Lancelot, J., 1982, U-Pb dating of an Early Paleozoic bimodal magmatism in the French Massif Central and of its further metamorphic evolution: Contrib. Mineral. Petrol., v. 79, p. 1-12.

Pin, C. and Carme, F., 1987, A Sm-Nd isotopic study of 500 Ma old oceanic crust in the Variscan belt of Western Europe: the Chamrousse ophiolite complex, Western Alps (France): Contrib. Min. Petrol., v.96, p.406-413.

Pin, C., 1990, Variscan oceans: ages, origins and geodynamic implications inferred from geochemical and radiometric data: Tectonophysics, v. 144, p. 215-228.

del Prado, C., 1884, Descripción física y geológica de la Provincia de Madrid: Junta General de Estadística, Madrid, pp. 219.

Prigmore, J.K.; Butler, A.J.; Woodcock, N.H., 1997, Rifting during separation of Eastern Avalonia from Gondwana: Evidence from subsidence analysis: Geology, v.25, p.203-206.

Quesada, C., 1990 a, Precambrian terranes in the Iberian Varsican foldbelt: in Strachan, R.A. and Taylor, G.K. (Eds.) Avalonian and Cadomian Geology of the North Atlantic. Blackie & Son Ltd., Glasgow-London, p. 109-133.

Quesada, C., 1990 b, Precambrian successions in southwest Iberia: their relationship to 'Cadomian' orogenic events: in D'Lemos, R.S.; Strachan, R.A. and Topley, C.G. (editors), 1990, The Cadomian Orogeny: Geol. Soc. London, Spec. Pub. 51, p. 353-362.

Quesada, C.; Robardet, M. and Gabaldon, V., 1990, Synorogenic phase (Upper Devonian-Carboniferous-Lower Permian) (Ossa Morena Zone, stratigraphy): in Dallmeyer, R.D. and Martínez García, E. (Eds.), Pre-Mesozoic geology of Iberia, Springer Verlag, p. 273-279.

Quesada, C., 1991, Geological constraints on the Paleozoic tectonic evolution of tectonostratigraphic terranes in the Iberian Massif: Tectonophysics, v. 185, p. 225-245.

Quesada, C., 1992, Evolución tectónica del Macizo Ibérico (una historia de crecimiento por acrecencia sucesiva de terrenos durante el Proterozoico Superior y el Paleozoico): in Gutíerrez Marco, J.G.; Saavedra, J. and Rábano, I. (Eds.). Paleozoico Inferior de Ibero-América, Univ. Extremadura, p. 173-189.

Quesada, C. and Dallmeyer, R.D., 1994, Tectonothermal evolution of the Badajoz-Córdoba shear zone (southwest Iberia): characteristics and $^{40}Ar/^{39}Ar$ mineral age constraints: Tectonophysics, v. 231, p. 195-213.

Rabu, D.; Thiéblemont, D.; Tegyey, M.; Guerrot, C.; Alsac, C.; Chauvel, J.J.; Murphy, J.B. and Keppie, J.D., 1996, Late Proterozoic to Paleozoic evolution of the St. Pierre and Miquelon Islands: a new piece in the Avalonian puzzle of the Canadian Appalachians: in Nance, R.D. and Thompson, M.D. Avalonian and related peri-Gondwanan terranes of the circum-North Atlantic: Geological Society of America Spec. paper 304, p. 65-94

Rapela, C.W. and Pankhurst, R.J., 1992, The granites of northern Patagonia and the Gastre Fault System in the relation to the break-up of Gondwana: in Storey, B.C., Alabaster, T. and Pankhurst, R.J. eds, Magmatism and the causes of continental break-up, Geol. Soc. Spec. Pub., 68, p. 209-220.

Rast, N. and Crimes, T.P., 1969, Caledonian orogenic episodes in the British Isles and northwestern France and their tectonic and chronological interpretation: Tectonophysics, v.7, p. 277-307.

Rast, N., 1988, Tectonic implications of the timing of the Variscan orogeny: in Harris, A.L. and Fettes, D.J. (Eds.), The Caledonian-Appalachian orogen, Geol. Soc. London Spec. Pub. 38, p.585-595.

Rast, N. and Skehan, J.W., 1988, Constituent terranes of the Avalon Superterrane in the Appalachian chain: IGCP project 233, Terranes in the Variscan Belt of France and Western Europe, Univ. Montpellier, Conference Abstracts, 70.

Rast, N.; Sturt, B.A. and Harris A.L., 1988, Early deformation in the Caledonian-Appalachian orogen: in Harris, A.L. and Fettes, D.J., (Eds.) The Caledonian-Appalachian Orogen. Geol. Soc. Spec. Publ., 38, p.111-122.

Ratschbacher, L.; Frisch, W.; Neubauer, F.; Schmid, S.M. and Neugebauer, J., 1989, Extension in compressional orogenic belts: The eastern Alps: Geology, v. 17, p.404-407.

Reinhardt, J. and Kleemand, U., 1994, Extensional unroofing of granulitic lower crust and related low-pressure, high temperature metamorphism in the Saxonian Granulite Massif, Germany: Tectonophysics, v. 238, p.71-94.

Ribeiro, M.L., 1987, Petrogenesis of Early Palezoic peralkaline rhyolites from the Macedo de Cavaleiros region (NE Portugal): Geol. Rundsch., v. 76/1, p. 147-168.

Ribeiro, A.; Quesada, C. and Dallmeyer, R.D., 1990, Geodynamic evolution of the Iberian Massif: in Dallmeyer, R.D. and Martínez García Eds, Pre-Mesozoic Geology of Iberia, Springer-Verlag, Berlin Heidelberg, p. 399-409.

Robardet, M.; Paris, F. and Racheboeuf, P.R., 1990, Palaeogeographic evolution of southwestern Europe during Early Palaeozoic times: in McKerrow, W. S. and Scotese, C.R. (Eds.) Palaeozoic Palaeogeography and Biogeography, Geol. Soc. Memoir 12, p. 411-420.

Robardet, M. and Gutiérrez Marco, J.C., 1990, Sedimentary and faunal domains in the Iberian Peninsula during Lower Paleozoic times: in Dallmeyer, R.D. and Martínez García Eds, Pre-Mesozoic Geology of Iberia, Springer-Verlag, Berlin Heidelberg, p. 383-398.

Robinson, P.; Tracy, R.J.; Santallier, D.S., Andréasson, P.G. and Gil Ibarguchi, J.L., 1988, Scandian-Acadian-Caledonian sensu stricto metamorphism in the range 450-360 Ma: in Harris, A.L. and Fettes, D.J., (Eds.) The Caledonian-Appalachian Orogen. Geol. Soc. Spec. Publ., 38, p. 453-467.

Rogers, J.J.W., 1996, A history of continents in the past three billion years: J. Geol., v. 104, p.91-107.

de San José, M.A.; Rábano, I.; Herranz, P. and Gutiérrez Marco, J.C., 1992, El Paleozoico Inferior de la Zona Centroibérica meridional: in Gutíerrez Marco, J.G.; Saavedra, J. and Rábano, I. (Eds.). Paleozoico inferior de Ibero-América, Universidad de Extremadura, p. 505-521.

Sánchez Carretero, R.; Eguiluz, L.; Pascual, E. and Carracedo, M., 1990, Igneous rocks (Ossa Morena Zone): in Dallmeyer, R.D. and Martînez García, E. (Eds.). Pre-Mesozoic geology of Iberia, Springer Verlag, Berlin, p. 292-313.

Sánchez Posada, L.C.; Martínez Chacon, M.L.; Mendez Fernández, C.; Menendez Alvarez, J.R.; Truyols and Villa, E., 1990, Carboniferous pre-Stephanian rocks in the Asturian-Leonese domain (Cantabrian Zone): in Dallmeyer, R.D. and Martínez García, E. (Eds.). Pre-Mesozoic geology of Iberia, Springer Verlag, Berlin, p. 24-33.

Santallier, D.; Briand, B.; Ménot, R.P.; Piboule, M., 1988, Les complexes leptyno-amphiboliques (C.L.A.): revue critique et suggestions pour un meilleur emploi de ce terme: Bull. Soc. Géol. France, v. 8, p. 3-12.

Santos Zalduegui, J.F.; Schärer, U. and Gil Ibarguchi, J.I., 1995, Isotope constraints on the age and origin of magmatism and metamorphism in the Malpica-Tuy allochthon, Galicia, NW Spain: Chem. Geol. v. 121, p. 91-103.

Santos Zalduegui, J.F.; Schärer, U.; Gil Ibarguchi, J.I. and Girardeau, J., 1996, Origin and evolution of the Paleozoic Cabo Ortegal ultramafic-mafic complex (NW Spain): U-Pb, Rb-Sr and Pb-Pb isotope data: Chem. Geol., v.129, p. 281-304.

Scotese, C.R. and McKerrow, W.S., 1990, Revised world maps and introduction: in McKerrow, W.S. and Scotese, C.R. ((Eds.)), Palaeozoic palaeogeography and biogeography, Geol. Soc. Memoir # 12, p.1-21

Schäfer, G., 1969, Geologie und petrographie in östlichen Kastilichen Kauptscheidegebirge (Sierra de Guadarrama, Spanien): Münst. Forsch. Geol.Paleont., v.10, pp.207.

Schäfer, H.J., 1990, Geochronological investigations in the Ossa-Morena Zone, southwest Spain: Ph.D. Diss.# 9246, E.T.H. (Zürich), pp. 153.

Schäfer, H.J.; Gebauer, D.; Gil Ibarguchi, J.I. and Peucat, J.J., 1993a, Ion-microprobe U-Pb dating on the HP/HT Cabo Ortegal Complex (Galicia, NW Spain): preliminary results: TERRA abstracts, EUG VII meeting, Strasbourg, v. 5(4).

Schäfer, H.J.; Gebauer, D.; Nägler, T.H. and Eguíluz, L., 1993, Conventional and ion-microprobe U-Pb dating of detrital zircons of the Tentudia Group (Serie Negra, southwest Spain): implications for zircon systematics, stratigraphy, tectonics and the Precambrian/Cambrian boundary; Contrib. Min. Petrol., v. 113, p.289-299.

Schaltegger, U.; Schneider, J.L.; Maurin, J.C. and Corfu, F., 1996, Precise U-Pb chronometry of 345-340 Ma old magmatism related to syn-convergence extension in the Southern Vosges (Central Variscan Belt): Earth Planet. Sci. Lett., v. 144, p. 403-419.

Schofield, D.I.; Winchester, J.A. and van Staal, C.R., 1993, The Isle aux Morts metabasalt, southwest Newfoundland: Current Research, part D, Geological Survey of Canada, paper 93-1D, p.39-46.

Scholfield, D. and D'Lemos, 1995, Unravelling regional exhumation histories from granite pluton analysis: Abstracts, Tectonic Studies Group, 26th meeting, Cardiff.

Schröder, G., 1930, Das Grenzgebiet von Guadarrama und Hesperischen Ketten (Zentral-Spanien): Münster. Forsch. Geol. Paläont., H., v. 10, pp.207

Serrano Pinto, M.; Casquet, C.; Ibarrola, E.; Corretgé, L.G. and Portugal Ferreira, M., 1987, Sintese geocronologica dos granitoides do Maçizo Hesperico: in Bea, F.; Carnicero, A.; Gonzalo, J.C.; López Plaza, M. and Rodriguez Alonso, M.D. (Eds.). Geologia de los granitoides y rocas asociadas del Macizo Hespérico, Rueda, Madrid, p. 68-86.

Sha, L.K., 1995, Genesis of zoned hydrous ultramafic/mafic-silicic intrusive complexes: an MHFC hypothesis: Earth Science Reviews, 39. p.59-90.

Shelley, D., 1993, Igneous and Metamorphic rocks under the Microscope. Chapman & Hall, London, pp.445.00

Shervais, J.W., 1982, Ti-V plots and the petrogenesis of modern and ophiolitic lavas: Earth Planet. Sci. Lett., v.59, p.101-118.

Silva, J.B.; Oliveira, J.T. and Ribeiro, A., 1990, Structural outline (South Portuguese Zone): in Dallmeyer, R.D. and Martínez García, E. (Eds.). Pre-Mesozoic geology of Iberia. Springer Verlag, Berlin, p.348-362.

Snoke, A.W.; Quick, J.E. and Bowman, H.R., 1981, Bear Mountain igneous complex, Klamath Mountains, California: an ultrabasic to silicic calc-alkaline suite: J. Petrol., v.22, p.501-552.

Smith, H.A. and Barreiro, B., 1990, Monazite U-Pb dating of staurolite grade metamorphism in pelitic schists: Contrib. Mineral. Petrol., v. 105, p. 602-615.

Soers, E., 1972, Stratigraphie et geologie structurale de la partie orientale de la Sierra de Guadarrama (Espagne Centrale): Studia Geologica, IV, p. 7-94.

Sommer, W., 1965, Stratigraphie und tektonik im östlichen Guadarrama-Gebirge: Arbeiten Geol. Paläont. Inst. West. Wilhems-Universität, Münster.

Soper, N.J., 1988, Timing and geometry of collision, terrane accretion and sinistral strike-slip events in the British Caledonides: in Harris, A.L. and Fettes, D.J. (Eds.), The Caledonian-Appalachian orogen, Geol. Soc. London Spec. Pub. 38, p.481-492.

Spear, F.S., 1993, Metamorphic phase equilibria and pressure-temperature-time paths: Mineralogical Soc. America. Monograph Series v. 1, pp. 799

Srivastava, S.P. and Tapscott, C.R., 1986, Plate kinematics in the North Atlantic: in Vogt, P.R. and Tucholke, B.E. (Eds.). The western North Atlantic region. The geology of North America, v. M, Geological Society of America, p. 379-404.

Stacey, J.S. and Kramers, J.D., 1975, Approximation of terrestrial lead isotope evolution by a two stage model: Earth Planet. Sci. Lett., v. 6, p. 15-25

Stevens, R.D.; Delabio, R.N. and Lachance, G.R., 1982, Age determinations and geological studies. K/Ar isotopic ages: Report 16, Geological Survey of Canada Spec. Paper 82-2.

Stewart, D.; Tucker, R.D. and West, D., Genesis of Silurian composite terrane in northern Penobscot Bay: in Hussey, A.M. and Johnston, R.A. (Eds.) Guidebook to the field trips in southern Maine and adjacent New Hampshire, 87th annual meeting NEIGC, Maine Geol. Survey - Dept. of Geology Bowdoin College, Brunswick (Maine, USA), p. 29-51.

Stille, H., 1924, Grundfragen der Vergleichenden. Tectonik: Gebrueder Borntragen, Berlin, pp. 322

Storey, B.C.; Alabaster, T.; Hole, M.J.; Pankhurst, R.J. and Wever, H.E., 1992, Role of subduction-plate boundary forces during the initial stages of Gondwana break-up: evidence from the proto-Pacific margin of Antartica: in Storey, B.C., Alabaster, T. and Pankhurst, R.J. eds, Magmatism and the causes of continental break-up, Geol. Soc. Spec. Pub., 68, p.149-163.

Strachan, R.A. and Taylor, G.K. (editors), 1990, Avalonian and Cadomian geology of the North Atlantic: Blackie & son Ltd., Glasgow-London, Chapman and Hall, New York, pp. 252.

Strachan, R.A. and Taylor, G.K., 1990, Introduction: in Strachan, R.A. and Taylor, G.K. (Eds.) Avalonian and Cadomian Geology of the North Atlantic, Blackie & Son Ltd., Glasgow-London, p. 1-3.

Strachan, R.A.; Nance, R.D.; Dallmeyer, R.D.; D'Lemos, R.S.; Murphy, J.B. and Watt, G.R., 1996, Late Precambrian tectonothermal evolution of the Malverns Complex: J. Geol. Soc. London, v.153, p.589-600.

Sturt, B.A., Pringle, I.R. and Ramsay, D.M., 1978, The Finnmarkian phase of the Caledonian orogeny: J. Geol. Soc. London, v. 135, p. 597-610.

Sun, S.-S., 1980, Lead isotopic study of young volcanic rocks from mid-ocean ridges, ocean islands and island arcs: Phil. Trans. R. Soc. Lond., v. A297, p. 409-445.

Sutcliffe, R.H.; Smith, A.R., Doherty, W. and Barnett, R.L., 1990, Mantle derivation of Archean amphibole-bearing granitoid and associated mafic rocks: evidence from the southern Superior Province, Canada: Contrib. Mineral. Petrol., v. 105, p. 255-274.

Swinden, H.S. and Thorpe, R.I., 1984, Variations in style of volcanism and massive sulphide deposition in island arc sequences of the Newfoundland Central Mobile Belt: Economic Geology, v. 79, p. 1596-1619.

Swinden, H.S.; Jenner, G.A.; Fryer, B.J.; Hertogen, J. and Roddick, J.C., 1990, Petrogenesis and paleotectonic history of the Wild Bight Group, an Ordovician rifted island arc in central Newfoundland: Contrib. Mineral. Petrol., v. 105, p. 219-241.

Talbot, C.J. and Sokoutis, D., 1995, Strain ellipsoids from incompetent dykes: application to volume loss during mylonitization in the Singö gneiss zone, central Sweden: J. Struct. Geol., v. 17, p. 927-948.

Thiéblemont, D.; Béchennec, F.; Cabanis, B. and Chantraine, J., 1989, Lithostratigraphie et géochimie des formations paléomagmatiques dans le secteur Moëlan-Concarneau (Bretagne méridionale). Nouvelles contraintes sur l'évolution géodynamique du domaine Sud-Armorican au cors du Paléozoïque: Geodinamica Acta, v. 3 (2) , p. 1-16.

Thompson, M.D.; Hermes, O.D.; Bowring, S.A.; Isachsen, C.E.; Besancon, J.R. and Kelly, K.L., 1996, Tectonostratigraphic implications of late Proterozoic U-Pb zircon ages in the Avalon Zone of Southeastern New England: in Nance, R.D. and Thompson, M.D. (Eds.) Avalonian and related peri-Gondwanan terranes of the circum-North Atlantic. Geological Society of America Spec. paper 304, p. 179-192.

Tobisch, O.T.; Saleeby, J.B.; Renne, P.R.; McNulty, B. and Tong, W., 1995, Variations in deformation fields during development of a large-volume magmatic arc, Central Sierra Nevada, California: Geological Society of America Bull., v. 107, p. 148-166.

Todt, W.; Cliff, R.A.; Hansen, A. and Hofman, A.W., 1993, Re-calibration of NBS lead standards using a $^{202}Pb + ^{205}Pb$ double spike: EUG VII, Strasbourg, Terra abstracts, 5 (1), p. 396.

Torsvik, T.H.; Smethurst, M.A.; Meert, J.G.; Van der Voo, R.; McKerrow, W.S.; Brasier, M.D.; Sturt, B.A. and Walderhaug, H.J., 1996, Continental break-up and collision in the Neoproterozoic and Palaeozoic - A tale of Baltica and Laurentia: Earth Sci. Reviews, v.40, p.229-258.

Truyols, J.; Arbizu, M.A.; García Alcalde, J.L.; García López, S.; Mendez Bedia, I.; Soto, F. and Truyols Massoni, M., 1990, Pre-Mesozoic geology of Iberia, Springer Verlag, Berlin, p. 10-19.

Tucker, R.D. and Pharaoh, T.C., 1991, U-Pb zircon ages for Late Precambrian igneous rocks in southern Britain: J. Geol. Soc. London, v. 148, p. 435-443.

Tucker, R.D.; O'Brien, S.J. and O'Brien, B.H., 1994, Age and implications of Early Ordovician (Arenig) plutonism in the type area of the Bay du Nord Group, Dunnage Zone, southern Newfoundland Appalachians: Can. J. Earth Sci., v. 31, p. 351-357.

Tucker, R.D. and McKerrow, W.S., 1995, Early Paleozoic chronology: A review in light of new U-Pb zircon ages from Newfoundland and Britain: Can. J. Earth Sci., v. 32, p. 368-379

Ugidos, J.M., 1990, Granites as a paradigm of genetic processes of granitic rocks: I-types vs. S-types (Central Iberian Zone): in Dallmeyer, R.D. and Martínez García, E. (Eds.). Pre-Mesozoic geology of Iberia. Springer Verlag, Berlin, p. 189-206.

Valverde-Vaquero, P., 1993, Permo-Carboniferous magmatic activity in the Cantabrian Zone (N.E. Iberian Massif, Asturias, NW Spain) - Boston College, M.Sc. thesis -: University Microfilms Inc., Ann Arbor (Michigan), pp. 198.

Valverde-Vaquero, P. and Hepburn, J.C., 1995, Pre- and post-Variscan magmatism in the northern Iberian Massif (Cantabrian Zone): Geochemical signatures and tectonic implications: Abstracts supplement N°.1 to TERRAnova, v.7, EUG 8, Strasbourg, p.141.

Valverde-Vaquero, P.; Hernaiz - Huerta P.P.; Escuder-Viruete, J. and Dunning, G.R., 1995, Comparision of the Precambrian and Paleozoic evolution of the Sierra de Guadarrama (Central Iberian Zone, Spain) and the Gondwanan Margin of the Newfoundland Appalachians (GMNA): Abstracts supplement N°.1 to TERRAnova, v.7, EUG 8, Strasbourg, p.278.

Valverde-Vaquero, P. and Fernández, F.J., 1996, Edad de enfriamiento U/Pb en rutilos del gneis de Chimparra (Cabo Ortegal, NO de España): IV Congreso Geologico de España, Alcala de Henares, Geogaceta 20 (2), p. 475-478.

van Breemen, O.; Aftalion, M.; Bowes, D.R.; Dudek, A.; Msar, Z.; Povondra, P. and Vrana, S., 1982, Geochronological studies of the Bohemian Massif, Czechoslovakia, and their significance in the evolution of Central Europe: Trans. R. Soc. Edinburgh: Earth Sciences, v. 75, p. 89-108.

van Calsteren, F.W.C; Boelrijk, N.A.I.M.; Hebeda, E.H.; Priem, H.N.A.; Den Tex, E.; Verdurmen, E.A. Th. and Verschure, R.H., 1979, Isotopic dating of older elements (including the Cabo Ortegal mafic-ultramafic complex) in the Hercynian orogen of NW Spain: manifestations of a presumed Early Paleozoic mantle-plume: Chem. Geol., v.24, p. 35-56.

van der Pluijm, B.A.; Van der Voo, R. and Torsvik, T.H., 1995, Convergence and subduction at the Ordovician margin of Laurentia: in Hibbard, J.P.; van Staal, C.R. and Cawood, P.A., eds, Current Perspectives in the Appalachian-Caledonian Orogen. Geol. Assoc. Can., Spec. Paper 41, p. 127-136.

van Staal, C.R.; Winchester, J.A. and Bedard, J.H., 1991, Geochemical variations in Middle Ordovician volcanic rocks of the northern Miramichi Highlands and their tectonic significance: Can. J. Earth Sci., v. 28, p. 1031-1049.

van Staal, C.R.; Winchester, J.A.; Brown, M. and Burgess, J.L., 1992, A reconnaissance geotraverse through southwestern Newfoundland: Current Research, part D, Geological Survey of Canada, paper 92-1D, p. 133-143.

van Staal, C.R., 1994, Brunswick subduction complex in the Canadian Appalachians: record of the Late Ordovician to Late Silurian collision between Laurentia and the Gander margin of Avalon: Tectonics, v. 13, p. 946-962.

van Staal, C.R.; Dunning, G.; Valverde, P.; Burgess, J. and Brown, M., 1994, Arenig and younger evolution of the Gander margin: a comparison of the New Brunswick and Newfoundland segments: New perspectives in the Appalachian-Caledonian orogen -a conference in honour of Dr. Harold Williams, Geological Association of Canada NUNA conference, 1994 Grand Falls, Newfoundland, program with abstracts, p. 28.

van Staal, C.R., and de Roo, J.A., 1995, Mid-Paleozoic tectonic evolution of the Appalachian Central Mobile Belt in Northern New Brunswick, Canada: collision,

extensional collapse and dextral transpression: in Hibbard, J.P.; van Staal, C.R. and Cawood, P.A. (Eds.) Current Perspectives in the Appalachian-Caledonian Orogen: Geol. Assoc. Can. Spec. paper 41, p. 367-390.

van Staal, C.R.; Sullivan, R.W. and Whalen, J.B., 1996a, Provenance and tectonic history of the Gander Zone in the Caledonian/Appalachian Orogen: implications for the origin and assembly of Avalon: in Nance, R.D. and Thompson, M.D. Avalonian and related peri-Gondwanan terranes of the circum-North Atlantic: Geological Society of America Spec. paper 304, p. 347-368.

van Staal, C.R.; Hall, L.; Scholfield, D and Valverde, P., 1996b, Geology of Port-aux-Basques area, Newfoundland (110/11); Geological Survey of Canada (Geological Survey of Canada) open file 3165, scale 1:25.000.

van Staal, C.R.; Lin, S.; Valverde, P.; Hall, L. and Genkin, M., 1996c, Geology of Rose Blanche area, Newfoundland (110/10); Geological Survey of Canada (Geological Survey of Canada) open file 3219, scale 1:25.000.

Vavra, G., 1990, On the kinematics of zircon growth and its petrogenetic significance: a cathodoluminescence study: Contrib. Mineral. Petrol., v. 106, p. 90-99.

Vialette, Y.; Bellido, F.; Fuster, J.M. and Ibarrola, E., 1981, Données geochronologiques sur les granites de la Cabrera: Cuad. Geol. Ibérica, v. 7, p. 327-335.

Vialette, Y.; Casquet, C.; Fuster, J.M.; Ibarrola, E.; Navidad, M., Peinado, M. and Villaseca, C., 1986, Orogenic granitic magmatism of pre-Hercynian age in the Spanish Central System (S.C.S.): Terra Cognita, v.6, 2, p. 143.

Vialette, Y.; Casquet, C.; Fuster, J.M.; Ibarrola, E.; Navidad, M.; Peinado, M. and Villaseca, C., 1987, Geochronological study of orthogneisses from the Sierra de Guadarrama (Spanish Central System): Neues Jahrb. Mineral. Monatsh , v.10, pp.465-479.

Villena, J. and Pardo, G., 1983, El Carbonífero de la Cordillera Ibérica: in Martínez Díaz, C. (Ed.). Carbonífero y Pérmico de España. X Congreso Internacional de Estratigrafia y geologia del Carbonífero. ITGE (Spanish Geol. Survey), Madrid, p. 189-206.

Villaseca, C., 1983, Evolución metamórfica del sector centro-septentrional de la Sierra de Guadarrama: Ph.D. thesis (unpublished), Univ. de Madrid, pp.331.

de Waard, D., 1950, Palingenetic structures in augen gneiss of the Sierra de Guadarrama, Spain: Bull. Com. Geol. Finlande, v. 23, p. 51-66.

Weber, K., 1984, Variscan events: early Paleozoic continental rift metamorphism and late Paleozoic crustal shortening: in Hutton, D.H.W. and Sanderson, D.J. (Eds), Variscan Tectonics of the North Atlantic Region: Geol. Soc. London, Spec. issue, 14, p. 3-22.

Wendt, J.I.; Kröner, A.; Fiala, J. and Todt, W., 1993, Evidence from zircon dating for existence of approximately 2.1 Ga old crystalline basement in southern Bohemia, Czech Republic: Geol. Rundsch., v. 82, p. 42-50.

Went, D. and Andrews, M., 1990, Post-Cadomian erosion, deposition and basin development in the Channel Islands and northern Brittany: in D'Lemos, R.S.; Strachan, R.A. and Topley, C.G. (Eds), The Cadomian Orogeny: Geol. Soc. London, Spec. Pub. 51, p

Whalen, J.B.; Currie, K.L and van Breemen, O., 1987, Episodic Ordovician-Silurian plutonism in the Topsails igneous terrane, western Newfounland: Trans. R. Soc. Edin. Earth Sci., v. 78, p. 17-28.

Whalen, J.B.; Jenner, G.A.; Currie, K.L.; Barr, S.M.; Longstaffe, F.J. and Hegner, E., 1994, Geochemical and isotopic characteristics of granitoids of the Avalon Zone, southern New Brunswick: possible evidence for repeated delamination events: J. Geol., v. 102, p. 269-282.

White, C.E. and Barr, S.M., 1996, Geology of the Brookville Terrane, Southern New Brunswick, Canada: in Nance, R.D. and Thompson, M.D. (Eds.) Avalonian and related peri-Gondwanan terranes of the circum-North Atlantic. Geological Society of America Spec. paper 304, p. 133-148.

Wiebe, R.A., 1991, Commingling of contrasted magmas and generation of mafic enclaves in granitic rocks: in Didier, J. and Barbarin, B. (Eds.). Enclaves and Granite petrology. Developments in Petrology, 13, Elsevier, Amsterdam, p.393-402.

Wildberg, H.D.H.; Bischoff, L.and Baumann, A., 1989, U-Pb ages of zircon from meta-igneous and meta-sedimentary rocks of the Sierra de Guadarrama: implications for the Central Iberian crustal evolution: Contrib. Mineral. Petrol. v.103, pp.253-262.

Williams, H., 1964, The Appalachians in Northeastern Newfoundland - a two sided symmetrical system: Am. J. Sci., v.262, p. 1137-1158.

Williams, H.; Kennedy, M.J. and Neale, E.R.W., 1970, The Hermitage Flexure, the Cabot Fault and the disappearance of the Newfoundland Central Mobile Belt: Geological Society of America Bull., v.81, p.1563-1568.

Williams, H.; Dallmeyer, R.D. and Wanless, R.K., 1976, Geochronology of the Twinllingate granite and Herring Neck Group, Notre Dame Bay, Newfoundland: Can. J. Earth Sci., v. 13, p. 1592-1601.

Williams, H. (compiler), 1978a, Tectonic-Lithofacies map of the Appalachian Orogen: Memorial University of Newfoundland. Map # 1.

Williams, H, 1978b, Geological development of the northern Appalachians: its bearing on the evolution of the British Isles. in Bowes, D.R. and Leake, B.E., (Eds.), Crustal evolution in northwestern Britain and adjacent regions, Seal House Press, Liverpool, England, p. 1-22.

Williams, H., 1979, Appalachian Orogen in Canada: Can. J. Earth Sci. v. 16, p. 792-807.

Williams, H. and Hatcher, R.D., 1983, Appalachian suspect terranes: Geological Society of America Memoir 158, p. 33-53.

Williams, H.; Colman-Sadd, S. and Swinden, H.S., 1988, Tectonic-stratigraphic subdivisions of central Newfoundland: in Current Research, Part B, Geological Survey of Canada. paper 88-1B, p. 91-98.

Williams, H. (eds and coordinator), 1995*, Geology of the Appalachian-Caledonian orogen in Canada and Greenland: Geological Survey of Canada, Geology of Canada, # 6, pp. 944. (*also*, Geological Society of America, The Geology of North America, v. F-1). * *in references refers to this volume.*

Williams, H., 1995a*, Introduction: Chapter 1., in *, p.1-19

Williams, H., 1995b*, Intruduction (Humber Zone): Chapter 3, in *, p. 50-61.

Williams, H., 1995c*, Taconic allochthons in Newfoundland, Chapter 3: in *, p. 99-114.

Williams, H., 1995d *, Preamble (Dunnage Zone), Chapter 3: in *, p. 139-142.

Williams, H., 1995e *, Dunnage Zone-Newfoundland, Chapter 3: in *, p. 142-166.

Williams, H., 1995f *, Preamble (Gander Zone), Chapter 3: in *, p.198-199.

Williams, H., 1995g *, Introduction: Middle Paleozoic rocks - Newfoundland, Chapter 4: in *, p. 383-384

Williams, H., 1995h*, Introduction: Springdale Belt, Chapter 4: in *, p.389.

Williams, H., 1995i*, Springdale Belt: summary and discussion, Chapter 4, in *, p.396-397.

Williams, H., 1995j*, Summary and overview, Chapter 11, in*, p. 843-890.

Williams, H.; Colman-Sadd, S.P. and O'Neill, P.P., 1995 *, Gander Zone-Newfoundland, Chapter 3, in *, p. 199-212.

Williams, H.; Coyle, M. and Strong, D.F., 1995a*, Springdale Belt-Halls Bay area, Chapter 4, in *, p.393-394.

Williams, H.; Dean, P.L. and Pickering, K.T., 1995b*, Botwood Belt, Chapter 4: in*, p.413-420.

Williams, H.; Fahraeus, L.E. and Stevens, R.K., 1995c*, Clam Bank Belt, Chapter 4 : in *, p. 384-388.

Williams, H; Kumarapeli; P.S. and Knight, I., 1995d, Upper Precambrian-Lower Cambrian clastic sedimentary and volcanic rocks (Humber Zone), chapter 3: in *, p. 61-67.

Williams, H.; Lafrance, B.; Dean, P.L.; Williams, P.F.; Pickering, K.T. and van der Pluijm, B.A., 1995e*, Badger Belt, Chapter 4, in *, p.403-413.

Williams, H. and O'Brien, S.J., 1995*, Fortune belt, Chapter 4: in*, p.423-425.

Williams, S.H.; Harper, D.A.T.; Neuman, R.B.; Boyce, W.D. and MacNiocaill, C., 1995, Lower Paleozoic fossils from Newfoundland and their importance in understanding the history of the Iapetus Ocean: in Hibbard, J.P.; van Staal, C.R. and Cawood, P.A. (Eds.) Current Perspectives in the Appalachian-Caledonian Orogen: Geol. Assoc. Can. Spec. paper 41, p. 115-126.

Wilson, J.T., 1966, Did the Atlantic close and then re-open?: Nature, v. 211, p. 676-681.

Wilson, M., 1989, Igneous Petrogenesis: Unwin Hyman, London, pp. 466.

Wilton, D.H.C., 1983, The geology and strcutural history of the Cape Ray Fault Zone in southwestern Newfoundland: Can. J. Earth Sci., v.20, p. 1119-1133.

Wilton, D.H.C., 1984, Metallogenic, tectonic and geochemical evolution of the Cape Ray Fault Zone with emphasis on electrum mineralization: Ph.D. thesis, Memorial University of Newfoundland, 618 pp.

Winchester, J.A. and Floyd, P.A., 1977, Geochemical discrimination of different magma series and their differentiation products using immobile elements: Chem. Geol., v.16, p.325-343.

Winchester, J.A.; Max, M.D. and Murphy, F.C., 1990, The Rosslare Complex: a displaced terrane in southeast Ireland: in Strachan, R.A. and Taylor, G.K. (Eds.) Avalonian and Cadomian Geology of the North Atlantic, Blackie & Son Ltd., Glasgow-London, p.49-64

Winchester, J.A. and van Staal, C.R., 1995, Volcanic and sedimentary terrane correlation between the Dunnage and Gander Zones of the Canadian Appalachians and the British Caledonides reviewed: in Hibbard, J.P.; van Staal, C.R. and Cawood, P.A. (Eds.) Current Perspectives in the Appalachian-Caledonian Orogen: Geol. Assoc. Can. Spec. paper 41, p.95-114.

Wonderley, P.F. and Neuman, R.B., 1984, The Indian Bay formation: fossiliferous Early Ordovician volcanigenic rocks in the northern Gander Terrane, Newfoundland, and their regional significance: Can. J. Earth Sci., v. 21, p.525-532.

Wood, D.A., 1980, The application of the Th-Hf-Ta diagram to problems tectonomagmatic classification and to the establishing the nature of crustal contamination of basaltic lavas of the Bristish Tertiary volcanic province: Earth Planet. Sci. Lett., v. 50, p. 11-30.

Yenes, M.; Gutiérrez-Alonso, G. and Alvarez, F., 1996, Dataciones K-Ar de los granitoides del área La Alberca-Béjar (Sistema Central Español): Geogaceta, v.20, p. 479-482.

York, D., 1969, Least squares fitting of a straight line with correlated errors: Earth and Planet. Sci. Lett., v. 5, p. 320-324.

Young, T.P., 1990, Ordovician sedimentary facies and faunas of southwest Europe: palaeogeographic and tectonic implications: in McKerrow, W. S. and Scotese, C.R. (Eds.) Palaeozoic Palaeogeography and Biogeography, Geol. Soc. Memoir 12, p. 421-430.

Ziegler, Z.A.. 1986, Geodynamic model for the Palaeozoic crustal consolidation of Western and Central Europe: Tectonophysics, v. 126, p. 303-328

APPENDIX

ANALYTICAL METHODS

A.1.- U-Pb PROCEDURE.-

This is a brief description of the analytical procedure used for the U-Pb analysis of zircon, monazite, xenotime, titanite and rutile.

A.1.1.- Sample preparation.

The rock sample (5 to 25 kg, average 10-15 kg) was washed and any dirt removed with running water and a wire brush. The sample was dried and pulverized using a hydraulic press, a jaw-crusher and a steel plate pulverizer. All crushing equipment was dismantled and cleaned using alcohol and compressed air; the crushing plates were scrubbed with a powerbrush and then cleaned between samples. A first separation of light and heavy minerals was done using a Wilfley panning table. The Wilfley table was previously cleaned with 1N HCl, soap and water and the accessory equipment was cleaned with soap and water, alcohol and compressed air. The heavy fraction and a portion of the light mineral fraction were kept; both fractions were washed with alcohol and dried on a hot plate. Highly magnetic minerals such as magnetite and small iron filings from the pulverizer plates were removed by dropping the sample past an electromagnet. The remaining heavy fraction was sieved to a -40 mesh size. The fine fraction was separated twice into light and heavy fractions using bromoform and methylene iodide. Finally the heavy fraction was separated according to magnetic character using a Frantz isodynamic magnetic separator. Separation of the different accessory mineral phases was achieved by changing the tilt and current intensity of the Frantz. This separation also yielded separate fractions with different

paramagnetic properties for some of the minerals of interest, like zircon. Mineral fractions for U-Pb analysis were hand-picked from the magnetic separates under a microscope on the basis of morphology, colour, size and crystal quality. Crystal selection was very strict to assure the homogeneity of the fractions. In several cases the purity of the monazite and xenotime fractions was checked by EDS analysis (CAMECA SX 50 microprobe) of the whole mineral fraction. In order to minimize discordance, due to the effects of alteration and Pb loss, most mineral fractions were air abraded (Krogh, 1982). The abraded and unabraded mineral fractions were washed with 4N HNO_3 (5 minutes on a hot plate at 120°C), H_2O and alcohol. A second selection of the best grains was done under the microscope after which they were placed in a clean Pyrex crystal beaker with alcohol.

A.1.2.- Sample cleaning, weighing, spiking, dissolution and U-Pb separation.

This part of the procedure took place in a clean air laboratory and within clean boxes with an outward laminar flow; all reagents were double distilled and clean-lab sample-handling procedures were observed.

The mineral fractions were washed with 2xH_2O, 4N HNO_3 (20 minutes on a hot plate at 100°-120°C), 2xH_2O and twice with acetone and 2xH_2O and dried; during each wash the sample was ultrasonic for 10 seconds. The mineral fractions were weighed with a five digit balance with an uncertainty of ±2 micrograms, mixed with a ^{205}Pb - ^{235}U spike (Parrish and Krogh, 1987) inside Teflon® Krogh-type dissolution bombs (Krogh, 1973) or Teflon® Savillex containers and dissolved (Table A.1). The samples were spiked according to the sample weight and the expected age and U concentration in the sample.

Table A.1.: Mineral dissolution procedure

Mineral phase	Dissolution vessel	Reagents	Temperature / time
Zircon, rutile	Krogh-type dissolution Teflon® bombs and minibombs	HF, 8N HNO_3	210°C oven / 5 days
Titanite	Savillex screw top Teflon® containers	HF, 8N HNO_3	120°C hot plate / 5 days
Monazite, xenotime	Savillex screw top Teflon® containers	6.2N HCl	120°C hot plate / 5 days

Once dissolved, the samples were dried on a hot plate (120°C) and re-dissolved with 3.1N HCl at the same temperature conditions of table A.1 for 24 hours. U and Pb were separated through ion exchange chemistry following modified procedures for zircon chemistry after Krogh (1973) and HBr chemistry after Manhès et al. (1978) for rutile, titanite, monazite and xenotime (Table A.2).

Procedure blanks during the period of analysis ranged from 1 pg U and 2 to 12 pg common Pb (depending on the minibomb set) for zircon and 1 pg U and 12 to 20 pg common Pb for rutile, titanite, monazite and xenotime.

A.1.3 .- U-Pb isotopic analysis and age determination.

The U and Pb isotopic ratios were measured by thermal ionization mass-spectrometry (TIMS) using a Finnigan MAT 262 mass spectrometer equipped with an ion-counting secondary electron multiplier (SEM). U and Pb were loaded together with H_3PO_4 and silica gel on a previously outgassed single rhenium filament in a clean box. Both U and Pb were measured in static mode on the Faraday cups, ^{204}Pb was measured in the previously calibrated, axial SEM/ion counter. The SEM is calibrated with respect to the Faraday cups before and after each analysis. Small Pb fractions (Less than 3mv signal of ^{205}Pb or ^{207}Pb

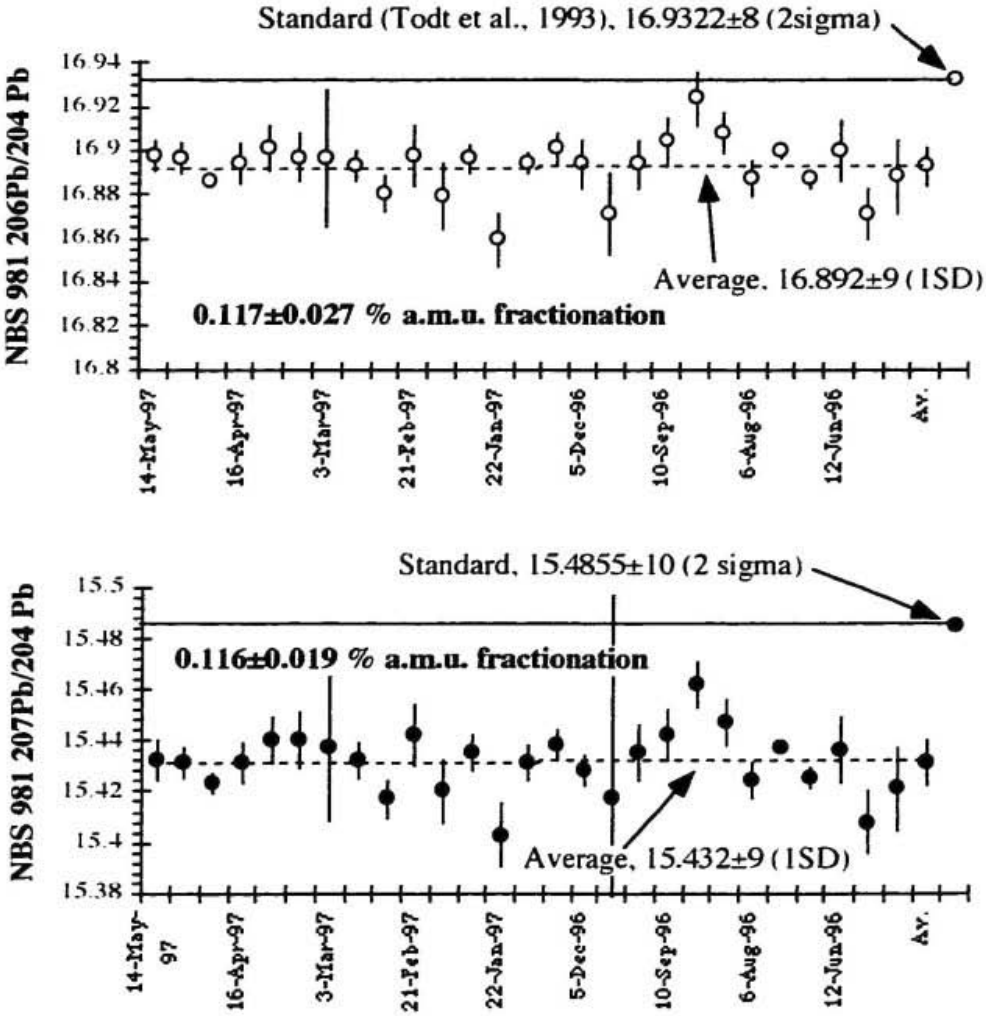

Fig.A.1.- Variation of the measurements of the 206Pb / 204Pb and 207Pb / 204Pb isotopic ratios of the NBS 981 common Pb standard with respect to the reported ratios (Todt, 1993), and calculated values of the Pb isotopic fractionation during mass spectrometry. The measured ratios were taken from 27 randomly selected analyses between May 14th 1997 and March 26th 1996. The calculated isotopic fractionation in the 206Pb/204Pb ratio is slightly higher but has a smaller error than the one used in the age calculations (0.1±0.04). The elimination of some of the outliers would bring the fractionation value closer to the one used in the age calculations. This new fractionation value, if applied, would not change the isotopic ages but it would result in narrower error ellipses.

in the Faraday cups) were measured in dynamic mode using the SEM (peak jumping on the SEM), these isotopic ratios were checked and calibrated against Faraday-derived data during the same run. These measurements were performed in single blocks of 10 scans each, outliers were identified and eliminated from the final mean of the measurement (Finnigan MAT 262 software). The best Pb emissions were usually obtained between 1400° and 1550°C, and for U between 1550°-1650°C. The intensity of the emission was monitored on a chart recorder, which allowed, in the case of static collection, manual increase or decrease of the temperature of the filament during the measurement to keep a stable emission.

The isotopic ages have been calculated using the accepted disintegration constants for ^{235}U and ^{238}U (Jaffey et al., 1971). The isotopic ages and the error on the isotopic ratios have been calculated using unpublished Royal Ontario Museum (ROM) software by Larry Heaman. The errors on the isotopic ratios are given at 2 sigma level and are the result of propagating two-sigma errors from the amount of isotopic fractionation (0.1±0.04 % a.m.u for Pb and 0.05±0.04% a.m.u for U; Fig. A.1), total blanks in the analysis, laboratory blanks ($^{206}Pb/^{204}Pb = 18.33$; $^{207}Pb/^{206}Pb = 0.855$; $^{208}Pb/^{206}Pb = 2.056$), amount of initial common Pb and uncertainties on the measurements. The initial common Pb was corrected after the model of Stacey and Kramers (1975). The U and Pb concentrations were estimated from the absolute sample and spike weights. The linear regressions for the discordia lines were calculated after the method of Davis (1982). The discordia line is defined by the best fit line, this method also provides the probability of fit of the data points to the discordia line and the probability of each individual data point fitting the line. If the U-Pb data does not fit the discordia line within error, the error ellipses of the data points are then expanded with an error proportional to the degree of discordance of each data point (v. Davis, 1982). The error on the intercepts of the discordia line are based on the Bayesian

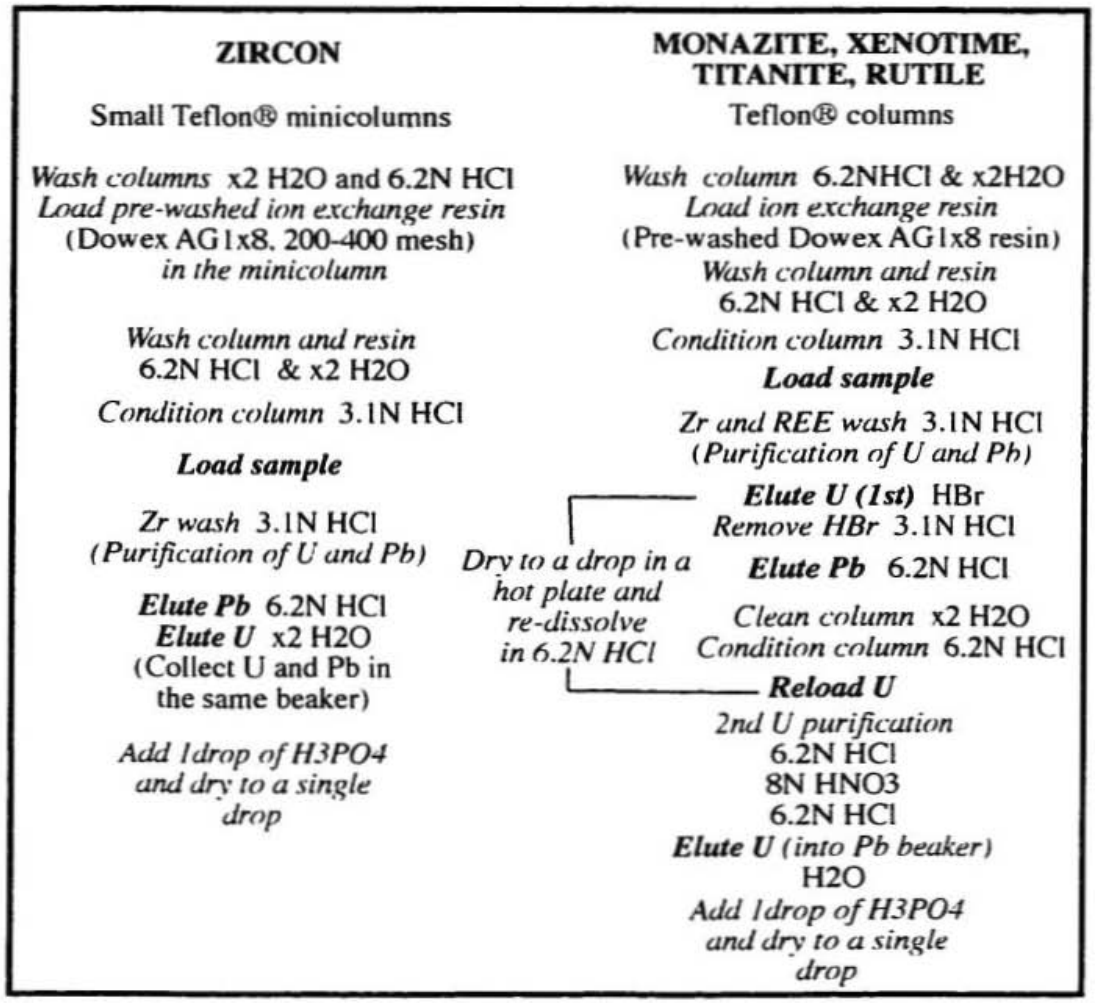

Table A.2.- Schematic U and Pb ion exchange chemical extraction procedure. The Teflon® columns are similar in dimension to those of Krogh (1973), the volume of Teflon® minicolumns was scaled down to 1/10 of the columns. All acids are double distilled (X2 H2O, double distilled H2O).

intervals of the probability function of the age of the best fit line (i.e. intercept of the discordia line with the concordia curve) at a 95% confidence level. This method is different from that of the commonly used program of Ludwig (1980), which estimates the age intercept error from the hyperbolic error band of the discordia line after a least-squares York fit (York, 1969) of the data points. In should be noted that for lower probabilities of fit, the Davis method generally gives larger age intercept errors than the program of Ludwig (1980). This is due to the fact that the method of Davis takes into account the degree of discordance of the individual data points, so the best fit line relies more on the less discordant data points (i.e. geologically, the more reliable data) even if other points are more precise. Age errors are given at a 95% confidence level.

A.2.- MAJOR AND TRACE ELEMENT ANALYSIS.-

This is a description of the analytical techniques used to obtain the major and trace element whole rock analyses presented in chapters III and IV of this thesis, including the sample preparation.

The rock samples weighed between 10 to 20 Kg depending on the average grain size (1.5 to 0.5 mm), resulting in sampling errors of around 5%. The weathering surfaces of the rock sample were removed prior to rock crushing. The rock crushers were cleaned between samples, and small portion of the sample was crushed and discarded prior to the final crushing to avoid cross-contamination. After crushing, the rock chips were quartered to assure the representativeness of the sample. Randomly selected rock chips were powered to <200 mesh size using a carbon-tungsten rock mill. The rock mill was cleaned between samples. Before the final powdering and to avoid cross-contamination, rock chips from the

sample were pulverized and the powder discarded. The final powder was stored in a clean plastic sample vial.

The loss on ignition were calculated by placing 2 g of fresh rock powder in a ceramic crucible. The powder and the crucible were weighed and then placed in an oven at 450°C for 12 hours and the weight loss measured afterwards.

A.2.1.- X-ray fluorescence (XRF) analysis.

The major elements were analyzed on fused glass beads (fused pellets). The glass beads were made by mixing 1.5000 g of ignited rock powder with a flux of 6.0000 g of Lithium metaborate and 1.5000 g of Lithium tetraborate. The half of the homogenized powder was placed in a clean, dry platinum crucible and 0.02 g of Lithium Bromide solution added to the powder, after which the remaining powder was placed in the crucible. The glass beads were automatically made with a LECO FX 200 burner in sets of six. The burner was programmed to progressively reach temperatures of 1500°C over 12.5 minutes.

The trace elements were analyzed on press pellets made of 5.00 g of fresh rock powder and 0.70 g of phenolic resin (BRP-5933 Bakelite phenolic resin). The rock powder and the resin were homogenized for 10 minutes in a roller mixer and the resulting mixed powder was pressed in a Herzog pellet press for 5 seconds at a pressure of 20 tons. The resulting pressed pellets were placed in a oven at 200°C for 15 minutes. Further details on the sample preparation can be obtained from the internal procedures of the XRF analytical facilities of the department of earth sciences at Memorial University of Newfoundland.

The XRF major and trace element analyses were performed using the Fisons/ARL 8420+ sequential wavelength-dispersive X-ray spectrometer. This spectrometer has one

goniometer and is capable of holding six analyzing crystals. For trace element analysis five crystals were used, including a LiF200H crystal specially treated for heavy element sensitivity. Also either an argon flow-proportional detector (FPC) or a scintillation (SC) detector was used with the rhodium anode end-window X-ray tube operated at 3 kw. The analytical procedure, including the calibration and matrix correction procedures, and the precision and accuracy have been described in detail by Longerich (1995). The limits of detection for the major elements are 0.02% for SiO_2, 0.01% for TiO_2, 0.06% for Al_2O_3, 0.01% for total Fe as Fe_2O_3, 0.00% for MnO, 0.03% for MgO, 0.01% for CaO, 0.04% for Na_2O, 0.01% for K_2O and 0.01% for P_2O_5. The analysis of five standards in each run has allowed to determine a precision and accuracy of <1% for concentrations above 1% and <3% for concentrations below 1%, for the major element analysis. The limits of detection for the trace elements are in brackets in ppm: Sc (6), V(6), Cr(7), Ni(5), Cu(4), Zn(3), Ga(3), Rb(0.7), Sr(1.2), Y(0.7), Zr(1.2), Nb(0.7), Ba(23), Pb(4). The precision and accuracy of the trace element analysis is below 1% for most elements, except for Zn (4%).

A.2.2.- Inductively coupled plasma mass spectrometry (ICP-MS) trace element analysis.

ICP-MS analysis using Na_2O_2 sinter sample dissolution was used for the determination of the Lanthanides (REE) and Th because it dissolves resistant accessory mineral phases, such as zircon, which contain significant concentrations of these elements. The linear fit between the XRF and the ICP-MS analyses for Y (Fig.A.2) shows the good agreements between the analytical techniques, and suggests that there were no dissolution problems with the heavy-REE. The high field strength elements (Zr, Nb, Hf and Ta) were also determined by ICP-MS analysis. But there is a scatter between the ICP-MS and the

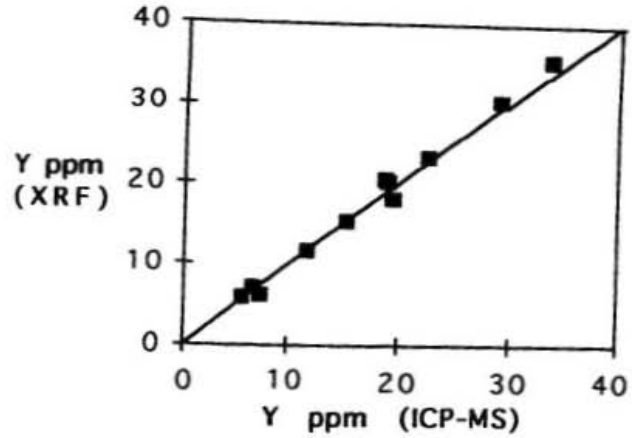

Fig.A.2.- Comparative chart of the Y XRF versus ICP-MS analyses (Margaree orthogneiss data).

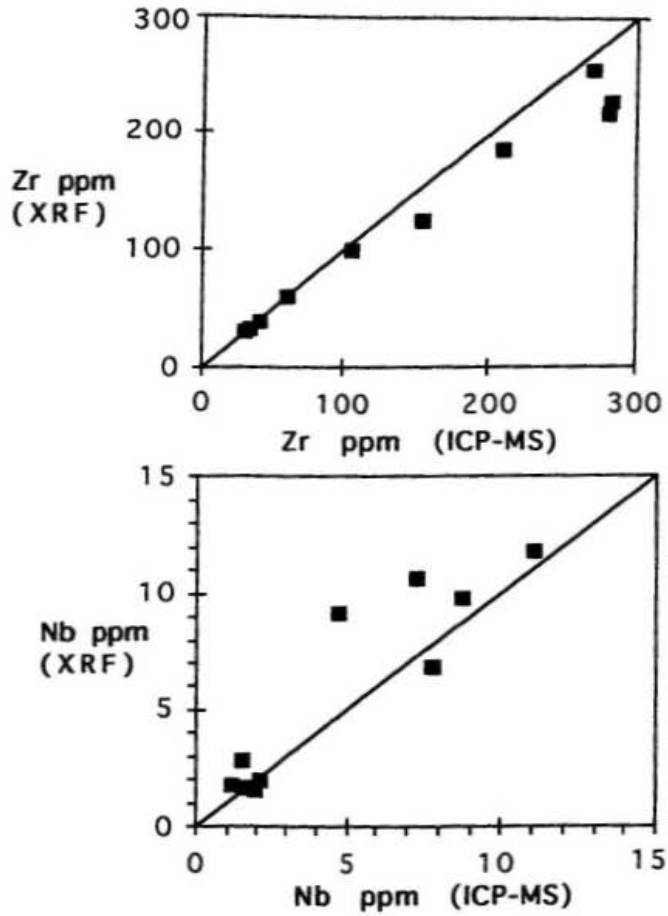

Fig. A.3.- Comparative chart of the XRF and ICP-MS Zr and Nb analyses (Margaree orthogneiss data).

XRF analyses (Fig.A.3) which could be due to solution instability and potential memory problems with these elements (Jenner et al., 1990). For this reason only the XRF results for Zr and Nb were reported in the analysis tables.

The samples were prepared by mixing 0.2 g of fresh rock powder in a Ni crucible with 0.8 g of Na_2O_2 and sintering the mixture in a muffle furnace at 480°C for 1.5 hours. The crucibles were cooled and 10 ml of distilled H_2O were added until reaction stopped. The mixture was diluted with distilled H_2O, centrifuged and dissolved in 8N HNO_3 and oxalic acid. The solution was diluted with distilled H_2O prior to ICP-MS analysis. This solution was latter mixed with an on-line standard spike.

The analytical data was acquired with an SCIEX ELAN 250 ICP-MS modified at Memorial University and equipped with an autosampler. Each run consisted of 56 unknown samples distributed in 8 cycles, each cycle containing 7 unknowns, 4 standards and 1 calibration blank. A "Y" tube was used to spike the samples with a standard solution of Rb, Cs, Tl and U at a 1 part of spike / 2 parts of sample ratio. The calibration blank was used to make the background correction, oxide interferences were corrected using the UO/U ratio in the standards and the mass interpolated ratio of the intensity of the spike in the samples and the standards was used to correct the matrix effects. Further details of the data acquisition and processing, including the calibration techniques, can be found in Jenner et al (1990). The analytical limits of detection are at the sub-ppm level: 0.02 ppm for Nd, Zr*, and Hf*; 0.01 ppm for Sm, Eu, Gd, Dy, Er, Yb and Ta*; below 0.00 ppm for Y*, La, Ce, Pr, Tb, Ho, Tm, Lu and Th (* elements analyzed but not reported in the final analysis tables). The precision of the technique is generally between 3 and 10% for the REE and Y, between 10 and 15% for Zr and Hf, more than 20% for Nb and Ta and in excess of 40% for Th (Longerich pers comm.). The low precision of the HFSE is due to a dissolution problem plus the added difficulty of keeping them in solution. The low

precision of Th is due mostly to machine memory problems (Longerich, pers comm.). Duplicates of two rock samples were dissolved and analyzed separately during the same run to show the reproducibility of the technique (Table A.3). The apparent good reproducibility of Th led to its use for tectonic discrimination purposes in some discrimination diagrams of chapters III and IV. These results were always backed up by diagrams using more reliable elements.

	Sample GMA-B (N=2)			Sample GMA-C (N=2)		
	Mean	*SD*	RSD (%)	*Mean*	*SD*	RSD (%)
Y	19.45	0.13	0.67	15.66	0.11	0.70
Zr	289.29	7.94	2.74	288.53	9.09	3.15
Nb	9.26	2.70	29.15	11.10	0.00	0.00
Ba	414.29	7.03	1.70	824.48	1.24	0.15
La	37.25	2.16	5.81	26.05	0.36	1.37
Ce	71.01	3.33	4.69	51.06	0.59	1.15
Pr	7.52	0.35	4.72	5.59	0.11	1.95
Nd	26.75	1.07	4.02	20.04	0.32	1.59
Sm	4.43	0.25	5.62	3.67	0.18	4.81
Eu	1.01	0.07	7.21	0.95	0.04	4.25
Gd	3.85	0.17	4.39	3.08	0.07	2.32
Tb	0.58	0.02	4.25	0.47	0.01	2.53
Dy	3.70	0.15	4.16	2.89	0.04	1.35
Ho	0.75	0.02	2.53	0.55	0.02	3.36
Er	2.13	0.06	2.65	1.66	0.03	1.88
Tm	0.33	0.01	3.26	0.26	0.00	1.37
Yb	2.10	0.15	7.00	1.79	0.01	0.36
Lu	0.28	0.01	3.25	0.28	0.00	0.51
Hf	7.28	0.10	1.40	7.16	0.27	3.81
Ta	2.79	0.36	12.98	3.00	0.05	1.60
Th	13.72	0.66	4.84	12.04	0.36	2.96

Table A.3. Results of the ICP-MS Na_2O_2 sinter duplicate analysis of samples G-MA-B and G-MA-C (Margaree Complex). The percentage RSD, although not statistically significant, offers an insight into the reproducibility of the technique but should not be taken as indicative of the technique's precision.

IMAGE EVALUATION
TEST TARGET (QA-3)

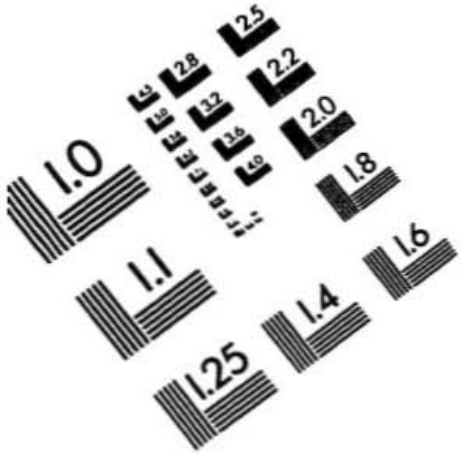

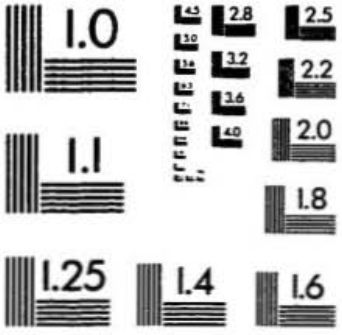

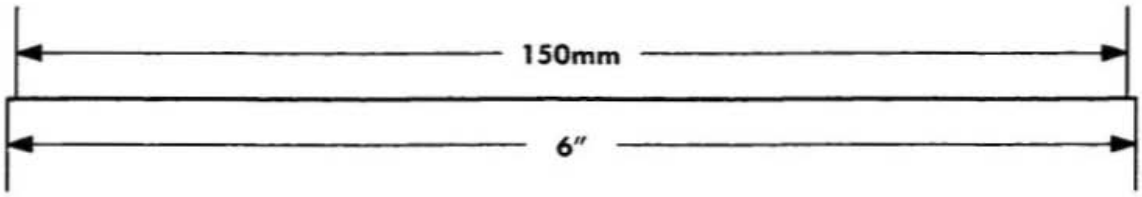

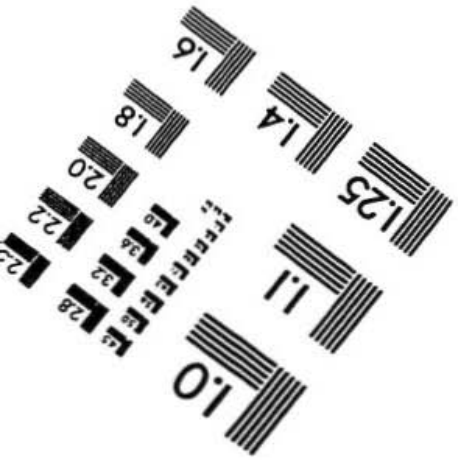

APPLIED IMAGE, Inc
1653 East Main Street
Rochester, NY 14609 USA
Phone: 716/482-0300
Fax: 716/288-5989

AN INTEGRATED FIELD, GEOCHEMICAL AND U-Pb GEOCHRONOLOGICAL STUDY OF THE SOUTHWEST HERMITAGE FLEXURE (NEWFOUNDLAND APPALACHIANS, CANADA) AND THE SIERRA DE GUADARRAMA (IBERIAN MASSIF, CENTRAL SPAIN): A CONTRIBUTION TO THE UNDERSTANDING OF THE GEOLOGICAL EVOLUTION OF CIRCUM-ATLANTIC PERI-GONDWANA

PABLO VALVERDE-VAQUERO

AN INTEGRATED FIELD, GEOCHEMICAL AND U-Pb GEOCHRONOLOGICAL STUDY OF THE SOUTHWEST HERMITAGE FLEXURE (NEWFOUNDLAND APPALACHIANS, CANADA) AND THE SIERRA DE GUADARRAMA (IBERIAN MASSIF, CENTRAL SPAIN): A CONTRIBUTION TO THE UNDERSTANDING OF THE GEOLOGICAL EVOLUTION OF CIRCUM-ATLANTIC PERI-GONDWANA

VOLUME II: Tables, Maps and Figures

By:

© PABLO VALVERDE-VAQUERO; Lic.; M.Sc.

A thesis submitted to the School of Graduate Studies
in partial fulfilment of the requirements for the degree
of Doctor of Philosophy

Department of Earth Sciences
Memorial University of Newfoundland

September 1997

St. John's Newfoundland

TABLE OF CONTENTS

VOLUME II: Tables, Maps and Figures

LIST OF TABLES

Volume II: Tables, Maps and Figures

LIST OF MAPS

Volume II: Table, Maps and Figures

CHAPTER III - THE CINQ-CERF GNEISS (SW Hermitage Flexure)

LIST OF FIGURES:

Volume II: Tables, Maps and Figures

CHAPTER I: INTRODUCTION.

CHAPTER II: THE NEWFOUNDLAND APPALACHIANS.

CHAPTER III.- THE CINQ-CERF GNEISS (SW Hermitage Flexure):

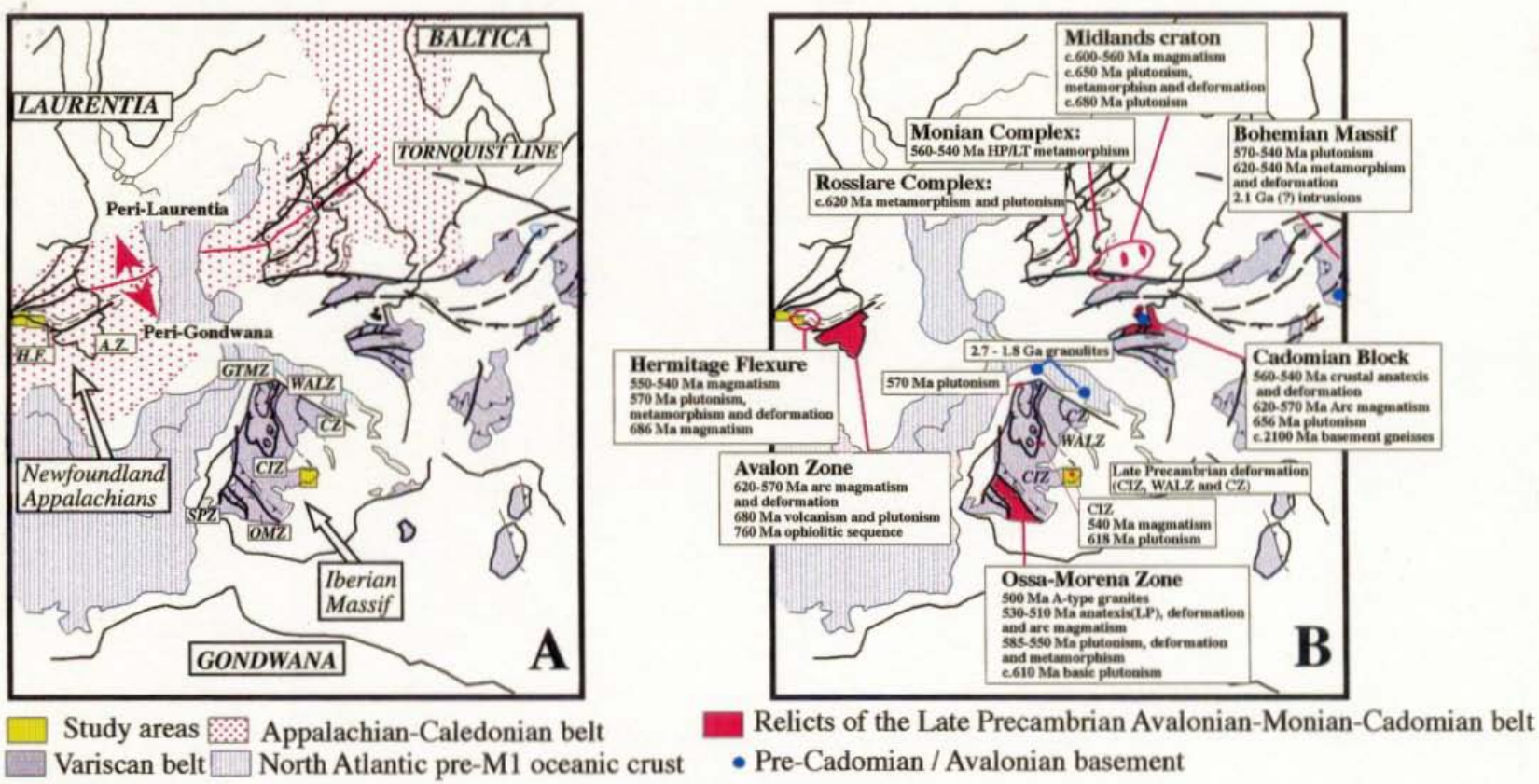

Fig.1.1.- (A) Paleogeographic reconstruction of the North Atlantic at M1 magnetic anomaly (131 Ma; Srivastava and Tapscott, 1986) showing the relative position of the Appalachian-Caledonian orogen, the Variscan Belt and the areas of study. The red line marks the separation between the peri-Laurentian and peri-Gondwanan margins of the Iapetus Ocean. Correlation between the Newfoundland Appalachians and the British Caledonides based on Colman-Sadd et al. (1992). Lithotectonic zones of the Iberian Massif after Farias et al. (1986): CZ, Cantabrian Zone; WALZ, West Asturian-Leonese Zone; CIZ, Central Iberian Zone; GTMZ, Galicia Tras-os-Montes Zone; OMZ, Ossa-Morena Zone; SPZ, South Portuguese Zone. Newfoundland Appalachians: A.Z., Avalon Zone; H.F., Hermitage Flexure.

(B) Distribution of the circum-North Atlantic Avalonian-Monian-Cadomian terranes and relicts of pre-Cadomian/Avalonian basement: *Avalonian belt*: Avalon Zone and Hermitage Flexure (O'Brien et al., 1996 and ref. within), Midlands Craton (Soper, 1988; Tucker and Pharaoh, 1991; Strachan et al., 1996), Rosslare Complex (Winchester et al., 1990); *Monian Complex* (Gibbons, 1990; Gibbons and Horak, 1990); *Cadomian belt*: Cadomian block (ref. in D'Lemos et al. eds. (1990) and Strachan and Taylor eds.(1990));Bohemian Massif (Chaloupsky, 1990; Kroner et al., 1994); Ossa-Morena Zone (Quesada, 1990a; 1990b; Oschner, 1993); CIZ, WALZ and CZ , references in Dallmeyer and Martinez Garcia eds. (1990). *Proterozoic basement* (Clavez and Vidal, 1978; Auvray et al., 1980; Guerrot et al., 1989; Wendt et al., 1993)

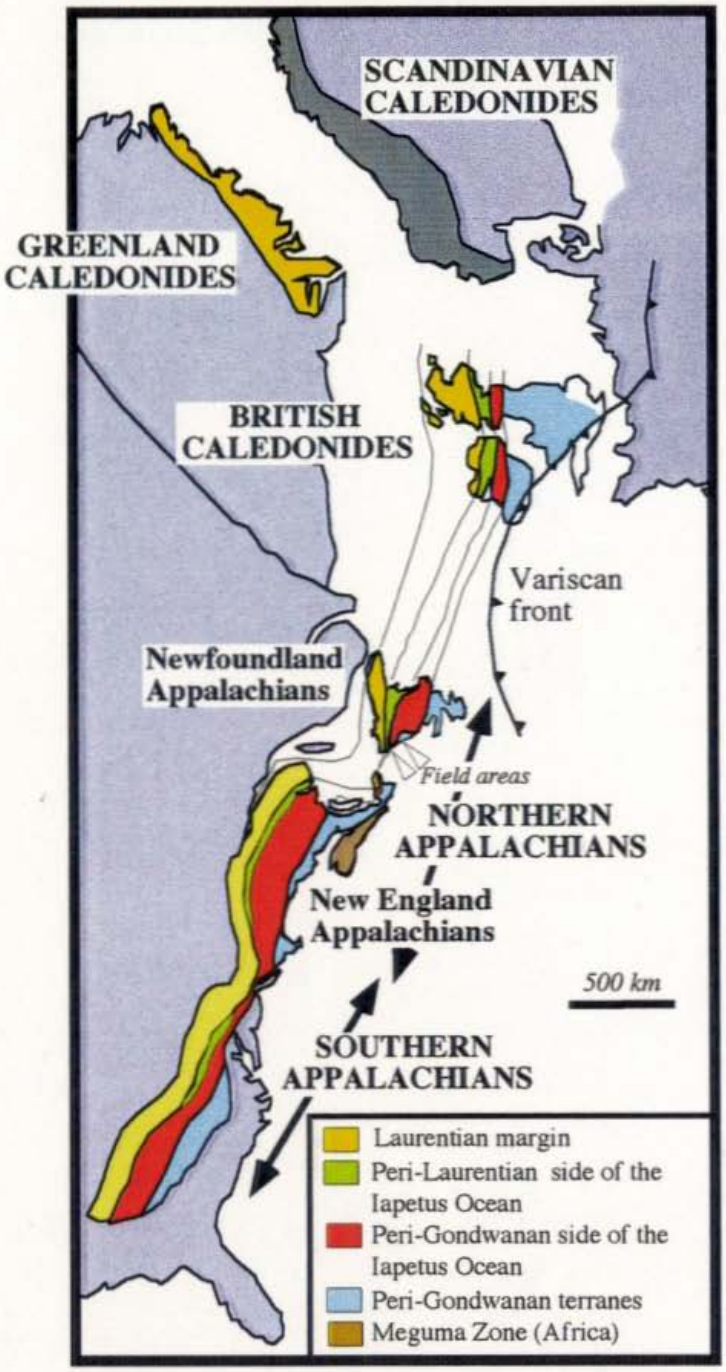

Fig. 1.2.- Map of the Appalachian-Caledonian orogen. Correlation between the Newfoundland Appalachians and the British Caledonides after Colman-Sadd et al. (1992). Correlation between Newfoundland and the Maritimes taken from Lin et al. (1994). U.S. Appalachians modified after Williams (compiler, 1978).

Fig.1.3. .- Distribution of the elements of the Variscan Belt. Areas with proven Cadomian tectonothermal events (plutonism, metamorphism and deformation) in red (Modified after Franke, 1989). Zonal division of the Central European Variscides (Kossmat, 1927): R-H.Z., Rheno-Hercynian Zone; S.Z., Saxothuringian Zone; M.Z., Moldanubiam Zone

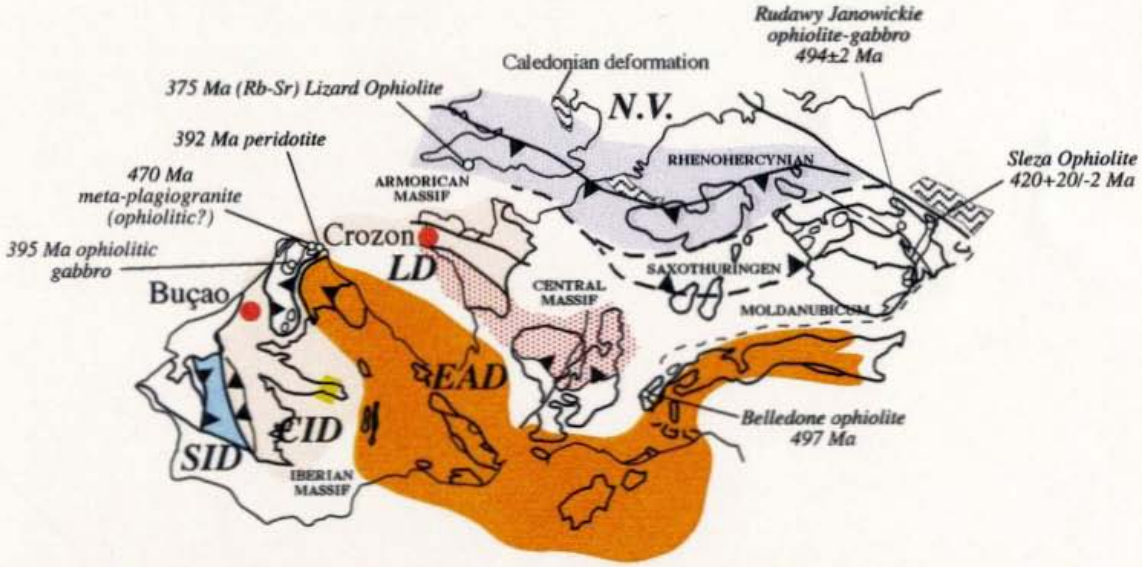

Fig.1.4.- Lower Paleozoic faunal domains of European Variscides and location of dated ophiolitic units. Faunal domains after Paris and Robardet (1990) and Robardet et al. (1990): N.V, Northern Variscides; SID, South Iberian Domain (Ossa-Morena); CID, Central Iberian Domain; LD, Ligerian Domain; EAD, Ebro-Aquitanian Domain. Red circles: matching Arenig to Asghill biostratigraphic successions (Young, 1990). Areas with Caledonian deformation after Franke (1989). Dated ophiolitic units after Menót et al. (1988), Peucat et al. (1990) Pin (1990), Oliver et al. (1993), Santos Zalduegui et al. (1996) and Dunning (unpublished). Ordovician mafic-ultramafic complexes with Silurian HP metamorphism (Ligerian Domain, Alps and NW Spain) omitted for simplicity (e.g., Pin, 1990; von Raumer and Neubauer, 1993)

Fig. 1.5.- Early Cambrian reconstruction of Gondwana showing the relative positions of Iberia and Avalonia (Courjault-Radé et al., 1992).

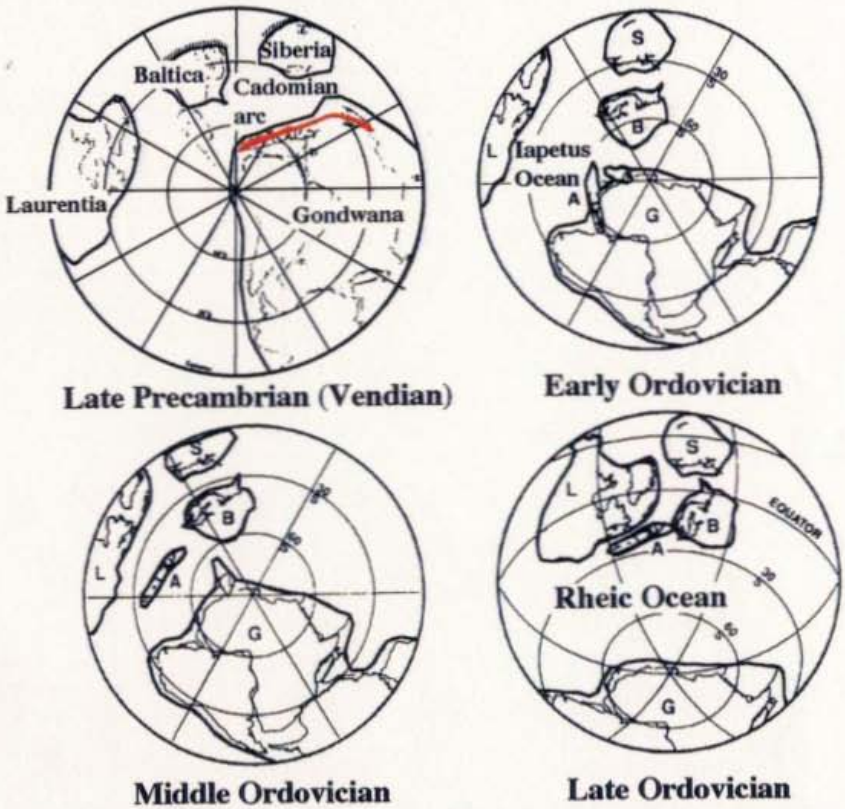

Fig. 1.6.- Paleogeographic reconstructions of Avalonia (A, Cadomian arc), Baltica (B), Gondwana (G) and Laurentia (L) in the Late Precambrian (Torsvik et al., 1996) and the Ordovician (van der Pluijm et al., 1995).

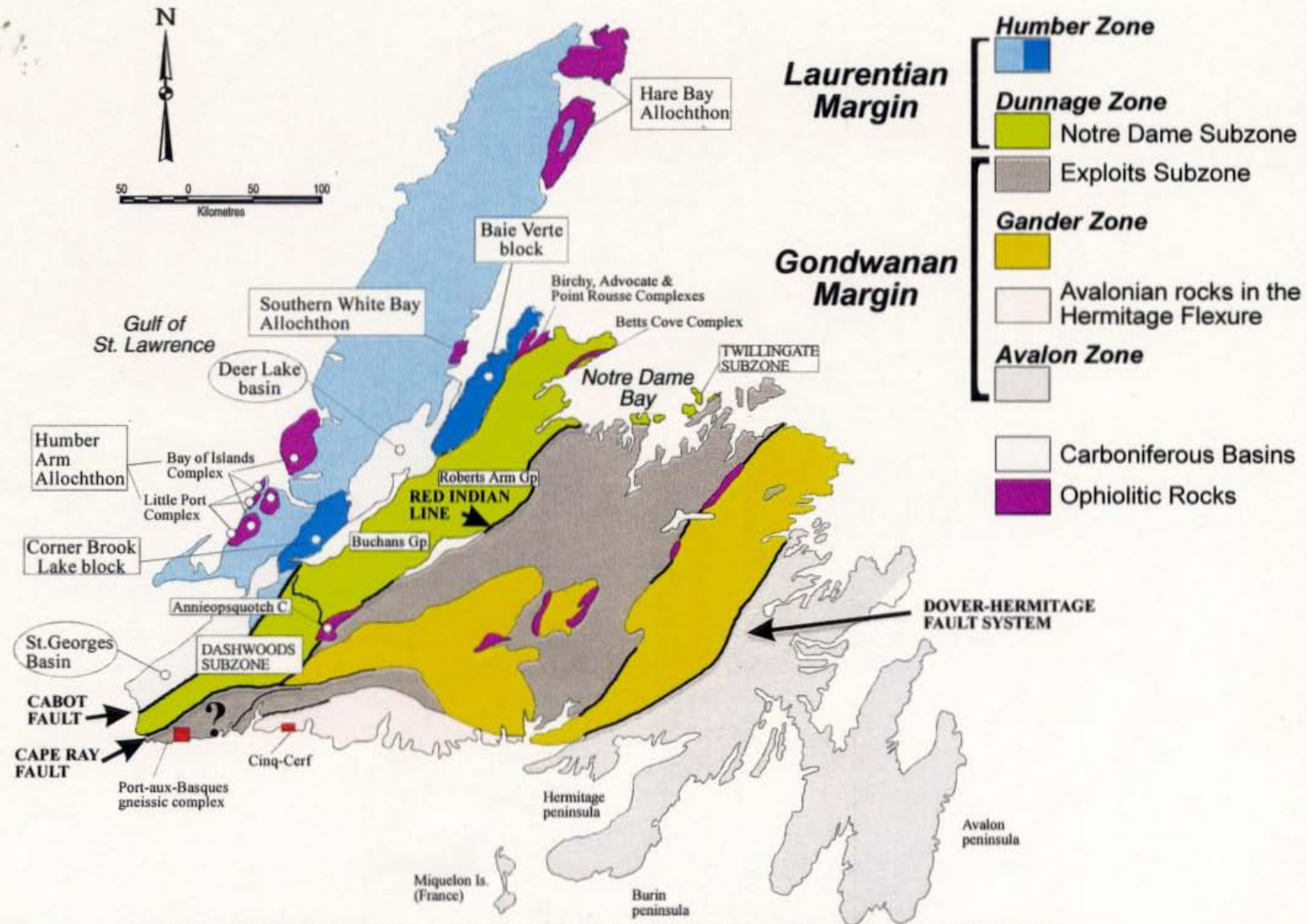

Fig.2.1.- Subdivisions of the peri-Laurentian zones of the Newfoundland Appalachians (modified after Williams et al., 1988). Red squares, field areas.

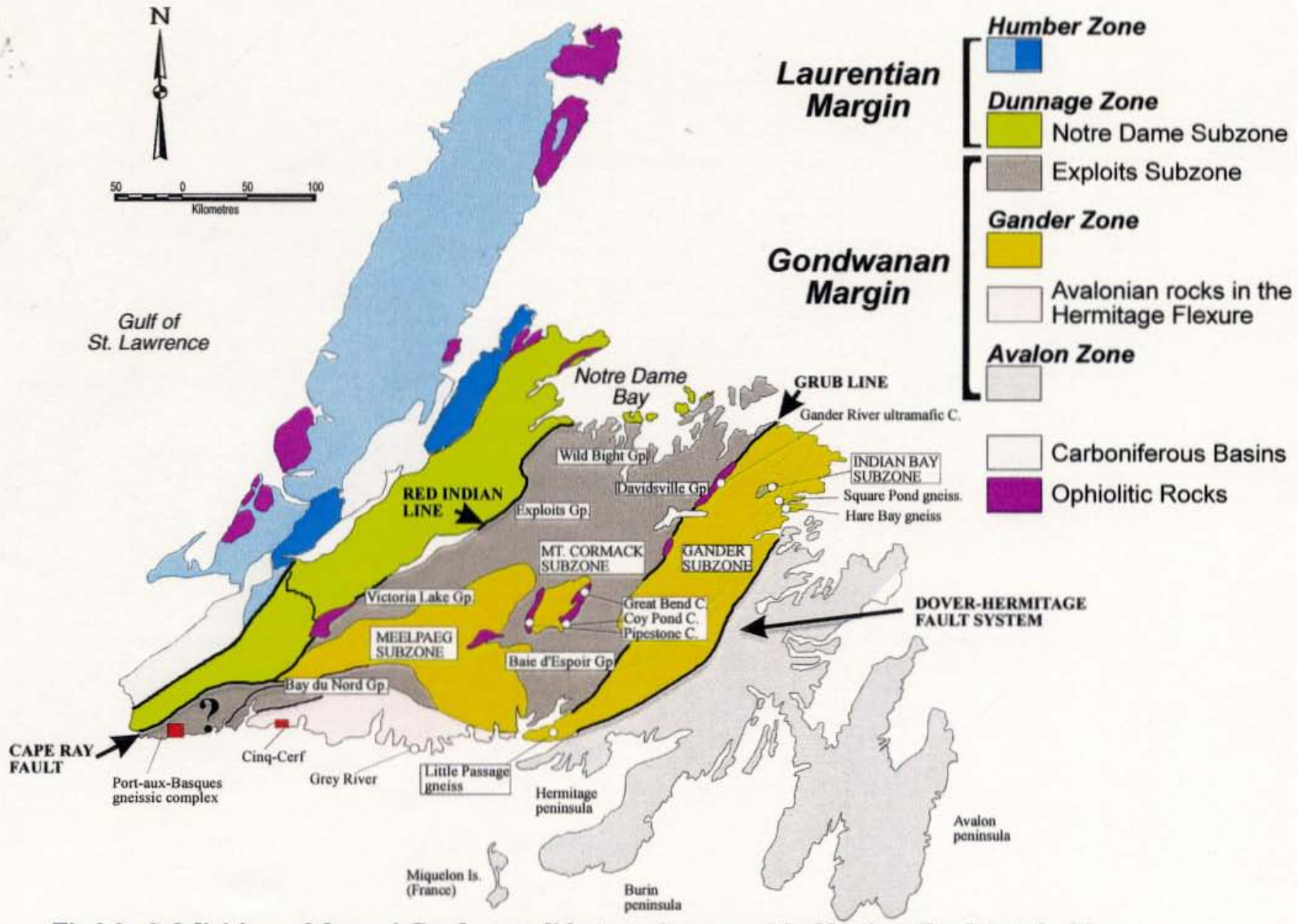

Fig.2.2.- Subdivisions of the peri-Gondwanan lithotectonic zones of the Newfoundland Appalachians (modified after Williams et al., 1988). Red squares, field areas.

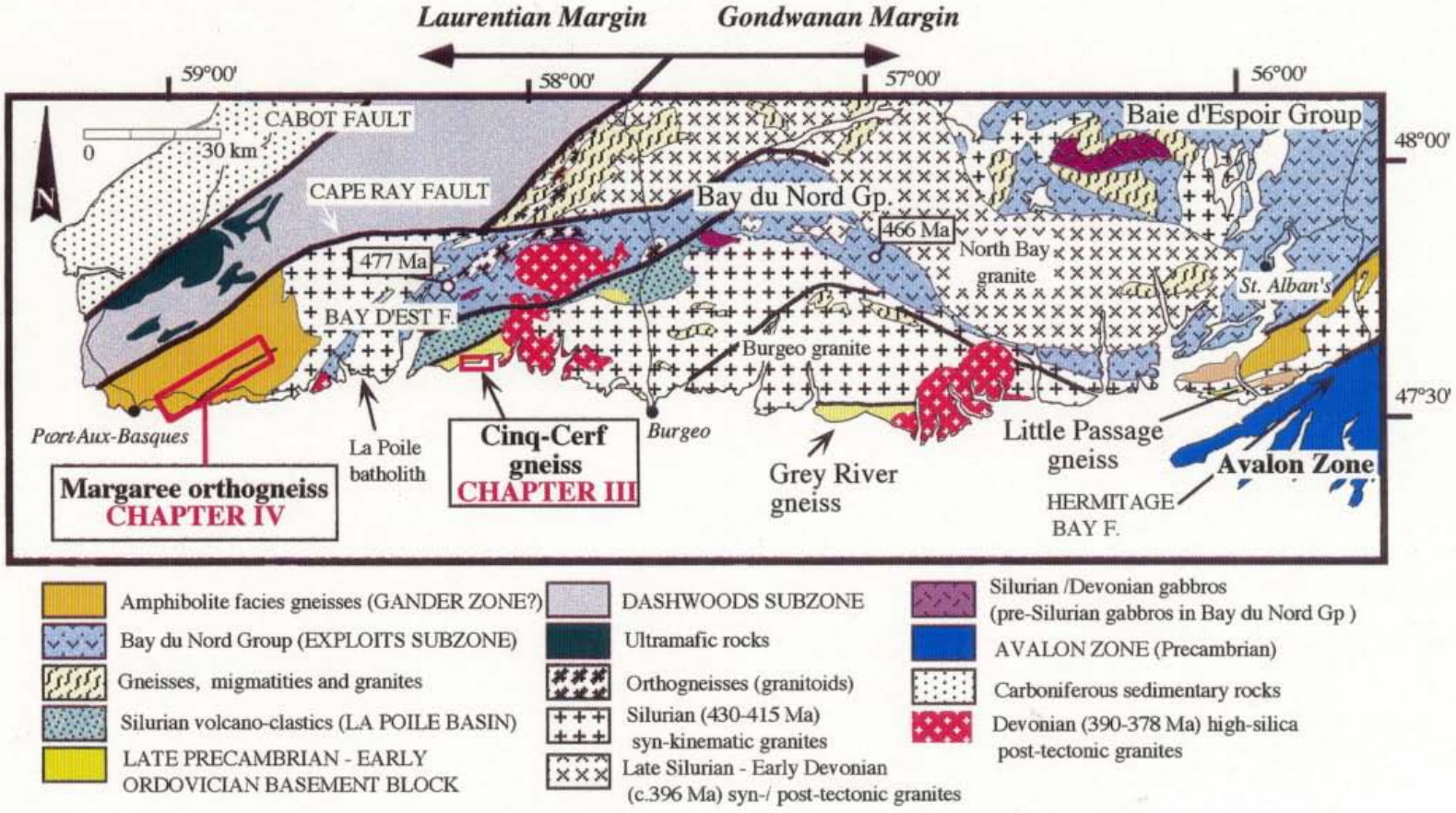

Fig.2.3.- Geological map of the Hermitage Flexure (modified after Dunning et al., 1990)

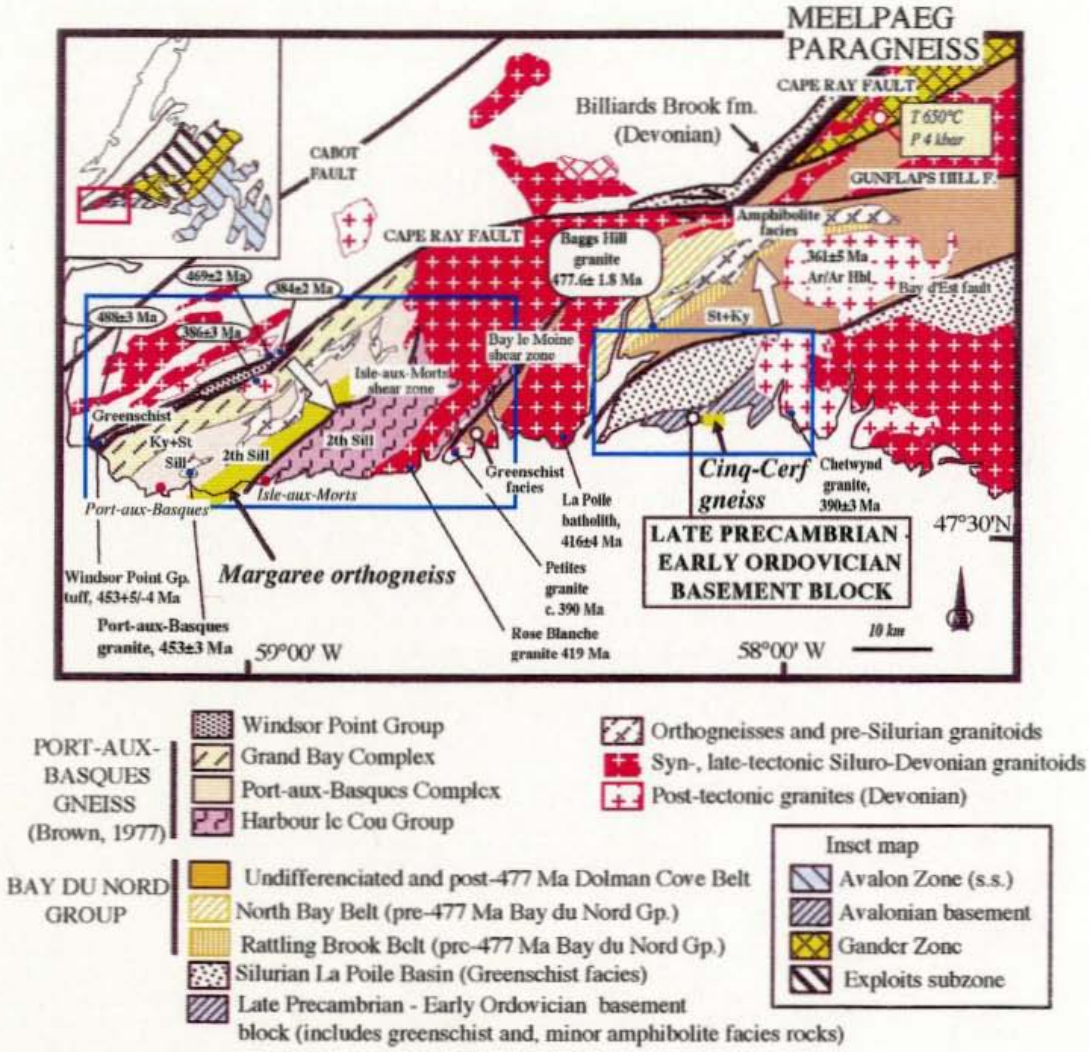

Fig. 2.4.-Generalized geological map of southwestern Newfoundland (modified from Lin et al., 1994; Tucker et al., 1994; Dubé et al., 1996). U/Pb zircon ages from Chorlton and Dallmeyer (1986), Dunning et al. (1990), Van Staal et al. (1994), Tucker et al. (1994) and Dubé et al. (1996). Ar/Ar data from Chorlton and Dallmeyer (1986). Metamorphic data after Brown (1975), Chorlton (1980), O'Neill (1985) and Owen (1992); open arrow, increasing metamorphic gradient. Field areas in yellow; blue rectangle, general study areas.

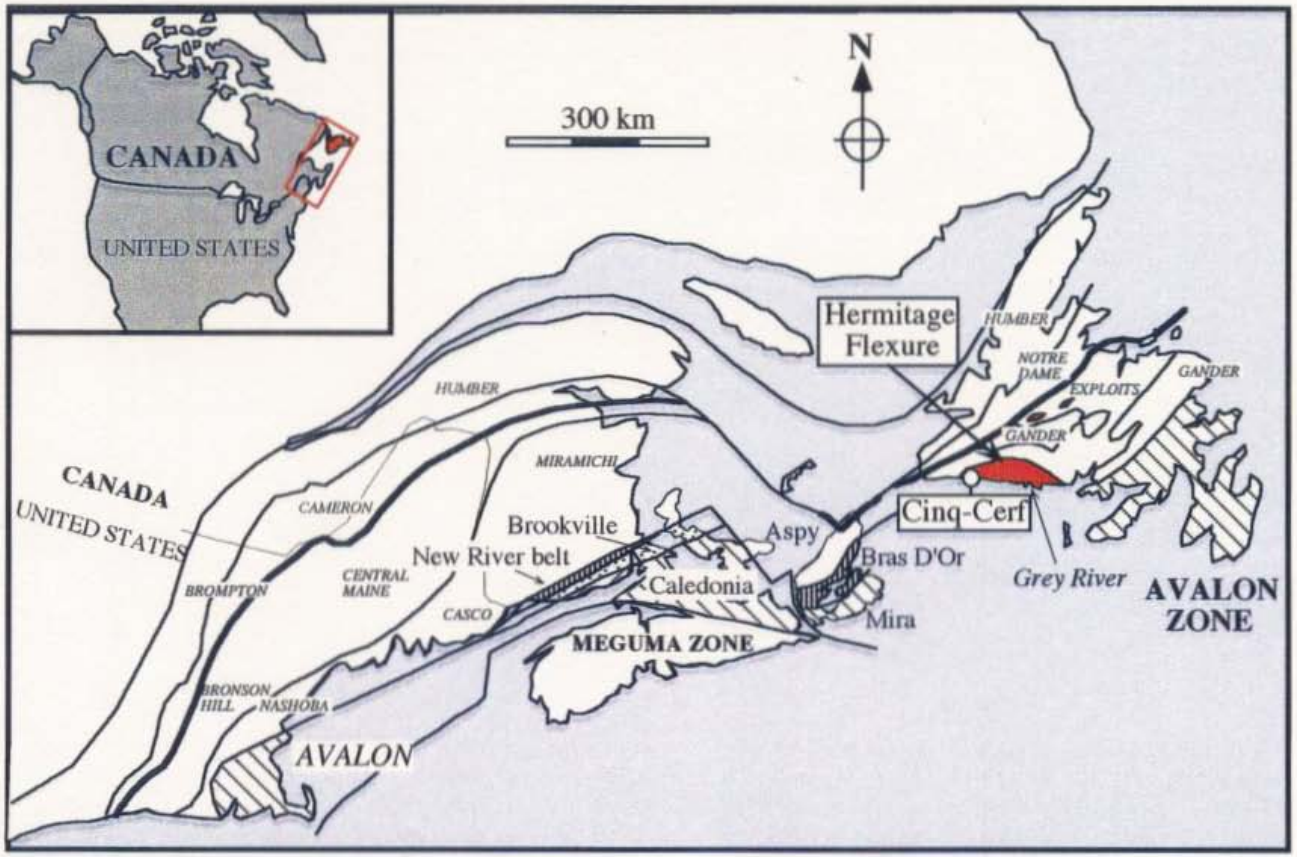

Fig. 3.1.- Distribution of Avalonian terranes (patterned) in the Northern Appalachians (modified after Barr and White, 1996), showing the position of the Cinq-Cerf gneiss and the Late Precambrian basement of the Hermitage Flexure and the Late Precambrian inliers in the Exploits subzone(red). The thick boundary line marks the separation between the peri-Laurentian and the peri-Gondwanan margins of the Iapetus Ocean.

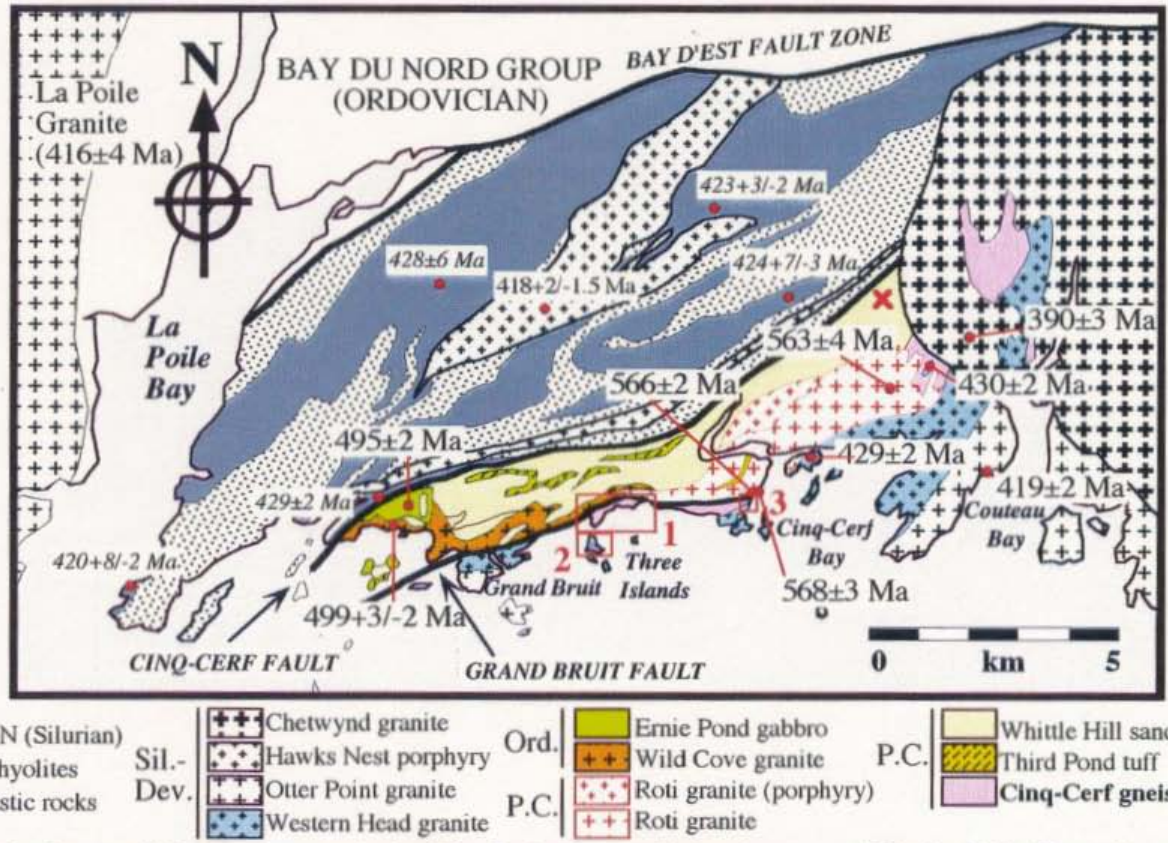

Fig. 3.2.- Geological map of the western extent of the Late Precambrian basement block of the Hermitage Flexure (area between La Poile Bay and Coteau Bay, modified after B.H.O'Brien, 1989; and B.H. O'Brien et al., 1991). U/Pb absolute ages after Chorlton and Dallmeyer, 1986; Dunning and O'Brien, 1989; B.H. O'Brien et al., 1991; B.H. O'Brien et al., 1993). Field areas (red numbers): 1) Sandbank-Point East Diver Head; 2) Three Islands; 3) Cinq-Cerf Bay. Red cross, Hope Brook gold mine. Dev, Devonian; Sil, Silurian; Ord, Ordovician; P.C., Precambrian

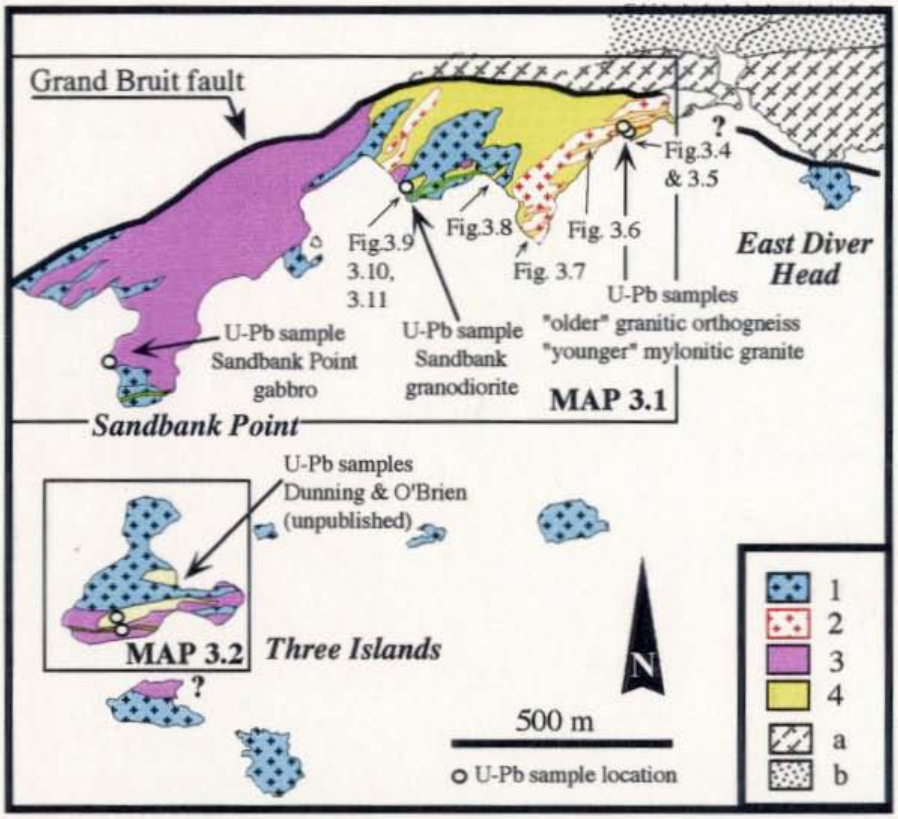

Fig.3.3.- Map of the main geological units in the Sandbank Point-East Diver Head and Three Islands sections, including location of maps 3.1 and 3.2, figure captions of the Cinq-Cerf gneiss (composite gneiss) and U-Pb sample locations.

Legend: 1) Western Head granite/granodiorite with mafic enclaves; 2) Felsic mylonitic granite (Western Head); 3) Sandbank metagabbro (diorite); 4) Composite Cinq-Cerf gneiss. a) Roti granite (Precambrian?); b) Whittle Hill sandstone (Precambrian). The map area outside maps 3.1 and 3.2 is after B.H. O'Brien (1990).

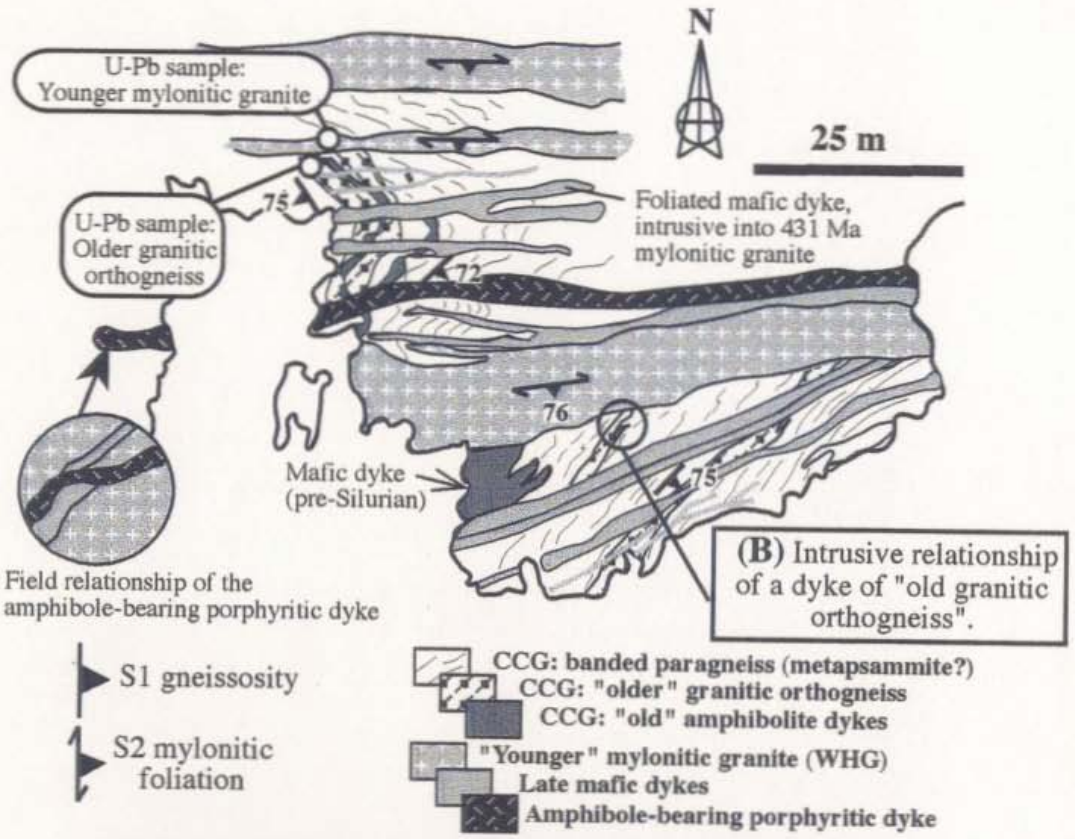

Fig. 3.4.- Outcrop plan view of the Cinq-Cerf gneiss, banded gneiss, showing the field realtionships between the older granitic orthogneisses and mafic dykes, the younger mylonitic granite and the late mafic dykes. (B) "Older" granitic orthogneiss intrusive into metasedimentary banded gneiss overprinted by D1 and cross-cut by "young" mylonitic granite with a D2 mylonitic fabric. CCG, Cinq-Cerf gneiss; WHG, Western Head granite.

Figure 3.5

Fig. 3.5.- Composite Cinq-Cerf gneiss, cross-cutting relationships in the outcrop of figure 3.4.

(A)Top left, late granitic dyke ("younger" mylonitic granite; U/Pb sample 94-PV-11, 431.5±1 Ma) cross cutting the composite Cinq-Cerf gneiss with a sliver of old granitic orthogneiss (U/Pb sample 94-PV-12; 675+12/-11 Ma).

(B)Top right, detail of the cross-cutting relationship between the gneissic mylonitic fabric in the banded gneiss (composite $S1^a$-$S1^c$ foliation), the late granite and the mylonitic foliation ($S2^b$) in the granite. Note that there is no D2 overprint in the gneiss, except for brittle offsets of the gneissic banding.

(C) Bottom left, old amphibolite dykes (undated) intrusive into older granitic orthogneiss (U/Pb sample 94-PV-12). These dykes have a weak fabric (S1) parallel to the composite S1a-S1c fabric in the orthogneiss and are cross-cut by the 431.5 Ma granite dyke.

(D) Bottom right, late mafic dyke cross-cutting a stretched enclave in the 431.5 Ma granite dyke. This mafic dyke is then cross-cut by late amphibole porphyry dyke in fig. 3.4.

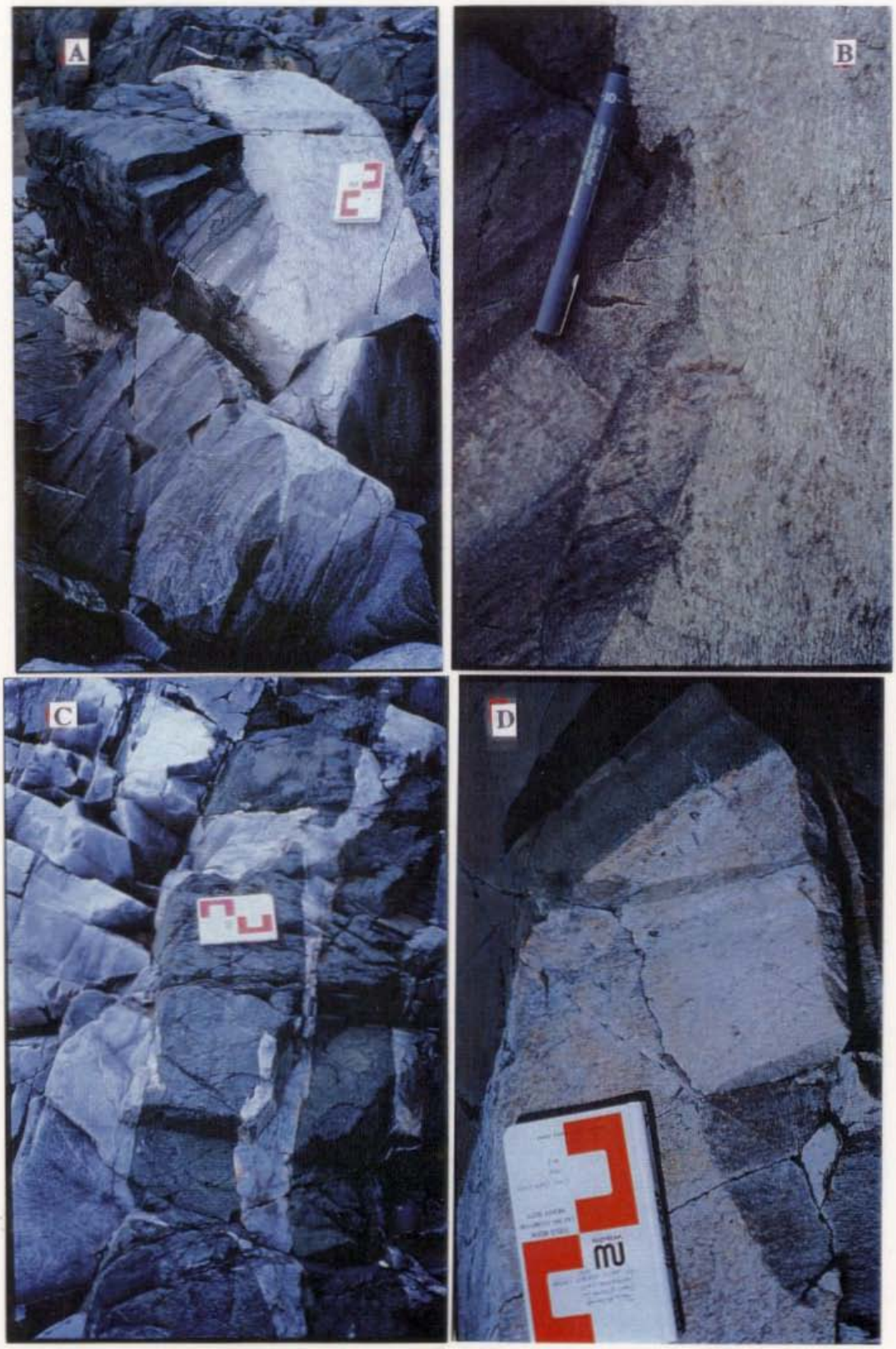
A
B
C
D

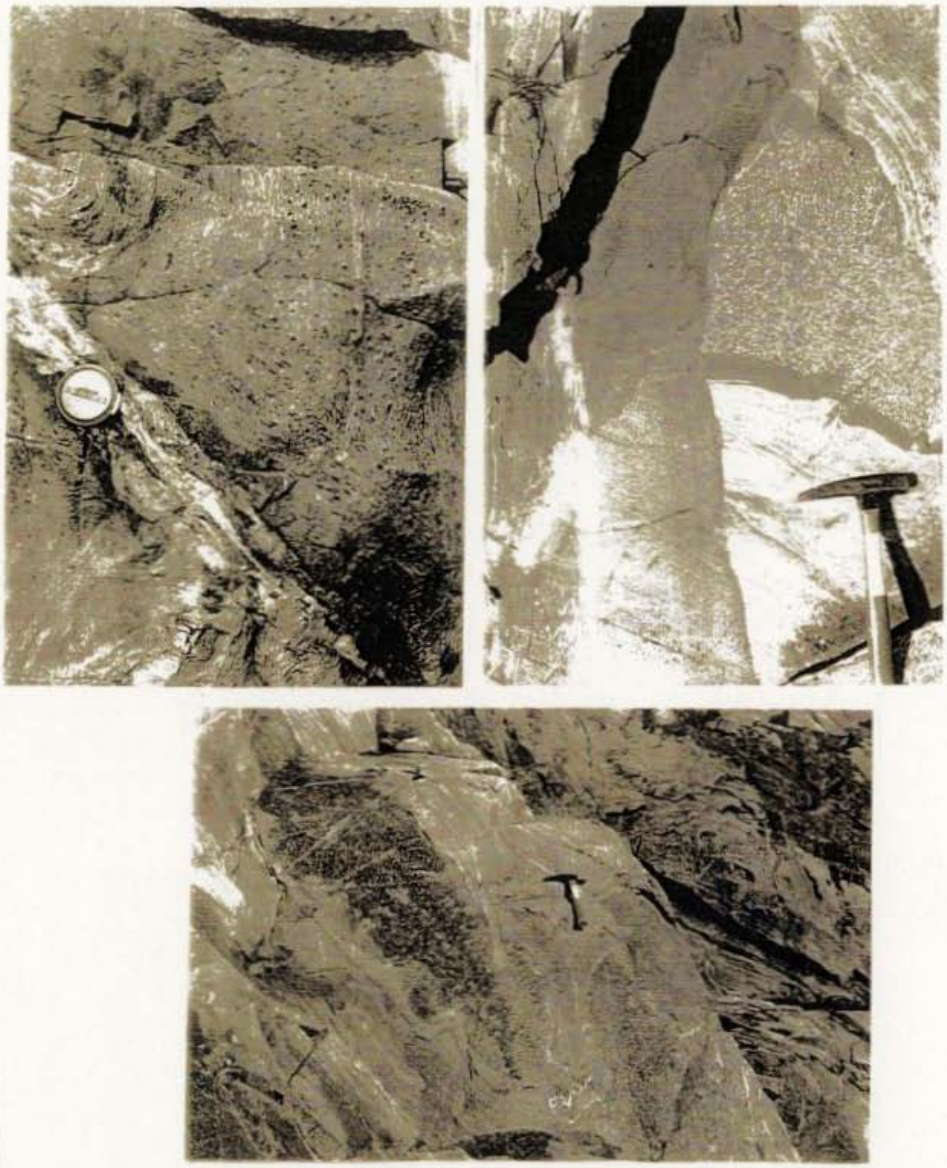

Fig.3.6.- Sandbank Point-East Diver Head section, amphibolitic banded gneiss. Top left: tuff-like level with green clinoamphibole porphyroblasts with diffuse contacts with the fine grain gneiss (upper left). The banding in the gneiss (S1) is offset by a discrete late, greenschist facies, shear zone (D2). **Top right:** Late mafic dyke (with a D2b fabric) cross-cutting gabbroic blob in the banded gneiss (without a penetrative internal fabric) and F1c isoclinal folds in the banded gneiss. The discontinuous mafic rim around the gabbroic blob suggests a metasomatic origin rather than a chill-margin. **Bottom:** Gneissic banding warping around coarse-grained gabbroic pods, boudinaged gabbroic apophysis?. Photos courtesy of B.H. O'Brien

Fig. 3.7.- Cinq-Cerf gneiss, disharmonic folding of granite injections (Western Head granite) and the country rock paragneiss suggesting a viscous non-linear rheological behaviour due to thermal softening and synmagmatic deformation. Hinge of an $F2^a$ fold in the rocky point west of East Diver Head (location in fig.3.3).

Fig. 3.8.- Banded quartzo-feldspathic gneiss, dome and basin interference pattern (D1?) overprinted by $F2^b$ folds. Note the axial planar foliation to the F2 folds in the granite vein (Western Head granite).

Fig. 3.9.- Veined gneiss resembling an anatectic migmatite. The felsic veins are variably folded aplitic injections. The country rock to the aplitic veins is a greenschist facies tourmaline-bearing schist. Cinq-Cerf gneiss near location in fig.3.10

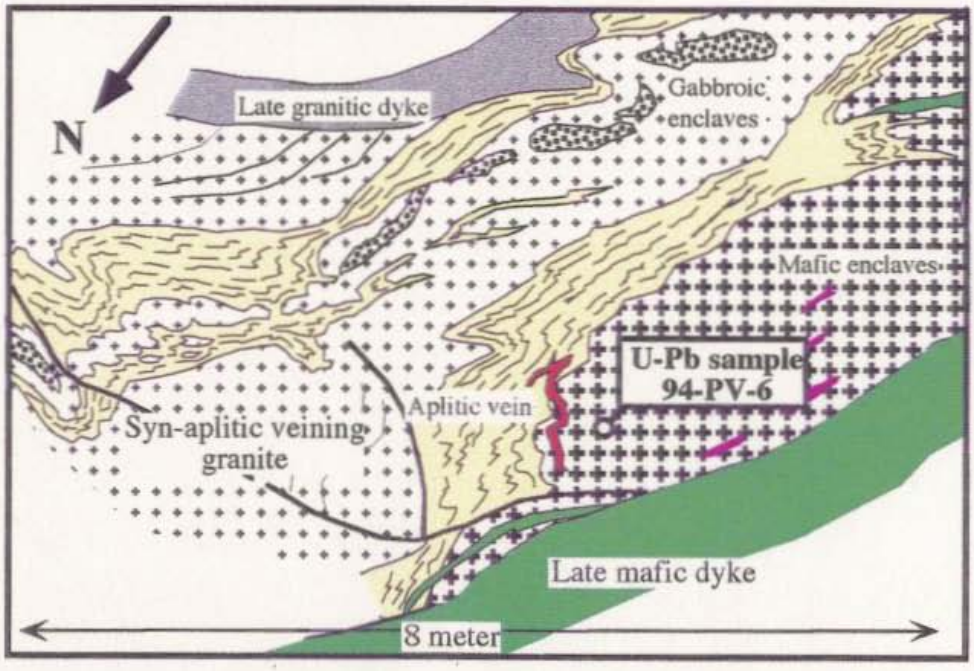

Fig.3.10.- Field relationships between the tourmaline-bearing veined paragneiss (yellow), weakly deformed Sandbank granodiorite with mafic enclaves (U-Pb sample 94-PV-6), an intrusive aplitic vein and the syn-veining granite (undated).

Fig.3.11.- Field relationships between tourmaline-bearing paragneiss, Sandbank granodiorite (D-Pb sample 94-PV-6), aplitic veins and the Western Head granite (granite/granodiorite with mafic enclaves), location as in Fig.3.10.

(A)Top left: Aplitic vein with ptygmatic folding intruding the Sandbank granodiorite (arrow) and the tourmaline-bearing paragneiss.

(B)Top right: Same aplitic vein merging with other veins in the schistose paragneiss and cross-cutting older fabric (S1; arrow) in the paragneiss.

(C)Bottom left: Contact between the Sandbank granodiorite and the country rock paragneiss. The strain gradient in the paragneiss increases towards the contact (compositie S1-S2 fabric) whereas the granodiorite remains almost undeformed.

(D)Bottom right: Reworked contact between the veined gneiss and the Western Head granite/granodiorite showing the composite D1-D2 character of the pre-existing veined-gneiss. The Western Head granite is apparently post-aplitic veins, but it can not be unequivocally confirmed by a clear field relationship.

Figure 3.11

Fig.3.11.- Field relationships between tourmaline-bearing paragneiss, Sandbank granodiorite (U-Pb sample 94-PV-6), aplitic veins and the Western Head granite (granite/granodiorite with mafic enclaves), location as in fig.3.10.

(A)Top left: Aplitic vein with ptygmatic folding intruding the Sandbank granodiorite (arrow) and the tourmaline-bearing paragneiss.

(B)Top right: Same aplitic vein merging with other veins in the schistose paragneiss and cross-cutting older fabric (S1; arrow) in the paragneiss.

(C)Bottom left: Contact between the Sandbank granodiorite and the country rock paragneiss. The strain gradient in the paragneiss increases towards the contact (composite S1-S2 fabric) whereas the granodiorite remains almost undeformed.

(D)Bottom right: Reworked contact between the veined gneiss and the Western Head granite/granodiorite showing the composite D1-D2 character of the gneissosity in the veined-gneiss. The Western Head granite is apparently post-aplitic veins, but it can not be unequivocally confirmed by a clear field relationship.


B

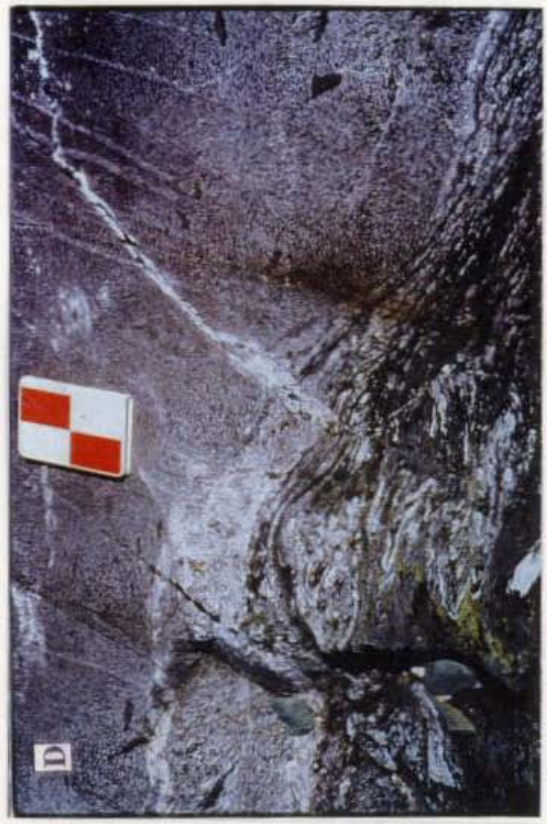
D


A


C

Fig.3.12.- Aspect of the Cinq-Cerf gneiss at Cinq-Cerf Bay (Field photograph courtesy of B.H. O'Brien). Note the lithological similarity between the gneiss and the country rock gneiss to the gabbroic pods in the Sandbank-East Diver Head section (Fig. 3.6).

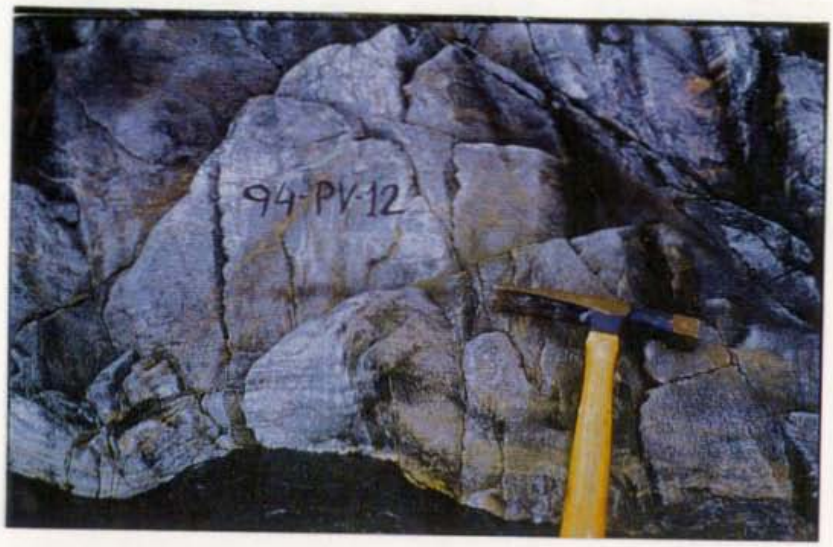

Fig.3.13.- Field appearance of sample 94-PV-12, granitic orthogneiss part of the banded gneiss in fig.3.4.

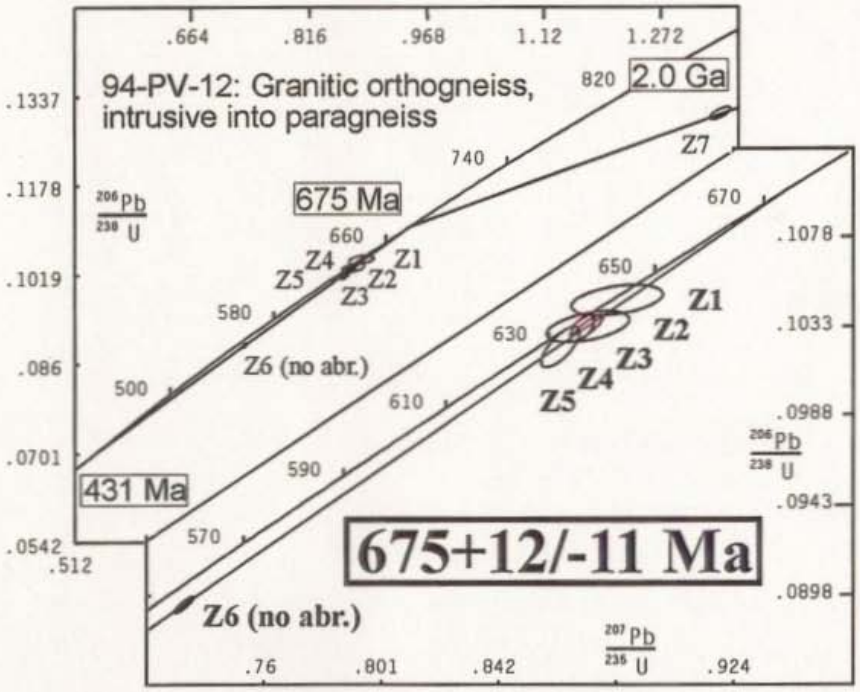

Fig.3.14 .- U/Pb concordia diagram for the old granitic orthogneiss; Cinq-Cerf gneiss, Sandbank Point-East Diver Head section. Upper inset, upper and lower intersections of the discordia line and reference line between the protolith age and 2.0 Ga (maximum age of inheretance). Lower half, detail of the upper intercept of the discordia line. Z, zircon

TABLE 3.1.- U-Pb DATA, CINQ-CERF GNEISS.

Description	Weight	Concentration		Measured		Corrected atomic ratios*						Age (Ma)		
Fraction	(mg)	U (ppm)	Pb rad (ppm)	Total common Pb (Pg)	$\frac{206}{204}\frac{Pb}{Pb}$	$\frac{208}{206}\frac{Pb}{Pb}$	$\frac{206}{238}\frac{Pb}{U}$	±	$\frac{207}{235}\frac{Pb}{U}$	±	$\frac{207}{206}\frac{Pb}{Pb}$	±	$\frac{206}{238}\frac{Pb}{U}$	$\frac{207}{235}\frac{Pb}{U}$	$\frac{207}{206}\frac{Pb}{Pb}$
1.-Western Head mylonitic granite(94-PV-11), 11500-81750†															
Z1 M. eu. prisms AB	0.1209	726	50	17	22740	0.1049	0.06846	26	0.5235	20	0.05547	06	427	428	431
Z2 M. eu. prisms AB	0.1030	705	48	10	31803	0.1163	0.06818	22	0.5213	18	0.05546	06	425	426	431
Z3 M. eu. prisms AB	0.0825	489	33	13	13194	0.1029	0.06818	28	0.5215	21	0.05547	10	425	426	431
Z4 M. eu. prisms NAB	0.2189	792	54	99	7466	0.1047	0.06797	22	0.5202	18	0.05551	06	424	425	433
Z5 M. eu. prisms AB	0.1776	622	42	16	29250	0.1135	0.06744	20	0.5157	17	0.05547	06	421	422	431
2.- Sandbank Point metagabbro (94-PV-4), 10200-81150.															
Z1 M. eu. prisms AB	0.0498	90	9	9	2856	0.2718	0.08962	26	0.7251	23	0.05868	08	553	554	555
Z2 M. eu. prisms AB	0.0390	71	7	12	1305	0.2917	0.08949	54	0.7202	66	0.05836	46	553	551	543
Z3 M. eu. gem pr. AB	0.1346	94	9	16	4570	0.2612	0.08859	34	0.7154	25	0.05857	14	547	548	551
Z4 S. eu. gem pr. NAB	0.1622	105	10	30	3117	0.2321	0.08603	36	0.6921	29	0.05835	10	532	534	543
3.- Sandbank granodiorite (94-PV-6), 11000-81600.															
Z1 M. stb. prisms AB	0.1353	112	12	17	5282	0.2580	0.09299	44	0.7611	34	0.05936	16	573	575	580
Z2 M. stb prisms AB	0.1295	111	11	73	1130	0.2518	0.09019	30	0.7351	29	0.05911	12	557	560	571
Z3 S. prisms NAB	0.2043	132	13	65	2323	0.2433	0.08822	32	0.7150	26	0.05878	12	545	548	559
Z4 S. prisms (1:3-1:5) AB	0.0366	205	25	9	3721	0.9143	0.07105	38	0.5571	27	0.05687	18	442	450	487
4.- Cinq-Cerf gneiss, old granitic orthogneiss (94-PV-12), 11500-81750.															
Z1 M. stb. eu. prisms AB	0.0112	76	7	9	664	n.d.	0.10470	64	0.8835	134	0.06120	82	642	643	646
Z2 M. stb. eu. prisms AB	0.0786	79	9	12	3277	0.2451	0.10327	58	0.8713	35	0.06119	28	634	636	646
Z3 M. stb. prisms AB	0.0293	76	9	23	653	0.2307	0.10335	64	0.8733	118	0.06128	72	634	637	649
Z4 M. stb. prisms AB	0.0651	69	8	11	2626	0.2399	0.10327	56	0.8729	48	0.06130	16	634	637	650
Z5 M. stb. prisms AB	0.0726	75	9	7	4998	0.2399	0.10232	84	0.8637	55	0.06122	34	628	632	647
Z6 S. stub. eu. pr. NAB	0.1276	159	15	38	3045	0.1359	0.08936	34	0.7322	28	0.05943	10	552	558	583
Z7 M. stb. prisms AB	0.0311	93	13	32	756	0.2225	0.13075	92	1.3481	109	0.07478	42	792	867	1062

1.- Z = zircon, s = small (<80 μm), m= medium (>80 and <150 μm), l = large (>150 μm), Ndl. = Needles (1:10 to 1:7 width/length ratio), pr = prisms (1:6 to 1:4), stb = stubby (1:3 to 1:1), clr = clear, eu. = euhedral, y.= yellow, AB = air abraded (Krogh, 1982), NAB = not abraded.

2.- Uncertainty in sample weight ± 0.001 mg (2 sigma)

3.- Atomic ratios corrected for fractionation and spike, 8 to12 pg Pb blank lab procedure, initial common Pb (Stacey and Kramers, 1975) and 1 pg U blank. 2 sigma errors reported for corrected isotopic ratios.

† Sample location in U.T.M. coordinates, 21TVC UTM zone and 100 km square.

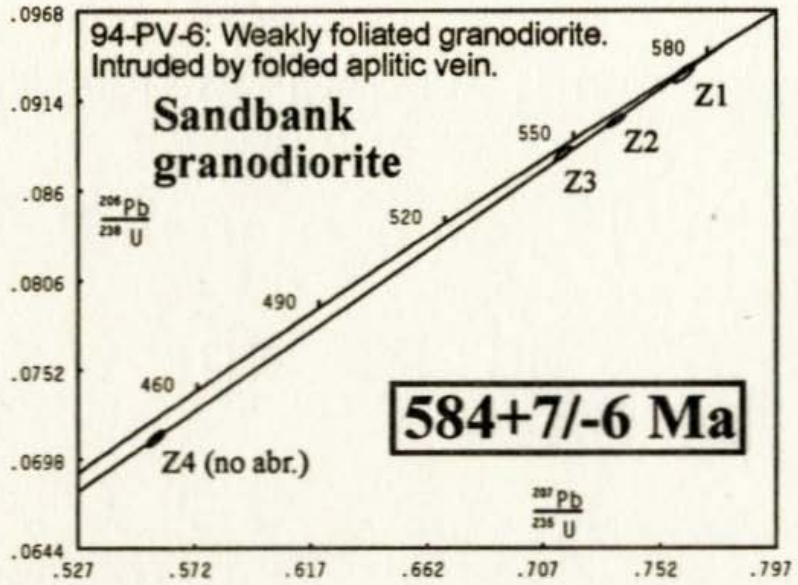

Fig.3.15.- U/Pb concordia diagram for the weakly foliated Sandbank granodiorite (sample 94PV6), intrusive into the tourmaline-bearing paragneiss (Cinq-Cerf gneiss). Z, zircon.

Fig. 3.16.- Sandbank Point metagabbro: Metagabbro intruded by metadiorite with mafic enclaves showing sharp to diffuse contacts, both are cross-cut by a late grey mafic-intermediate dyke (NW side of the cobble bar at Sandbank Point).

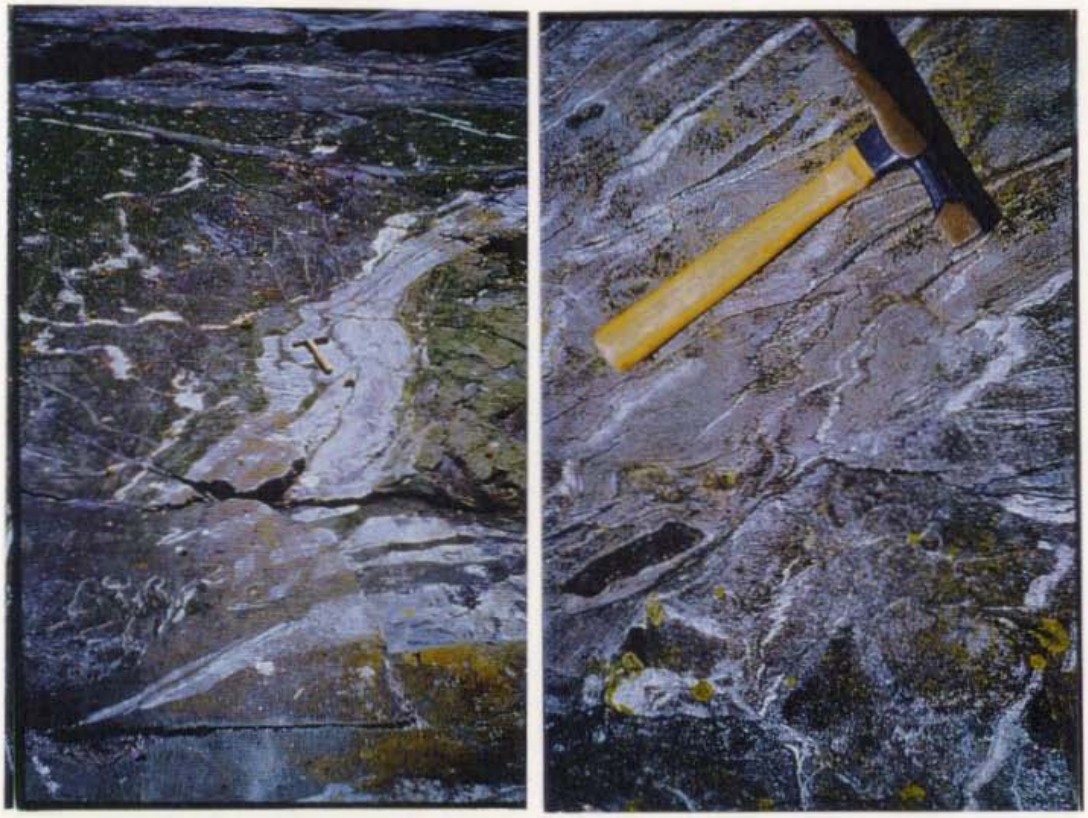

Fig.3.17.- Sandbank Point metagabbro (Three Islands). Left: Late mafic dykes cross-cutting folded felsic dykes intrusive into mafic metagabbro. Right: Old granitoid/intermediate dykes intrusive into metagabbro, showing refolded compositional banding like the 547 Ma U-Pb sample from Three Islands of Dunning and B.H. O'Brien (unpublished).

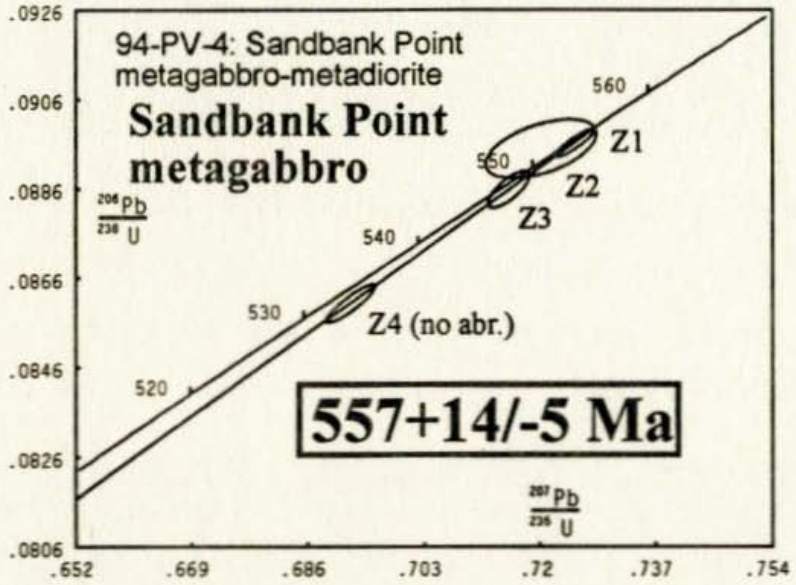

3.18.- U/Pb concordia diagram for the mafic metagabbro-diorite at Sandbank Point (sample 94PV4). Z, zircon.

Fig.3.19.- Western Head granite/granodiorite (undated) with mafic and gneissic enclaves cross-cut by late mafic dykes (Sandbank Point-East Diver Head section). Note the weak solidus foliation in the granite and the sharp dyke boundaries, suggesting brittle behaviour of the granite during dyke emplacement.

Fig.3.20.- Mingling of coeval (?) mafic and felsic magmas and high temperature deformation, Western Head granite at Sandbank Point.

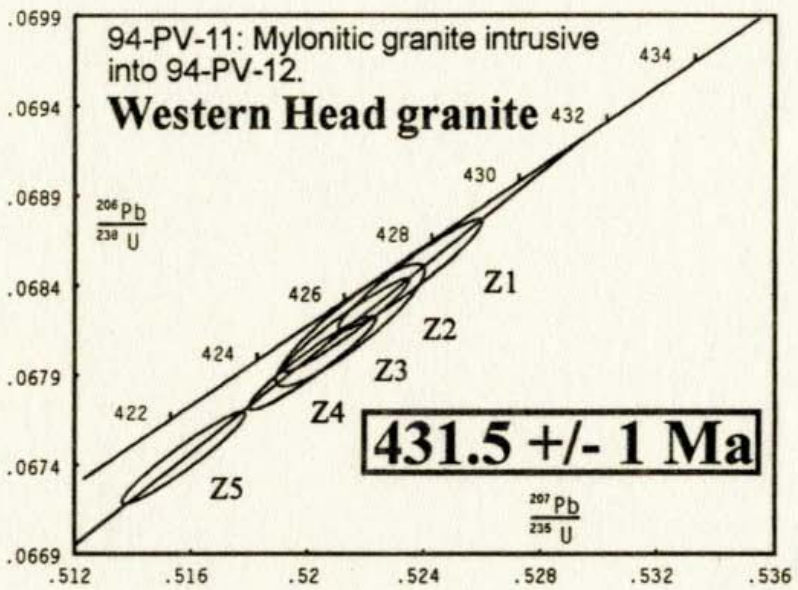

Fig. 3.21 .- U/Pb concordia diagram for the mylonitic facies of the Western Head granite. Granitic dyke intrusive into the Cinq-Cerf gneiss, Sandbank Point-East Diver Head. Z, zircon.

Figure 3.22

Fig. 3.22.- Microfabric in the 675 Ma orthogneiss.

Top: $F1^c$ folded polycrystalline quartz ribbon ($S1^b$?) cross-cutting earlier $S1^a$ fabric. The $S1^c$ axial planar foliation is weakly developed. View perpendicular to the intersection lineation. Parallel light, field of view is 5.21 mm wide.

Bottom: View parallel to the intersection lineation, cross polars. Composite $S1^a$-$S1^c$ fabric showing oriented biotite and a partially recrystallized quartz-feldspathic matrix with irregular grain boundaries and abundant subgrains. Field of view is 1.32 mm wide.

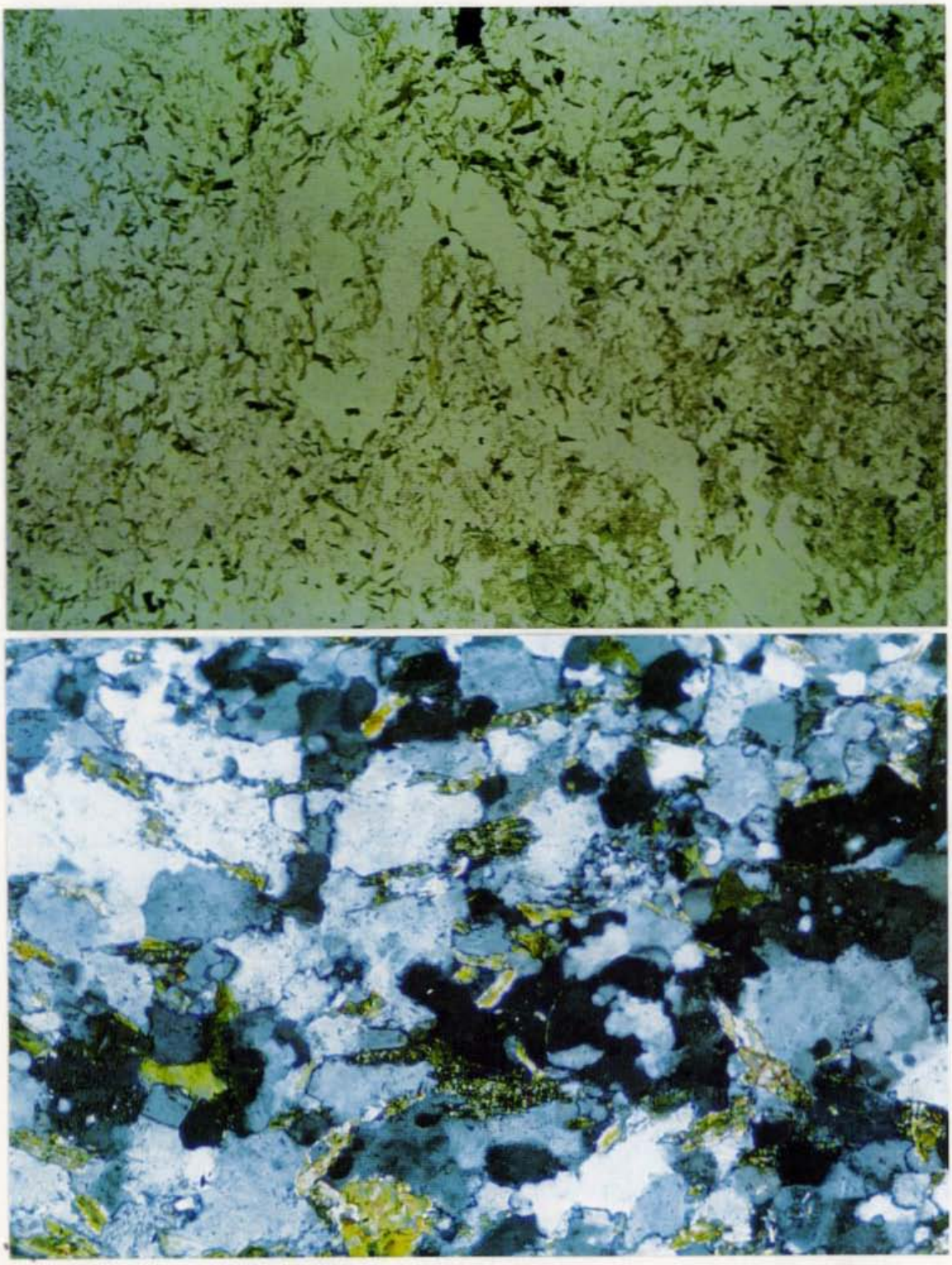

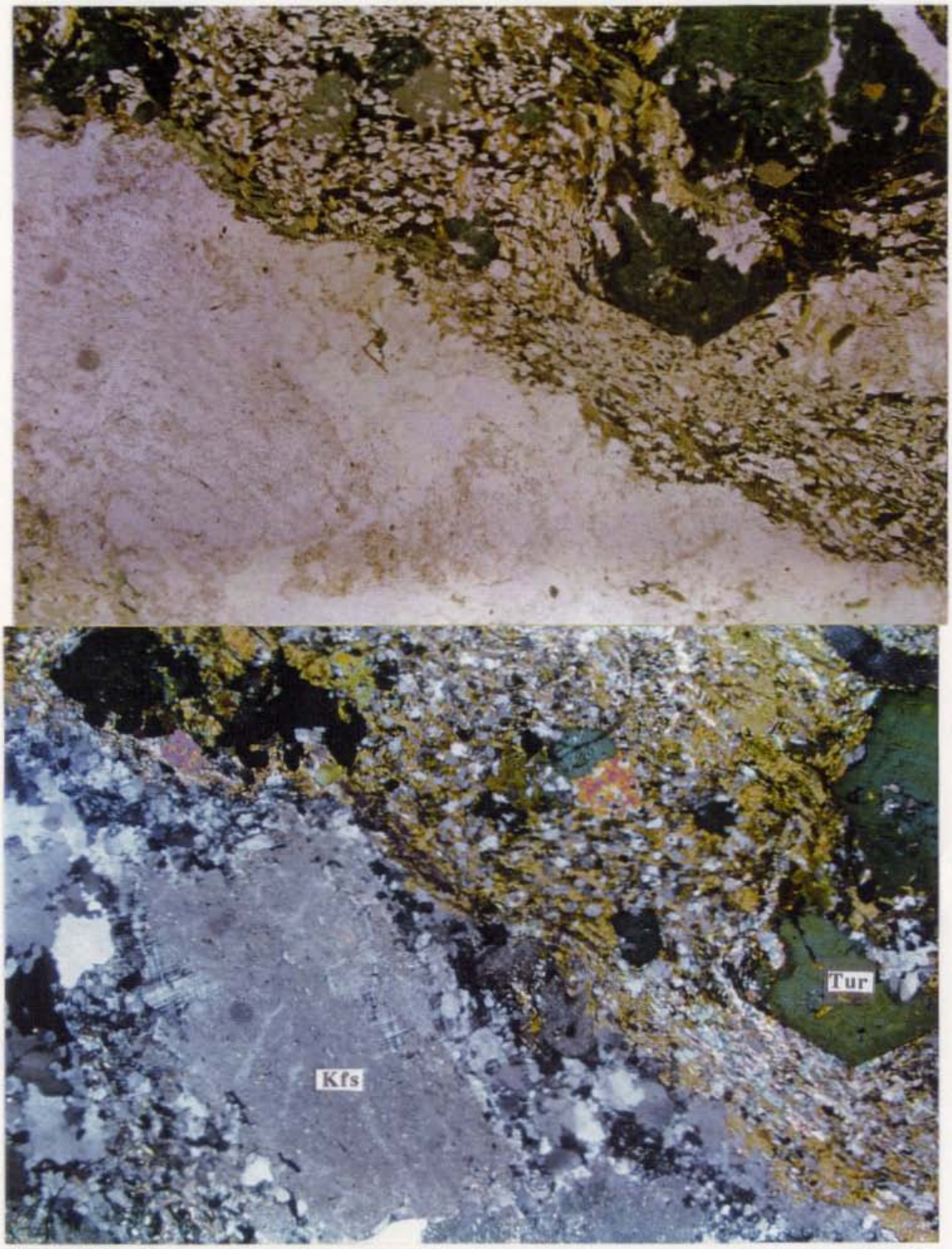

Fig. 3.23.- Tourmaline-bearing veined gneiss, country rock to the 584 Ma granodiorite. Contact between an aplitic/pegmatitic vein and the tourmaline-bearing schist. Tourmaline growths late overprinting the composite S1-S2 foliation defined by the phyllosilicates (chlorite, white mica and biotite) in the schist. This fabric is parallel to the contact with the aplite. The aplite (post-584 Ma) shows a partial collapse of the primary igneous framework (bottom): grain reduction, dynamic recrystallization of quartz and mantle structures with recrystallization of microcline around primary feldspar phenocrysts. Field of view is 5.21 mm wide

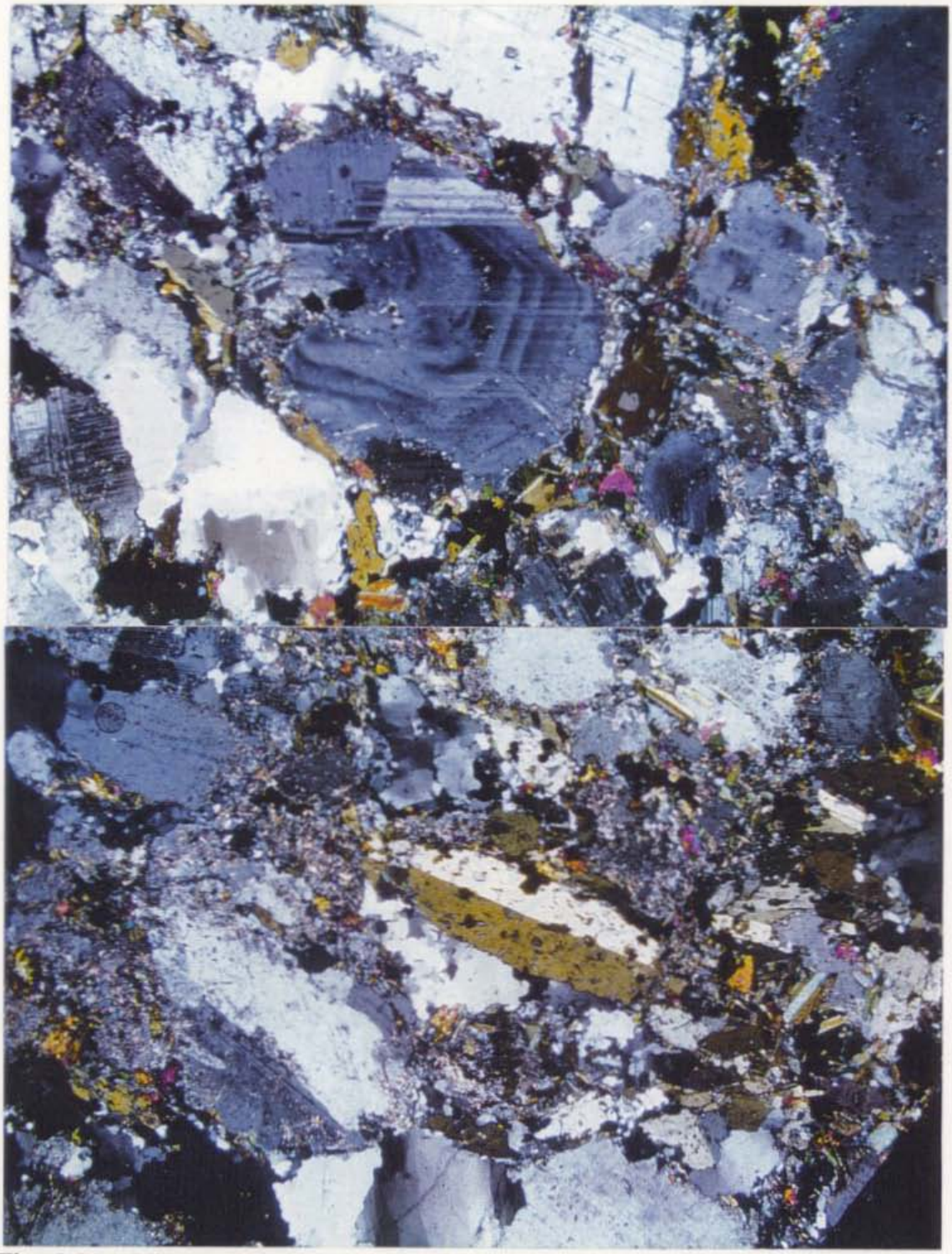

Fig. 3.24.- Microtexture of the 584 Ma Sandbank granodiorite. Top: Primary igneous concentric zoning in plagioclase, grain reduction in the intergranular spaces with growth of epidote, white mica, chlorite, green clinoamphibole and biotite. **Bottom:** Primary hornblende (?). Field of view is 1.32 mm wide

Fig. 3.25.- Microtexture of the 557 Ma Sandbank Point metagabbro/diorite. Top: D2 greenschist overprint of the earlier metamorphic fabric. Note: grain reduction, growth of chlorite and brittle offset of amphibole along a discrete shear band (Arrow). Other deformational features are discussed in the text. Field of view is 5.21 mm wide. **Bottom:** mantle-core structure in plagioclase with subgrain rotation recrystallization. Field of view is 1.32 mm.

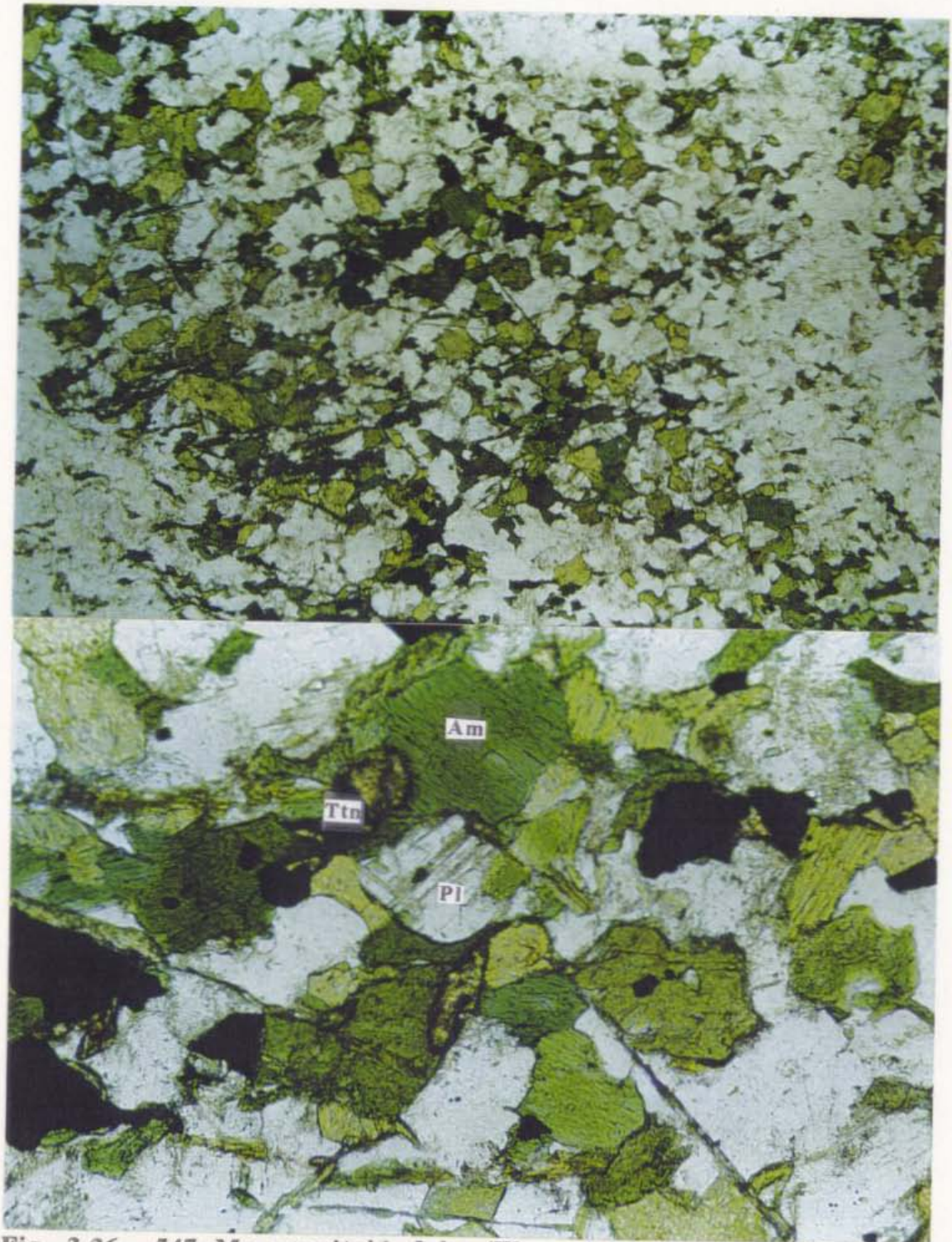

Fig. 3.26.- 547 Ma granitoid dyke (Three Islands, unpublished U/Pb sample of B.H. O'Brien and Dunning). Top: $S1^a$ compositional banding and biotite defining a second foliation ($S1^b$). Field of view is 5.21 mm wide **Bottom:** Titanite (448+9/-3 Ma; Dunning, unpublished) in interstitial positions with recrystallized plagioclase and green hornblende. Field of view is 1.32 mm.

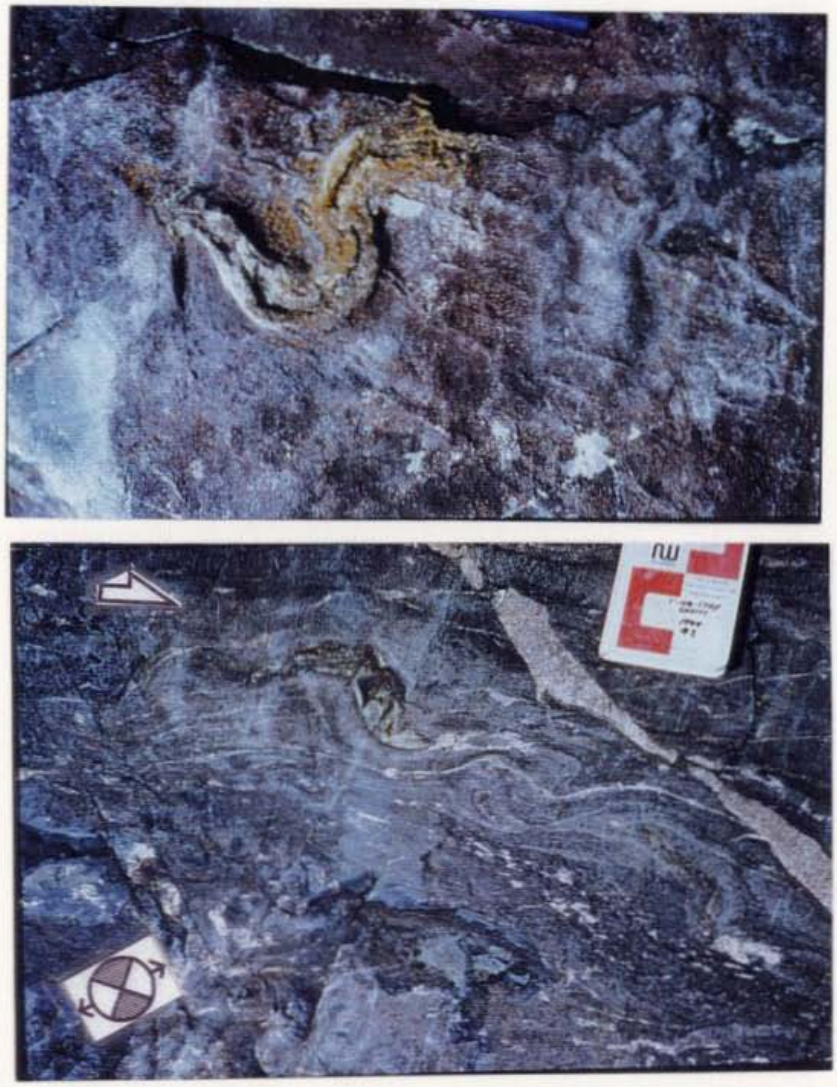

Fig.3.27.- Cinq-Cerf gneiss, paragneiss, Cinq-Cerf Bay section. Top: Epidote-rich layer showing F2 refolding of an F1 basin interference pattern ($F1^a$-$F1^b$). **Bottom:** Syn-D2 granitic dyke (Western Head?) and F2 folding of the S1 compositional banding by rotation of competent layers. The en echelon intrusion of the granite dyke along tensional cracks and the sense of rotation of the competent layers indicate a dextral shear sense.

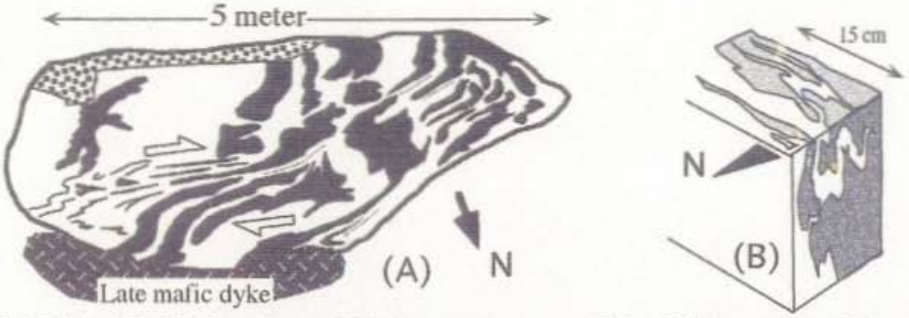

Fig.3.28 .- Field sketches of high temperature D2a deformational features, Sandbank Point, Western Head granite. A) Plan view of ductile shearing of mafic dykes in Western Head granite. B) F2a folding of felsic veins in mafic-rich area (fig.3.21).

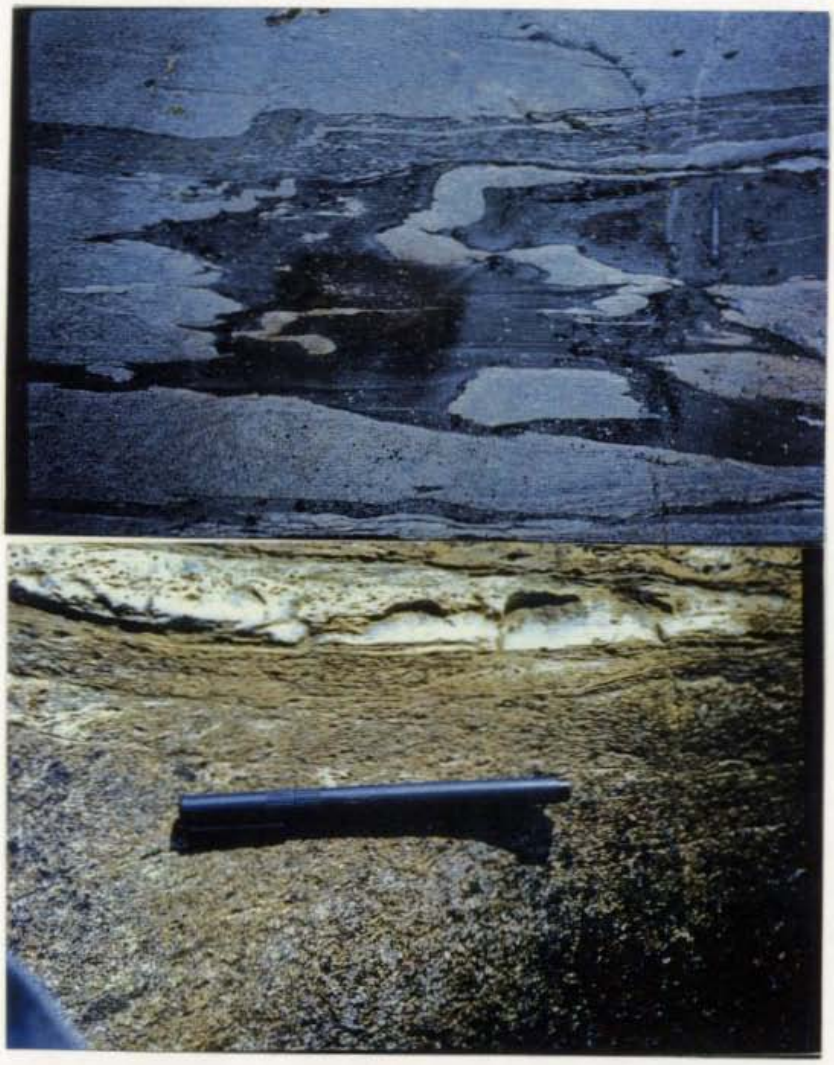

Fig.3.29.- Top: High temperature sub-solidus folding (F2a) of the Western Head granite at Three Islands. Cuspate and lobate folds and boudins of the granite veins suggest that the granite was more competent than the amphibolite during the F2a folding. The 2-D strain ellipsoid indicates an apparent dextral shear sense.
Bottom: D2b low grade S-C and C' (shear bands) structures in the Western Head granite indicating an apparent dextral shear sense (Sandbank Point-East Diver Head section)

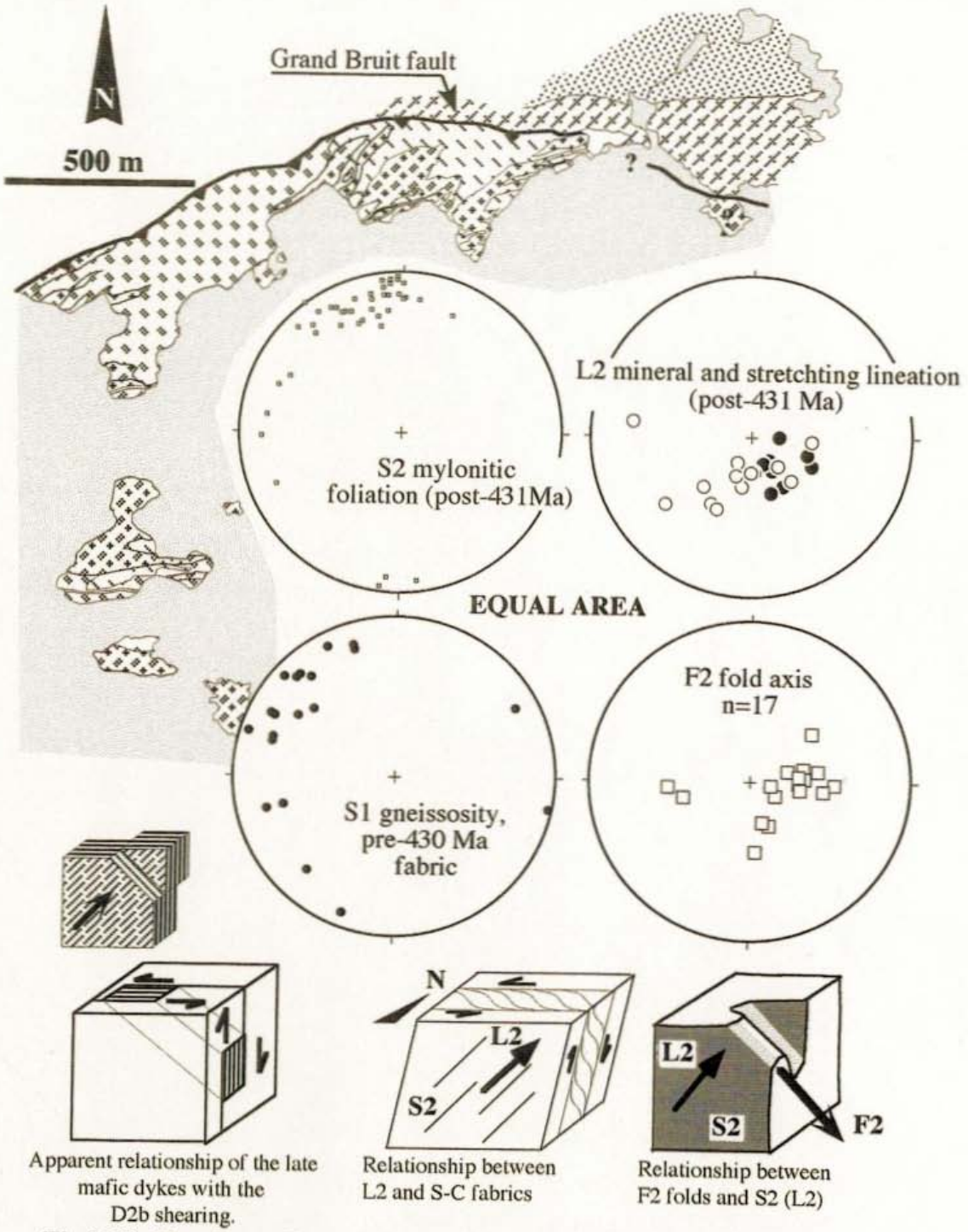

Fig.3.30.- Equal area lower hemisphere stereonet projections of the S2b mylonitic fabric, L2 lineation, S1 gneissosity (compositional banding) and plunge of the F2 folds (both F2a and F2b). Block diagrams show the relationships between the D2 folds, lineation, and mylonitic foliation and the late mafic dykes. Geological map as in fig.3.3.

Fig.3.31.- Sandbank Point metagabbro: Discrete greenschist facies retrograde shear zone (10 cm thick) with top to the left (i.e. thrusting) shear sense. Sandbank Point -East Diver Head section.

Fig.3.32.- D2 retrograde greenschist facies deformation of the Sandbank Point metagabbro, small dyke of leuco-diorite and country rock metagabbro deformed by late-D2 shear bands and fractures overprinted by a final set of joints. Upper left, intrusive contact with Western Head granite. Sandbank Point-East Diver Head section.

Fig. 3.33.- $S2^b$ mylonitic fabric in the 431.5±1 Ma mylonitic granite dyke (Western Head granite, sample location in fig.3.4 & 3.5).

Top: $S2^b$ retrograde greenschist facies mylonitic fabric with S-C and C' planes indicating a dextral shear sense (i.e. thrusting). Field of view is 5.21 mm wide

Bottom: Dynamic recrystallization of the quartzo-feldspathic mylonitic matrix and quartz (SR recrystallization?) in the tail of an asymmetric porphyroclast. Phyllosilicates (white mica and biotite) and grain elongation in the matrix define the S-C and C' planes Field of view is 0.76 mm wide.

Figure 3.33

Fig. 3.33.- $S2^b$ mylonitic fabric in the 431.5±1 Ma mylonitic granite dyke (Western Head granite, sample location in fig.3.4 & 3.5).

Top: $S2^b$ retrograde greenschist facies mylonitic fabric with S-C and C' planes indicating a dextral shear sense (i.e. thrusting). Field of view is 5.21 mm wide

Bottom: Dynamic recrystallization of the quartzo-feldspathic mylonitic matrix and quartz (SR recrystallization?) in the tail of an asymmetric porphyroclast. Phyllosilicates (white mica and biotite) and grain elongation in the matrix define the S-C and C' planes Field of view is 0.76 mm wide.

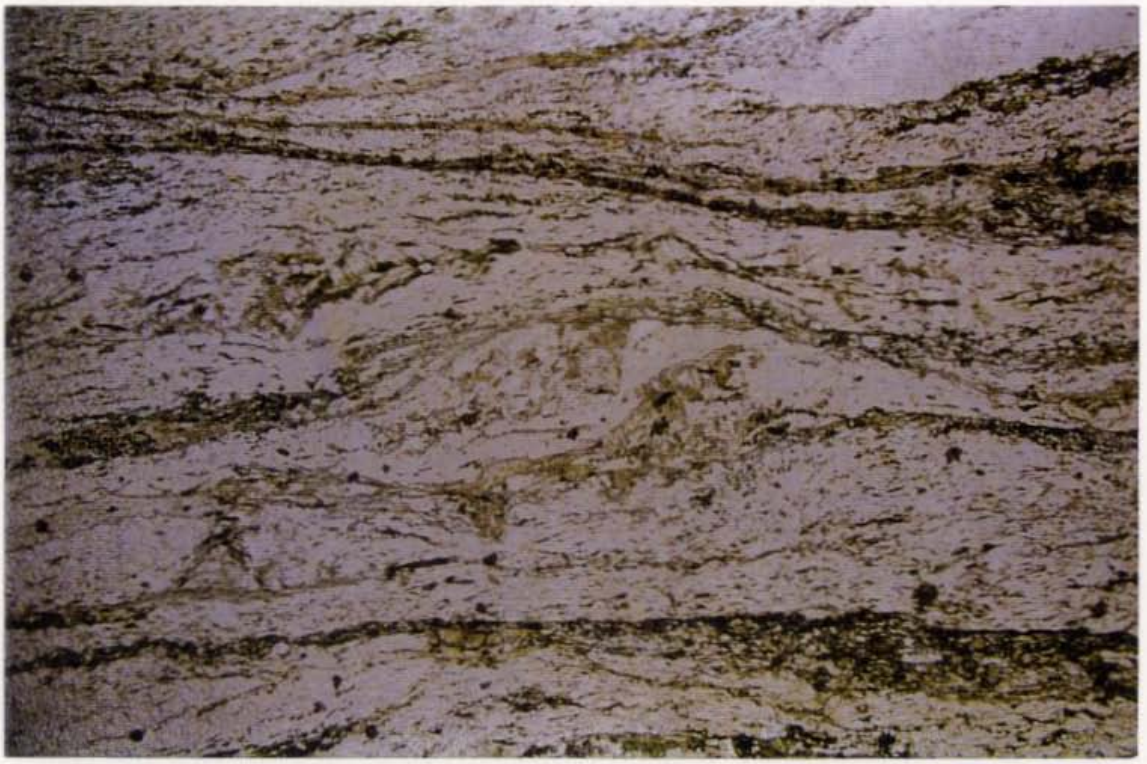

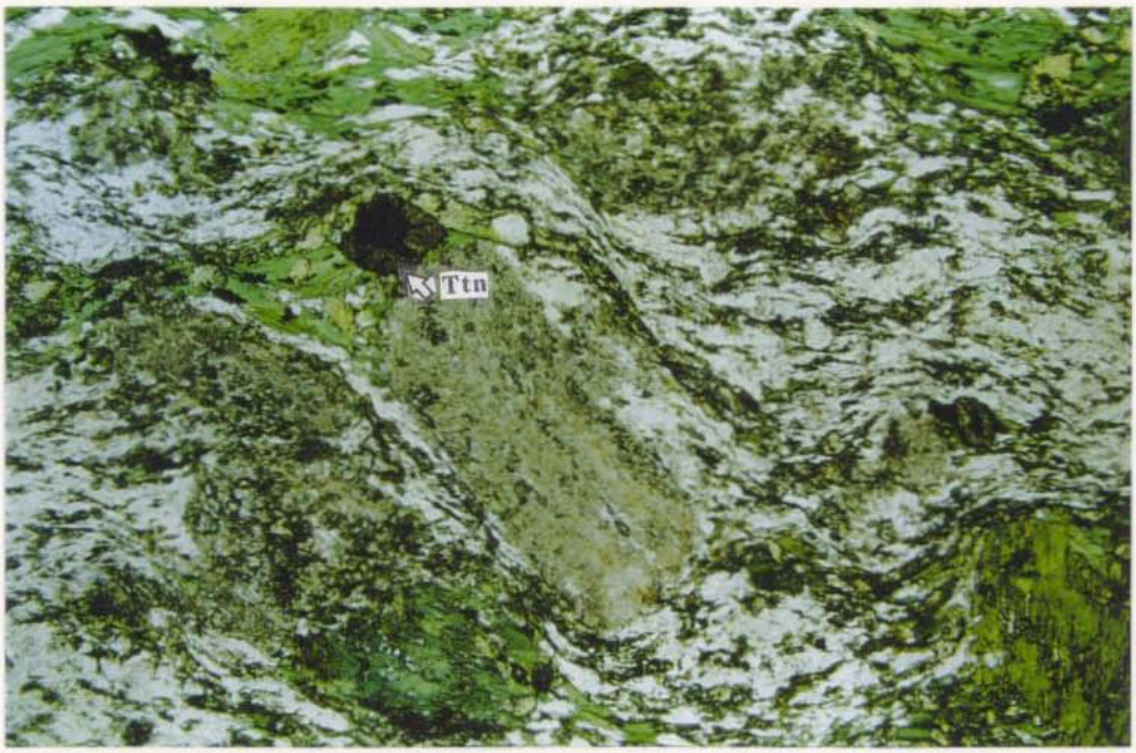

Fig.3.34.- Late mafic porphyritic dyke (post-431 Ma) showing greenschist facies overprint of the primary magmatic fabric. Chlorite + epidote+titanite form asymmetric tails around partially retrogressed (sericitized) plagioclase phenocrysts. The primary mafic phenocrysts are replaced by accumulations of actinolite (bottom right). Titanite is growing late after opaques (ilmenite?). Titanite from a similar dyke has been dated at 420±3 Ma (Dunning and B.H. O'Brien, unpublished).

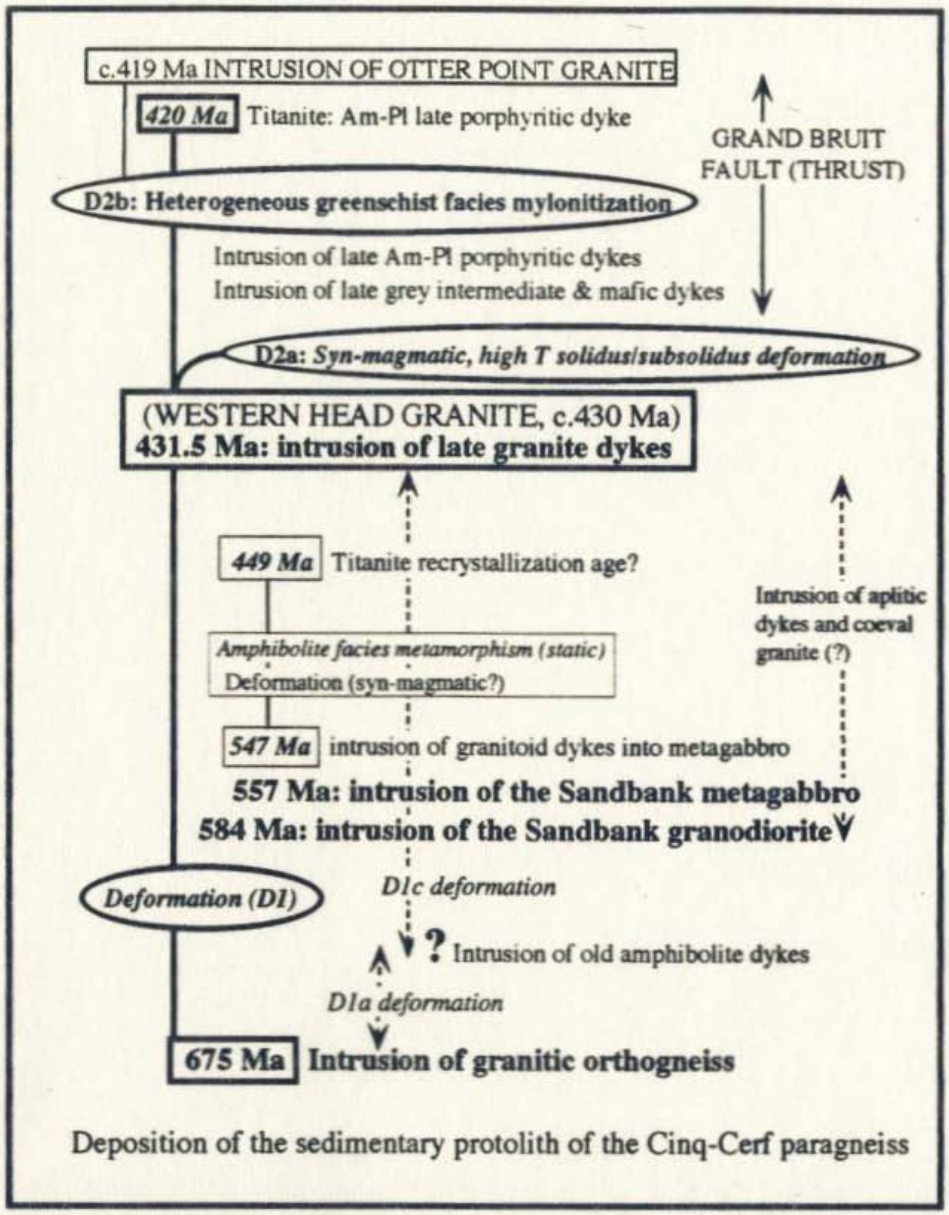

Fig. 3.35.- Time and field constraints on the tectonothermal evolution and timing of deformation in the Cinq-Cerf gneiss. Ages in bold (this study); ages in bold italics (Dunning and B.H. O'Brien, unpublished). Other ages: Western Head granite (429±2 Ma; 430±2 Ma; B.H. O'Brien et al., 1991); Otter Point granite (419±2 Ma; B.H. O'Brien et al., 1991). Thick lines mark the absolute time constraints provided by this study. Discontinuous lines, relative time constraints provided by individual field relationships.

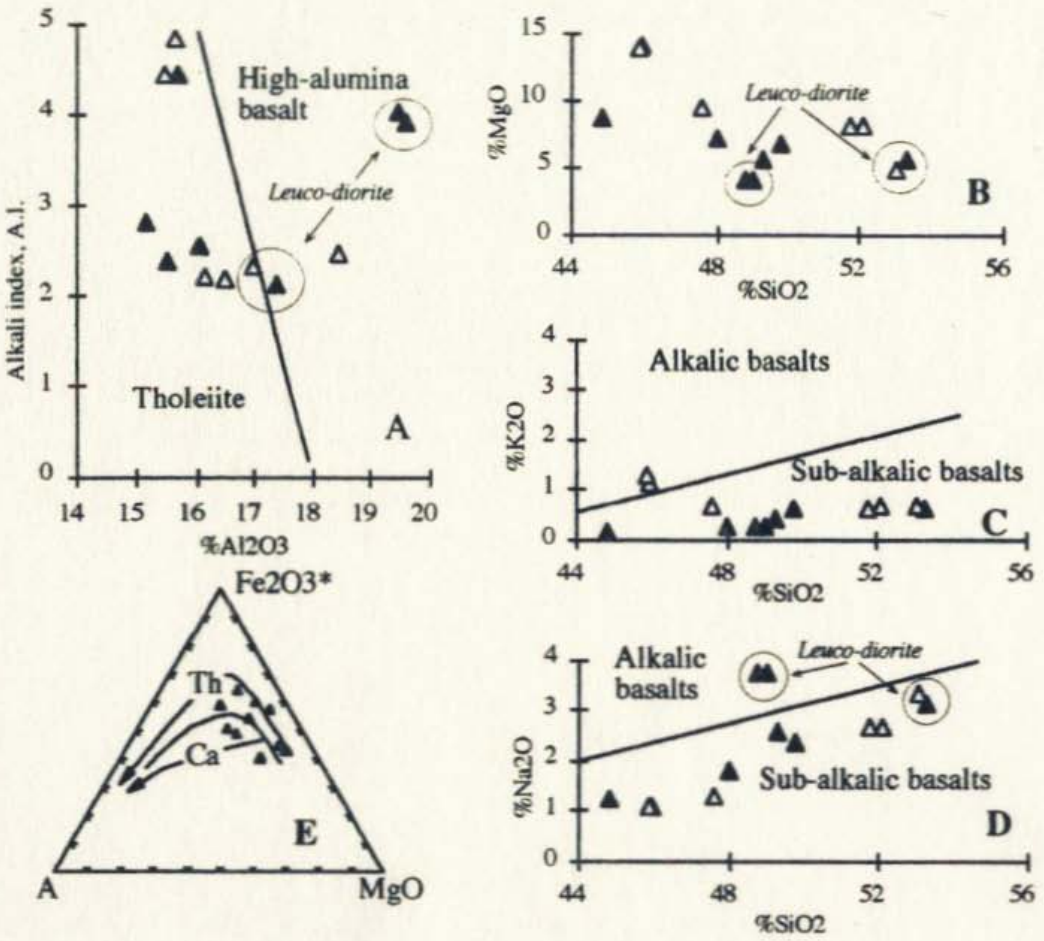

Fig.3.36.- Cinq-Cerf gneiss, metadiorites-metagabbros major element series discrimination diagrams. **A**) alkali index, A.I. vs % Al2O3 (Middlemost, 1975). **B**) %MgO vs %SiO2. **C**) %K2O vs % SiO2 (Middlemost, 1975). **D**) % Na2O vs % SiO2 (Middlemost, 1975). **E**) AFM ternary diagram (Miyashiro, 1978). Closed triangles, Sandbank Point; open triangles, Three Islands

TABLE 3.2.- MAJOR AND TRACE ELEMENT ANALYSES OF THE SANDBANK METAGABBRO/ DIORITE.

Sample	GCQ7A	GCQ10A	GCQ10	GCQ13	GCQ5	GCQ6	GCQ7B	GCQ3	GCQ1	GCQ12	GCQ12A	GCQ11	GCQ4
Rock type	Mafic meta-gabbro	Hornblendite	Mafic meta-gabbro	Mafic meta-gabbro	Mafic meta-gabbro/ diorite	Leuco-meta-gabbro / diorite	Leuco-meta-gabbro / diorite	Mafic meta-gabbro	Mafic meta-gabbro/ diorite	Meta-gabbro/ diorite	Leuco-meta-gabbro/ diorite	Meta-gabbro/ diorite	Mafic meta-diorite (U-Pb)
SiO_2	44.86	45.87	45.93	47.6	48.03	48.78	49.01	49.29	49.81	51.78	52.13	53.07	53.32
TiO_2	1.31	0.74	0.69	0.47	1.21	1.45	1.43	1.65	1	0.62	0.61	1.14	0.89
Al_2O_3	15.7	15.66	15.47	18.45	15.55	19.46	19.59	15.2	16.05	16.17	16.5	16.98	17.41
Fe_2O_3T	13.45	12.13	12.1	9.09	13.65	11.42	11.27	15.07	11.24	7.68	7.53	8.87	8.76
MnO	0.21	0.2	0.19	0.17	0.26	0.18	0.18	0.22	0.18	0.14	0.15	0.21	0.19
MgO	8.64	13.81	13.96	9.34	7.08	4.07	3.99	5.52	6.67	8.01	8	4.79	5.59
CaO	13.64	8.56	8.73	12.54	11.29	9.76	9.71	9.79	11.07	10.76	10.77	9.05	9.44
Na_2O	1.22	1.07	1.1	1.27	1.79	3.7	3.75	2.57	2.35	2.65	2.68	3.3	3.13
K_2O	0.18	1.28	1.11	0.65	0.25	0.26	0.25	0.42	0.6	0.64	0.68	0.67	0.61
P_2O_5	0.07	0.09	0.1	0.07	0.1	0.38	0.38	0.2	0.08	0.07	0.06	0.17	0.13
Total	99.28	99.41	99.38	99.65	99.21	99.46	99.56	99.93	99.05	98.52	99.11	98.25	99.47
L.O.I.	1.27	2.2	2.18	4.18	0.81	0.62	0.59	0.69	0.44	1.12	1.13	0.58	0.97
Ba	54	188	112	78	64	78	82	88	80	131	116	164	118
Rb	1	61	50	28	2	6	6	9	11	22	26	18	17
Sr	252	154	163	215	252	391	388	272	232	190	203	293	300
Y	31	12	10	10	41	23	22	38	19	18	19	32	44
Zr	32	53	49	27	126	48	38	45	51	50	49	73	151
Nb	3	3	3	2	5	4	4	9	4	3	3	9	6
Pb	6	-	4	5	-	5	5	5	5	5	6	10	6
Ga	16	14	13	15	21	26	26	21	19	15	15	19	19
Zn	56	72	65	17	105	29	29	68	39	-	-	36	47
Cu	113	39	45	-	61	23	35	24	18	41	23	22	40
Ni	50	354	355	59	29	5	9	19	35	105	102	17	40
V	469	140	148	149	377	267	265	463	357	177	171	215	206
Sc	60	19	19	40	58	34	28	46	45	33	40	37	40
Cr	250	705	755	205	89	27	28	26	111	264	271	31	129
La	3.7	-	4.2	3.4	-	7.9	8.2	-	7.6	-	5.5	-	9.8
Ce	13	-	10	8	-	19.7	20.2	-	17.8	-	13.4	-	27.1
Pr	2.3	-	1.4	1.1	-	2.8	2.9	-	2.4	-	1.9	-	4.3
Nd	13.2	-	6.4	5.1	-	14	14	-	10.2	-	8.3	-	22.4
Sm	4.1	-	1.7	1.5	-	3.5	3.5	-	2.5	-	2.4	-	6.1
Eu	1.2	-	0.7	0.5	-	1.3	1.4	-	0.8	-	0.8	-	1.8
Gd	5.2	-	2	1.7	-	4.2	3.9	-	3	-	2.8	-	7.3
Tb	0.9	-	0.3	0.3	-	0.6	0.6	-	0.5	-	0.5	-	1.2
Dy	5.6	-	1.9	1.9	-	4	4.1	-	3.2	-	3.2	-	7.7
Ho	1.2	-	0.4	0.4	-	0.9	0.9	-	0.7	-	0.7	-	1.6
Er	3.3	-	1.2	1.2	-	2.5	2.4	-	2.1	-	2.1	-	4.8
Tm	0.5	-	0.2	0.2	-	0.4	0.3	-	0.3	-	0.3	-	0.7
Yb	3	-	1.2	1	-	2.3	2.2	-	2.2	-	2.1	-	4.5
Lu	0.4	-	0.2	0.1	-	0.3	0.3	-	0.3	-	0.3	-	0.7
Th	0.1	-	0.6	0.4	-	0.7	0.8	-	2.4	-	0.9	-	0.7

Major element concentrations in weight % (XRF fused pellet analyses). All Fe is given as Fe2O3. Trace element concentration in ppm. Ba, Rb, Sr, Y, Zr, Nb, Pb, Ga, Zn, Cu, Ni, V, Sc and Cr were analyzed by XRF (press pellets). The REE and Th were analyzed by Na2O2 sinter ICP-MS analyses. Details of the analytical techniques, including limits of detection and precision, are given in the appendix.

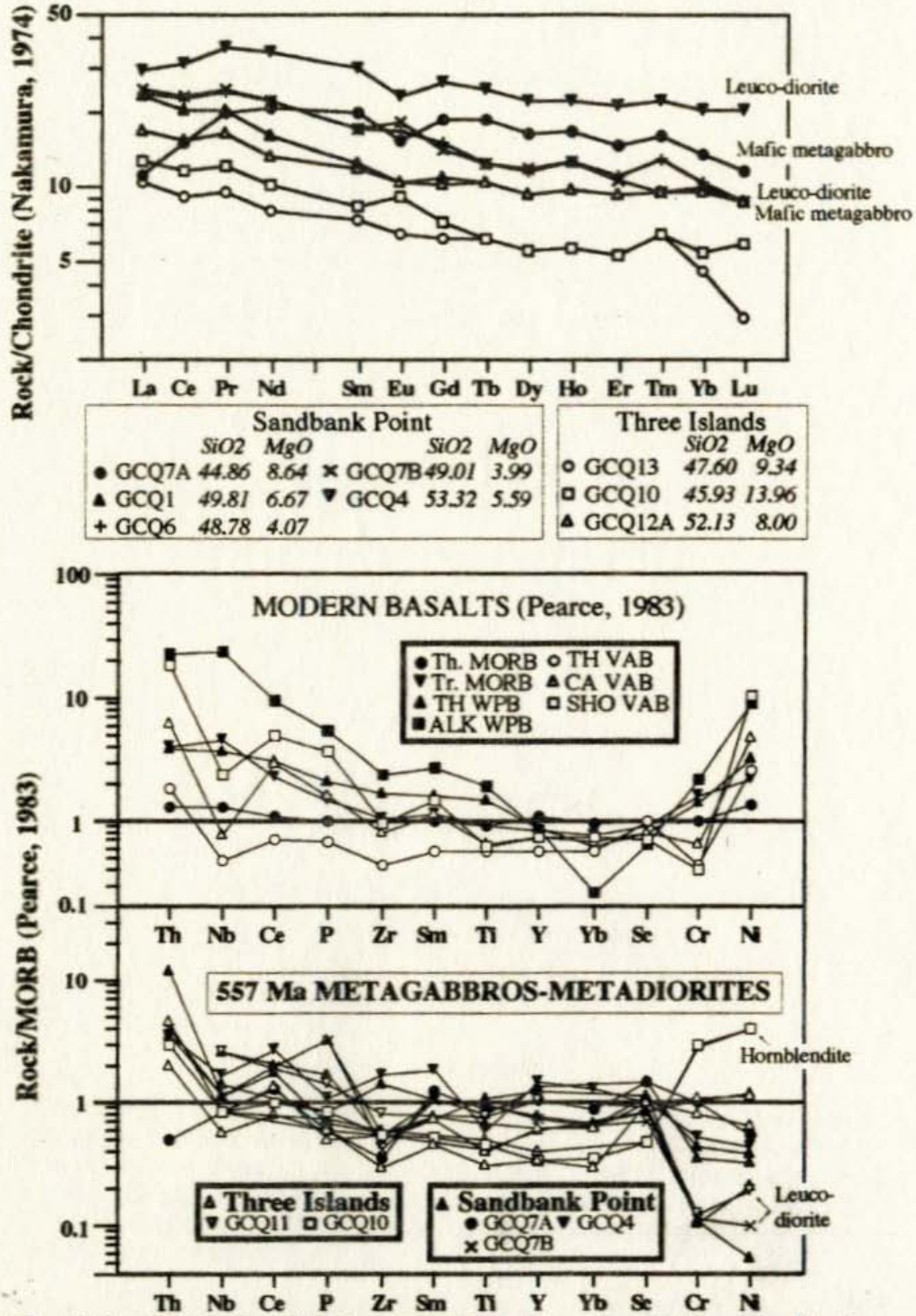

Fig. 3.37.- 557 Ma Sandbank metagabbro. Top: chondrite-normalized multielement pattern. Sample symbols and SiO2 and MgO concentrations in the table below. **Bottom: MORB (Pearce, 1983) - normalized multielement patterns for the Sandbank Point and Three Islands samples and modern day basalts (Pearce, 1983).** Th, tholeiite; Tr, transitional; ALK, alkaline; CA, calc-alkaline; SHO, shoshonitic; VAB, volcanic arc basalt; WPB, within plate basalt; MORB; Mid Ocean Ridge basalt.

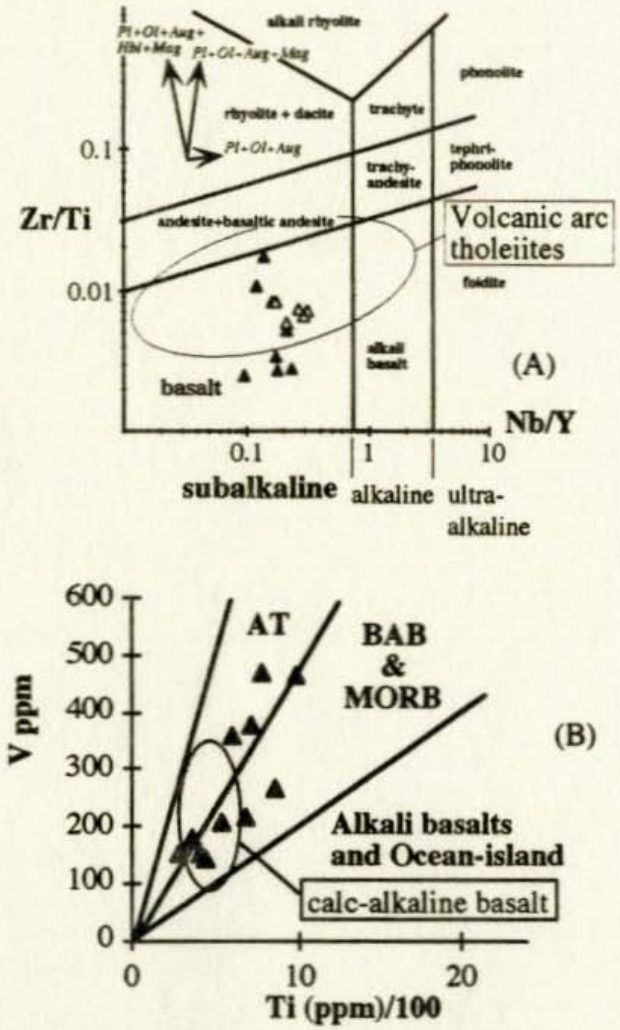

Fig.3.38.- Bivariate series discrimination diagrams: (A) Zr/Ti vs. Nb/Y diagram of Winchester and Floyd (1977) modified by Pearce (1996). The arrows correspond to fractionation vectors; mineral symbols after Kretz (1983); filled triangles, Sandbank Point; open triangles, Three Islands. **(B) V vs. Ti diagram (Shervais, 1982).** AT, arc tholeiite; BAB back arc basalt; MORB, Mid Ocean Ridge basalt

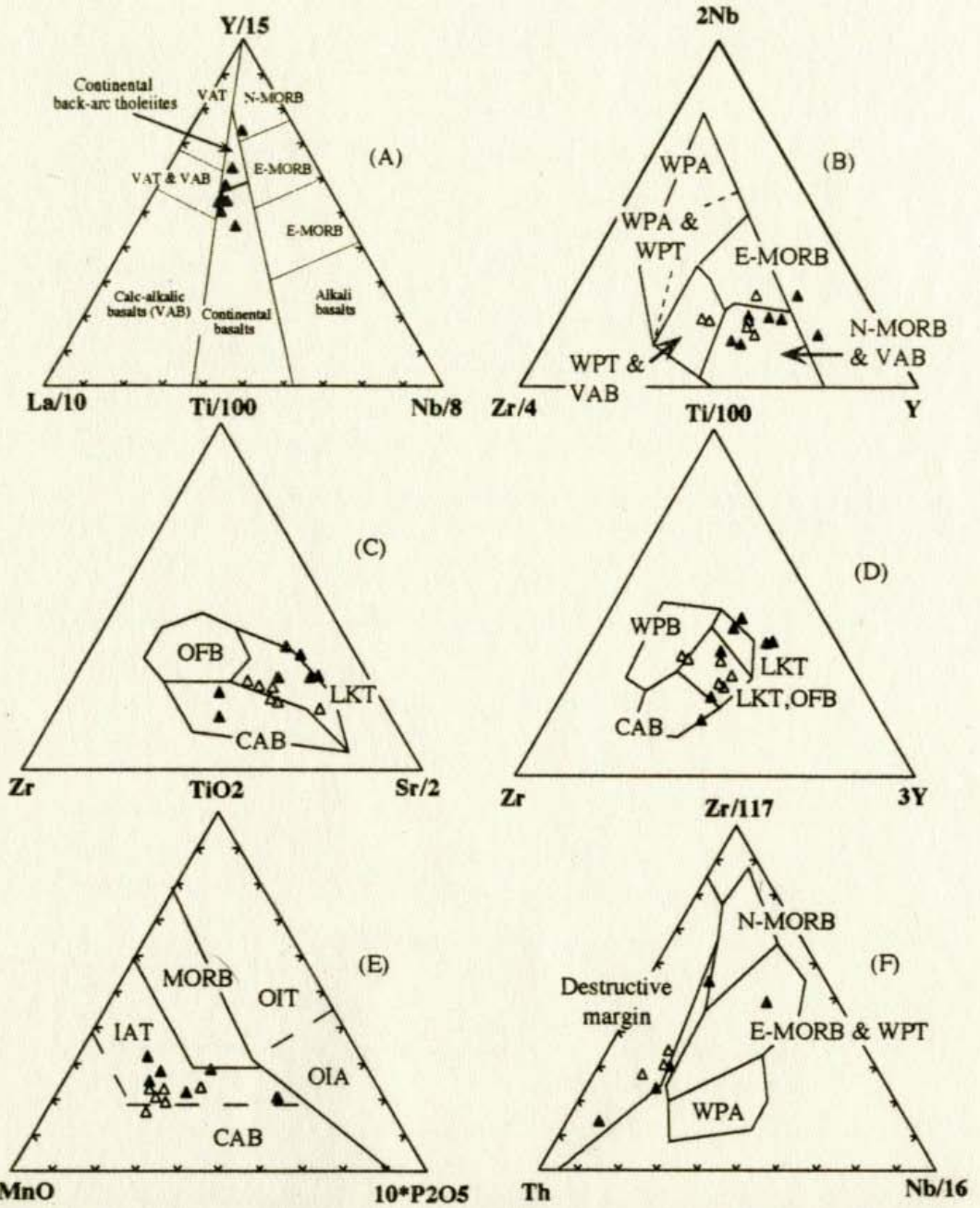

Fig.3.39.- Ternary tectonic discrimination diagrams for the 557 Ma Sandbank metagabbro/diorite. **(A)** La/10-Y/15-Nb/8 diagram (Cabanis and Lecolle, 1989). **(B)** Zr/4-2Nb-Y diagram (Meschede, 1986). **(C)** Zr-Ti/100-Sr/2 diagram (Pearce and Cann, 1973). **(D)** Zr-Ti/100-3Y diagram (Pearce and Cann, 1973). **(E)** 10MnO - TiO2 - 10P2O5 diagram (Mullen, 1983). **(F)** Th-Zr/117-Nb/16 diagram (modification of the Th-Hf/3-Ta diagram of Wood, 1980). Filled triangles, Sandbank Point; open triangles, Three Islands, except diagram A (not differentiated).

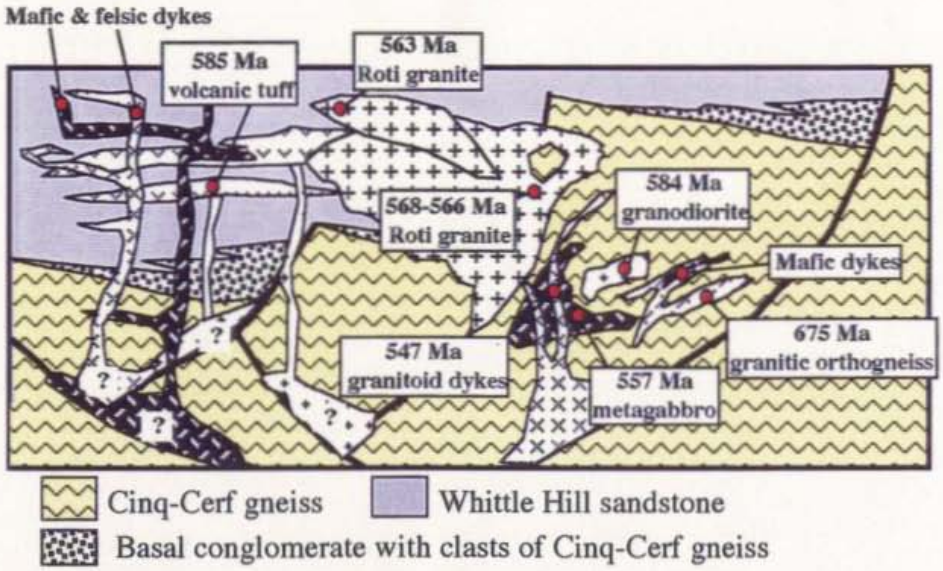

Fig.3.40.- Model of the Late Precambrian-Early Cambrian basement-cover relationship between the Cinq-Cerf gneiss and the Whittle Hill sandstone.

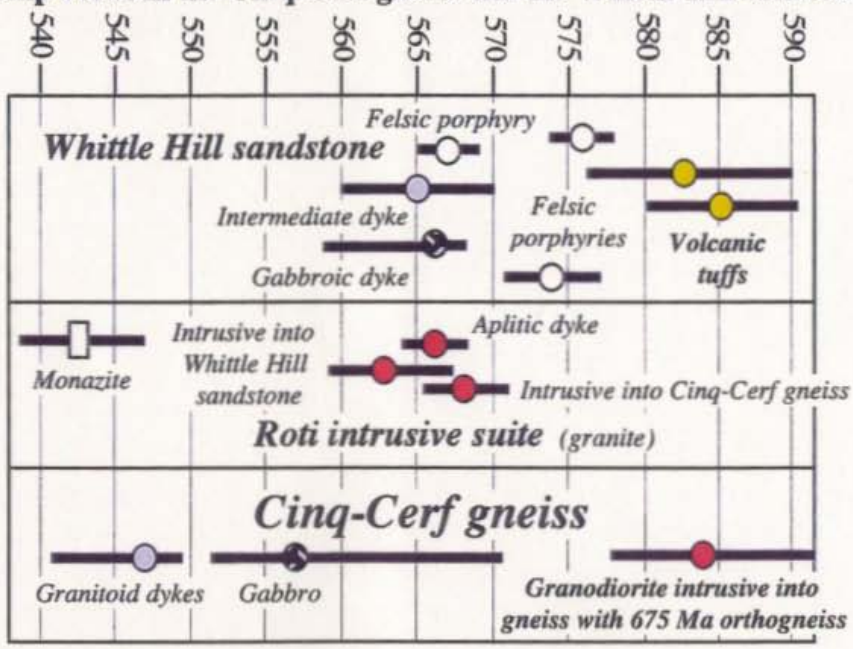

Table 3.3.- Comparative table of the post-675 Ma, Late Precambrian-Early Cambrian U-Pb absolute ages from the Cinq-cerf gneiss (This study and Dunning and B.H. O'Brien, unpublished) and the adjacent Roti suite (Dunning and S.J. O'Brien, 1989; B.H. O'Brien et al, 1991; B.H. O'Brien et al., 1993) and the Whittle Hill sandstone (Dubé and Dunning, in press) .

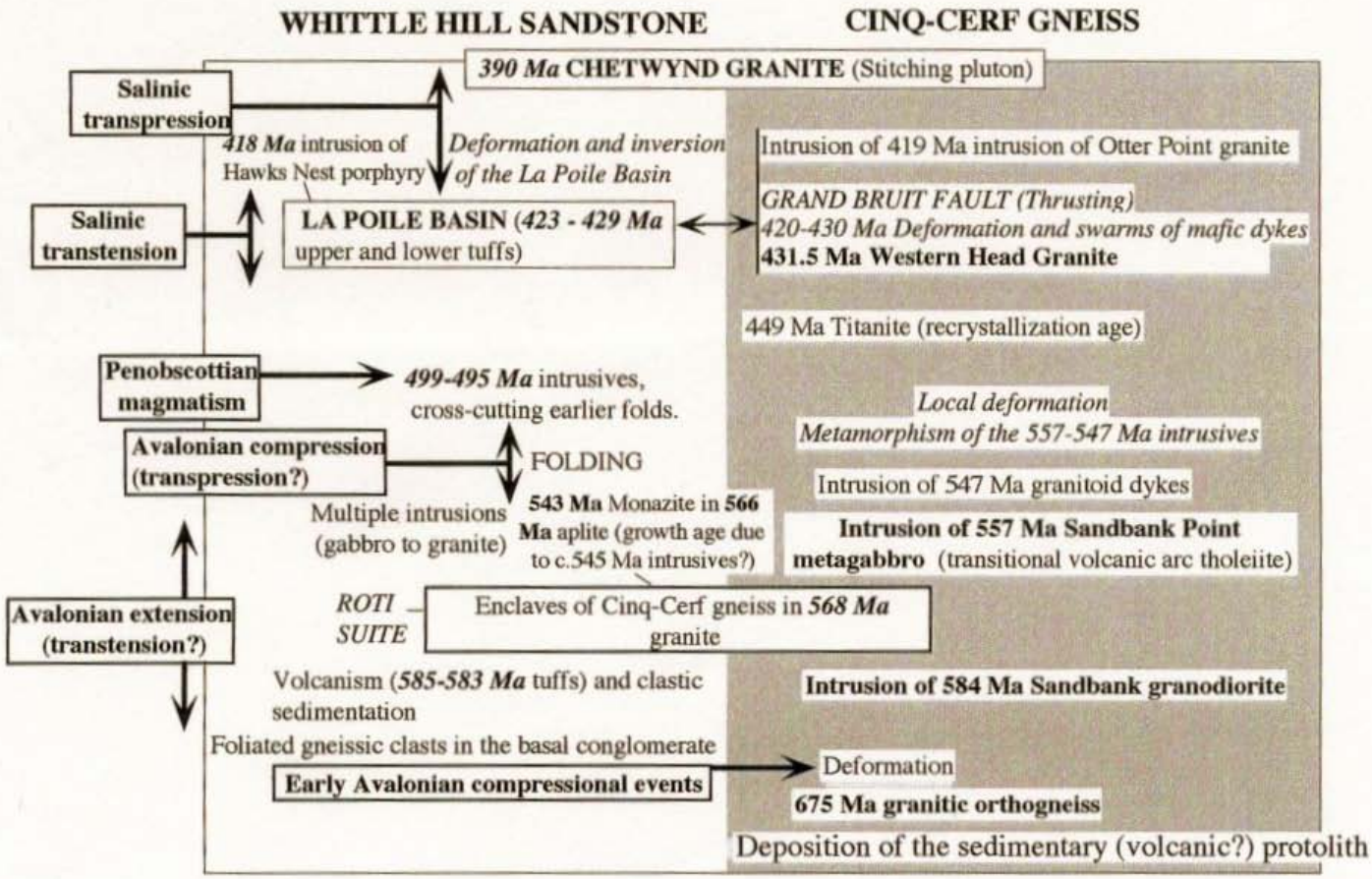

Fig.3.41.- Late Precambrian to Late Paleozoic geological evolution of the Avalonian basement of the La Poile Bay-Coteau Bay area of the Hermitage Flexure (Central mobile belt, SW Newfoundland Appalachians)

MAP A.1.- SANDBANK POINT-EAST DIVER HEAD SECTION

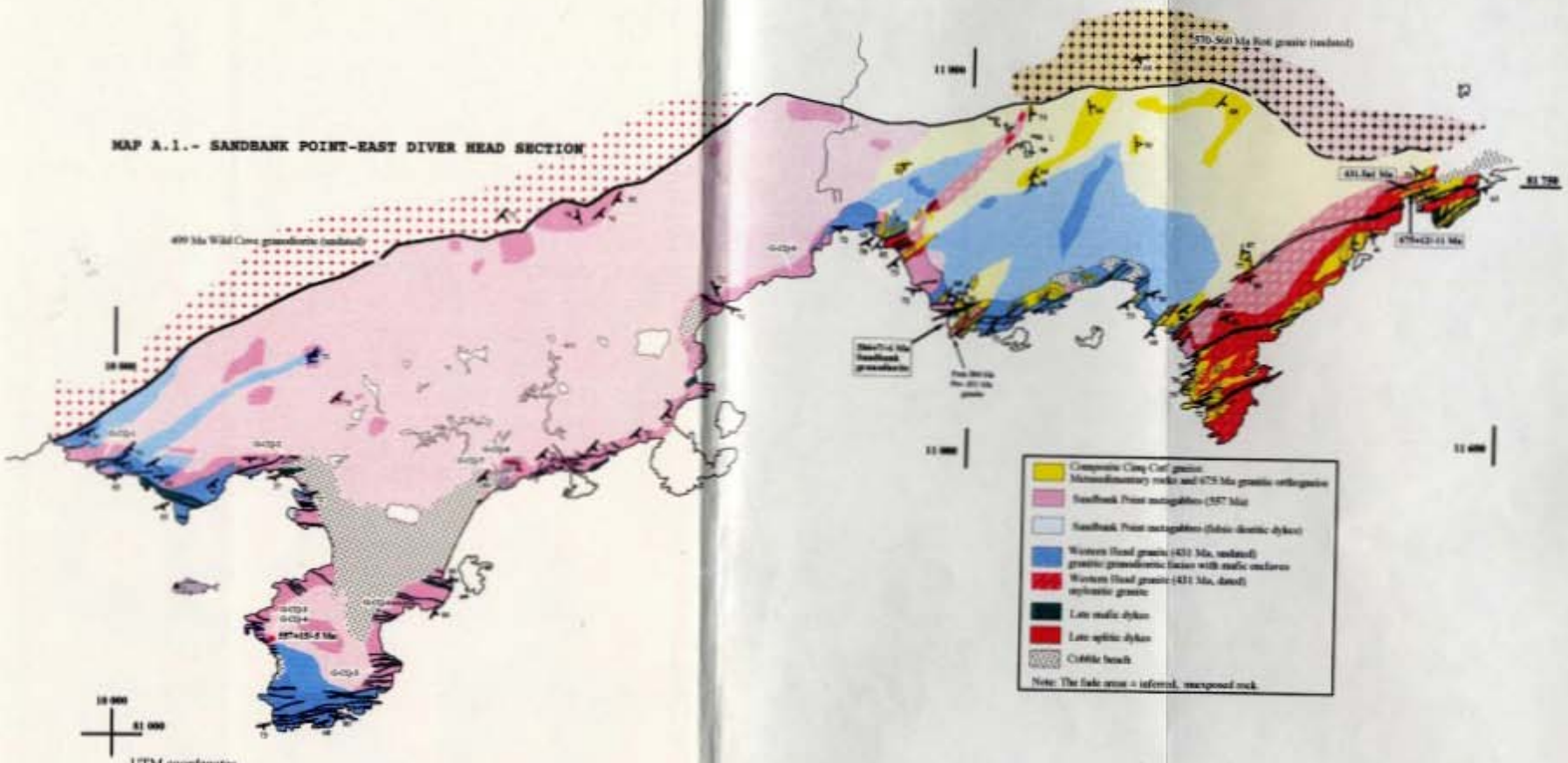

UTM coordenates
21T Grid zone
VC 100,000 m square

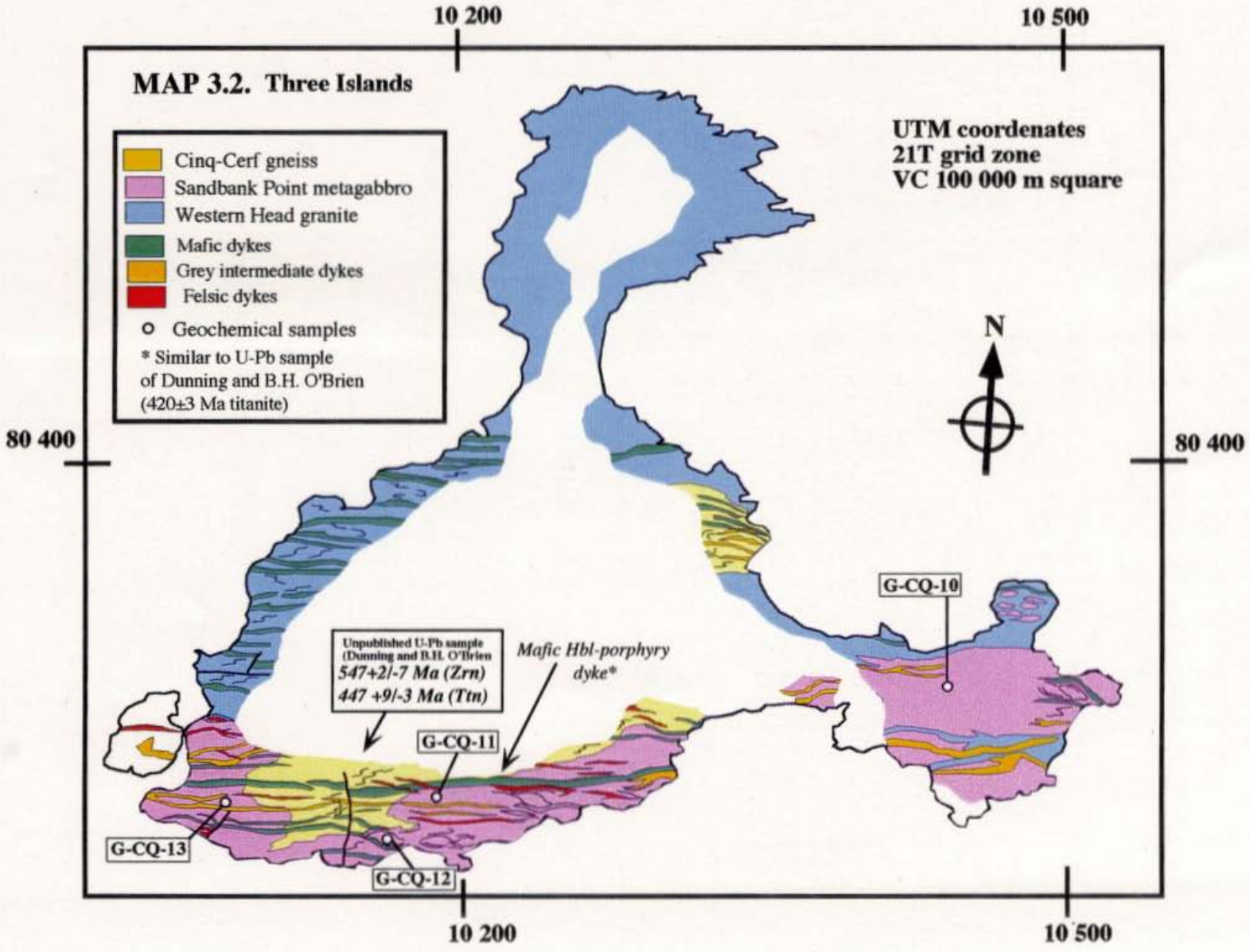
MAP 3.2. Three Islands
Cinq-Cerf gneiss
Sandbank Point metagabbro
Western Head granite
Mafic dykes
Grey intermediate dykes
Felsic dykes
Geochemical samples
* Similar to U-Pb sample of Dunning and B.H. O'Brien (420±3 Ma titanite)
UTM coordenates
21T grid zone
VC 100 000 m square
N
10 200
10 500
80 400
Unpublished U-Pb sample (Dunning and B.H. O'Brien
547+2/-7 Ma (Zrn)
447 +9/-3 Ma (Ttn)
Mafic Hbl-porphyry dyke*
G-CQ-10
G-CQ-11
G-CQ-13
G-CQ-12

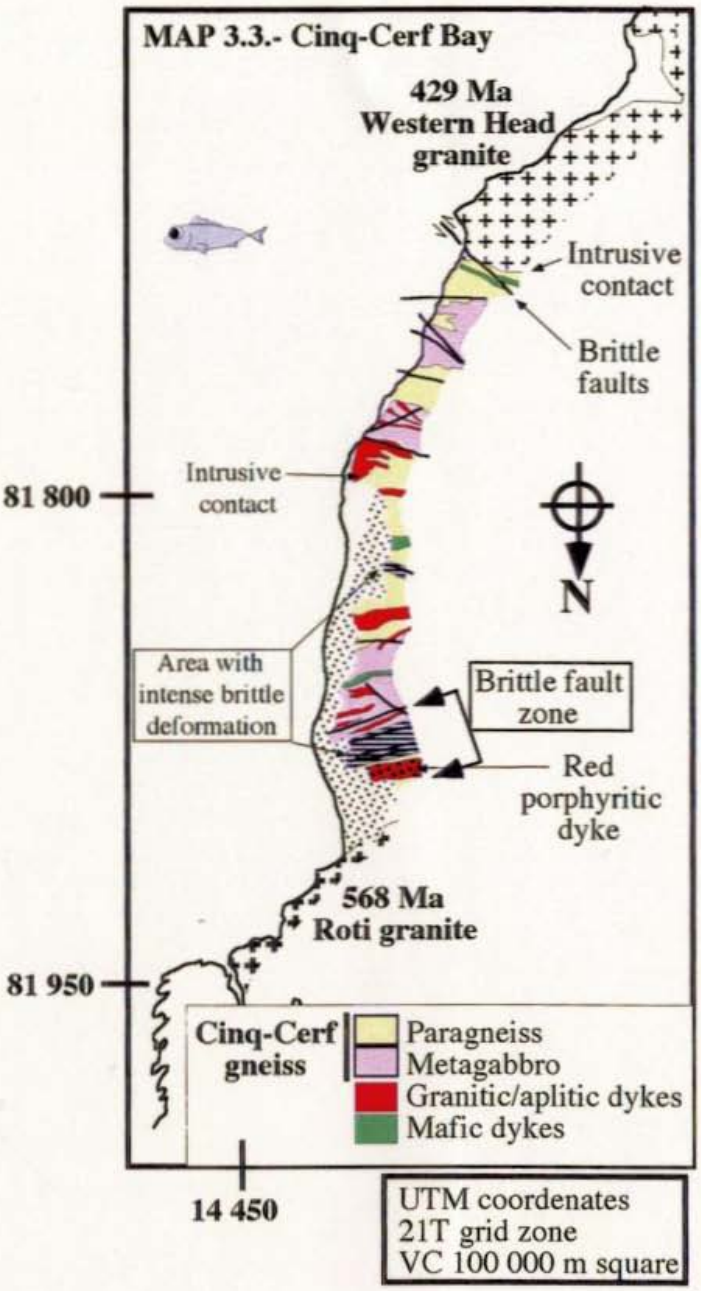
MAP 3.3.- Cinq-Cerf Bay
429 Ma
Western Head
granite
Intrusive
contact
Brittle
faults
81 800
Intrusive
contact
N
Area with
intense brittle
deformation
Brittle fault
zone
Red
porphyritic
dyke
568 Ma
Roti granite
81 950
Cinq-Cerf
gneiss
Paragneiss
Metagabbro
Granitic/aplitic dykes
Mafic dykes
14 450
UTM coordenates
21T grid zone
VC 100 000 m square

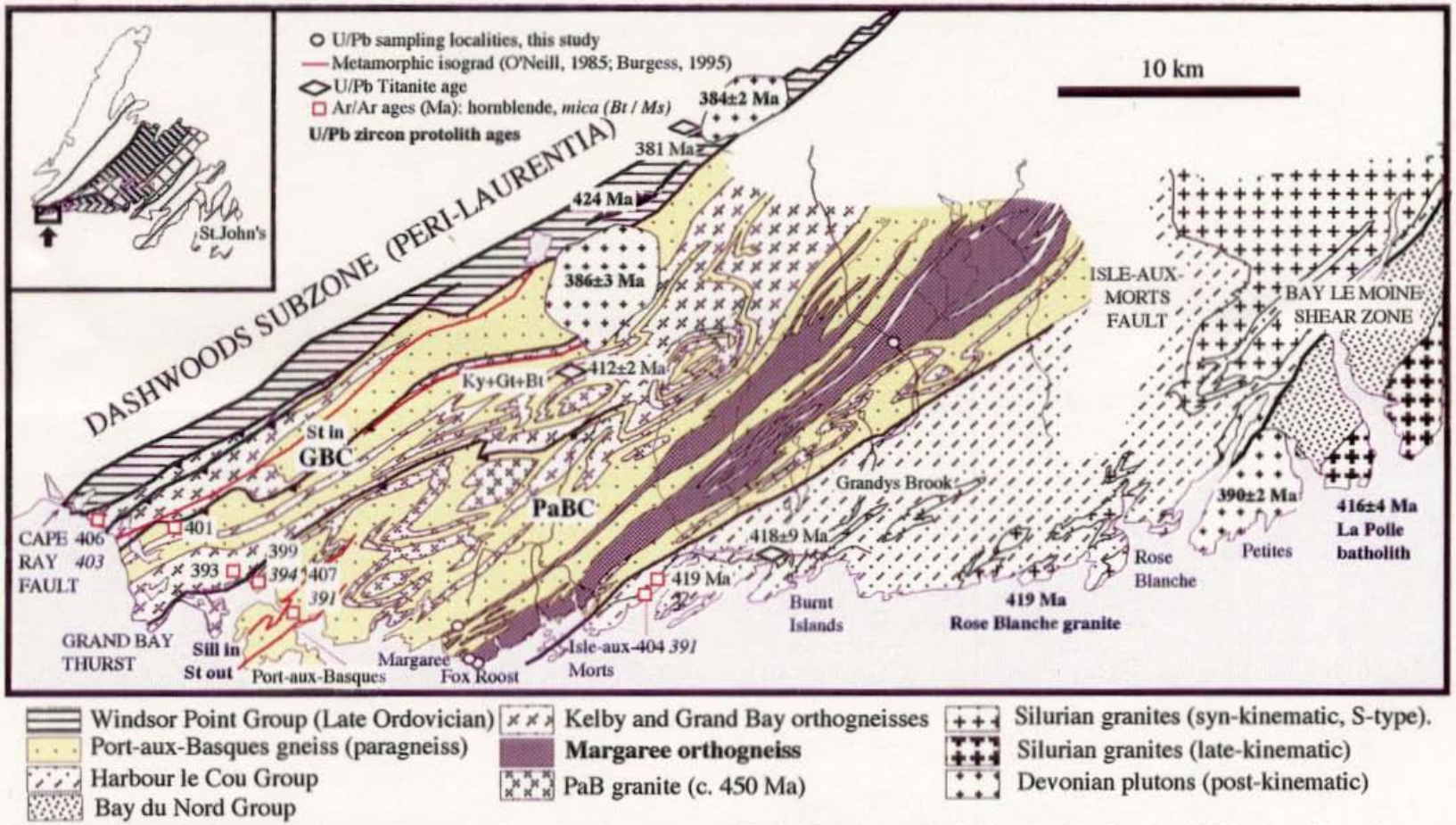

Fig.4.1.- Geological map of the area between Port aux Basques and Garia Bay (compiled after van Staal et al., 1996 b, c and Dubé et al., 1996). Geochronological data after Chorlton and Dallmeyer (1986), Dunning et al. (1990), Van Staal et al. (1994), Burgess et al. (1995) and Dubé et al. (1996). Metamorphic isograds after O'Neill (1985) and Burgess et al. (1995), in red. GBC, Grand Bay complex; PaBC, Port-aux-Basques complex.

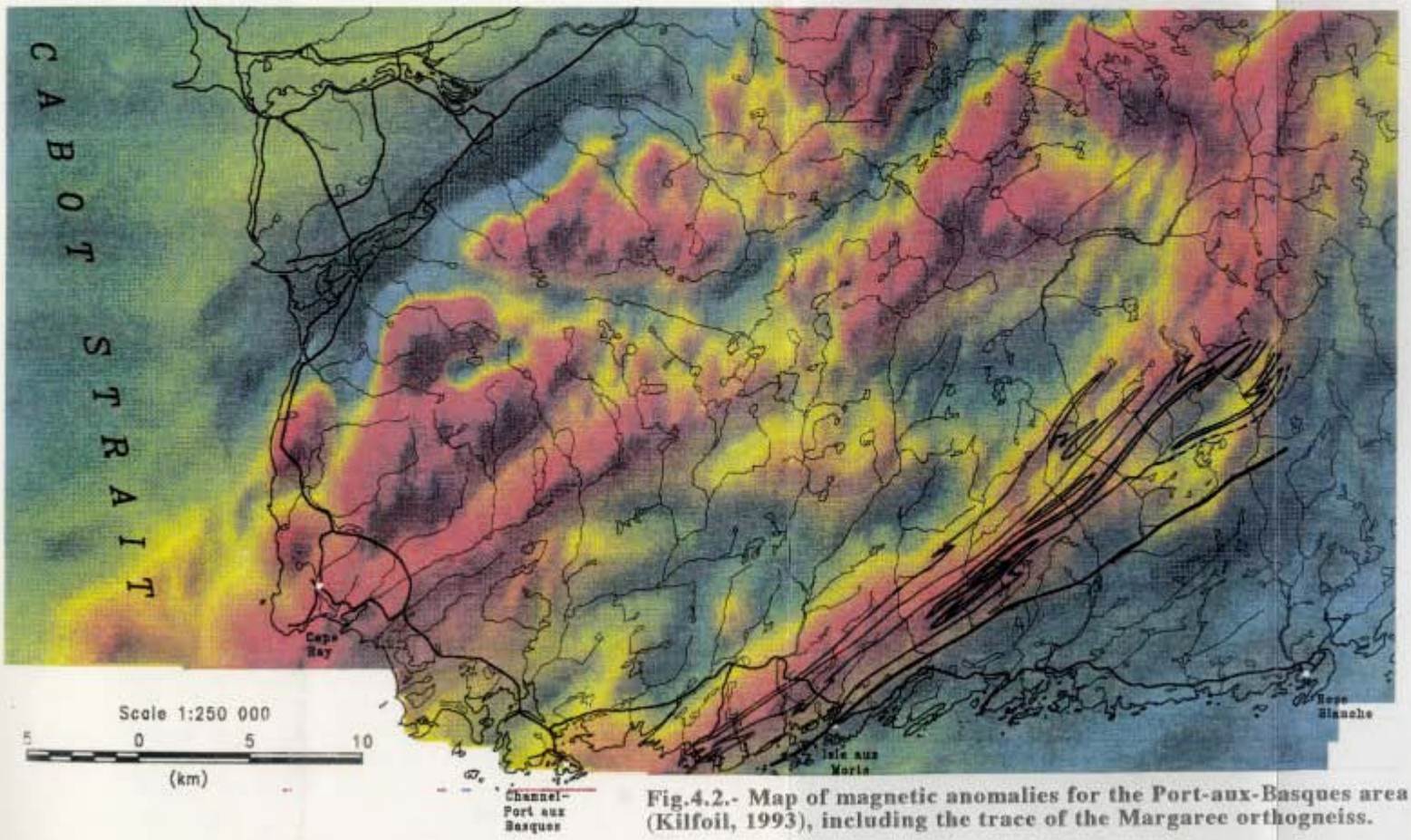

Fig.4.2.- Map of magnetic anomalies for the Port-aux-Basques area (Kilfoil, 1993), including the trace of the Margaree orthogneiss.

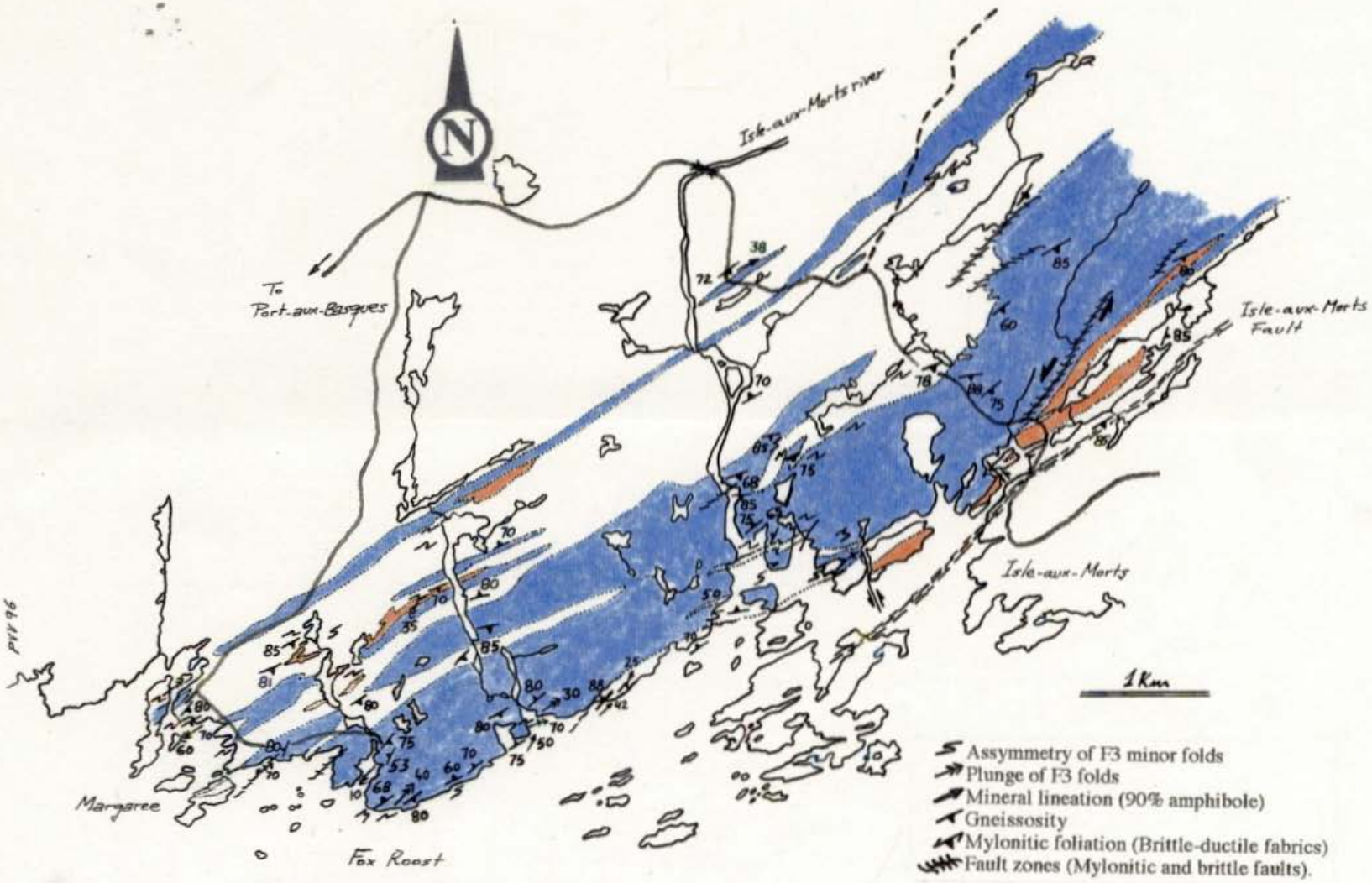

Fig. 4.3.- Geological map of the Margaree/Isle-aux-Morts portion of the Margaree orthogneiss. Blue, Margaree orthogneiss; orange, Port-aux-Basques granite (pre-D3 foliated granite).

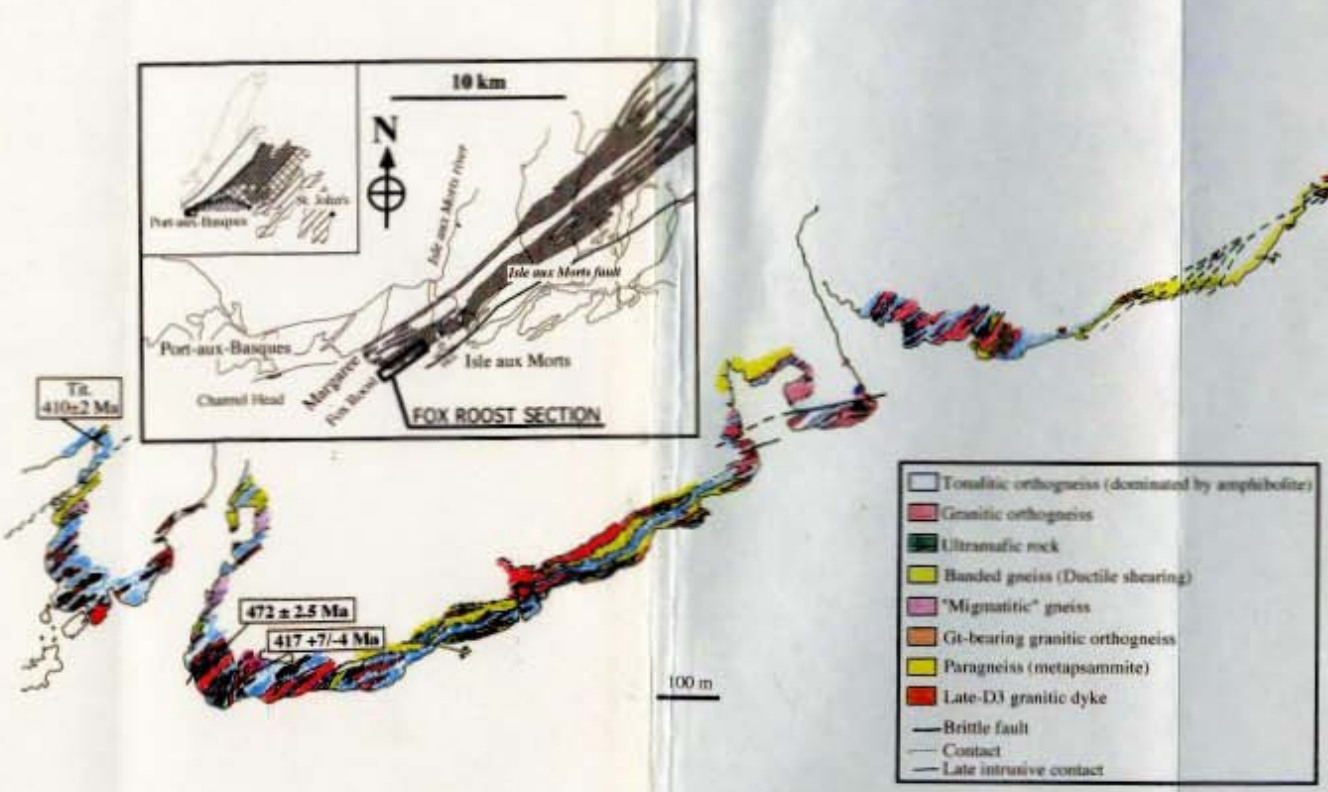

Fig.4.4.- Lithological map of the Fox Roost section of the Margaree orthogneiss including U/Pb sampling locations.

Fig. 4.5.- Macro- and mesoscopic relationships between the amphibolite-rich "tonalitic" gneisses and the granitic orthogneisses of the Margaree orthogneiss, Fox Roost.

A) Contact between amphibolite-rich "tonalitic" orthogneisses and granitic orthogneisses (L.Hall for scale). Felsic granitic veins in the "tonalitic" orthogneiss merge with the granitic orthogneisses.

B) Cross-section view of a stained contact between "tonalitic" orthogneiss and granitic orthogneiss with some pegmatitic pockets (Hammer for scale). Note minor asymmetric folds with vertical limbs and ductile absorbing in the fold limbs (D3 deformation).

C) Detail of back-veining of the amphibole-rich " mafic tonalitic" orthogneiss by the granitic orthogneiss (A72 Ma).

Figure 4.5

D) Plan view, straight contact between "tonalitic" and granitic orthogneisses with a late pegmatitic; with an undeformed core, cross-cutting the previous Felsic veins in the mafic "tonalitic" merge with the granitic orthogneiss. Well developed compositional banding in the granitic orthogneiss (bottom) is isoclinally folded and is partially transposed by an axial planar fabric. At the top the compositional banding is transposed into parallelism. The pegmatitic intruded late during the ductile shearing approximately perpendicular to the extension direction (note small asymmetric folded felsic pegmatitic vein, upper left corner).

Fig.4.5.- Macro- and mesoscopic relationships between the amphibolite-rich "tonalitic" gneisses and the granitic orthogneisses of the Margaree orthogneiss, Fox Roost.

A) Contact between amphibolite-rich "tonalitic" orthogneisses and granitic orthogneisses (L.Hall for scale). Felsic granitic veins in the "tonalitic" orthogneiss merge with the granitic orthogneisses.

B) Cross-section view of a strained contact between "tonalitic" orthogneiss and granitic orthogneiss with some pegmatitic patches (Hammer for scale). Note minor asymmetric folds with vertical limbs and ductile shearing in the fold limbs (D3 deformation).

C) Detail of back-veining of the amphibole-rich " mafic tonalitic" orthogneiss by the granitic orthogneiss (472 Ma).

D) Plan view, straight contact between "tonalitic" and granitic orthogneisses with a late pegmatite, with an undeformed aplitic core, cross-cutting the gneissosity. Felsic veins in the mafic "tonalite" merge with the granitic orthogneiss. Well developed compositional banding in the granitic orthogneiss (bottom) is isoclinally folded and is partially transposed by an axial planar fabric. At the top the compositional banding is transposed into parallelism. The pegmatite intruded late during the ductile shearing, approximately perpendicular to the extension direction (note small stretched felsic pegmatitic vein, upper left corner).


A


B


C


D

Fig.4.6.- Margaree orthogneiss, hornblende-bearing granodioritic orthogneiss (U/Pb sample 93-PV-3). Location: quarry outside Margaree (UTM, 21T UC 345200 5271400). Typical aspect of the gneiss showing a hornblende-bearing felsic vein (metamorphic differentiation) isoclinally folded and transposed into parallelism with the rest of the gneissosity. Pen for scale is 13 cm long.

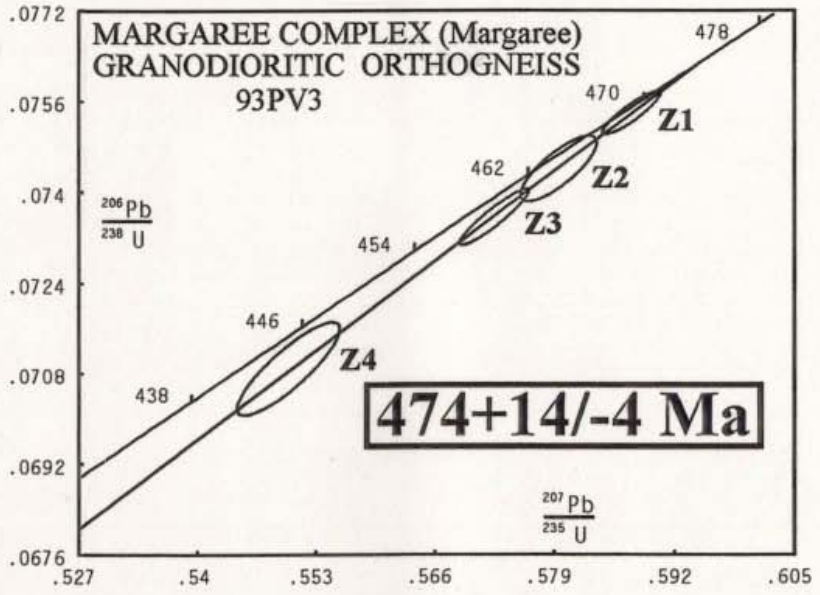

Fig.4.7.- U-Pb concordia diagram for the granodioritic orthogneiss (Sample 93-PV-3). Z; zircon.

TABLE 4.1.- U-Pb DATA, MARGAREE ORTHOGNEISS.

Description	Weight	Concentration		Measured		Corrected atomic ratios*							Age (Ma)		
Fraction	(mg)	U (ppm)	Pb rad (ppm)	Total common Pb (Pg)	$\frac{206Pb}{204Pb}$	$\frac{208Pb}{206Pb}$	$\frac{206Pb}{238U}$	±	$\frac{207Pb}{235U}$	±	$\frac{207Pb}{206Pb}$	±	$\frac{206Pb}{238U}$	$\frac{207Pb}{235U}$	$\frac{207Pb}{206Pb}$
1. -Hbl-bearing granodioritic orthogneiss (93-PV-3, Quarry outside Margaree) 45200-71400 †															
Z1 Pr. w/ rounded tips AB	0.0498	350	30	31	2690	0.2662	0.07540	32	0.5874	26	0.05650	10	469	469	472
Z2 NM needles AB	0.0208	346	29	7	5040	0.2790	0.07441	48	0.5795	34	0.05649	22	463	464	472
Z3 M1 needles AB	0.0880	414	34	18	9336	0.2580	0.07356	40	0.5725	31	0.05645	12	458	460	470
Z4 Needles w/cracks NAB	0.0873	547	43	18	11547	0.2380	0.07089	68	0.5500	46	0.05627	28	441	445	463
2. -Granitic orthogneiss (93-PV-5, Fox Roost) 46350-70125															
Z1 M0 Needles AB	0.0257	307	24	10	3600	0.1416	0.07600	40	0.5918	31	0.05648	16	472	472	471
Z2 Pr. w/ rounded tips AB	0.0397	239	18	28	1644	0.1237	0.07515	32	0.5874	25	0.05670	14	467	469	480
Z3 Ndl. w/ rounded tips AB	0.0119	256	19	14	1039	0.1347	0.07563	38	0.5946	28	0.05702	24	470	474	492
Z4 Needles & small pr. AB	0.0433	314	24	10	6474	0.1413	0.07450	52	0.5817	33	0.05663	24	463	466	477
Z5 Ndl. w/ rounded tips NAB	0.0558	308	22	16	4954	0.1142	0.07234	46	0.5619	37	0.05633	18	450	453	465
3. -Amphibolite dyke (93-PV-6, Fox Roost) 46125-70600															
T1 Brown, clr, Ttn AB	0.3287	141	15	391	506	0.8621	0.06558	40	0.4975	34	0.05502	20	409	410	413
4. -Late syn-D3 cross-cutting granitic dyke (92GD11, Fox Roost) 46400-70125															
Z1 MO clr. cracked pr. AB	0.0060	572	53	18	768	0.6388	0.06413	30	0.4878	25	0.05517	20	401	403	419
Z2 MO cracked pr. AB	0.0738	531	43	111	1441	0.4285	0.06442	156	0.4877	115	0.05491	56	402	403	408
Z3 Needles & pr. AB	0.1940	472	36	124	1687	0.3399	0.06375	50	0.4845	38	0.05513	14	398	401	417
Z4 Needles & pr. AB	0.0346	505	41	14	5040	0.4560	0.06363	24	0.4829	19	0.05504	12	398	400	414
Z5 Sm. cracked pr. NAB	0.1747	562	46	124	3181	0.4508	0.06342	20	0.4820	17	0.05512	08	396	399	417
Z6 Frag. & pr. AB	0.1973	348	23	21	13732	0.1167	0.06589	24	0.5042	18	0.05551	10	411	415	433
T1 Pale brown Ttn AB	0.4650	65	7	763	179	1.0140	0.06513	24	0.5000	42	0.05568	38	407	412	440
5. -Granitic orthogneiss (94-PV-2, Grandy's Brook) 64150-83525															
Z1 M0 sm. pr w/ rd. tips AB	0.0454	355	32	11	6683	0.3392	0.07488	58	0.5804	43	0.05622	24	465	465	461
Z2 M0 pr & frag. AB	0.1586	295	25	28	7793	0.2987	0.07413	32	0.5763	25	0.05638	10	461	462	467
Z3 M0 needles & pr. AB	0.0535	372	33	19	4891	0.3325	0.07340	28	0.5705	23	0.05637	08	457	458	467
T1 Clr. brown Ttn AB	0.4740	241	23	1018	482	0.5942	0.06589	28	0.4989	27	0.05492	14	411	411	409
T2 Clr. brown Ttn AB	0.5086	176	17	789	484	0.6622	0.06562	32	0.4980	31	0.05502	20	410	410	413

1.- Z = zircon; T= titanite; NM = non magnetic(Frantz separation), M0= 0° magnetic, M1= 1° magnetic; s = small (<80 μm), m= medium (>80 and <150 μm), l = large (>150 μm), Ndl. = Needles (1:10 to 1:7 width/length ratio), pr = prisms (1:6 to 1:4), stb = stubby (1:3 to 1:1), clr = clear, eu. = euhedral, y.= yellow, AB = air abraded (Krogh, 1982), NAB = not abraded, rd = rounded, w/ = with, inc = inclusions, frag.= fragment

2.- Uncertainty in sample weight ± 0.001 mg (2 sigma)

3.- Atomic ratios corrected for fractionation and spike, 8 to12 pg Pb blank lab procedure (25 pg- titanite), initial common Pb (Stacey and Kramers, 1975) and 1 pg U blank. 2 sigma errors reported for corrected isotopic ratios.

† Sample location in U.T.M. coordinates, 21TUC UTM zone and 100 km square.

Figures 4.8, 4.9, 4.10

Fig.4.8.- Top: Granitic orthogneiss (Fox Roost, U\Pb sample 93-PV-5) and folded amphibolite enclave. Plan view, folded amphibolite enclave in granitic orthogneiss with mullion-like structures at its terminations. In the bottom half (arrow), an axial planar fabric is partially developed in the granitic orthogneiss. Weak gneissic compositional banding in the orthogneiss is also folded and locally transposed by an apparent dextral shear (D3 deformation).

Fig. 4.9.- Middle: Partially mingled amphibolite dyke intrusive into granitic orthogneiss (Fox Roost). 472 Ma granitic orthogneiss and partially disrupted amphibolite dyke back-veined by felsic magma in a low strain area; the front of the dyke (bottom right) is disrupted as small enclaves in the surrounding felsic material, some enclaves show a compositional banding suggesting mingling. This field relationship could be interpreted either as anatectic melting of the amphibolite or as a mafic dyke intruding into a partially crystallized felsic magma chamber (Fernandez and Barbarin, 1991). The lack of evidence for amphibole-out reactions and anatexis in the 472 Ma granitic orthogneiss favours the second hypothesis. Note high-strain ductile shear zone (D3) in the left of the picture.

Fig.4.10.-Bottom: U\Pb concordia diagram for sample 93-PV-5, granitic orthogneiss (Fox Roost): Z. zircon.

Fig.4.8.- Top: Granitic orthogneiss (Fox Roost, U/Pb sample 93-PV-5) and folded amphibolite enclave. Plan view, folded amphibolite enclave in granitic orthogneiss with mullion-like structures at its terminations. In the bottom half (arrow), an axial planar fabric is partially developed in the granitic orthogneiss. Weak gneissic compositional banding in the orthogneiss is also folded and locally transposed by an apparent dextral shear (D3 deformation).

Fig. 4.9.- Middle: Partially mingled amphibolite dyke intrusive into granitic orthogneiss (Fox Roost). 472 Ma granitic orthogneiss and partially disrupted amphibolite dyke back-veined by felsic magma in a low strain area; the front of the dyke (bottom right) is disrupted as small enclaves in the surrounding felsic material, some enclaves show a compositional banding suggesting mingling. This field relationship could be interpreted either as anatectic melting of the amphibolite or as a mafic dyke intruding into a partially crystallized felsic magma chamber (Fernandez and Barbarin, 1991). The lack of evidence for amphibole-out reactions and anatexis in the 472 Ma granitic orthogneiss favours the second hypothesis. Note high-strain ductile shear zone (D3) in the left of the picture.

Fig.4.10.-Bottom: U/Pb concordia diagram for sample 93-PV-5, granitic orthogneiss (Fox Roost): Z. zircon.

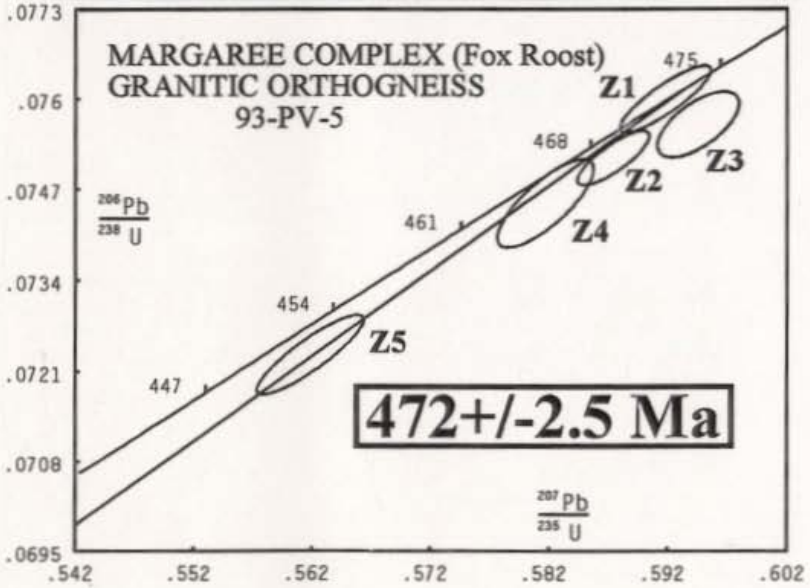
MARGAREE COMPLEX (Fox Roost)
GRANITIC ORTHOGNEISS
93-PV-5
Z1
Z2
Z3
Z4
Z5
475
468
461
454
447
472+/-2.5 Ma
$\frac{206}{238}$ Pb U
$\frac{207}{235}$ Pb U
.0773
.076
.0747
.0734
.0721
.0708
.0695
.542
.552
.562
.572
.582
.592
.602

Margaree orthogneiss , Grandys Brook section:

Fig.4.11.- (Top) Geological map of the lower part of the Grandys Brook section showing the location of the U/Pb sample and the intrusive contact between the Margaree orthogneiss (M.O.) and the country rock Port-aux-Basques gneiss. Small insets: A) Field sketch of the F2-F3 folding of the compositional banding, including leucosomes, in the Port-aux-Basques gneiss (not to scale). B) Field relationships between the metasedimentary Port-aux-Basques gneiss, the Port-aux-Basques granite and a late syn-D3 granite (not to scale). C) Boudinaged and folded amphibolite dyke intrusive into the granitic members of the Margaree orthogneiss at the U-Pb sampling location. (Legend: PaB, Port-aux-Basques).

Figures 4.11, 4.12, 4.13

Fig.4.12.- (Bottom left) U/Pb concordia diagram for the granitic orthogneiss at Grandys Brook (U/Pb sample 94-PV-2). Z, zircon; T, titanite.

Fig.4.13. (Bottom right)- Amphibolite dyke intrusive into 465 Ma granitic orthogneiss. The dyke on right of the picture has been boudinaged during ductile shearing (D3?). The pegmatite patches in the boudin necks are evidence for high-temperature shearing. Field notebook for scale is 20.5 cm long and 12 cm wide.

Margaree orthogneiss , Grandys Brook section:

Fig.4.11.- (Top) Geological map of the lower part of the Grandys Brook section showing the location of the U/Pb sample and the intrusive contact between the Margaree orthogneiss (M.O.) and the country rock Port-aux-Basques gneiss. Small insets: A) Field sketch of the F2-F3 folding of the compositional banding, including leucosomes, in the Port-aux-Basques gneiss (not to scale). B) Field relationships between the metasedimentary Port-aux-Basques gneiss, the Port-aux-Basques granite and a late syn-D3 granite (not to scale). C) Boudinaged and folded amphibolite dyke intrusive into the granitic members of the Margaree orthogneiss at the U-Pb sampling location. (Legend: PaB, Port-aux-Basques).

Fig.4.12.- (Bottom left) U/Pb concordia diagram for the granitic orthogneiss at Grandys Brook (U/Pb sample 94-PV-2). Z, zircon; T, titanite.

Fig.4.13. (Bottom right)- Amphibolite dykes intrusive into 465 Ma granitic orthogneiss. The dyke on right of the picture has been boudinaged during ductile shearing (D3?). The pegmatite patches in the boudin necks are evidence for high-temperature shearing. Field notebook for scale is 20.5 cm long and 12 cm wide.

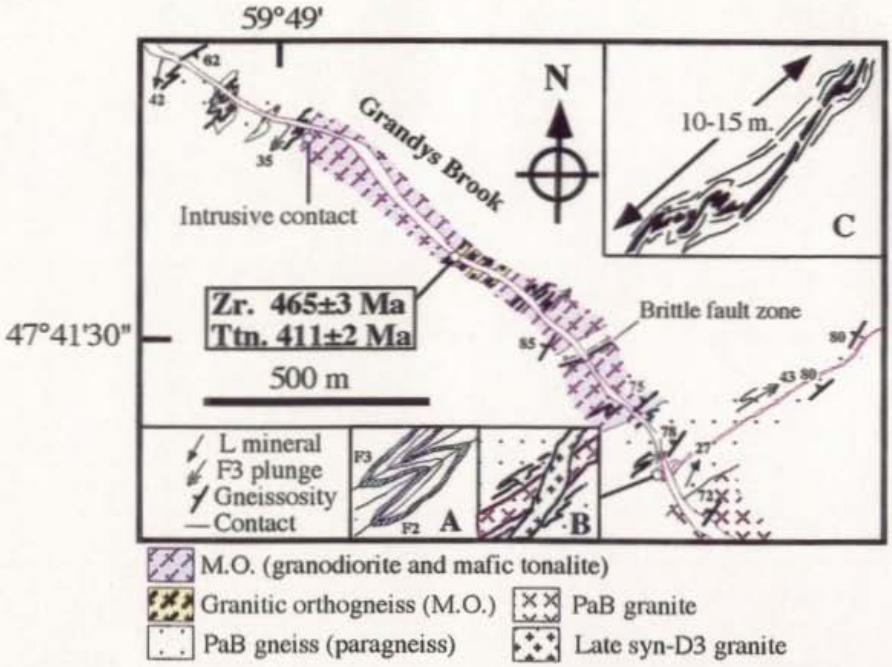
59°49'
47°41'30"
Grandys Brook
N
10-15 m.
C
Intrusive contact
Zr. 465±3 Ma
Ttn. 411±2 Ma
500 m
Brittle fault zone
L mineral
F3 plunge
Gneissosity
Contact
F3
F2
A
B
M.O. (granodiorite and mafic tonalite)
Granitic orthogneiss (M.O.)
PaB granite
PaB gneiss (paragneiss)
Late syn-D3 granite

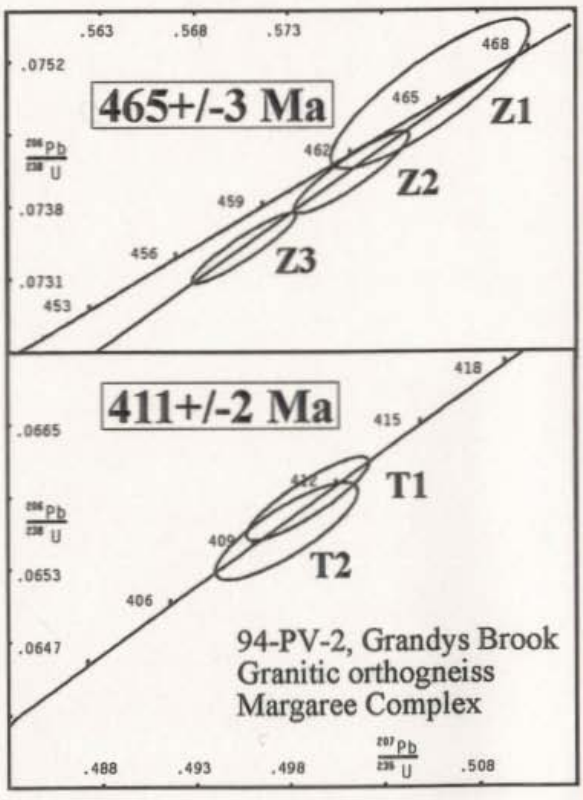
465+/-3 Ma
Z1
Z2
Z3
411+/-2 Ma
T1
T2
94-PV-2, Grandys Brook
Granitic orthogneiss
Margaree Complex
206Pb/238U
207Pb/235U

Figures 4.14, 4.15, 4.16

Fig.4.14. (Top left) - Fox Roost-Margaree, amphibolite (U-Pb sample 93-PV-6) intrusive into hornblende-bearing felsic granodioritic orthogneiss.

Fig.4.15. (Top right) - U-Pb concordia diagram for titanite from sample 93-PV-6.

Fig.4.16. (Bottom) - Titanite (410 Ma U-Pb cooling/recrystallization age) aligned with green hornblende and biotite defining the fabric in sample 93-PV-6. Mineral assemblage: hornblende + plagioclase (≈An 30) + biotite+ titanite + quartz. Most titanites occupy interstitial positions (arrow) and have straight boundaries suggesting that they have recrystallized with the rest of the mineral assemblage following D3. L mineral (amphibole) in this sample is parallel to the plunge of the F3 folds.

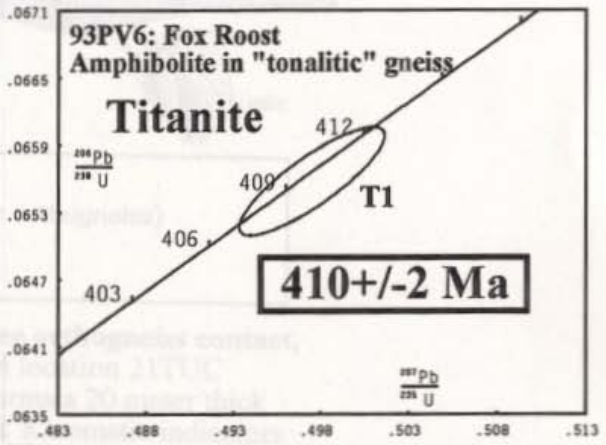
93PV6: Fox Roost
Amphibolite in "tonalitic" gneiss
Titanite
412
409
406
403
T1
410+/-2 Ma
.0671
.0665
.0659
.0653
.0647
.0641
.0635
.483
.488
.493
.498
.503
.508
.513

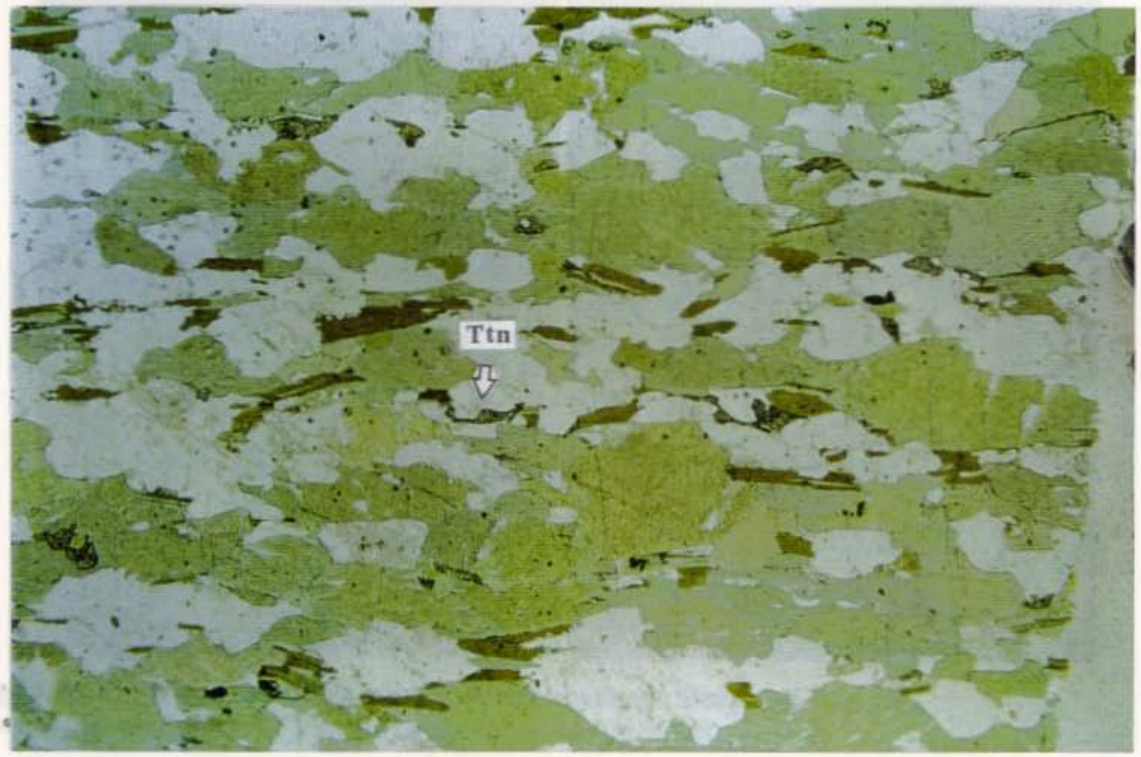
Ttn

Fig.4.19.(Top) - Late syn-D3 granitic dyke intrusive into "migmatitic" gneiss (Fox Roost, U/Pb sample 92-GD-11). Pen for scale is 14 cm long.

Fig.4.20. (Middle) - Detail of the intrusive contact and the syn-magmatic fabric in the granitic dyke.

Fig.4.21. (Bottom) - U/Pb concordia diagram for the late-syn D3 granitic dyke (sample 92-GD-11): Z, zircon; T, titanite.

Figures 4.19, 4.20, 4.21

Fig.4.19.(Top) - Late syn-D3 granitic dyke intrusive into "migmatitic" gneiss (Fox Roost, U/Pb sample 92-GD-11). Pen for scale is 14 cm long.

Fig.4.20. (Middle) - Detail of the intrusive contact and the syn-magmatic fabric in the granitic dyke.

Fig.4.21. (Bottom) - U/Pb concordia diagram for the late-syn D3 granitic dyke (sample 92-GD-11): Z, zircon; T, titanite.

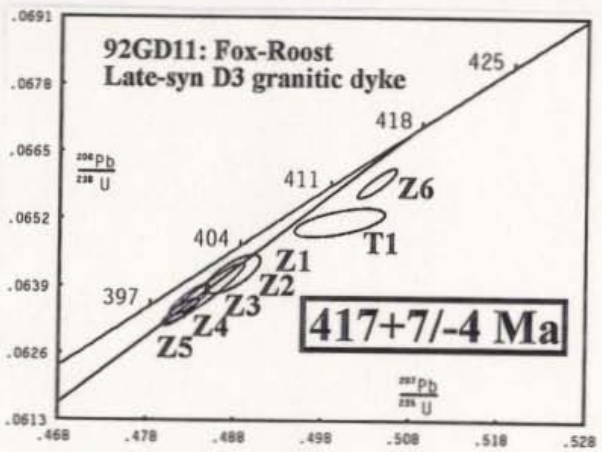
92GD11: Fox-Roost
Late-syn D3 granitic dyke
425
418
411
404
397
Z6
T1
Z1
Z2
Z3
Z4
Z5
417+7/-4 Ma
.0691
.0678
.0665
.0652
.0639
.0626
.0613
.468
.478
.488
.498
.508
.518
.528

Fig. 4.22. (Top left) - Cross-view, Margaree orthogneiss, Fox Roost: F2-F3 interference folding cross-cut by late pegmatites.

Fig.4.23. (Top right)-Plan view, F3 overprint of a D2 boudin in a quartzo-feldspathic paragneiss, contact between the Port-aux-Basques gneiss and the Margaree orthogneiss at Margaree.

Fig.4.24. (Bottom right)- Plan view, closure of an F2 fold overprinted by F3 folding in migmatitic Port-aux-Basques gneiss. Dolphin road, only 20 m apart from Margaree orthogneiss outcrops. Both the anatectic granitic dyke and the leucosomes are aligned with gneissosity (S0-S2?). The leucosomes were produced by muscovite-out reactions (Burgess et al., 1995), note the contrast in the abundance of felsic material in the "migmatitic" gneiss at Fox Roost (fig. 4.19).

Figures 4.22, 4.23, 4.24, 4.25

Fig.4.25. (Bottom left)- **Plan view, amphibolite in F3 ductile shear zone (Margaree orthogneiss, Margaree-Fox Roost).** Asymmetric amphibolite boudin/enclave indicates an apparent dextral shear sense, this is also supported by the small C'-like offsets of the amphibolite.

Fig. 4.22. (Top left) - **Cross-view, Margaree orthogneiss, Fox Roost: F2-F3 interference folding cross-cut by late pegmatites.**

Fig.4.23. (Top right)-**Plan view, F3 overprint of a D2 boudin in a quartzo-feldspathic paragneiss, contact between the Port-aux-Basques gneiss and the Margaree orthogneiss at Margaree.**

Fig.4.24. (Bottom right)- **Plan view, closure of an F2 fold overprinted by F3 folding in migmatitic Port-aux-Basques gneiss**. Dolphin road, only 20 m apart from Margaree orthogneiss outcrops. Both the anatectic granitic dyke and the leucosomes are aligned with gneissosity (S0-S2?). The leucosomes were produced by muscovite-out reactions (Burgess et al., 1995), note the contrast in the abundance of felsic material in the "migmatitic" gneiss at Fox Roost (fig. 4.19).

Fig.4.25. (Bottom left)- **Plan view, amphibolite in F3 ductile shear zone (Margaree orthogneiss, Margaree-Fox Roost)**. Asymmetric amphibolite boudin/enclave indicates an apparent dextral shear sense, this is also supported by the small C'-like offsets of the amphibolite.


1

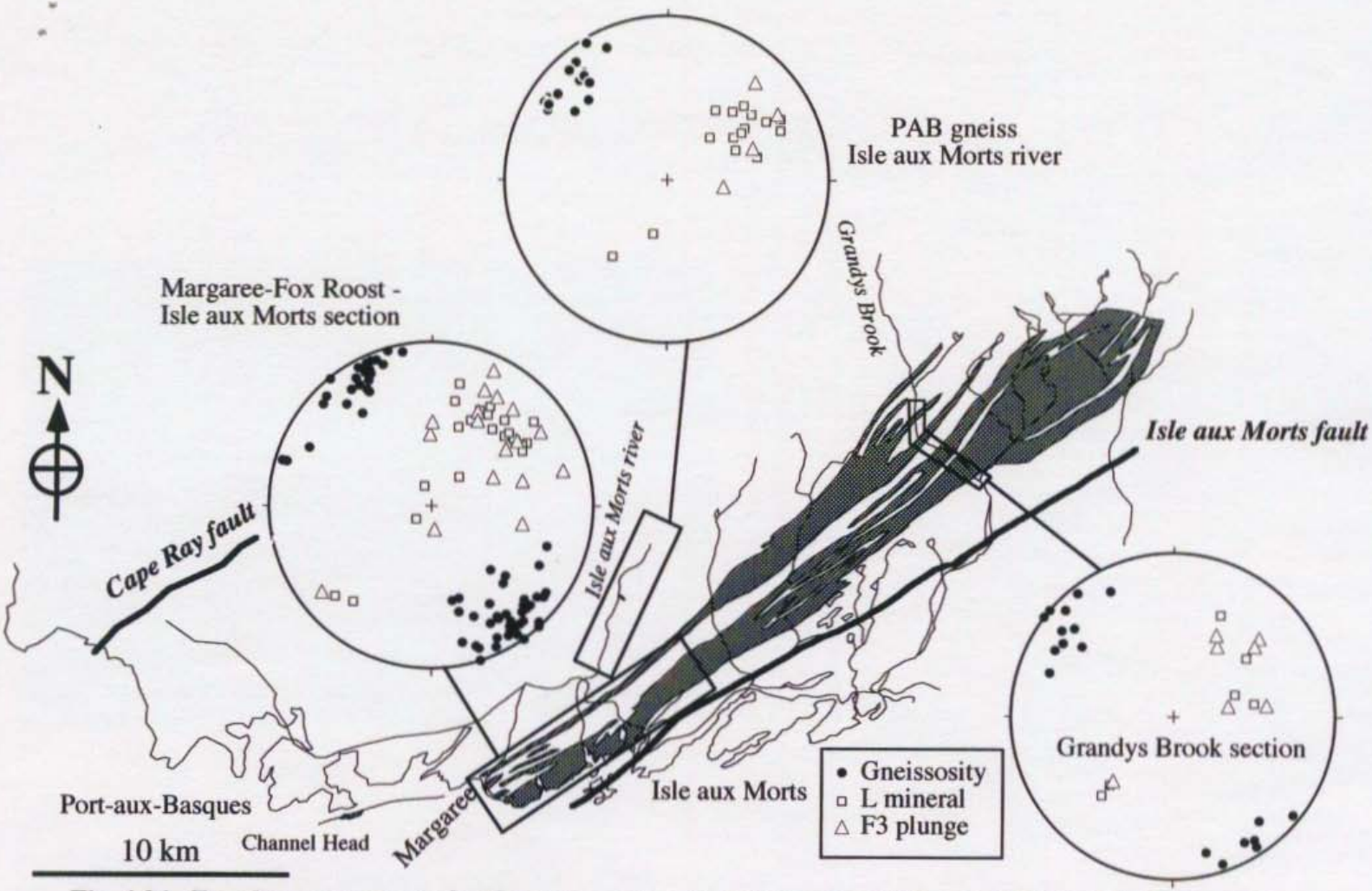

Fig. 4.26.- Equal area stereonets for the gneissosity, mineral lineation (90% amphibole) and plunge of F3 folds in the Margaree orthogneiss and the surrounding Port-aux-Basques gneiss.

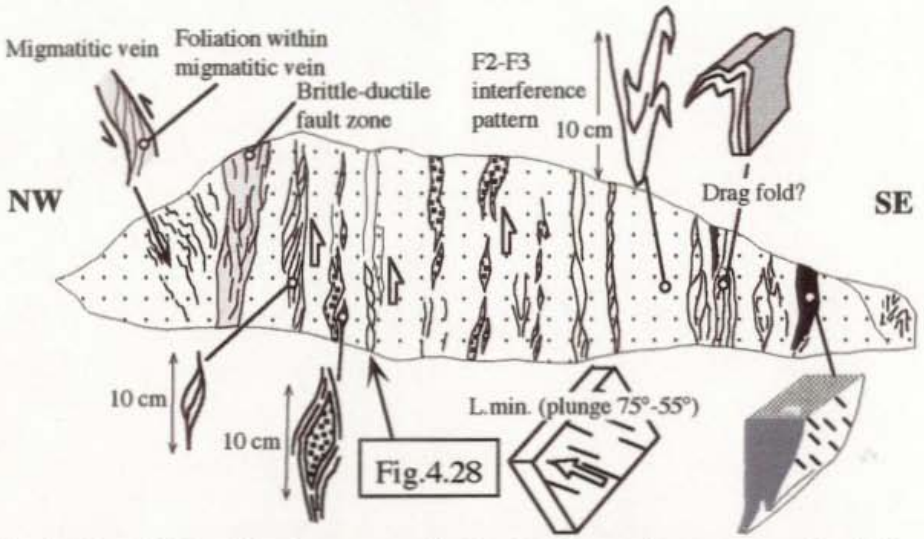

Fig. 4.27 .- D3 ductile shear zone in the Port-aux-Basques gneiss. Kinematic indicators suggest an oblique top to the southwest motion. Black, amphibolite; pattern, pegmatite (pre-D3). Location: road cut before the Isle-aux-Morts welcome post. Approximate total length of the outcrop is 30 meters.

Fig.4.28.- D3 deformation, detail of back rotated segments of a competent quartzo-feldspathic layer in the Port aux Basques gneiss. Asymmetrical extensional shear bands indicating a relative thrusting motion are responsible for the asymmetric boudinage.

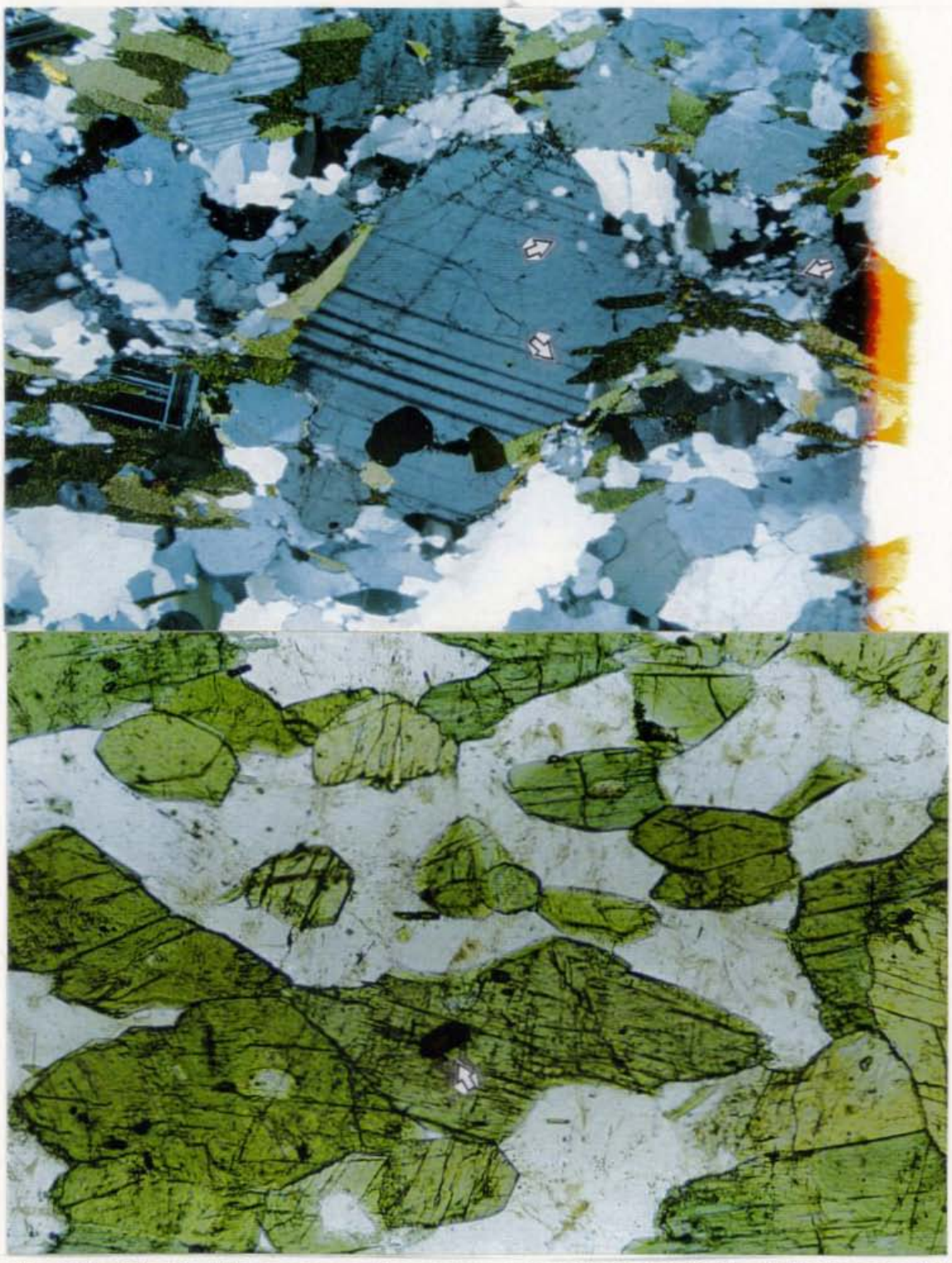

Fig.4.29 (Top).- Margaree orthogneiss, microtexture of the 472 Ma granitic orthogneiss. Large plagioclase crystal pinning small quartz and biotite (arrows), suggesting high temperature grain boundary migration recrystallization. The quartz grains show parallel deformation bands (recovery) and small areas with dynamic recrystallization (arrow). Field of view 5.2 mm long.

Fig.4.30 (Bottom).- Margaree orthogneiss, granoblastic texture in amphibolite. Mineral assemblage: green hornblende, plagioclase (andesine) and rutile. Arrow: rutile inclusion in hornblende. Field of view 1.3 mm long.

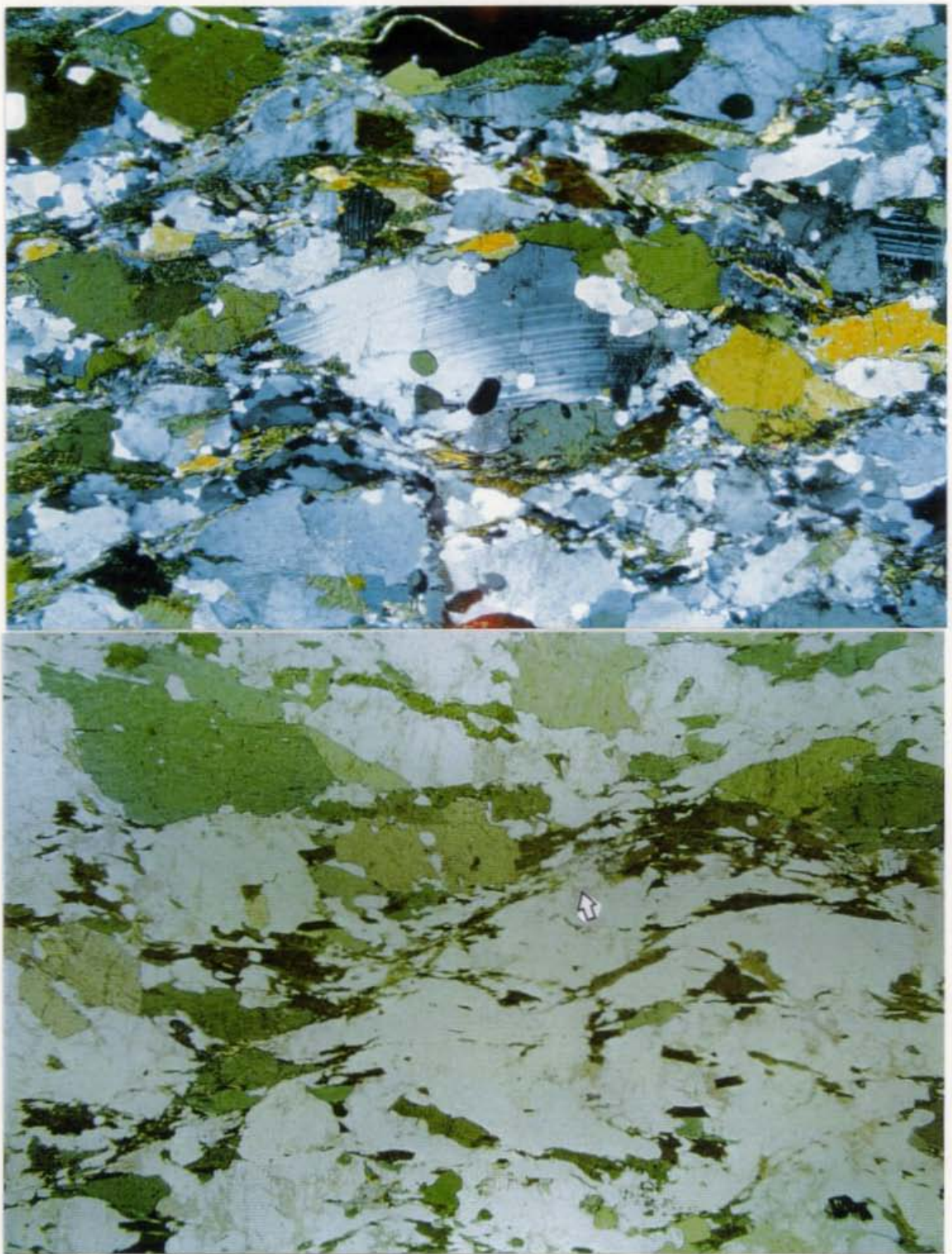

Fig.4.31.- Margaree orthogneiss, D3 microstructural features in weakly recrystallized banded gneiss: (Top) C'-like high strain bands with grain reduction and dynamic recrystallization of quartz. The plagioclase in the center shows slightly bent and tapered twins indicating intracrystalline deformation. Field of view is 5.2 mm long. **(Bottom)** Shear band, antithetic to the C'-like bands, showing associated growth of biotite and epidote Field of view is 5.2 mm long.

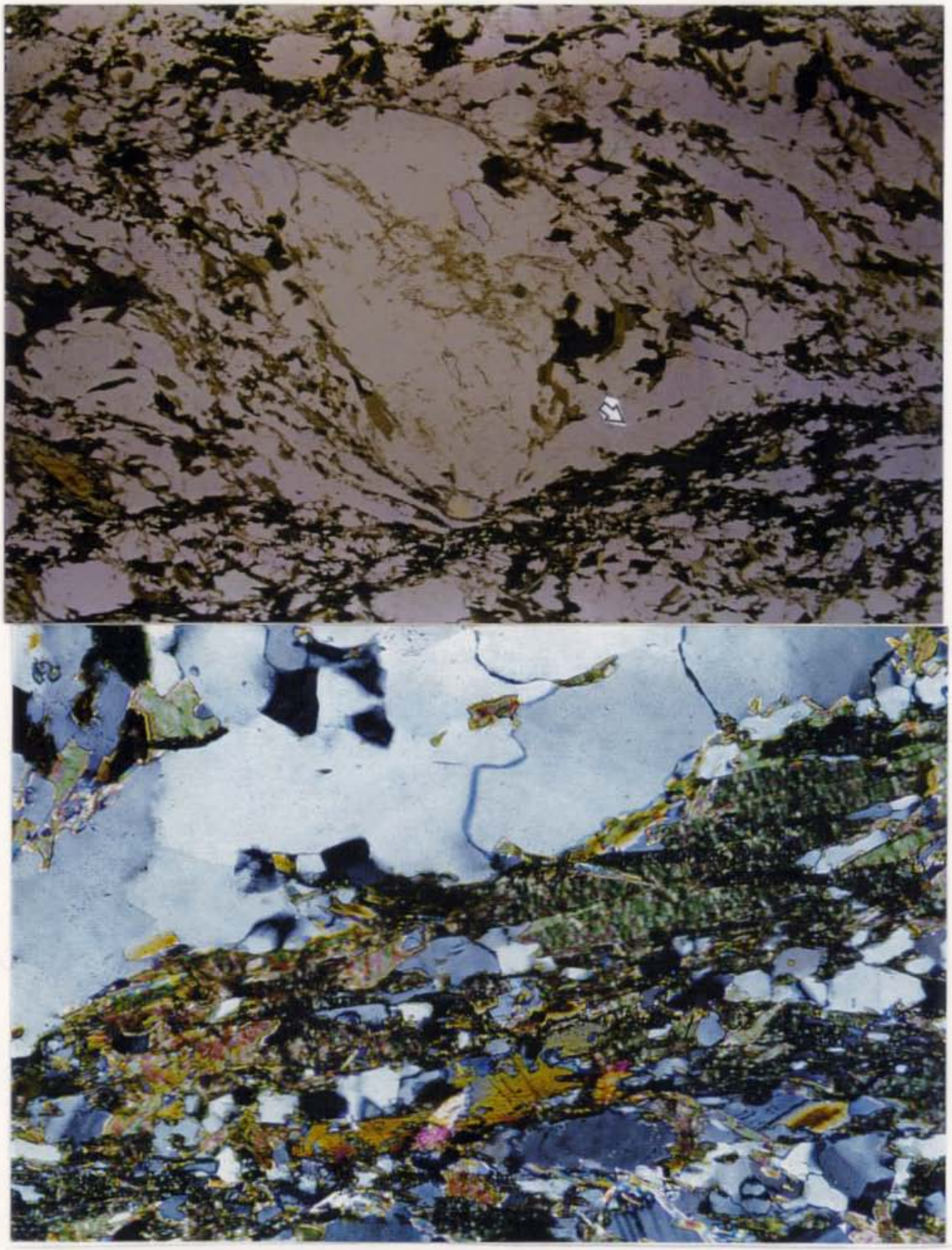

Fig.4.32.- Margaree orthogneiss, microtexture of late-/post-D3 mylonites: **(Top)** Plagioclase porphyroclast with winged quartz-rich ribbons surrounded by a small grain mylonitic matrix. Arrow, detailed area shown in bottom figure. Field of view is 5.2 mm long. **(Bottom)** Detail of quartz subgrains and ameboid-lobate quartz-quartz contacts suggesting dynamic recrystallization in the quartz ribbons. Lower portion, fine grain matrix formed by aligned biotite, epidote and white mica, and quartz, plagioclase and feldspar (?). Field of view is 1.32 mm long.

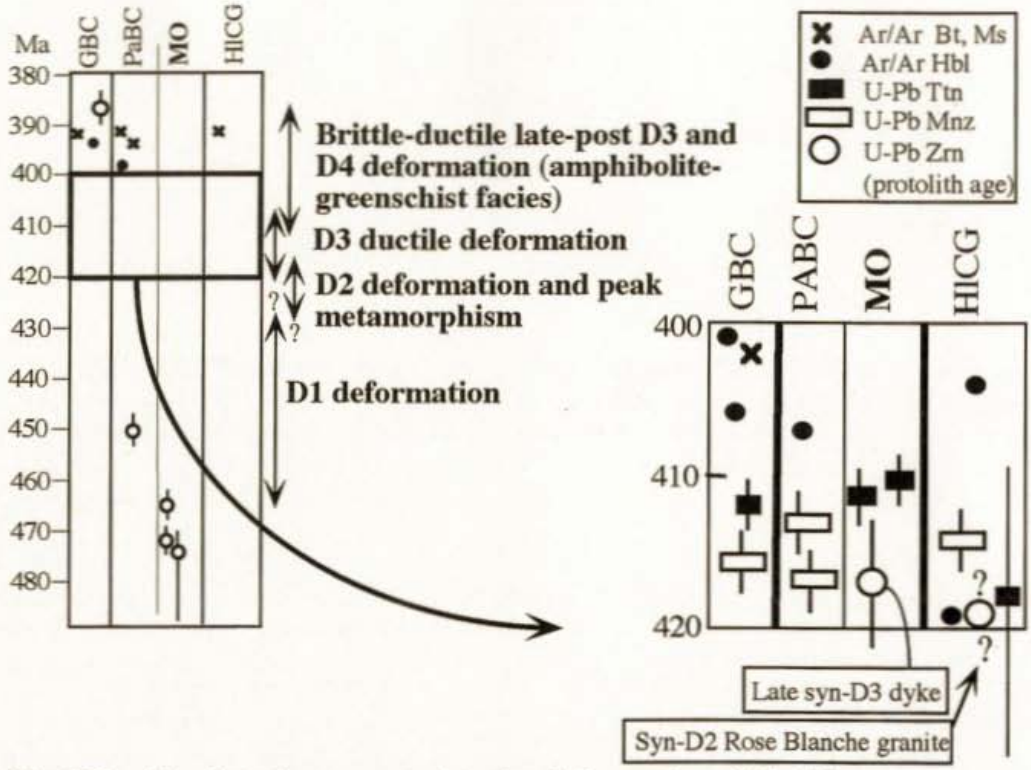

Fig.4.33.- Absolute time constraints for deformation of the Margaree orthogneiss and the associated Port-aux-Basques gneiss. GBC, Grand Bay Complex, PaBC, Port-aux-Basques complex; **MO, Margaree orthogneiss**; HlCG, Harbour le Cou Group. Ar/Ar data after Burgess et al. (1995) and Dubé et al. (1996). Zr data: MO, this study; PaBC (Van Staal et al., 1994 and Dubé et al., 1996). Mnz data: Dunning unpublished. Ttn data: GBC (Dunning et al., 1990); MO, this study ; HlCG (Burgess et al., 1995).

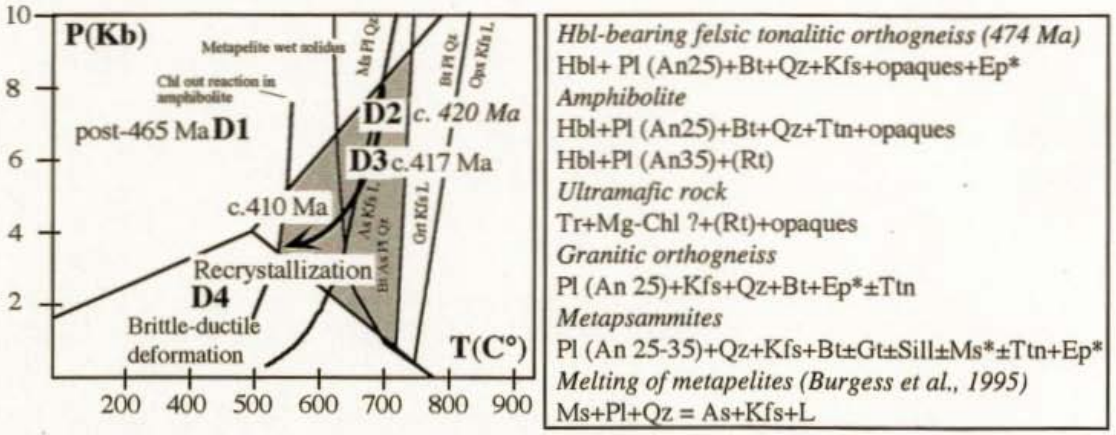

Fig.4.34.- P-T-t-d path for the Margaree orthogneiss and stable mineral assemblages: P-T-t path after Burgess et al. (1995). Pattern area, stability field for the mineral assemplages of the Margaree orthogneiss and surrounding PaB gneiss. Triple point and reaction curves after figures 10-16 and 11-16 of Spear (1993). (*) Growth during D3.

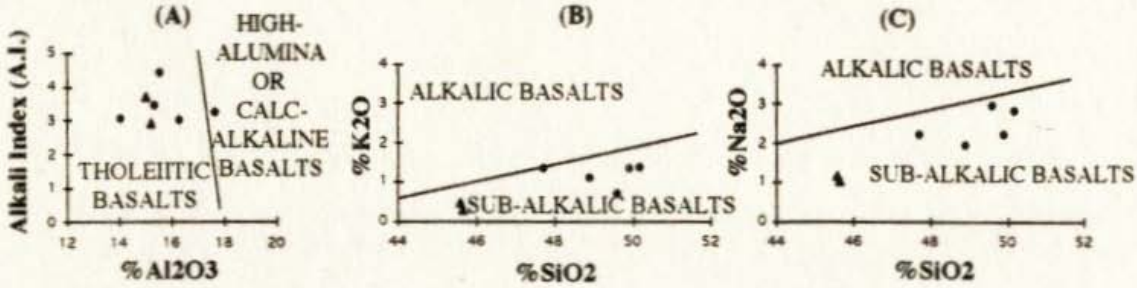

Fig.4.35.- Margaree orthogneiss: mafic and ultramafic rocks: (**A**) Alkalic Index (A.I.) vs. Al2O3 basalt classification (Middlemost, 1975), G-MA-3 is the sample classified in the high-alumina field. Classification of alkalic and subalkalic basalts (**B**) K2O vs. SiO2 and (**C**) Na2O vs. SiO2 (Middlemost, 1975). Triangles, ultramafic rocks; filled circles, amphibolites.

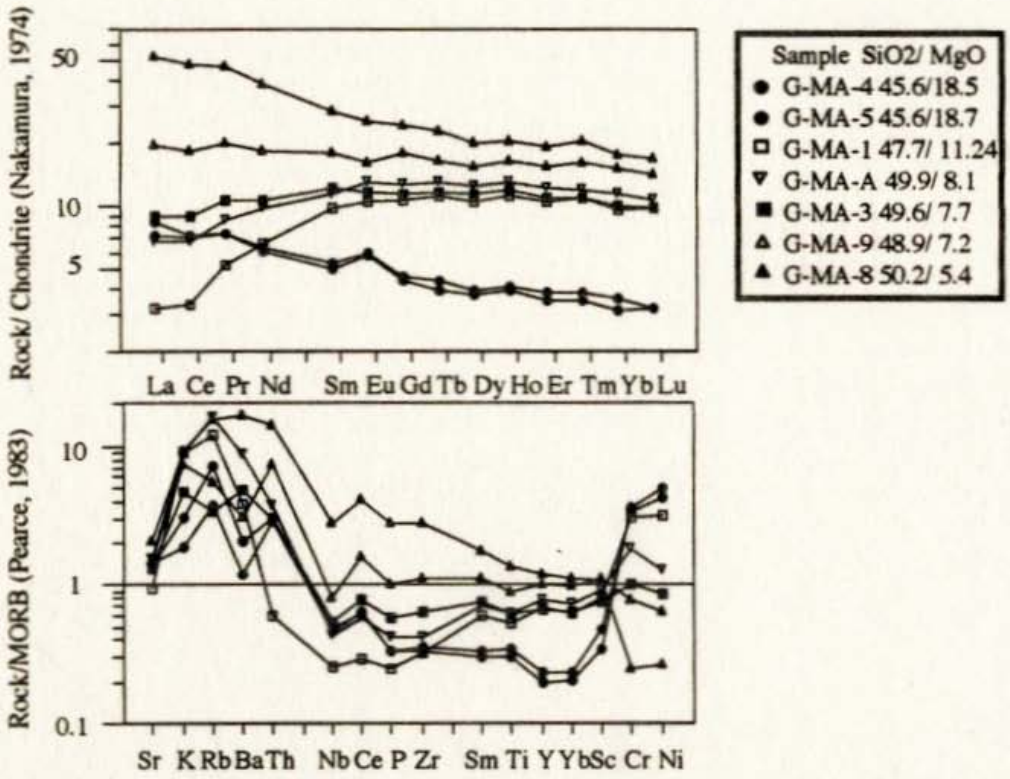

Fig. 4.36.- Margaree orthogneiss: mafic and ultramafic rocks. (**A**) REE multielement patterns. (**B**) MORB (Pearce, 1983) normalized multielement patterns. Filled circles, ultramafics; other symbols, amphibolites.

TABLE 4.2.- MAJOR AND TRACE ELEMENT ANALYSES, MARGAREE ORTHOGNEISS.

Sample	G-MA-4	G-MA-5	G-MA-1	G-MA-9	G-MA-3	G-MA-A	G-MA-8	G-MA-B	G-MA-C	G-MA-2	G-MA-6
Rock type	*ultra-mafic*	*ultra-mafic*	*amphi-bolite*	*amphi-bolite*	*amphi-bolite*	*amphi-bolite*	*amphi-bolite*	*grano-diorite*	*grano-diorite*	*granite*	*granite*
SiO_2	45.58	45.64	47.71	48.9	49.6	49.9	50.18	62.17	64.85	71.12	74.07
TiO_2	0.52	0.45	0.79	1.31	0.92	0.93	2.02	0.61	0.5	0.37	0.32
Al_2O_3	15	15.2	15.52	14.02	17.63	16.26	15.34	17.01	16.25	14.46	12.92
Fe_2O_3T	10.58	10.29	9.7	12.38	8.95	9.93	12.83	5.46	4.76	3.44	1.9
MnO	0.15	0.15	0.19	0.2	0.14	0.19	0.2	0.1	0.1	0.07	0.03
MgO	18.47	18.67	11.24	7.24	7.69	8.14	5.37	2.73	2.11	1.02	0.54
CaO	8.61	8.55	10.57	10.47	11.07	10.18	8.65	5.31	4.35	3.21	1.5
Na_2O	1.16	1.03	2.2	1.94	2.93	2.2	2.82	3.58	3.01	3.86	2.79
K_2O	0.46	0.28	1.33	1.1	0.69	1.34	1.37	1.62	2.49	1.32	4.06
P_2O_5	0.04	0.04	0.03	0.12	0.07	0.05	0.33	0.2	0.19	0.08	0.05
Total	100.57	100.3	99.28	97.68	99.69	99.12	99.11	98.79	98.61	98.95	98.18
L.O.I.	3.49	3.77	1.02	0.73	0.59	0.72	0.71	0.87	0.82	0.36	0.27
Ba	42	24	77	62	96	175	338	519	1007	364	896
Rb	14	7	24	11	7	32	31	73	94	45	91
Sr	163	173	113	178	156	185	252	351	353	182	147
Y	7	6	20	30	20	23	35	18	15	12	6
Zr	32	30	29	99	58	37	253	227	215	123	185
Nb	2	2	-	3	2	2	10	11	12	9	7
Pb	-	-	4	9	-	7	6	9	18	-	15
Ga	12	11	14	17	16	17	21	19	17	14	13
Zn	49	40	61	78	51	63	82	32	30	12	-
Cu	15	5		127	29		103	5	6	7	-
Ni	382	452	283	57	78	116	24	10	9	-	-
V	101	88	212	350	213	245	387	132	103	43	23
Sc	19	14	32	44	30	37	43	17	14	12	8
Cr	846	888	772	196	254	451	62	29	26	8	25
La	2.4	2.8	1.1	6.5	3.0	2.2	17.3	38.8	25.8	20.2	16.9
Ce	6.1	6.3	3.0	15.9	7.8	5.9	41.0	73.4	50.6	40.6	47.7
Pr	0.9	0.9	0.6	2.3	1.2	1.0	5.5	7.8	5.5	4.8	3.8
Nd	4.0	3.8	4.2	11.5	6.7	6.1	24.0	27.5	19.8	18.6	13.7
Sm	1.1	1.0	2.0	3.7	2.5	2.3	5.7	4.6	3.5	3.9	2.8
Eu	0.5	0.4	0.8	1.2	0.9	1.0	2.0	1.1	0.9	0.8	0.7
Gd	1.2	1.2	2.9	4.9	3.1	3.5	6.7	4.0	3.0	3.4	2.3
Tb	0.2	0.2	0.5	0.8	0.6	0.6	1.1	0.6	0.5	0.5	0.3
Dy	1.4	1.3	3.6	5.3	3.9	4.2	6.9	3.8	2.9	2.6	1.8
Ho	0.3	0.3	0.8	1.2	0.8	0.9	1.4	0.8	0.6	0.5	0.4
Er	0.9	0.8	2.3	3.5	2.4	2.7	4.3	2.2	1.7	1.4	0.9
Tm	0.1	0.1	0.3	0.5	0.3	0.4	0.6	0.3	0.3	0.2	0.1
Yb	0.8	0.7	2.1	3.3	2.2	2.5	3.8	2.2	1.8	0.9	0.7
Lu	0.1	0.1	0.3	0.5	0.3	0.4	0.6	0.3	0.3	0.1	0.1
Th	0.6	0.6	0.1	1.5	0.6	0.7	2.8	14.2	11.8	6.0	10.9

Major element concentrations in weight % (XRF fused pellet analyses). All Fe is given as Fe3+ oxide. Trace element concentration in ppm. Ba, Rb, Sr, Y, Zr, Nb, Pb, Ga, Zn, Cu, Ni, V, Sc and Cr were analyzed by XRF (press pellets). The REE and Th were analyzed by Na2O2 sinter ICP-MS analysis. Details of the analytical techniques, including limits of detection and precision, are given in the appendix.

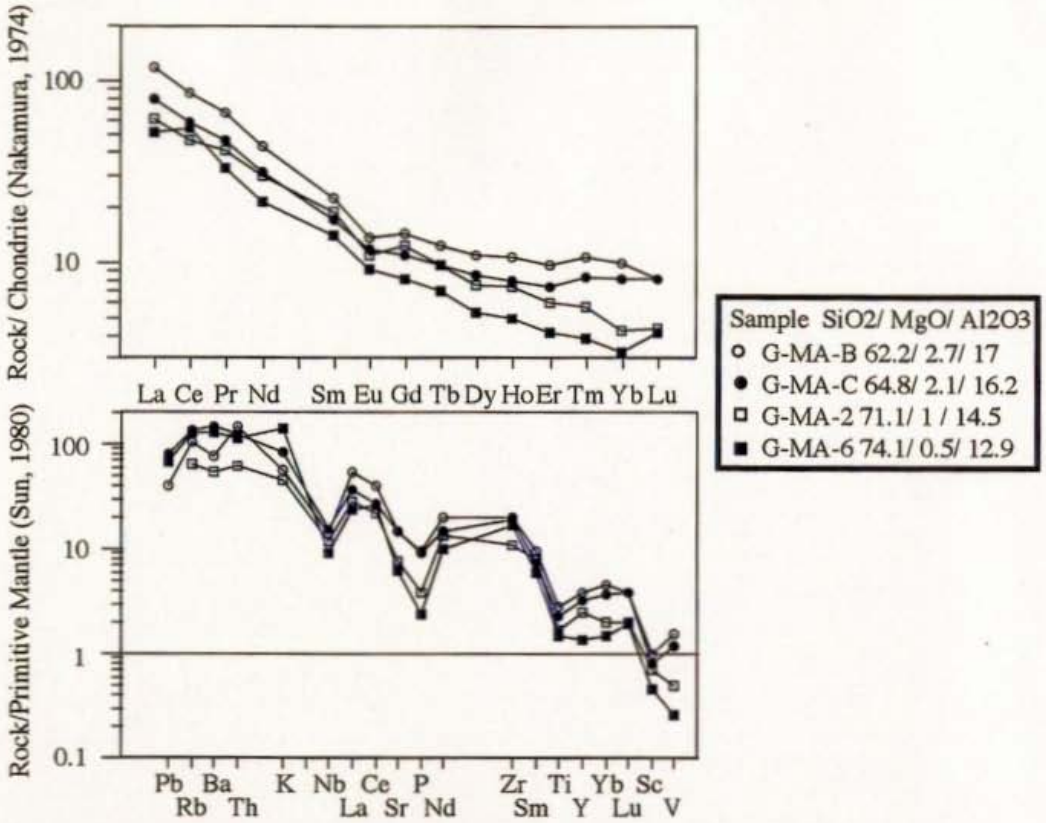

Fig. 4.37.- Margaree orthogneiss, tonalitic and granitic orthogneisses. (**A**) REE element multielement patterns. (**B**) Primitive mantle (Sun, 1980)normalized multielement pattern. Circles, Hbl-bearing tonalitic orthogneiss (474+4/-14 Ma); squares, Bt-bearing granitic orthogneiss (472±2.5 Ma).

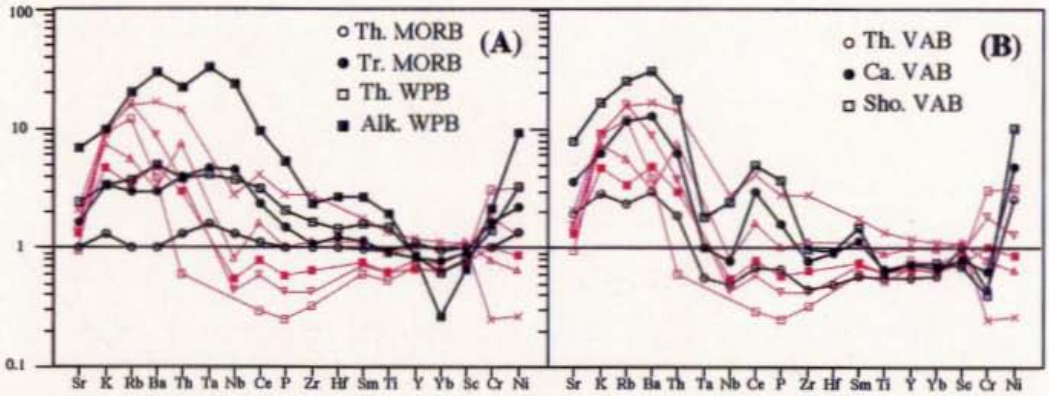

Fig. 4.38. - MORB (Pearce, 1983) - normalized multielement patterns from modern tectonic environments (black; after Pearce, 1983) superposed to the amphibolites from the Margaree orthogneiss (red). Th., tholeiitic; Tr., transitional; Alk, alkaline; Ca, calc-alkaline; Sho, shoshonitic; MORB, mid ocean ridge basalt; WPB, within plate basalt; VAB, volcanic arc basalt. Symbols for the Margaree amphibolites as in fig. 4.36.

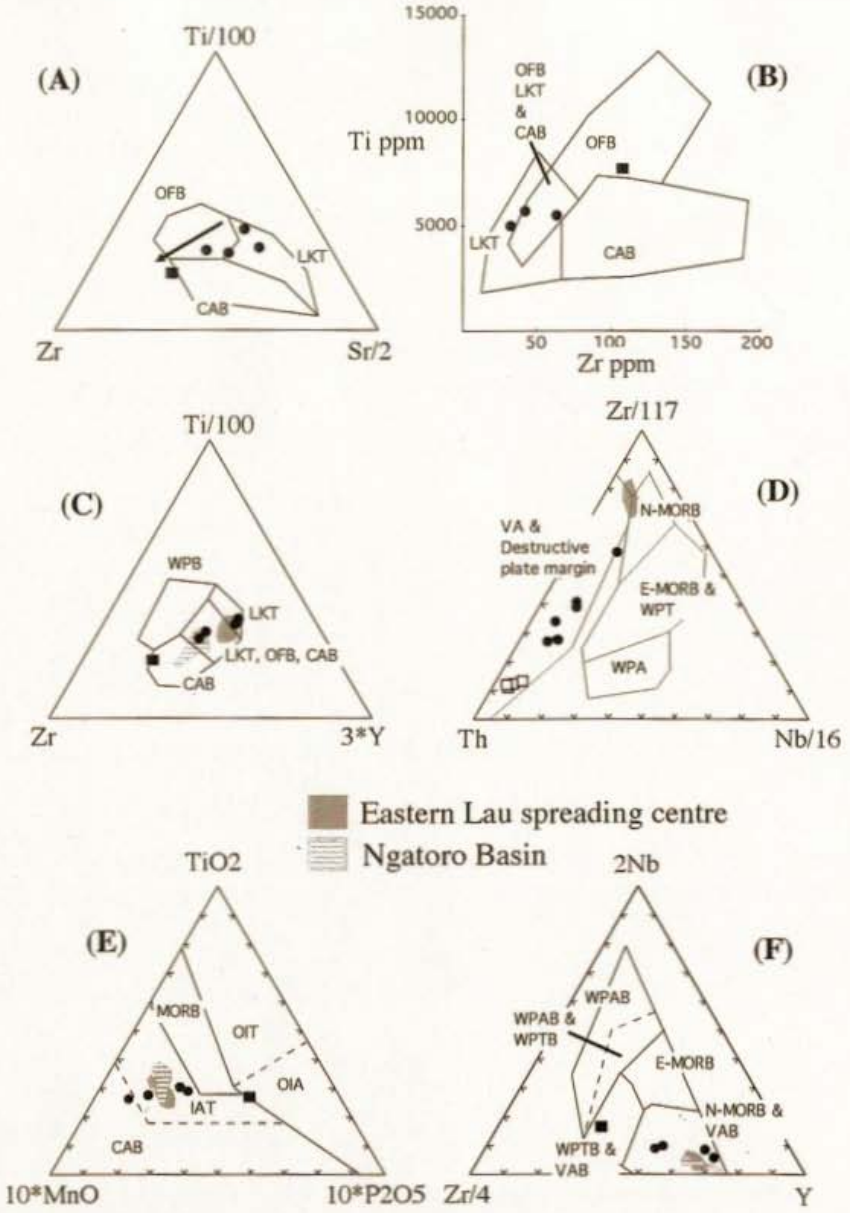

Fig. 4.39.- Tectonic discrimination diagrams for the amphibolites of the Margaree orthogneiss: (A) Ti-Zr-Sr diagram (Pearce and Cann, 1973); (B) Ti vs. Zr diagram (Pearce and Cann, 1973); (C) Ti-Zr-Y diagram (Pearce and Cann, 1973); (D) Zr-Th-Nb diagram (Wood, 1980 with modifications in Jenner, 1996); (E) TiO2-MnO-P2O5 diagram (Mullen, 1983); (F) Nb-Zr-Y diagram (Mechesde, 1986). Amphibolites, filled circles; filled square, LREE enriched amphibolite (50.2% SiO2, 5.4% MgO). Tonalitic and granitic orthogneisses, open squares in diagram **D**. Ultramafics also included in D. Modern back-arc basalts from the SW Pacific Eastern Lau spreading centre (Lau Basin; Pearce et al., 1995) and the Ngatoro Basin (Gamble et al., 1995) for comparison.

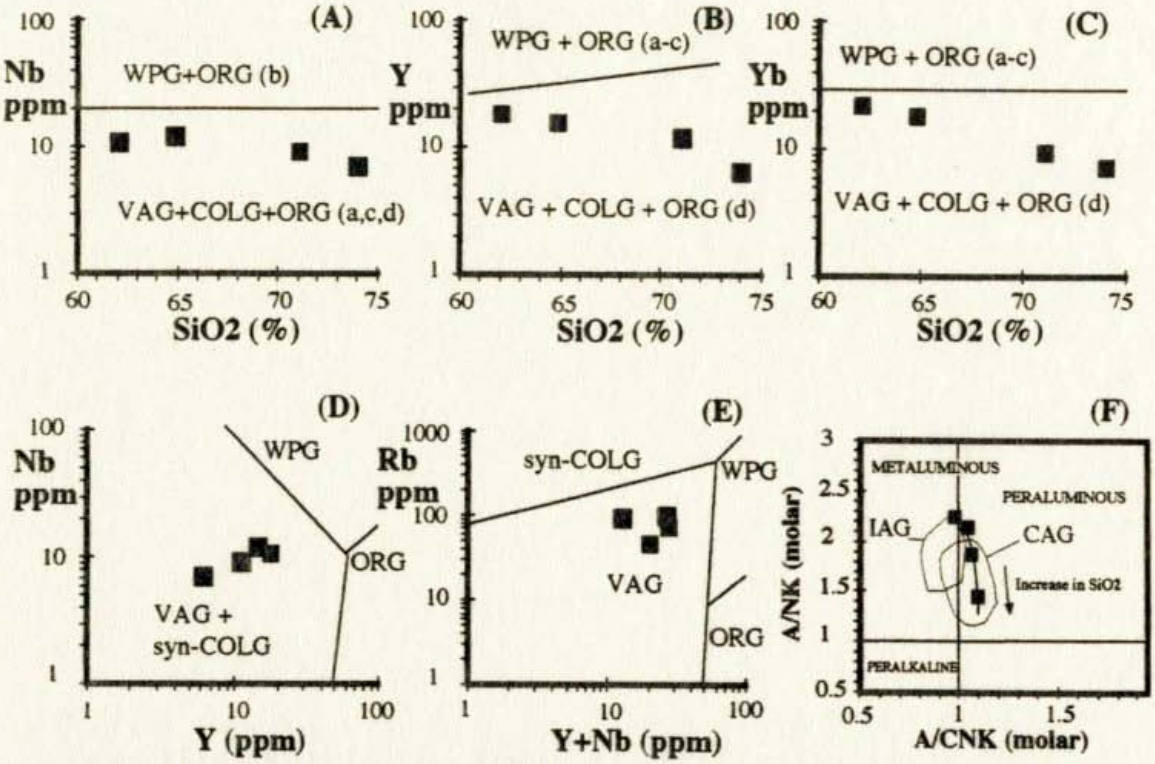

Fig.4.40.- Tectonic discrimination diagrams for granitic rocks, Margaree tonalitic and granitic orthogneisses. Diagrams **A, B, C, D, E** after Pearce et al. (1984). VAG, volcanic arc granitoid; WPG, within plate granitoid; ORG, ocean ridge granitoid; syn-COLG, syn-collisional granitoid. Diagram **F** (Maniar and Piccoli, 1989). A/NK, Al2O3 / (Na2O + K2O)(molar) ; A/CNK, Al2O3 / (CaO+ Na2O+ K2O) (molar).

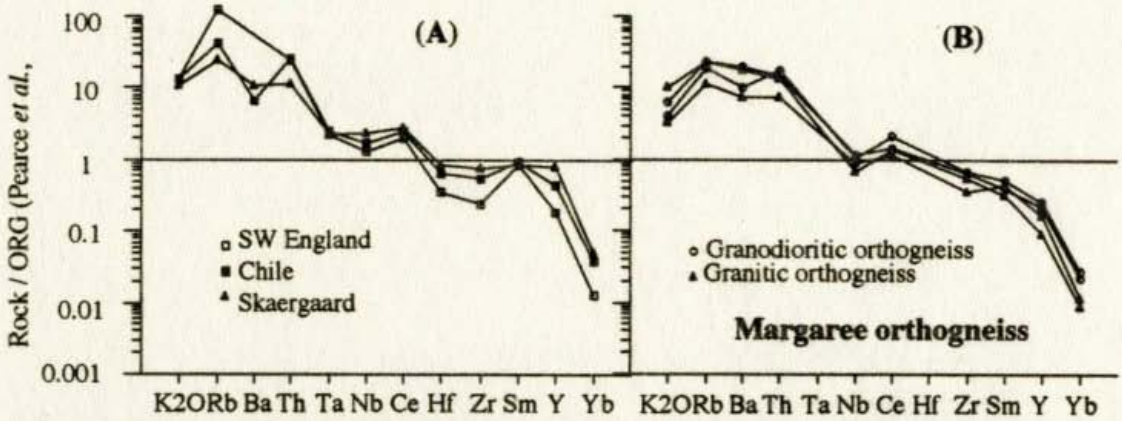

Fig.4.41.- ORG (Ocean Ridge granite; Pearce et al., 1984) - normalized multielement diagram: (A) open squares, Collisional granite from SW England (COLG, continent-continent collision); filled squares, volcanic arc granite from Chile (VAG, active continental margin); filled triangle, Skaergaard granite (WPG, attenuated continental crust) (B) Margaree tonalitic (granodioritic) and granitic orthogneisses.

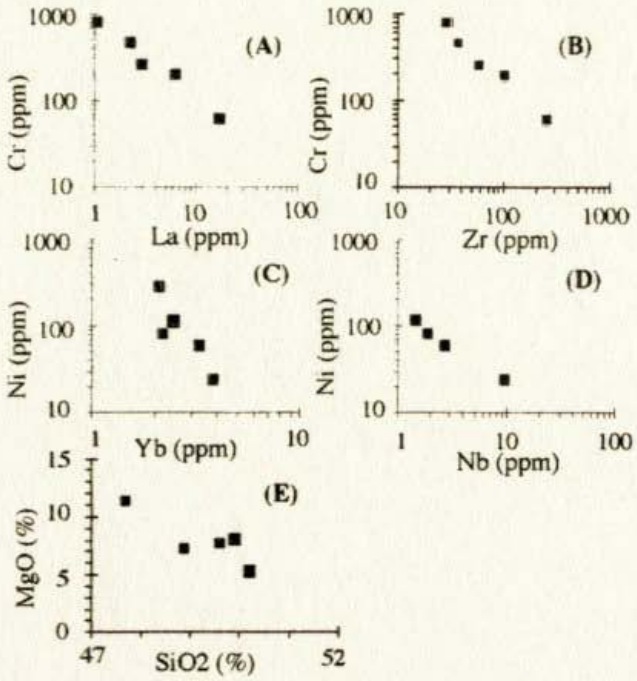

Fig.4.42. .- Margaree orthogneiss, amphibolites: (A, B,C,D) log-log highly compatible (Ni, Cr) vs. incompatible (La, Zr, Yb, Nb) diagrams. Note the linear, fractionation-like trends defined by the samples. **(E) MgO vs. SiO2 diagram.**

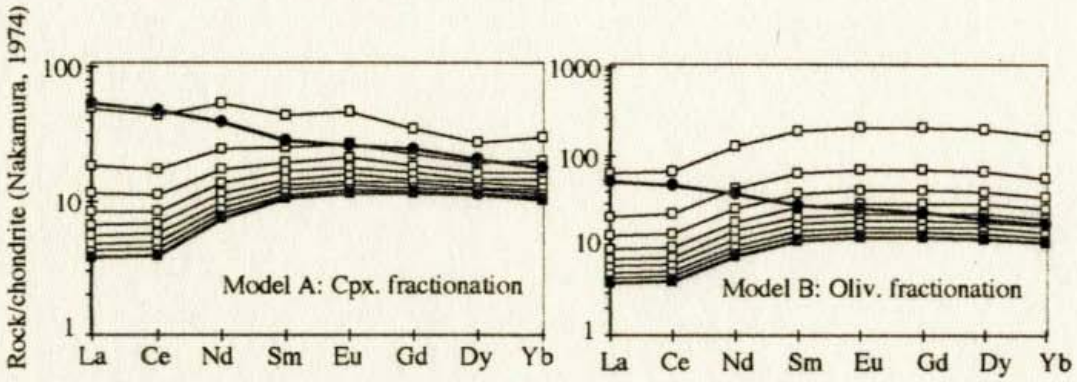

Fig. 4.43. .- Crystal fractionation REE element modelling: REE element patterns normalized to chondrite (Nakamura, 1974). Crystal fractionation equations after Hanson (1989); Kd's for olivine and clinopyroxene after Henderson (1984). Source (sample G-MA-1, 11.2% MgO), filled squares; model fractionates (15% fractionation intervals), open squares; Sample G-MA-8 (50.2% SiO2, 5.4% MgO), filled circles.

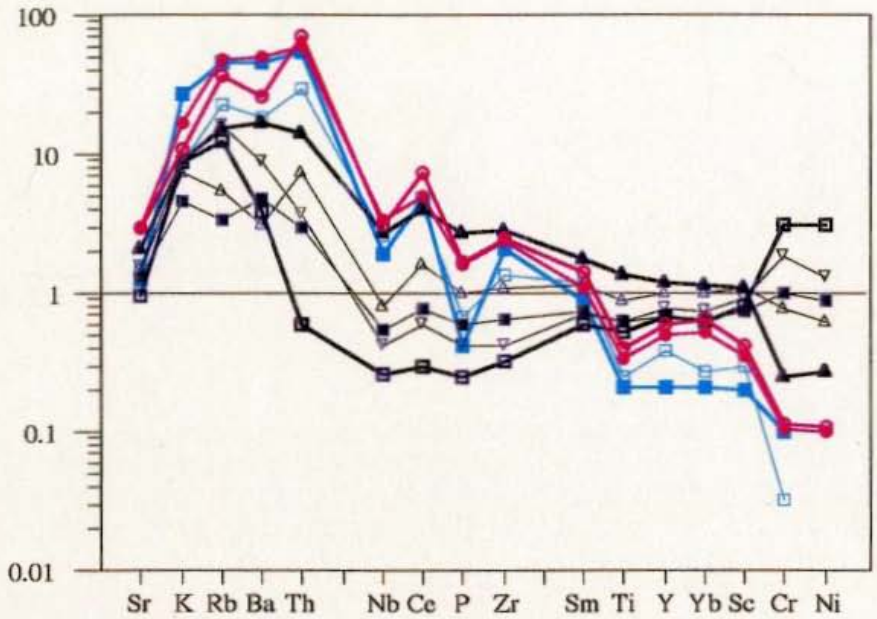

Fig.4.44.- MORB (Pearce, 1983) - normalized multielement diagram for the Margaree orthogneisses (ultramafic rocks excluded). Black, amphibolites; blue, granitic orthogneisses; red, tonalitic orthogneisses. The tonalitic orthogneisses have the most enriched patterns indicating that they are not a product of simple binary mixing between mafic and felsic (granitic) magmas. The amphibolite G-MA-8 is enriched in HFSE, mid and HREE with respect to the rest of the samples, indicating that was not contaminated by the tonalitic and/or granitic sources (or magmas).

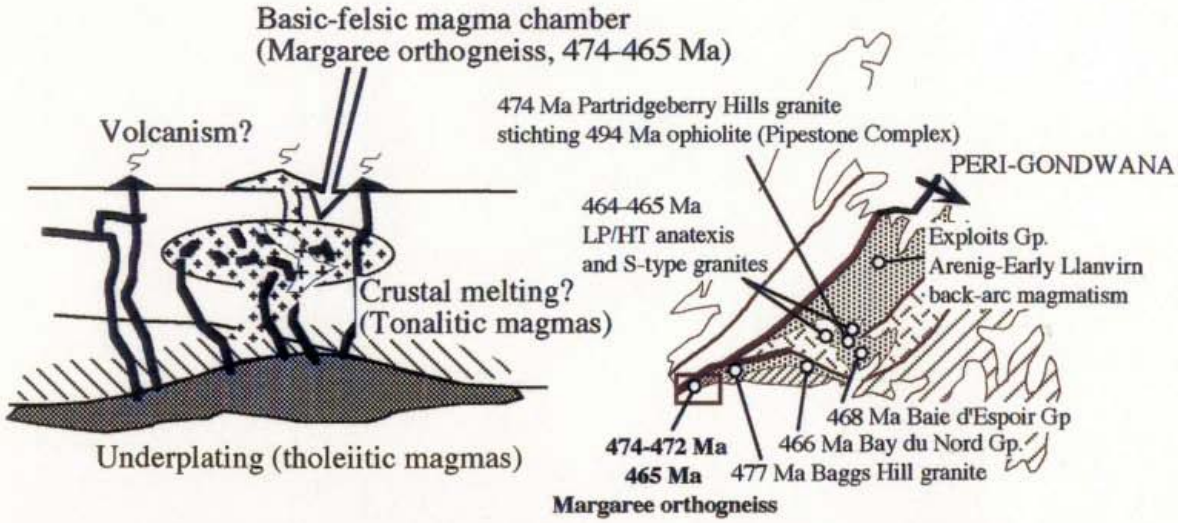

Fig.4.45.-(Left) **Interpretative model for the generation of the mafic-felsic igneous complex, Margaree orthogneiss.** (Right) **Coeval magmatism along the peri-Gondwanan margin of the Newfoundland Appalachians (Exploits subzone and Gander Zone)**. Avalonian basement, striped pattern.

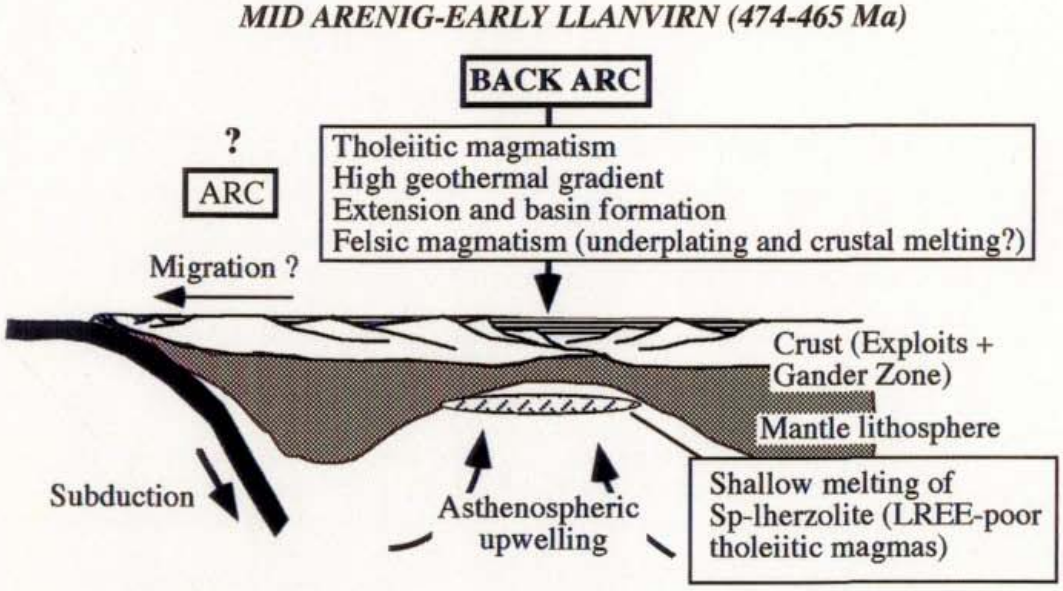

Fig.4.46.- Hypothetical Mid Arenig - Early Llanvirn tectonic setting for the Margaree orthogneiss (igneous complex) : Shallow melting of asthenospheric mantle in an arc/back-arc setting with coeval crustal extension and basin formation. Subduction polarity based on Van Staal (1994).

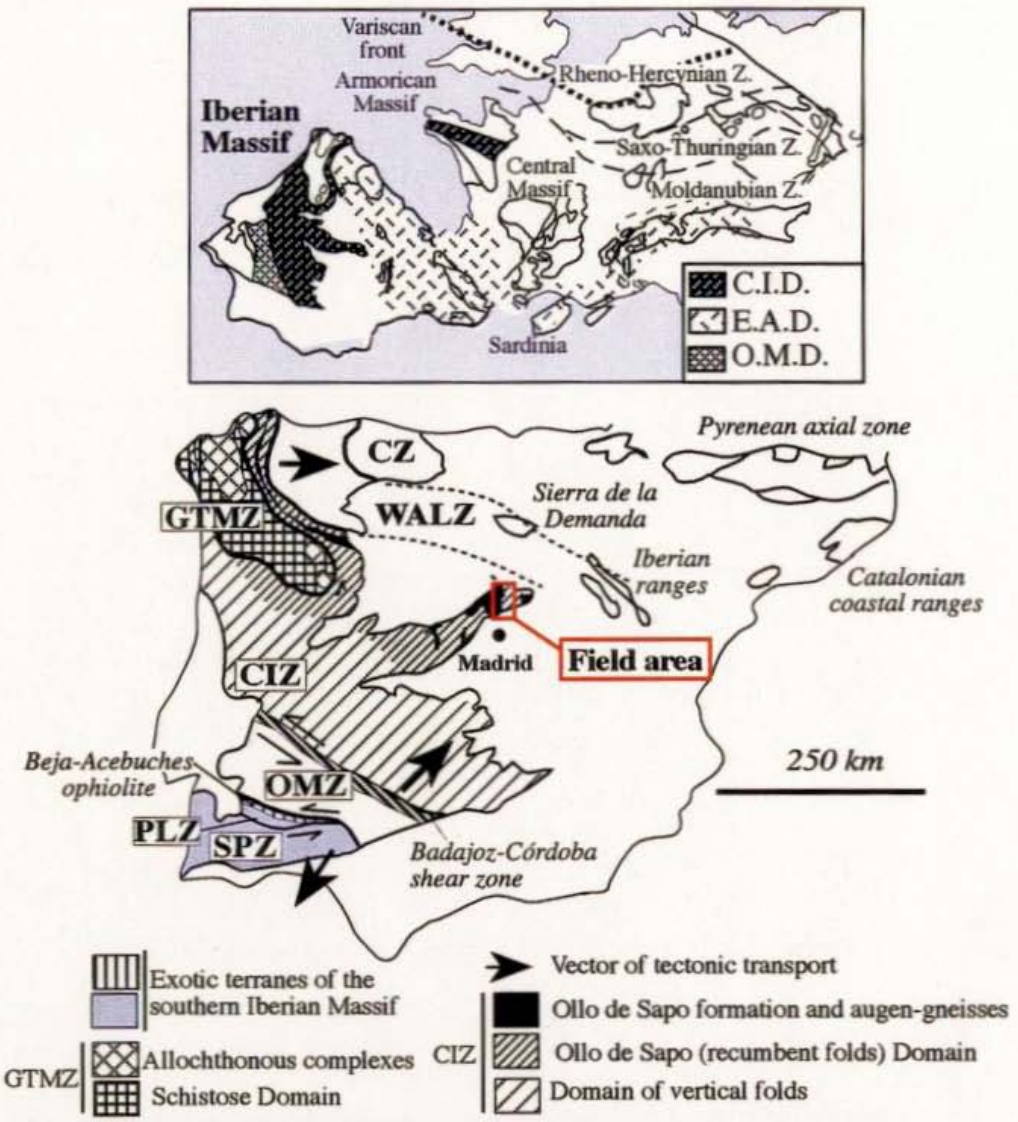

Fig. 5.1.- Location of the Iberian Massif in the European Variscides and lithotectonic zones of the Iberian Massif.
Ordovician faunistical domains in the Southern Variscides after Paris and Robardet (1990) and Robardet et al. (1990): CID, Central Iberian Domain; EAD, Ebro-Aquitanian Domain; OMZ, Ossa-Morena Domain.
Lithotectonic zones of the Iberian Massif (Julivert et al, 1972; Farias et al, 1986): SPZ, South Portuguese Zone; PLZ, Pulo do Lobo Zone (former SPZ); OMZ, Ossa-Morena Zone; CIZ, Central Iberian Zone: Ollo de Sapo (recumbent folds) domain and domain of vertical folds (Diez Balda et al., 1990); GTMZ; Galicia Tras-os-Montes zone: domains after Farias et al. (1987); WALZ, West Asturian-Leonese Zone; CZ, Cantabrian Zone.

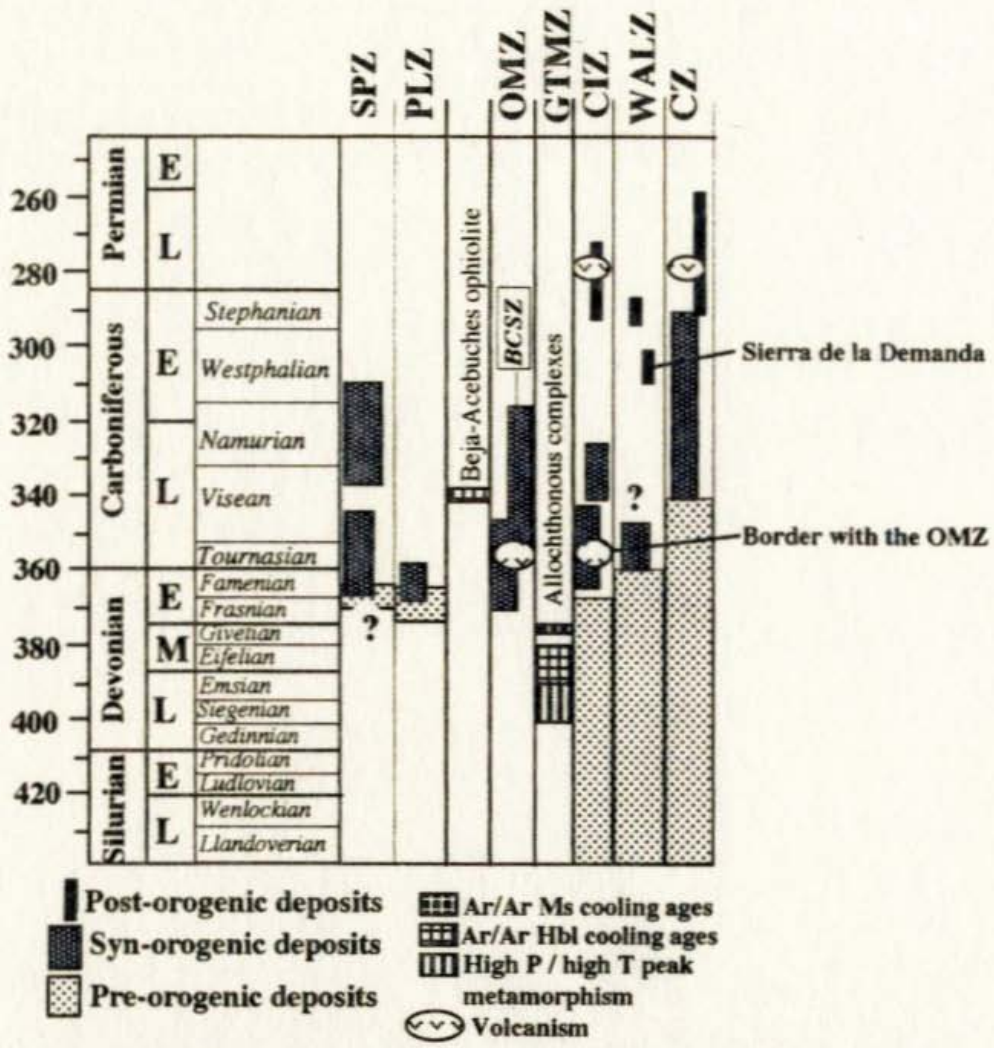

Fig. 5.2.- Geological constraints on the timing of the Variscan orogeny in the Iberian Massif: SPZ, South Portuguese Zone; PLZ, Pulo do Lobo Zone; OMZ, Ossa-Morena Zone; BCSZ, Badajoz-Cordoba shear zone; GTMZ, Galicia Tras-os-Montes Zone; CIZ, Central Iberian Zone; WALZ, West Asturian-Leonese Zone; CZ, Cantabrian Zone. References in text. Time scale Odin et al. (1990)

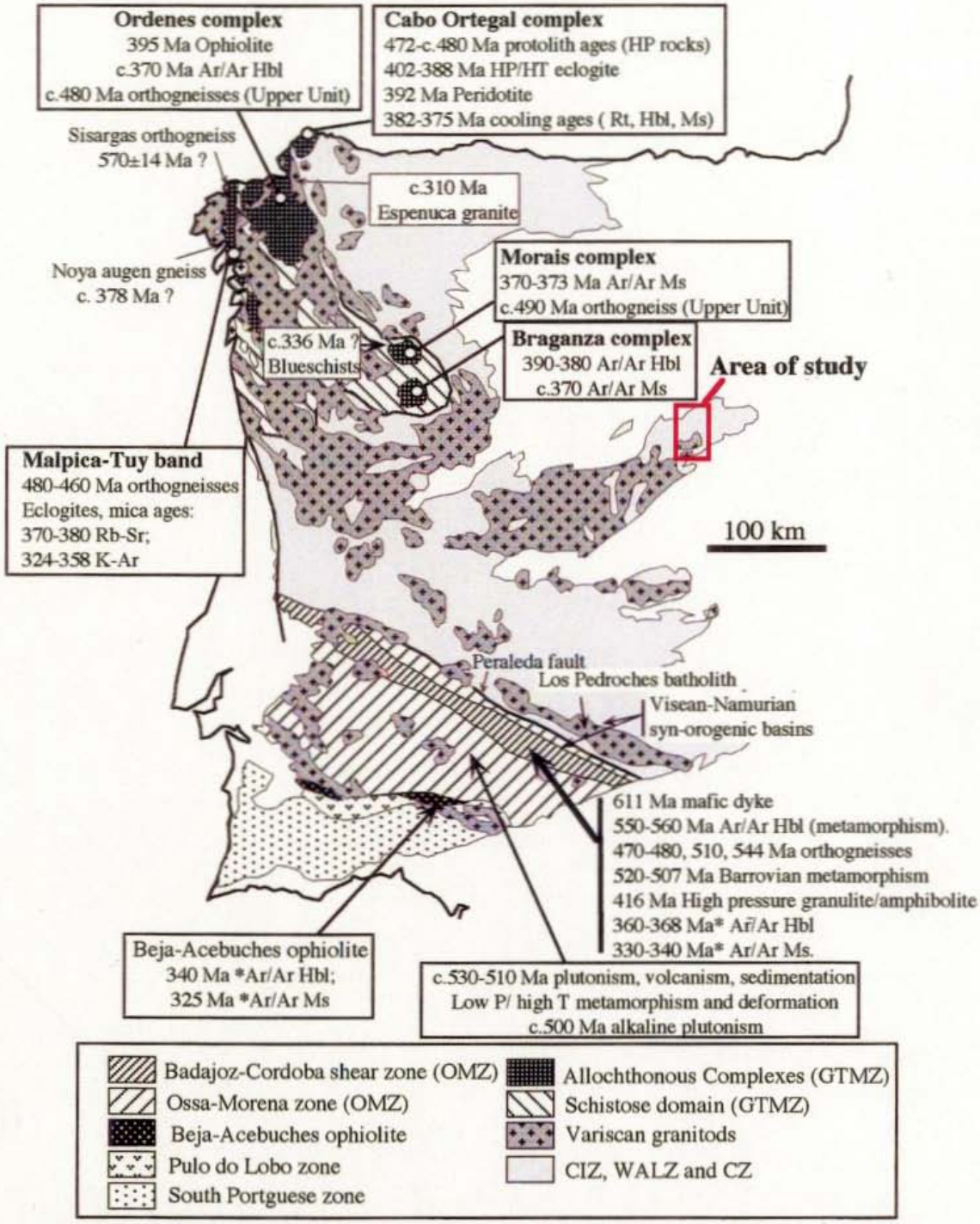

Fig. 5.3.- Lithotectonic units of the Iberian Massif with the location of the geological elements described in sections 5.2.1 to 5.2.3. (* cooling age).

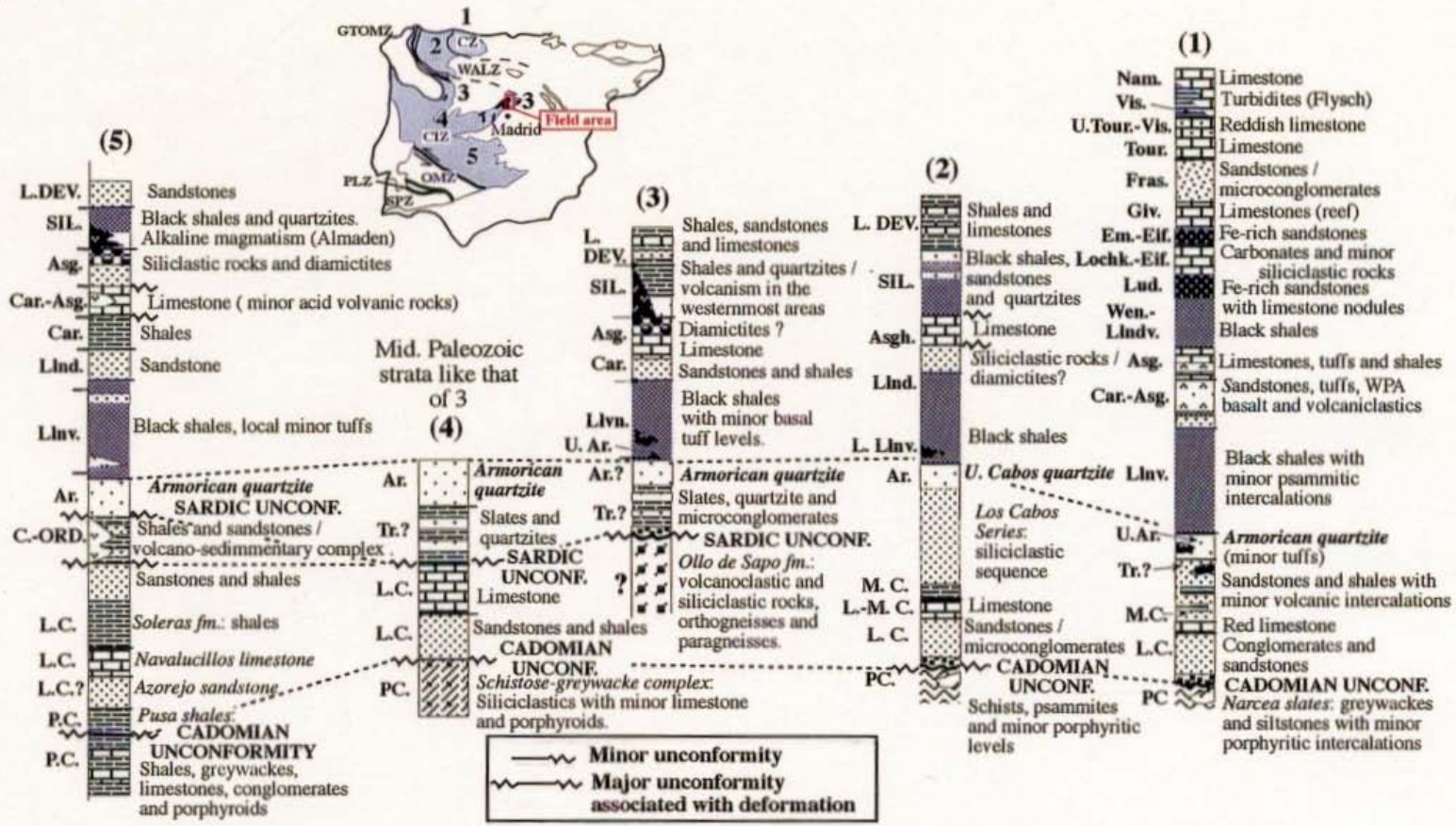

Fig. 5.4.- Compiled pre-Variscan stratigraphic sequences of the CIZ, WALZ and CZ. (1) CZ: Cantabrian Zone (e.g., Truyols et al., 1990; Sanchez Posada et al., 1990); (2) WALZ: West Asturian -Leonese Zone (e.g., Perez Estaun et al., 1990); (3): CIZ: Central Iberian Zone, Ollo de Sapo domain (e.g., Gutierrez Marco et al., 1990); (4) CIZ: Central Iberian Zone, northern Domain of Vertical Folds in the Salamanca area (e.g., Gutierrez Marco et al., 1990); (5) CIZ: Central Iberian Zone, southern Domain of Vertical Folds (e.g., Gutierrez Marco et al., 1990). L., Lower; M., Medium; U., Upper; P.C., Precambrian; C., Cambrian. ORD., Ordovician: Tr., Tremadoc; Ar., Arenig; Llnv., Llanvirn; Llnd., Llandeilo; Car., Caradoc; Asg., Asghill; SIL., Silurian; Llandv., Llandovery; Wen.; Wenlock; Lud., Ludlow. DEV., Devonian: Lochk., Lochkovian; Em., Emsian; Eif., Eifelian; Giv., Givetian; Fras., Frasnian. Carboniferous: Tour., Tournasian; Vis., Visean; Nam.; Namurian.

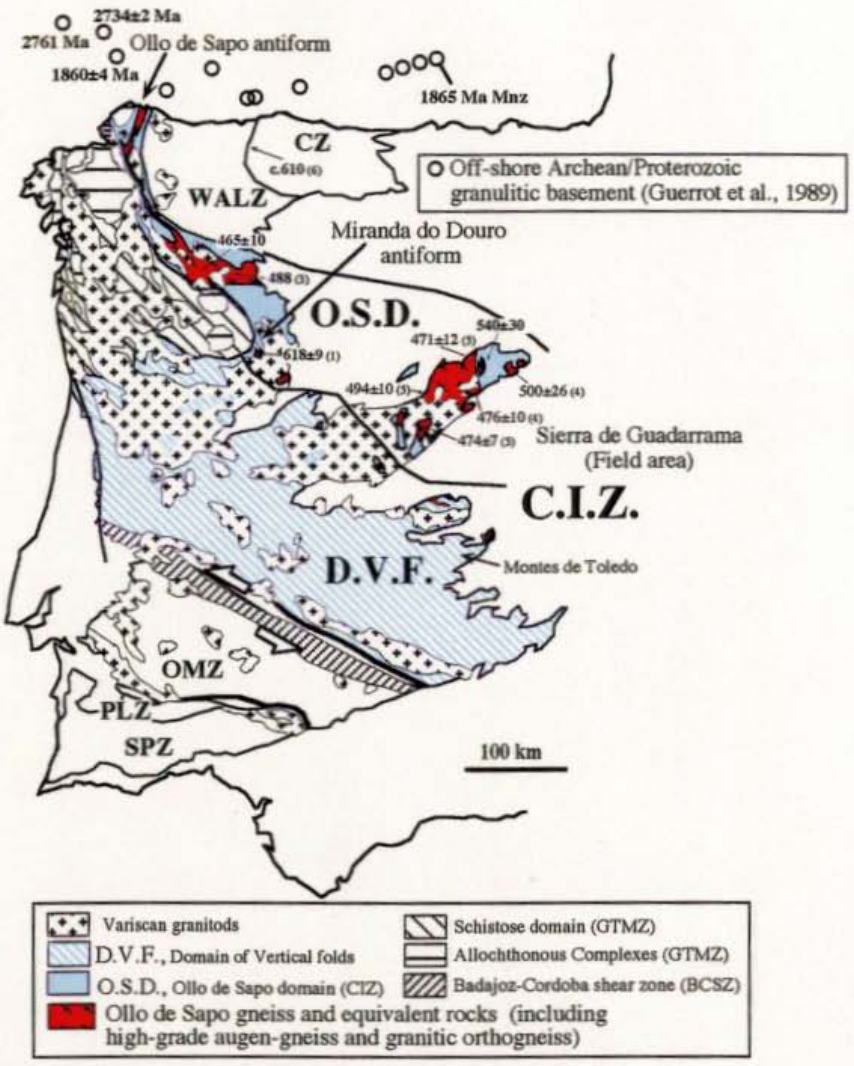

Fig. 5.5.- Domains of the Central Iberian Zone (CIZ) and localition of the main outcrops of pre-variscan orthogneisses, including the available pre-variscan absolute ages (Ma) in the CIZ and the CZ, and the off-shore granulitic basement. Bold, U-Pb ages; Plain, Rb-Sr ages. (1)U-Pb Zrn, Lancelot et al. (1985); (2) U-Pb Zrn, Wildberg et al. (1989); (3) U-Pb Zrn SHRIMP, Gebauer et al., 1993; (4) WR Rb-Sr, Vialette et al. (1986); (5)WR Rb-Sr, Vialette et al. (1987); (6) U-Pb Zrn LAM ICP-MS (J. Fernandez Suarez, per comm.)

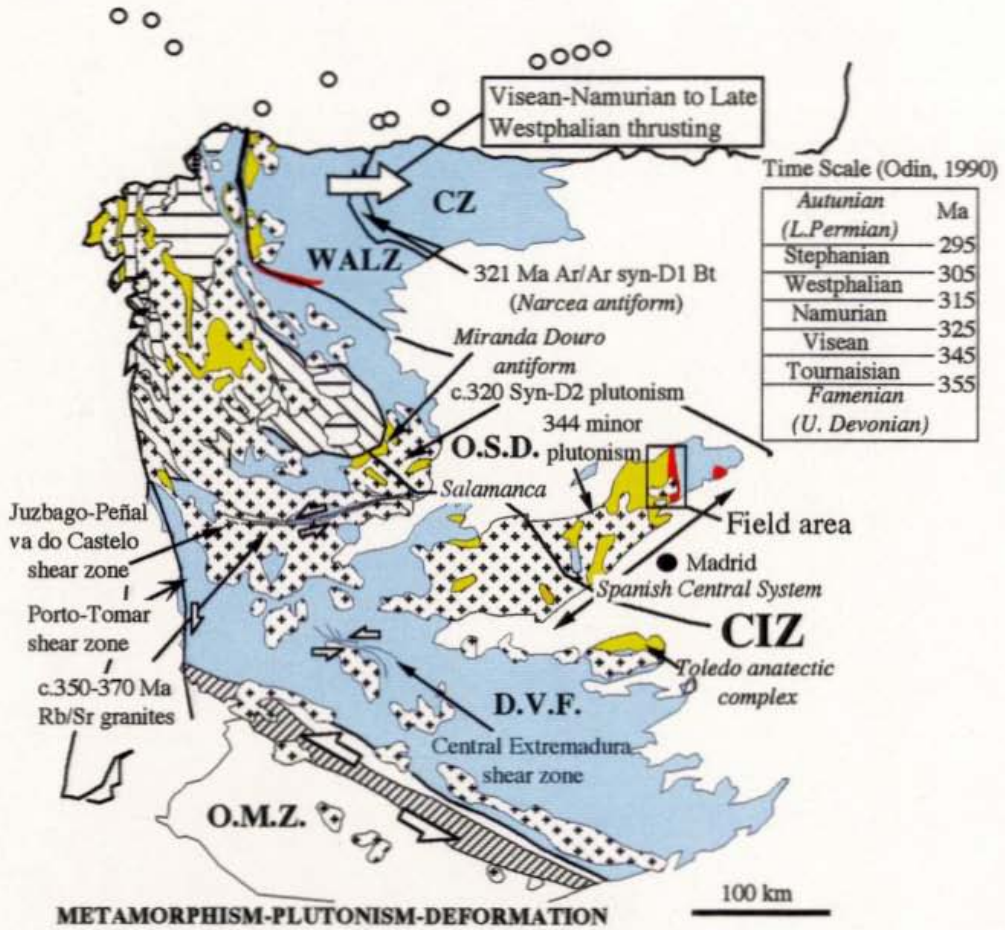

METAMORPHISM-PLUTONISM-DEFORMATION RELATIONSHIPS IN THE CENTRAL IBERIAN ZONE
(Julivert and Martinez, 1987)

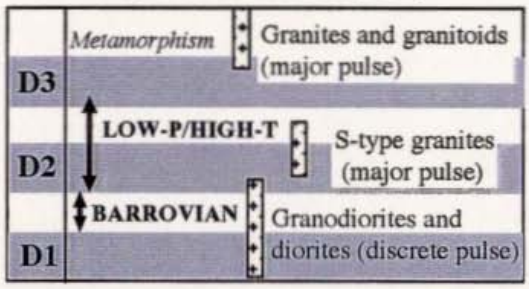

Fig. 5.6.- Distribution of Sill-bearing metamorphic complexes (yellow) and Barrovian metamorphic sequences (red) in the CIZ, WALZ and CZ (blue) after Martinez et al. (1990a, b) and Martinez Catalan et al. (1990); location of the Archean basement granulites off-shore the Cantabrian Sea (Guerrot et al., 1989); and relative relationships between deformation, metamorphism and plutonism in the CIZ. Major wrench shear zones in the CIZ after Diez Balda et al. (1990). Note: most plutonism is 315-270 Ma (Rb-Sr; K-Ar; e.g., Serrano Pinto et al., 1987), except for pointed exceptions. Timing of deformation in the WALZ after Martinez Catalan et al. (1990) and Martinez Catalan et al. (1993) and in the CZ after Perez Estaun et al. (1990).

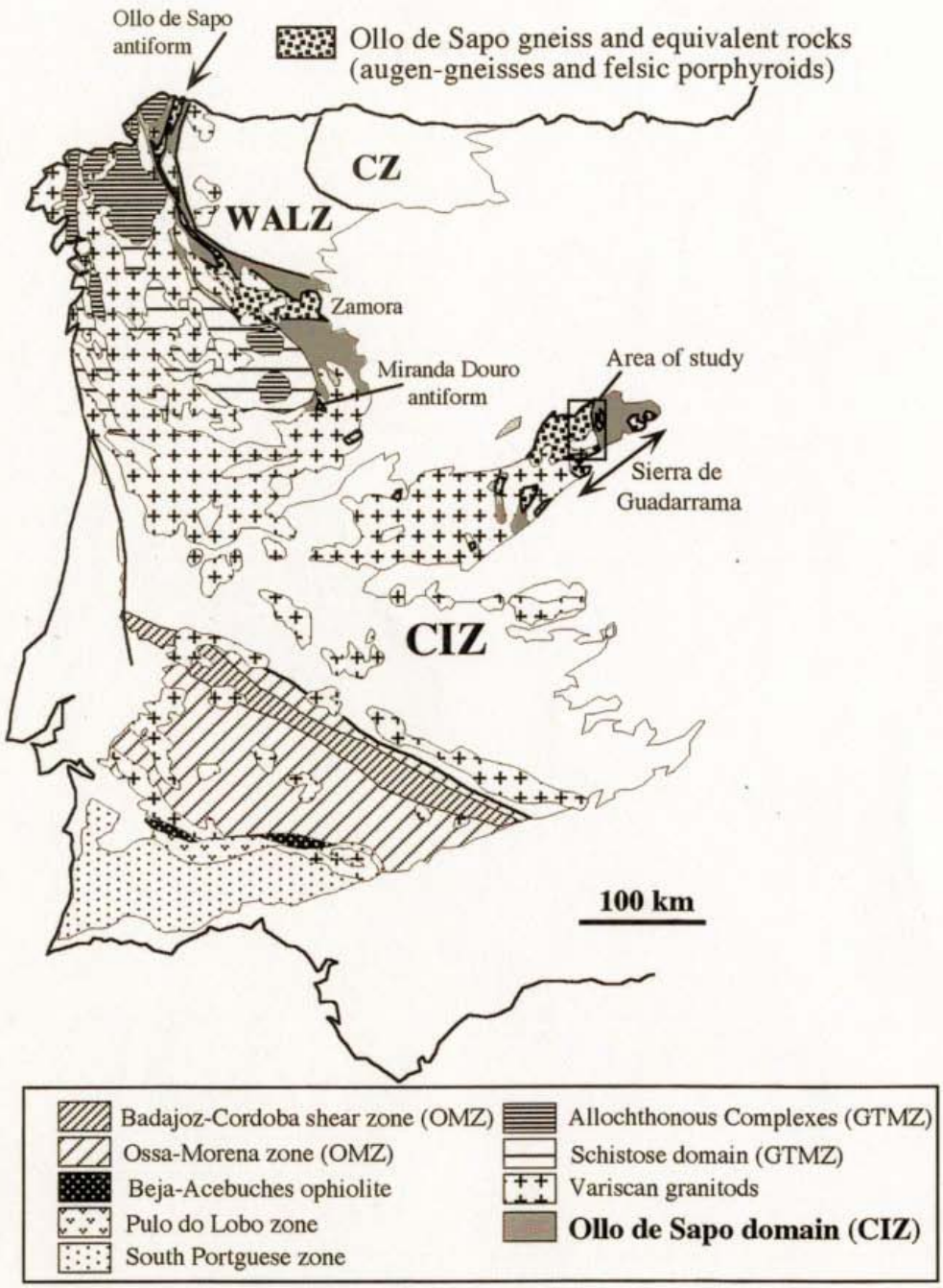

Fig. 6.1.- Map of the lithotectonic zones of the Iberian Massif showing the distribution of the Ollo de Sapo pre-variscan gneisses and the location of the area of study.

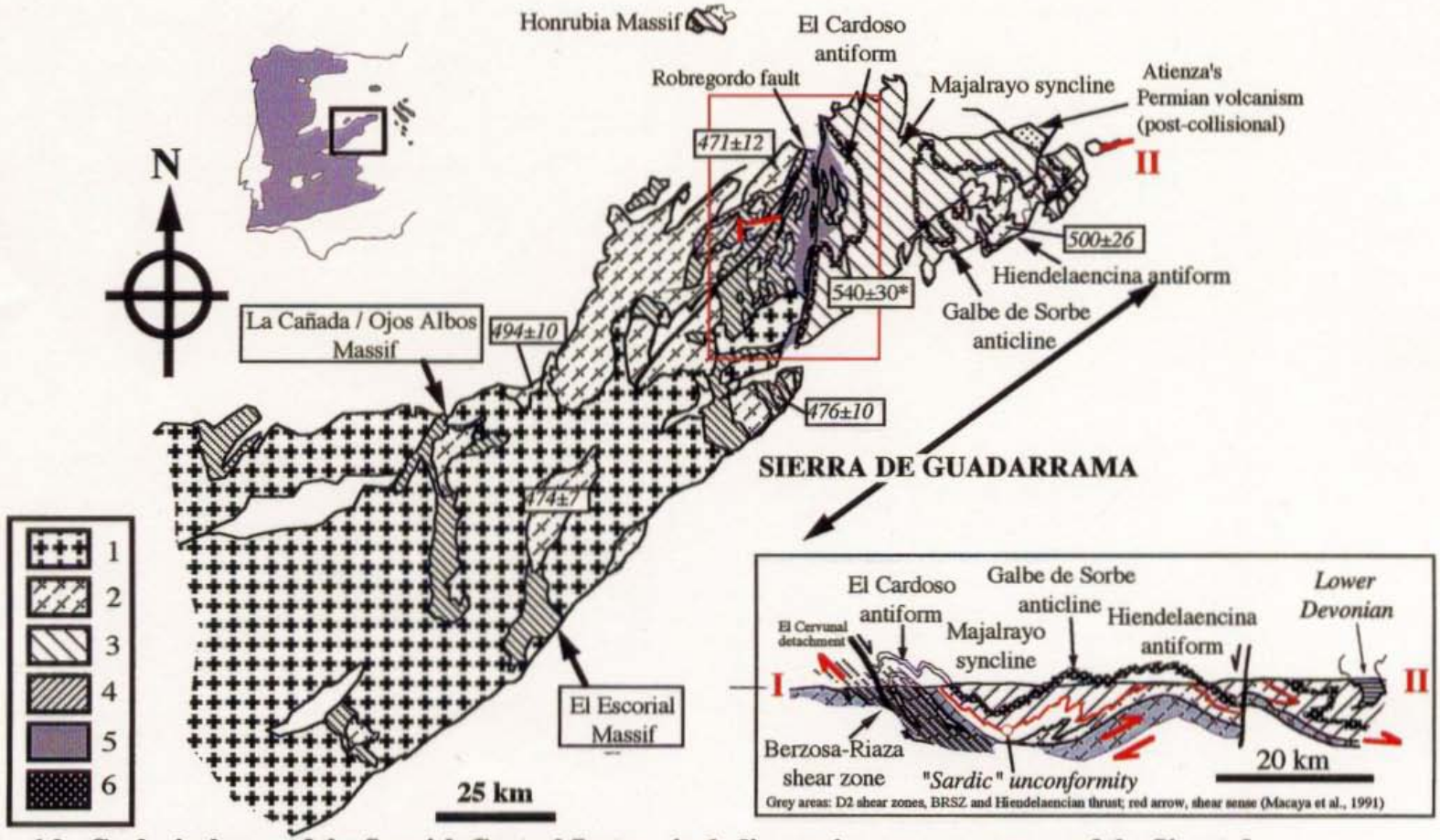

Fig. 6.2.- Geological map of the Spanish Central System, including main macrostructures of the Sierra de Guadarrama, also shown in cross section (I-II, mainly Eastern Domain; modified from Macaya et al., 1991). Legend: (1) Variscan granites; (2) Pre-Variscan orthogneiss; (3) Paleozoic of the Eastern Guadarrama Domain; (4) Metasedimentary rocks; (5) Berzosa-Riaza shear zone; (6) Armorican quartzite (Arenig?); red square, area of study. Location of previous absolute age determinations in Ma: *, U-Pb lower intercept (Wildberg et al., 1989); italics, WR Rb-Sr (Vialette et al, 1986; 1987).

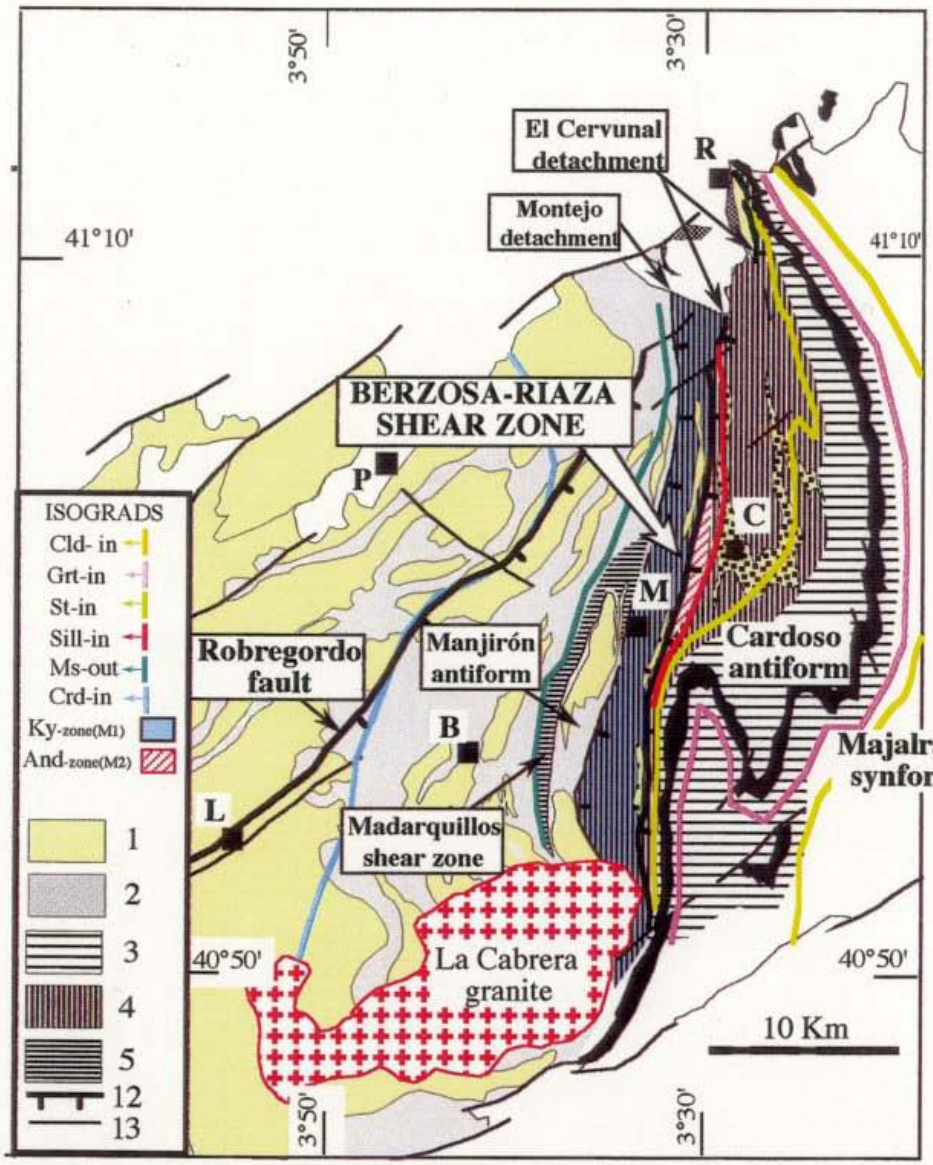

Fig. 6.3.- Main structural elements (Fernandez Casal, 1979; Azor et al., 1991b; Hernaiz Huerta et al., 1996) and distribution of the metamorphic isograds (eg Lopez Ruiz et al., 1975; Gonzalez Casado, 1987; Escuder Viruete et al., 1996) of the Somosierra area of the Sierra de Guadarrama. Legend: pre-variscan orthogneisses (1) and metasedimentary rocks (2) of the Western Domain; 3) D2 crenulation band; 4) Berzosa-Riaza shear zone (BRSZ, ductile mylonitic fabrics); 5) Madarquillos synform (high strain zone, shear zone). B, Buitrago; C, El Cardoso; M, Montejo; L, Lozoya; P, Pradena; R, Riaza.

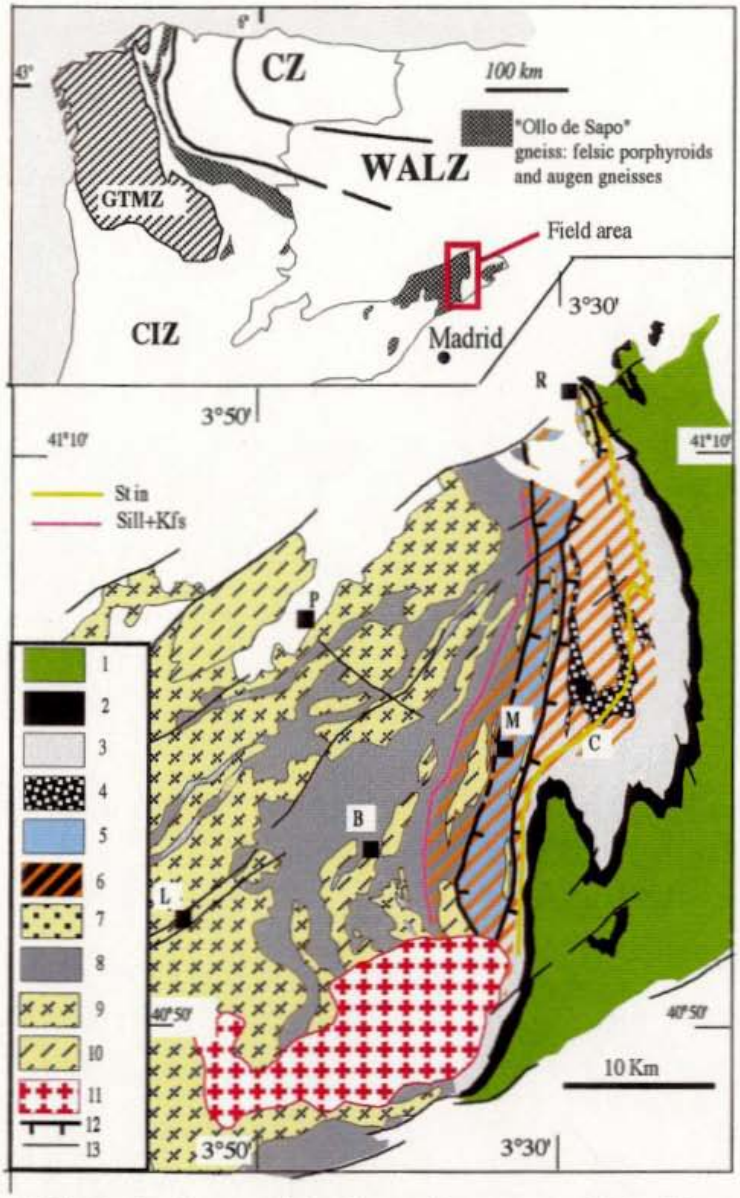

Fig. 6.4.- Lithological map of the Somosierra area of the Sierra de Guadarrama. Legend: Eastern Domain: 1) Rodada Gp. (Llanvirn); 2) Armorican Quartzite, Alto rey fm.(Arenig?); 3) Micaschist, metapsammite, quartzite and minor para-amphibolite (Constante formation); 4) Cardoso gneiss, felsic metavolcanoclastic rock. Berzosa-Riaza shear zone: 5) metasedimentary rocks of the Sill+Ky zone; 6) Ductile mylonitic fabrics; 7) Foliated megacrystic granite, Riaza-Nazaret- Berzosa-Pedrezuela gneisses. Western Domain: 8) Paragneiss, schist and anatectic migmatite; 9) Augen-gneisse, foliated megacrystic granite; 10) Leucogneiss, mainly pre-Variscan leucogranite. 11) Post-tectonic La Cabrera granite. 12) Late extensional detachments; 13), Late faults (Paleozoic and Mesozoic). B, Buitrago; C, El Cardoso; L, Lozoya; M, Montejo; P, Pradena; R, Riaza.

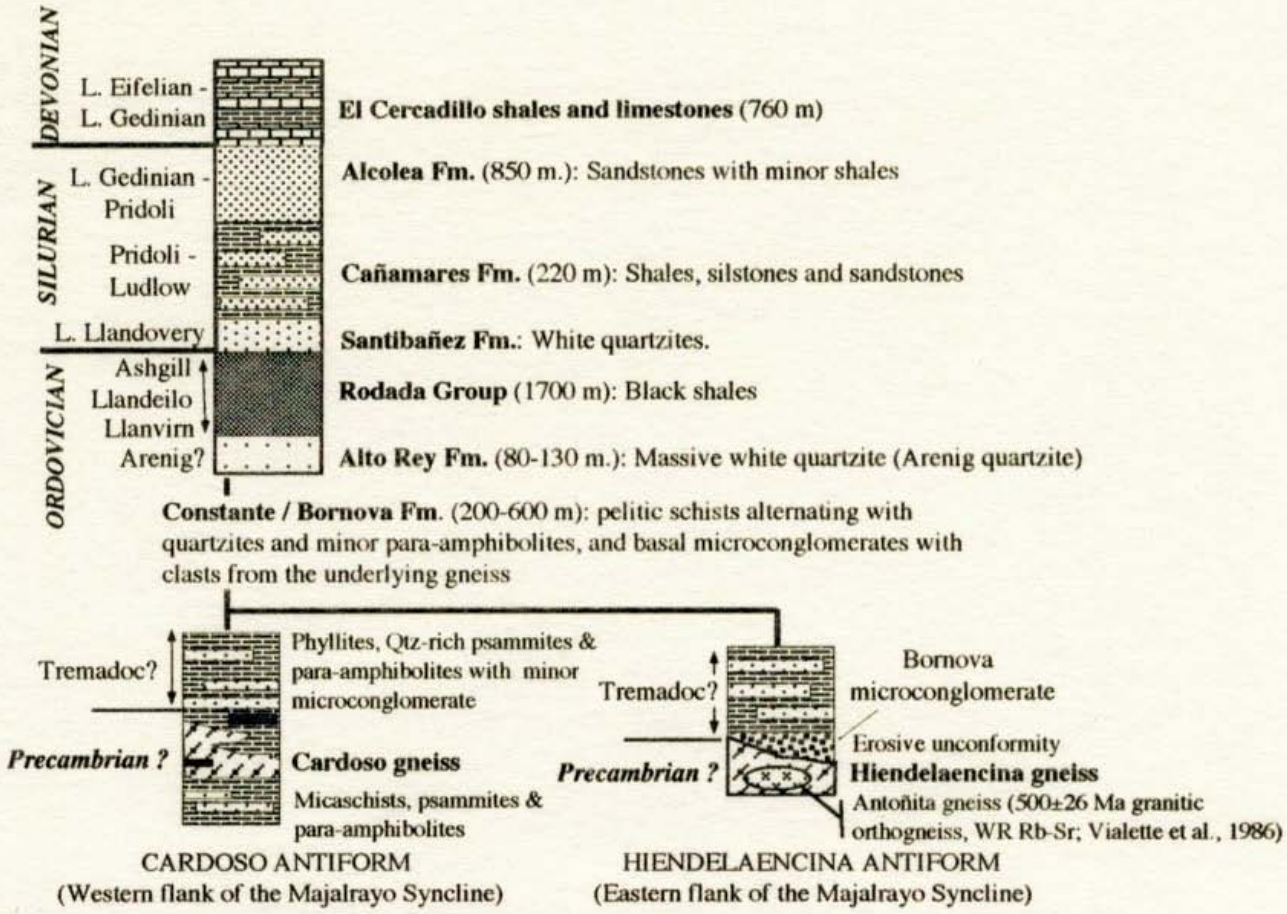

Fig. 6.5.- Paleozoic stratigraphic sequence of the Eastern Guadarrama Domain. Ref. in text, for geographic locations see fig. 6.2.

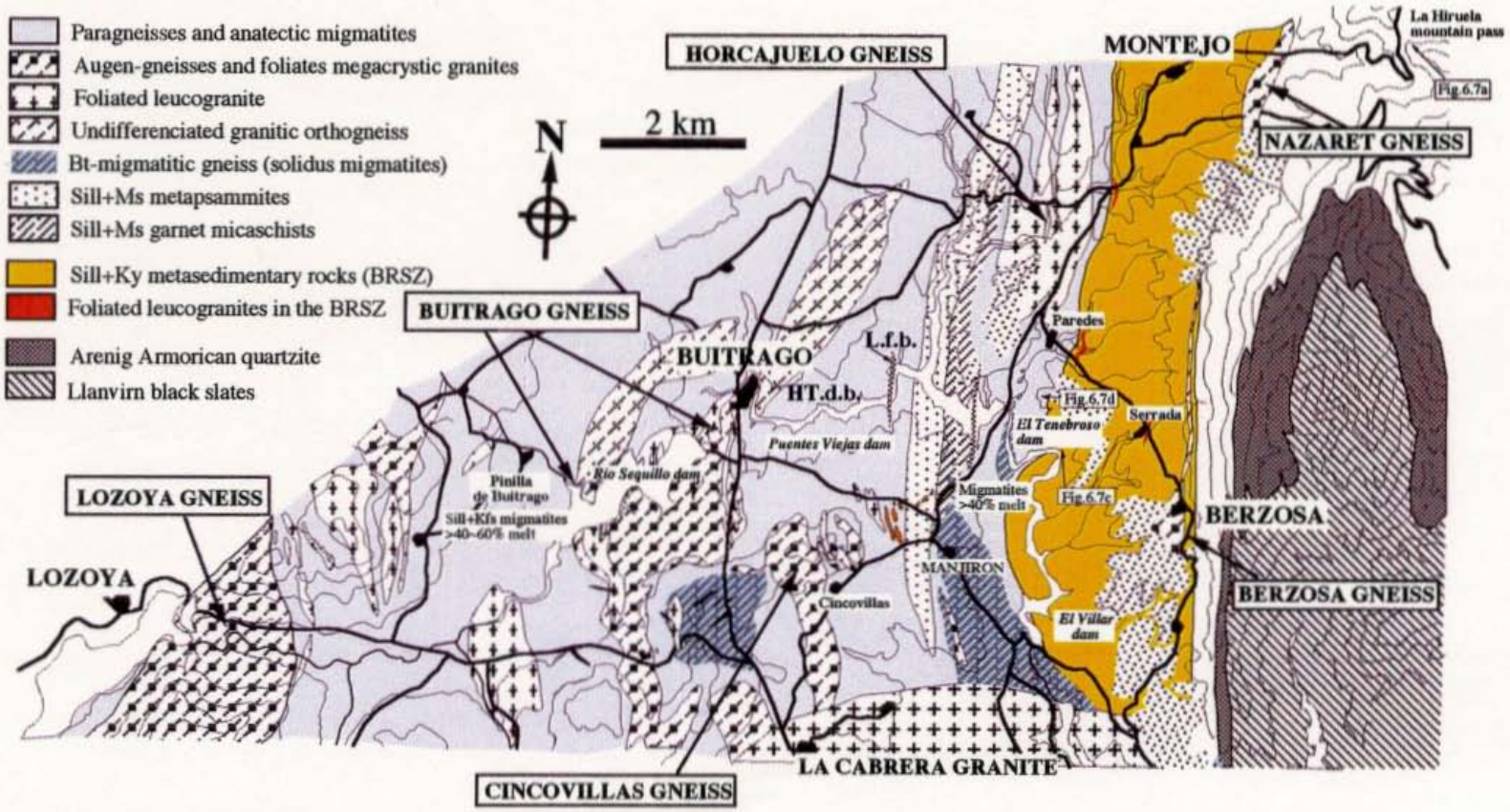

Fig. 6.6.- Lithological map of the Montejo-Berzosa-Buitrago-Lozoya area. Topographic base after Fernandez Casals (1979). Geological map west of the Rio Sequillo dam and the trace of the Armorican quartzite after Fernandez Casals (1979). HT.d.b., high temperature deformation band; L.f.b., L-fabric band. Calc-silicates (blue)

Fig.6.7.- Lithological changes along the Berzosa-Riaza shear zone.

(A) Eastern Cuadramma domain. Chloritoid micaschist between the Cardoso gneiss and the Armuncia Granite, top of the Berzosa-Riaza shear zone. Note the penetrative S2 mylonitic fabric with pressure shadows around the chloritoid porphyroblasts. S1-Cd1 transition, shear sense of top down to the SE. Location in Fig.6.6.

(B) Basal Eastern Cuadarrama Domain. St-Grt micaschist, structurally below the Cardoso gneiss. S2 foliation plane showing a well defined L2 mineral (St) and stretching lineation.

(C) Base of the Sill+Ky zone, Berzosa-Riaza shear zone. Ky-Grt bearing metapsammite showing E1 isoclinal folds in a D2 bundle. Tail of El Villar dam, at the contact with the migmatitic gneisses of the Manjirón anticline. Location in Fig. 6.6.

(D) Sill+Ms zone, migmatitic gneiss at the footwall of the Berzosa-Riaza shear zone, with D2 shear bands indicating a shear sense of top down to the SE (Manjirón anticline, location in Fig. 6.6).

Figure 6.7

Fig.6.7.- Lithological changes along the Berzosa-Riaza shear zone.

(A) Eastern Guadarrama domain, Chloritoid micaschist between the Cardoso gneiss and the Armorican Quartzite, top of the Berzosa-Riaza shear zone. Note the penetrative S2 mylonitic fabric with pressure shadows around the chloritoid porphyroblasts. St-Cld transition, shear sense of top down to the SE. Location in Fig. 6.6.

(B) Basal Eastern Guadarrama Domain, St-Grt micaschist, structurally below the Cardoso gneiss. S2 foliation plane showing a well defined L2 mineral (St) and stretching lineation.

(C) Base of the Sill+Ky zone, Berzosa-Riaza shear zone. Ky-Grt bearing metapsammite showing F1 intrafolial folds in a D2 boudin. Tail of El Villar dam, at the contact with the migmatitic gneisses of the Manjirón antiform. Location in Fig. 6.6.

(D) Sill+Ms zone, migmatitic gneiss at the footwall of the Berzosa-Riaza shear zone, with D2 shear bands indicating a shear sense of top down to the S-SE (Manjirón antiform, location in Fig. 6.6).

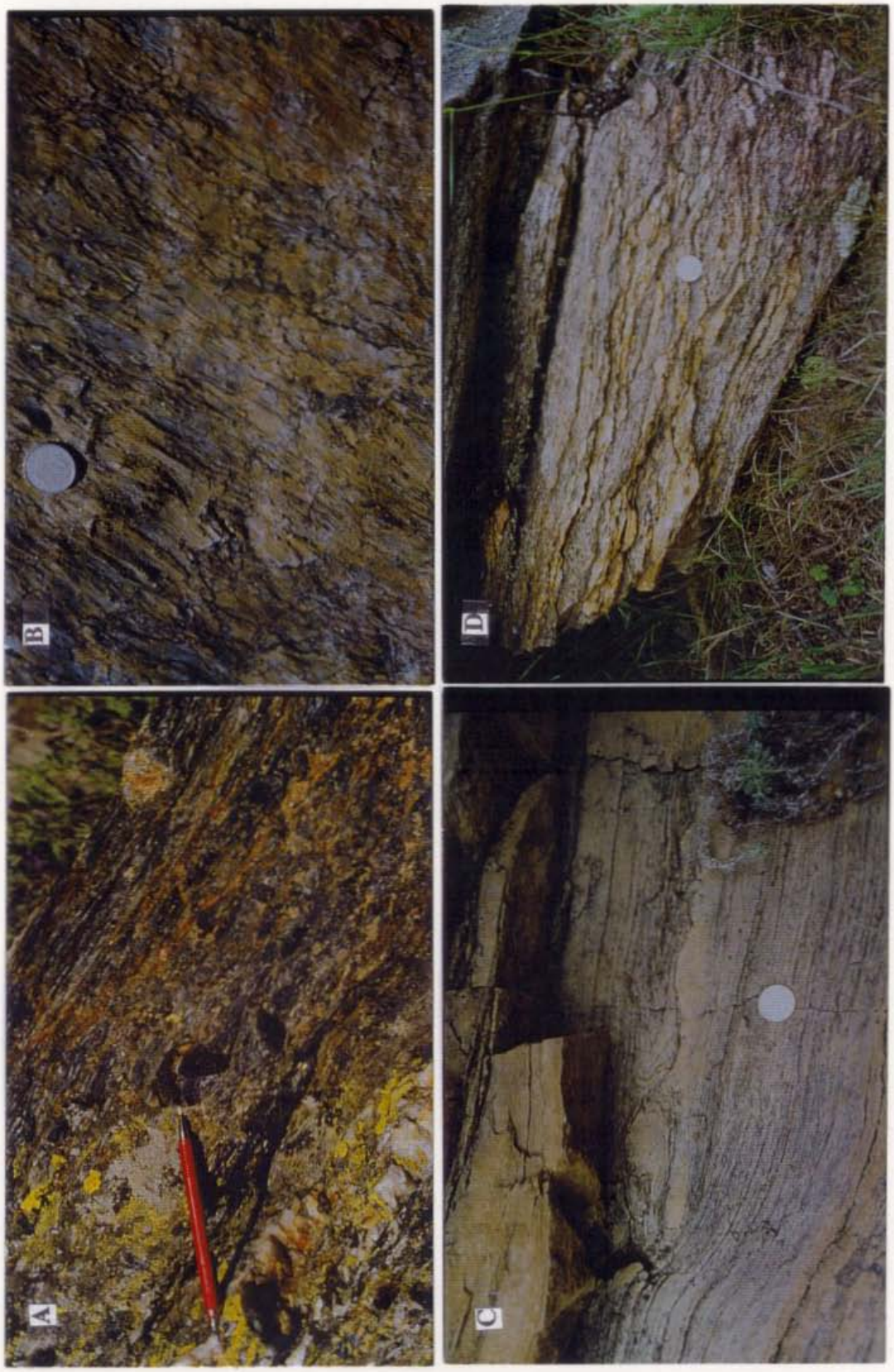
B
D
A
C

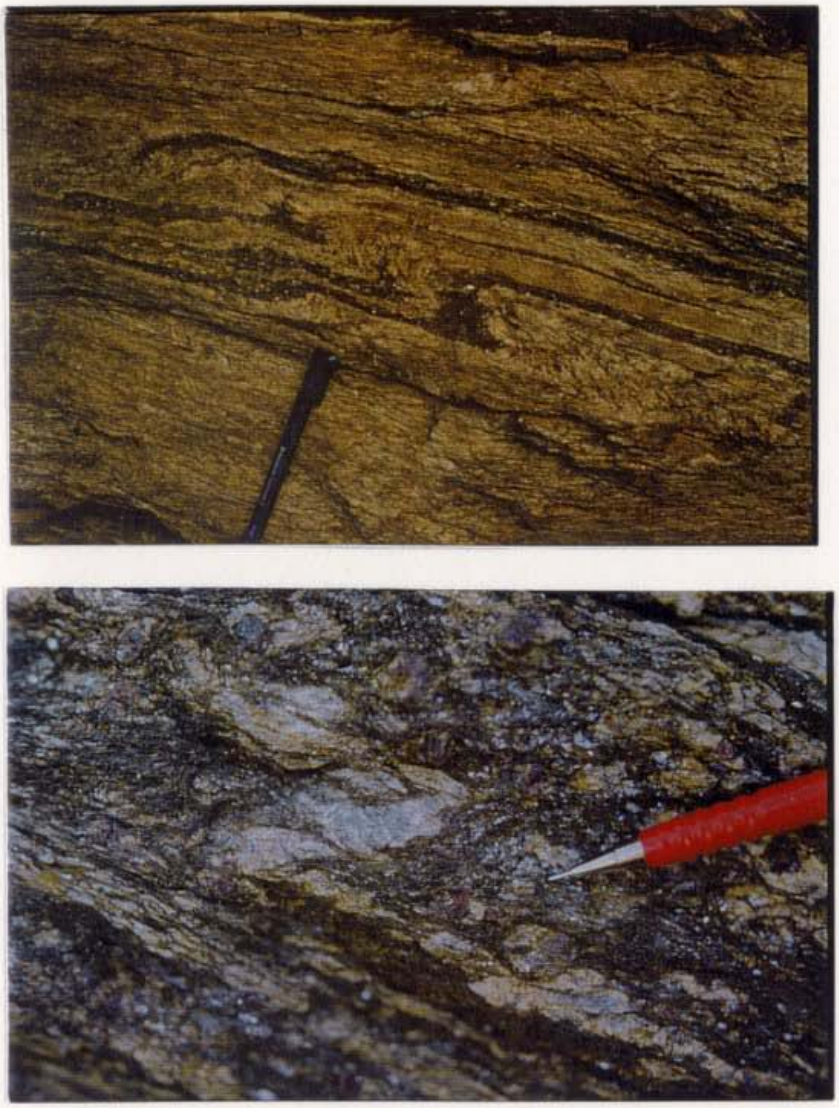

Fig.6.8.- Metasediments in the Manjiron antiform, Sill+Ms zone. Top: Quartzo-feldspathic paragneiss showing D1-D2 refolding of the S0 compositional banding, plan view. **Bottom:** Asymmetric Z-folds in garnet-micaschist (Grt-Bt-Ms-Pl-Qtz) indicating a top-down to the SE shear sense. View parallel to Ls.

Fig.6.9.- Cuarzo-feldspathic paragneisses of the Western Cuadarrama Domain. Buitrago area (Sill+Kfs zone, western side of the Puentes Viejas dam).

Top: Cuarzo-feldspathic paragneiss of granitic composition with continuous compositional banding and refolding of the leucocratic and biotite-rich layers.

Figure 6.9

Middle: F1-F2 refolding of the compositional banding (S0) in the competent quartz-feldspathic levels. The main foliation (S2) is axial planar to the tight F2 folds.

Bottom: Massive megaboudin of migmatitic quartzo-feldspathic gneiss, the compositional banding in the boudin suggests a sedimentary protolith.

Fig.6.9.- Quartzo-feldspathic paragneisses of the Western Guadarrama Domain, Buitrago area (Sill+Kfs zone, western side of the Puentes Viejas dam).

Top: Quartzo-feldspathic paragneiss of granitic composition with continuous compositional banding and refolding of the leucocratic and biotite-rich layers.

Middle: F1-F2 refolding of the compositional banding (S0) in the competent quartz-feldspathic levels. The main foliation (S2) is axial planar to the tight F2 folds.

Bottom: Massive megaboudin of migmatitic quartzo-feldspathic gneiss, the compositional banding in the boudin suggests a sedimentary protolith.

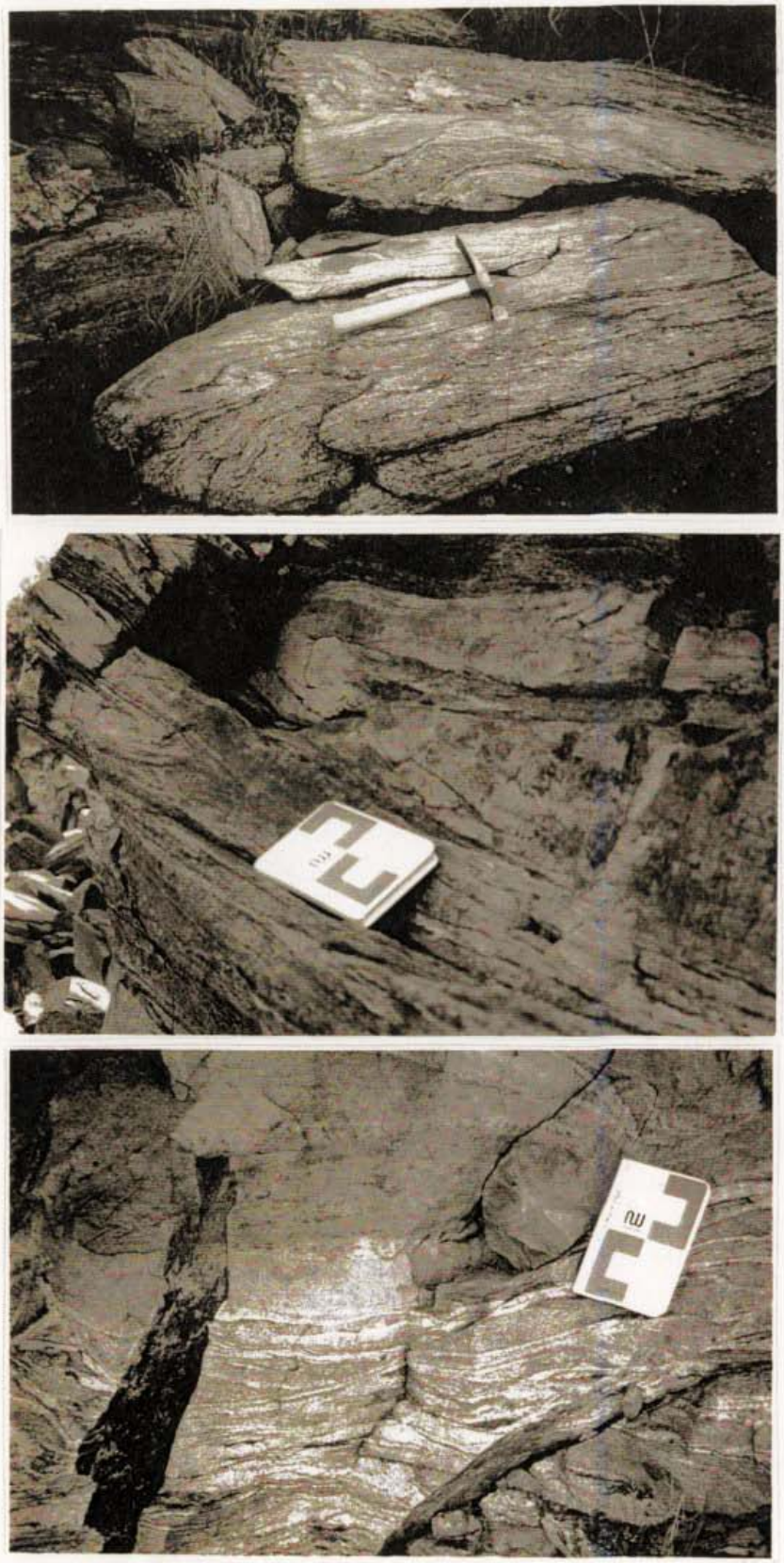

Fig.6.10.- Anatectic melts in the Buitrago area, Sill+Kfs zone. Top: Pre-early syn-D2 stromatic migmatite with granitic leucosomes and Bt+Sill melanosomes defining the gneissosity. **Bottom:** Late post-D2 granitic melt intruding along a shear band in the Buitrago gneiss. Western side of the Rio Sequillo dam.

Fig.6.11.- Anatectic migmatites of the Western Cinderarrena domain.

Top.- Migmatites in the Silt+Ms zone. Mantiform anticline. Head of the Pumeles Viejas dam.

(A) F2 folding of granitic leucosomes concordant with the paleosomes. It is uncertain if these are anatectic melts or metamorphic differentiates. The melanosomes are formed by silliminanite + biotite + muscovite ± garnet.

(B) Diatexitic migmatite with interconnected leucosomes showing a complex disharmonic refolding. The leucosomes contain minor garnet. They have granitic composition and preserve relicts of paragneiss texture. View perpendicular to L2.

Bottom.- Migmatites in the Silt+Ms zone, western side of the Rio Seguillo dam.

(C) Garnet-bearing stromatic migmatite folded by F2 with more than 40 leucosome, migmatitic paragneiss. Note the disharmonic refolding of the leucosomes.

(D) Detail of leucosome in the hinge of a D2 fold suggesting melt migration during F2-folding.

Figure 6.11

Fig.6.11.- Anatectic migmatites of the Western Guadarrama domain.

Top.- Migmatites in the Sill+Ms zone, Manjiron antiform, head of the Puentes Viejas dam.

(**A**) F2 folding of granitic leucosomes concordant with the gneissosity in the paleosome. It is uncertain if these are anatectic melts or metamorphic differentiates. The melanosomes are formed by sillimanite + biotite + muscovite ± garnet.

(**B**) Diatexitic migmatite with interconnected leucosomes showing a complex disharmonic refolding. The leucosomes contain minor garnet, have granitic compositions and preserve relicts of magmatic textures. View perpendicular to Ls.

Bottom.- Migmatites in the Sill+Kfs zone, eastern side of the Rio Sequillo dam.

(**C**) Garnet-bearing stromatic migmatite folded by F2 with more than 40% leucosome, migmatitic paragneiss. Note the disharmonic refolding of the leucosomes.

(**D**) Detail of leucosome in the hinge of a D2 fold suggesting melt migration during F2 folding.

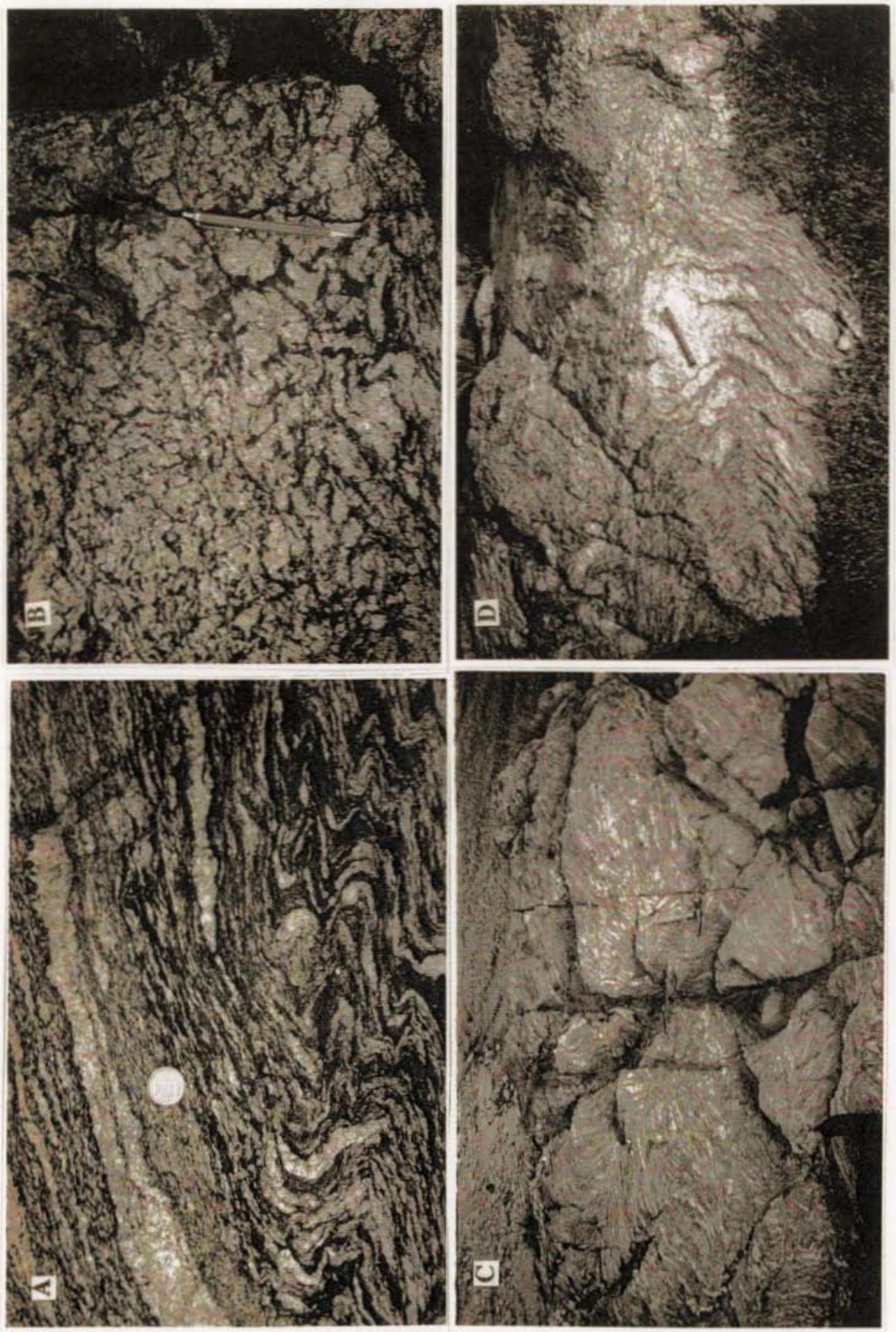
B
D
A
C

Fig. 6.12.- Calc-silicate lithologies.-

Top: Complex F1 folding of garnet and clinopyroxene-rich layers (S0-S1) inside a D2 boudin, late tension cracks (D2) are filled with plagioclase. The grey centimetric speckles in the rock are composed of calcite, plagioclase and epidote. Manjiron antiform (Sill+Ms zone), base of the Puentes Viejas dam.

Middle: Calc-silicate, quartz-free, garnet-clinopyroxene assemblage with new growth of plagioclase (Pl) after clinopyroxene. The inclusions in the garnet are zoisite and rutile. Titanite is restricted to the matrix. Field of view is 1.32 mm long. Manjiron antiform, Puentes Viejas dam.

Bottom: Isolated calc-silicate lense, deformed boudin, surrounded by migmatitic paragneisses showing D2 strain partitioning. Note F2 folding and D2 shearing and transposition of the compositional banding. View oblique to L2. Buitrago area (Sill+Kfs zone), high temperature deformation band, western Puentes Viejas dam.

Figure 6.12

Fig. 6.12.- Calc-silicate lithologies.-

Top: Complex F1 folding of garnet and clinopyroxene-rich layers (S0-S1) inside a D2 boudin, late tension cracks (D2) are filled with plagioclase. The grey centimetric speckles in the rock are composed of calcite, plagioclase and epidote. Manjiron antiform (Sill+Ms zone), base of the Puentes Viejas dam.

Middle: Calc-silicate, quartz-free, garnet-clinopyroxene assemblage with new growth of plagioclase (Pl) after clinopyroxene. The inclusions in the garnet are zoisite and rutile. Titanite is restricted to the matrix. Field of view is 1.32 mm long. Manjiron antiform, Puentes Viejas dam.

Bottom: Isolated calc-silicate lense, deformed boudin, surrounded by migmatitic paragneisses showing D2 strain partitioning with F2 folding and D2 shearing and transposition of the compositional banding. View oblique to Ls. Buitrago area (Sill+Kfs zone), high temperature deformation band, western Puentes Viejas dam.

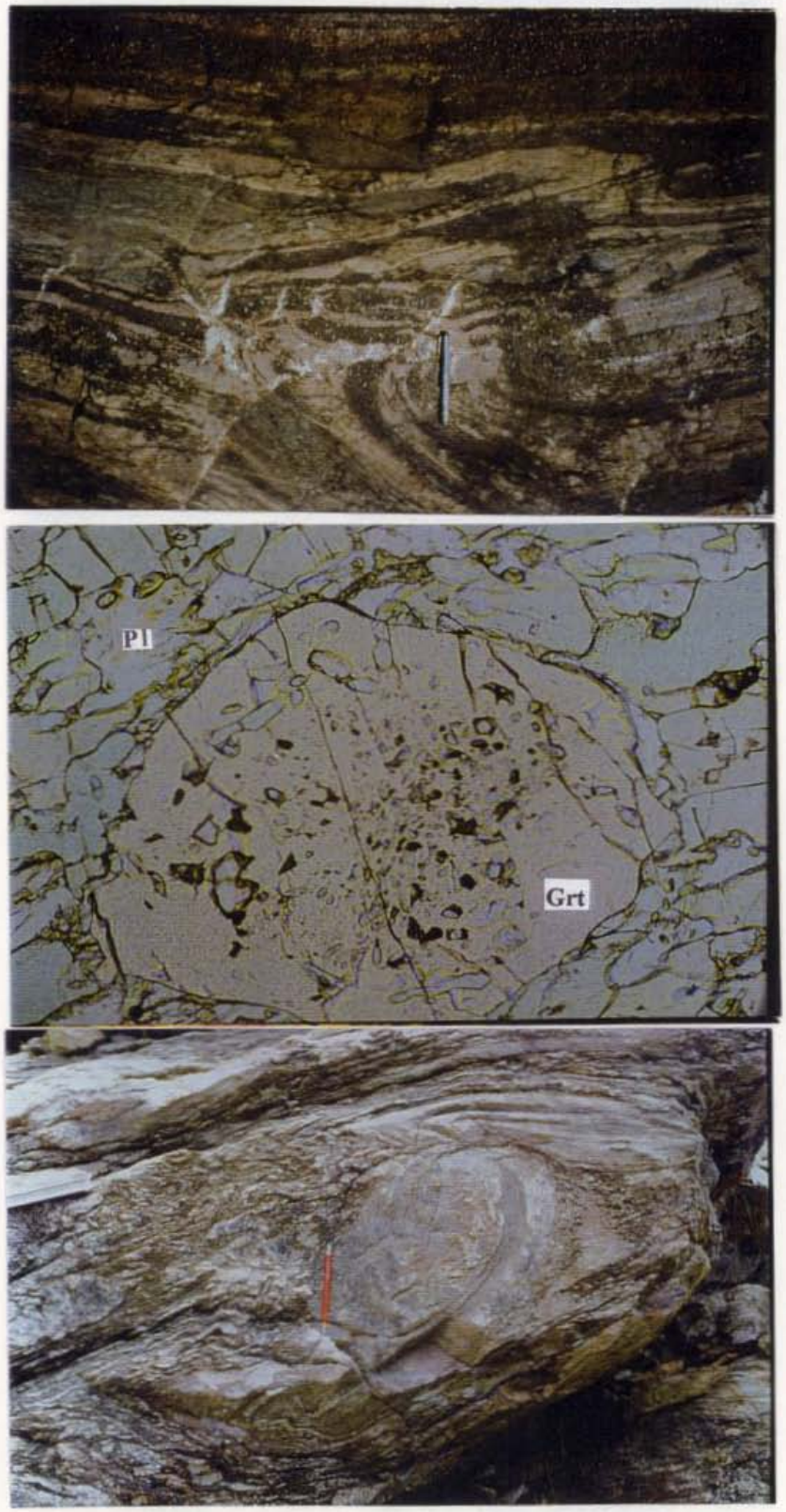
Pl
Grt

Figure 6.13

Fig.6.13.- El Villar biotite-bearing migmatites, non-anatectic migmatites, Western Guadarrama Domain.

A) Foliated aplitic dyke subparallel to the gneissosity defined by quartz + K-feldspar + plagioclase rich domains. El Villar dam. SE border of the Manjirón antiform (Sill+Ms zone).

B) Sub-solidus migmatites near el Cuadrón (Sill+Kfs zone). The absence of well defined melanosomes and the pegmatoid character of the leucosomes suggest that they are derived from strained pegmatitic veins or deformed and recrystallized feldspar porphyroclasts.

C) El Villar dam, coarse-grained leucosome with no melanosome in a highly strained granitic paleosome with leucocratic domains suggesting that this is a sub-solidus migmatite. The rock consists of biotite + muscovite + plagioclase (An15-20) + quartz, with very scarce garnet and no sillimanite.

Fig.6.13.- El Villar biotite-bearing migmatites, non-anatectic migmatites, Western Guadarrama Domain.

A) Foliated aplitic dyke subparallel to the gneissosity defined by quartz + K-feldspar + plagioclase rich domains. El Villar dam, SE border of the Manjiron antiform (Sill+Ms zone).

B) Sub-solidus migmatites near el Cuadrón (Sill+Kfs zone). The absence of well defined melanosomes and the pegmatoid character of the leucosomes suggest that they are derived from strained pegmatitic veins or deformed and recrystallized feldspar porphyroclasts.

C) El Villar dam, coarse-grained leucosome with no melanosome in a highly strained granitic paleosome with leucocratic domains suggesting that this is a sub-solidus migmatite. The rock consists of biotite + muscovite + K-feldspar + plagioclase (An15-20) + quartz, with very scarce garnet and no sillimanite.

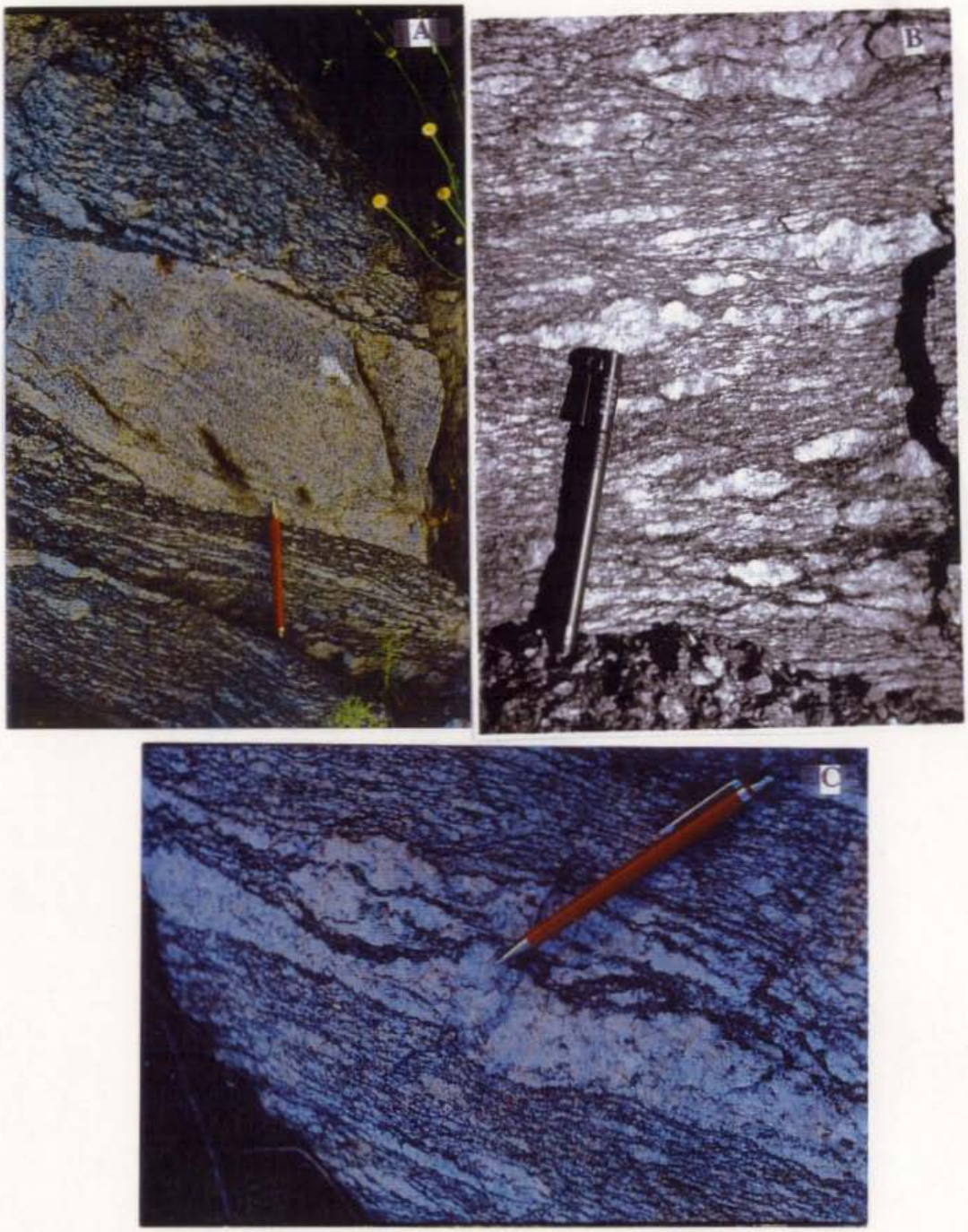
A
B
C

Fig. 6.14.- Argyra gracilicornis and foliated megacrystic granites of the Wedgetail Quadrangle domain.

A) Heterogeneously deformed foliated megacrystic granite. Cinnovillia grexis.

B) Argyra-grexis, megacrystic facies of the Bunbugo grexis showing primary feldspar porphyroclasts surrounded by a ductily deformed stilpnomelic-bearing quartzo-feldspathic matrix. Weakly developed S-C structures and discrete shear bands (below the pen) indicate a top down to the SE (dextral) D2 shear sense.

C) Highly strained argyra-grexis, Cinnovillia grexis, showing an intense D2 foliation and deformation of the primary feldspar megacrysts. The strain partitioning around the feldspar megacrysts and the asymmetry of the porphyroclast tails do not allow reliable determination of the shear sense; view parallel to the stretching lineation.

Figure 6.14

Fig. 6.14.- Augen gneisses and foliated megacrystic granites of the Western Guadarrama domain.

A) Heterogeneously deformed foliated megacrystic granite, Cincovillas gneiss.

B) Augen-gneiss, megacrystic facies of the Buitrago gneiss showing primary feldspar porphyroclasts surrounded by a ductily deformed sillimanite-bearing quartzo-feldspathic matrix. Weakly developed S-C structures and discrete shear bands (below the pen) indicate a top down to the SE (dextral) D2 shear sense.

C) Highly strained augen-gneiss, Cincovillas gneiss, showing an intense D2 flattening and deformation of the primary feldspar megacrysts. The strain partitioning around the feldspar megacrysts and the symmetry of the porphyroclast tails do not allow reliable determination of the shear sense; view parallel to the stretching lineation.

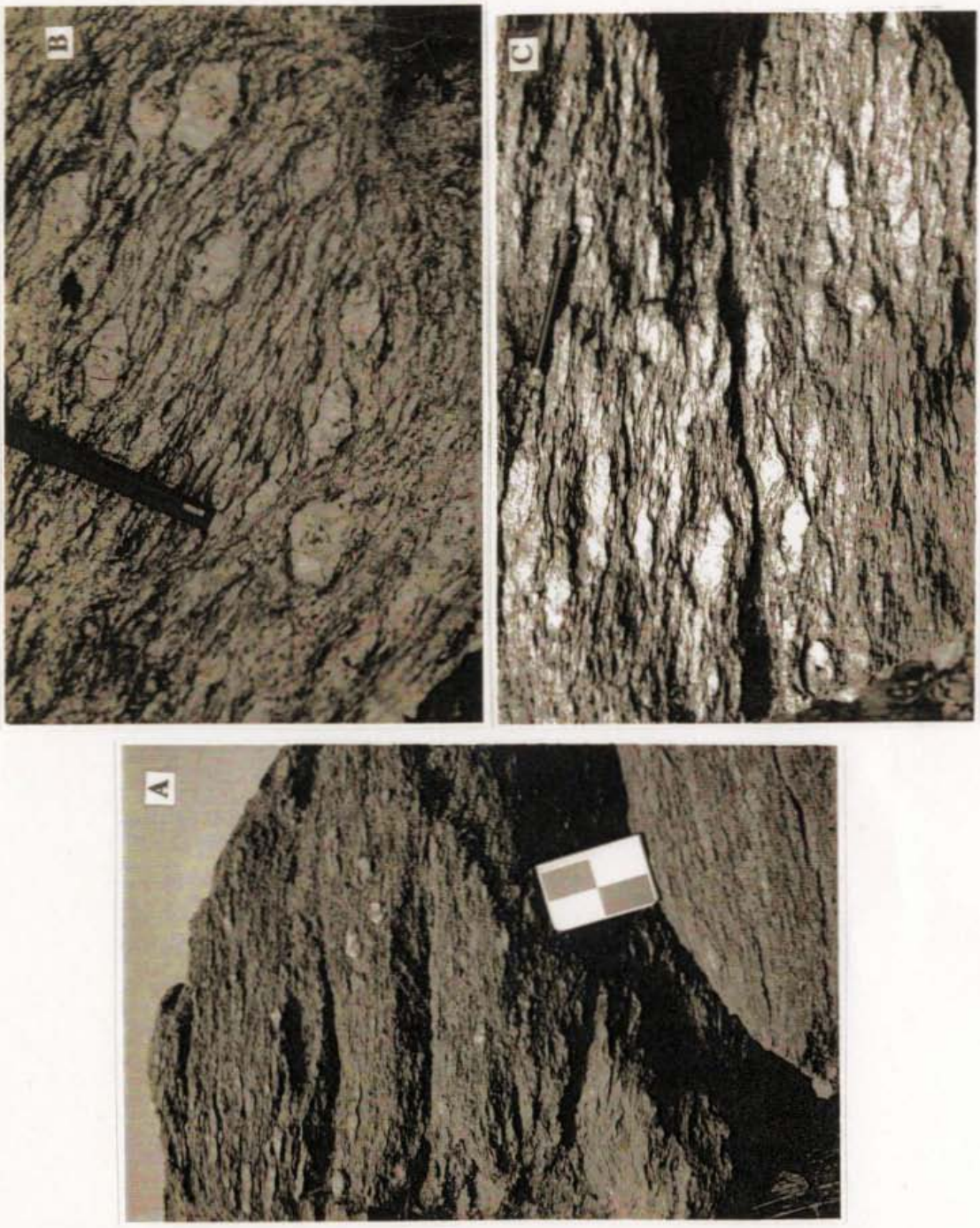
B
C
A

Fig.6.15.- Gneissic leucogranites of the Western Guadarrama Domain, Manjiron antiform (Ms+Sill zone). Top: Foliated leucogranite with a diatexitic apperance, Horcajuelo gneiss, Rio Cocinillas section. **Bottom:** Garnet-bearing strongly foliated leucogranite, Puentes Viejas dam.

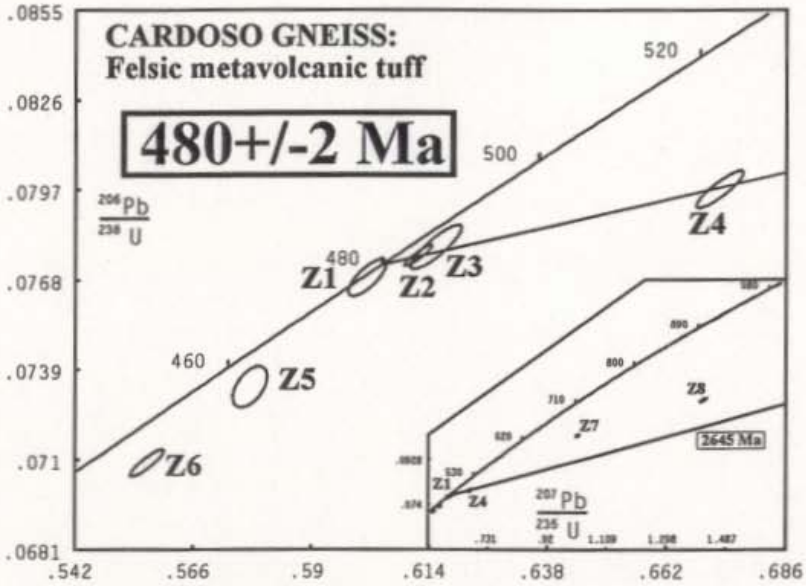

Fig.6.16.-U-Pb concordia diagram for the Cardoso gneiss and a weakly deformed hand sample showing the volcaniclastic character of this rock.

TABLE 6.1.- U-Pb DATA, PRE-VARISCAN PROTOLITH AGES, SIERRA DE GUADARRAMA

Description / Fraction	Weight (mg)	Concentration U (ppm)	Concentration Pb rad (ppm)	Measured Total common Pb (Pg)	Measured $^{206}Pb/^{204}Pb$	Corrected atomic ratios* $^{208}Pb/^{206}Pb$	$^{206}Pb/^{238}U$	±	$^{207}Pb/^{235}U$	±	$^{207}Pb/^{206}Pb$	±	Age (Ma) $^{206}Pb/^{238}U$	Age (Ma) $^{207}Pb/^{235}U$	Age (Ma) $^{207}Pb/^{206}Pb$
1.- Cardoso gneiss, volcaniclastic rock, 60950-49720†															
Z1 Needles AB	0.0416	412	31	12	7049	0.0811	0.07688	50	0.6013	32	0.05673	24	477	478	481
Z2 Clr. needles w/small incl. AB	0.1290	372	28	37	6321	0.0835	0.07760	28	0.6117	23	0.05717	08	482	485	498
Z3 Needles AB	0.0240	327	25	12	3322	0.0779	0.07787	58	0.6153	42	0.05731	20	483	487	503
Z4 Needles w/ small incl. AB	0.0590	474	37	26	5349	0.0695	0.07972	48	0.6727	38	0.06120	18	494	522	646
Z5 Needles NAB	0.0561	285	20	30	2504	0.0791	0.07335	54	0.5776	28	0.05711	36	456	463	496
Z6 pencil-like ndl NAB	0.0821	324	22	12	3861	0.0682	0.07090	36	0.5566	28	0.05694	14	441	449	489
Z7 Stb eu. multifaced pr AB	0.0721	304	32	41	3454	0.1101	0.10289	36	1.0177	38	0.07173	10	631	713	978
Z8 Stb eu. multifaced pr AB	0.0712	265	32	46	3033	0.1197	0.11773	60	1.4159	74	0.08723	14	717	896	1365
2.- Riaza gneiss, mylonitic granite, 61750-66150															
Z1 Needles AB	0.0068	404	29	11	1191	0.0505	0.07541	60	0.5808	72	0.05673	58	469	471	481
Z2 Sm. pr. AB	0.0452	456	31	12	7609	0.0502	0.07171	38	0.5567	29	0.05631	14	446	449	465
Z3 Ndl w/ few incl AB	0.0134	558	37	59	582	0.0431	0.07107	48	0.5519	47	0.05633	36	443	446	465
Z4 Ndl AB	0.0283	392	25	11	4252	0.0439	0.06818	32	0.5294	22	0.05631	16	425	431	465
Z5 Sm pr & ndl AB	0.0274	464	33	36	1696	0.0557	0.07495	34	0.5869	29	0.05679	12	466	469	483
Z6 Eu. pr. AB	0.0561	333	24	36	2517	0.0492	0.07699	30	0.6369	24	0.06000	16	478	500	604
Z7 Ndl AB	0.0148	406	29	13	2127	0.0635	0.07338	58	0.5974	38	0.05904	32	456	476	569
Z8 Large eu pr AB	0.0595	543	38	34	4411	0.0449	0.07312	28	0.6068	24	0.06019	10	455	482	610
3.- Buitrago gneiss, foliated megacrystic granite, 45675-37575															
Z1 Clr. ndl w/ incl. AB	0.0316	676	47	15	6610	0.0350	0.07432	32	0.5808	25	0.05667	12	462	465	479
Z2 Ndl AB	0.0198	373	26	8	4067	0.0419	0.07352	62	0.5724	42	0.05647	28	457	460	471
Z3 0°M clr ndl w/ rd tips AB	0.1170	700	46	218	1680	0.0318	0.07074	36	0.5552	30	0.05692	10	441	448	489
Z4 Clr. ndl w. incl NAB	0.0887	901	54	69	4705	0.0260	0.06499	22	0.5013	18	0.05594	06	406	413	450
Z5 Ndl NAB	0.0687	846	51	67	3518	0.0278	0.06480	26	0.4998	21	0.05594	08	405	412	450
Z6 Ndl NAB	0.0373	1822	108	68	4015	0.0252	0.06360	56	0.4905	43	0.05593	12	398	405	449
4.-Buitrago gneiss, foliated aplitic vein, 45675-37575															
Z1 Clr. eu. ndl AB	0.0134	3056	203	36	5059	0.0314	0.07171	58	0.5540	44	0.05654	14	443	448	473
Z2 Ndl. w/ incl &cracks AB	0.0472	2046	123	124	3181	0.0176	0.06520	36	0.5068	29	0.05638	10	407	416	467
Z3 Ndl. AB	0.0113	1825	108	23	3583	0.0188	0.06376	40	0.4968	29	0.05652	18	398	410	473
Z4 Clr. incl. free ndl NAB	0.0317	2614	147	242	1309	0.0248	0.06034	36	0.4657	29	0.05597	12	378	388	451
Z5 Ndl. NAB	0.0244	2443	134	258	872	0.0221	0.05920	84	0.4581	84	0.05613	10	371	383	457
5.-Buitrago gneiss, Pinilla de Buitrago, foliated leucogranite, 43200-36575															
Z1 Sm pr & ndl AB	0.0347	717	46	53	2050	0.0367	0.06836	26	0.5310	22	0.05634	12	426	432	466
Z2 Eu. pr. AB	0.0188	699	43	30	1833	0.0364	0.06624	44	0.5118	32	0.05603	22	413	420	454
Z3 Ndl (20 xtals) AB	0.0137	780	48	39	1134	0.0354	0.06545	44	0.5073	34	0.05622	20	409	417	461
Z4 1:5 Sm pr AB	0.0580	1072	64	190	1333	0.0312	0.06389	20	0.4949	19	0.05617	10	399	408	459
Z5 Ndl AB	0.0796	1569	86	393	1193	0.0218	0.05890	22	0.4532	19	0.05581	08	369	380	445
6.-Lozoyuela gneiss, augen gneiss, 35550-33500															
Z1 single xtal AB	0.0256	288	22	9	4085	0.0924	0.07683	58	0.5999	36	0.05663	28	477	477	477
Z2 Ndl & sm pr. AB	0.0282	472	32	8	7018	0.0514	0.07084	40	0.5487	26	0.05618	20	441	444	459
Z3 Eu. ndl AB	0.0150	413	27	14	1970	0.0463	0.06936	46	0.5368	33	0.05612	24	432	436	457
Z4 Eu. gem pr. AB	0.0774	404	29	12	12216	0.0584	0.07493	28	0.6023	22	0.05830	10	466	479	541
Z5 Eu. gem pr. AB	0.2165	306	33	18	24698	0.1016	0.10706	32	1.2316	40	0.08344	08	656	815	1279
M1 2 large xtals AB	0.0378	11553	1120	141	9987	1.1326	0.05136	26	0.3744	19	0.05288	08	323	323	324
M2 Medium eu. pale y. AB	0.0438	10180	1280	89	16694	1.6997	0.05286	24	0.3876	18	0.05318	04	332	333	338
M3 Pale y. ABR	0.0200	5803	878	25	16025	2.0962	0.05555	20	0.4114	15	0.05372	06	348	350	359
X1 Clr eu. y.-green NAB	0.0440	2722	288	101	3844	1.3412	0.05126	26	0.3733	20	0.05281	08	322	322	321

1.- Z = zircon, M = monazite, X = xenotime, s = small (<80 μm), m= medium (>80 and <150 μm), l = large (>150 μm), Ndl. = Needles (1:10 to 1:7 width/length ratio), pr = prisms (1:6 to 1:4), stb = stubby (1:3 to 1:1), clr = clear, eu. = euhedral, y.= yellow, AB = air abraded (Krogh, 1982), NAB = not abraded, rd = rounded, w/ = with, inc = inclusions, xtal = crystal

2.- Uncertainty in sample weight ± 0.001 mg (2 sigma)

3.- Atomic ratios corrected for fractionation and spike, 8 to12 pg Pb blank lab procedure (25 pg- monazite and xenotime), initial common Pb (Stacey and Kramers, 1975) and 1 pg U blank. 2 sigma errors reported for corrected isotopic ratios.

† Sample location in U.T.M. coordinates, 30TVL UTM zone and 100 km square.

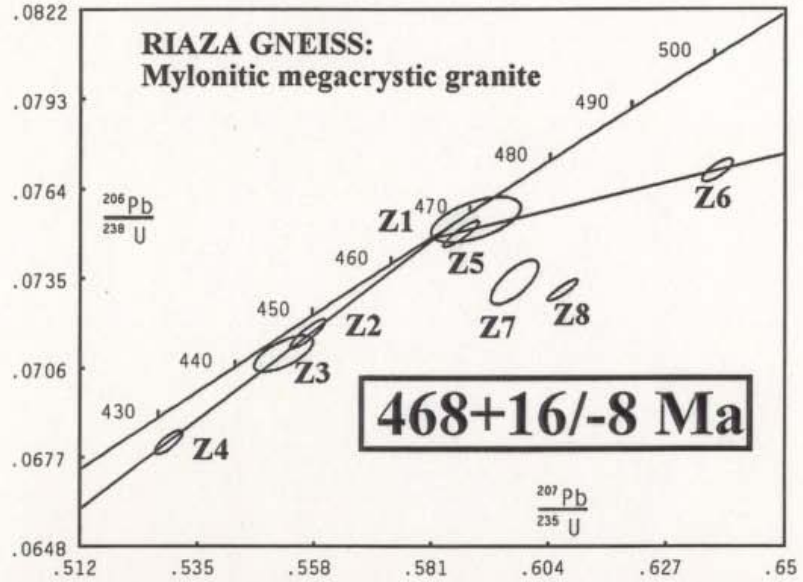

Fig.6.17.- U-Pb concordia diagram for the Riaza gneiss and field apperance of the strongly mylonitized facies. Hammer shaft is approximately 60 cm. long.

Fig.6.18.- Buitrago gneiss. Left: Sampling site for samples BU-1 (foliated megacrystic granite) and BU-2 (foliated aplitic vein) showing BU-2 intrusive into BU-1, the view is orthogonal to the stretching lineation. **Right: Concordant deformation of the thin end of the aplitic dyke (BU-2) and the country rock (BU-1).** This relationship indicates that the apparent fabric/dyke cross-cutting relationship on the sampling site (left) is an effect of the contrast of competencies and the composite character of the fabric in the megacrystic sample BU-1. Both pictures are from the same continuous outcrop, abandoned quarry SW of Buitrago.

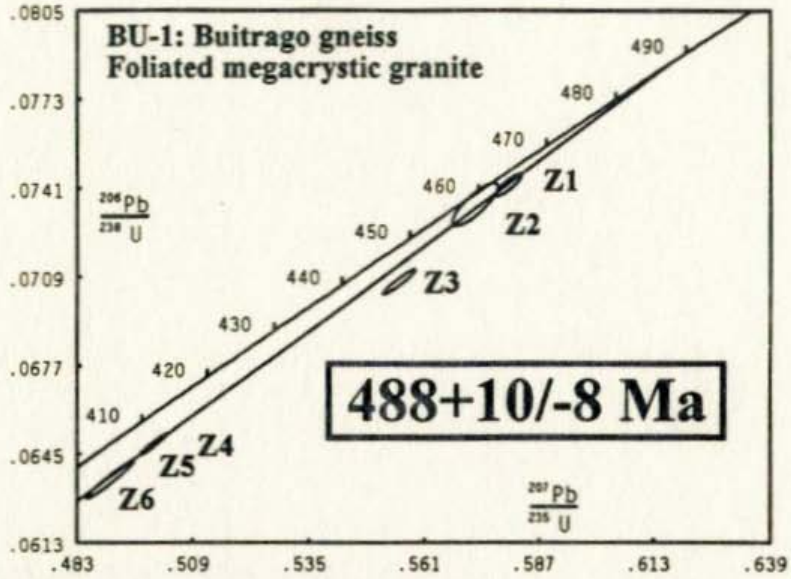

Fig. 6.19.- U-Pb concordia diagram for the foliated megacrystic granite facies of the Buitrago gneiss, sample BU-1. Z., zircon.

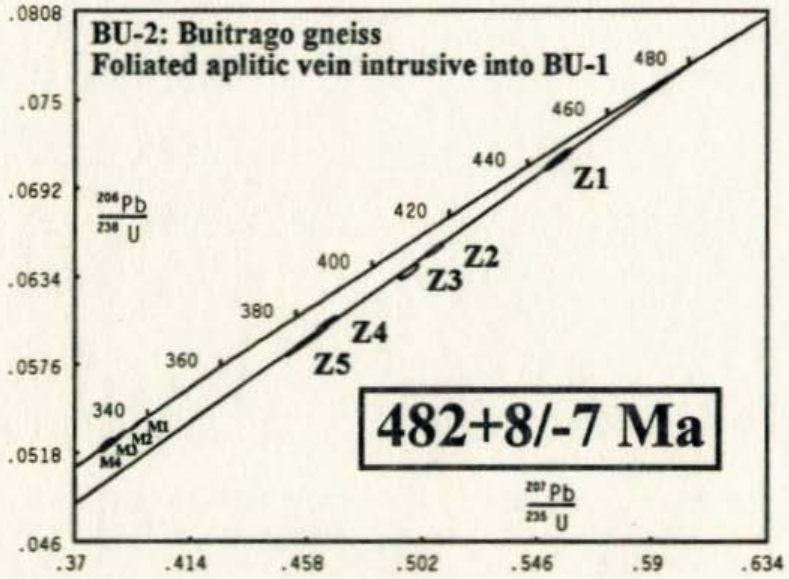

Fig. 6. 20.- U-Pb concordia diagram for sample BU-2, foliated aplitic vein intrusive into BU-1, Buitrago gneiss. Z., zircon; M, monazite.

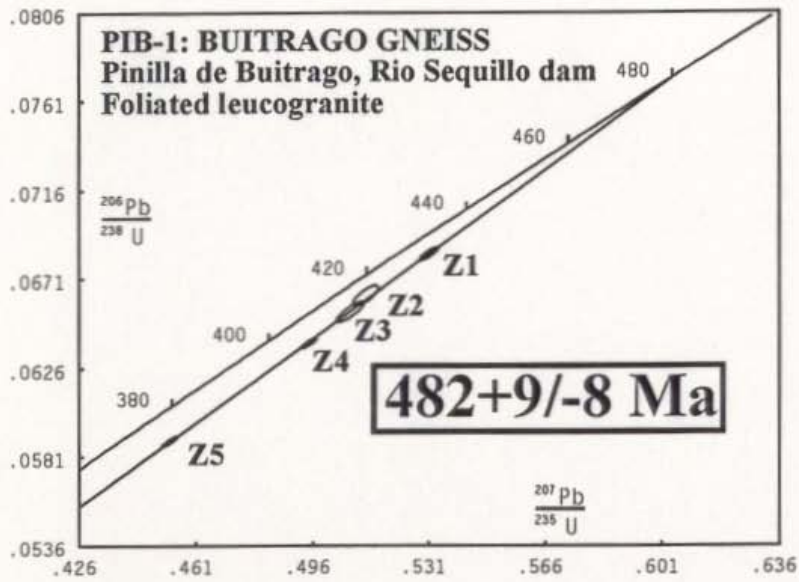

Fig.6.21.- U-Pb concordia diagram for sample PIB-1, garnet-bearing foliated leucogranite in the Buitrago gneiss, and field character of the dated sample. Pen for scale is 13.5 cm long. Location: western side of the Rio Sequillo dam in the vicinity of Pinilla de Buitrago.

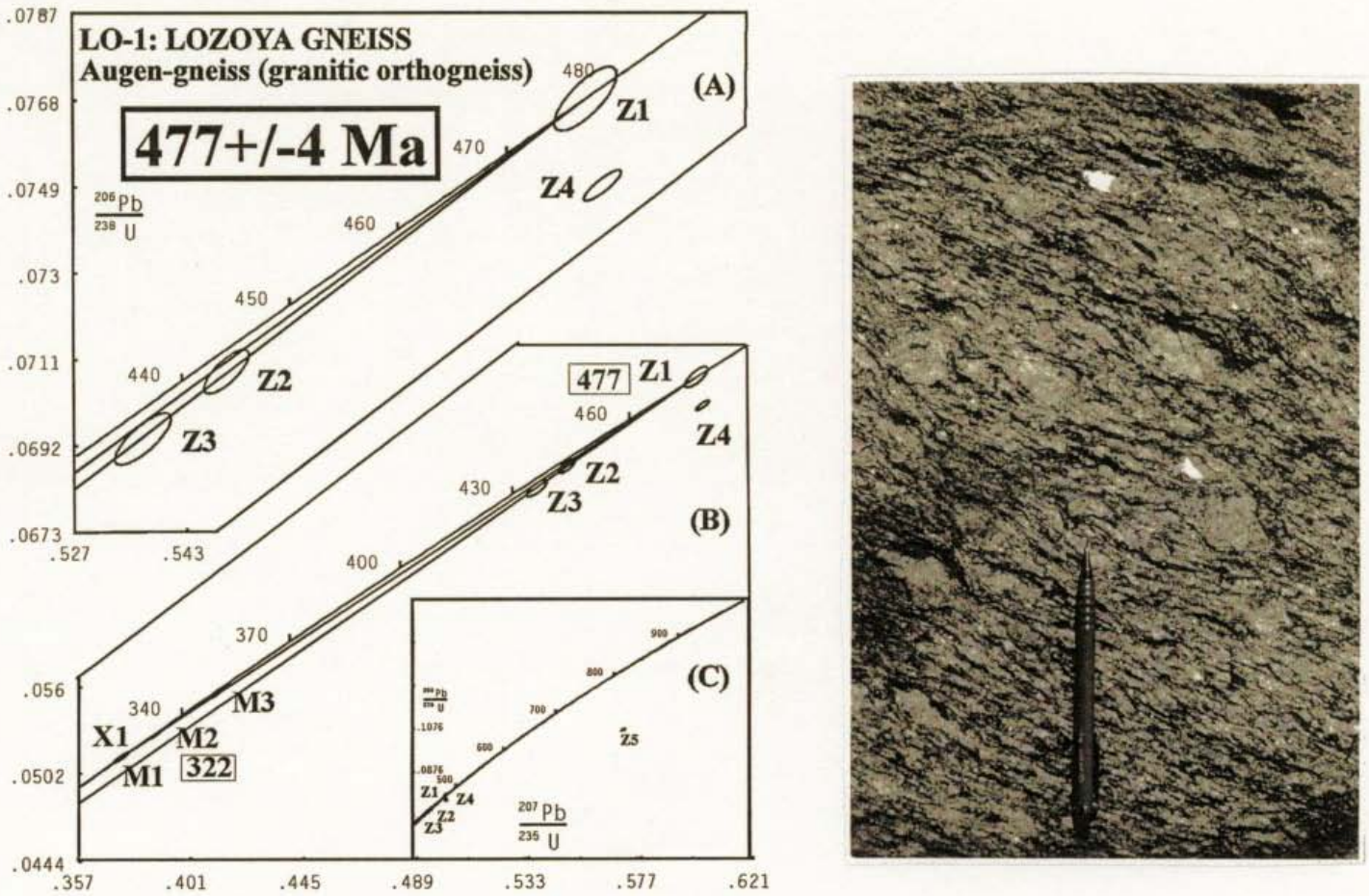

Fig.6.22.- U-Pb concordia diagram for the Lozoya gneiss: (A) Detail of the upper intercept of the two independent zircon and monazite discordia lines and the concordant single crystal analysis Z1. (B) Zircon and monazite discordia lines. (C) Inset concordia diagram showing the position of the highly discordant zircon fraction Z5. Right: Field aspect of sample LO-1. Pen for scale is 14 cm long.

Figure 6.23

Fig. 6.23.-Location of the new protolith U-Pb ages for the pre-Variscan orthogneisses of the Sierra de Guadarrama. (**A**) Tectono-stratigraphic zones of the northern Iberian Massif showing the distribution of pre-Mid Ordovician augen-gneisses and coarse felsic volcaniclastics (Ollo de Sapo gneisses) and the location of relevant published geochronological data: bold, U-Pb data (Lancelot et al., 1985; Gebauer et al., 1993); bold italics, Rb-Sr data (Vialette et al., 1987). (**B**) Geological map of the field area (modified after Hernaiz Huerta et al., in press) with the location of the new U-Pb zircon ages.

Legend:

1, Mesozoic deposits. Eastern Guadarrama Domain: 2, Rodada series, black shales and siliciclastic rocks (Llanvirn-Ashgill); 3, Armorican quartzite (Alto Rey fm., Arenig?); 4, pre-Mid Ordovician micaschists, metapsammites and metaquartzites with minor para-amphibolite (including the Constante formation); 5, metavolcanic Cardoso gneiss. Berzosa-Riaza shear zone (BRSZ): 6, mylonitic fabrics in the BRSZ; 7, mylonitic megacrystic granites within the BRSZ (Riaza, Nazaret and Berzosa gneisses). Western Guadarrama domain: 8, micaschists, paragneisses and migmatites; 9, augen-gneisses and foliated megacrystic granites; 10, leucogneisses (might include undated Variscan foliated S-type granites). 11, post-collisional (La Cabrera) granite-granodiorite. 12, Variscan greenschist facies extensional detachments. 13, brittle faults including both Variscan and Mesozoic faults. B, Buitrago; C, El Cardoso; L, Lozoya; M, Montejo; P, Pradena; R, Riaza

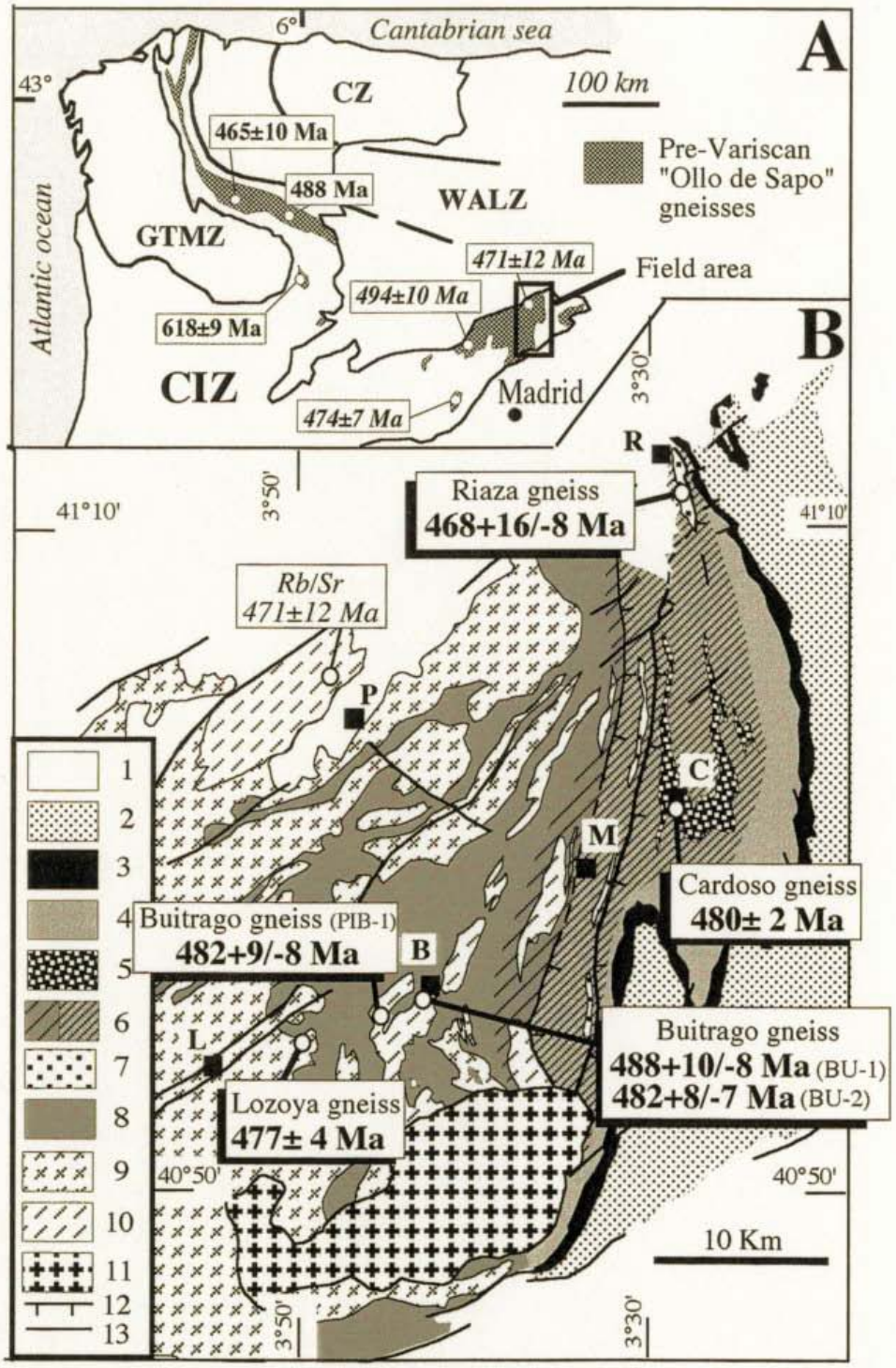
A
B
Cantabrian sea
6°
43°
Atlantic ocean
CZ
100 km
465±10 Ma
488 Ma
WALZ
GTMZ
Pre-Variscan
"Ollo de Sapo"
gneisses
471±12 Ma
Field area
494±10 Ma
618±9 Ma
CIZ
Madrid
474±7 Ma
3°30'
3°50'
41°10'
R
Riaza gneiss
468+16/-8 Ma
Rb/Sr
471±12 Ma
P
C
M
Cardoso gneiss
480± 2 Ma
Buitrago gneiss (PIB-1)
482+9/-8 Ma
B
L
Buitrago gneiss
488+10/-8 Ma (BU-1)
482+8/-7 Ma (BU-2)
Lozoya gneiss
477± 4 Ma
40°50'
10 Km
1
2
3
4
5
6
7
8
9
10
11
12
13

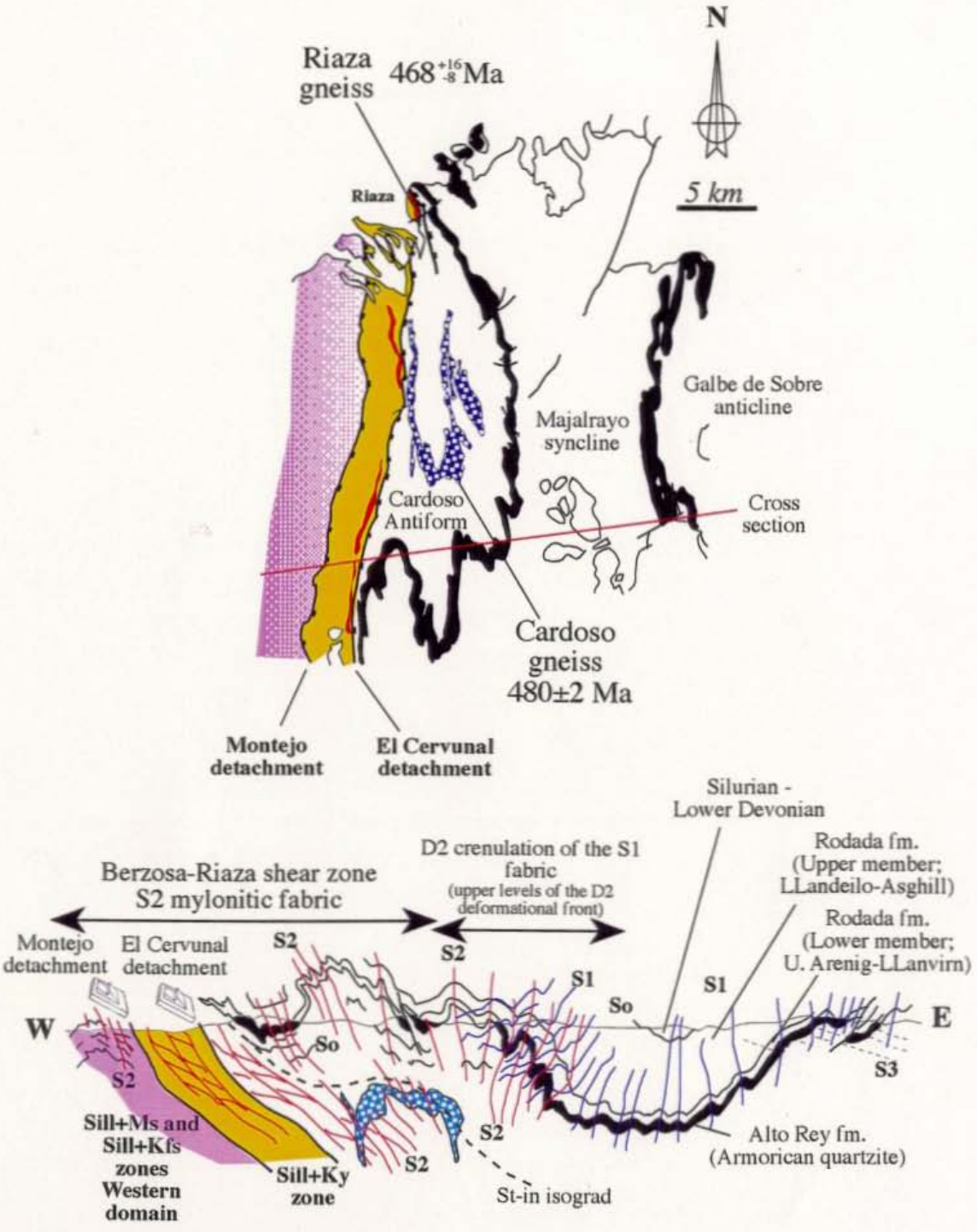

Fig. 6.24.- Schematic geological map and interpretative cross-section of the Berzosa-Riaza shear zone (BRSZ), the Cardoso antiform, the Majalrayo syncline and the western flank of the Galbe de Sorbe antiform (After Hernaiz Huerta et al., 1996).

Figure 6.25

II-1 : cross section (Fig. 6.43)

Fig. 6.25.- Geological map of the Benivengo-Montelo-Barcena area. Topographic base after Fernandez Casals (1979)

Fig. 6.25.- Geological map of the Buitrago-Montejo-Berzosa area. Topographic base after Fernandez Casals (1979)

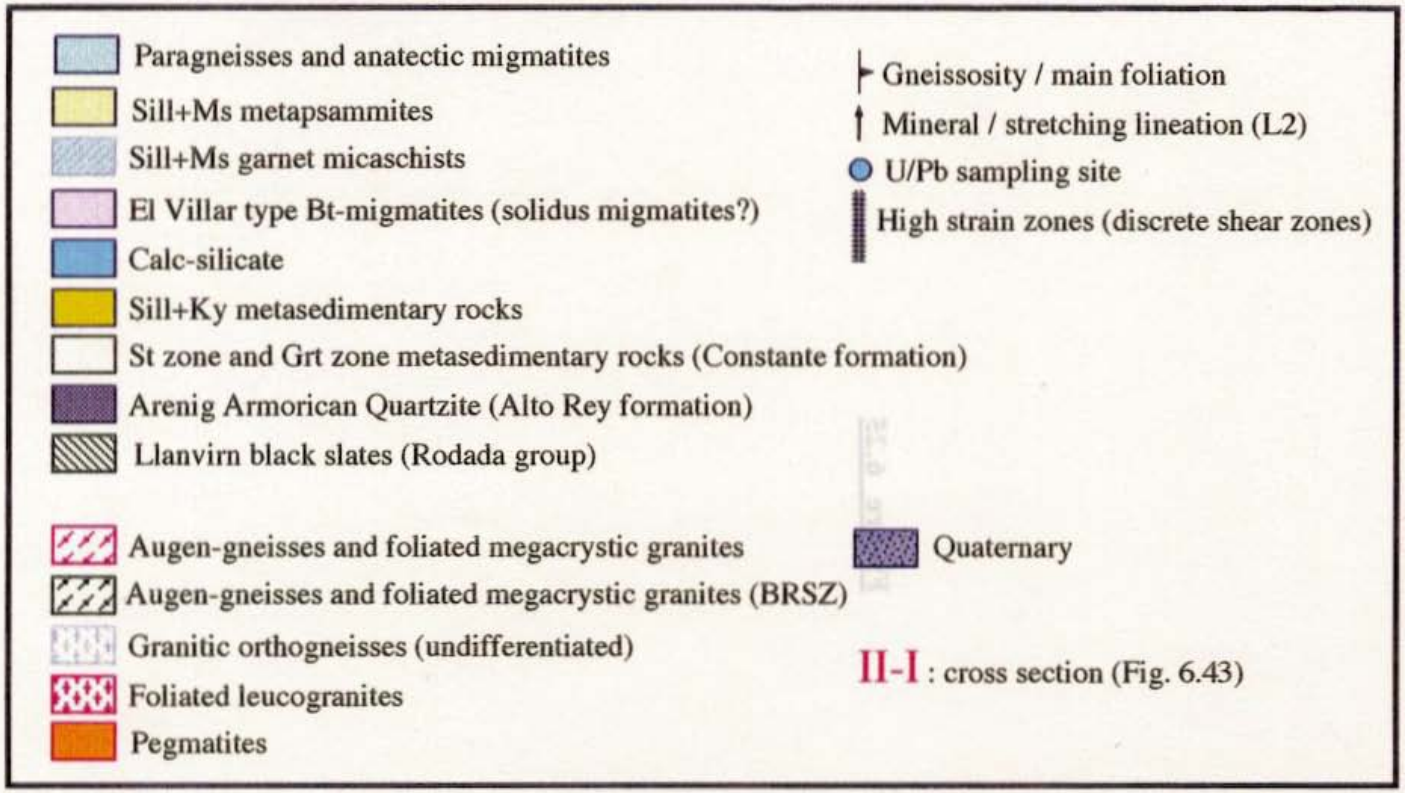

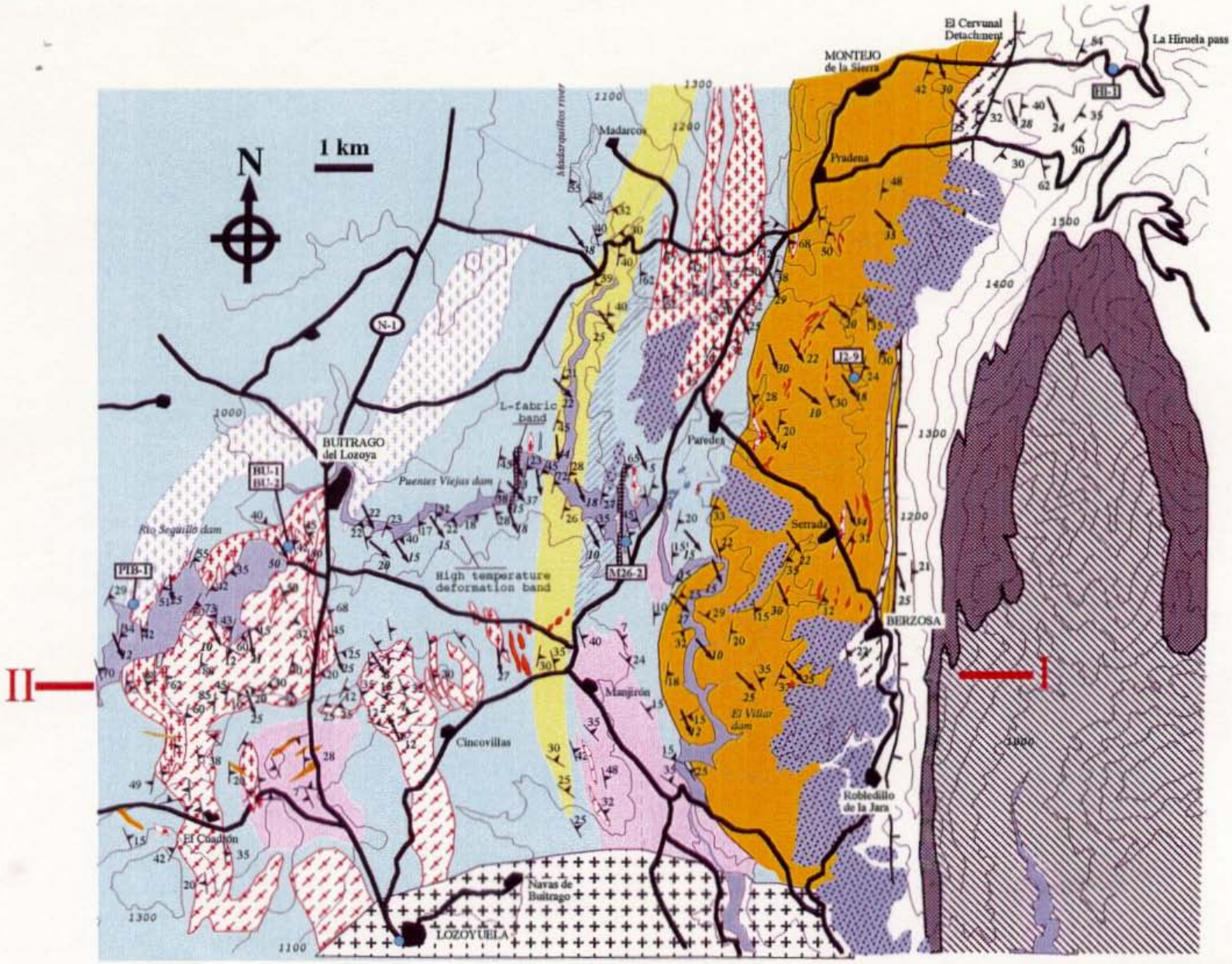
N
1 km
El Cervunal Detachment
La Hiruela pass
MONTEJO de la Sierra
Madarcos
Pradena
Paredes
Serrada
BERZOSA
BUITRAGO del Lozoya
Puentes Viejas dam
Río Sequillo dam
L-fabric band
High temperature deformation band
El Villar dam
Manjirón
Cincovillas
El Cuadrón
Navas de Buitrago
LOZOYUELA
Robledillo de la Jara
N-1
BU-1
BU-2
PTB-1
M26-2
P2-9
HI-1
II
I
1000
1100
1200
1300
1400
1500

Figure 6.26

Fig.6.26.- Microtextures along the metamorphic zones of the lower levels of the Eastern Guadarrama domain and the upper levels of the Western domain (BRSZ).

Top: Chloritoid-bearing black slate showing a spaced S2 crenulation cleavage affecting the S1 fabric and the inter D1-D2 chloritoid (Cld) porphyroblasts. Eastern Guadarrama domain, D2 crenulation of the S1 fabric, Bt-zone (Llanvirn black slates of the Rodada group 1 km east of Robledillo de la Jara; Fig.6.25). Field of view is 5.21 mm long.

Middle: Eastern Guadarrama domain, upper levels of the BRSZ, St-zone, late-D2 growth of staurolite and partial D2 transposition of the S1 fabric. U-Pb sample Hi-1 (Fig.6.25), La Hiruela mountain pass. Field of view is 9 mm long.

Bottom: Western Guadarrama domain, BRSZ, Sill (Ky) zone. quartz + muscovite-bearing micaschist with relict staurolite and kyanite. The winged kyanite porphyroblasts are inter D1-D2, indicate a top down to the SE shear sense (ie. dextral) and show D2 pressure shadows with new growth of sillimanite (fibrolite) and biotite. The D2 fabric is defined by oriented Bt+Sill (fibrolite)+Ms. U-Pb sample J2-9 (Fig.6.25). Field of view is 5.2 mm long.

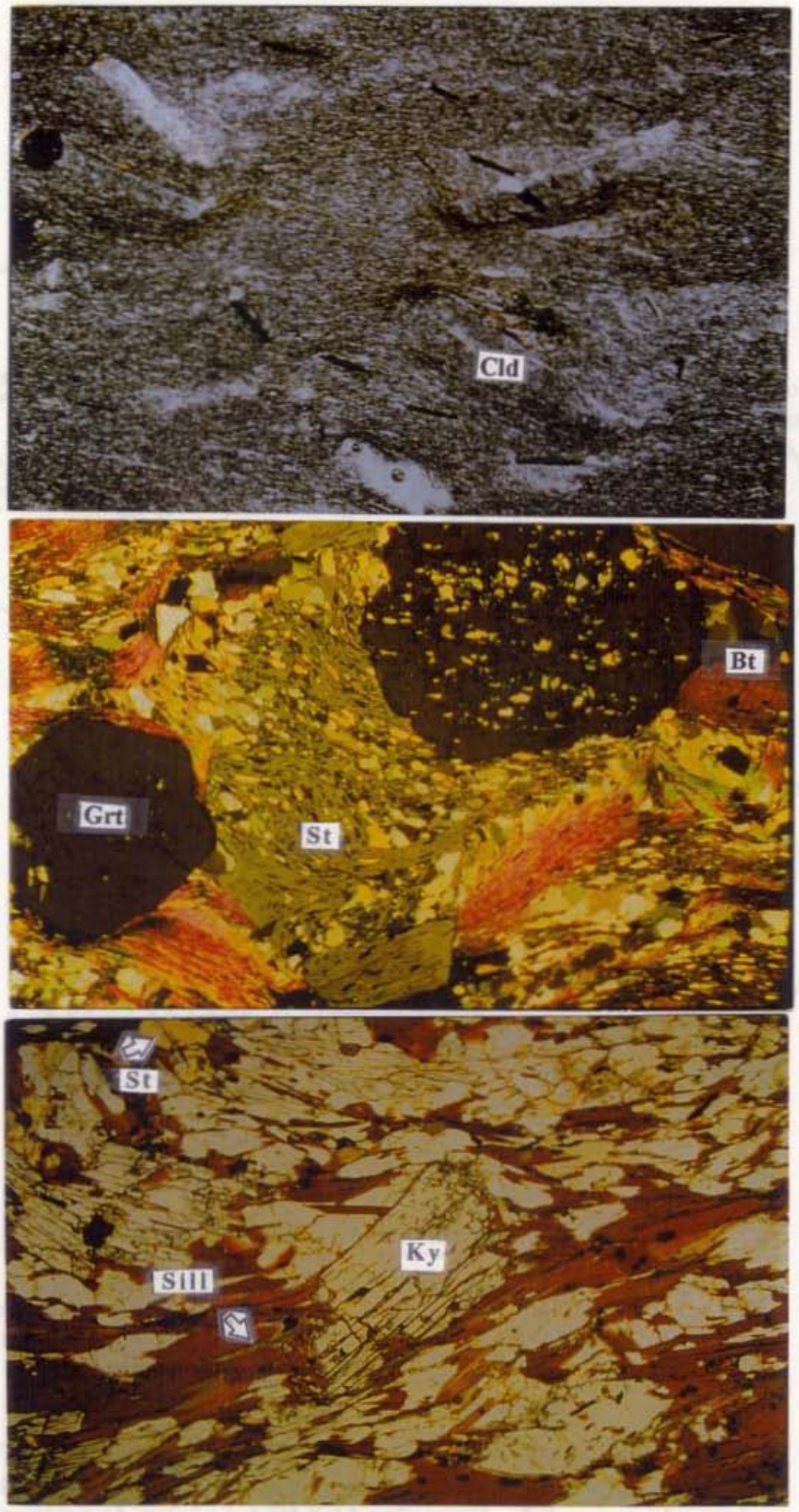
Cld
Bt
Grt
St
St
Ky
Sill

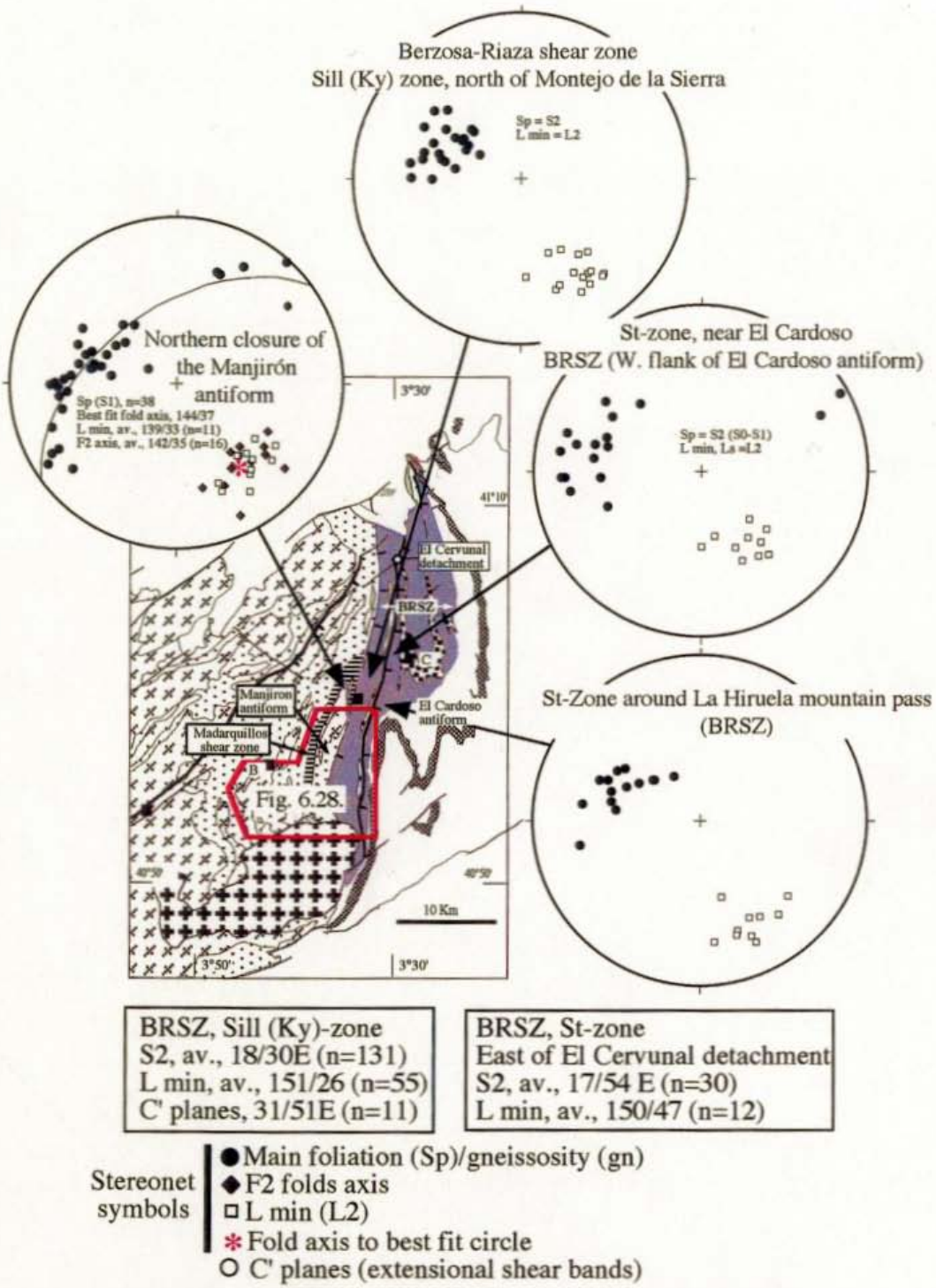

Fig. 6.27.- Equal area, lower hemisphere stereonet projections of the main foliation/gneissosity, mineral and stretching lineation (L min) and F2 fold axis north of the area shown in detail in Fig. 6.25 (red area). B, Buitrago; C, El Cardoso.

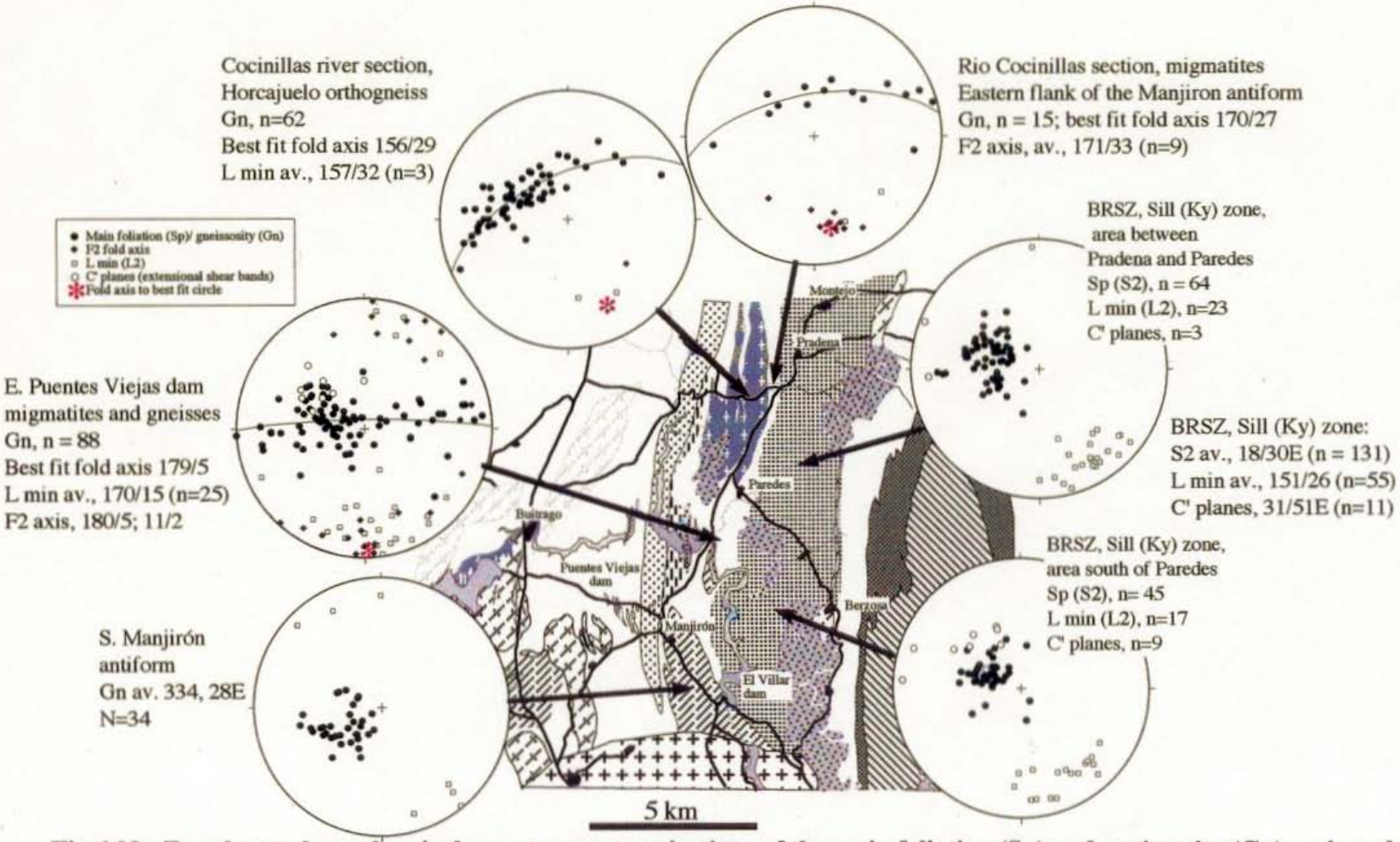

Fig.6.28.- Equal area, lower hemisphere, stereonet projections of the main foliation (Sp) and gneissosity (Gn), mineral lineation (Lmin), F2 fold axis, C' planes (extensional shear bands) and best fit plane and theoretical fold axis for the Berzosa-Riaza shear zone (BRSZ; Sill (Ky) zone) and the Manjirón antiform.

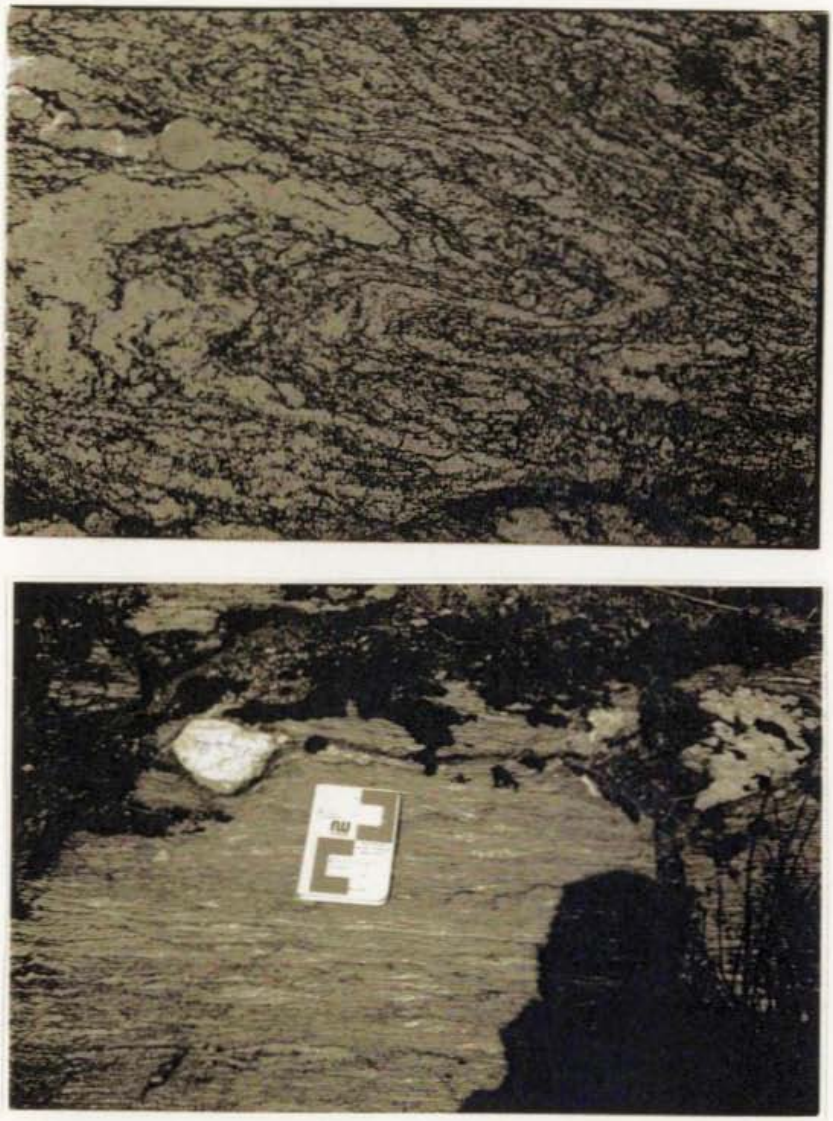

Fig.6.29.- Deformation in the southern part of the Manjiron antiform. Top: Isoclinal folding (D2?) of the gneissosity in the El Villar biotite-bearing migmatites (solidus migmatites), SE border of the Manjiron antiform. **Bottom: Apparently dextral D2 ductile shear zone in the granitic orthogneisses at the SW border of the Manjiron antiform.** View slightly oblique to the stretching lineation.

Figure 6.30

Fig.6.30.- Microtextures along the metamorphic zones of Western Guadarrama domain in the area of study.

Top: Manjiron antiform, sillimanite+muscovite micaschist showing refolded fibrolite (Sill) patches and recrytallized muscovite defining D2 microfolds. Field of view is 9 mm long.

Middle: Madarquillos shear zone, sillimanite+muscovite metapsammites, oriented sample. D2 fabric with S-C structures with stable biotite+sillimanite+ muscovite indicating a shear sense of top down to the SE (ie.dextral). Field of view is 11 mm long.

Bottom: Buitrago area, Sill+Kfs zone. D2 fabric in migmatitic paragneiss with alternating biotite+sillimanite and K-feldspar+quartz+(plagioclase) layers, and elongated and flattened garnet porphyroblasts. Field of view is 5.2 mm long.

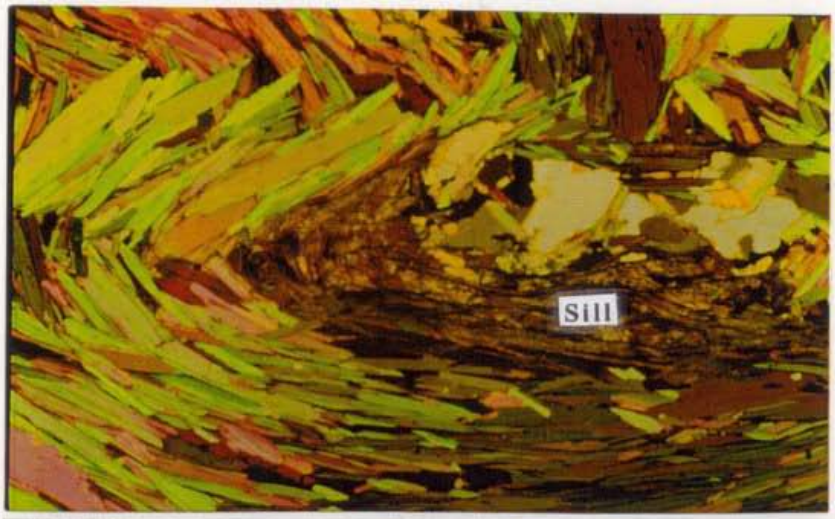
Sill


Sill

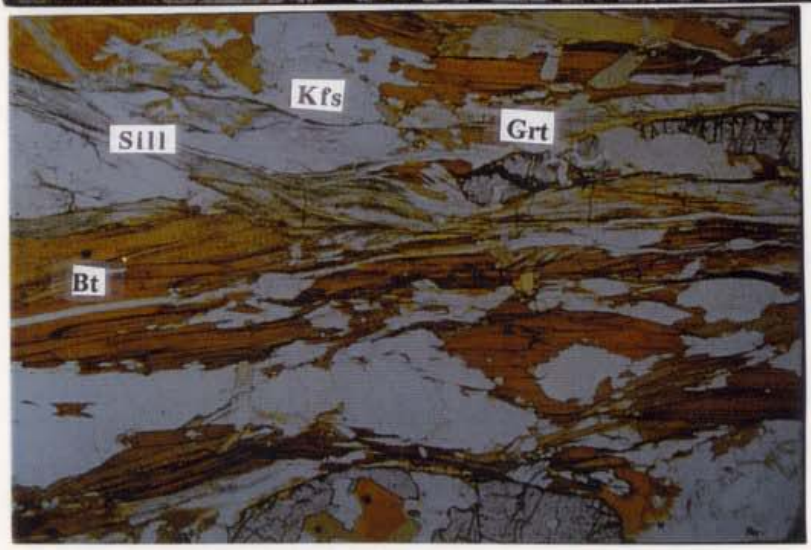
Kfs
Sill
Grt
Bt

Fig.6.31.- F2 folds and D1-D2 relationships in the Madarquillos shear zone. Top: Isoclinal F2 fold in Sill+Ms metapsammites. **Bottom:** Sill+Ms metapsammites. Asymmetrical F2 fold with axial planar S2 foliation overprinting S0 compositional banding and oblique S1 foliation (parallel to quartz veins).

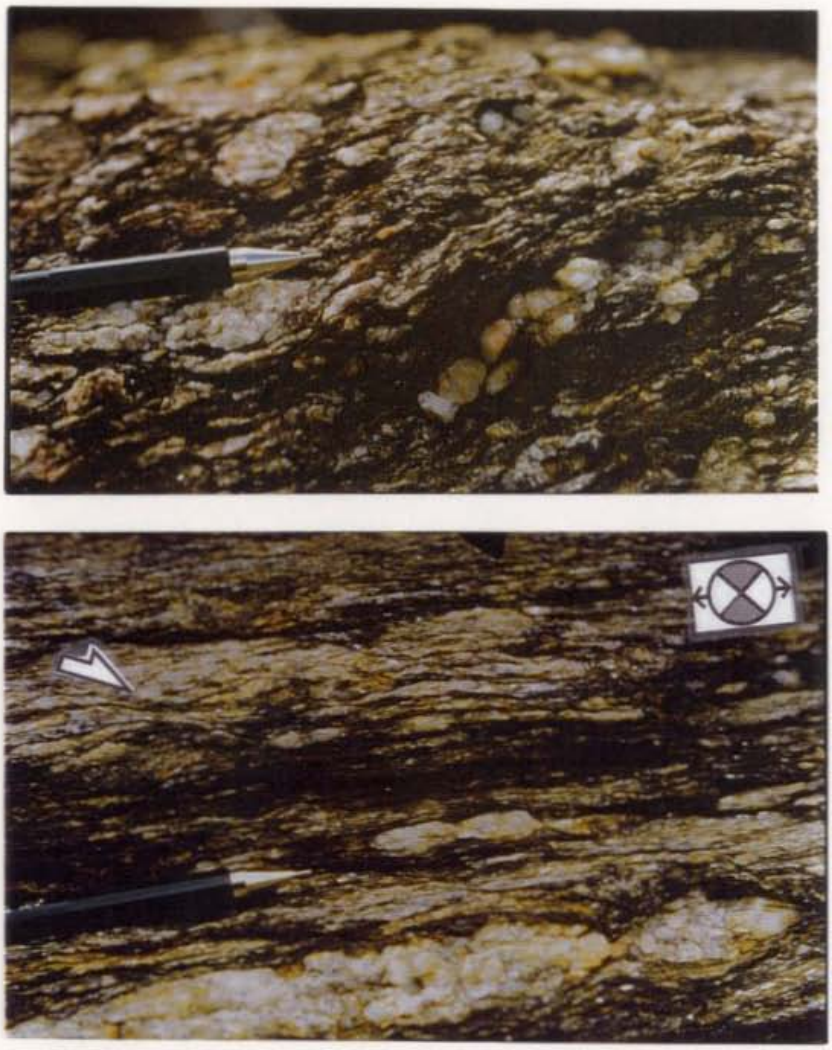

Fig.6.32.- D2 microstructures in Sill+Ms micaschists. Top: Orthogonal view to the mineral lineation (centimetric fibrolite patches) showing D2 crenulation of an earlier foliation (S1?). **Bottom:** Same outcrop, parallel view to the mineral lineation (Sill) showing flattened D2 S-C structures, D2 boudinage of quartz veins and associated D2 shear bands (C'planes, arrow showing the shear sense) with stable fibrolite. Top to the S-SE (dextral) shear sense.

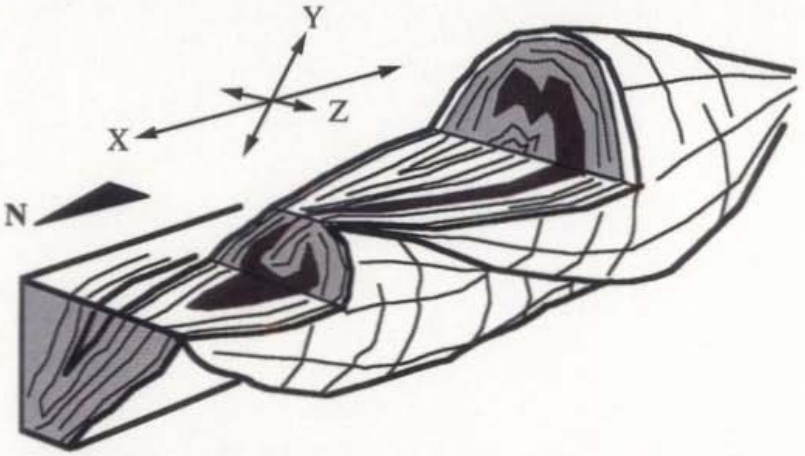

Fig. 6.33.- Relationships between D2 boudinage (X directed) **and F2** (X-Y) **folding of a competent layer during top down to the SE shearing.** In the field photograph, the shaft of the hammer is oriented parallel to the stretching lineation. Manjiron antiform-Madarquillos shear zone border, Sill + Ms micaschists in the eastern Puentes Viejas dam.

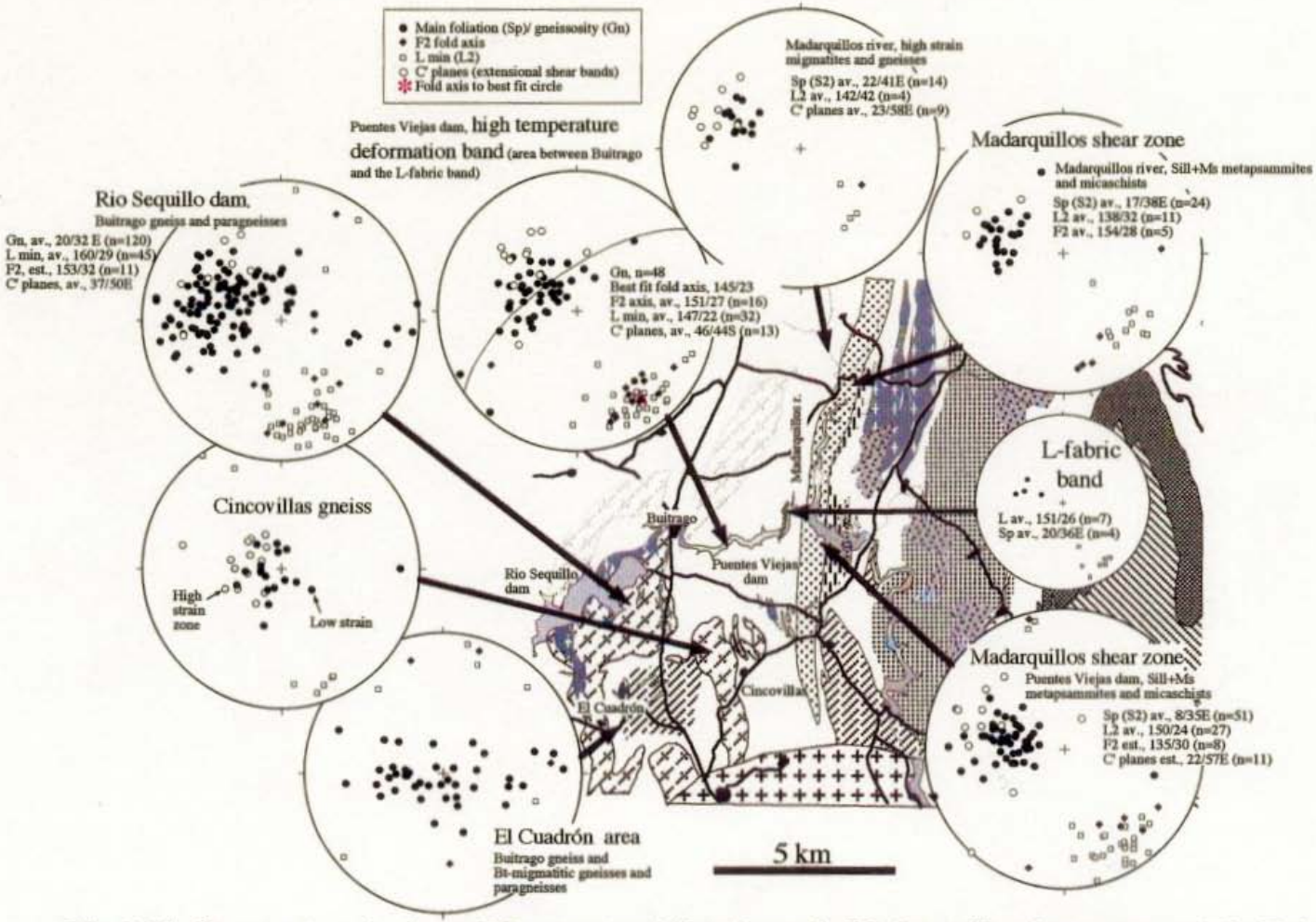

Fig. 6.34.- Stereonet projections of the structural data from the Madarquillos shear zone and the Buitrago area.

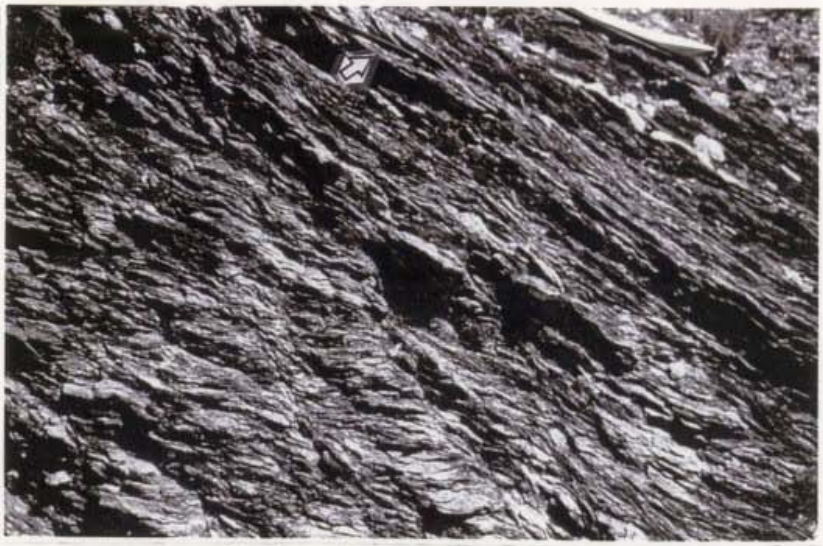

Fig.6.35.- Shear bands (C'planes) in the Madarquillos shear zone indicating a shear sense of top down to the SE. Pen for scale (top) is 15 cm long.

Fig.6.36.- L-fabric band: L-fabric and associated quartz-rods. Puentes Viejas dam.

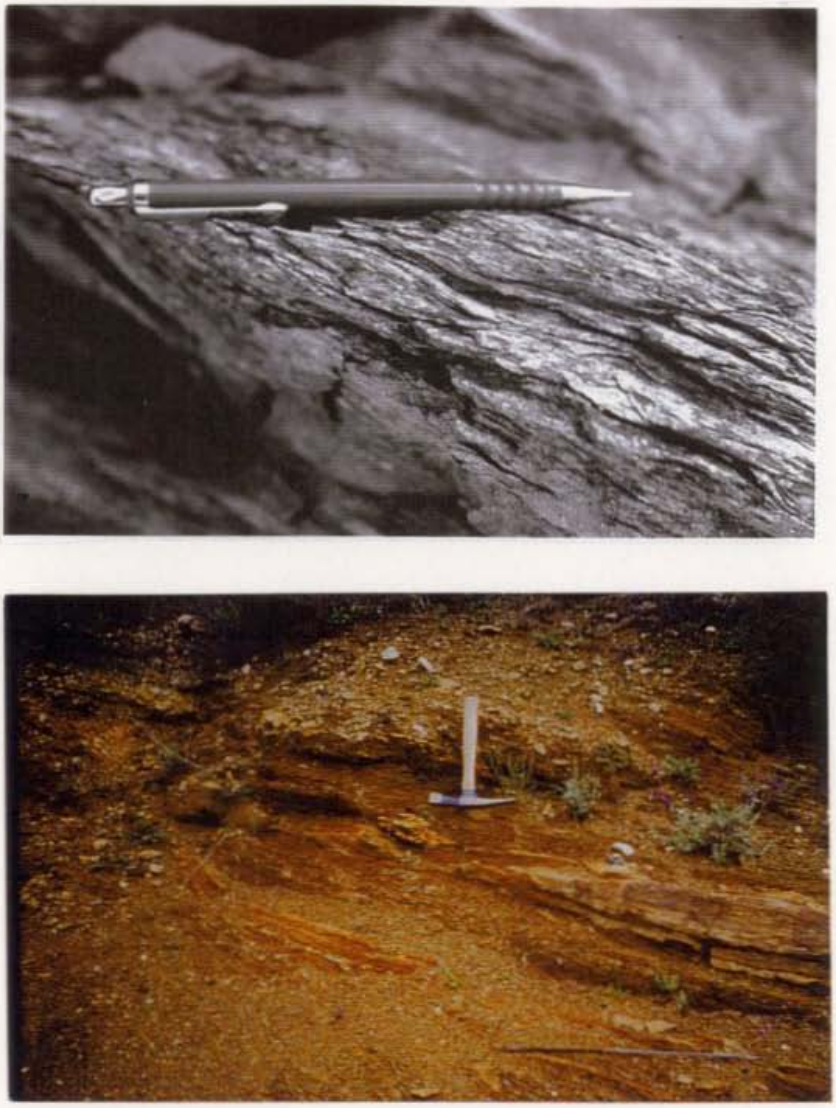

Fig.6.37.- Kinematic indicators with opposite top to the NW D2 shear sense (ie. sinistral) in the western margin of the Madarquillos shear zone, view parallel to Ls. Top: Discrete level with opposite shear sense in a top to the SE dominated area, Madarquillos river road section. **Bottom:** Sinistral asymmetrical boudinage in the Puentes Viejas dam, area dominated by top to the NW shear sense. The head of the hammer is oriented parallel to the stretching lineation.

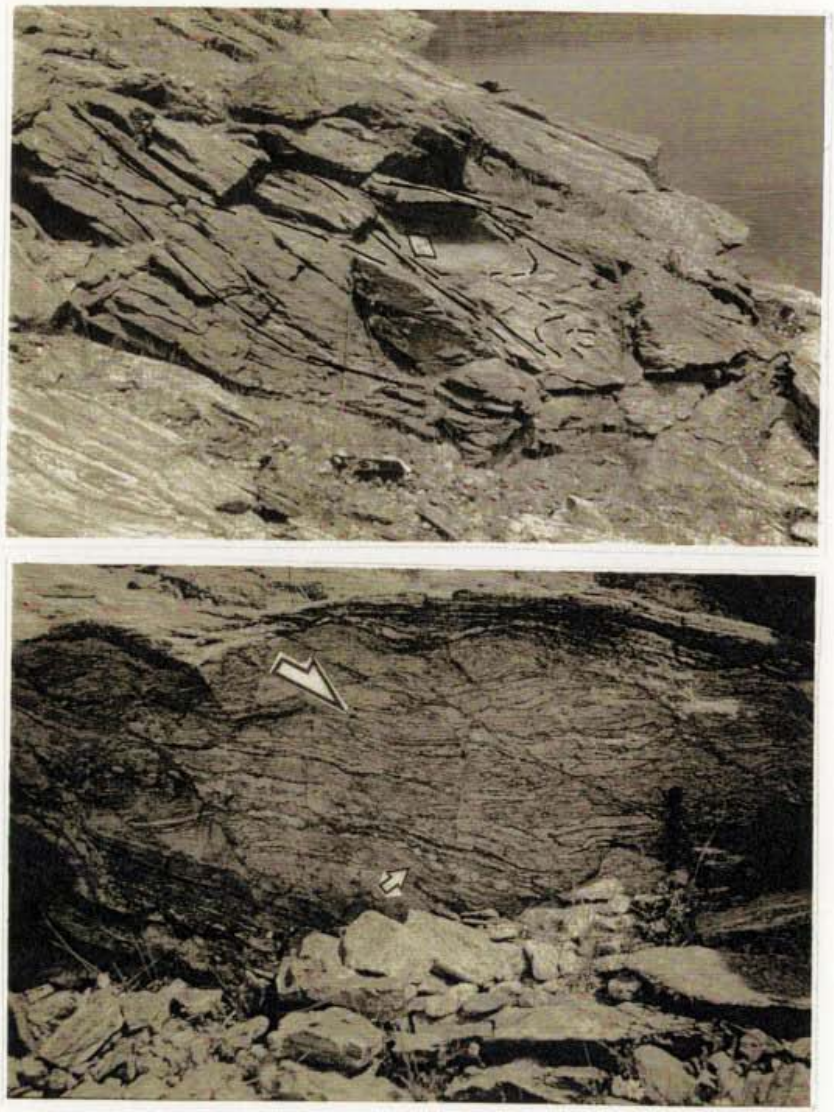

Fig.6.38.- D2 High temperature deformation band in the Buitrago area, Puentes Viejas dam (Sill+Kfs zone). Top: Lenses of quartzo-feldspathic paragneiss separated by anastomosed ductile high strain zones, showing the strong strain partitioning associated with the D2 deformation. The compositional banding (notebook location) is folded inside the lenses, with the F2 fold axis parallel to the stretching lineation. The book for scale is 18 cm long. **Bottom:** D2 shear bands (C'planes), with top down to the SE (dextral) shear sense, developed inside a competent quartzo-feldspathic lense bounded by a high strain D2 shear zone (top of the picture). Note the complex deformation inside the lense with rootless, isoclinal intrafolial folds (D1?, early D2?) and a sheared pegmatite (arrow). Pen for scale is 13.5 cm long.

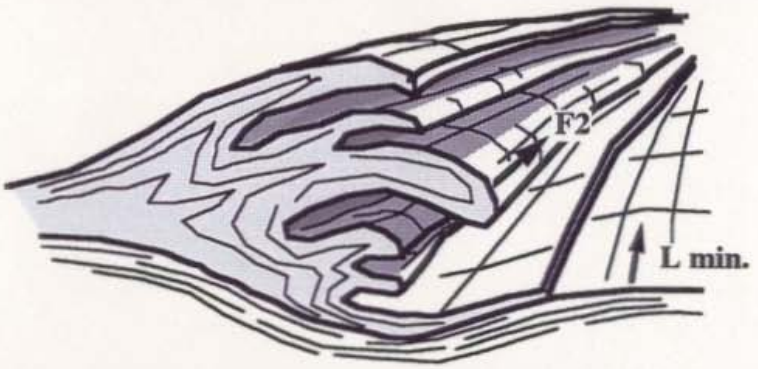

Fig.6.39.- Relationship between F2 fold axis and mineral (stretching) lineation inside the lenses of quartzo-feldspathic gneiss of the high temperature deformation band. Field photograph: metric lense of competent quartzo-feldspathic paragneiss showing asymmetric F2 folding and D2 coaxial flattening. (View perpendicular to the mineral lineation and F2 fold axis, Western Puentes Viejas dam).

Fig.6.40.- Top to the SE shear bands in the quartzo-feldspathic gneisses of the Western Guadarrama domain. Left: Discrete shear band offsetting a leucosome in the high strain zone in the Rio Madarquillos, boundary with the Madarquillos shear zone. The leucosomes are parallel to the main mylonitic fabric (S2). **Right:** Well developed shear bands cross-cutting the main foliation (S2), note the presence of a small pegmatitic patch at the bottom of the shear band (arrow). Western Puentes Viejas dam, high temperature deformation band.

Figure 6.41

Fig.6.41.- Late D2 pegmatitic patches in the Buitrago area, Sill+Kfs zone.

A) Tourmaline-bearing pegmatitic patch cross-cutting the main foliation in the migmatitic paragneisses. Western Puentes Viejas dam, high temperature deformation band.

B) Undeformed, centimetric scale, tourmaline-rich pegmatitic patch with diffuse boundaries in the 488 Ma Buitrago gneiss. Sampling location for U/Pb samples BU-1 and BU-2.

C) Tourmaline-free, undeformed, granitic pegmatitic patch in the neck of a D2 boudin, Buitrago gneiss.

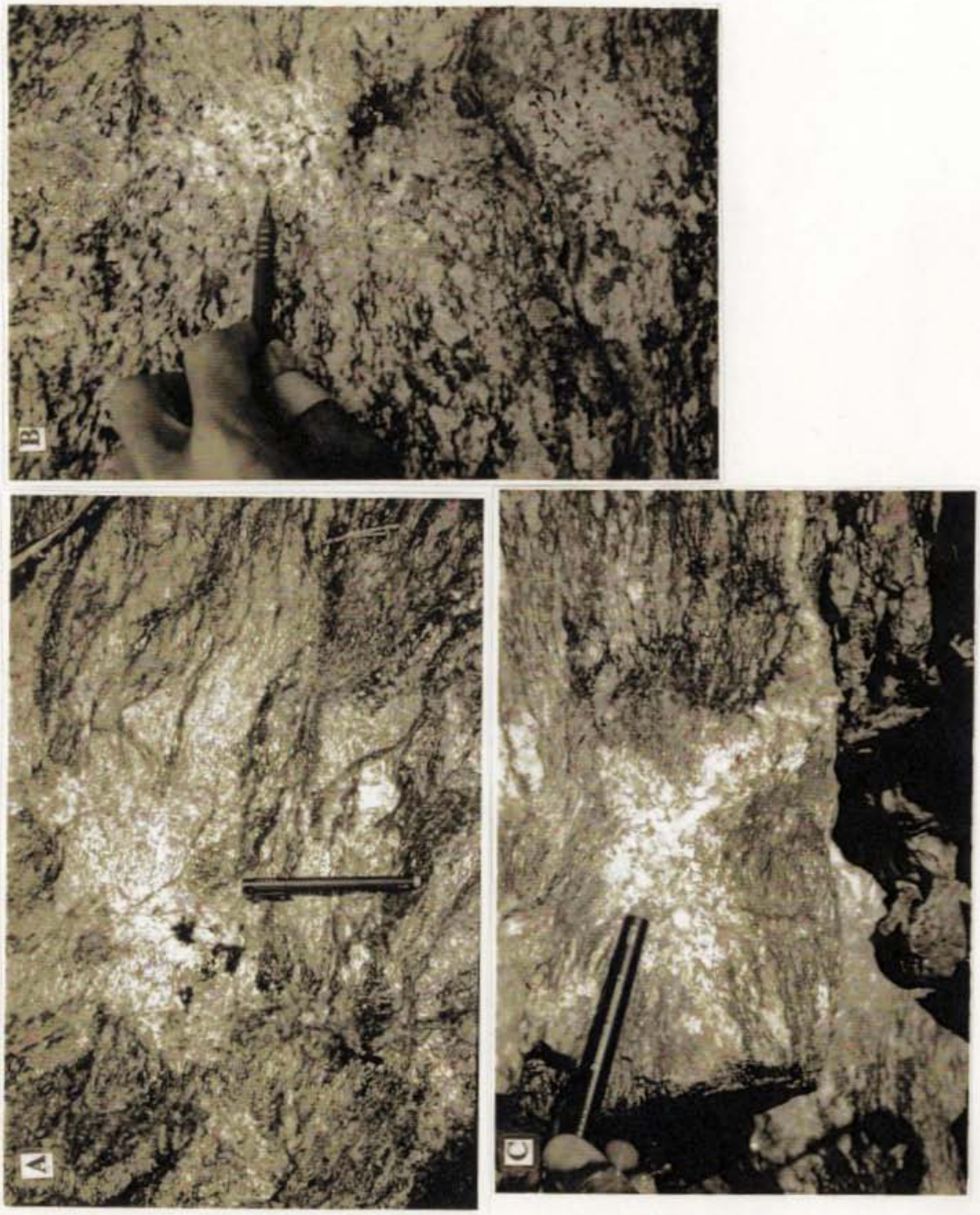
B
A
C

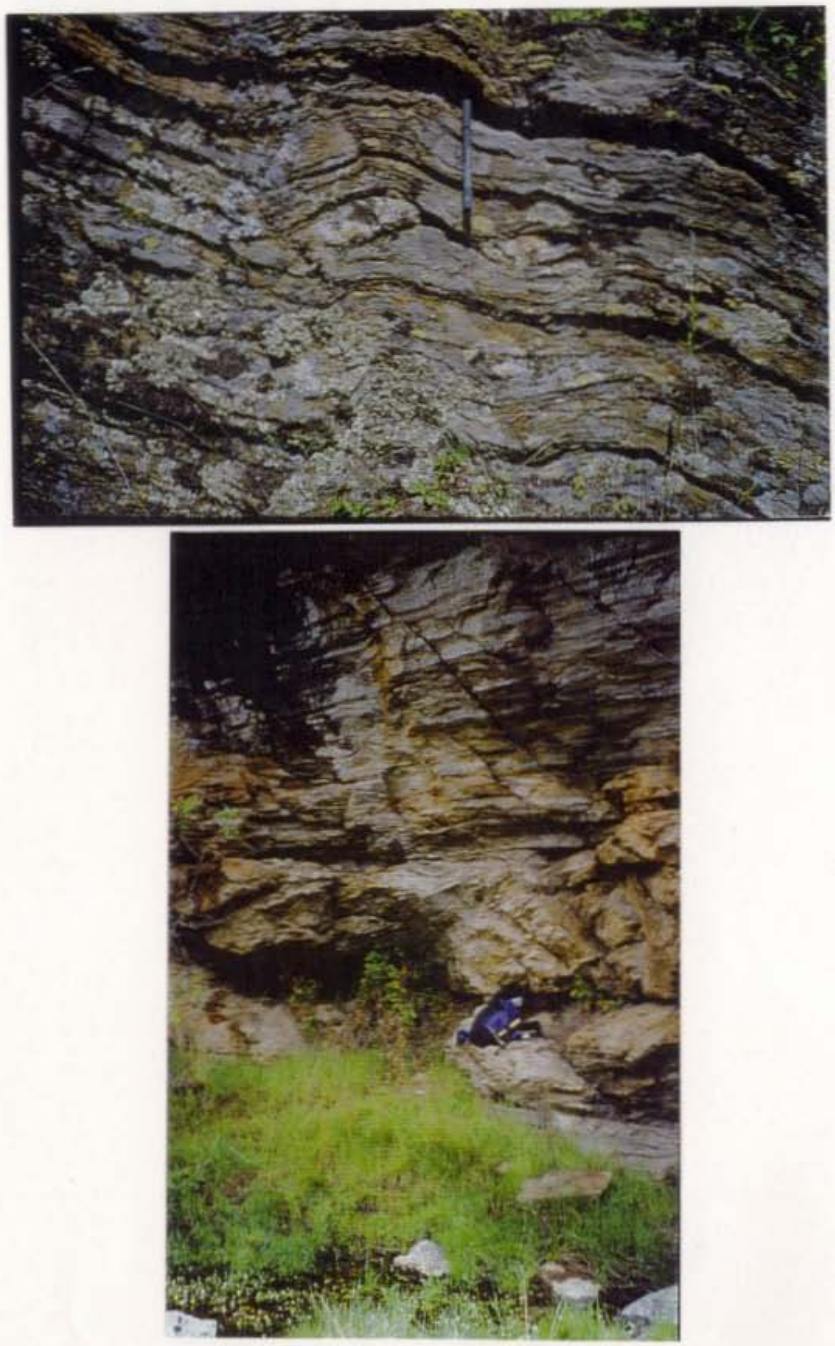

Fig.6.42.- D3 structural features, Berzosa-Riaza shear zone. Top: D3 upright crenulation of the D2 extensional fabric (note sheared quartz vein), Sill (Ky) zone. **Bottom:** 1.5 m thick brittle/ductile greenschist facies fault zone (near the pack) affecting the metasediments of the Sill (Ky) zone west of El Villar dam. Late Variscan reactivation along the Montejo detachment?

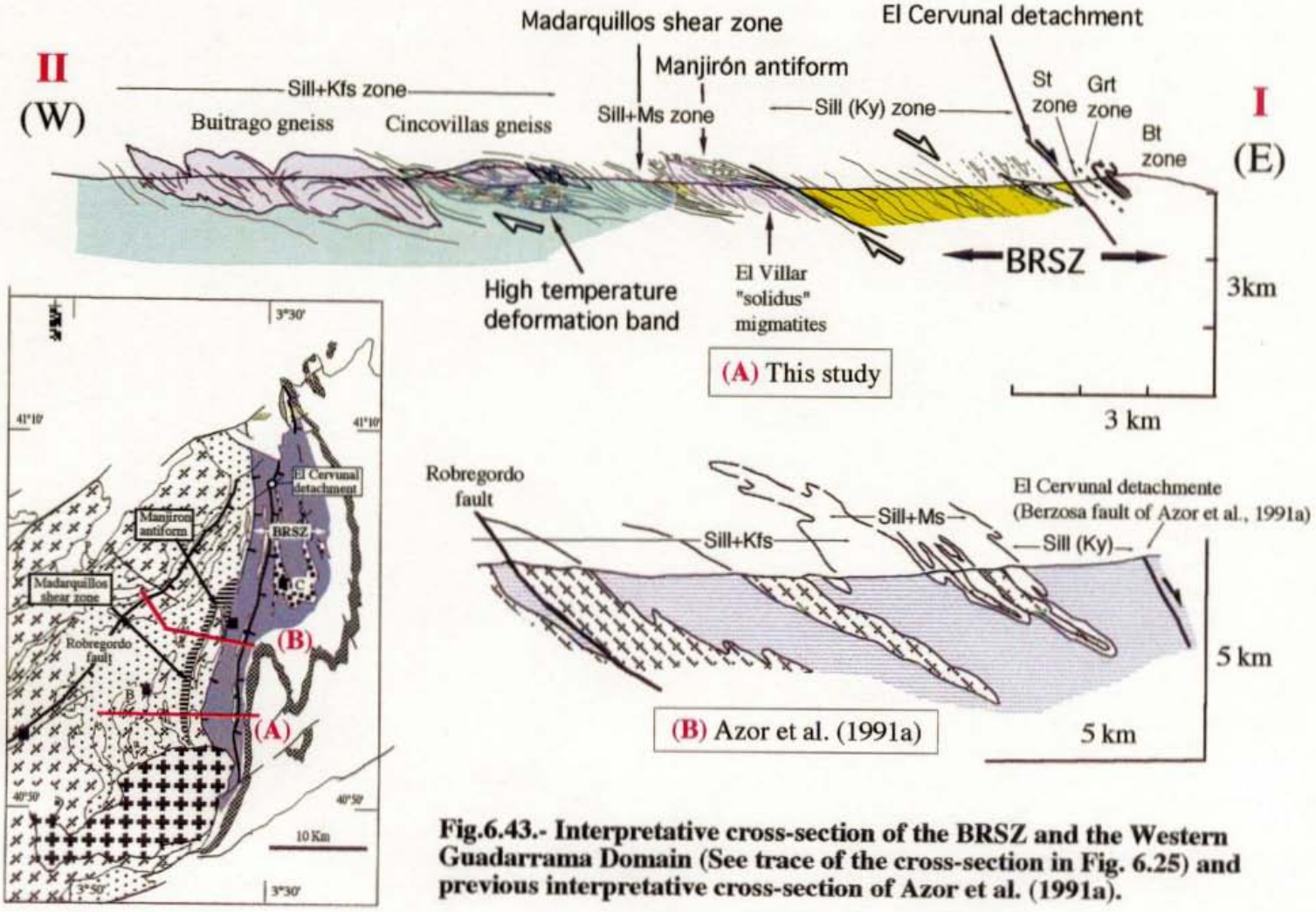

Fig.6.43.- Interpretative cross-section of the BRSZ and the Western Guadarrama Domain (See trace of the cross-section in Fig. 6.25) and previous interpretative cross-section of Azor et al. (1991a).

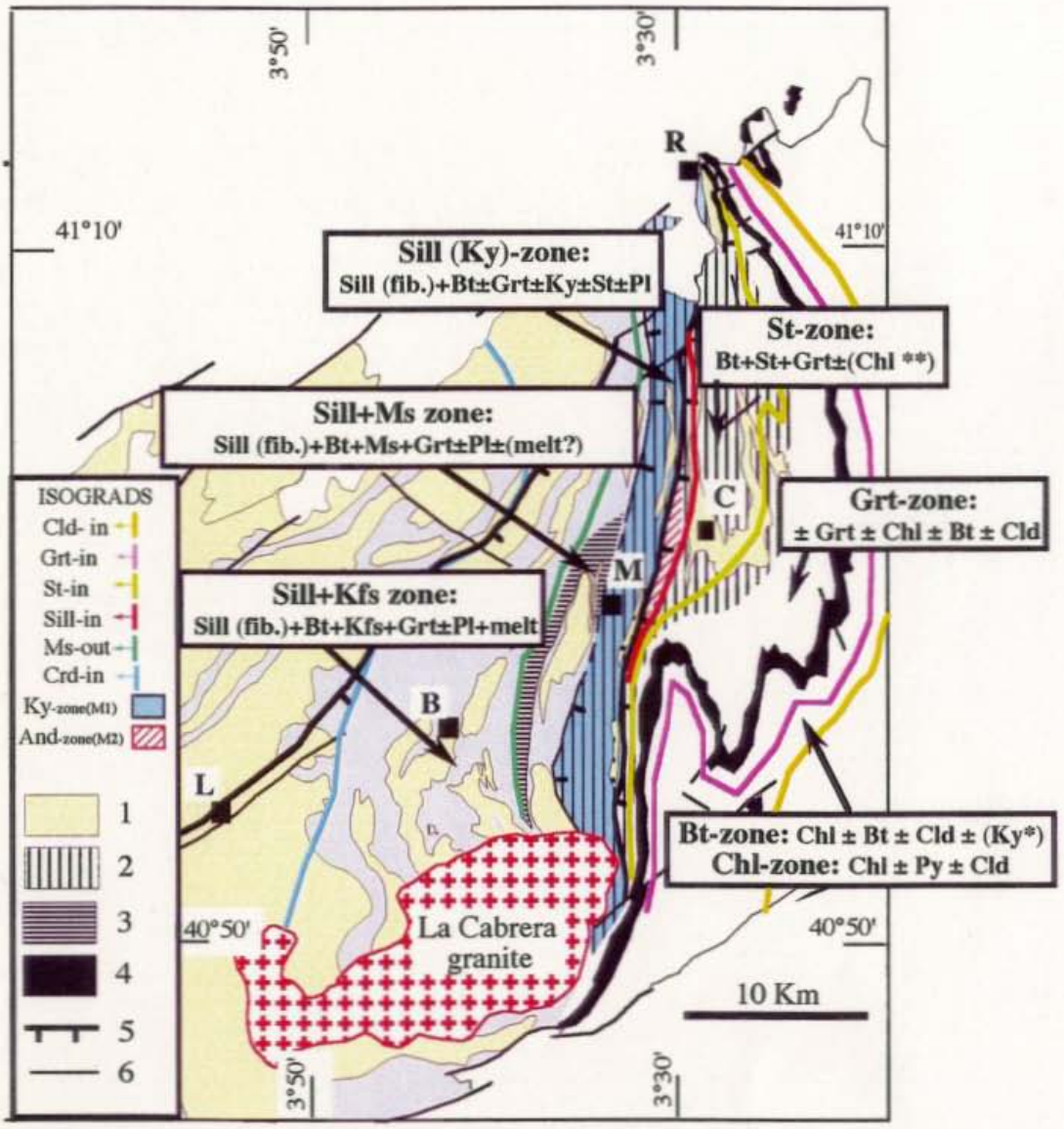

Fig. 6.44.- Distribution of mineral isograds (Lopez Ruiz, 1975; Gonzalez Casado, 1987; Escuder Viruete et al., 1996) **and mineral assemblages in metapelites**. (*) Ky in the Bt-zone after Garcia Cacho (1973, in Lopez Ruiz et al.; 1975), unconfirmed in this study. (**) Chl is consumed in the lower part of the St zone. Legend: 1) Pre-Variscan orthogneisses; 2) Berzosa-Riaza shear zone; 3) Madarquillos synform (D2 shear zone); 4) Armorican Quartzite (Arenig?); 5) Late extensional detachments; 6) Late Variscan and Mesozoic faults. B, Buitrago; C, El Cardoso; M , Montejo; L, Lozoya; R, Riaza.

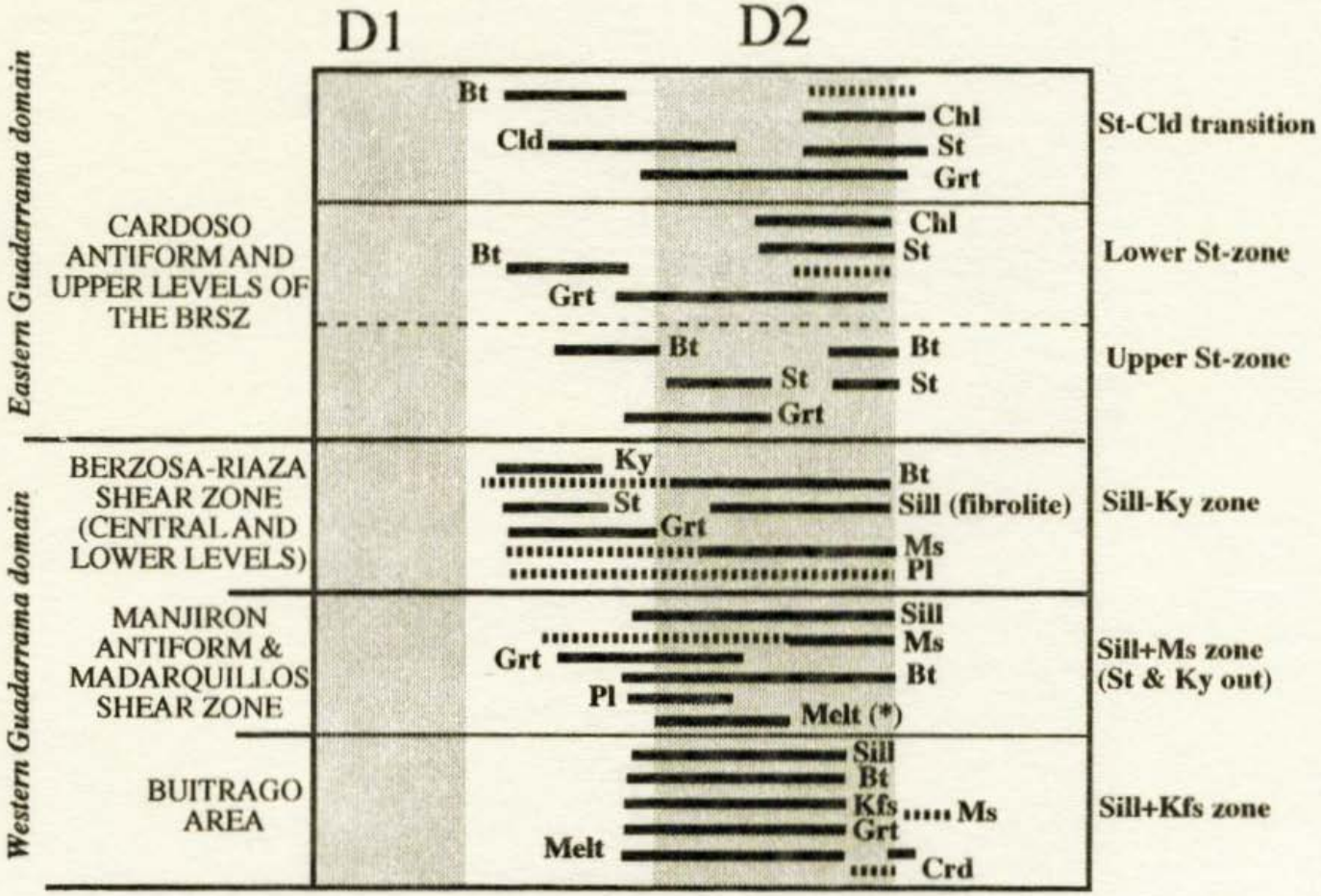

Fig. 6.45.- Mineral growth / deformation relationships in the area of study.

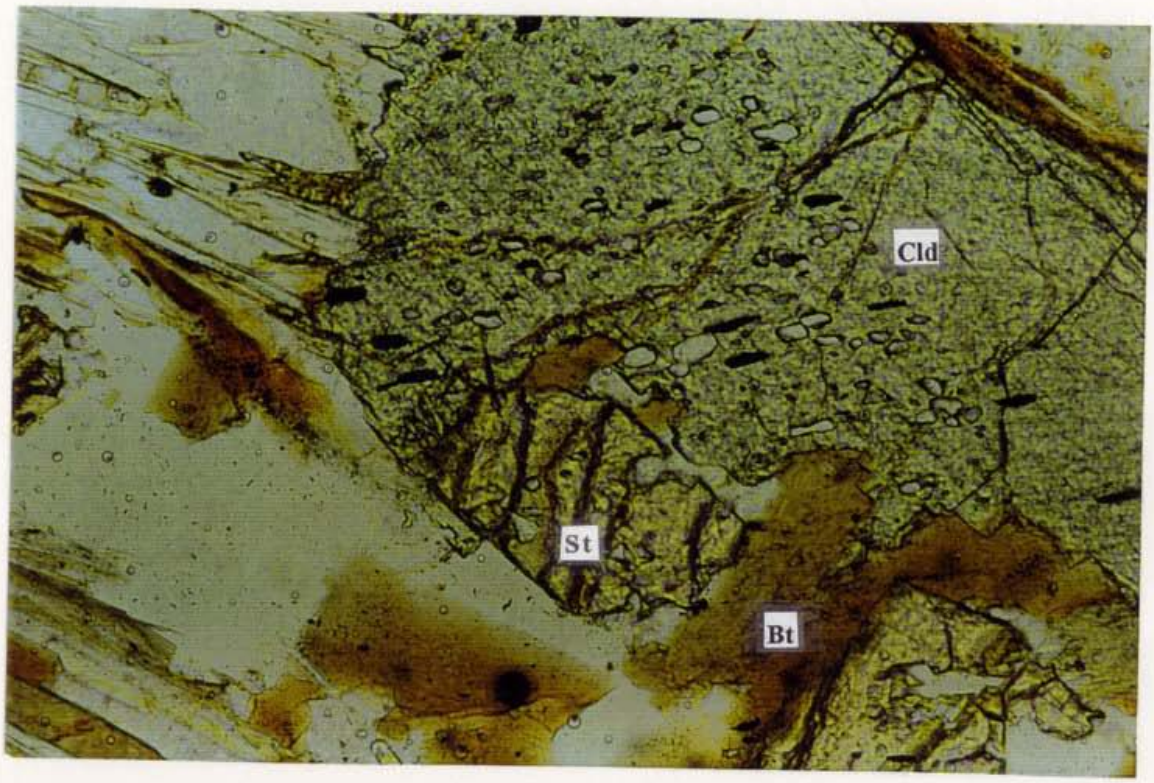

Fig.6.46.- Staurolite growing at the expense of chloritoid while biotite apparently remains stable, staurolite-chloritoid transition. This staurolite-chloritoid micaschist contains quartz, muscovite, garnet, chlorite and opaques. Garnet and chlorite are also in contact with chloritoid. Location: La Hiruela mountain pass. The field of view is 1.32 mm long.

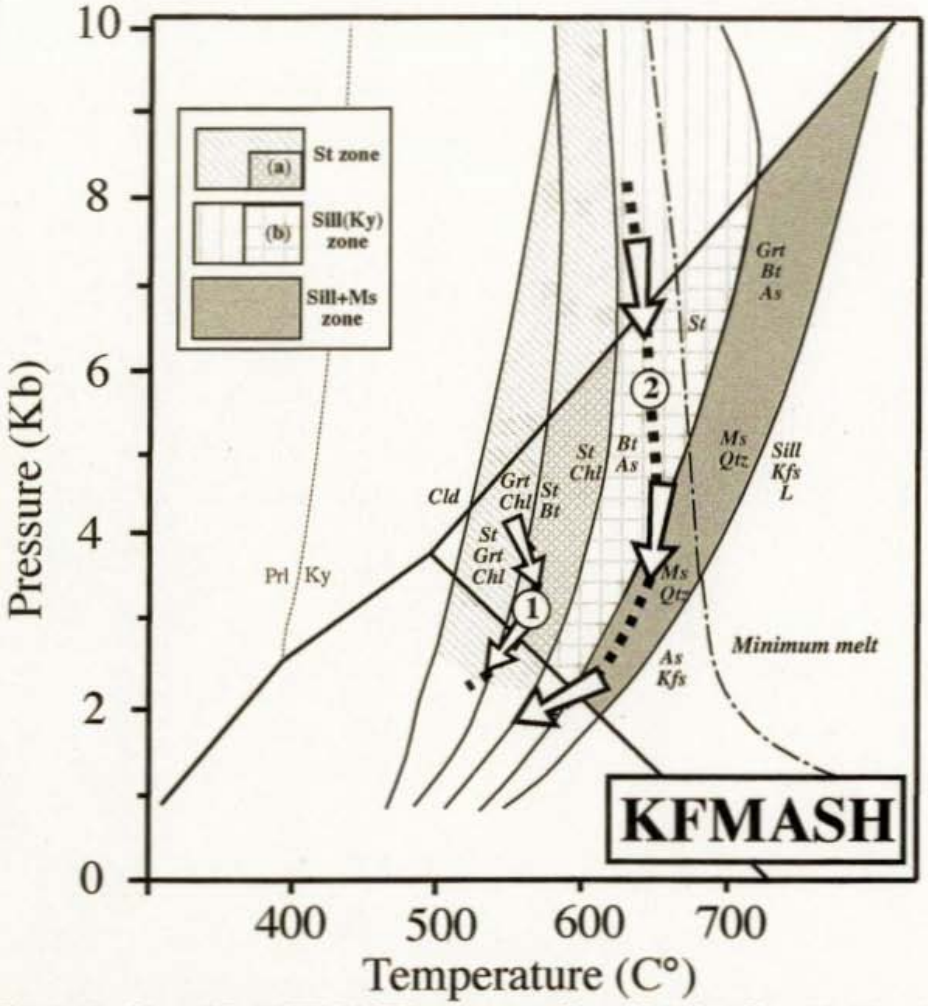

Fig. 6.47.- Simplified KFMASH petrogenetic grid (after figs. 10-15 and 10-16 in chapter 10 of Spear, 1993) for the metapelites of the Berzosa-Riaza shear zone. (a) Post-D2 growth of sillimanite in the deeper parts of the St-zone, east of the Cervunal detachment. (b) Syn-D2 conditions in the Sill (Ky) zone.The arrows indicate the parts of qualitative P-T path deduced for the lower levels of the Eastern Guadarrama domain (Path 1; St zone) and the upper levels of the Western Guadarrama domain (Path 2; BRSZ, Sill (Ky) zone).

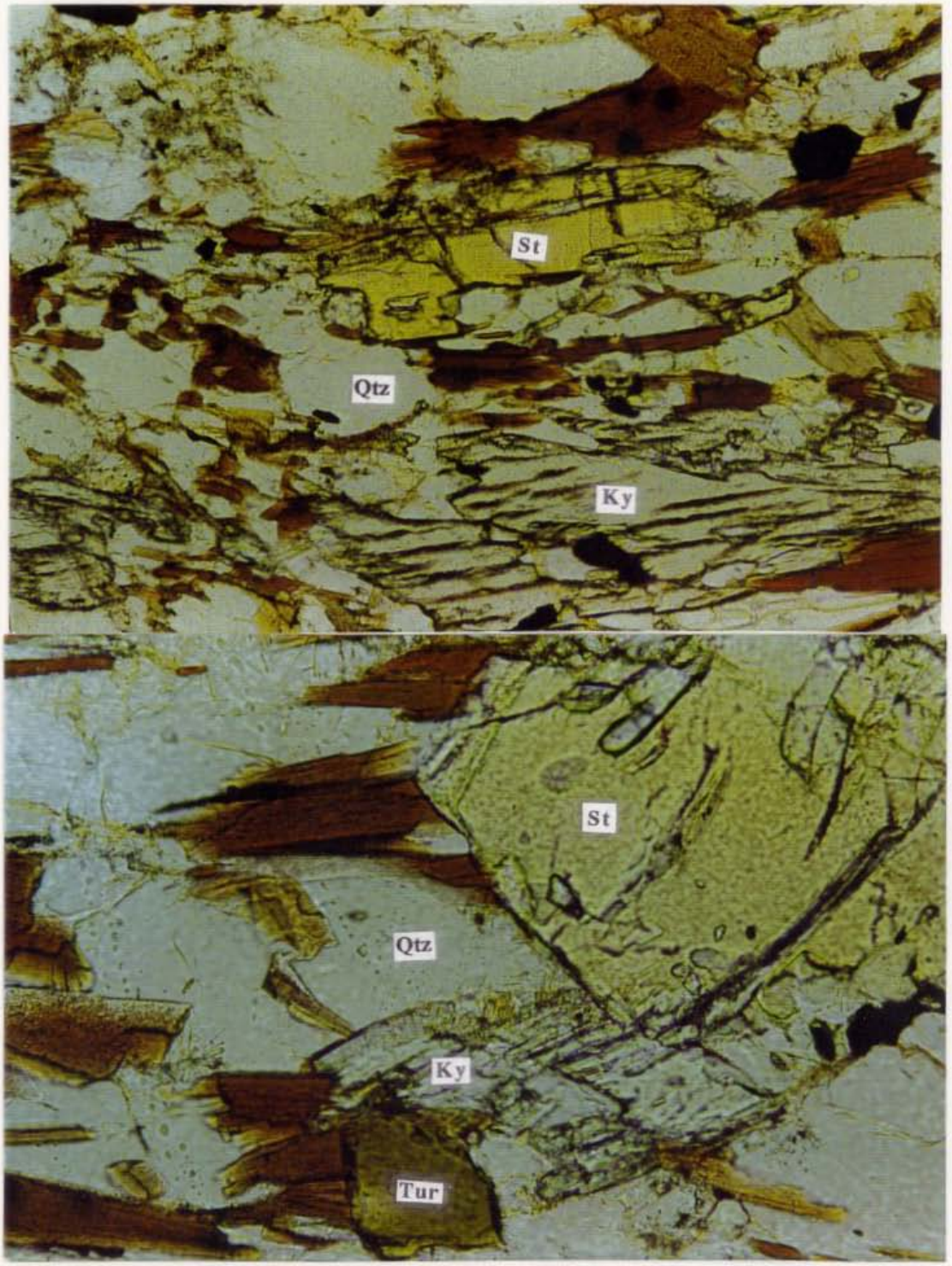

Fig.6.48.- Kyanite and staurolite relicts in the Sill+Ky micaschists of the BRSZ.
Top: Staurolite and kyanite relicts in contact with quartz. Field of view is 1.32 mm long.
Bottom: Mutual contact between quartz, staurolite and kyanite. Field of view is 0.76 mm long.

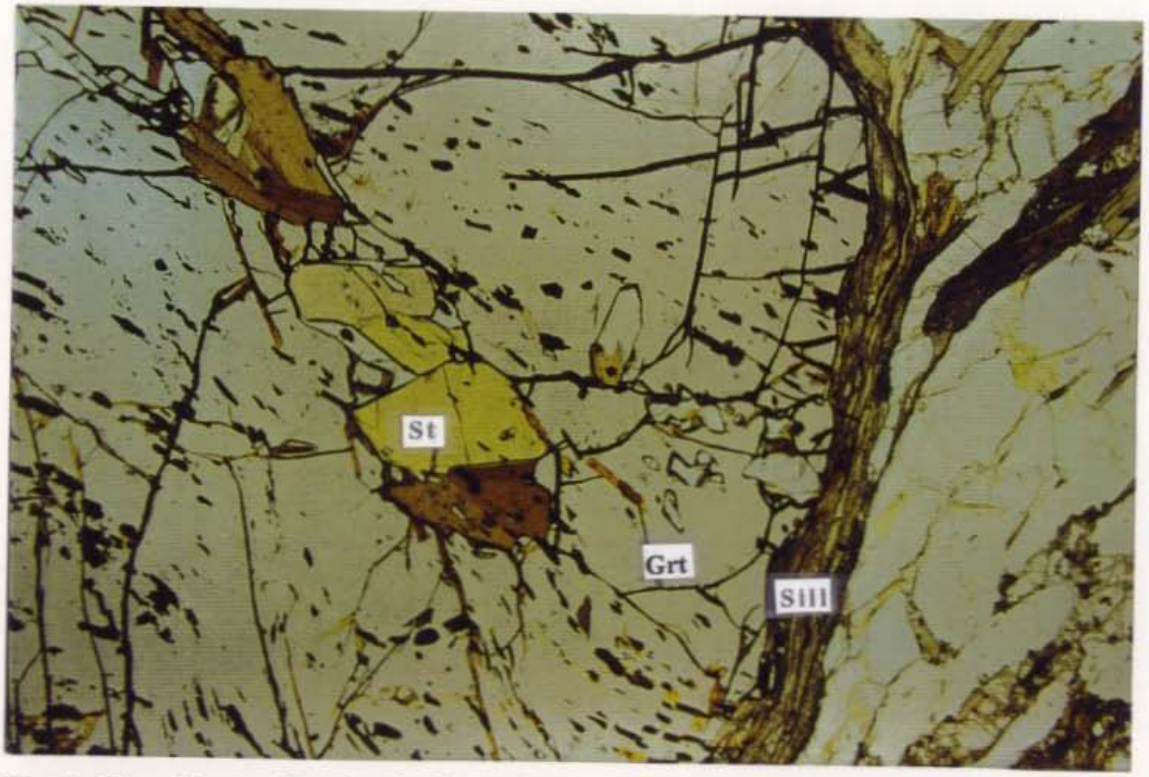

Fig.6.49.- Staurolite inclusions in a garnet porphyroblast rimmed by fibrolitic sillimanite. Deeper structural levels of the BRSZ. Field of view is 1.32 mm long.

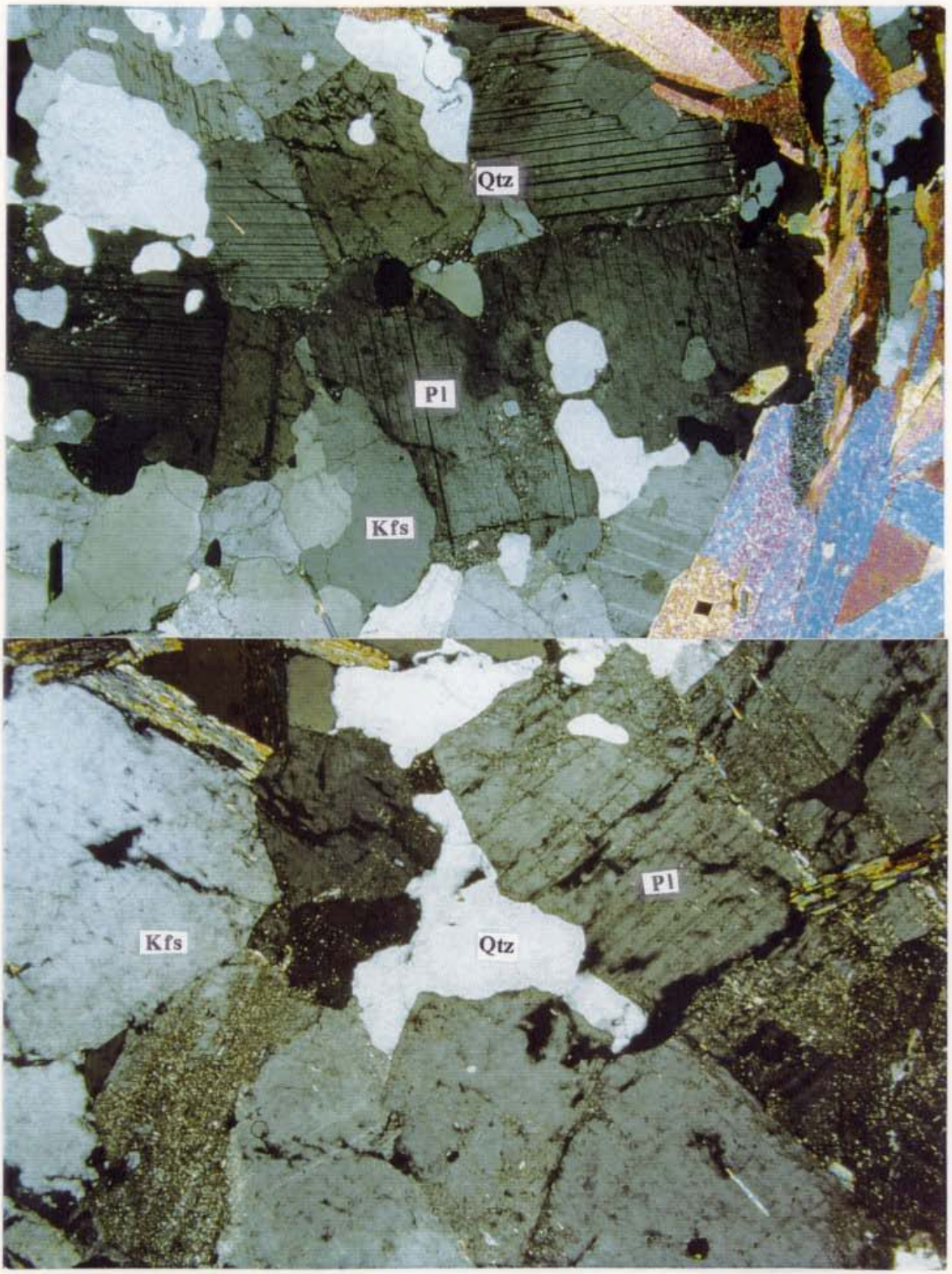

Fig.6.50.- Granitic leucosomes in the Sill+Ms zone (Manjirón antiform) showing interstitial quartz in contact with subhedral plagioclase (An10-15) laths and K-feldspar. Top, field of view is 5.21 mm long; bottom, field of view is 1.32 mm long

Fig. 6.51.- Biotite micafish with monazite inclusions (pleocroic haloes) in a Cld-St micaschist. The micafish was formed during the D2 transposition of the S1 fabric and indicates a D2 shear sense of top down to the SE (ie. dextral). Therefore, the monazite inclusions are syn-D2 (ie.syn-biotite) or pre-D2 (ie. pre-biotite). Using the most conservative interpretation (as in this study), U/Pb dating of this monazite would provide an older age constraint for the lower amphibolite facies, D2 extensional fabric. Field of view is 17 mm long.

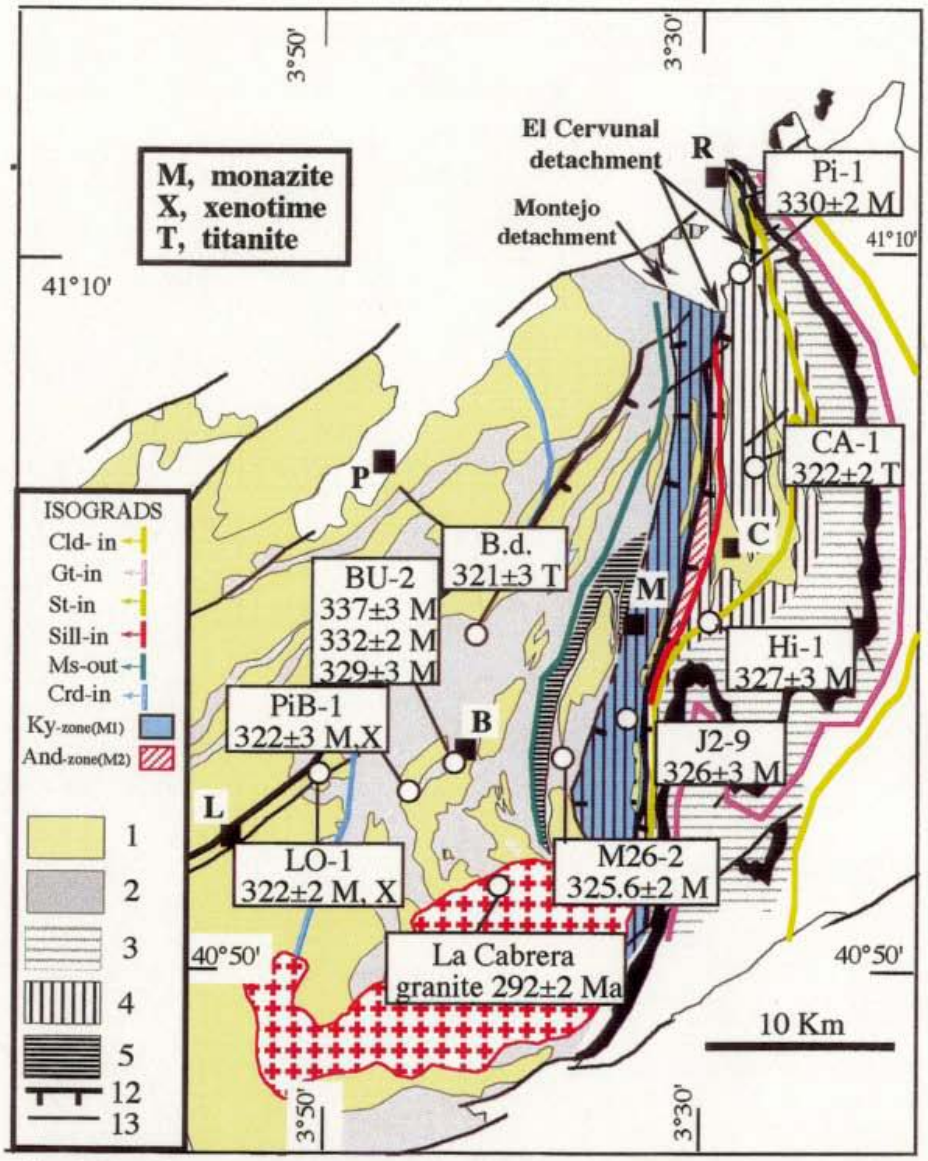

Fig. 6.52.- Sample distribution and Variscan U-Pb protolith and metamorphic ages (Ma) for the Somosierra area of the Sierra de Guadarrama. Legend: Western Domain, (1) pre-variscan orthogneisses, (2) metasediments; 3) D2 crenulation band; 4) Berzosa-Riaza shear zone (BRSZ, ductile mylonitic fabrics); 5) Madarquillos synform (high strain zone, shear zone). B.d., Braojos dyke. B, Buitrago; C, El Cardoso; M, Montejo; L, Lozoya; P; Pradena; R, Riaza.

TABLE 6.2.- U-Pb DATA, VARISCAN AGES, SIERRA DE GUADARRAMA.

Description / Fraction	Weight (mg)	Concentration U (ppm)	Pb rad (ppm)	Measured Total common Pb (Pg)	$^{206}Pb/^{204}Pb$	Corrected atomic ratios* $^{208}Pb/^{206}Pb$	$^{206}Pb/^{238}U$	±	$^{207}Pb/^{235}U$	±	$^{207}Pb/^{206}Pb$	±	Age (Ma) $^{206}Pb/^{238}U$	$^{207}Pb/^{235}U$	$^{207}Pb/^{206}Pb$
1.-Hi-1. La Hiruela mountain pass. St-Cld transition . 59700-45850†																
M1 platy y. NAB	0.0469	3532	795	213	2529	3.9728	0.05171	24	0.3787	18	0.05531	06	325	326	334
M2 platy y. AB	0.0050	6995	1306	66	1771	3.0544	0.05252	40	0.3807	32	0.06072	20	330	328	310
2.-Pi-1, road to La Pinilla (ski resort). St zone. 61400-63350																
M1 Eu. platy y. AB	0.0053	3901	895	69	1003	3.9995	0.05244	48	0.3855	36	0.05333	28	330	331	343
M2 Eu. platy y. NAB	0.014	3274	710	102	1503	3.6977	0.05269	118	0.3882	86	0.05343	30	331	333	347
3.-CA-1, para-amphibolite, St zone. 63800- 52600																
T1 colourless AB	0.3600	19	1	759	48	0.1180	0.05114	30	0.3850	12	0.05461	17	321	331	396
T2 pale br. AB	0.4528	87	7	1477	104	0.6515	0.05136	18	0.3841	60	0.05425	86	323	330	381
4.- J2-9, Ky-Sill micaschist, Berzosa-Riaza shear zone . 55300-40500																
M1 platy NAB	0.0050	9487	1944	105	1473	3.5376	0.05157	40	0.3783	28	0.05320	14	324	326	337
M2 platy NAB	0.005	7150	1214	76	1551	2.7020	0.05231	38	0.3801	27	0.05271	20	329	327	316
5.- M26-2, Folded migmatite, Sill+Ms zone. 51500-37750																
M1 y. clr. incl free AB	0.2124	8156	980	364	15440	1.6352	0.05173	26	0.3772	19	0.05289	04	325	325	324
M2 y. clr. incl. free lrg. AB	0.2579	7887	913	222	29622	1.5400	0.05164	24	0.3765	19	0.05287	04	325	324	323
Z1 20 needles AB	0.0137	1208	66	26	2408	0.0253	0.05915	48	0.4486	35	0.05501	16	370	376	412
Z2 3 small pr. AB	0.0042	975	56	11	1415	0.0262	0.06144	28	0.4693	25	0.05540	16	384	391	428
Z3 Needles & sm pr. AB	0.0182	683	39	14	3375	0.0394	0.06116	46	0.4708	32	0.05584	20	382	392	446
Z4 Eu. pr. & tips AB	0.0779	787	45	79	3038	0.0322	0.06177	18	0.4725	16	0.05547	06	386	393	431
Z5 Eu. sm. pr. AB	0.0277	728	43	52	1564	0.0401	0.06328	28	0.4857	22	0.05567	12	396	402	439
Z6 Eu. needles AB	0.2830	856	55	26	3948	0.0355	0.06777	28	0.5761	24	0.06165	10	423	462	662
6.- Buitrago gneiss, BU-2, 482 Ma foliated aplitic vein, Sill+Kfs zone. 45675-37575																
M1 pale y. clr. lrg. AB	0.0850	11783	1806	142	23651	2.2477	0.05370	28	0.3937	22	0.05318	04	337	337	337
M2 pale y. clr. lrg. AB	0.0629	10016	1430	314	6663	2.0697	0.05290	26	0.3869	19	0.05305	06	332	332	331
M3 y. platy NAB	0.0050	30765	4000	65	7742	1.8050	0.05262	38	0.3851	28	0.05308	08	331	331	332
M4 sm. platy NAB	0.0521	14465	1831	513	4833	1.7454	0.05232	34	0.3820	23	0.05295	18	329	329	327
7.-Buitrago gneiss, PIB-1, 482 Ma foliated leucogranite, Sill+Kfs zone. 43200-36575																
M1 pale y. ABR	0.0599	27503	2330	626	8510	0.8544	0.05146	30	0.3750	22	0.05284	04	323	323	322
M2 y. ABR	0.1165	22959	2690	1033	8265	1.6009	0.05094	30	0.3712	23	0.05286	04	320	321	323
X1 greenish stubby prisms NAB	0.0617	4888	411	402	2326	0.9338	0.04907	18	0.3576	14	0.05285	08	309	310	322
8.- Lozoya gneiss, LO-1, 477 Ma augen gneiss, Sill+Kfs zone. 35550-33500																
MONAZITE AND XENOTIME DATA IN TABLE 6.1. (PRE-VARISCAN U-Pb PROTOLITH AGES)																
9.- Braojos dyke, Cpx-Pl-Am. amphibolite, Sill+Kfs zone. 45400-44500																
T1 Pale brown AB	0.2785	19	1.4	134	147	0.6320	0.05095	32	0.3813	47	0.05428	60	320	328	382
T2 clear AB	0.3515	14	1	210	97	0.5697	0.05115	32	0.3782	69	0.05363	90	322	326	356
10.- La Cabrera granite, post-collisional intrusion. 47625-31150																
M1 Sm pale y. inc. free AB	0.0168	1044	540	47	1096	11.83	0.04631	32	0.3325	19	0.05208	30	292	291	289
M2 pale y. AB	0.0256	417	267	46	693	14.85	0.04638	28	0.3331	25	0.05210	34	292	292	290
M3 pale y. NAB	0.0384	790	484	174	511	14.70	0.04662	50	0.3352	35	0.05214	34	294	293	292
Z1 euh. prisms AB	0.1916	651	30	48	7490	0.1004	0.04578	20	0.3305	15	0.05235	08	289	290	301
Z2 lrg. eu. prisms AB	0.1797	654	30	31	10803	0.0998	0.04587	16	0.3335	12	0.05273	06	289	292	317
Z3 small prisms AB	0.0280	701	32	49	1178	0.1068	0.04604	40	0.3358	29	0.05291	18	290	294	325

1.- Z = zircon, M = monazite, X = xenotime, s = small (<80 μm), m= medium (>80 and <150 μm), l = large (>150 μm), Ndl. = Needles (1:10 to 1:7 width/length ratio), pr = prisms (1:6 to 1:4), stb = stubby (1:3 to 1:1), clr = clear, eu. = euhedral, y.= yellow, AB = air abraded (Krogh, 1982), NAB = not abraded, rd = rounded, w/ = with, inc = inclusions, xtal = crystal

2.- Uncertainty in sample weight ± 0.001 mg (2 sigma)

3.- Atomic ratios corrected for fractionation and spike. 8 to12 pg Pb blank lab procedure (25 pg- monazite, xenotime and titanite), initial common Pb (Stacey and Kramers, 1975) and 1 pg U blank. 2 sigma errors reported for corrected isotopic ratios.

† Sample location in U.T.M. coordinates, 30TVL UTM zone and 100 km square.

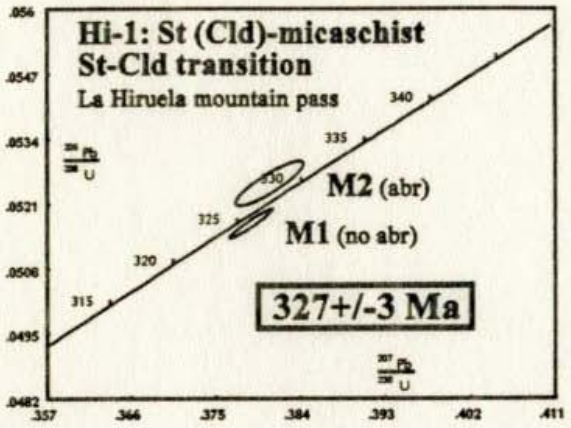

Fig. 6.53.- U-Pb concordia diagram for monazite from sample Hi-1, St+Grt+(Cld) micaschist. Lower staurolite zone (Eastern Guadarrama domain).

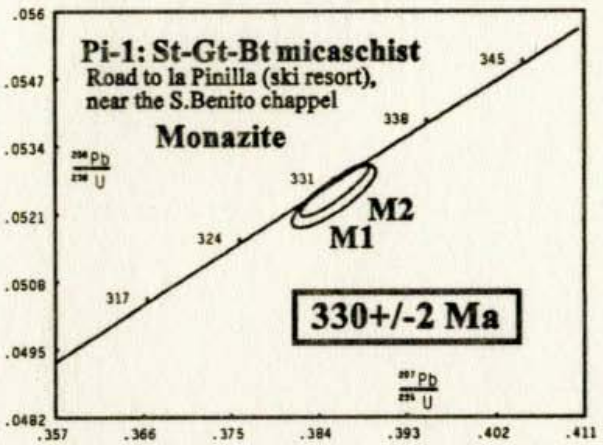

Fig. 6.54.- U-Pb concordia diagram for monazite from sample Pi-1, St+Grt+Bt micaschist. Upper staurolite zone (Eastern Guadarrama domain).

Fig.6.55.- Sample Pi-1, St-Grt micaschist.

Top: The S2 fabric, defined by muscovite and biotite, wraps around staurolite and garnet with inclusions defining an Si (S1). Field of view is 15.5 mm long.

Middle: Monazite inclusions in S2 biotites. Field of view is 3.5 mm long.

Bottom: Platy, subhedral monazite parallelograms, fraction M1. Field of view is 3.5 mm long. Human hair for scale.

Figure 6.55

Fig.6.55.- Sample Pi-1, St-Grt micaschist.

Top: The S2 fabric, defined by muscovite and biotite, wraps around staurolite and garnet with inclusions defining an Si (S1). Field of view is 15.5 mm long.

Middle: Monazite inclusions in S2 biotites. Field of view is 3.5 mm long.

Bottom: Platy, subhedral monazite parallelograms, fraction M1. Field of view is 3.5 mm long, human hair for scale.


St
Grt
Bt
Mnz

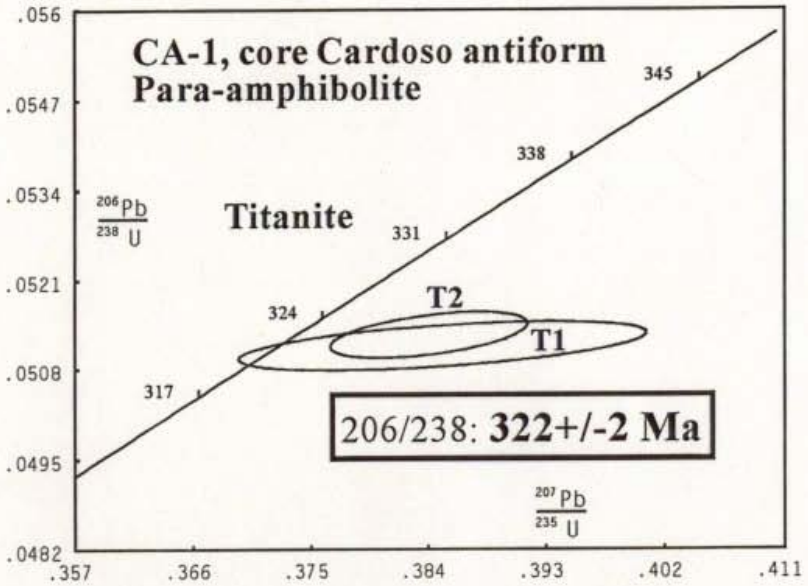

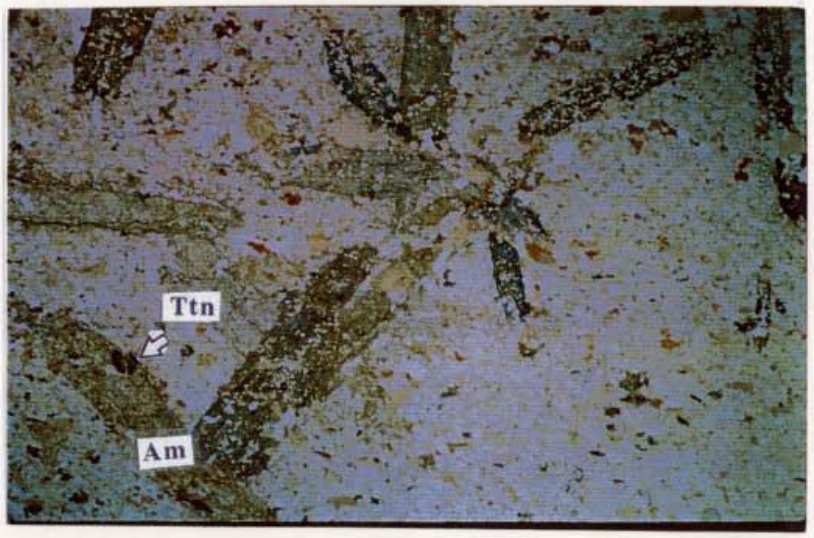

Fig.6.56.- U-Pb concordia diagram for titanite from sample CA-1, para-amphibolite from the core of the Cardoso antiform and microtexture showing titanite associated with the randomly oriented amphibole porphyroblasts (static post-tectonic porphyroblastesis). Field of view is 5.2 mm long.

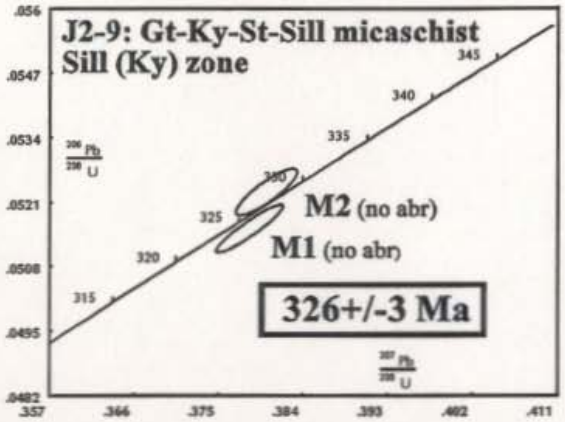

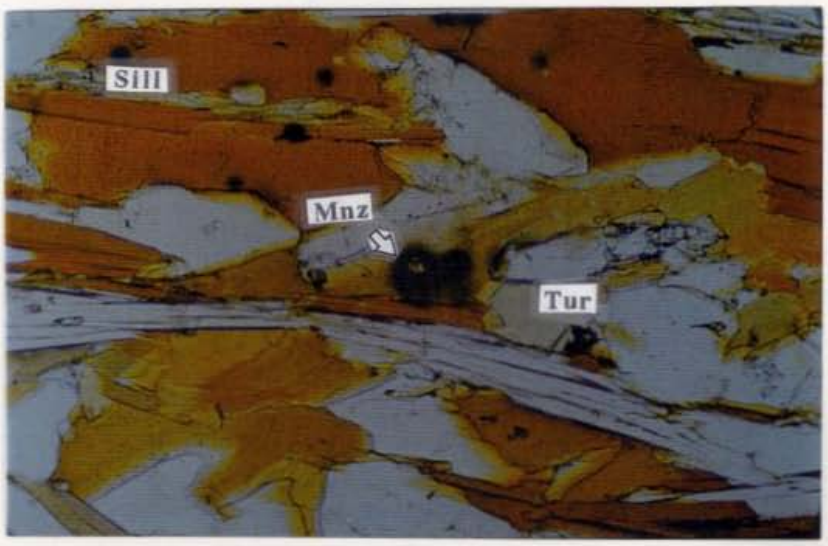

Fig. 6.57.- U-Pb concordia diagram for sample J2-6, Ky+St+Grt+Sill micaschist (Fig.6.26c) from the Sill (Ky) zone. Berzosa-Riaza shear zone (BRSZ), upper levels of the Western Guadarrama domain. Detail of a monazite inclusion in a D2 biotite next to a subhedral tourmaline. Field of view is 1.32 mm long.

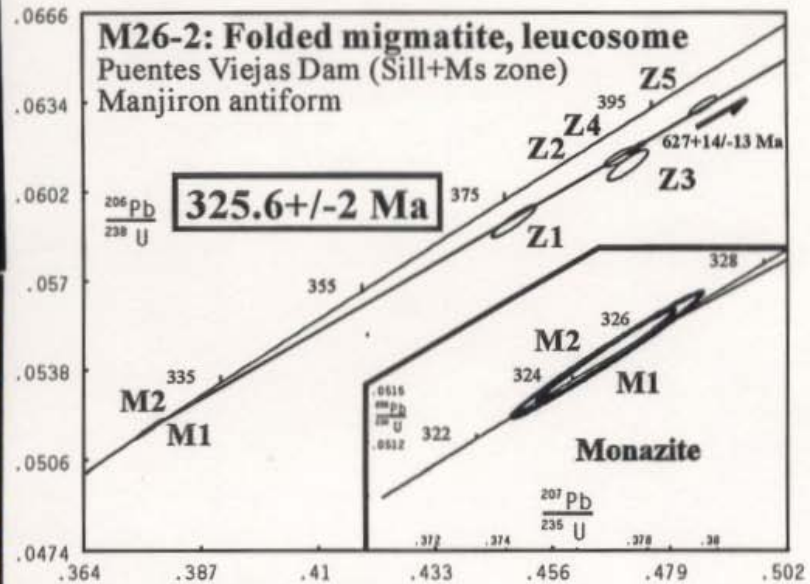

Fig.6.58.- U-Pb concordia diagram for sample M26-2, leucosome from a folded (F2) migmatite. Outcrop photograph of the sampled leucosome and detail of a monazite inclusion in a biotite from the melanosome (Field of view is 1.32 mm. long). Sill+Ms zone, Manjiron antiform (Puentes Viejas dam).

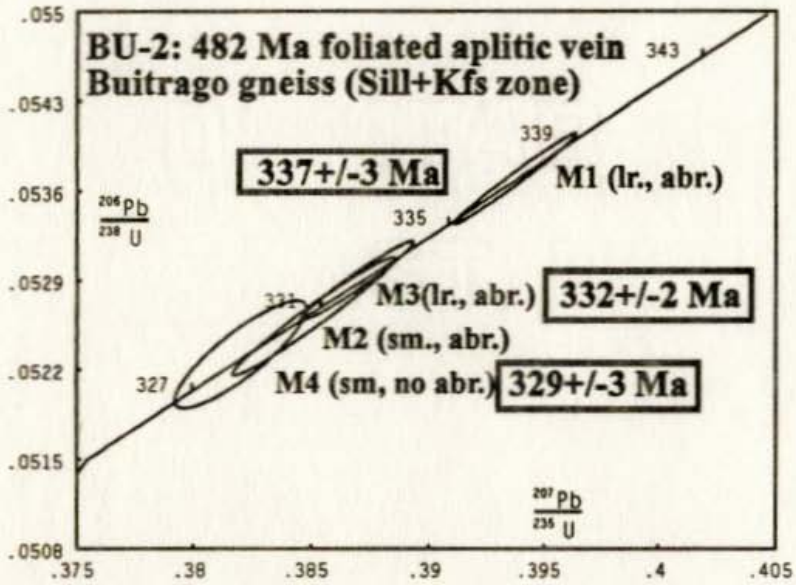

Fig.6.59.- U-Pb concordia diagram of monazite fractions from sample BU-2 (482 Ma foliated aplitic vein, Buitrago gneiss; fig.6.18 and 6.20). M, monazite; lr., large; sm., small; abr., air abraded. Sillimanite-bearing sample, Sill+Kfs zone, Western Guadarrama domain.

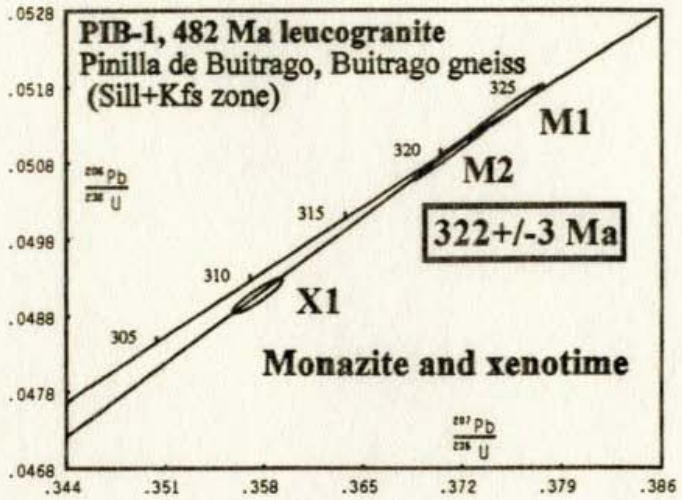

Fig.6.60.- U-Pb concordia diagram of monazite and xenotime fractions from sample PiB-1 (482 Ma foliated leucogranite, Buitrago gneiss; fig. 6.21). Sill+Kfs zone, Western Guadarrama domain. M, monazite; X, xenotime.

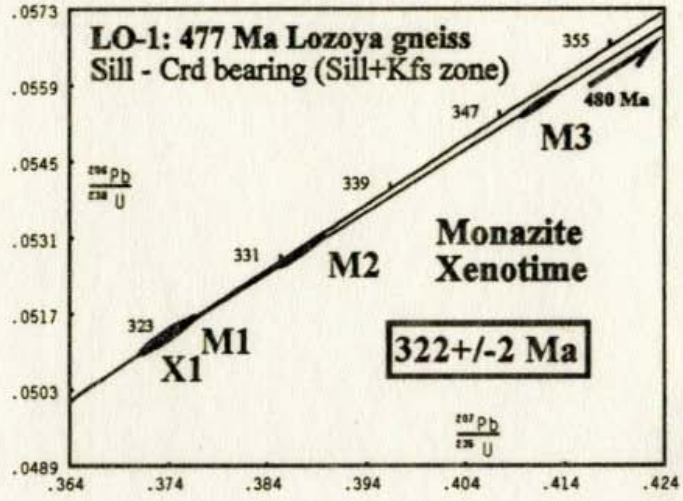

Fig.6.61.- U-Pb concordia diagram of monazite and xenotime fractions from the 477 Ma Lozoya gneiss (augen gneiss; fig. 6.22). Sill+Kfs zone, sillimanite+cordierite-bearing sample, Western Guadarrama domain. M, monazite; X, xenotime.

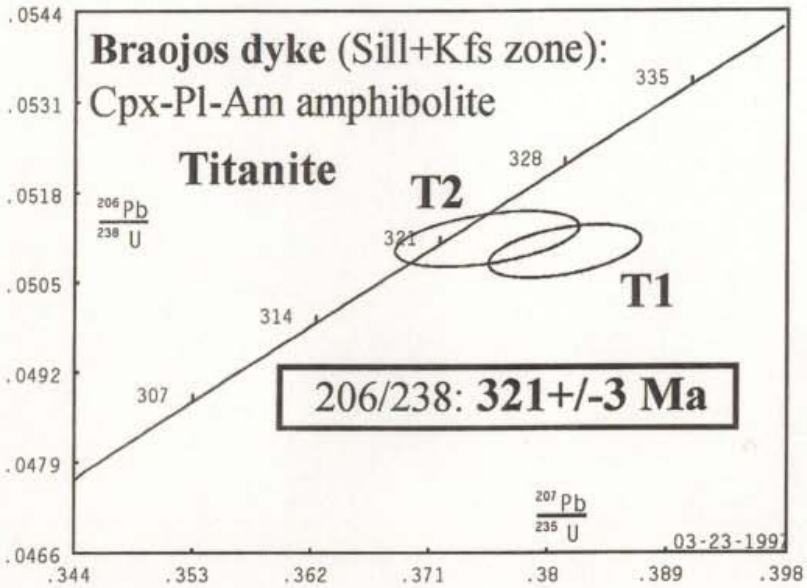

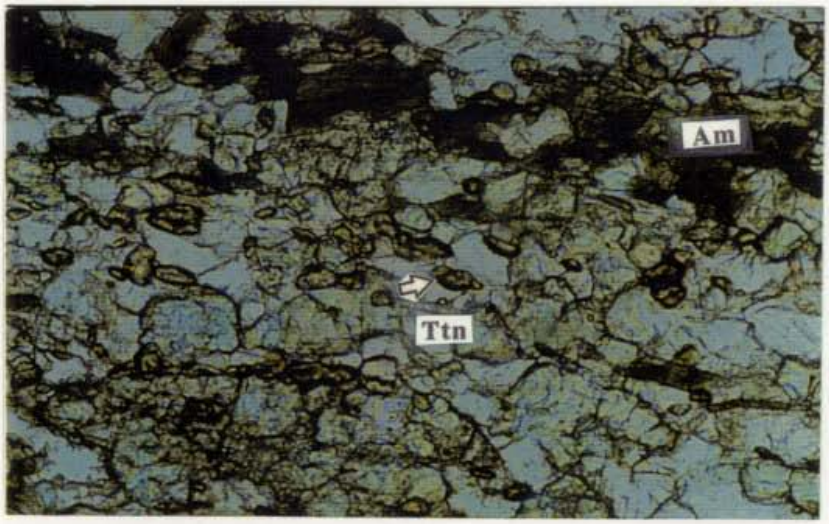

Fig. 6.62.- U-Pb concordia diagram for titanite separates from the Braojos dyke and microtexture of the U-Pb sample. Amphibole is growing after syn-D2 amphibolitization of clinopyroxene. Titanite is associated with both amphibole and the Pl+Cpx levels. Field of view is 1.32 mm long

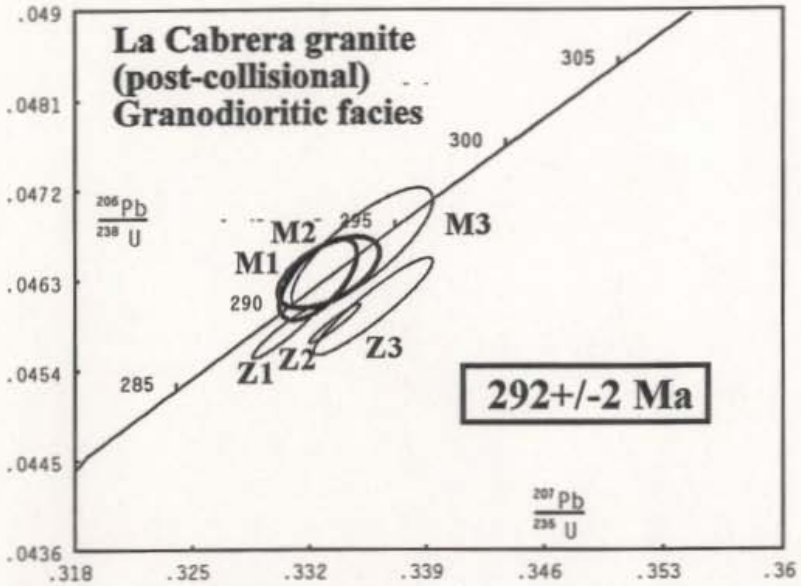

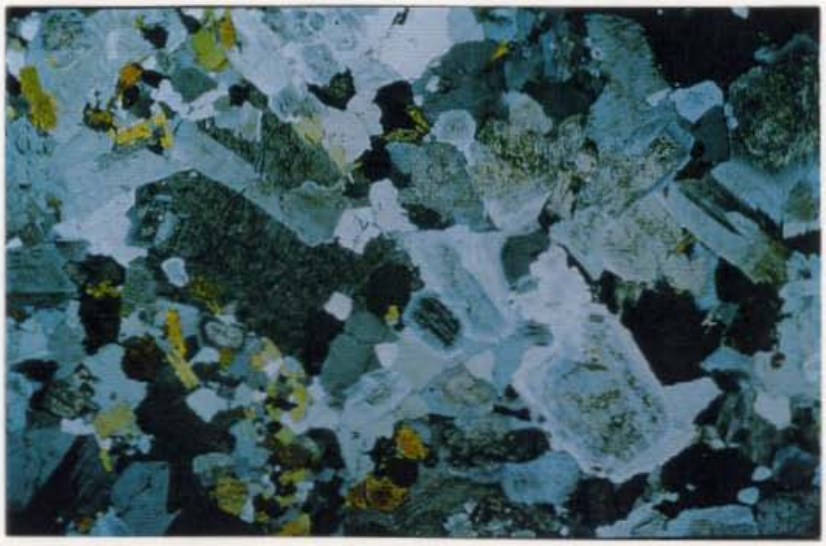

Fig.6.63.- U-Pb concordia diagram for the post-tectonic La Cabrera granite (M, monazite; Z, zircon) and microstructure of the U-Pb sample. Undeformed Bt-granite/granodiorite with a heterogranular igneous texture. Field of view is 17mm long.

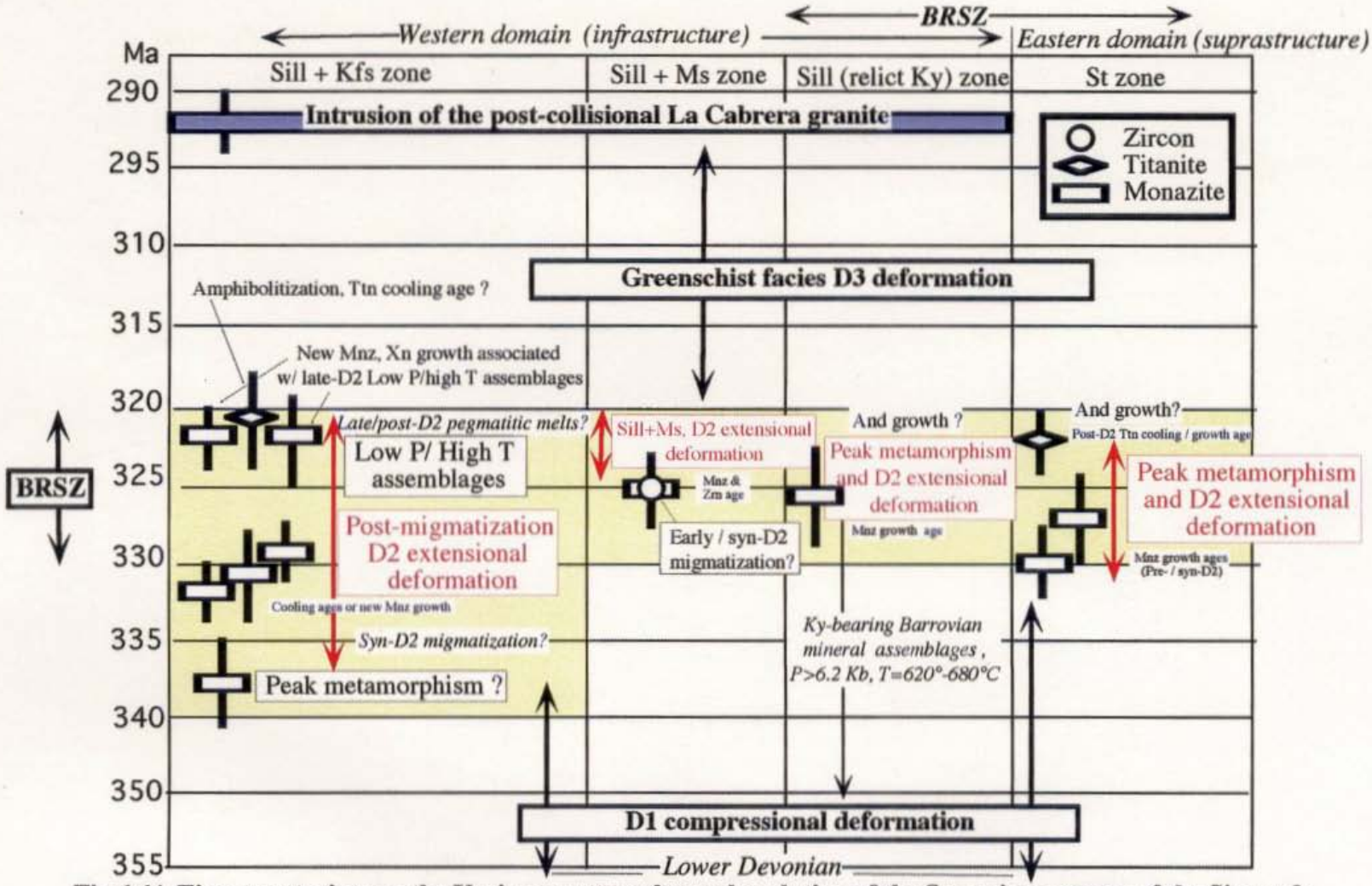

Fig.6.64. Time constraints on the Variscan tectonothermal evolution of the Somosierra sector of the Sierra de Guadarrama

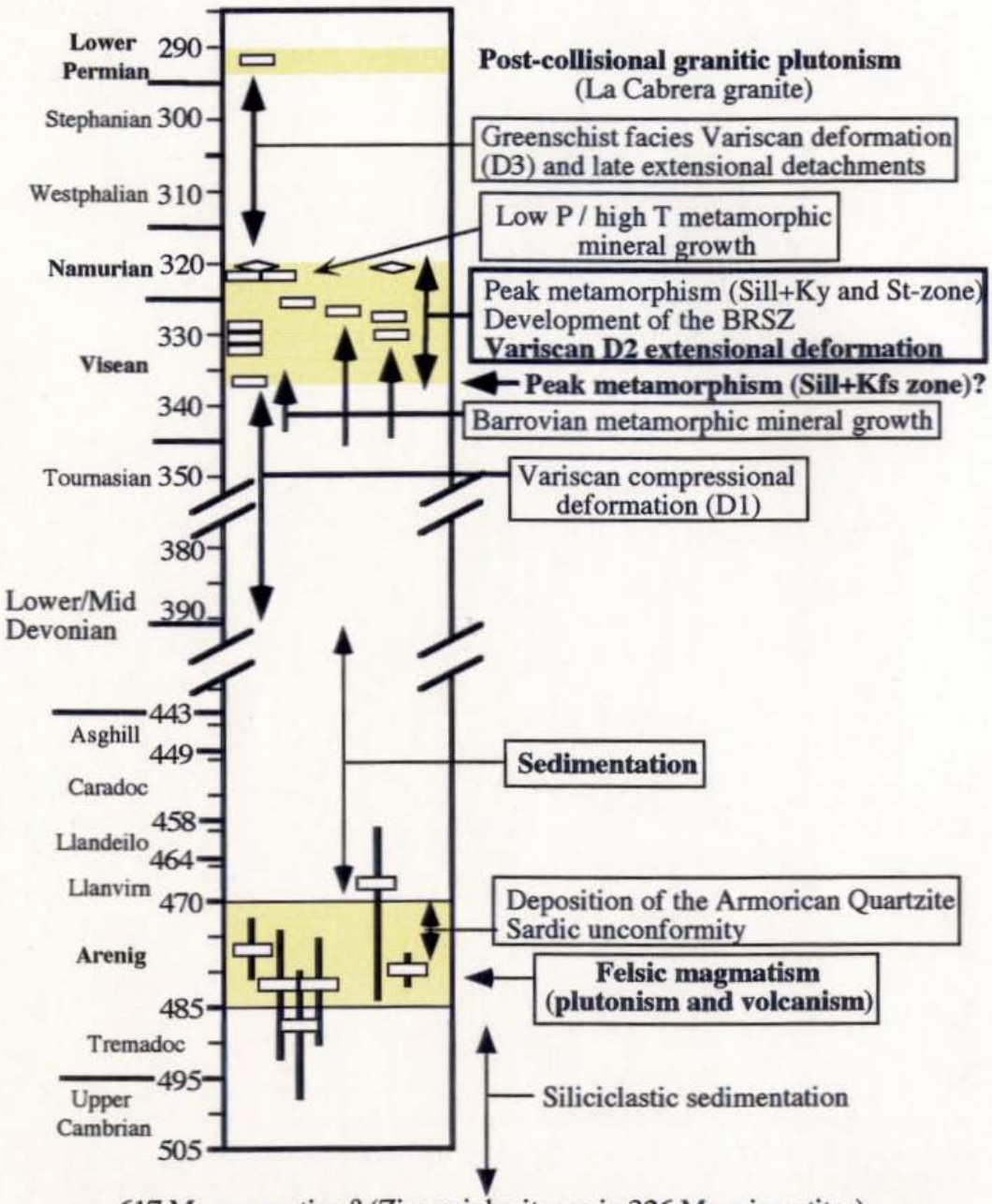

Fig.6.65.- Tectonothermal evolution of the Somosierra sector of the Sierra de Guadarrama, Ollo de Sapo domain, Central Iberian Zone, Iberian Massif (Central Spain).

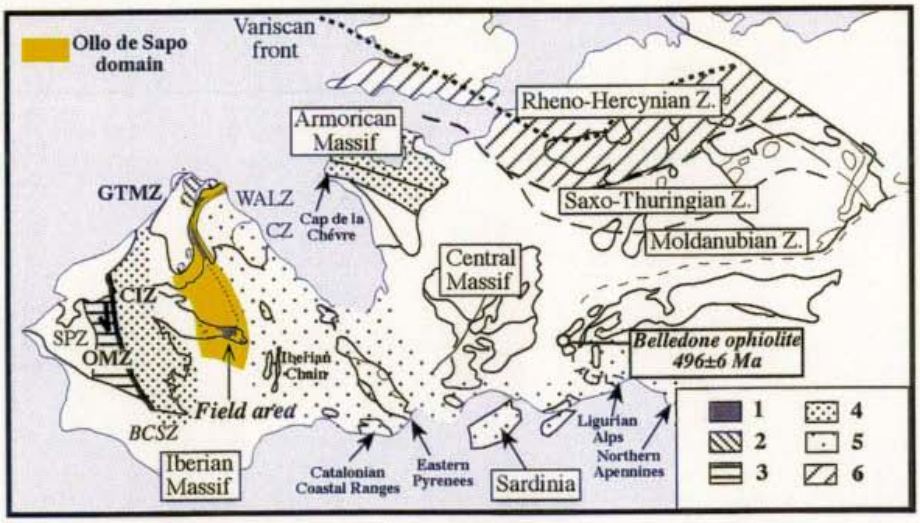

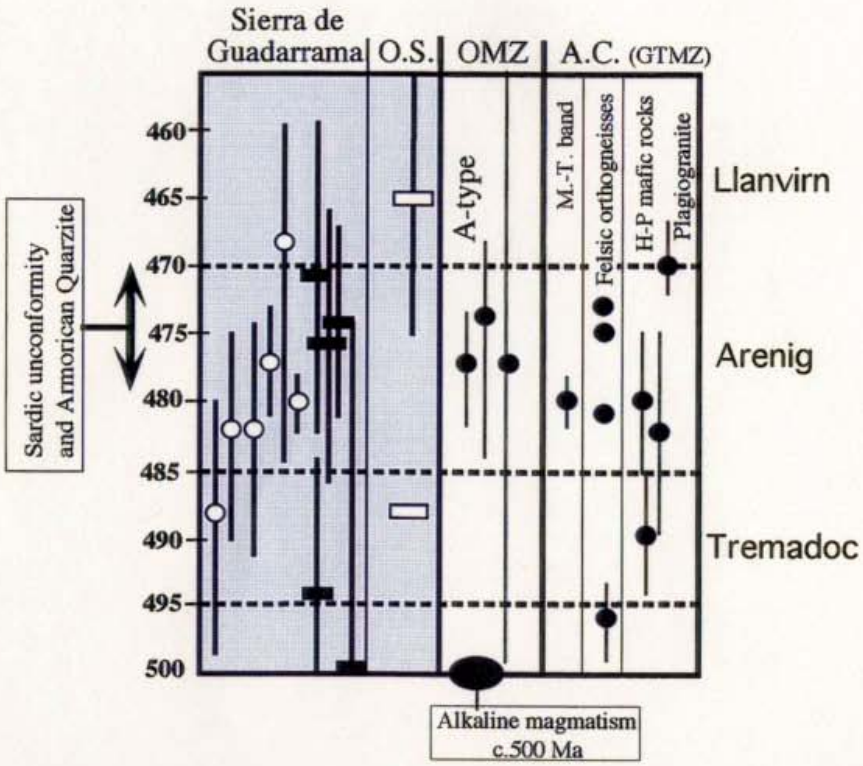

Fig.6.66.- Comparative table of Ordovician U-Pb and Rb-Sr absolute ages from the Central Iberian Zone (grey area) and U-Pb ages from other parts of the Iberian Massif (Time scale of Tucker and McKerrow, 1995) and location of these areas within the European Variscides. Table: open circles, U-Pb ages this study; open rectangles, U-Pb ages of Lancelot et al (1985) and Gebauer et al (1993); filled rectangles, Rb-Sr ages (Vialette et al., 1986; 1986); filled circles, U-Pb ages from the OMZ and the allochthonous complexes (A.C.) of the GTMZ (References in chapter V).
Map legend: 1) Pre-Variscan orthogneisses of the Ollo de Sapo domain; 2) Allocthonous complexes of the GTMZ. Early-Mid Paleozoic faunal domains (Paris and Robardet, 1990): 3) Ossa-Morena domain; 4) Central Iberian domain; 5) Ebro-Aquitanian domain.

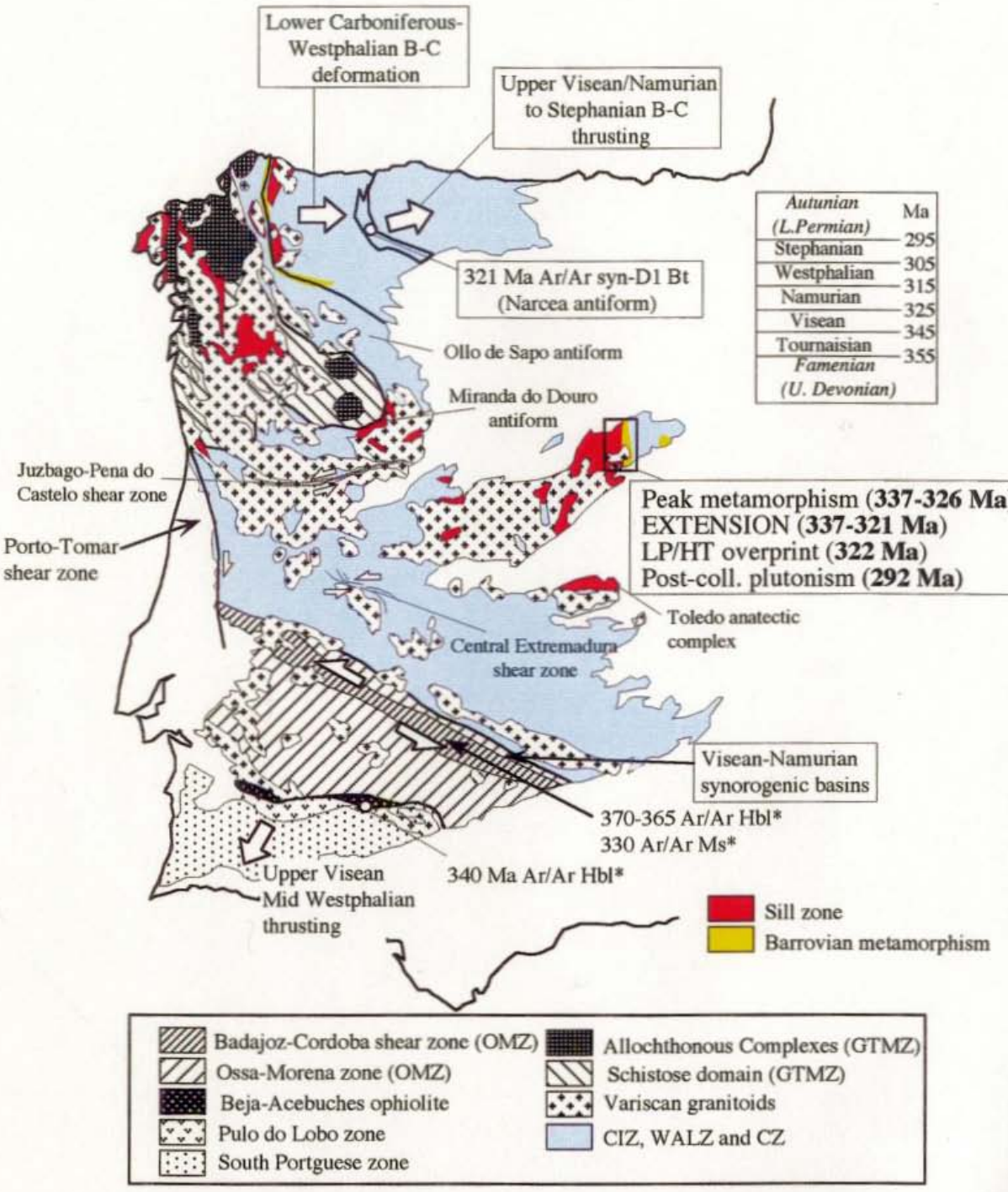

Fig. 6.67.- Map of the Iberian Massif showing the new time constraints on the Variscan tectonothermal events from the Somosierra sector of the Sierra de Guadarrama, other time constraints on the timing of the Variscan deformation and the distribution of the Carboniferous Variscan metamorphism and plutonism. (References in chapter V, * metamorphic cooling ages; time scale after Odin, 1990).

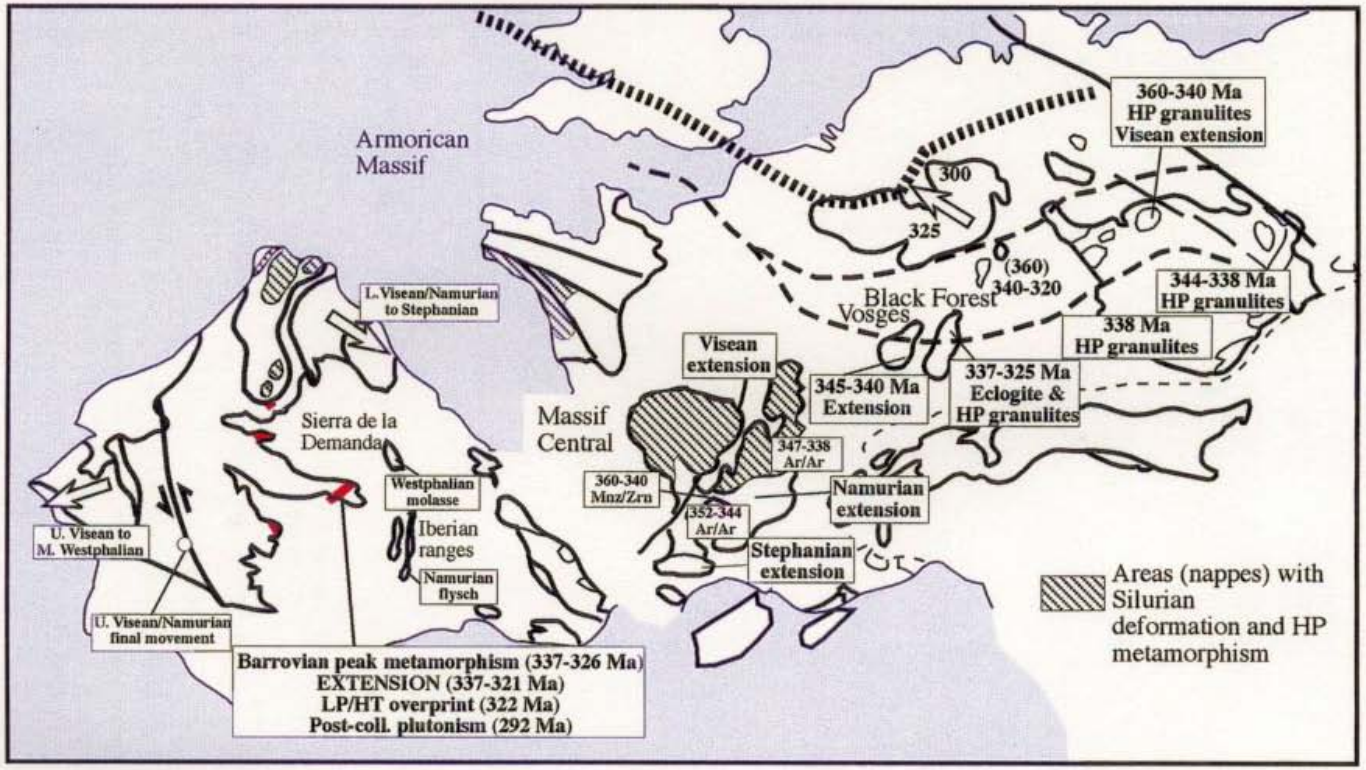

Fig.6.68.- Timing and distribution of the Early-Mid Carboniferous syncollisional extension and metamorphism along the Variscan belt (Burg et al., 1994; Krohe, 1996).- Data from the Massif Central (Faure, 1995; Costa, 1991); Vosges (Schaltegger et al., 1996); Black Forest (Kalt et al., 1994); Saxonian granulites (Reinhardt and Kleeman, 1994); Bohemian Massif (Aftalion et al., 1989; van Breemen et al., 1982); Iberian Massif (ref. in text except: Sierra de la Demanda, Villena and Pardo, 1983 ; Iberian ranges, Melendez et al., 1983). Red areas of reported syn-collisional extension in the CIZ. HP, high-pressure; LP, low-pressure; HT, high-temperature.

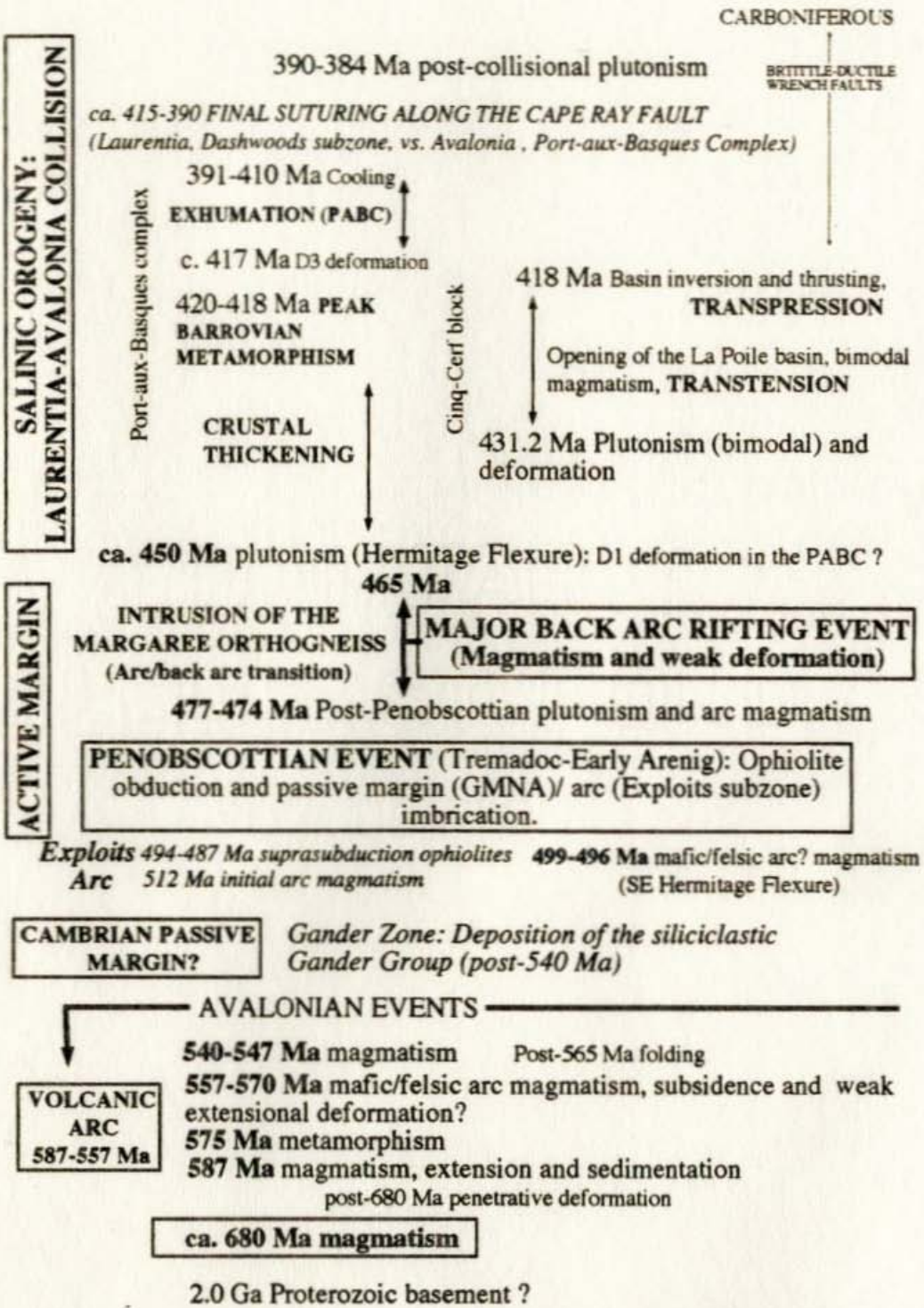

Fig. 7.1.- Tectonothermal evolution of the Gondwanan margin of the Newfoundland Appalachians, Hermitage Flexure.

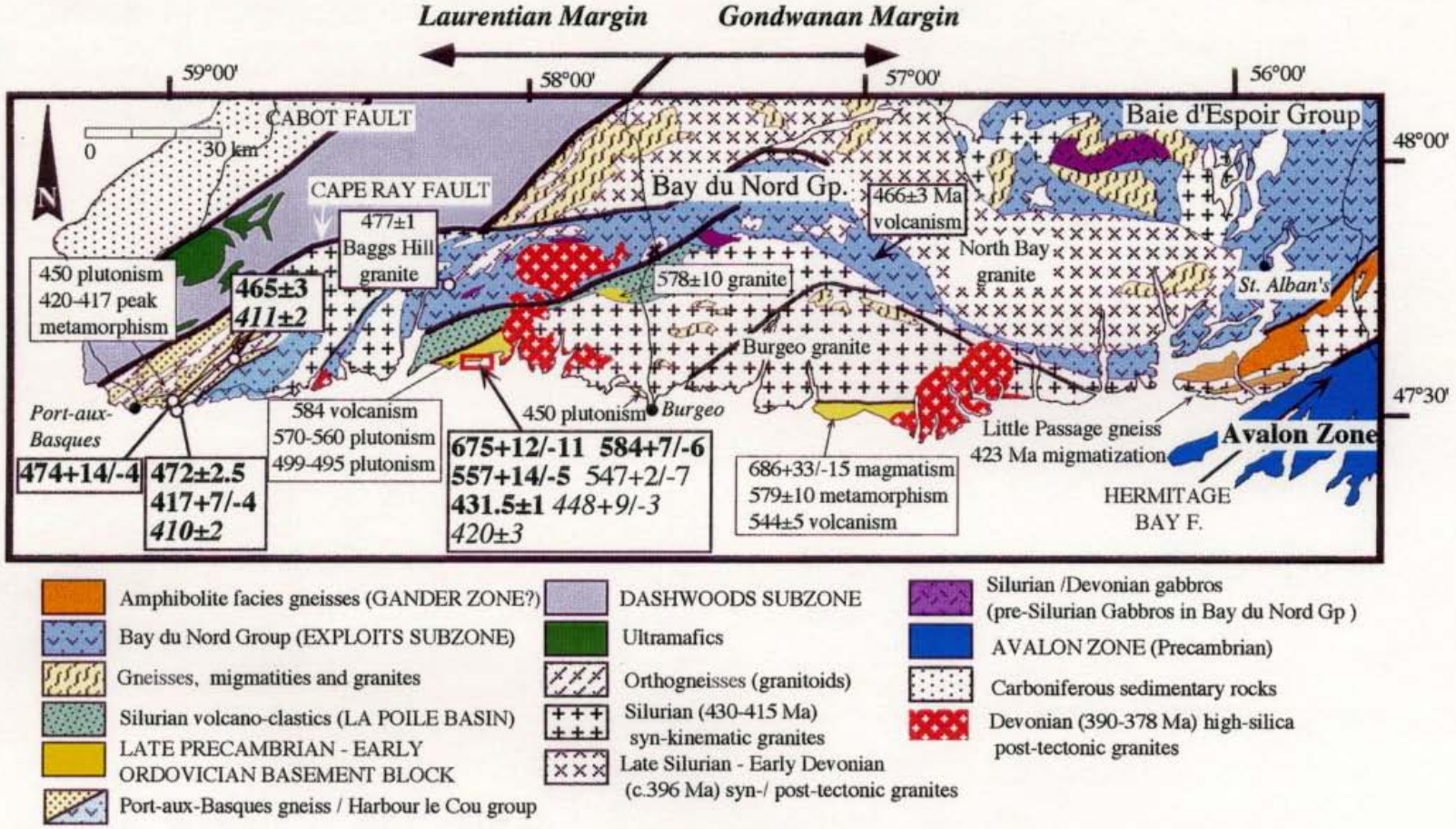

Fig.7.2.- Geological map of the Hermitage Flexure (modified after Dunning et al., 1990) showing the location of the new U-Pb data (Ma protolith ages; italics, titanite ages; plain, unpublished data of Dunning and O'Brien from the Cinq-Cerf gneiss) and the geological data discussed in the text.

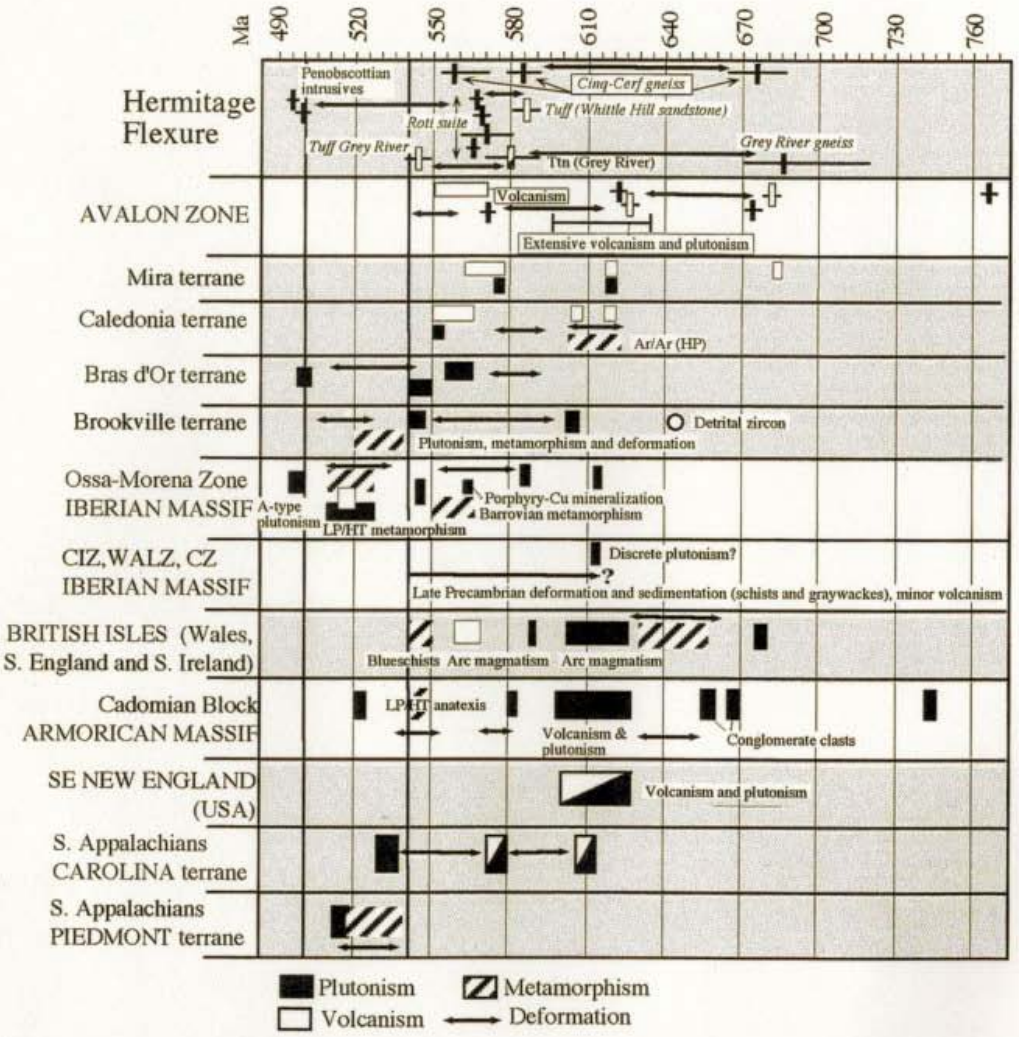

Fig. 7.3.- Comparative table of events in the Late Precambrian, peri-Gondwanan, Cadomian / Avalonian belt and the Hermitage Flexure of the Newfoundland Appalachians. Sources of data: Hermitage Flexure (This study; Dunning and O'Brien, 1989; O'Brien et al., 1996; Dubé and Dunning, in press); Avalon Zone (Newfoundland Appalachians; O'Brien et al., 1996); Mira, Caledonia, Bras d'Or and Brookville terranes (Northern Appalachians, Nova Scotia and Cape Breton; Barr and White, 1996; White and Barr, 1996); Iberian Massif: Ossa Morena Zone (Schafer, 1990; Oschner, 1993); CIZ, WALZ, CZ (Lancelot et al., 1985; Julivert and Martinez, 1987); British Avalon (Tucker and Pharaoh, 1991; Strachan et al., 1996; Gibbons and Horák, 1996); Armorican Massif (Cadomian block, Guerrot and Peucat, 1990; Egal et al., 1996); New England Appalachians (Thompson et al., 1996); Southern Appalachians: Carolina and Piedmont terranes (Hibbard and Samson, 1995).

Fig. 7.4.- Distribution of the Late Precambrian Cadomian / Avalonian terranes on pre-drift reconstruction of the circum-North Atlantic. G.Z., Gander Zone; E.S., Exploits subzone. Iberian Massif: CZ, Cantabrian Zone; WALZ; West Asturian-Leonese Zone; CIZ, Central Iberian Zone; OMZ, Ossa-Morena Zone; black pattern, pre-Variscan orthogneisses of the CIZ.

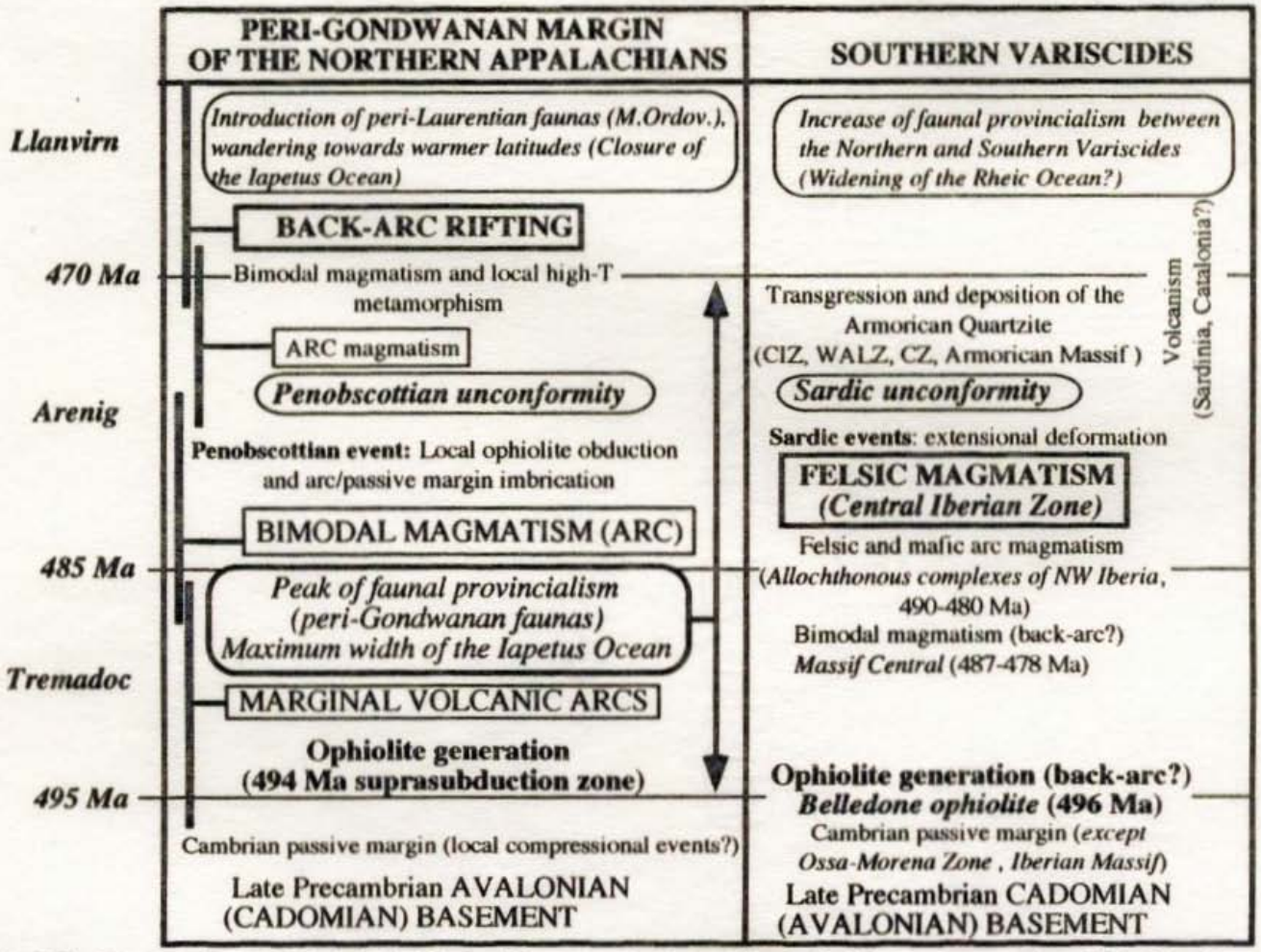

Fig.7.5.- Comparison of the Early Ordovician events in the Peri-Gondwanan margin of the Northern Appalachians and the Southern Variscides. Time scale after Tucker and McKerrow (1995).

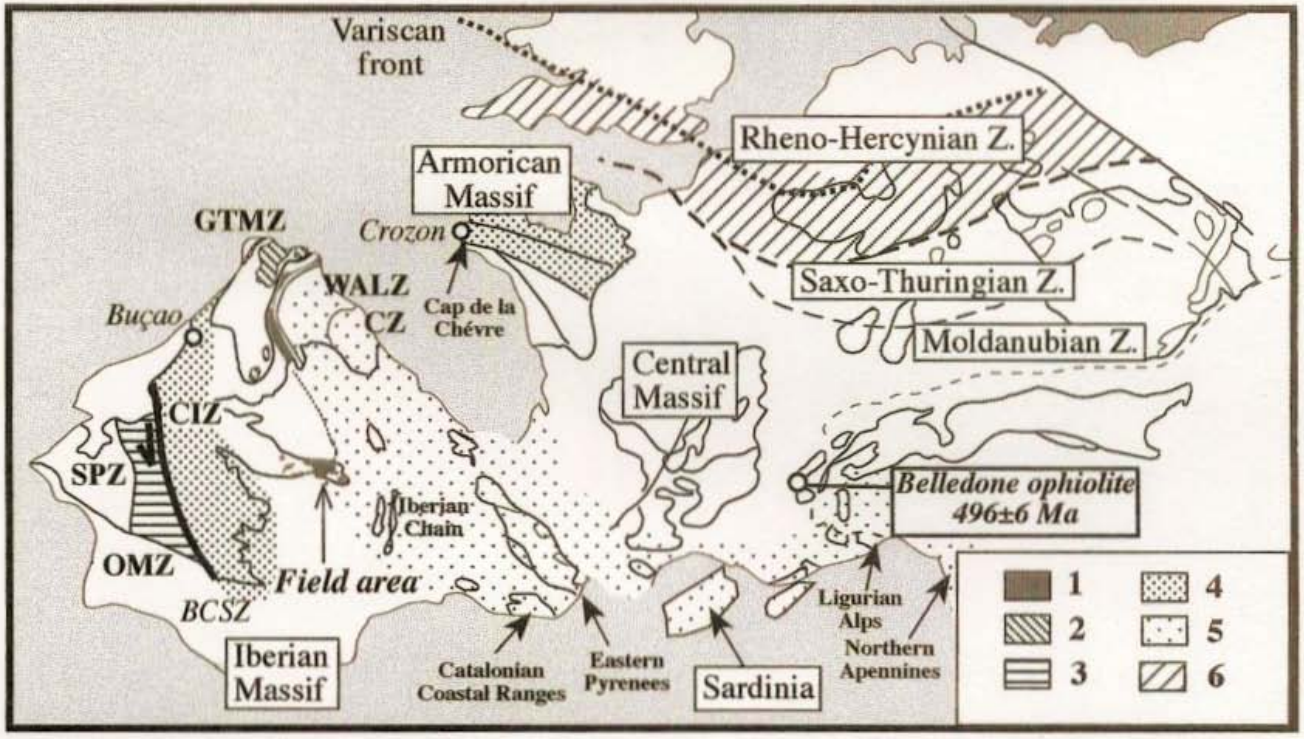

Fig. 7.6.- Location of the interpreted relict Arenig felsic magmatic arc of the CIZ in the Southern Variscides. Legend: 1) Pre-Variscan orthogneisses of the Sierra de Guadarrama and correlatives along the Ollo de Sapo Domain (Arenig magmatic arc?); 2) Allochthonous complexes of NW Iberia; Ordovician faunal domains (Robardet et al., 1990): (3) South Iberian (OMZ), (4) Central Iberian and (5) Ebro-Aquitanian domains; 6) Northern Variscides (Paris and Robardet, 1990). Open circles, matching Arenig to Ashgill stratigraphic sequences (Buçao and Crozon; Young, 1990) and location of the Belledone ophiolite (U-Pb age; Ménot et al., 1988). Cap de la Chévre, Early Ordovician volcaniclastics (continuation in the Armorican Massif of the Ollo de Sapo domain?). Lithotectonic zones of the Iberian Massif (Julivert et al., 1977; Farias et al., 1987): (SPZ) South Portuguese, (OMZ) Ossa-Morena, (CIZ) Central Iberian, (GTMZ) Galicia Tras-os-Montes, (WALZ) West Asturian Leonese and (CZ) Cantabrian zones.

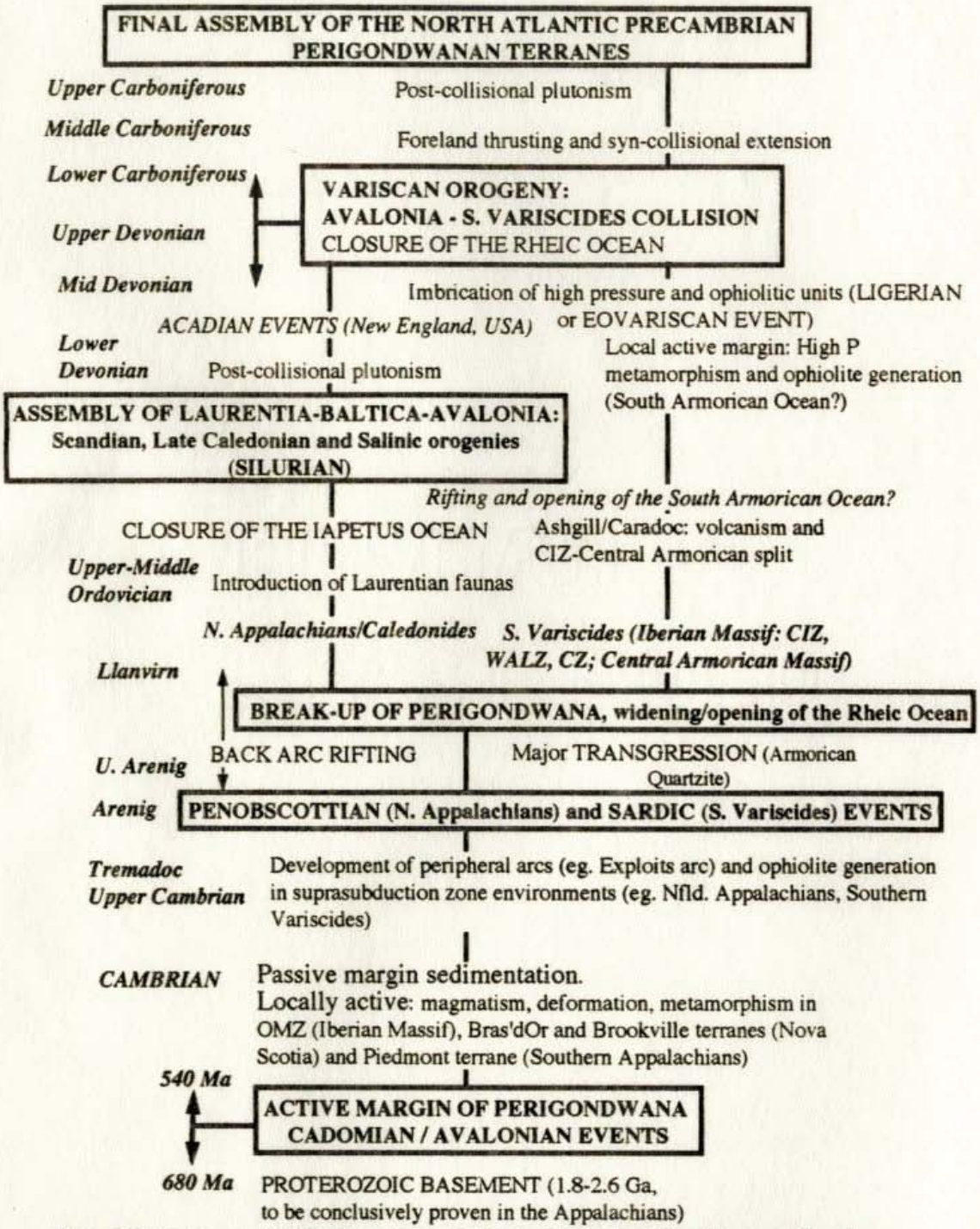

Fig. 7.7.- Interpreted Paleozoic evolution of North Atlantic peri-Gondwana.
Note (conceptual oceans); Iapetus Ocean, Laurentia-Perigondwana (eg. Williams, 1978); Rheic Ocean, Avalonia-Southern Variscides (Paris and Robardet, 1991); South Armorican Ocean: northern Iberia-Armorica (Hanmer, 1977; Paris and Robardet, 1991)

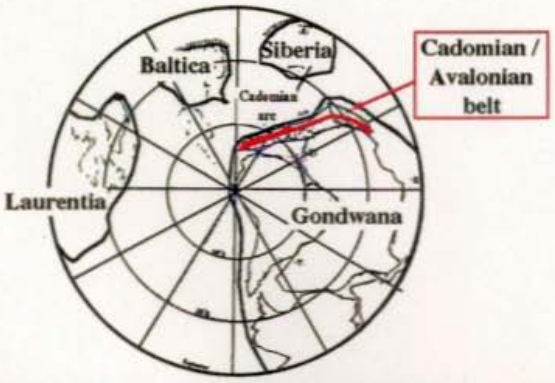

Late Precambrian (Vendian): development of the peri-Gondwanan Cadomian/Avalonian belt (red)

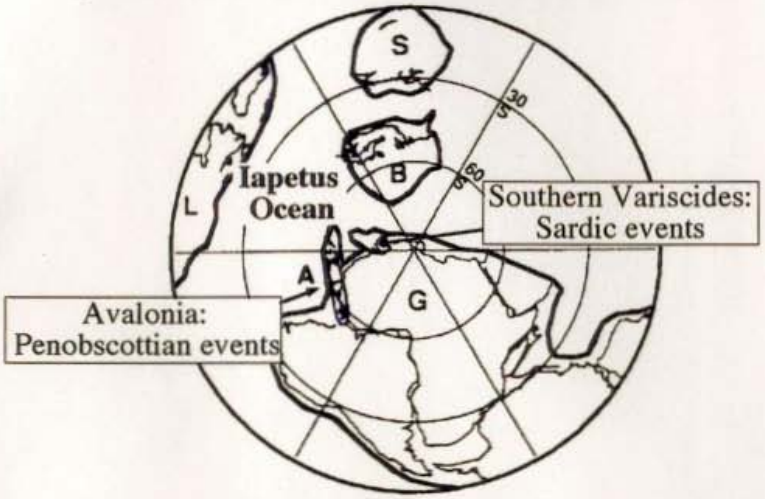

EARLY ORDOVICIAN

Middle Ordovician: Rifting of Avalonia

Late Ordovician: Avalonia-Laurentia collision

Fig. 7.8.- Paleogeographic reconstructions of Avalonia (A, Cadomian arc), Baltica (B), Gondwana (G) and Laurentia (L) in the Late Precambrian (Torsvik et al., 1996) and the Ordovician (van der Pluijm et al., 1995) and rationale for the Mid Paleozoic events discussed in fig. 7.7.